frontiers | Research Topics

# Advances in the discovery of natural molecules and their analogues against microbial infection-related biofilms

**Edited by**
Laura Quintieri, Giovanni Lentini, Sridhar Mani and Giuseppantonio Maisetta

**Published in**
Frontiers in Microbiology

ISSN 1664-8714
ISBN 978-2-83251-011-7
DOI 10.3389/978-2-83251-011-7

## About Frontiers

Frontiers is more than just an open access publisher of scholarly articles: it is a pioneering approach to the world of academia, radically improving the way scholarly research is managed. The grand vision of Frontiers is a world where all people have an equal opportunity to seek, share and generate knowledge. Frontiers provides immediate and permanent online open access to all its publications, but this alone is not enough to realize our grand goals.

## Frontiers journal series

The Frontiers journal series is a multi-tier and interdisciplinary set of open-access, online journals, promising a paradigm shift from the current review, selection and dissemination processes in academic publishing. All Frontiers journals are driven by researchers for researchers; therefore, they constitute a service to the scholarly community. At the same time, the *Frontiers journal series* operates on a revolutionary invention, the tiered publishing system, initially addressing specific communities of scholars, and gradually climbing up to broader public understanding, thus serving the interests of the lay society, too.

## Dedication to quality

Each Frontiers article is a landmark of the highest quality, thanks to genuinely collaborative interactions between authors and review editors, who include some of the world's best academicians. Research must be certified by peers before entering a stream of knowledge that may eventually reach the public - and shape society; therefore, Frontiers only applies the most rigorous and unbiased reviews. Frontiers revolutionizes research publishing by freely delivering the most outstanding research, evaluated with no bias from both the academic and social point of view. By applying the most advanced information technologies, Frontiers is catapulting scholarly publishing into a new generation.

## What are Frontiers Research Topics?

Frontiers Research Topics are very popular trademarks of the *Frontiers journals series*: they are collections of at least ten articles, all centered on a particular subject. With their unique mix of varied contributions from Original Research to Review Articles, Frontiers Research Topics unify the most influential researchers, the latest key findings and historical advances in a hot research area.

Find out more on how to host your own Frontiers Research Topic or contribute to one as an author by contacting the Frontiers editorial office: frontiersin.org/about/contact

# Advances in the discovery of natural molecules and their analogues against microbial infection-related biofilms

**Topic editors**

Laura Quintieri — Institute of Sciences of Food Production, National Research Council (CNR), Italy

Giovanni Lentini — University of Bari Aldo Moro, Italy

Sridhar Mani — Albert Einstein College of Medicine, United States

Giuseppantonio Maisetta — University of Pisa, Italy

**Citation**

Quintieri, L., Lentini, G., Mani, S., Maisetta, G., eds. (2022). *Advances in the discovery of natural molecules and their analogues against microbial infection-related biofilms*. Lausanne: Frontiers Media SA. doi: 10.3389/978-2-83251-011-7

# Table of contents

frontiers | Frontiers in Microbiology

TYPE Editorial
PUBLISHED 25 November 2022
DOI 10.3389/fmicb.2022.1092209



OPEN ACCESS

EDITED AND REVIEWED BY
Rustam Aminov,
University of Aberdeen,
United Kingdom

*CORRESPONDENCE
Laura Quintieri
laura.quintieri@ispa.cnr.it
Giuseppantonio Maisetta
giuseppantonio.maisetta@unipi.it

SPECIALTY SECTION
This article was submitted to Antimicrobials, Resistance and Chemotherapy, a section of the journal Frontiers in Microbiology

RECEIVED 07 November 2022
ACCEPTED 09 November 2022
PUBLISHED 25 November 2022

CITATION
Quintieri L, Mani S, Lentini G and Maisetta G (2022) Editorial: Advances in the discovery of natural molecules and their analogues against microbial infection-related biofilms. *Front. Microbiol.* 13:1092209. doi: 10.3389/fmicb.2022.1092209



# Editorial: Advances in the discovery of natural molecules and their analogues against microbial infection-related biofilms

Laura Quintieri[1]*, Sridhar Mani[2], Giovanni Lentini[3] and Giuseppantonio Maisetta[4]*

[1]Institute of Sciences of Food Production, National Research Council (CNR), Bari, Italy, [2]Department of Medicine, Molecular Pharmacology and Genetics, Albert Einstein College of Medicine, The Bronx, NY, United States, [3]Department of Pharmacy-Pharmaceutical Sciences, University of Bari Aldo Moro, Bari, Italy, [4]Department of Translational Research and New Technologies in Medicine and Surgery, University of Pisa, Pisa, Italy

KEYWORDS

**biofilm, antibiotics, Quorum-Sensing, natural compounds, resistance**

Editorial on the Research Topic
Advances in the discovery of natural molecules and their analogues against microbial infection-related biofilms

Bacterial biofilms are clusters of bacteria attached to a surface and embedded in a self-produced matrix. Biofilm formation can cause several infections of living tissues including wounds, lungs, and dental plaque, as well as infection of external devices such as contact lenses, prosthetic joints, and catheters (Vestby et al., 2020). The resistance of biofilm to antimicrobial agents is due to different mechanisms, such as the presence of persister cells, reduced bacterial growth rate, and limited antibiotic penetration (Ciofu et al., 2022). Despite intensive work, the therapy of biofilm-associated infections is still problematic to date. It relies on high doses of systemic antibiotic combinations to eradicate pre-formed biofilms. Nature has been always the source of inspiration for the finding of novel medicinal drugs. Natural compounds such as phytochemicals and antimicrobial peptides are promising molecules in the development of novel antibiofilm treatments (Mishra et al., 2020). Some of these are less prone to induce resistance, exhibit a wide spectrum of actions, and are suitable for chemical modification to improve pharmacological and pharmacokinetic properties. In this context, this Research Topic aimed to gather a collection of papers focused on the anti-biofilm activity of new natural molecules and synthetic analogs. A total of 13 research articles were collected disclosing new and interesting aspects of the promising approaches to prevent or eradicate microbial biofilms formed by human pathogens using plant extracts, essential oils, and nanoparticles prepared using natural compounds.

Five articles described natural compounds with antibiofilm activity against *Pseudomonas aeruginosa*, which is an opportunistic Gram-negative bacterium and a leading cause of nosocomial infections, highly contributing to morbidity and mortality of patients with cystic fibrosis (CF) or with severe burns (Reynolds and Kollef, 2021). *P. aeruginosa* readily acquires antimicrobial resistance determinants, resulting in multidrug-resistant or pan-drug-resistant strains (Reynolds and Kollef, 2021). An attempt to inhibit the biofilm formation is to quench the Quorum-Sensing (QS), which is a cell-to-cell signaling process involved in both the biofilm formation and the expression of genes associated with bacterial virulence (Rather et al., 2022; Wang et al., 2022). The QS system of *P. aeruginosa* is mainly regulated by four QS network subsystems, including lasI/lasR, rhlI/rhlR, PQS, and IQS systems (Rather et al., 2022).

In a mouse model of *P. aeruginosa*-induced acute lung infection, Tang et al. demonstrated that the phenolic compound epigallocatechin-3-gallate (EGCG), one of the richest ingredients in green tea-derived polyphenols, protected mice against *P. aeruginosa*-induced lung damage by inhibiting the virulence controlled by QS systems. In particular, EGCG decreased the expression of both QS-system genes (*las, rhl* and *pqs*) and biofilm-related genes (*pela, pila*, and *pslb*). Choi et al. observed that the Rhl QS system was selectively inhibited by curvularin, an aromatic compound isolated from the soil fungus *Phoma macrostoma*. Curvularin inhibited the production of pyocyanin and rhamnolipid and reduced the *in vivo* virulence of *P. aeruginosa* in the infection model *of Caenorhabditis elegans*.

Jia et al. observed that PQS QS system was inhibited by phthiocol (Pht), a metabolite produced by *Mycobacterium tuberculosis*. The binding of Pht and its analogs (Vitamin K1, K2 and K3) to PQS receptors of *P. aeruginosa* caused the reduction of both biofilm formation and pyocyanin production.

A standardized extract of cultured mycelium of *Lentinula edodes* (AHCC), which is available as a dietary supplement, was found by Garitaonaindia et al. to inhibit the biofilm formation of *P. aeruginosa* and to Garitaonaindia the levels of exotoxin A.

*P. aeruginosa* plays a crucial role in chronic wound infections, Di Lodovico et al. propose the *C. spinose* aqueous extract as an innovative eco-friendly strategy to prevent and control wound microbial infections. In this study authors demonstrated that such extract significantly reduced the biofilm formed by *P. aeruginosa* and *S. aureus* in the Lubbock system. This model mimics the *in vivo* microbial spatial distribution in wounds.

Although much less investigated than bacterial biofilms, also fungal biofilms play a major role in human infections (Cavalheiro and Teixeira, 2018). An increasing number of people are affected by fungal biofilm-based infections, which are resistant to the majority of currently used antifungal drugs. Only a few antifungal drugs including echinocandins and liposomal formulations of amphotericin B are available to treat biofilm-based fungal infections. In three papers on this Research Topic, the authors studied the effects of different natural compounds on fungi.

Khadke et al. demonstrated that *trans*-4-methylcinnamaldehydes which are present in the bark of trees, were able to down-regulate several genes involved in biofilm formation such as genes for hyphal development and matrix production of *Candida albicans*.

The new sodium houttuyfonate (SNH) is a compound derived from the plant *Houttuynia cordata*, an herbal drug clinically used in Asia. Zhang et al. demonstrated that SNH inhibited fungal sporulation, conidial germination, and biofilm formation. Interestingly, daily gastric gavage of SNH significantly decreased the fungal burden and local tissue damage in a mouse model of disseminated infection of *Aspergillus fumigatus*.

Wei et al. isolated from the endophytic fungus *Xylaria curta* E10 new dimeric chromanones (Paecilins) and several Paecilins showed antifungal activity against *C. albicans*.

Nanobiotechnology has gained attention in the pharmaceutical and medical fields, and the nano-sizing of antimicrobial agents seems to be a promising treatment for biofilm-related infections. In two papers on this Research Topic, antibiofilm of different chitosan formulations were studied. Chitosan (CS) is a cost-effective biopolymer suitable for preparing biocompatible, biodegradable, and non-cytotoxic nanoparticles (Kumar et al., 2022).

In the paper of Tan et al., amphotericin B (AmpB)-loaded chitosan nanoparticles (CSNP) functioned with β-1,3 glucanase (Gls), and their antibiofilm activity was evaluated against *C. albicans* biofilm *in vitro*. CSNP-AmpB-Gls inhibited biofilm formation and exhibited high efficacy in the disruption of a mature biofilm. Such nanoparticles were able to penetrate the biofilm and disassemble the biofilm matrix.

In their paper, Lin et al., combined chitosan with EDTA and the antimicrobial peptide Nile tilapia piscidin 4 (TP4). Such a formulation was tested against biofilm formed by *Gardnerella vaginalis* and *Streptococcus anginosus*, two vaginitis-associated pathogens. In addition to an antibiofilm activity *in vitro*, the TP4-chitosan formulation significantly decreased the amount of *G. vaginalis* and *S. anginosus* recovered from mice vaginal lavage, after infection with the two microorganisms. Interestingly, the TP4-chitosan formulation did not act against vaginal lactobacilli, representing an important protective component in the vaginal district.

In the paper of Lahiri et al. nanoparticles of ZnO were synthesized using the floral extract of *Clitora ternatea*, a traditionally used medicinal plant. Such nanoparticles showed stability for a long period. They were effective in the eradication

of the oral biofilm formed by *Porhpyromonas gingivalis* or *Alcaligenes faecalis*, reducing the carbohydrate and protein content of the extracellular polymeric substance of biofilm.

*Melissa officinalis* is associated with phytotherapy for its sedative, antispasmodic, antimicrobial, and antioxidative activities. Yu et al. tested the essential oil of *M. officinalis* (MOEO) toward *Vibrio parahaemolyticus* that can lead to vibriosis in different species of aquatic animals, along with septicemia and gastroenteritis in humans. The Authors observed that MOEO could inhibit the biofilm formation and extracellular polysaccharide production.

Finally, Rao et al. tested SYG-180-2-2, an amide-containing compound widely present in natural products and pharmaceuticals, against methillin-resistant *Staphylococcus aureus* strains and showed that such a compound suppressed the biofilm-formation, reducing the bacterial adhesion and the production of polysaccharide intercellular adhesin.

In summary, this Research Topic provides a better understanding of the main natural and alternative components that exhibit activity in the biofilm control of pathogenic species. It is also becoming evident that the problem of biofilm-related infections can only be tackled by using interdisciplinary approaches that involve different expertise from clinicians, microbiologists, chemists, and bio-materialists. In this way, we hope that this Research Topic can generate knowledge and open ways for the construction of new strategies to combat biofilm-related infections.

## Author contributions

GM: draft preparation. LQ, SM, and GL: revision and modification. All authors contributed to the article and approved the submitted version.

## Acknowledgments

We thank all of the contributors to this topic collection. We also appreciate the efforts of the reviewers for their comprehensive manuscript evaluations and suggestions.

## Conflict of interest

The authors declare that the research was conducted in the absence of any commercial or financial relationships that could be construed as a potential conflict of interest.

## Publisher's note



## References

Cavalheiro, M., and Teixeira, M. C. (2018). *Candida* biofilms: threats, challenges, and promising strategies. *Front. Med.* 5, 28. doi: 10.3389/fmed.2018.00028

Ciofu, O., Moser, C., Jensen, P. Ø., and Høiby, N. (2022). Tolerance and resistance of microbial biofilms. *Nat. Rev. Microbiol.* 20, 621–635. doi: 10.1038/s41579-022-00682-4

Kumar, S., Dhiman, R., Prudencio, C. R., da Costa, A. C., Vibhuti, A., Leal, E., et al. (2022). Chitosan: applications in drug delivery system. *Mini Rev. Med. Chem.* doi: 10.2174/1389557522666220609102010

Mishra, R., Panda, A. K., De Mandal, S., Shakeel, M., Bisht, S. S., and Khan, J. (2020). Natural anti-biofilm agents: strategies to control biofilm-forming pathogens. *Front. Microbiol.* 11:566325. doi: 10.3389/fmicb.2020.566325

Rather, M. A., Saha, D., Bhuyan, S., Jha, A. N., and Mandal, M. (2022). Quorum quenching: a drug discovery approach against *Pseudomonas aeruginosa*. *Microbio. Res.* 264, 127173. doi: 10.1016/j.micres.2022.127173

Reynolds, D., and Kollef, M. (2021). The epidemiology and pathogenesis and treatment of *pseudomonas aeruginosa* infections: an update. *Drugs*. 81, 2117–2131. doi: 10.1007/s40265-021-01635-6

Vestby, L. K., Grønseth, T., Simm, R., and Nesse, L. L. (2020). Bacterial biofilm and its role in the pathogenesis of disease. *Antibiotics*. 9, 59. doi: 10.3390/antibiotics9020059

Wang, Y., Bian, Z., and Wang,.Y. (2022). Biofilm formation and inhibition mediated by bacterial quorum sensing. *Appl. Microbiol. Biotechnol.* 106, 365–638. doi: 10.1007/s00253-022-12150-3

frontiers in Microbiology

ORIGINAL RESEARCH
published: 07 January 2022
doi: 10.3389/fmicb.2021.770657

# Small-Molecule Compound SYG-180-2-2 to Effectively Prevent the Biofilm Formation of Methicillin-Resistant *Staphylococcus aureus*

*Lulin Rao[1], Yaoguang Sheng[2], Jiao Zhang[1], Yanlei Xu[3], Jingyi Yu[4], Bingjie Wang[4], Huilin Zhao[4], Xinyi Wang[4], Yinjuan Guo[4], Xiaocui Wu[4], Zengqiang Song[2], Fangyou Yu[1,4]* and Lingling Zhan[1]**

[1] Department of Laboratory Medicine, The First Affiliated Hospital of Wenzhou Medical University, Wenzhou, China, [2] School of Pharmaceutical Sciences, Wenzhou Medical University, Wenzhou, China, [3] Jiangxi Provincial Key Laboratory of Preventive Medicine, School of Public Health, Nanchang University, Nanchang, China, [4] Department of Clinical Laboratory, School of Medicine, Shanghai Pulmonary Hospital, Tongji University, Shanghai, China

OPEN ACCESS

**Edited by:**
Giuseppantonio Maisetta,
University of Pisa, Italy

**Reviewed by:**
Silke Niemann,
University Hospital Münster, Germany
Lucinda Janete Bessa,
Centro de Investigação Interdisciplinar Egas Moniz (CiiEM), Egas Moniz - Cooperativa de Ensino Superior, CRL, Portugal

***Correspondence:**
Fangyou Yu
wzjxyfy@163.com
Lingling Zhan
zll6560@126.com

**Specialty section:**
This article was submitted to Antimicrobials, Resistance and Chemotherapy, a section of the journal Frontiers in Microbiology

**Received:** 04 September 2021
**Accepted:** 08 December 2021
**Published:** 07 January 2022

**Citation:**
Rao L, Sheng Y, Zhang J, Xu Y, Yu J, Wang B, Zhao H, Wang X, Guo Y, Wu X, Song Z, Yu F and Zhan L (2022) Small-Molecule Compound SYG-180-2-2 to Effectively Prevent the Biofilm Formation of Methicillin-Resistant Staphylococcus aureus. Front. Microbiol. 12:770657. doi: 10.3389/fmicb.2021.770657

The resistance of methicillin-resistant *Staphylococcus aureus* (MRSA) has augmented due to the abuse of antibiotics, bringing about difficulties in the treatment of infection especially with the formation of biofilm. Thus, it is essential to develop antimicrobials. Here we synthesized a novel small-molecule compound, which we termed SYG-180-2-2 ($C_{21}H_{16}N_2OSe$), that had antibiofilm activity. The aim of this study was to demonstrate the antibiofilm effect of SYG-180-2-2 against clinical MRSA isolates at a subinhibitory concentration (4 μg/ml). In this study, it was showed that significant suppression in biofilm formation occurred with SYG-180-2-2 treatment, the inhibition ranged between 65.0 and 85.2%. Subsequently, confocal laser scanning microscopy and a bacterial biofilm metabolism activity assay further demonstrated that SYG-180-2-2 could suppress biofilm. Additionally, SYG-180-2-2 reduced bacterial adhesion and polysaccharide intercellular adhesin (PIA) production. It was found that the expression of *icaA* and other biofilm-related genes were downregulated as evaluated by RT-qPCR. At the same time, *icaR* and *codY* were upregulated when biofilms were treated with SYG-180-2-2. Based on the above results, we speculate that SYG-180-2-2 inhibits the formation of biofilm by affecting cell adhesion and the expression of genes related to PIA production. Above all, SYG-180-2-2 had no toxic effects on human normal alveolar epithelial cells BEAS-2B. Collectively, the small-molecule compound SYG-180-2-2 is a safe and effective antibacterial agent for inhibiting MRSA biofilm.

**Keywords: MRSA, SYG-180-2-2, biofilm, cell adhesion, *icaA***

## INTRODUCTION

*Staphylococcus aureus* is a pathogen that causes a variety of infections ranging from relatively benign to life-threatening infections including pneumonia, endocarditis, osteomyelitis, and sepsis (Cassat et al., 2007). Due to the use of antibiotics, drug-resistant strains have increased rapidly, especially methicillin-resistant *Staphylococcus aureus* (MRSA) which is difficult to treat and has a

high mortality rate (Mole, 2013). It was reported that some MRSA had even developed resistance to vancomycin which is the most effective antibiotic for the treatment of MRSA (Cong et al., 2020). With the introduction of biomaterials such as artificial catheters and artificial joints, implant material-related infections frequently develop (Biedlingmaier et al., 1998), and they are usually persistent and multidrug-resistant, which brings a heavy burden to patients (Aslan and Yapar, 2015). The main cause of such infections is biofilm formation (Uruen et al., 2020). Biofilm is a kind of special colony structure formed by the encapsulation of a microorganism in its own secreted polymer (Hoiby et al., 2010), which will tend to resist both host clearance mechanisms and antibiotic therapy (Reed et al., 1986). Treatment with traditional antibiotics is ineffective to cope with the current severe drug resistance situation (Basnyat et al., 2015). Therefore, it is urgent to develop new drugs that cannot only effectively inhibit biofilm formation but also prevent bacterial mutations from developing drug resistance.

The formation of biofilm is a dynamic process, including initial adhesion, proliferation, maturation, and diffusion (Dufour et al., 2010). Initial adhesion is the first stage of biofilm formation. The most prominent cell wall-anchored proteins are microbial surface components that recognize adhesive matrix molecules (MSCRAMMs) that promote the binding of *S. aureus* to the host surface (Achek et al., 2020). MSCRAMMs including but not limited to fibronectin binding protein B (*fnbB*), laminin binding protein (*eno*), fibrinogen binding protein (*fib*), and encoding elastin binding protein (*ebpS*) promote the binding of *S. aureus* to the host surface (Nemati et al., 2009). The next stage of biofilm formation is the production of the extracellular matrix and cell proliferation. The extracellular polymeric substance (EPS) is mainly composed of polysaccharides, proteins, and extracellular DNA (eDNA) to protect cells (Lopez et al., 2010). A main component of the EPS is polysaccharide intercellular adhesin (PIA), which is mediated by the intercellular adhesin (*ica*) locus in *S. epidermidis* and *S. aureus* (Rohde et al., 2001; Fluckiger et al., 2005). In *S. aureus* ATCC 35556, mutation of the *ica* operon attenuated the production of PIA and lost the ability to form a strong biofilm (Cramton et al., 1999). *IcaR* is a negative regulator of the *ica* operon; inactivation of *icaR* augmented the transcription of the *icaAD* (Jefferson et al., 2004). In addition to *icaADBC*, *codY* also had an impact on PIA-dependent biofilm formation (Mlynek et al., 2020). The mutation of *codY* in *S. aureus* led to lower PIA production and less biofilm formation (Tu Quoc et al., 2007). The *S. aureus* Sae two component system involves the SaeS sensor histidine kinase and the SaeR response regulator, the former regulates the expression of exoproteins such as FnbA and FnbB, the latter is essential for the maturation of biofilms (Liu et al., 2016; Schilcher and Horswill, 2020). Besides, the accessory gene regulator (Agr) quorum sensing (QS) system is the most researched on the regulation system of staphylococcal biofilm formation (Yarwood et al., 2004). Part of QS-regulated genes are directly regulated by AgrA, for example, *psm*α and *psm*β (Jenul and Horswill, 2019). Phenol soluble modulins (PSM) expression can lead to the spread of biofilms, which in turn results in the systemic spread of biofilm infections (Peschel and Otto, 2013).

SYG-180-2-2 is a small molecule which consists of an indole ring, a selenyl group, and an amido group. Indoles have been identified as a privileged scaffold for the design of medicinal drugs (O'Connor and Maresh, 2006; Liu et al., 2009; Biersack and Schobert, 2012), 3-selenylindoles are a significant class of indole compounds as they are bioactive (Nogueira et al., 2004), and the amido group is a very important substituent in medicinal chemistry. Amide-containing compounds are widely present in natural products and pharmaceuticals, displaying a wide range of biological activities, such as anticancer and antiviral properties (Fatahala et al., 2017). Considering the dominance of 3-selenylindole and the amido group in nature and their impact in medicinal chemistry, we designed a novel compound SYG-180-2-2 containing these two frameworks. With our continuing interest in the discovery of new antibacterial agents (Yu et al., 2021), we have great interest in the exploration of the antibacterial activity of this novel compound. SYG-180-7 is similar to SYG-180-2-2 in structure and has strong hydrophobicity.

The purpose of this study was to investigate the effect of SYG-180-2-2 at a subinhibitory concentration (4 μg/ml) on the formation of MRSA biofilms and antibacterial mechanisms in order to evaluate the clinical potential of SYG-180-2-2 in the prevention and treatment of MRSA chronic infection.

## MATERIALS AND METHODS

### The Synthesis of SYG-180-2-2 and SYG-180-7

A mixture of *N*-pivaloyl indoles 1 (0.2 mmol), 3-phenyl-1,4,2-dioxazol-5-one (0.6 mmol), $[RuCl_2(p\text{-cymene})]_2$ (5 mol%), $AgSbF_6$ (20 mol%), PivOH (3 equiv), and HFIP (2 ml) was added in a 5 mL glass tube, which was stirred at room temperature for 24 h (Sheng et al., 2021). The reaction was stopped, and it was mixed with water and dichloromethane. The reaction mixture was extracted three times with dichloromethane. The combined organic layer was washed twice with a small amount of water, dried over anhydrous magnesium sulfate, and filtered. The filtrate was evaporated under a vacuum, and the residue was purified by flash column chromatography on silica gel (eluting with petroleum ether-ethyl acetate) to provide the desired product 2. A mixture of 7-amido indoles 2 (0.2 mmol), diphenyl diselenide (0.22 mmol), *t*-BuOK (0.4 mmol), and DMF (2 ml, 0.1 M) was added in a 5 mL glass tube, which was stirred at room temperature for 0.5 h. When the reaction was completed, the next steps were the same as those described above to obtain the desired product SYG-180-2-2 (**Figure 1**). The full name of SYG-180-2-2 is *N*-(3-(phenylselanyl)-1-pivaloyl-1*H*-indol-7-yl) benzamide.

Next, 7-amido indoles 2 (0.2 mmol), Pd $(TFA)_2$ (5 mol%), AgOAc (0.6 mmol), and PivOH (1.2 mmol) were added into a 12 mL screw capped tube with 2 mL of benzene at room temperature. The reaction mixture was allowed to warm up to 110°C and stirred for 4 h. When the reaction was completed, the next steps were the same as those described above to obtain the desired product SYG-180-7 (**Supplementary Figure 1**). The full name of SYG-180-7 is *N*-(2-phenyl-1-pivaloyl-1*H*-indol-7-yl) benzamide.

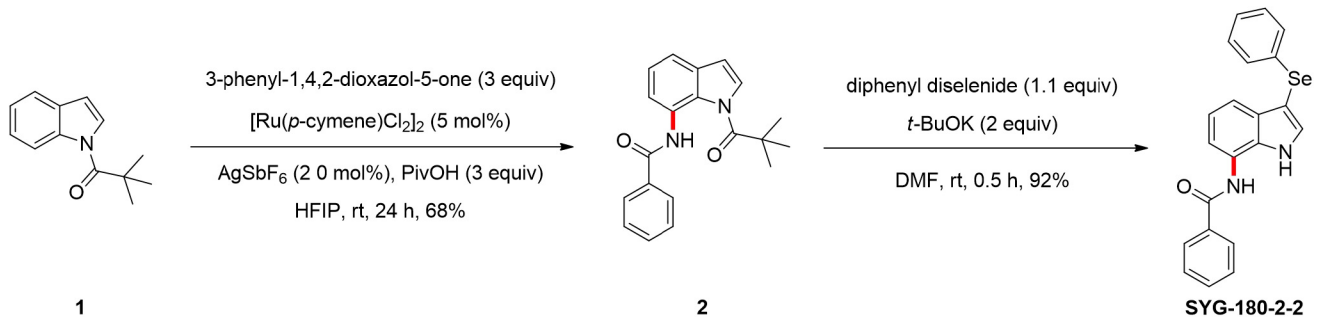


**FIGURE 1 |** Synthetic process of SYG-180-2-2. 1: *N*-pivaloyl indoles. 2: *N*-(1-pivaloyl-1*H*-indol-7-yl) benzamide. SYG-180-2-2: desired product.

**TABLE 1 |** Bacterial strains used in this study.

| Strain | SYG-180-2-2 MIC (μg/ml) | Source | Ward | Antibiotic resistance/susceptibility profiles |
|---|---|---|---|---|
| JP5023 | >128 | Blood | Emergency rescue | PG[1] (R); OX[2] (R); EM[3] (R); CC[4] (R); CIP[5] (I) |
| JP4856 | >128 | Pus | Otolaryngology department | PG (R); OX (R); EM (R); CC (R); CIP (S) |

*1: Penicillin G; 2: Oxacillin; 3: Erythromycin; 4: Clindamycin; 5: Ciprofloxacin.*

## Bacterial Strains, Cells, and Growth Conditions

Bacterial strains used in this study are described at **Table 1**. Methicillin-resistant *S. aureus* strains JP5023 and JP4856 were isolated from patients with different infection sites at the First Affiliated Hospital of Wenzhou Medical University. On the basis of their ability to form potent biofilm, we used them to carry out biofilm research. We used Trypticase soy broth (TSB, BD Biosciences, Franklin Lakes, NJ, United States) medium without antibiotics to culture all strains at 37°C with shaking at 220 rpm.

Human normal alveolar epithelial cells BEAS-2B were a gift from the Clinical Transformation Center, Shanghai Pulmonary Hospital, Tongji University School of Medicine and cultured in Dulbecco's Modified Eagle's Medium [DMEM, Thermo Fisher Biochemical Products (Beijing) Co., Ltd.].

## Determination of Minimum Inhibitory Concentration

SYG-180-2-2 was diluted with dimethyl sulfoxide (DMSO, Biosharp, Beijing, China) to the concentration of 20 mg/ml. The MIC values of SYG-180-2-2 against JP5023 and JP4856 were determined by the microtiter broth dilution method (van Hal et al., 2011). The colonies were cultured for 16–18 h and directly extracted to prepare a 0.5 MacFarland turbidity standard bacterial suspension, and then diluted with cation-adjusted Mueller-Hinton broth (CAMHB) 1:100. A total of 100 μl of medium containing SYG-180-2-2 (1–128 μg/ml) and 100 μl of suspension were added into a 96-well microfilter plate. In the experiment, we used DMSO as a control. After that the plate was incubated for 16–18 h at 37°C. All assays were performed in triplicate. The minimum concentration at which no bacterial growth was observed by the naked eye was defined as the MIC.

## Growth Inhibition Assay

Methicillin-resistant *S. aureus* strains were grown in TSB for 4–6 h and made into a bacterial suspension with a turbidity of 0.5 MacFarland standard. Then we performed 1:100 dilution into TSB medium containing SYG-180-2-2, so that the final concentrations of the medium were 4 and 8 μg/ml. No drug was added as a positive control, TSB was the negative control. An equivalent volume of DMSO to the 4 and 8 μg/ml SYG-180-2-2 samples was used as a control in the experiment in order to exclude the influence of solvent on bacterial growth. A 200 μl mixed liquor was added to a sterile bioscreen honeycomb plate. We used an automatic microbial growth curve analyzer (OY Growth Curves, Finland) to measure $OD_{600}$ every 1 h for 24 h and obtain a growth curve according to the measured values. The test was performed in triplicate.

## Biofilm Formation Assessment

Overnight-cultured MRSA strains JP5023 and JP4856 were diluted 1:100 in different drug concentrations (0–32 μg/ml) with TSB containing 0.5% glucose (TSBG), and each concentration was added to three parallel wells in 96-well microplates. After incubation for 24 h, the wells were washed carefully three times with 200 μl of phosphate-buffered saline [PBS, Sangon Biotech (Shanghai) Co., Ltd.]. Removing unattached bacteria, biofilms were fixed with 200 μl of 99% methanol for 15 min and stained with 200 μl of 1% crystal violet for 8 min (Chaieb et al., 2011). The excess dye was gently washed off the wells with running water until the water was colorless. The absorbance was measured at 600 nm after adding 30% acetic acid.

## Biofilms Observed by Laser Scanning Confocal Microscopy

Strains were incubated by TSBG in 20 mm glass-bottomed cell culture dishes (NEST, Wuxi, China). After 24 h, we washed the dishes twice with PBS to remove floating cells and then

added SYTO-9 (0.02%, Thermo Fisher Scientific, Waltham, MA, United States) and PI (0.067%, Thermo Fisher Scientific, Waltham, MA, United States) to stain biofilms for 30 min in the dark. After staining, samples were scanned by CLSM (TCS SP5; Leica, Wetzlar, Germany) using a 63 × oil immersion objective lens directly.

## Bacterial Biofilm Metabolism Activity

3-(4,5-Dimethylthiazol-2-yl)-2,5-diphenyltetrazolium bromide, also called MTT, is reduced to the water-insoluble blue-purple formazan by amber dehydrogenase in the mitochondria of living cells. Formazan is dissolved by DMSO, and then its absorbance can indirectly reflect the number of living bacteria. We used MTT to detect the biofilm metabolism activity. In brief, overnight-cultured MRSA strains JP5023 and JP4856 were diluted 1:100 with TSBG containing 4 μg/ml of SYG-180-2-2 in 96-well plates, wells without SYG-180-2-2 were control. Each condition was tested in three replicate wells. Plates were incubated at 37°C for 6, 12, 24, and 48 h, respectively. We removed the supernatant and washed the wells twice with PBS. Then, 100 μl of TSBG containing 0.25 mg/ml MTT (Beijing Solarbio Science and Technology Co., Ltd.) was added into each well and incubated at 37°C for 0.5 h in dark. Subsequently, the supernatant was discarded and 100 μl of DMSO was added to wells to dissolve biofilms, and then the optical density of the wells was measured at $OD_{490}$.

## Cell Adhesion Assay

The experimental method was slightly modified according to the previously described method (Wang et al., 2021). Briefly speaking, after MRSA strains were cultured overnight in TSB containing 2% glucose, 100 μl of the overnight culture was added to 96-well plates. Subsequently, the equal volume of TSB including SYG-180-2-2 and SYG-180-7 was added, respectively, to realize the desired final concentration of 4 μg/ml. The plates were incubated at 37°C for 4 h. After this, the plate was washed with PBS to discard the floating cells and the absorbance was measured at 600 nm. SYG-180-7 was severed as a control compound to exclude the possibility that the hydrophobicity of the compound itself inhibits the interaction between MRSA and the sold surface.

## Polysaccharide Intercellular Adhesin and Extracellular DNA Detection

For polysaccharide intercellular adhesin (PIA) detection, we diluted the overnight culture 1:100 in 3 ml TSBG containing a concentration of 4 μg/ml SYG-180-2-2 into a six-well plate at 37°C for 24 h, wells without SYG-180-2-2 served as the control. Planktonic cells were removed and washed with PBS, then biofilms were resuspended with 500 μl of 0.5 M EDTA [PH 8.0, Sangon Biotech (Shanghai) Co., Ltd.] using a scraper. Cells were incubated at 100°C for 5 min and centrifuged at 12,000 rpm for 2 min. Then, 40 μl of supernatant was added to 20 μl of proteinase K (20 mg/ml) at 37°C for 2 h. A total of 10 μl of the treated PIA sample was spotted onto the polyvinylidene fluoride (PVDF) membrane which was activated by methanol. The membrane was kept moist and smooth during the spotting process. After drying, the membrane was blocked with 3.5% bovine serum albumin (BSA) (Biosharp, Beijing, China) in PBS with 0.1% Tween 20 (PBST) [Sangon Biotech (Shanghai) Co., Ltd.] at 4°C overnight, and incubated at 37°C with Wheat Germ Agglutinin-HRP (WGA-HRP) conjugate for 1 h at a Universal Antibody Diluent (New Cell and Molecular Biotech Co., Ltd.) of 1:5,000. The membrane was washed thoroughly three times with PBST and detected using enhanced chemiluminescence (ECL) (Affinity Bio, San Francisco, CA, United States).

For extracellular DNA (eDNA) detection, MRSA strains were cultured in six-well plates as described above. After incubation at 37°C for 24 h, the eDNA was extracted as previously described (Rice et al., 2007). The amount of eDNA was measured using a UV Nanodrop 2000 (ThermoFisher Scientific Ltd.). The experiment was repeated three times.

## Isolation of RNA and Quantitative RT-PCR

We followed the manufacturer's instructions [(Spin Column Bacteria Total RNA Purification Kit and Sangon Biotech (Shanghai) Co., Ltd.] for RNA extraction. Briefly, MRSA strains were cultured in TSB with and without SYG-180-2-2 at 37°C for 16 h. The bacterial mass was collected by centrifugation and suspended in lysozyme (20 mg/ml) and lysostaphin (1 mg/ml) at 37°C for 1 h. Then total RNA was extracted and cDNA was

**TABLE 2 |** Primes used in this study.

| Primer | Sequence (5′–3′) |
|---|---|
| *gyrB*-RT-F | ACATTACAGCAGCGTATTAG |
| *gyrB*-RT-R | CTCATAGTGATAGGAGTCTTCT |
| *icaA*-RT-F | GTTGGTATCCGACAGTATA |
| *icaA*-RT-R | CACCTTTCTTACGTTTTAATG |
| *icaR*-RT-F | GGATGCTTTCAAATACCAACT |
| *icaR*-RT-R | TTATCTAATACGCCTGAGGAAT |
| *codY*-RT-F | GACAATGTATTAACAGTATTCC |
| *codY*-RT-R | TAGCAGCATATTCACCTA |
| *fnbB*-RT-F | GCGAAGTTTCTACTTTTG |
| *fnbB*-RT-R | CAACCATCACAATCAACA |
| *eno*-RT-F | CTCCAATTGCATTCCAAG |
| *eno*-RT-R | GCATCTTCAGTACCTTCA |
| *fib*-RT-F | GTGCTTTACGGTGTGTTG |
| *fib*-RT-R | CTGCTATTAGTTTAACGGTATCAA |
| *ebpS*-RT-F | GTGTGATGATTCGACTTG |
| *ebpS*-RT-R | CAGGATACAATAGAGAATACG |
| *saeR*-RT-F | GTCGTAACCATTAACTTCTG |
| *saeR*-RT-R | ATCGTGGATGATGAACAA |
| *psmα*-RT-F | ATGGAATTCGTAGCAAAATTATTC |
| *psmα*-RT-R | TAGTTGTTACCTAAAAATTTACC |
| *psmβ*-RT-F | CCTAGTAAACCCACACCG |
| *psmβ*-RT-R | GCTGCACAACAACATGATA |
| *agrA*-RT-F | GCAGTAATTCAGTGTATGTTCA |
| *agrA*-RT-R | TATGGCGATTGACGACAA |

synthesized using a Primescript$^{TM}$ RT reagent Kit with gDNA Eraser (Takara, Tokyo, Japan).

Quantitative real-time PCR (qPCR) was performed using the Fast Start DNA Master SYBR Green II Mixture (Takara, Tokyo, Japan) and QuantStudio® 5 Applied Biosystems (ABI) Fluorescence quantitative PCR instrument (Thermo Fisher Scientific). The reaction used the DNA sequence of gyrB as an internal reference and was performed in a 20 μl reaction volume per well. **Table 2** shows the primer pairs used for RT-PCR. The cycling conditions were 95°C for 30 s, followed by 40 cycles, with 1 cycle consisting of 95°C for 5 s and 60°C for 34 s. The cycle threshold (Ct) measurements were calculated by the QuantStudio$^{TM}$ Design and Analysis SE software version 1.6.0. First, the relative expression levels of biofilm-related genes treated with and without SYG-180-2-2 were normalized to the *gyrB* reference gene to obtain $\Delta Ct_1$ and $\Delta Ct_2$, respectively. $\Delta\Delta Ct$ was acquired by subtracting $\Delta Ct_2$ from $\Delta Ct_1$. Then we used the relative quantification method ($2^{-\Delta\Delta Ct}$) to analyze the transcription level of the target gene in the sample with SYG-180-2-2. Three replicates were performed for each condition.

## Assessment of SYG-180-2-2 Cytotoxicity

The Cell Counting Kit-8 (CCK-8) solution was used to evaluate the proliferation and cytotoxicity of SYG-180-2-2 to BEAS-2B (Yu et al., 2017). WST-8 is reduced by cellular dehydrogenase to an orange formazan product which can dissolve in culture medium. The amount of formazan product is directly proportional to the number of living cells. In short, the cells were seeded in a 96-well plate at different cells/well for 12 h. Then we discarded the supernatant and added a final concentration of 4 μg/ml of SYG-180-2-2 DMEM containing 10% fetal bovine serum (FBS, Sigma-Aldrich, St. Louis, MO, United States) and 1% penicillin/streptomycin solution (sterile), wells without SYG-180-2-2 were used as a positive control. After 24 h, the supernatant was removed and wells were washed twice with PBS. Then 100 μl of DMEM and 10 μl of cck8 were added to wells at 37°C for 1–2 h. Finally, 450 nm absorbance was measured. Three independent experiments were carried out.

## Statistical Analysis

Statistical analysis was performed using GraphPad Prism (version 8.0). Multiple *t*-tests were used for the growth curve. Biofilm formation assessment was analyzed using one-way analysis of variance (ANOVA) followed by Tukey's multiple-comparison test. Unpaired two-tailed *t*-tests were used for the other experiments. $P$ values $< 0.05$ were considered statistically significant. $^{*}P < 0.05$, $^{**}P < 0.01$,

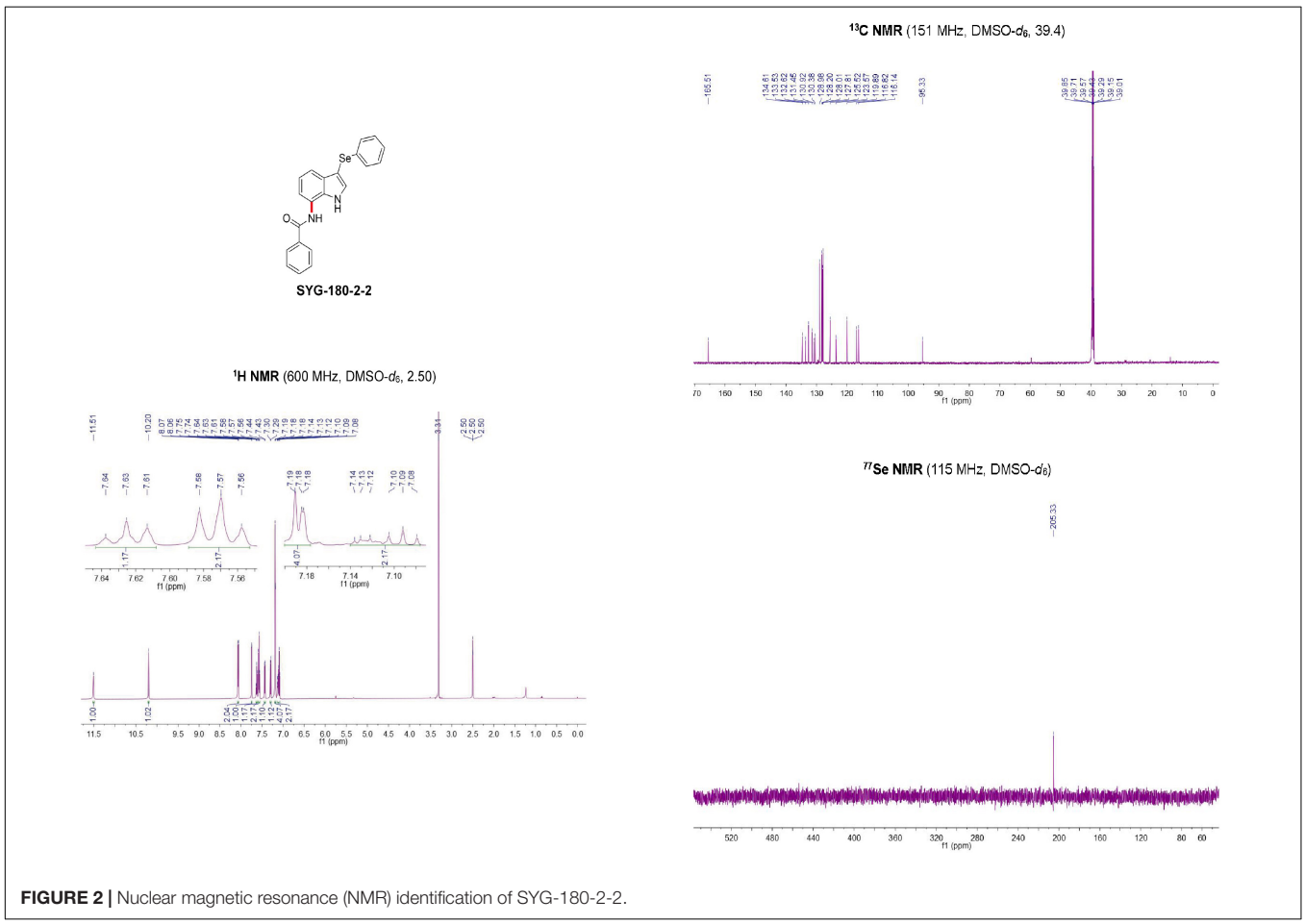


**FIGURE 2 |** Nuclear magnetic resonance (NMR) identification of SYG-180-2-2.

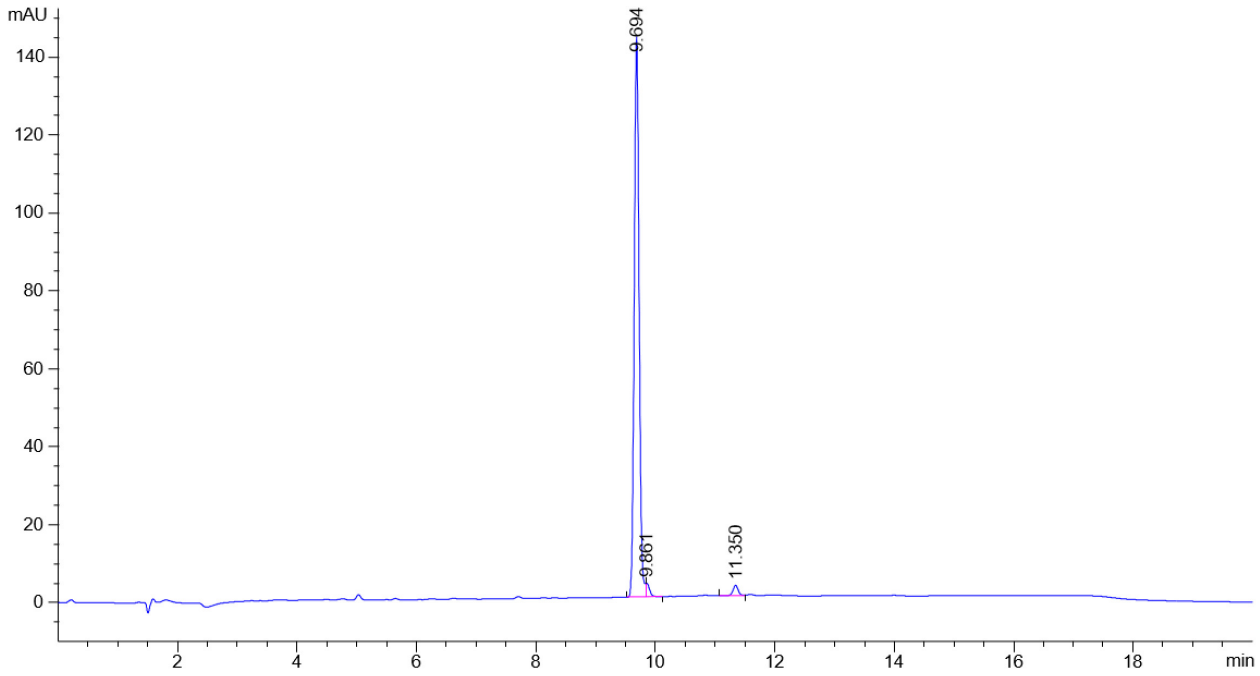


Signal 1: VWD1 A, Wavelength=250nm

| Peak # | RetTime [min] | Type | Width [min] | Area [mAU*s] | Height [mAU] | Area % |
|---|---|---|---|---|---|---|
| 1 | 9.694 | BV | 0.0881 | 814.11682 | 143.68512 | 96.0527 |
| 2 | 9.861 | VB | 0.0747 | 17.37427 | 3.51296 | 2.0499 |
| 3 | 11.350 | BV | 0.0929 | 16.08193 | 2.64640 | 1.8974 |
| Totals : | | | | 847.57302 | 149.84448 | |

**FIGURE 3 |** High-resolution mass spectrometry (HRMS) identification of SYG-180-2-2.

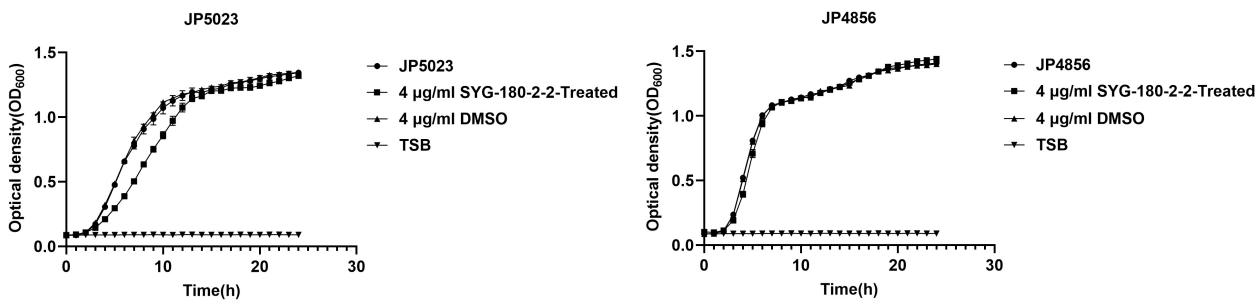


**FIGURE 4 |** Growth curves of methicillin-resistant *Staphylococcus aureus* (MRSA) strains treated with SYG-180-2-2. Strains JP5023 and JP4856 were cultured with 4 μg/ml of or without SYG-180-2-2. Trypticase soy broth (TSB) was used as a blank control. Dimethyl sulfoxide (DMSO) was used as a control in order to exclude the influence of solvent on bacterial growth.

$^{***}P < 0.001$, and $^{****}P < 0.0001$. All figures were presented as mean ± standard deviation.

## RESULTS

### Characterization of Products SYG-180-2-2 and SYG-180-7

SYG-180-2-2 was a white solid (96.0527% purity) after purification by chromatography (elution: 35% EtOAc in petroleum ether) with a melting point of 230–231°C. SYG-180-2-2 was characterized by nuclear magnetic resonance (NMR, **Figure 2**) spectroscopy and high-resolution mass spectrometry (HRMS, **Figure 3**), obtaining the following results: $^{1}$H NMR (600 MHz, DMSO-$d_6$) δ 11.51 (brs, 1H), 10.20 (brs, 1H), 8.07 (d, $J$ = 7.3 Hz, 2H), 7.74 (d, $J$ = 2.6 Hz, 1H), 7.63 (t, $J$ = 7.3 Hz, 1H), 7.57 (t, $J$ = 7.5 Hz, 2H), 7.43 (d, $J$ = 7.5 Hz, 1H), 7.29 (d, $J$ = 7.9 Hz, 1H), 7.20–7.18 (m, 4H), 7.14–7.08 (m, 2H) ppm;$^{13}$C NMR (151 MHz, DMSO-$d_6$) δ 165.51, 134.61, 133.53, 132.62, 131.45, 130.92, 130.38, 128.98, 128.20, 128.01, 127.81, 125.52, 123.57, 119.89, 116.82, 116.14, and 95.33 ppm; $^{77}$Se NMR (115 MHz, DMSO-$d_6$) δ 205.33 ppm; HRMS: calc. for $C_{21}H_{17}N_2OSe^+$ $[M + H]^+$: 393.05061, found: 393.05005.

SYG-180-7 was a white solid (100% purity) after purification by chromatography (elution: 15% EtOAc in petroleum ether) with a melting point of 125–126°C. SYG-180-7 was characterized by nuclear magnetic resonance (NMR, **Supplementary Figure 2**) spectroscopy and high-resolution mass spectrometry (HRMS, **Supplementary Figure 3**), obtaining the following results: $^{1}$H NMR (600 MHz, $CDCl_3$) δ 8.27 (brs, 1H), 8.04 (d, $J$ = 7.3 Hz, 2H), 7.97 (d, $J$ = 7.8 Hz, 1H), 7.60–7.53 (m, 5H), 7.48 (d, $J$ = 7.8 Hz, 1H), 7.45 (t, $J$ = 7.6 Hz, 2H), 7.39 (t, $J$ = 7.4 Hz, 1H), 7.29–7.26 (m, 1H), 6.77 (s, 1H), 0.75 (s, 9H) ppm. $^{13}$C NMR (151 MHz, $CDCl_3$) δ 193.1, 164.8, 139.9, 134.1, 133.0, 131.9, 130.5, 129.1, 128.8, 128.7, 128.6, 128.1, 127.1, 123.0, 122.1, 119.6, 117.9, 106.2, 46.6, and

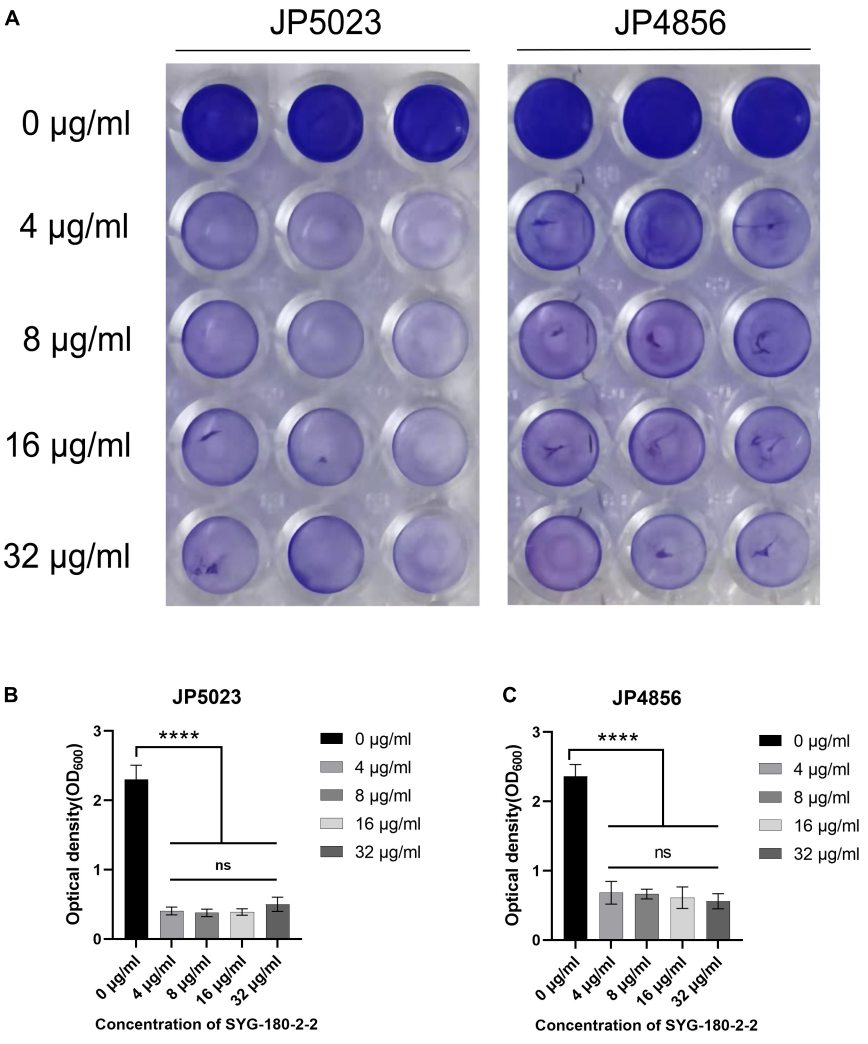


**FIGURE 5 |** The effect of SYG-180-2-2 on the formation of biofilm. **(A)** Biofilm formation in a 96-well plate. At $OD_{600}$, there was a significant difference in the biofilm formation of JP5023 **(B)** and JP4856 **(C)** cultured with or without SYG-180-2-2. $^{****}P < 0.0001$.

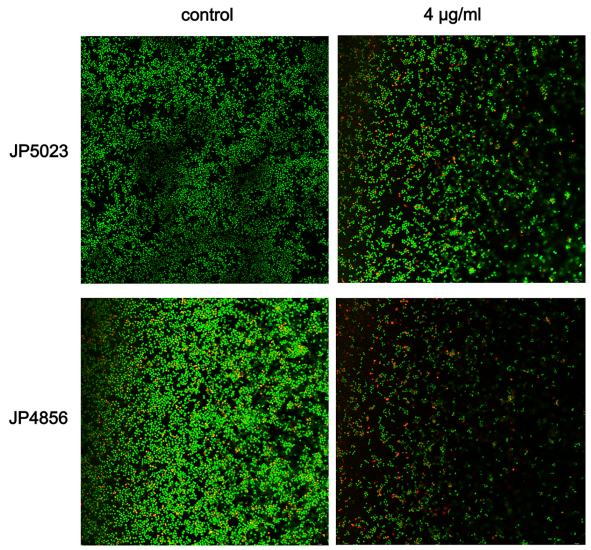


**FIGURE 6 |** Biofilm formation was observed by CLSM. JP5023 and JP4856 treated with SYG-180-2-2 (4 μg/ml).

27.6 ppm. HRMS (ESI) m/z: $[M + H]^+$ calc. for $C_{26}H_{25}N_2O_2$: 397.1916; found, 397.1914.

## Influence of Subinhibitory Concentrations of SYG-180-2-2 on the Growth of Methicillin-Resistant *Staphylococcus aureus* Strains

The minimum inhibitory concentration (MIC) values of SYG-180-2-2 against MRSA JP5023 and JP4856 were >128 μg/ml. According to the growth curve we drew, the amount of MRSA strain JP4856 in the late logarithmic growth period was consistent at the subinhibitory concentration of 4 μg/ml. But, at 4 μg/ml, MRSA strain JP5023 grew more slowly than bacteria in the control wells at 4–11 h, and the growth was consistent in the late logarithmic phase (**Figure 4**). The high concentration of SYG-180-2-2 (8 μg/ml) inhibited the growth of MRSA JP5023 (**Supplementary Figure 4**).

## SYG-180-2-2 Inhibits Methicillin-Resistant *Staphylococcus aureus* Biofilm Formation

Bacterial biofilms are difficult to eradicate and resistant to antibacterial drugs (Tan et al., 2012). We used semi-quantitative biofilm to detect the effect of subinhibitory concentrations of SYG-180-2-2 on MRSA biofilm. Treatment with SYG-180-2-2 at a concentration of 4 μg/ml decreased the JP5023 and JP4856 biofilm by 82.9 ± 2.3 and 71.9 ± 6.8%, respectively, when compared with the untreated group (**Figure 5**). Similarly, treatment with SYG-180-2-2 at concentrations of 8, 16, and 32 μg/ml had a significant reduction effect on biofilms. These results showed that sub-MICs of SYG-180-2-2 (4, 8, 16, and 32 μg/ml) were not affected by dose. We observed in the bacterial biofilm treated with SYG-180-2-2 by CLSM at 4 μg/ml that the density of the biofilm was lower and sparser (**Figure 6**), compared with the untreated group.

## SYG-180-2-2 Reduces the Metabolic Activity of Methicillin-Resistant *Staphylococcus aureus* Biofilm

Under the action of a subinhibitory concentration of SYG-180-2-2 (4 μg/ml), the bacterial metabolic activity of the strains was measured in four time points by MTT staining. Reduction of the metabolic activity of JP5023 strain in the presence of SYG-180-2-2 at 4 μg/ml after 6, 12, 24, and 48 h were 47.2 ± 0.6, 53.3 ± 3.6, 40.3 ± 6.6, and 57.6 ± 9.9%, respectively, when compared to the untreated groups. At the same time, reduction of the metabolic activity of JP4856 strain after 6, 12, 24, and 48 h of SYG-180-2-2 treatment with 4 μg/ml were 71.0 ± 2.7, 64.8 ± 3.5, 57.0 ± 8.5, and 71.2 ± 7.3%, respectively, compared to the control (**Figure 7**).

## SYG-180-2-2 Affects the Adhesion of Methicillin-Resistant *Staphylococcus aureus*

We observed the effect of a subinhibitory concentration of SYG-180-2-2 (4 μg/ml) on the initial adhesion stage of MRSA

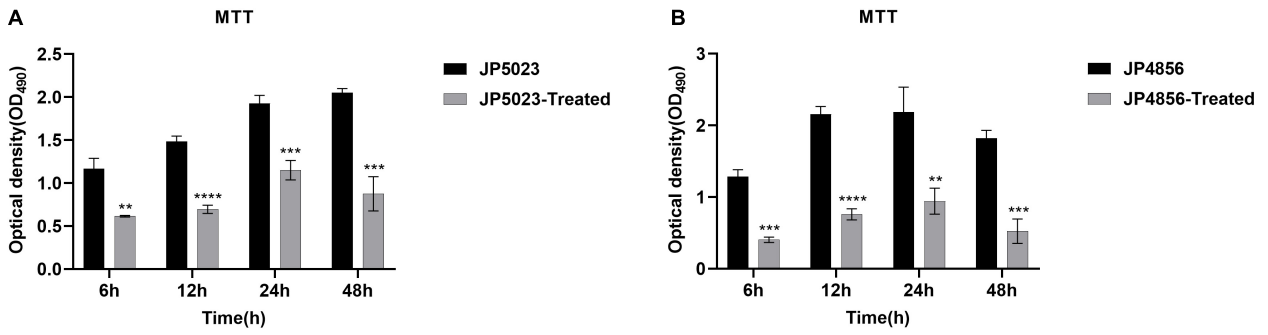


**FIGURE 7 |** The effect of subinhibitory concentration of SYG-180-2-2 on the metabolic activity of MRSA strains JP5023 **(A)** and JP4856 **(B)** biofilm. $^{**}P < 0.01$, $^{***}P < 0.001$, and $^{****}P < 0.0001$.

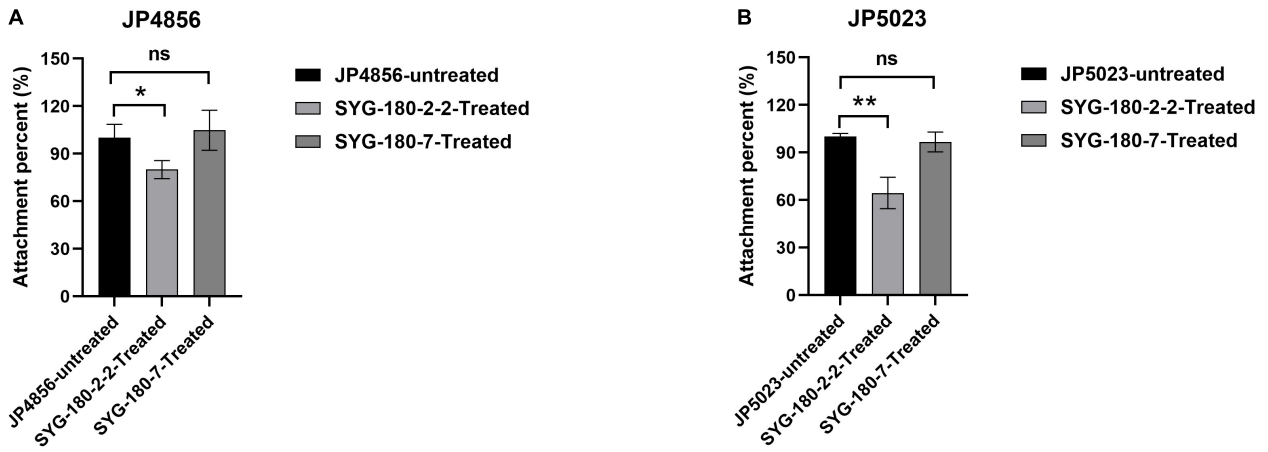


**FIGURE 8 |** Attachment percent of JP5023 **(A)** and JP4856 **(B)** explored by attachment assay (the control was set to 100%). *$P < 0.05$ and **$P < 0.01$.

biofilm by an attachment assay. The results showed that SYG-180-2-2 significantly suppressed the adhesion of JP5023 and JP4856 to the solid surface at 4 μg/ml by 37.6 ± 9.3 and 21.4 ± 5.1%, respectively (**Figure 8**). Meanwhile, SYG-180-7 showed no significant difference in cell adhesion, when compared with the untreated strains (**Figure 8**).

## The Effect of SYG-180-2-2 on the Production of Polysaccharide Intercellular Adhesin and Extracellular DNA in Methicillin-Resistant *Staphylococcus aureus*

In order to study the effect of SYG-180-2-2 on the biofilm matrix of MRSA, the release of PIA and eDNA was detected. Compared with the untreated group, the production of PIA with SYG-180-2-2-treated strains was decreased significantly (**Figure 9**), however, there was no significant difference in eDNA (**Supplementary Figure 5**).

## Effect of SYG-180-2-2 on the Expression of Biofilm-Related Genes

The transcript levels of biofilm-related genes treated with the concentration of 4 μg/ml of SYG-180-2-2 were determined using RT-PCR to clarify the effect of SYG-180-2-2 on the formation of biofilm. In general, the results showed that in JP5023 and JP4856, except for the expression of *icaR* and *codY* genes which was upregulated, the expression of *icaA*, *icaD*, *icaR*, *fnbB*, *eno*, *fib*, *ebps*, *saeR*, *psmα*, *psmβ*, and *agrA* genes was downregulated to varying degrees with the treatment of SYG-180-2-2 (**Figure 10**). These results were consistent with the adhesion of bacteria and the detection of PIA.

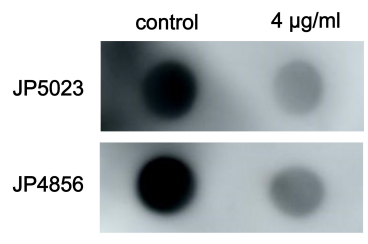


**FIGURE 9 |** Effect of the subinhibitory concentration of SYG-180-2-2 on MRSA PIA production.

## Subinhibitory Concentration of SYG-180-2-2 Is Non-toxic to Human Alveolar Epithelial Cells

In order to study the effect of SYG-180-2-2 on human cytotoxicity, we used BEAS-2B in our experiments to evaluate the cytotoxicity of SYG-180-2-2 with the CCK-8 assay. There was no effect on the cytotoxicity when SYG-180-2-2 was used (**Figure 11A**). When the cells were seeded at 3,000 cells/well, the cell morphology was not abnormal under the microscope (**Figure 11B**). Obviously, SYG-180-2-2 is not cytotoxic at a subinhibitory concentration.

# DISCUSSION

When MRSA strains acquire resistance to antibiotics and form robust biofilm, this leads to higher mortality, especially when they infect patients in the intensive care unit (ICU; Turner et al., 2019). Fortunately, we synthesized a new small-molecule compound SYG-180-2-2 that possessed significant inhibitory activity against the biofilm of MRSA ranging from different types.

In recent years, there have been many reports on the effect of antibacterial drugs with subinhibitory concentrations on biofilms (Goneau et al., 2015). SYG-180-2-2 has a higher MIC, however, at low concentrations, proving it has remarkable anti-biofilm activity. At 4 μg/ml, the amount of JP5023 slowed down in the logarithmic phase; the possible reason was that the bacteria incurred the cost of adaptability for growth. A higher concentration of SYG-180-2-2 suppressed the growth of JP5023, while at 4 μg/ml, it had no effect on the later growth of

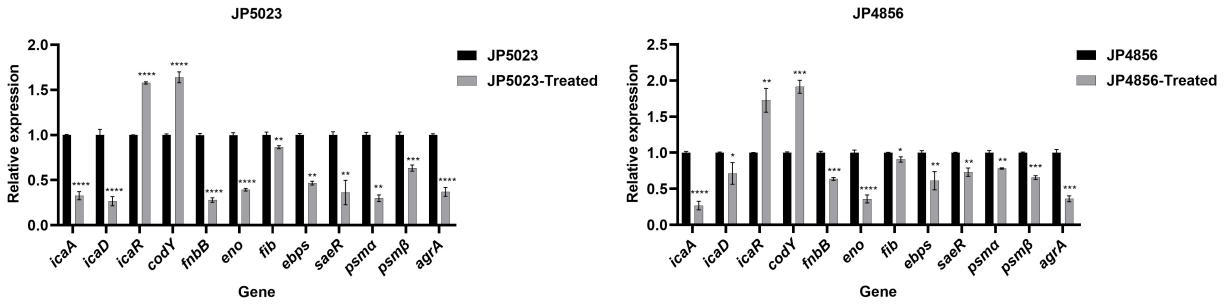


**FIGURE 10 |** The effect of MRSA strains with SYG-180-2-2 treatment on biofilm-related gene expression. *$P < 0.05$, **$P < 0.01$, ***$P < 0.001$, and ****$P < 0.0001$.

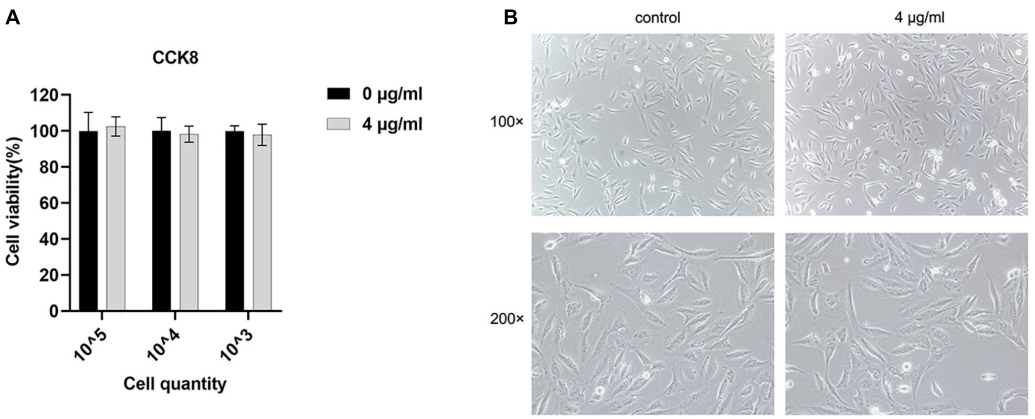


**FIGURE 11 |** The effect of SYG-180-2-2 on BEAS-2B. **(A)** The activity of different amounts of BEAS-2B with or without SYG-180-2-2 treatment. **(B)** Microscopic cell morphology.

the bacteria. Hence, the growth curve proved that the biofilm inhibitory effects of SYG-180-2-2 (4 μg/ml) were not due to its bactericidal efficacy. We speculate that the higher the sub-MICs (8, 16, and 32 μg/ml) of SYG-180-2-2, the more likely bactericidal efficacy is to attenuate the biofilms. In biofilm formation assessment, there were no significant differences among the subinhibitory concentrations (4, 8, 16, and 32 μg/ml). Therefore, through the growth curve and biofilm formation assay, we focused on the lower concentration of 4 μg/ml in the experiment in order to exclude that SYG-180-2-2 inhibits MRSA biofilm formation by preventing cell proliferation. In addition to semi-quantitative biofilm experiments, CLSM further confirmed that the subinhibitory concentration of SYG-180-2-2 could reduce biofilm formation significantly in clinical isolates of MRSA. A metabolic assay is a brilliant method to quantify the viability of bacteria in biofilms. The number of living bacteria in the biofilm and the metabolic activity of individual bacteria determine the quantity of metabolites produced by the biofilm (Kot et al., 2019). As CV-stained biomass contains dead bound bacteria instead of live bacteria, we used MTT to detect the amount of live bacteria in the biofilm at the same time, which proved that SYG-180-2-2 has anti-biofilm activity.

Primary attachment is the first step for bacteria to bind to the host surface. In our experiment, SYG-180-7, which has a similar structure to SYG-180-2-2, was used as the control, indicating that SYG-180-2-2 inhibits the binding of MRSA to the host surface due to its anti-adhesion rather than hydrophobicity. The decreased expression of *fnbB*, *fib*, *ebpS,* and *eno* genes involved in adhesion further proved that SYG-180-2-2 could prevent the initiation of host tissue colonization. PIA and eDNA are essential for biofilm formation (Lopez et al., 2010). It was reported that PIA-dependent biofilm often appears in methicillin-sensitive *S. aureus* (MSSA), while PIA-independent biofilm is common in MRSA (Nguyen et al., 2020). In contrast, the strains we used in the experiment produced large amounts of PIA. PIA-dependent biofilm formation results in a stronger and steadier biofilm than those whose biofilm is PIA-independent (Rohde et al., 2007; Dice et al., 2009). In our study, we found that SYG-180-2-2 could reduce the PIA production to inhibit biofilm formation, while the production of eDNA was not significantly decreased. These results indicate that the formation of *S. aureus* biofilm may be prevented by affecting the PIA production rather than eDNA. Both *ica*-negative and *ica*-positive MRSA can produce biofilm, and the extracellular matrix of *ica*-positive MRSA is mainly composed of PIA, while those of *ica*-negative MRSA is mostly formed of eDNA (Chopra et al., 2015). It is well known that the *ica* operon affects the formation of PIA (Nguyen et al., 2020), which is confirmed by the decrease in the expression of *icaA* and *icaD* according to the RT-qPCR method. Meanwhile, the expression of *icaR* was upregulated. PIA is the main influence

of low CodY activity bacteria on biofilm formation, and most recent works showed that *codY* regulated the PIA-dependent biofilm (Majerczyk et al., 2008; Atwood et al., 2015; Waters et al., 2016; Schilcher and Horswill, 2020). In our study, we guess the upregulation of *codY* prevented PIA production. Moreover, *saeR* is not only a key regulator of virulence gene expression (Nagel et al., 2018), but also affects the maturation process of biofilm (Mashruwala et al., 2017). The downregulation of its expression indicated that SYG-180-2-2 may also have an effect on biofilm maturation and virulence. *Psms* including *psm*α and *psm*β are considered to disperse biofilm resulting in persistent infection (Periasamy et al., 2012). Furthermore, the *psms* gene is positively regulated by the *agrA* gene (George et al., 2019). Our results were consistent with the above, when the expression of *agrA* decreased, as did the expression of *psms*. Taken together, SYG-180-2-2 inhibits biofilm formation by preventing the adhesion of bacteria and the production of PIA.

More importantly, the subinhibitory concentration of SYG-180-2-2 (4 μg/ml) is not only non-toxic to human cells but can also inhibit the formation of biofilm. We concluded that SYG-180-2-2 had the potential to become a new type of antimicrobial drug used in clinical practice.

## DATA AVAILABILITY STATEMENT

The original contributions presented in the study are included in the article/**Supplementary Material**, further inquiries can be directed to the corresponding authors.

## AUTHOR CONTRIBUTIONS

LR, YS, and YX designed the work and analyzed and interpreted the data for the work. LR and JY drafted the work and revised it critically for important intellectual content. BW, HZ, XWa, XWu, YG, and ZS participated in the experimental design and data analysis. FY and LZ provided approval for publication of the content and agreed to be accountable for all aspects of the work in ensuring that questions related to the accuracy or integrity of any part of the work are appropriately investigated and resolved. All authors read and approved the final manuscript.

## ACKNOWLEDGMENTS

We are grateful to Haipeng Liu of Clinical Transformation Center, Shanghai Pulmonary Hospital, Tongji University School of Medicine for providing human normal alveolar epithelial cells BEAS-2B for this study.

## SUPPLEMENTARY MATERIAL

The Supplementary Material for this article can be found online at: https://www.frontiersin.org/articles/10.3389/fmicb.2021.770657/full#supplementary-material

**Supplementary Figure 1 |** Synthetic process of SYG-180-7. 1: *N*-pivaloyl indoles. 2: *N*-(1-pivaloyl-1*H*-indol-7-yl) benzamide. SYG-180-7: desired product.

**Supplementary Figure 2 |** Nuclear magnetic resonance (NMR) identification of SYG-180-7.

**Supplementary Figure 3 |** High-resolution mass spectrometry (HRMS) identification of SYG-180-7.

**Supplementary Figure 4 |** Growth curves of MRSA strains cultured with SYG-180-2-2 (8 μg/ml).

**Supplementary Figure 5 |** Effect of the subinhibitory concentration of SYG-180-2-2 on MRSA eDNA production.

## REFERENCES

Achek, R., Hotzel, H., Nabi, I., Kechida, S., Mami, D., Didouh, N., et al. (2020). Phenotypic and molecular detection of biofilm formation in *staphylococcus aureus* isolated from different sources in Algeria. *Pathogens* 9:153. doi: 10.3390/pathogens9020153

Aslan, H., and Yapar, N. (2015). [Comparison of tigecycline and vancomycin activities in an in vitro biofilm model generated with methicillin-resistant *Staphylococcus aureus*]. *Mikrobiyol. Bul.* 49, 475–483.

Atwood, D. N., Loughran, A. J., Courtney, A. P., Anthony, A. C., Meeker, D. G., Spencer, H. J., et al. (2015). Comparative impact of diverse regulatory loci on *Staphylococcus aureus* biofilm formation. *Microbiologyopen* 4, 436–451. doi: 10.1002/mbo3.250

Basnyat, B., Pokharel, P., Dixit, S., and Giri, S. (2015). Antibiotic use, its resistance in Nepal and recommendations for action: a situation analysis. *J. Nepal Health Res. Counc.* 13, 102–111.

Biedlingmaier, J. F., Samaranayake, R., and Whelan, P. (1998). Resistance to biofilm formation on otologic implant materials. *Otolaryngol. Head Neck Surg.* 118, 444–451. doi: 10.1177/019459989811800403

Biersack, B., and Schobert, R. (2012). Indole compounds against breast cancer: recent developments. *Curr. Drug Target.* 13, 1705–1719. doi: 10.2174/138945012804545551

Cassat, J. E., Lee, C. Y., and Smeltzer, M. S. (2007). Investigation of biofilm formation in clinical isolates of *Staphylococcus aureus*. *Methods Mol. Biol.* 391, 127–144.

Chaieb, K., Kouidhi, B., Jrah, H., Mahdouani, K., and Bakhrouf, A. (2011). Antibacterial activity of Thymoquinone, an active principle of Nigella sativa and its potency to prevent bacterial biofilm formation. *BMC Complement. Altern. Med.* 11:29. doi: 10.1186/1472-6882-11-29

Chopra, S., Harjai, K., and Chhibber, S. (2015). Antibiotic susceptibility of ica-positive and ica-negative MRSA in different phases of biofilm growth. *J. Antibiot. (Tokyo)* 68, 15–22. doi: 10.1038/ja.2014.96

Cong, Y., Yang, S., and Rao, X. (2020). Vancomycin resistant *Staphylococcus aureus* infections: a review of case updating and clinical features. *J. Adv. Res.* 21, 169–176. doi: 10.1016/j.jare.2019.10.005

Cramton, S. E., Gerke, C., Schnell, N. F., Nichols, W. W., and Gotz, F. (1999). The intercellular adhesion (ica) locus is present in *Staphylococcus aureus* and is required for biofilm formation. *Infect. Immun.* 67, 5427–5433. doi: 10.1128/IAI.67.10.5427-5433.1999

Dice, B., Stoodley, P., Buchinsky, F., Metha, N., Ehrlich, G. D., and Hu, F. Z. (2009). Biofilm formation by ica-positive and ica-negative strains of *Staphylococcus epidermidis* in vitro. *Biofouling* 25, 367–375. doi: 10.1080/08927010902803297

Dufour, D., Leung, V., and Lévesque, C. M. (2010). Bacterial biofilm: structure, function, and antimicrobial resistance. *Endodontic Topics* 22, 2–16.

Fatahala, S. S., Khedr, M. A., and Mohamed, M. S. (2017). Synthesis and structure activity relationship of some indole derivatives as potential anti-inflammatory agents. *Acta Chim. Slov.* 64, 865–876. doi: 10.17344/acsi.2017.3481

Fluckiger, U., Ulrich, M., Steinhuber, A., Doring, G., Mack, D., Landmann, R., et al. (2005). Biofilm formation, icaADBC transcription, and polysaccharide intercellular adhesin synthesis by staphylococci in a device-related infection model. *Infect. Immun.* 73, 1811–1819. doi: 10.1128/IAI.73.3.1811-1819.2005

George, S. E., Hrubesch, J., Breuing, I., Vetter, N., Korn, N., Hennemann, K., et al. (2019). Oxidative stress drives the selection of quorum sensing mutants in the *Staphylococcus aureus* population. *Proc. Natl. Acad. Sci. U.S.A.* 116, 19145–19154. doi: 10.1073/pnas.1902752116

Goneau, L. W., Hannan, T. J., MacPhee, R. A., Schwartz, D. J., Macklaim, J. M., Gloor, G. B., et al. (2015). Subinhibitory antibiotic therapy alters recurrent urinary tract infection pathogenesis through modulation of bacterial virulence and host immunity. *mBio* 6:e00356-15. doi: 10.1128/mBio.00356-15

Hoiby, N., Bjarnsholt, T., Givskov, M., Molin, S., and Ciofu, O. (2010). Antibiotic resistance of bacterial biofilms. *Int. J. Antimicrob. Agents* 35, 322–332.

Jefferson, K. K., Pier, D. B., Goldmann, D. A., and Pier, G. B. (2004). The teicoplanin-associated locus regulator (TcaR) and the intercellular adhesin locus regulator (IcaR) are transcriptional inhibitors of the ica locus in *Staphylococcus aureus*. *J. Bacteriol.* 186, 2449–2456. doi: 10.1128/JB.186.8.2449-2456.2004

Jenul, C., and Horswill, A. R. (2019). Regulation of *Staphylococcus aureus* virulence. *Microbiol. Spectrum.* 7:10.

Kot, B., Sytykiewicz, H., Sprawka, I., and Witeska, M. (2019). Effect of trans-Cinnamaldehyde on Methicillin-resistant *Staphylococcus aureus* biofilm formation: metabolic activity assessment and analysis of the biofilm-associated genes expression. *Int. J. Mol. Sci.* 21:102. doi: 10.3390/ijms21010102

Liu, Q., Yeo, W. S., and Bae, T. (2016). The SaeRS two-component system of *Staphylococcus aureus*. *Genes (Basel)* 7:81.

Liu, X., Wang, L., Steffan, N., Yin, W. B., and Li, S. M. (2009). Ergot alkaloid biosynthesis in *Aspergillus fumigatus*: FgaAT catalyses the acetylation of fumigaclavine B. *Chembiochem* 10, 2325–2328. doi: 10.1002/cbic.200900395

Lopez, D., Vlamakis, H., and Kolter, R. (2010). Biofilms. *Cold Spring Harb. Perspect. Biol.* 2:a000398.

Majerczyk, C. D., Sadykov, M. R., Luong, T. T., Lee, C., Somerville, G. A., and Sonenshein, A. L. (2008). *Staphylococcus aureus* CodY negatively regulates virulence gene expression. *J. Bacteriol.* 190, 2257–2265. doi: 10.1128/JB.01545-07

Mashruwala, A. A., Gries, C. M., Scherr, T. D., Kielian, T., and Boyd, J. M. (2017). SaeRS is responsive to cellular respiratory status and regulates fermentative biofilm formation in *Staphylococcus aureus*. *Infect. Immun.* 85:e00157-17. doi: 10.1128/IAI.00157-17

Mlynek, K. D., Bulock, L. L., Stone, C. J., Curran, L. J., Sadykov, M. R., Bayles, K. W., et al. (2020). Genetic and biochemical analysis of CodY-mediated cell aggregation in *Staphylococcus aureus* reveals an interaction between extracellular dna and polysaccharide in the extracellular matrix. *J. Bacteriol.* 202:e00593-19. doi: 10.1128/JB.00593-19

Mole, B. (2013). MRSA: farming up trouble. *Nature* 25, 398–400. doi: 10.1038/499398a

Nagel, A., Michalik, S., Debarbouille, M., Hertlein, T., Gesell Salazar, M., Rath, H., et al. (2018). Inhibition of Rho activity increases expression of SaeRS-dependent virulence factor genes in *Staphylococcus aureus*, showing a link between transcription termination, antibiotic action, and virulence. *mBio* 18:e01332-18. doi: 10.1128/mBio.01332-18

Nemati, M., Hermans, K., Devriese, L. A., Maes, D., and Haesebrouck, F. (2009). Screening of genes encoding adhesion factors and biofilm formation in *Staphylococcus aureus* isolates from poultry. *Avian Pathol.* 38, 513–517. doi: 10.1080/03079450903349212

Nguyen, H. T. T., Nguyen, T. H., and Otto, M. (2020). The staphylococcal exopolysaccharide PIA - Biosynthesis and role in biofilm formation, colonization, and infection. *Comput. Struct. Biotechnol. J.* 18, 3324–3334. doi: 10.1016/j.csbj.2020.10.027

Nogueira, C. W., Zeni, G., and Rocha, J. B. (2004). Organoselenium and organotellurium compounds: toxicology and pharmacology. *Chem. Rev.* 104, 6255–6285. doi: 10.1021/cr0406559

O'Connor, S. E., and Maresh, J. J. (2006). Chemistry and biology of monoterpene indole alkaloid biosynthesis. *Nat. Prod. Rep.* 23, 532–547. doi: 10.1039/b512615k

Periasamy, S., Joo, H. S., Duong, A. C., Bach, T. H., Tan, V. Y., Chatterjee, S. S., et al. (2012). How *Staphylococcus aureus* biofilms develop their characteristic structure. *Proc. Natl. Acad. Sci. U.S.A.* 109, 1281–1286. doi: 10.1073/pnas.1115006109

Peschel, A., and Otto, M. (2013). Phenol-soluble modulins and staphylococcal infection. *Nat. Rev. Microbiol.* 11, 667–673. doi: 10.1038/nrmicro3110

Reed, W. P., Moody, M. R., Newman, K. A., Light, P. D., and Costerton, J. W. (1986). Bacterial colonization of hemasite access devices. *Surgery* 99, 308–317.

Rice, K. C., Mann, E. E., Endres, J. L., Weiss, E. C., Cassat, J. E., Smeltzer, M. S., et al. (2007). The cidA murein hydrolase regulator contributes to DNA release and biofilm development in *Staphylococcus aureus*. *Proc. Natl. Acad. Sci. U.S.A.* 104, 8113–8118. doi: 10.1073/pnas.0610226104

Rohde, H., Burandt, E. C., Siemssen, N., Frommelt, L., Burdelski, C., Wurster, S., et al. (2007). Polysaccharide intercellular adhesin or protein factors in biofilm accumulation of *Staphylococcus epidermidis* and *Staphylococcus aureus* isolated from prosthetic hip and knee joint infections. *Biomaterials* 28, 1711–1720.

Rohde, H., Knobloch, J. K., Horstkotte, M. A., and Mack, D. (2001). Correlation of *Staphylococcus aureus* icaADBC genotype and biofilm expression phenotype. *J. Clin. Microbiol.* 39, 4595–4596. doi: 10.1128/JCM.39.12.4595-4596.2001

Schilcher, K., and Horswill, A. R. (2020). *Staphylococcal* biofilm development: structure, regulation, and treatment strategies. *Microbiol. Mol. Biol. Rev.* 84:e00026-19. doi: 10.1128/MMBR.00026-19

Sheng, Y., Zhou, J., Gao, Y., Duan, B., Wang, Y., Samorodov, A., et al. (2021). Ruthenium(II)-Catalyzed direct C7-selective amidation of indoles with dioxazolones at room temperature. *J. Org. Chem.* 86, 2827–2839. doi: 10.1021/acs.joc.0c02779

Tan, H., Peng, Z., Li, Q., Xu, X., Guo, S., and Tang, T. (2012). The use of quaternised chitosan-loaded PMMA to inhibit biofilm formation and downregulate the virulence-associated gene expression of antibiotic-resistant *Staphylococcus*. *Biomaterials* 33, 365–377. doi: 10.1016/j.biomaterials.2011.09.084

Tu Quoc, P. H., Genevaux, P., Pajunen, M., Savilahti, H., Georgopoulos, C., Schrenzel, J., et al. (2007). Isolation and characterization of biofilm formation-defective mutants of *Staphylococcus aureus*. *Infect. Immun.* 75, 1079–1088.

Turner, N. A., Sharma-Kuinkel, B. K., Maskarinec, S. A., Eichenberger, E. M., Shah, P. P., Carugati, M., et al. (2019). Methicillin-resistant *Staphylococcus aureus*: an overview of basic and clinical research. *Nat. Rev. Microbiol.* 17, 203–218.

Uruen, C., Chopo-Escuin, G., Tommassen, J., Mainar-Jaime, R. C., and Arenas, J. (2020). Biofilms as promoters of bacterial antibiotic resistance and tolerance. *Antibiotics (Basel)* 10:3. doi: 10.3390/antibiotics10010003

van Hal, S. J., Barbagiannakos, T., Jones, M., Wehrhahn, M. C., Mercer, J., Chen, D., et al. (2011). Methicillin-resistant *Staphylococcus aureus* vancomycin susceptibility testing: methodology correlations, temporal trends and clonal patterns. *J. Antimicrob. Chemother.* 66, 2284–2287. doi: 10.1093/jac/dkr280

Wang, F., Liu, H., Li, J., Zhang, W., Jiang, B., and Xuan, H. (2021). Australian propolis ethanol extract exerts antibacterial activity against methicillin-resistant *Staphylococcus aureus* by mechanisms of disrupting cell structure, reversing resistance, and resisting biofilm. *Braz. J. Microbiol.* 7, 1651–1664. doi: 10.1007/s42770-021-00547-7

Waters, N. R., Samuels, D. J., Behera, R. K., Livny, J., Rhee, K. Y., Sadykov, M. R., et al. (2016). A spectrum of CodY activities drives metabolic reorganization and virulence gene expression in *Staphylococcus aureus*. *Mol. Microbiol.* 101, 495–514. doi: 10.1111/mmi.13404

Yarwood, J. M., Bartels, D. J., Volper, E. M., and Greenberg, E. P. (2004). Quorum sensing in *Staphylococcus aureus* biofilms. *J. Bacteriol.* 186, 1838–1850.

Yu, J., Rao, L., Zhan, L., Zhou, Y., Guo, Y., Wu, X., et al. (2021). Antibiofilm activity of small-molecule ZY-214-4 Against *Staphylococcus aureus*. *Front. Microbiol.* 12:618922. doi: 10.3389/fmicb.2021.618922

Yu, T., Guo, F., Yu, Y., Sun, T., Ma, D., Han, J., et al. (2017). *Fusobacterium nucleatum* promotes chemoresistance to colorectal cancer by modulating autophagy. *Cell* 170, 548–563.e16. doi: 10.1016/j.cell.2017.07.008

**Conflict of Interest:** The authors declare that the research was conducted in the absence of any commercial or financial relationships that could be construed as a potential conflict of interest.

**Publisher's Note:** All claims expressed in this article are solely those of the authors and do not necessarily represent those of their affiliated organizations, or those of the publisher, the editors and the reviewers. Any product that may be evaluated in this article, or claim that may be made by its manufacturer, is not guaranteed or endorsed by the publisher.

frontiers in Microbiology

ORIGINAL RESEARCH
published: 10 March 2022
doi: 10.3389/fmicb.2022.812792

# The Antimicrobial Effect of *Melissa officinalis* L. Essential Oil on *Vibrio parahaemolyticus*: Insights Based on the Cell Membrane and External Structure

*Huijie Yu*[1], *Juxin Pei*[1], *Weiqiang Qiu*[1,2,3,4], *Jun Mei*[1,2,3,4]* *and Jing Xie*[1,2,3,4]*

[1] College of Food Science and Technology, Shanghai Ocean University, Shanghai, China, [2] Shanghai Professional Technology Service Platform on Cold Chain Equipment Performance and Energy Saving Evaluation, Shanghai Ocean University, Shanghai, China, [3] National Experimental Teaching Demonstration Center for Food Science and Engineering, Shanghai Ocean University, Shanghai, China, [4] Shanghai Engineering Research Center of Aquatic Product Processing and Preservation, Shanghai Ocean University, Shanghai, China

OPEN ACCESS

**Edited by:**
Giuseppantonio Maisetta,
University of Pisa, Italy

**Reviewed by:**
Xiaodong Xia,
Dalian Polytechnic University, China
Arunachalam Muthaiyan,
University of New Mexico Gallup,
United States

***Correspondence:**
Jun Mei
jmei@shou.edu.cn
Jing Xie
jxie@shou.edu.cn

**Specialty section:**
This article was submitted to Antimicrobials, Resistance and Chemotherapy, a section of the journal Frontiers in Microbiology

**Received:** 10 November 2021
**Accepted:** 11 January 2022
**Published:** 10 March 2022

**Citation:**
Yu H, Pei J, Qiu W, Mei J and Xie J (2022) The Antimicrobial Effect of Melissa officinalis L. Essential Oil on Vibrio parahaemolyticus: Insights Based on the Cell Membrane and External Structure. Front. Microbiol. 13:812792. doi: 10.3389/fmicb.2022.812792

The study was to evaluate the antimicrobial impacts on *Melissa officinalis* L. essential oil (MOEO) against *Vibrio parahaemolyticus*. The minimum inhibitory concentration (MIC) of MOEO on *Vibrio parahaemolyticus* was 1 $\mu L \cdot mL^{-1}$. The kill-time curve exhibited that MOEO had good antimicrobial activity. The analysis of cellular ingredients leakage and cell viability illustrated that MOEO has destruction to the morphology of the cell membrane. The damage to the membrane integrity by MOEO has been confirmed by transmission and scanning electron microscopy, obvious morphological and ultrastructural changes were observed in the treated bacterial cells. The MOEO at 0.5 $\mu L \cdot mL^{-1}$ can inhibit the biofilm formation, biofilm motility, and extracellular polysaccharide production. Meanwhile, the qPCR results exhibited MOEO inhibited the expression of virulence genes. The findings showed that MOEO exerted its antimicrobial effect mainly by destroying the membrane, which indicated its potential as a natural food preservative.

**Keywords: *Melissa officinalis* L., *Vibrio parahaemolyticus*, antimicrobial mechanism, biofilm, virulence genes**

## INTRODUCTION

*Vibrio parahaemolyticus* can lead to vibriosis in different species of aquatic animals, along with septicemia and gastroenteritis in humans (Ning et al., 2021). It is the most common *Vibrio* genus and has recently become a primary food safety issue in many Asian countries (Zhu et al., 2022). *V. parahaemolyticus* is recognized as a new species because of vibriosis related to the consumption of contaminated raw or undercooked seafood (Ashrafudoulla et al., 2021). Sepsis has also been reported when wounds were exposed to the pathogen (Zhong et al., 2021).

Adding natural preservatives are the common methods to control the growth and reproduction of *V. parahaemolyticus* (Semeniuc et al., 2017). Essential oils (EO), a complex mixture of aromatic and volatile consisting secondary metabolites of aromatic plants, is usually obtained from plant material such as flowers, fruits, and leaves (Spadaccino et al., 2021). *Melissa officinalis* L. (MO) is a plant that has been used to give fragrance to foods and beverages. As a medicinal plant, it has been given various therapeutic roles (anticonvulsant, energizer, sedative, etc.) (Serra et al., 2020). *Melissa officinalis* L. essential oil (MOEO) primarily contains terpene aldehydes (citronellal, citral, and geranial) and terpenic alcohols (dimethylocta-2, dimethyl-3-octanol, etc.) (Rădulescu et al., 2021), which demonstrated good potential for antimicrobial activity.

Biofilms on microorganisms are referred to as a dense network structure made up of exopolysaccharides (EPS) and multifarious microorganisms embedded in them (Popławski et al., 2008). Biofilms may form on medical devices, the surfaces of food, and the equipment to transport raw materials. The biofilm environment acts just like a physical barricade and drives both metabolic and physiological changes, adapting microorganisms to a slow growth and situation of starvation, and increasing their resistance to various preservatives (Sahal et al., 2020). The purpose of the study was to detect the possible mechanism of antimicrobial action that *V. parahaemolyticus* treated by MOEO. The effect of *V. parahaemolyticus* treated by MOEO was decided by electric conductivity, glucose content, field emission Fourier transform infrared (FTIR) spectroscopic analysis, transmission electron microscope (TEM), field emission scanning electron microscope (SEM), biofilm formation, and the virulence genes expression.

## MATERIALS AND METHODS

### Gas Analysis by Gas Chromatography-Mass Spectrometry

The analysis of MOEO is carried out by Gas Chromatography-Mass Spectrometry (GC-MS) (Trace DSQ II, United States). A DB-5H capillary fused silica column was used. The temperatures of injector and detector were adjusted to 250 and 230°C, correspondingly. The ion source temp was set to 230°C. The oven temperature was maintained at 45°C for 1 min, followed by adjustment to 300°C at a speed of 20°C/min. The injection sample volume was 1 μL, the ionization energy was 70 EV, and the scan range was 35–500 m/z. Identification of MOEO was a comparison of retention times and mass spectral libraries.

### Chemicals and Bacterial Culture

MOEO was purchased from Tokyo Chemical Industry Co., Ltd. (Tokyo, Japan). *V. parahaemolyticus* ATCC 33847 was used in this study. There was 100 μL stock culture inoculated into 10 mL TSB medium (Hopebio, Qingdao) containing 3% NaCl (w/v). The strain was propagated in TSB medium (Hopebio, Qingdao) containing 3% NaCl (w/v) at 37°C with shaking at 200 r/min to receive the initial culture which concentration was $10^8$ CFU/mL. MOEO was dissolved with 5% Tween-80 (v/v) proportionally, and then sonicated for 30 min until completely dissolved.

### Minimum Inhibitory Concentration and Minimum Bactericidal Concentration Measurements

The MIC and MBC of *V. parahaemolyticus* treated with MOEO were ensured by the broth microdilution method according to the slightly modified method from Wang L. et al. (2020). There were 96-well microtiter plates added with the diluted bacterial culture at a concentration of $1 \times 10^8$ cfu/mL. Serial dilutions of MOEO were made up and the mixture was added to each well with final concentration range from 0.125 to 256 μL/mL. All plates were followed 24 h incubation at 37°C, then assessed for growth by turbidimetric method. Defined MIC as the lowest MOEO concentration that no visible growth was detected (OD600 $\leq$ 0.05). To evaluate the bacterial growth further, the cultures with no visible bacteria growth were subcultured on nutrient agar to determine that the minimum concentration of MOEO was defined as MBC, with no colony growth (Liu W. et al., 2020).

### Kill-Time Analysis

To study the effect of *V. parahaemolyticus* growth kinetics by MOEO treated, we used the kill-time assay according to a former research report with some modifications (Guo et al., 2019). *V. parahaemolyticus* was treated with different concentrations of MOEO (2×, 1×, 0.5× and 0.25× MIC) and 5% Tween-80. The culture cultured at 37°C and monitored $OD_{600}$. The experiments were carried out in triplicate.

### Measurements of Electric Conductivity and Glucose Content

The electric conductivity was measured based on Chen et al. (2021) with some modifications. *V. parahaemolyticus* was treated with MOEO 10 h at 37℃, then the mixture was centrifugated. The supernatant was diluted 40-fold and measured the conductivity every 2 h with an electrical conductivity facility (CN121-A, Nuclear Instrument Co., Ltd., China). The glucose content was determined every 2 h with a glucose assay kit (No. 361510, Jiancheng, Nanjing, China).

### Integrity of Cell Membrane

MOEO with the range of concentration ranges (2×, 1×, 0.5× and 0.25× MIC) was added to the initial culture ($1 \times 10^8$ cfu/mL), then the mixed culture was shaking incubated 4 h at 37°C. The supernatant was collected by centrifugating at 8,000 × g, 10 min at 4°C. Using a UV spectrophotometer (UV-2100, UNICO Instrument Co., Ltd., China), we monitored nucleic acid and protein levels, respectively (Wang N. et al., 2020).

### Scanning Electron Microscope Analysis

MOEO with the range of concentration ranges (2×, 1×, 0.5×, and 0.25× MIC) were added to the initial culture ($1 \times 10^8$ cfu/mL), then the mixed culture was shaking incubated 4 h at 37°C. The culture was subjected to centrifugation to collect

the bacteria cells. The *V. parahaemolyticus* samples were fixed in 2.5% glutaraldehyde solution over 4 h and cleaned with 0.01 mol/L PBS solution. The *V. parahaemolyticus* samples were then eluted with ethanol. After air-drying on coverslips, the sediment was sputtered with gold and imaged with SEM (S-3400, Hitachi, Tokyo, Japan).

## Transmission Electron Microscope Analysis

MOEO with the range of concentration ranges (1× MIC) were added to the initial culture ($1 \times 10^8$ cfu/mL), then the mixed culture was shaking incubated 4 h at 37°C. The culture was subjected to centrifugation to collect the bacteria cells. The *V. parahaemolyticus* samples were fixed in 2.5% glutaraldehyde solution over 4 h. The following treatments refer to Tan et al. (2018), using a JEM-2100 TEM (JEOL Ltd., Japan) observed.

## Fourier Transform Infrared Spectroscopic Analysis

MOEO with the range of concentration ranges (2×, 1×, 0.5×, and 0.25× MIC) were added to the initial culture ($1 \times 10^8$ cfu/mL), then the mixed culture was shaking incubated 4 h at 37°C. The culture was subjected to centrifugation to collect the bacteria cells. The *V. parahaemolyticus* samples were fixed in 2.5% glutaraldehyde solution over 4 h and cleaned with 0.01 mol/L PBS three times. The sediment was freeze-dried for 48 h and then subjected to FTIR spectroscopy (Nicolet, Thermo Fisher Scientific, United States) (Li et al., 2016).

## Crystal Violet Quantitative Assay

The influence of MOEO on biofilm was assessed indirectly by crystal violet staining (Zhang et al., 2017a). MOEO with the range of concentration ranges (2×, 1×, 0.5×, and 0.25× MIC) was added to the initial culture ($1 \times 10^8$ cfu/mL), and then cultured in a 48-well plate for 48 h, the presence of biofilm growth was assayed. After 24 h cultured in TSB, the cell culture was seeded to another plate in TSB and allowed to adhere. The suspending cells were then aspirated and 200 μL of fresh TSB with MOEO was added, incubated for a further 24 h, and then measured the biofilm production. The supernatant was removing floating cells, washing, and drying twice, the biofilm was stained with crystal violet. The solutions were taken to a new well and the absorbance was sensed at 570 nm. The experimental procedure was carried out in triplicate.

## Motility Assay

The impact of MOEO on the motility assay were assessed swimming and swarming. For swarming motility assay, 5 μL of $1 \times 10^8$ CFU/mL *V. parahaemolyticus* bacterial culture was added to the LB dishes with 1.5% (w/v) agar with MOEO at concentrations of 0.5× and 0.25× MIC, incubating at 37°C for 24 h. To the swimming motility assay, 5 μL of $1 \times 10^8$ CFU/mL bacterial culture was added to the center of the LB dishes with 0.3% (w/v) agar with MOEO at concentrations of 0.5× and 0.25× MIC, incubating at 37°C for 12 h.

## Exopolysaccharides Assay

MOEO with the range of concentration ranges (0.5× and 0.25× MIC) was added to the initial culture ($1 \times 10^8$ cfu/mL) and cultured in a 48-well plate 6 h at 37°C in an anaerobic environment to observe the amount of biofilm. The effects of MOEO were explored through the phenol-sulfuric acid (PSA) method (Cao et al., 2021).

## Confocal Laser Scanning Microscopy Assay

MOEO with the range of concentration ranges (0.5× and 0.25× MIC) was added to the initial culture and cultured in a 48-well plate 24 h at 37°C under anaerobic condition. We visualized the effect of MOEO on biofilm using confocal laser scanning microscopy (CLSM). After 24 h of biofilm formation, we removed the culture, and cleaned plastic panels three times with 0.1 M PBS. The 48-well plates were fixed with glutaraldehyde, and then the plastic panel was rinsed three times with 0.1 M PBS to eliminate glutaraldehyde. Subsequently, plastic panels were stained with SYBR Green I (Sangon Biotech, Co., Ltd., Shanghai, China) under dark conditions for 30 min. The plastic panels used 0.1 M PBS cleaned to remove extra stain. Last, the biofilm was studied with a CLSM (LSM710, Carl Zeiss AG, Germany) at 488 nm excitation light and 525 ± 25 nm emitting light, following a 20 × microscope objective (Jun and Jing, 2020).

## Quantitative Realtime PCR

MOEO (0.5 × and 0.25 × MIC) was added to the initial culture, oscillation cultured 6 h, then the culture was centrifuged to collect the bacteria cells. The total RNA was extracted. Of the total RNA, 1,000 ng, 1 μL of the primers oligo (dT), and 1 μL of 10 mmol/L dNTP mix was used to obtain the cDNA. MA-6000 Real Time PCR (Suzhou Yarui Biotechnology Co., Ltd., China) was used for quantitative realtime PCR (qPCR) assay. The relative expression levels were counted using the comparative threshold cycle ($2^{-\Delta\Delta Ct}$) method, and gapdh was defined as the reference gene. The gene sequences are in **Table 1**.

## Statistical Analysis

In all experiments, three simultaneous parallel dimensions were carried out. Statistical analysis was conducted with the software SPSS 22.0. Results are expressed as mean ± SD. A *P*-value of 0.05 or less was a difference that was statistically significant.

# RESULTS AND DISCUSSION

## Gas Chromatography-Mass Spectrometry Analyses

The compositions of MOEO were determined by GC-MS, and 11 main components were identified and quantified (**Table 2**). The main active constituents of MOEO were geraniol, citronella, and citronellol. Geraniol constituted 38.31% of the total amount. Citronella constituted 27.87% of the total amount, and was the second volatile component in MOEO, followed by citronellol (11.38%). The results were similar with the

**TABLE 1 |** The sequence of primers.

| Target gene | Sequence of primers (5′–3′) |
|---|---|
| Trh | F, ACGCGGTTGATGTTCGTAGT |
| | R, ACCTCATATCATCGCGCAGG |
| vopS | F, CTGGCAAGAACCTCAAAGCG |
| | R, GCCCTTCAATATGTCGCTGC |
| vscF | F, GAGCAACAAGCGAAAGACGC |
| | R, AGTGGTGGTTGCGTTGATGT |
| VP1388 | F, CAACATCAAACATGCCGCGT |
| | R, AGCTACACGCATGTCCCTTC |
| VP1407 | F, TCTTACGAGCGTAGTTGGCG |
| | R, CGGCTGATGAAGTACAACCG |
| toxR | F, TGAACCAGAAGCGCCAGTAG |
| | R, TTGTCCGCCAGTGGCAATTA |
| toxS | F, CCCGTTACGTCGTGTGAATG |
| | R, TTGTCGATTCAGCCGTCGAG |
| opaR | F, AGCTCGATCATCGCATTGGT |
| | R, TCAACCATGTTGTCCGTCAGT |
| aphA | F, GGCTTGTGCTGTTCAACCAT |
| | R, GTTACGACGAAGCGTTAGGC |
| luxM | F, ACCTGAGGTCAGTTCATGCTT |
| | R, TTCCGTTCCTGCGTGTCC |
| luxS | F, GCAGGGTTTGACTCCACACT |
| | R, TGATGGCTGCTGCAATGAGT |
| luxN | F, CAAACTCGGCGGGCATTGAT |
| | R, GGACGACGCAAAAGATCCTC |
| luxU | F, TTTCGGAGCCGACAGTTTGT |
| | R, CGTCGCGTGTTTCATTCAAG |
| luxO | F, GCGTCATGGCTCTCAAGACT |
| | R, TAGCGGCAGAGTCAATGGTG |

**TABLE 2 |** The formulation of MOEO.

| No. | Compounds | RT (min) | PA (%) |
|---|---|---|---|
| 1 | D-limonene | 4.74 | 4.13 |
| 2 | 3,7-dimethylocta-1,6-dien-3-ol | 5.335 | 1.1 |
| 3 | Citronellal | 5.815 | 27.87 |
| 4 | Citronellol | 6.4 | 11.38 |
| 5 | Geraniol | 6.6 | 38.31 |
| 6 | β-Citronellol | 7.335 | 2.75 |
| 7 | Eugenol | 7.415 | 1.05 |
| 8 | Geranyl acetate | 7.555 | 7.42 |
| 9 | β-elemene | 7.73 | 1.96 |
| 10 | D-iso macrogeradiene | 8.425 | 1.24 |
| 11 | α-copaene | 8.64 | 2.79 |

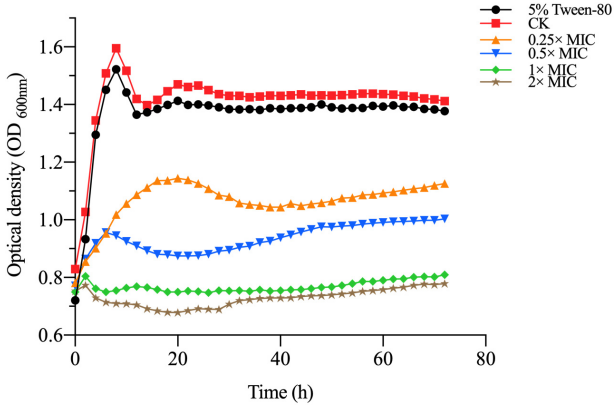


**FIGURE 1 |** The *V. parahaemolyticus* growth curves. CK is the *V. parahaemolyticus* without *Melissa officinalis* L. essential oil treated.

research reported by Miraj et al. (2017). MOEO was found in the presence of numerous phytochemicals such as phenolic components (tannins, flavonoids, and phenolic acids) and terpenes (triterpenes, sesquiterpenes, and monoterpenes) (Ilić et al., 2021). Miraj et al. (2017) found the predominant character of MOEO was present as oxygen-containing monoterpenes such as geranial, citronellal, and citral isomers which were the antimicrobial ingredient. Actually, the main ingredients of MOEO, citronellal and geranial, have been shown to be in charge of its antimicrobial activity which were proved to be responsible for its antimicrobial activity (Božović et al., 2018). Neda et al. (2004) found that the citral and citronellol content were 12 and 13%, respectively. Also, the MOEO showed a better antimicrobial effectiveness. The difference of MOEO levels was likely caused by different growing environments or different extraction methods (Caleja et al., 2017; Silva et al., 2021).

## Minimum Inhibitory Concentration and MBC of *Melissa officinalis* L. Essential Oil Against *Vibrio parahaemolyticus*

The MIC and MBC of MOEO against *V. parahaemolyticus* were 1 and 2 μL/mL, correspondingly. To further prove the antimicrobial activity of MOEO against *V. parahaemolyticus*, the influence of *V.* parahaemolyticus growth in the existence of levels (0.25×, 0.5×, 1×, 2× MIC and 5% Tween-80) were plotted. In **Figure 1**, there was no obvious difference between the growth value of 5% Tween-80 and CK. This result was consistent with Orafidiya et al. (2001) and illustrated 5% Tween-80 was not antimicrobial to *V. parahaemolyticus* (Rizvi et al., 2013). The increase of *V. parahaemolyticus* was inhibited with different concentrations of MOEO and the effect was a dose-dependent and time-dependent manner. This result was consistent with Chen et al. (2021). There was no obvious difference between the growth value of 1 × MIC and 2 × MIC, and the growth of *V. parahaemolyticus* was completely controlled. These findings indicated that MOEO had an antimicrobial effect on *V. parahaemolyticus* and increased with the dose. The antimicrobial activities of MOEO may probably be due to the citronellol, geranial, and D-limonene. Geranial and citronellal have been implicated in the antimicrobial and antifungal activities of the EO (Božović et al., 2018).

## Cell Membrane Permeability

The experiment of MOEO about electric conductivity was carried out to determine, in a greater degree, the disruption of cell architecture. In **Figure 2A**, the leakage degree was positively

correlated with the treated time at 0.25 × MIC MOEO. The electrical conductivity values of *V. parahaemolyticus* with MOEO treatment at levels of 1 × MIC and 2 × MIC were significantly increased after 2 h and decreased after 2 h. The cell membrane was destroyed and small molecules of $Na^+$ and $K^+$ leaked from the cells. Fluctuations in the conductivity of the control may be caused by autolysis and bacterial cell death (Zhang et al., 2017b). The immediate increase of the culture electrical conductivity upon the addition of the MOEO can be attributed to the high reactivity and volatility of the natural essential oil (Cui et al., 2016; Zhang et al., 2018). The mentioned phenomena were consistent with the results of TEM analysis, which gave further evidence of the disruption caused by MOEO to the cell membrane and wall of *V. parahaemolyticus*.

## Cell Membrane Integrity

Nucleic acids, proteins, and glucose were the essential substances presenting throughout the cell membrane and cytoplasm of bacteria, and they flowed out as the bacterial membrane was damaged (Xu et al., 2018). Therefore, the leakage of these substances can reflect the integrity of the membrane. In **Figure 2B**, the amount of extracellular glucose also went up with concentration, and the impact was time dependent. Conductivity values of *V. parahaemolyticus* by 1 × MIC MOEO treated increased obviously from 0 to 2 h and decreased after 4 h. The trend was the same at 2 × MIC concentrations, which can be owned to the stress response of mycelium (Zhang et al., 2018). As shown in **Figures 2C,D**, nucleic acids and proteins leaked from *V. parahaemolyticus* cells after the treatment of MOEO, the effect was dose related. There was no obvious difference between $OD_{260}$ and $OD_{280}$ value of 0.25 × MIC and 0.5 × MIC with the control. The nucleic acids and proteins treated with 0.25 × MIC MOEO increased by 1.47, 1.25 times compared to control, respectively. These results were consistent with Dai et al. (2021) that they found *Litsea cubeba* essential oils disrupted the integrity of *Escherichia coli* and caused the leakage of nucleic acids

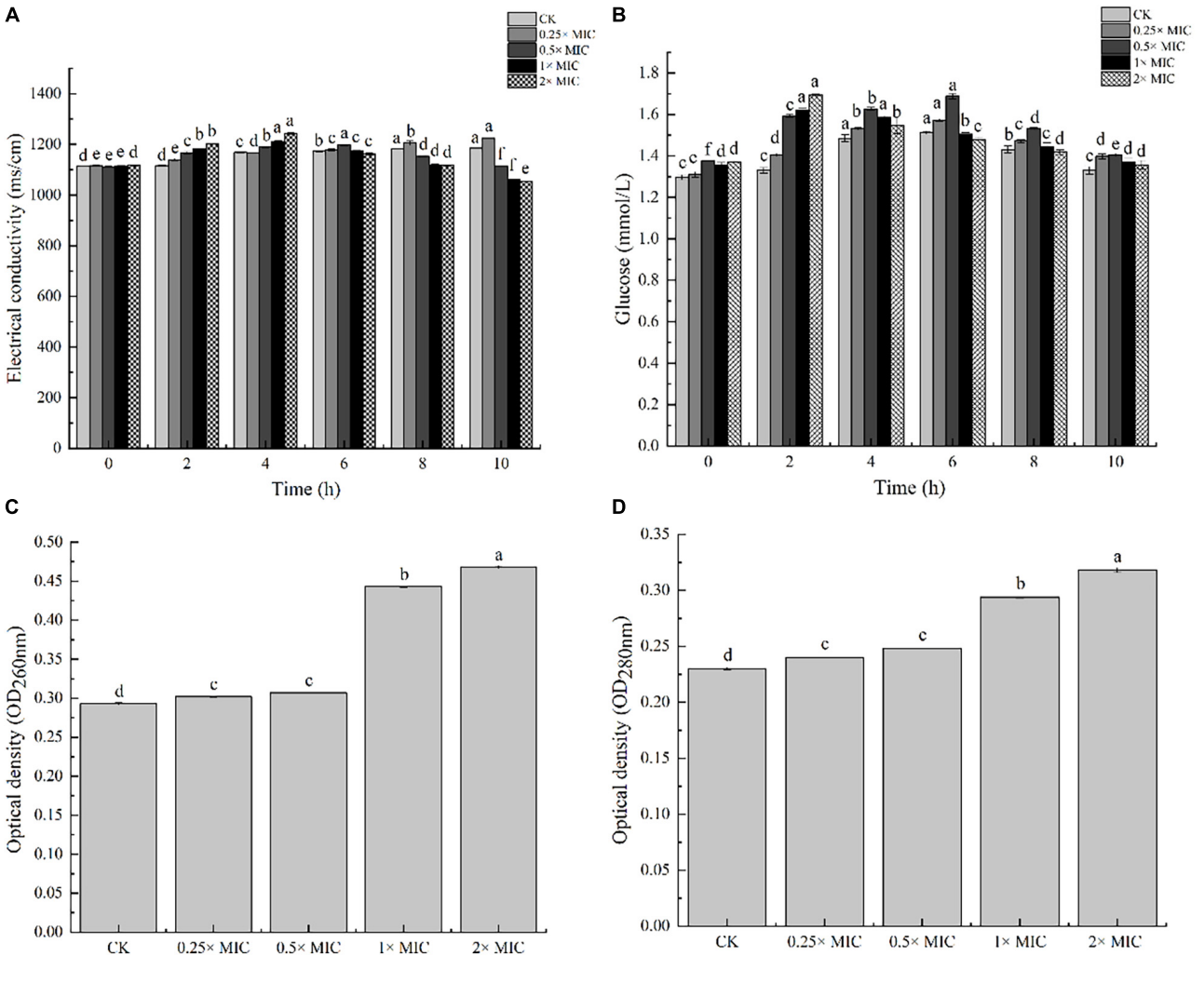


**FIGURE 2 |** The effects of electric conductivity **(A)**, and intracellular glucose spillage **(B)**, nucleic acids **(C)** and proteins **(D)** from *V. parahaemolyticus* treated with *Melissa officinalis* L. essential oil. CK is the *V. parahaemolyticus* without *Melissa officinalis* L. essential oil treated.

and proteins. This finding suggested that MOEO destroyed the cell membrane leading to the increase in extracellular proteins and nucleic acids.

## Electron Microscopic Observations

The morphological alterations of the cells and spores treated with different concentrations of MOEO (2×, 1×, 0.5×, and 0.25× MIC, respectively) were observed by SEM. In **Figure 3A**, the control showed rod-shaped cells with intact morphology and smooth surface, the cell had intact and dense protoplasm. In contrast, the cell structure changed significantly after treatment with different concentrations of MOEO. Irregular and distinct wrinkled with pucker and small holes appeared on the surface of *V. parahaemolyticus* treated with 0.25 × MIC MOEO. More cells became distorted and shriveled in 0.5 × MOEO treatment. The 1 × and 2 × MIC MOEO treated samples caused more severe membrane damage and the surface had many dents and wrinkles. Together, these results were consistent with the conclusions above, confirming that the bacterial cell membrane was damaged by treatment with MOEO. A similar change of *Shewanella putrefaciens* in SEM images after phenyllactic acid treated was reported (Fang et al., 2021). Ferreira et al. (2011)

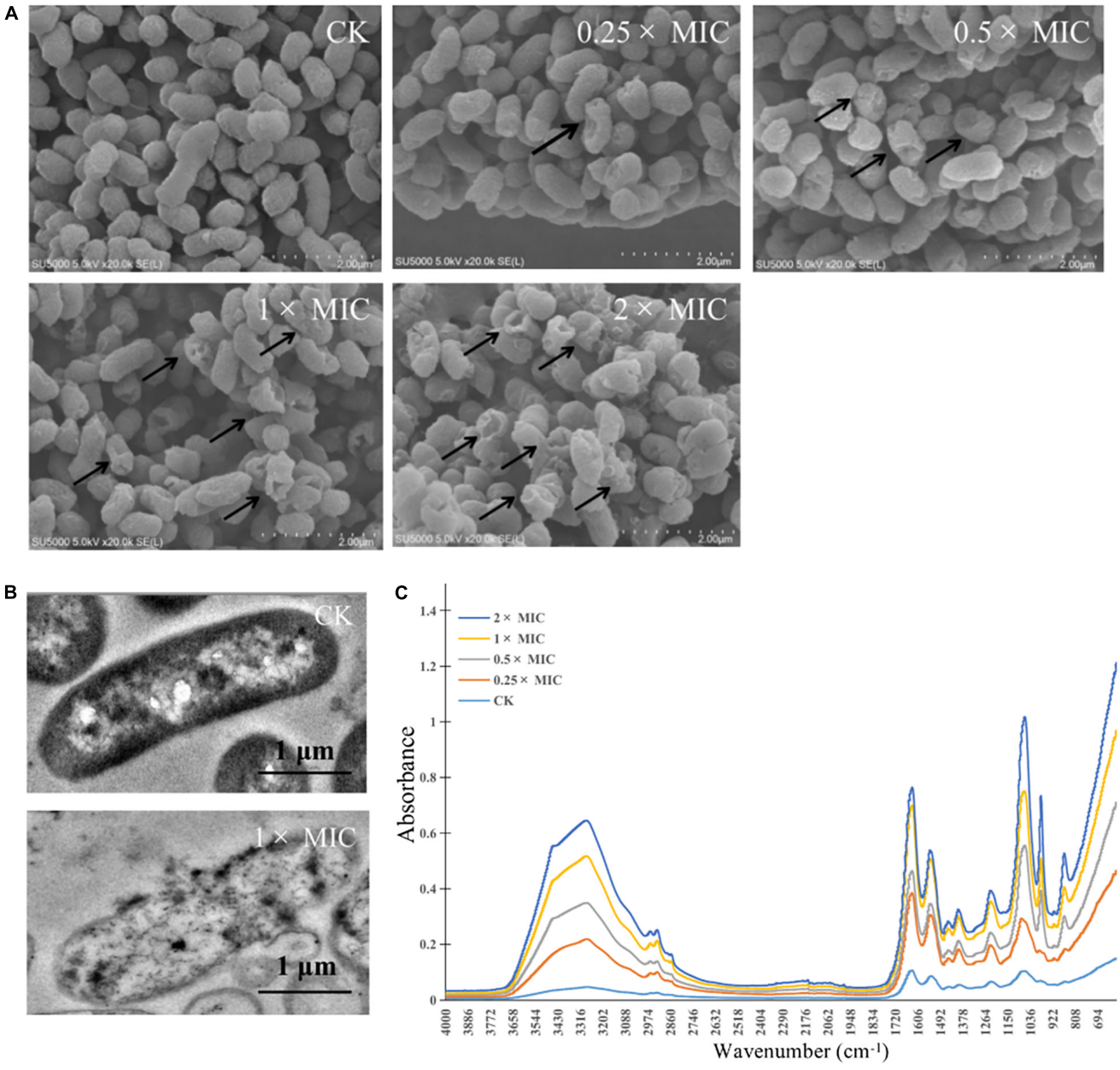


**FIGURE 3 |** Effects of *Melissa officinalis* L. essential oil on *V. parahaemolyticus* shown in SEM [**(A)** The magnification is 50,000×], TEM **(B)** images, and the FTIR spectroscopy **(C)**. CK is the *V. parahaemolyticus* without *Melissa officinalis* L. essential oil treated.

found that the *Pseudomonas fluorescens* appeared rougher with wrinkles and membrane deformed after citral treatment. All these results indicated that MOEO treatment disrupted the cell walls and cell membranes of the bacteria at different levels. Cells were disrupted and divided as a result of the loss of cell integrity.

Morphological changes of *V. parahaemolyticus* after treatment with MOEO (1 × and 0 × MIC, respectively) were observed by TEM. Cellular secretions in treated cells were found to leak in the surrounding medium by TEM studies (Guo et al., 2018). The controlling group kept the typical bacterial morphology with clear cytoplasm, cell wall, cell membrane, and nuclei (**Figure 3B**). Cells that were treated with 1 × MIC MOEO (**Figure 3B**) showed a marked variability. Bacterial cell membranes and walls were disrupted, lysed, and broken. In addition, the cytoplasm of the bacteria extravasated, appearing as a clear cavity, slightly deformed, cell wall broken, and cytoplasm leaked from the treated *V. parahaemolyticus*. Deng et al. (2021) demonstrated that anthocyanins inhibited the growth of *E. coli* by disrupting the bacterial cell wall and plasma membrane making cell dissolution and cytoplasmic released. Dai et al. (2021) reported that the strain cells treated with *Litsea cubeba* essential oil lead to disordered function of cell membranes and obvious intracellular injury appeared. Zhou et al. (2021) showed that treatment of *E. coli* with *Alpinia galanga rhizomes* essential oil can stimulate the efflux of intracellular material. Liu W. et al. (2020) interpreted that cell membranes and walls of *P. fluorescens* and *S. putrefaciens* treated with Daphnetin were disrupted and resolved, and the cytoplasm of the bacteria leaked, creating a clear cavity. Such phenomena suggested that adding polyphenols may disrupt cell division, leading to cells changing from classic long rod shape to short rod shape (Yi et al., 2010.). Apparently, the cells of strains that were treated with MOEO sustained major injury due to induced cell membrane dysfunction, according to the results (Chen et al., 2017).

## Fourier Transform Infrared Spectroscopic

Secondary structure was measured using the FTIR technique, with the purpose of exploring the antimicrobial effect of MOEO against *V. parahaemolyticus* (**Figure 3C**). The slight changes at 982 $cm^{-1}$ were attributed to the cyclic oscillation of oligosaccharides and polysaccharides (Salman et al., 2019). The 1,185–1,485 $cm^{-1}$ region bands were dominated by the protein, lipids, and phosphate compounds contribution, so the peak changed at 1,386 $cm^{-1}$ and showed the growth of *V. parahaemolyticus* was inhibited by MOEO. Changes in the characteristic peaks of absorbed at 3,260 and 1,218 $cm^{-1}$ showed that MOEO may destroy cell membrane phospholipid structure (Kos et al., 2003). The 1,080$cm^{-1}$ is due to symmetric phosphate stretching modes (Fujioka et al., 2004), and the decrease is probably because of the leakage of carbohydrates, nucleic acids, and polysaccharides (Salman et al., 2019). The characteristic absorption bands reduced at 1,061 $cm^{-1}$ also indicating the leakage of nucleic acids. Meanwhile, the characteristic absorption bands reduced at 1,629 $cm^{-1}$ suggested that protein leaked. These discoveries were the same as the result of cell membrane integrity analysis.

## Effect of *Melissa officinalis* L. Essential Oil on *Vibrio parahaemolyticus* Biofilm Formation

Anti-biofilm action of MOEO was evaluated by a crystalline violet test. It was shown that MOEO prevented biofilm generation and the effect was in a dose dependent manner (**Figure 4A**). Biofilm quantities were reduced after subinhibitory concentrations (SICs) MOEO treated. There were 90.31 and 98.27% inhibition ratio in 0.25 × MIC and 0.5 × MIC MOEO treatments for 8 h, respectively, and no biofilm formed after 24 h. MOEO disturbed the biofilm formation from the initiation stage. As a result, MOEO demonstrated excellent suppression of biofilm formation.

Cao et al. (2021) and Ruan et al. (2021) found that citral essential oil and resveratrol can suppress the biofilm formation in *V. parahaemolyticus* and *E. coli*. The biofilm formation in the control group decreased at 36 h may arise from cell apoptosis cutting down the amounts of bacteria that can form biofilms. The antimicrobial effect of MOEO may be related to its refrained formation of biofilm. In addition to environmental factors, the formation of biofilm was also influenced by the control of bacterial quorum sensing system (QS) (He et al., 2019). A classic two-component signal transduction system, the Lux system in Vibrio species, had been shown to contribute to biofilms' growth (Deborah and Groisman, 2013). Liu et al. (2021) demonstrated that LuxQ, LuxU, and LuxO were critical for biofilm formation control in *V. parahaemolyticus* and the deletion mutants among them displayed analogous biomembrane-forming. It can be concluded that MOEO inhibited the expression of *LuxQ*, *LuxU*, and *LuxO*, thus reducing the formation of biofilms (**Figure 5**).

## Inhibition of Motility by *Melissa officinalis* L. Essential Oil

In **Figure 6**, MOEO decreased swimming and swarming motilities of *V. parahaemolyticus* with a dose-dependent effect. With increasing MOEO concentration, the colony's diameters of *V. parahaemolyticus* reduced. Swimming motility of *V. parahaemolyticus* was markedly suppressed at 0.25 × MIC compared to the control. When the concentration was 0.5 × MIC, smaller colonies of bacteria were observed, illustrating higher inhibition of swimming motility. In addition, the active effect of MOEO to control swarming motility was also shown. The swarming motility of bacteria was suppressed by 0.25 × and 0.5 × MIC MOEO. As the diameter of bacterial colonies decreased, bacterial colonies progressively grew thinner. Jin et al. (2021) revealed that the garlic essential oil prevented the motility of Bacillus cereus ATCC 14579, and this experiment has indicated that MOEO could also restrict swarming and swimming motility of *V. parahaemolyticus*. The ability to swarm enabled *V. parahaemolyticus* cells to move through the

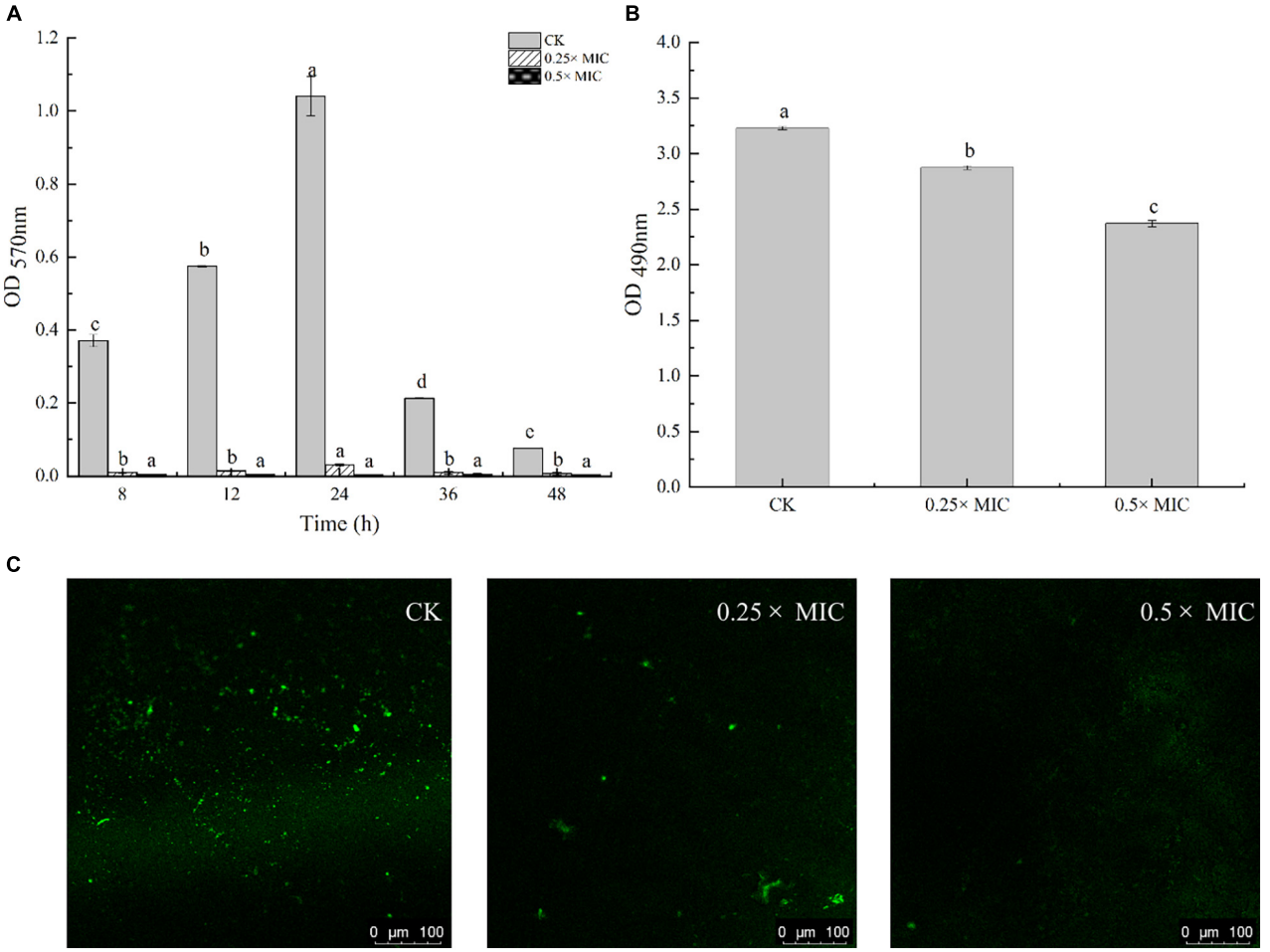


**FIGURE 4 |** Effect of *Melissa officinalis* L. essential oil on biofilm formation **(A)**, EPS production **(B)**, and CLSM **(C)**. CK is the *V. parahaemolyticus* without *Melissa officinalis* L. essential oil treated.

environment, making it possible for them to get a suitable surface to stick to Jin et al. (2021).

## Exopolysaccharides Production

Adhering to a solid surface, bacteria allowed bacteria to keep growing and secreting a matrix of biofilm outside the polymer, which included nucleic acids, proteins, and EPS. Extracellular polymeric matrix constituted 80% of the biofilm and formed a mature biofilm architecture. EPS is one of the main constituents of the extrapolymeric matrix. Therefore, it is important to suppress or decrease the production of EPS to control the biofilm formation (Liu F. et al., 2020).

Detection of EPS level in *V. parahaemolyticus* biofilms by quantification assay. In **Figure 4B**, adding 0.25 × and 0.5 × MIC MOEO markedly suppressed EPS contents in *V. parahaemolyticus* biofilms and EPS production decreased 4.87 and 17.48% in 0.25 × MIC and 0.5 × MIC MOEO treated samples, respectively. Thus, treatment with 0.25 × and 0.5 × MIC MOEO can suppress EPS production of *V. parahaemolyticus* cells in biofilms. The decrease of EPS was consistent with the result of the decreased biofilm production. Extracellular polymers of biofilms played an important part during the initial stages of adherence and biofilm formation by bacteria (Colagiorgi et al., 2016). Bacterial biofilms gave bacteria cells protection against harsh environments (Stoodley et al., 2002), and the inhibition of MOEO on *V. parahaemolyticus* growth can also be explained.

## Confocal Microscopy Observations (Confocal Laser Scanning Microscopy)

In **Figure 4C**, *V. parahaemolyticus* cells are not exposed (a, control) and exposed to 0.25 × and 0.5 × MIC MOEO. The amount of biofilm production was observed by treating the biofilm with SYBR Green I (Morozov et al., 2021). The results showed that the formation of biofilm matrix can be controlled by MOEO. According to CLSM images, biofilms were tightly attached to each other, and more cells fluoresced green in the visual field. In MOEO treated samples, biofilm structure was thin and shape appeared turbid. Compared with other groups, hardly any green in the visual field with 0.5 × MIC MOEO treated, showing that bacteria leaked the extrapolymeric matrix in the

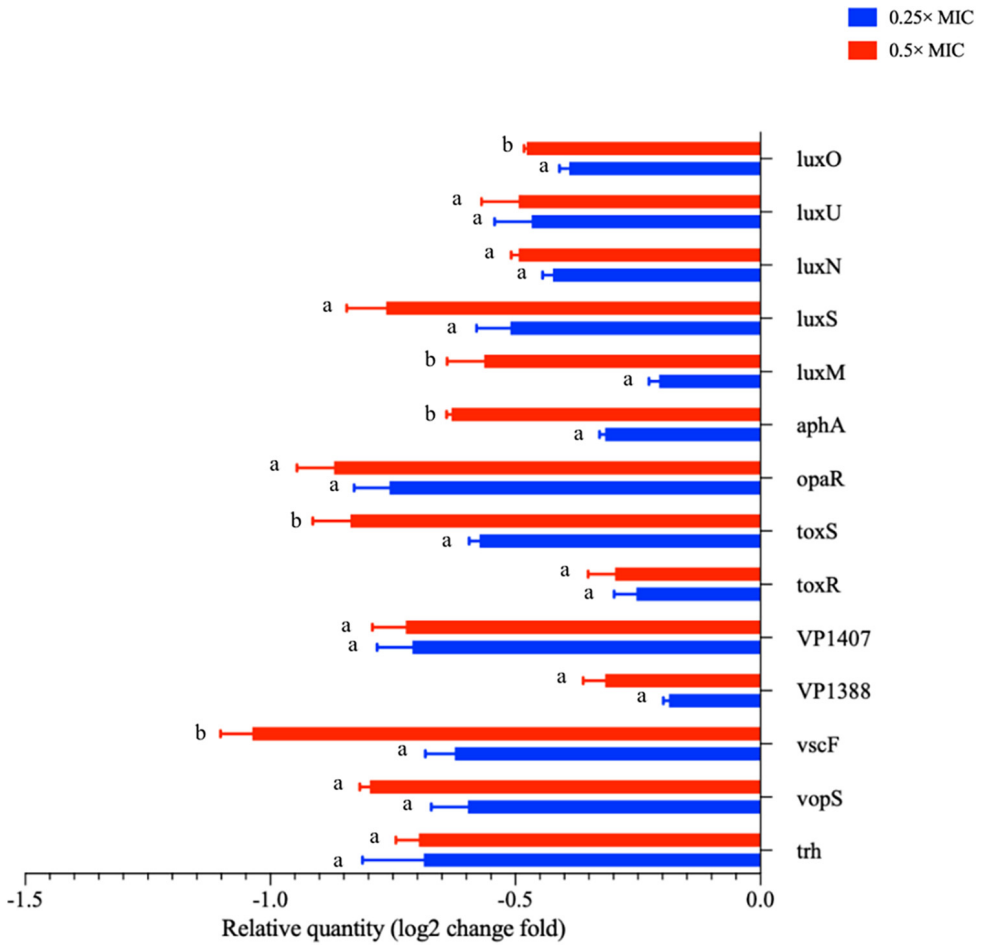


**FIGURE 5 |** The transcription levels of virulence related genes of *V. parahaemolyticus* treated with *Melissa officinalis* L. essential oil. CK is the *V. parahaemolyticus* without *Melissa officinalis* L. essential oil treated.

biofilm. These above phenomena were consistent with crystal violet quantitative assay.

## *Melissa officinalis* L. Essential Oil Suppressed the Virulence Gene Presentation

Under the influence of MOEO, virulence factor-associated genes in *V. parahaemolyticus* were displayed in **Figure 5**. The regulator gene T3SS (*vopS*, *vscF,* and *trh*), T6SS (*VP1388* and *VP1407*), ToxRS system (*toxR* and *toxS*), and the relation genes of QS (*luxU*, *luxS*, *luxN*, *luxO*, *luxM*, *opaR,* and *aphA*) were obviously lowered due to the treatment of MOEO. A greater suppression has been observed at 0.5 × MIC compared to 0.25 × MIC.

QS molecules have been shown to be implicated in the forming of bacterial biofilms (Rodolfo et al., 2016). *V. parahaemolyticus* mainly exploited the classical LuxI/LuxR system to create acyl homologous lactones (AHL) as signaling molecules to QS. AHL facilitated the formation of biofilm in *V. parahaemolyticus* (Ding et al., 2018). In **Figure 5**, it can be seen that MOEO controlled the expression of *luxM*, *luxS*, *luxN*, *luxU*, *luxO,* and *opaR* that were connected with QS. Liu et al. (2021) built the double deletion strains ΔluxUΔluxQ and ΔluxUΔluxO and assessed the number of biofilms, the result suggested that *luxQ*, *luxO*, and *luxU* were linked in the same signaling route regulating *V. parahaemolyticus* biofilm formation. Regarding additional *Vibrio* species, a recent study indicated that *Vibrio cholerae* used the Lux pathway by which to regulate biofilm formation (Jung et al., 2015). Ray and Visick (2012) proposed that *luxQ* exerted its function through *luxU* to regulate biofilm formation in *Vibrio fischeri*. *LuxU* controlled the transcription of syp loci (symbiotic polysaccharides) through the SypG-dependent pathway and *luxO*. Ray and Visick (2012) concluded that the Lux route influenced the formation of biofilms with *luxU* and *luxU* had a greater effect on biofilm formation than *luxO*, probably because the functions of *luxU* cognate appeared diverse in different *Vibrio* species. In general, Lux systems can affect the formation of biofilms in *Vibrio* species.

D-limonene, linalool, and citronellol were the main components of MOEO, which have been shown to inhibit

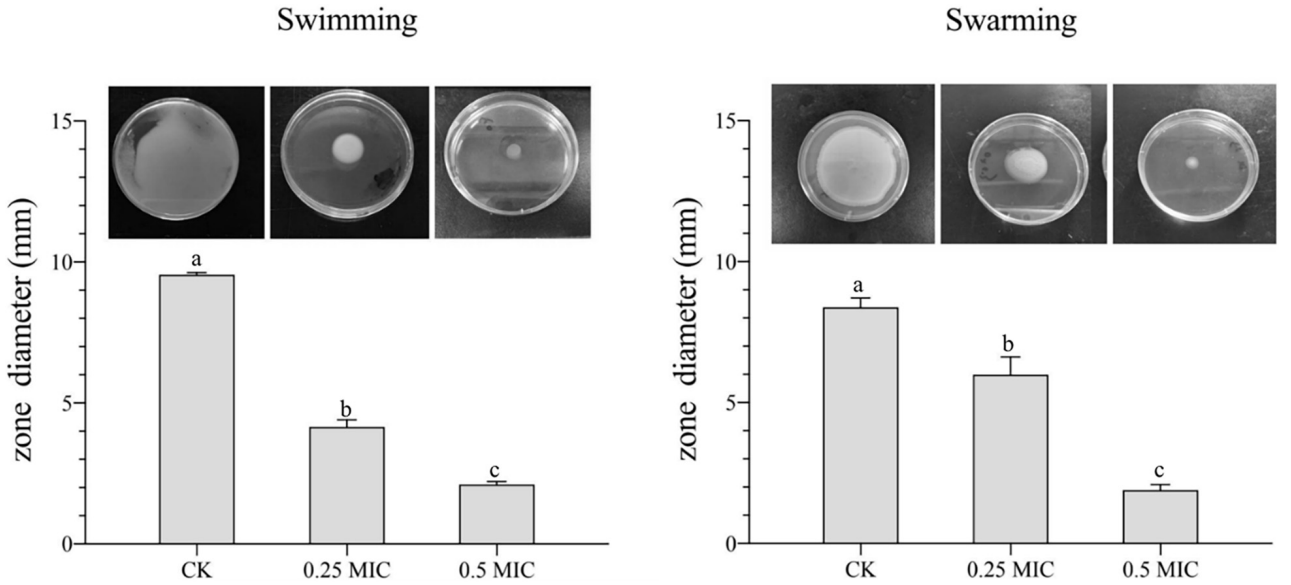


**FIGURE 6 |** Effects of *Melissa officinalis* L. essential oil on the motility of *V. parahaemolyticus*. CK is the *V. parahaemolyticus* without *Melissa officinalis* L. essential oil treated.

the QS system of bacteria (Deborah and Groisman, 2013; Ding et al., 2018; Zhang et al., 2018; He et al., 2019; Dai et al., 2021; Liu et al., 2021; Zhou et al., 2021). D-limonene can inhibit the activity of signaling molecules by degrading them or reducing their production (He et al., 2019). Linalool was able to reduce the activity of signal molecule synthase or signal molecule receptor protein and block the QS pathway (Stewart and McCarter, 2003). In addition, *opaR* can encode the key regulator at high cell density (Deborah and Groisman, 2013), *tdh* was the particular element of virulent *V. parahaemolyticus* strain (Liu et al., 2021). They were all inhibited by the gene expression.

Previous study on this bacterium revealed that T3SS system and T6SS system assisted the existence and multiplication of the bacterium in the human gastrointestinal tract. Furthermore, some effector proteins were produced by these secretion systems that were involved in immunosuppression, cytotoxicity, and dysregulation to the actin network (Burdette et al., 2008; Hubbard et al., 2016). Xiaohui et al. (2010) discovered that *VP1686* secreted from T3SS was accountable for the cytotoxicity of the host cell. Toshio et al. (2008) identified *vopD2* and *vopB2*, two effector proteins under T3SS, in charge of pore formation and cytotoxicity from infected cells. After treatment with MOEO, the relation genes of T3SS system and T6SS system expression were downmodulated, which may cause suppression of biofilm generation and virulence.

ToxRS is a chromosomally encoded gene with the primary function of regulating the virulence factors expression. The two-component regulator ToxRS proved to be critical to bacterial persistence and virulence of *V. parahaemolyticus* at the time of host infection (Yiquan et al., 2018). This study revealed that MOEO significantly repressed the *toxR* and *toxS* genes transcription from a dose-dependent manner.

## CONCLUSION

This research investigated the antimicrobial activity of MOEO against *V. parahaemolyticus* and its mechanism. The MIC of MOEO action on *V. parahaemolyticus* was 1 $\mu L \cdot mL^{-1}$. MOEO disrupted cell wall and membrane integrity, resulting in nucleic acid and protein efflux. SEM, TEM, and CLSM outcomes illustrated that MOEO altered the morphology of bacterial cells, allowing the efflux of materials in bacteria. FTIR spectra revealed that MOEO broke the phospholipid structure on the membrane, leading to nucleic acid and protein efflux, inhibiting the *V. parahaemolyticus* growth. At SICs, MOEO reduced the quantity of biofilm, slackened the biofilm structure, inhibited motility, as well as significantly reduced its potential virulence. MOEO impeded the process of QS in *V. parahaemolyticus*, downmodulated the regulatory genes T3SS, T6SS, and ToxRS system and the relational genes of QS to inhibit biofilm production. Those results demonstrated that MOEO can reduce the virulence risk even if the MOEO concentrations in food or packaging have not reached MIC for *V. parahaemolyticus*. Thus, MOEO is a promising natural preservative for the food industry, becoming a viable solution to decrease microbial growth.

## DATA AVAILABILITY STATEMENT

The original contributions presented in the study are included in the article/supplementary material, further inquiries can be directed to the corresponding author/s.

## AUTHOR CONTRIBUTIONS

HY: conceptualization, methodology, software, investigation, and writing. JP: methodology and investigation. WQ: conceptualization and software. JM: validation, formal analysis, writing—review, and editing. JX: examination and funding acquisition. All authors contributed to the article and approved the submitted version.

## FUNDING

This research was financially supported by the National Natural Science Foundation of China (Grant No. 31972142).

## REFERENCES

Ashrafudoulla, M., Na, K. W., Hossain, M. I., Mizan, M. F. R., Nahar, S., Toushik, S. H., et al. (2021). Molecular and pathogenic characterization of Vibrio parahaemolyticus isolated from seafood. *Mar. Pollut. Bull.* 172:112927. doi: 10.1016/j.marpolbul.2021.112927

Božović, M., Garzoli, S., Baldisserotto, A., Romagnoli, C., Pepi, F., Cesa, S., et al. (2018). Melissa officinalis L. subsp. altissima (Sibth. & Sm.) Arcang. essential oil: chemical composition and preliminary antimicrobial investigation of samples obtained at different harvesting periods and by fractionated extractions. *Ind. Crops Prod.* 117, 317–321. doi: 10.1016/j.indcrop.2018.03.018

Burdette, D. L., Yarbrough, M. L., Orvedahl, A., Gilpin, C. J., and Orth, K. (2008). Vibrio parahaemolyticus Orchestrates a Multifaceted Host Cell Infection by Induction of Autophagy, Cell Rounding, and Then Cell Lysis. *Proc. Natl. Acad. Sci. U.S.A.* 105, 12497–12502. doi: 10.1073/j.pnas.2008.0802773105

Caleja, C., Barros, L., Prieto, M. A., Barreiro, M. F., Oliveira, M. B. P. P., and Ferreira, I. C. F. R. (2017). Extraction of rosmarinic acid from Melissa officinalis L. by heat-, microwave- and ultrasound-assisted extraction techniques: a comparative study through response surface analysis. *Sep. Purif. Technol.* 186, 297–308. doi: 10.1016/j.seppur.2017.06.029

Cao, J., Liu, H., Wang, Y., He, X., Jiang, H., Yao, J., et al. (2021). Antimicrobial and antivirulence efficacies of citral against foodborne pathogen Vibrio parahaemolyticus RIMD2210633. *Food Control* 120:107507. doi: 10.1016/j.foodcont.2020.107507

Chen, F., Miao, X., Lin, Z., Xiu, Y., Shi, L., Zhang, Q., et al. (2021). Disruption of metabolic function and redox homeostasis as antibacterial mechanism of Lindera glauca fruit essential oil against *Shigella* flexneri. *Food Control* 130:108282. doi: 10.1016/j.foodcont.2021.108282

Chen, M., Zhao, Z., Meng, H., and Yu, S. (2017). The antibiotic activity and mechanisms of sugar beet (Beta vulgaris) molasses polyphenols against selected food-borne pathogens. *LWT Food Sci. Technol.* 82, 354–360. doi: 10.1016/j.lwt.2017.04.063

Colagiorgi, A., Ciccio, P. D., Zanardi, E., Ghidini, S., and Ianieri, A. (2016). A Look inside the Listeria monocytogenes Biofilms Extracellular Matrix. *Microorganisms* 4:22. doi: 10.3390/j.microorganisms.2016.4030022

Cui, H., Li, W., Li, C., Vittayapadung, S., and Lin, L. (2016). Liposome containing cinnamon oil with antibacterial activity against methicillin-resistant Staphylococcus aureus biofilm. *Biofouling* 32, 215–225. doi: 10.1080/j.bio.2015.08927014.1134516

Dai, J., Li, C., Cui, H., and Lin, L. (2021). Unraveling the anti-bacterial mechanism of Litsea cubeba essential oil against E. coli O157:H7 and its application in vegetable juices. *Int. J. Food Microbiol.* 338:108989. doi: 10.1016/j.ijfoodmicro.2020.108989

Deborah, C. H., and Groisman, E. A. (2013). The Biology of the PmrA/PmrB Two-Component System: the Major Regulator of Lipopolysaccharide Modifications. *Ann. Rev. Microbiol.* 67, 83–112. doi: 10.1146/annurev-micro-092412-155751

Deng, H., Zhu, J., Tong, Y., Kong, Y., Tan, C., Wang, M., et al. (2021). Antibacterial characteristics and mechanisms of action of Aronia melanocarpa anthocyanins against *Escherichia coli*. *LWT* 150:112018. doi: 10.1016/j.lwt.2021.112018

Ding, T., Li, T., and Li, J. (2018). Identification of natural product compounds as quorum sensing inhibitors in *Pseudomonas fluorescens* P07 through virtual screening. *Bioorg. Med. Chem.* 26, 4088–4099. doi: 10.1016/j.bmc.2018.06.039

Fang, M., Wang, R., Agyekumwaa, A. K., Yu, Y., and Xiao, X. (2021). Antibacterial effect of phenyllactic acid against Vibrio parahaemolyticus and its application on raw salmon fillets. *LWT* 112586 [preprint] doi: 10.1016/j.lwt.2021.112586

Ferreira, C., Pereira, A. M., Pereira, M. C., Melo, L. F., and Simões, M. (2011). Physiological changes induced by the quaternary ammonium compound benzyldimethyldodecylammonium chloride on *Pseudomonas* fluorescens. *J. Antimicrob. Chemotherapy* 66, 1036–1043. doi: 10.1093/j.jac/dkr028

Fujioka, N., Morimoto, Y., Arai, T., and Kikuchi, M. (2004). Discrimination between normal and malignant human gastric tissues by Fourier transform infrared spectroscopy. *Cancer Detect. Prev.* 28, 32–36. doi: 10.1016/j.cdp.2003.11.004

Guo, J., Gao, Z., Li, G., Fu, F., Liang, Z., Zhu, H., et al. (2019). Antimicrobial and antibiofilm efficacy and mechanism of essential oil from Citrus Changshan-huyou Y. B. chang against Listeria monocytogenes. *Food Control* 105, 256–264. doi: 10.1016/j.foodcont.2019.06.014

Guo, Z.-Y., Zhang, Z.-Y., Xiao, J.-Q., Qin, J.-H., and Zhao, W. (2018). Antibacterial Effects of Leaf Extract of Nandina domestica and the Underlined Mechanism. *Evid. Based Complementary Altern. Med.* 2018:8298151. doi: 10.1155/2018/8298151

He, L., Le, K. Y., Khan, B. A., Nguyen, T. H., Hunt, R. L., Bae, J. S., et al. (2019). Resistance to leukocytes ties benefits of quorum sensing dysfunctionality to biofilm infection. *Nature Microbiol.* 4, 1114–1119. doi: 10.1038/j.naturemicr.s41564-019-0413-x

Hubbard, T. P., Chao, M. C., Abel, S., Blondel, C. J., Abel Zur Wiesch, P., Zhou, X., et al. (2016). Genetic analysis of Vibrio parahaemolyticus intestinal colonization. *Proc. Natl. Acad. Sci. U.S.A.* 113, 6283–6288. doi: 10.1073/pnas.1601718113

Ilić, Z. S., Milenković, L., Tmušić, N., Stanojević, L., Stanojević, J., and Cvetković, D. (2021). Essential oils content, composition and antioxidant activity of lemon balm, mint and sweet basil from Serbia. *LWT* 153:112210. doi: 10.1016/j.lwt.2021.112210

Jin, Z., Li, L., Zheng, Y., and An, P. (2021). Diallyl disulfide, the antibacterial component of garlic essential oil, inhibits the toxicity of Bacillus cereus ATCC 14579 at sub-inhibitory concentrations. *Food Control* 126:108090. doi: 10.1016/j.foodcont.2021.108090

Jun, Y., and Jing, X. (2020). Comparative Proteome Analysis of Shewanella putrefaciens WS13 Mature Biofilm Under Cold Stress. *Front. Microbiol.* 11:1225. doi: 10.3389/fmicb.2020.01225

Jung, S. A., Chapman, C. A., and Wai-Leung, N. (2015). Quadruple quorum-sensing inputs control *Vibrio cholerae* virulence and maintain system robustness. *PLoS Pathog.* 11:e1004837. doi: 10.1371/j.ppat.2015.1004837

Kos, G., Lohninger, H., and Krska, R. (2003). Development of a method for the determination of Fusarium fungi on corn using mid-infrared spectroscopy with attenuated total reflection and chemometrics. *Anal. Chem.* 75, 1211–1217. doi: 10.1021/j.ac.2003.0260903

Li, H., Gao, Y., Li, C., Ma, G., Shang, Y., and Sun, Y. (2016). A comparative study of the antibacterial mechanisms of silver ion and silver nanoparticles by Fourier transform infrared spectroscopy. *Vib. Spectrosc.* 85, 112–121. doi: 10.1016/j.vibspec.2016.04.007

Liu, F., Jin, P., Gong, H., Sun, Z., Du, L., and Wang, D. (2020). Antibacterial and antibiofilm activities of thyme oil against foodborne multiple antibiotics-resistant Enterococcus faecalis. *Poult. Sci.* 99, 5127–5136. doi: 10.1016/j.psj.2020.06.067

Liu, M., Zhu, X., Zhang, C., and Zhao, Z. (2021). LuxQ-LuxU-LuxO pathway regulates biofilm formation by Vibrio parahaemolyticus. *Microbiol. Res.* 250:126791. doi: 10.1016/j.micres.2021.126791

Liu, W., Mei, J., and Xie, J. (2020). Elucidating Antibacterial Activity and Mechanism of Daphnetin against *Pseudomonas* fluorescens and Shewanella putrefaciens. *J. Food Quality* 2020, 1–10. doi: 10.1155/j.foodq.2020.6622355

Miraj, S., Rafieian-Kopaei, and Kiani, S. (2017). Melissa officinalis L: a Review Study With an Antioxidant Prospective. *J. Evid. Based Complementary Altern. Med.* 22, 385–394. doi: 10.1177/j.2017.2156587216663433

Morozov, V. N., Kolyvanova, M. A., Dement'eva, O. V., Rudoy, V. M., and Kuzmin, V. A. (2021). Comparison of quenching efficacy of SYBR Green I and PicoGreen fluorescence by ultrasmall gold nanoparticles in isotropic and liquid-crystalline DNA systems. *J. Mol. Liquids* 321:114751. doi: 10.1016/j.molliq.2020.114751

Neda, M.-D., Biljana, B., Marina, S., and Natasa, S. (2004). Antimicrobial and antioxidant activities of Melissa officinalis L. (Lamiaceae) essential oil. *J. Agricult. food chem.* 52, 2485–2489. doi: 10.1021/jf030698a

Ning, H., Cong, Y., Lin, H., and Wang, J. (2021). Development of cationic peptide chimeric lysins based on phage lysin Lysqdvp001 and their antibacterial effects against Vibrio parahaemolyticus: a preliminary study. *Int. J. Food Microbiol.* 358:109396. doi: 10.1016/j.ijfoodmicro.2021.109396

Orafidiya, L. O., Oyedele, A. O., Shittu, A. O., and Elujoba, A. A. (2001). The formulation of an effective topical antibacterial product containing Ocimum gratissimum leaf essential oil. *Int. J. Pharm.* 224, 177–183. doi: 10.1016/S0378-5173(01)00764-5

Popławski, N. J., Abbas, S., Maciej, S., and Glazier, J. A. (2008). Simulation of single-species bacterial-biofilm growth using the Glazier-Graner-Hogeweg model and the CompuCell3D modeling environment. *Mathematical biosciences and engineering. MBE* 5, 355–388. doi: 10.3934/j.mbe.2008.5.355

Rădulescu, M., Jianu, C., Lukinich-Gruia, A. T., Mioc, M., Mioc, A., Şoica, C., et al. (2021). Chemical Composition, In Vitro and In Silico Antioxidant Potential of Melissa officinalis subsp. *Officinalis Essential Oil*. Antioxidants 10:1081. doi: 10.3390/antiox10071081

Ray, V. A., and Visick, K. L. (2012). LuxU connects quorum sensing to biofilm formation in V ibrio fischeri. *Mol. Microbiol.* 86, 954–970. doi: 10.1111/mmi.12035

Rizvi, M., Ahmed, J., Khan, F., Shukla, I., and Malik, A. (2013). Assessment of combination therapy by time kill curve analysis and chequerboard assay for treatment of multi-drug resistant *Pseudomonas aeruginosa* isolates. *J. Global Antimicrob. Resist.* 1, 103–108. doi: 10.1016/j.jgar.2013.04.001

Rodolfo, G.-C., Toshinari, M., and Wood, T. K. (2016). Can resistance against quorum-sensing interference be selected? *ISME J.* 10, 4–10. doi: 10.1038/j.ismej.2015.84

Ruan, X., Deng, X., Tan, M., Wang, Y., Hu, J., Sun, Y., et al. (2021). Effect of resveratrol on the biofilm formation and physiological properties of avian pathogenic *Escherichia coli*. *J Proteom.* 249:104357. doi: 10.1016/j.jprot.2021.104357

Sahal, G., Woerdenbag, H. J., Hinrichs, W. L. J., Visser, A., Tepper, P. G., Quax, W. J., et al. (2020). Antifungal and biofilm inhibitory effect of Cymbopogon citratus (lemongrass) essential oil on biofilm forming by Candida tropicalis isolates; an in vitro study. *J. Ethnopharmacol.* 246:112188. doi: 10.1016/j.jep.2019.112188

Salman, A., Shufan, E., Sharaha, U., Lapidot, I., Mordechai, S., and Huleihel, M. (2019). Distinction between mixed genus bacteria using infrared spectroscopy and multivariate analysis. *Vib. Spectros.* 100, 6–13. doi: 10.1016/j.vibspec.2018.10.009

Semeniuc, C. A., Pop, C. R., and Rotar, A. M. (2017). Antibacterial activity and interactions of plant essential oil combinations against Gram-positive and Gram-negative bacteria. *J. Food Drug Anal.* 25, 403–408. doi: 10.1016/j.jfda.2016.06.002

Serra, E., Saubade, F., Ligorio, C., Whitehead, K., Sloan, A., Williams, D. W., et al. (2020). Methylcellulose Hydrogel with Melissa officinalis Essential Oil as a Potential Treatment for Oral Candidiasis. *Microorganisms* 8:215. doi: 10.3390/microorganisms8020215

Silva, T. C., Bertolucci, S. K. V., Carvalho, A. A., Tostes, W. N., Alvarenga, I. C. A., Pacheco, F. V., et al. (2021). Macroelement omission in hydroponic systems changes plant growth and chemical composition of Melissa officinalis L. essential oil. *J. Appl. Res. Med. Arom. Plants* 24:100297. doi: 10.1016/j.jarmap.2021.100297

Spadaccino, G., Frabboni, L., Petruzzi, F., Disciglio, G., Mentana, A., Nardiello, D., et al. (2021). Essential oil characterization of Prunus spinosa L., Salvia officinalis L., Eucalyptus globulus L., Melissa officinalis L. and Mentha x piperita L. by a volatolomic approach. *J. Pharm. Biomed. Anal.* 202:114167. doi: 10.1016/j.jpba.2021.114167

Stewart, B. J., and McCarter, L. L. (2003). Lateral flagellar gene system of Vibrio parahaemolyticus. *J. Bacteriol.* 185, 4508–4518. doi: 10.1128/j.jb.2003.185.15.4508-4518

Stoodley, P., Sauer, K., Davies, D. G., and Costerton, J. W. (2002). BIOFILMS AS COMPLEX DIFFERENTIATED COMMUNITIES. *Ann. Rev. Microbiol.* 56, 187–209. doi: 10.1146/annurev.micro.56.012302.160705

Tan, Z., Bo, T., Guo, F., Cui, J., and Jia, S. (2018). Effects of ε-Poly-l-lysine on the cell wall of Saccharomyces cerevisiae and its involved antimicrobial mechanism. *Int. J. Biol. Macromol.* 118, 2230–2236. doi: 10.1016/j.ijbiomac.2018.07.094

Toshio, K., Hirotaka, H., Kazuyoshi, G., Yukihiro, A., Shigeaki, M., Kwon-Sam, P., et al. (2008). Identification of two translocon proteins of Vibrio parahaemolyticus type III secretion system 2. *Infect. Immun.* 76, 4282–4289. doi: 10.1128/j.IAI.2008.01738-07

Wang, L., Zhang, K., Zhang, K., Zhang, J., Fu, J., Li, J., et al. (2020). Antibacterial Activity of Cinnamomum camphora Essential Oil on *Escherichia coli* During Planktonic Growth and Biofilm Formation. *Front. Microbiol.* 11:561002. doi: 10.3389/fmicb.2020.561002

Wang, N., Liu, X., Li, J., Zhang, Q., Li, X., An, Q., et al. (2020). Antibacterial mechanism of the synergistic combination between streptomycin and alcohol extracts from the Chimonanthus salicifolius S. *Y. Hu. leaves*. *J. Ethnopharmacol.* 250:112467. doi: 10.1016/j.jep.2019.112467

Xiaohui, Z., Konkel, M. E., and Call, D. R. (2010). Vp1659 is a Vibrio parahaemolyticus type III secretion system 1 protein that contributes to translocation of effector proteins needed to induce cytolysis, autophagy, and disruption of actin structure in HeLa cells. *J. Bacteriol.* 192, 3491–3502. doi: 10.1128/j.jb.01493-09

Xu, D., Sun, L., Li, C., Wang, Y., and Ye, R. (2018). Inhibitory effect of glucose oxidase from Bacillus sp. *LWT Food Sci. Technol.* 92, 339–346. doi: 10.1016/j.lwt.2018.02.025

Yi, S.-M., Zhu, J.-L., Fu, L.-L., and Li, J.-R. (2010). Tea polyphenols inhibit *Pseudomonas aeruginosa* through damage to the cell membrane. *Int. J. Food Microbiol.* 144, 111–117. doi: 10.1016/j.ijfoodmicro.2010.09.005

Yiquan, Z., Lingfei, H., George, O. A., Ying, Z., Wenhui, Y., Zhe, Y., et al. (2018). Autoregulation of ToxR and Its Regulatory Actions on Major Virulence Gene Loci in Vibrio parahaemolyticus. *Front. Cell. Infect. Microbiol.* 8:291. doi: 10.3389/j.fcimb.2018.00291

Zhang, N., Lan, W., Wang, Q., Sun, X., and Xie, J. (2018). Antibacterial mechanism of Ginkgo biloba leaf extract when applied to Shewanella putrefaciens and Saprophytic staphylococcus. *Aquacul. Fish.* 3, 163–169. doi: 10.1016/j.aaf.2018.05.005

Zhang, Y., Wang, Y., Zhu, X., Cao, P., Wei, S., and Lu, Y. (2017a). Antibacterial and antibiofilm activities of eugenol from essential oil of Syzygium aromaticum (L.) Merr. & L. M. Perry (clove) leaf against periodontal pathogen Porphyromonas gingivalis. *Microbial. Pathogenesis* 113, 396–402. doi: 10.1016/j.micpath.2017.10.054

Zhang, Y., Wu, Y.-T., Zheng, W., Han, X.-X., Jiang, Y.-H., Hu, P.-L., et al. (2017b). The antibacterial activity and antibacterial mechanism of a polysaccharide from Cordyceps cicadae. *J. Fun. Foods* 38, 273–279. doi: 10.1016/j.jff.2017.09.047

Zhong, X., Lu, R., Liu, F., Ye, J., Zhao, J., Wang, F., et al. (2021). Identification of LuxR Family Regulators That Integrate Into Quorum Sensing Circuit in Vibrio parahaemolyticus. *Front. Microbiol.* 12:691842. doi: 10.3389/j.fmicb.2021.691842

Zhou, C., Li, C., Siva, S., Cui, H., and Lin, L. (2021). Chemical composition, antibacterial activity and study of the interaction mechanisms of the main compounds present in the Alpinia galanga rhizomes essential oil. *Ind. Crops Products* 165:113441. doi: 10.1016/j.indcrop.2021.113441

Zhu, W., Gao, J., Liu, H., Liu, J., Jin, T., Qin, N., et al. (2022). Antibiofilm effect of sodium butyrate against Vibrio parahaemolyticus. *Food Control* 131:108422. doi: 10.1016/j.foodcont.2021.108422

**Conflict of Interest:** The authors declare that the research was conducted in the absence of any commercial or financial relationships that could be construed as a potential conflict of interest.

**Publisher's Note:** All claims expressed in this article are solely those of the authors and do not necessarily represent those of their affiliated organizations, or those of the publisher, the editors and the reviewers. Any product that may be evaluated in this article, or claim that may be made by its manufacturer, is not guaranteed or endorsed by the publisher.

frontiers in Microbiology

ORIGINAL RESEARCH
published: 16 March 2022
doi: 10.3389/fmicb.2022.814448

# A Standardized Extract of *Lentinula edodes* Cultured Mycelium Inhibits *Pseudomonas aeruginosa* Infectivity Mechanisms

*Mireia Tena-Garitaonaindia[1†], Diego Ceacero-Heras[1†], María Del Mar Maldonado Montoro[2,3], Fermín Sánchez de Medina[4,5], Olga Martínez-Augustin[1,3,5,6*] and Abdelali Daddaoua[1,3,6]*

[1] Department of Biochemistry and Molecular Biology II, Pharmacy School, University of Granada, Granada, Spain, [2] Clinical Analysis Service, Hospital Campus de la Salud, Granada, Spain, [3] Instituto de Investigación Biosanitaria (IBS), Granada, Spain, [4] Department of Pharmacology, School of Pharmacy, University of Granada, Granada, Spain, [5] Department of Pharmacology, Pharmacy School, University of Granada, Granada, Spain, [6] Institute of Nutrition and Food Technology "José Mataix," Center of Biomedical Research, University of Granada, Granada, Spain

OPEN ACCESS

**Edited by:**
Giuseppantonio Maisetta, University of Pisa, Italy

**Reviewed by:**
Piyush Baindara, University of Missouri, United States
Sunil D. Saroj, Symbiosis International University, India

***Correspondence:**
Olga Martínez-Augustin
omartine@ugr.es

[†] These authors have contributed equally to this work

**Specialty section:**
This article was submitted to Antimicrobials, Resistance and Chemotherapy, a section of the journal Frontiers in Microbiology

**Received:** 13 November 2021
**Accepted:** 14 February 2022
**Published:** 16 March 2022

**Citation:**
Tena-Garitaonaindia M, Ceacero-Heras D, Montoro MDMM, de Medina FS, Martínez-Augustin O and Daddaoua A (2022) A Standardized Extract of Lentinula edodes Cultured Mycelium Inhibits Pseudomonas aeruginosa Infectivity Mechanisms. Front. Microbiol. 13:814448. doi: 10.3389/fmicb.2022.814448

The priority pathogen list of the World Health Organization classified *Pseudomonas aeruginosa* as the second top critical pathogen. Hence, the development of novel antibacterial strategies to tackle this bacterium is highly necessary. Herein we explore the potential antibacterial effect of a standardized extract of cultured mycelium of *Lentinula edodes* (AHCC®) on *P. aeruginosa*. AHCC® was found to inhibit the growth rate and biofilm formation of strain PAO1. No change in swarming was observed, but AHCC® hampered swimming and twitching motility. In accordance, a decreased expression of metabolism, growth, and biofilm formation genes was shown. AHCC® also diminished the levels of exotoxin A and bacteria inside IEC18 cells and the secretion of IL-6, IL-10 and TNF by infected macrophages. This effect was related to a reduced phosphorylation of MAPKs and to bacteria internalization. Taken together, our data suggest that AHCC® has a potential role to prevent *P. aeruginosa* infections and may lead to the development of new therapies.

**Keywords: prebiotic, AHCC®, *Pseudomonas aeruginosa*, motility and biofilm, secretion system and adhesion, immune response, PCR real time (qPCR), internalization**

## INTRODUCTION

The gram-negative *Pseudomonas aeruginosa* is a versatile and opportunistic nosocomial pathogen able to infect different animals and plants, and ubiquitously present due to its phenomenal capacity to adapt to different environments (Goldberg, 2010). *P. aeruginosa* is one of the major pathogens causing hospital-acquired infections, including ventilator associated pneumonia (Chastre and Fagon, 2002), catheter infections in immuno-compromised patients and respiratory infections in cystic fibrosis patients (CF) (Hassett et al., 2010) and severely burned people (Montie et al., 1982a,b). Furthermore, conditions like prolonged antibiotic treatment, metabolic syndrome and intestinal inflammatory diseases, that compromise the intestinal barrier function and cause dysbiosis, facilitate the establishment of *P. aeruginosa* in the intestinal ecosystem

(Von Klitzing et al., 2017). This pathogen possesses a high level of intrinsic resistance to most antibiotics and, consequently, *P. aeruginosa* infections have become a worldwide health concern (Tacconelli and Magrini, 2017), the development of novel antibacterial strategies to tackle this pathogen being of critical importance. In fact, *P. aeruginosa* ranks second in the World Health Organization (WHO) priority pathogen list; a list of 12 species of bacteria highly resistant to antibiotics, elaborated to help prioritizing the research and development of new and effective antibiotic treatments.

*Pseudomonas aeruginosa* has developed a series of mechanisms to resist the effect of antibiotics and enhance virulence, including the synthesis of exotoxin A, a virulent factor (Iglewski and Kabat, 1975; Ortiz-Castro et al., 2014) that induces eukaryotic cell death (Hamood et al., 2004) and the formation of biofilms (Mah et al., 2003; Zhang and Mah, 2008; Taylor et al., 2014). Other virulence factors allow this pathogen to interact with epithelial cell monolayers and cross them. In this sense, its single polar flagellum facilitates near-surface swimming and attachment, and retractile type 4 pili power adhesion to and movement across biotic surfaces. Different secretion systems are then used to inject virulence factors into the cytoplasm of eukaryotic cells, allowing bacterial replication within macrophages or intestinal cells and the subsequent evasion from the immune system. In this context, six different classes of secretion systems [type I (TS1SS) to VI (TIVSS)] have been described so far (Durand et al., 2009; Bleves et al., 2010).

The different types differ in their molecular mechanisms and operate on different substrates. The type III secretion system (T3SS) of many bacterial pathogens injects a subset of bacterial "effector" proteins into host cells and in turn triggers a complete cytoskeletal reorganization, thereby preventing further uptake of bacteria. Further, ExsA, a member of the AraC/XylS family of transcriptional regulators (Hauser, 2009; Parsot, 2009), controls the transcription of T3SS genes.

In addition, another secretion system, termed type VI (T6SS) (Llosa et al., 2009), which shows similarities with the type III system (Cossart and Sansonetti, 2004; Merrell and Falkow, 2004), induces the expression of genes that encode the haemolysin-coregulated protein (Hcp) and the valine glycine repeat G (VgrG) family of proteins VgrG1, VgrG2 and VgrG3, that form part of the T6SS gene cluster (Suarez et al., 2008, 2010).

Different strategies are being developed to identify new drugs with direct and effective antibacterial activity that could be used as agents against *P. aeruginosa* (Siles et al., 2013; Rangel-Vega et al., 2015; Wilkinson and Pritchard, 2015; Torres et al., 2016), or as combinatorial drugs increasing the effectiveness of conventional antibacterials (Delattin et al., 2014; Van den Driessche et al., 2017). A significant number of natural compounds have been found to inhibit bacterial growth, although their mechanisms of action, in many cases, remain unclear (Johansson et al., 2008; Amer et al., 2010; Ortega-González et al., 2014; Rubio-Gómez et al., 2020). Among proposed foods or food components, prebiotics have been shown to perform an antagonistic role against gastrointestinal pathogenic bacteria (Oelschlaeger, 2010). Indirect mechanisms exerted by prebiotic on non-pathogenic bacteria or eukaryotic cells to inhibit bacterial growth have been described. These include the modulation of the host immunity or the induction of beneficial bacteria that compete for nutrients, produce antimicrobial peptides, or block the adhesion of pathogens to intestinal epithelial cells (Collado et al., 2007). Direct effects on specific pathogenic bacteria have been also studied. In this sense, we have described that inulin derived oligosaccharides modulates *P. aeruginosa* gene expression regulating biofilm formation and motility interfering with different signaling pathways (Ortega-González et al., 2014; Rubio-Gómez et al., 2020).

The standardized extract of cultured mycelium of *Lentinula edodes* (AHCC®) is a fermented extract that is available as a dietary supplement. AHCC® contains a mixture of oligosaccharides (∼74% of dry weight, ∼20% being of the α-1,4-glucan type), amino acids, lipids, and minerals (Kidd, 2005). The acetylated forms of α-1,4-glucans are resistant to digestion, have low molecular masses (∼5 kDa) and are believed to constitute its main active ingredient (Matsui et al., 2002). In addition, AHCC also contains β-(1, 3)-glucans with β-(1, 6) branches, also resistant to digestion. In fact, we have previously shown that AHCC® has intestinal anti-inflammatory and prebiotic effects in animal models of colitis, inhibiting the growth of pathogenic bacteria (Daddaoua et al., 2006, 2007). AHCC® is well tolerated both as a human nutritional supplement and as a therapeutic agent (Ghoneum et al., 1995; Kidd, 2005). As such, it is used to reduce adverse effects observed in advanced cancer patients during chemotherapy and growing evidence indicates multiple roles of AHCC® in cancer [including breast (Ito et *al.*, 2014), ovary (Choi et al., 2018) and pancreas (Yanagimoto et al., 2016)], host protection during viral (Roman et al., 2013) or bacterial infections (Aviles et al., 2008), chronic diseases, diabetes (Ye et al., 2003) and cardiovascular pathologies (Corradetti et al., 2019).

Our research group has described that AHCC® directly regulates the immune system acting on macrophage and intestinal epithelial cells (IEC18), an effect that involves toll like receptors and the adaptor molecule MyD88 and signaling pathways that include NF-κB/MAPK activation (Daddaoua et al., 2013). Based on these observations, and its prebiotic effects, here we have tested the hypothesis that AHCC® could be useful in the regulation of the growth and virulence of *P. aeruginosa.* With this aim, we have characterized its direct effect on *P. aeruginosa* growth, mobility, biofilm formation, and gene expression of virulence factors. Moreover, intestinal epithelial cells (IEC18) cultures have also been used to assess the effect of AHCC® on the capacity of *P. aeruginosa* to infect innate immune cells and produce an inflammatory response.

# MATERIALS AND METHODS

## Materials

AHCC® (Amino Up Co., Ltd., Sapporo, Japan) is a standardized extract of cultured *Lentinula edodes* mycelia. The solutions were made at 50 g/L in modified LB medium and, in the case of the eukaryotic cells, in Dulbecco's Modified Eagle's Medium (DMEM Sigma®) containing fetal bovine serum (FBS, 10%),

2 mM L-glutamine, and 2.5 mg/mL amphotericin B. Solutions were filtered using 0.22 μm cut-off filters.

## Bacterial Strains Used in This Study

*Pseudomonas aeruginosa* PAO1 was grown in LB, modified M9 minimal medium (Abril et al., 1989) or complete Brain Heart Infusion (BHI) medium. When required, antibiotics were added to the culture medium to reach a final concentration of 50 μg/mL ampicillin.

## Cell Lines

To isolate macrophages, female Wistar rats were sacrificed and the spleen was extracted aseptically. Cell suspensions were obtained by disrupting the spleen between dissecting forceps in physiological in medium. After centrifugation (1,000 × *g*/5 min), cells were cleared of erythrocytes by resuspension in hypotonic lysis buffer (15 mM NH4Cl, 10 mM KHCO3, 0.1 mM Na2EDTA, pH 7.3) for 30 min on ice. Mononuclear cells were washed and resuspended in MACs buffer (PBS containing 0.5% (w/v) BSA, 2 mM and EDTA, pH 7.2). To obtain a monocellular suspension, cells were passed through 70 μm nylon mesh prior to magnetic labeling and subsequently isolated by negative selection. To remove lymphocytes, CD161.1-biotin (1:200), CD45RA-PE (1:200) and CD3 (1:150) (Biosciences), were added and incubated at 4°C for 30 min. Cells were washed and sedimented by centrifugation at 1,000 × *g* for 5 min. After resuspension in MACs buffer, 25 μL of each Microbeads and anti-PE-microbeads (Miltenyi Biotec), were added and the resulting suspension incubated at 4°C during 30 min. Cells were washed, centrifuged and dissolved in DMEM medium (Dulbecco's Modified Eagle Medium). CD161.1 + , CD45RA + and CD3 + cells were discarded using an LD column (Miltenyi Biotec). Macrophages in the flow-through were centrifuged at 1,000 × *g* for 5 min and resuspended in Dulbecco's Modified Eagle Medium (DMEM) supplemented with 10% FBS (Sigma), 2.5 mg/L amphotericin B and 2 mM L-glutamine.

Intestinal epithelial IEC18 cells (passages 20–32) were obtained from the Cell Culture Service of the University of Granada and cultured in DMEM containing 10% FBS, 2 mM l-glutamine, 100 mg/L streptomycin, 100,000 U/L penicillin and 2.5 mg/L amphotericin B, in standard conditions.

## Effects of AHCC® on *P. aeruginosa* Growth

Individual colonies of *P. aeruginosa* PAO1 were picked from the surface of freshly grown LB plates and grown overnight in M9 minimum medium supplemented with 5 mM of citrate or in complete Brain Heart Infusion (BHI) medium at 37°C. The overnight culture was diluted to an $OD_{660nm}$ of 0.05 or 0.6 with M9 minimum medium and of 0.05 with BHI medium. Ninety-six well flat-bottomed polystyrene microtiter plates were filled with 180 μL of bacterial suspensions. AHCC® was added to bacteria grown in M9 from OD = 0.05 and BHI media, to reach final concentrations of 5, 15 and 30 mg/mL, while 5 mg/mL of AHCC was added to bacteria grown in M9 medium at OD = 0.6. Plates were incubated at 37°C under continuous agitation in a Bioscreen C MBR analyser type system FP-1100-C (OY Growth Curves Ab Ltd., Raisio, Finland). The turbidity was measured at 580 nm, using a wideband filter at 420–660 nm every 60 min, over a 24 h period for M9 medium starting at OD = 0.05. A 660 nm filter and a follow up period of 8 h was used when bacteria were cultured in BHI or M9 medium starting at OD = 0.6. Both procedures are equivalent for measuring bacterial growth in suspension and one or the other were used for purely practical reasons.

## Semiquantitative Determination of Biofilm Formation

The inhibitory effect of AHCC® on *P. aeruginosa* biofilm formation was measured as described (Christensen et al., 1985). The growth was initiated by inoculating 500 μL of M9 medium with 5 μL of suspended bacteria from an overnight culture, to reach a $DO_{660nm}$ of 0.05. Bacteria were cultured in individual wells of a 24-well microtiter plate at 37°C for different times in the absence and in the presence of different concentrations (up to 20 mg/mL) of AHCC®.

Biofilm formation was quantified using the crystal violet (CV) method (Fredheim et al., 2009). The structure of biofilm was observed under contrast-phase microscopy using a Zeiss Axioscope fluorescence microscope coupled to a Nikon DSS-Mc CCD camera and a 100-fold magnifier. Data reported are means from two independent experiments each conducted in quadruplet repeats.

## Motility Assays

Assays were carried out to determine the effect of AHCC® (5, 15 and 30 mg/mL) on swimming, twitching and swarming motility. In all assays these compounds were added at identical concentrations to the plates containing AHCC. For swimming assays bacteria were placed with the help of a sterile tooth-pick at the center of plates containing a 5 mm layer of LB medium with 0.3% (w/v) Bacto agar, 0.2% casamino acids (w/v) and 30 mM glucose. Plates were incubated at 37°C for 24 h and the radial diffusion of bacteria, due to swimming, was inspected. To monitor twitching motility bacteria were placed with a toothpick into a 2 mm thick layer containing 1.5% (w/v) Bacto agar, 0.2% (w/v) casamino acids and 30 mM glucose. After incubation for 24 h at 37°C, the expansion of bacteria on the plate was observed. For swarming assays 5 μL of an overnight culture of bacteria in minimum medium M9 were diluted to OD 0.6 and placed into the center of swarm plates (composed of 0.5% (w/v) Bacto agar supplement with 0.2% (w/v) casamino acids and 30 mM glucose). Plates were incubated at 37°C for 24 h, followed by an inspection of the surface movement of the bacteria. All the motility assays were performed in triplicates.

## Measurement of AHCC®-Induced Lactate Dehydrogenase Release in Macrophages and IEC18 Epithelial Cells

Cellular toxicity was quantified by the measurement of lactate dehydrogenase (LDH) release using non-radioactive Pierce LDH Cytotoxicity Assay Kit (Thermo Scientific), following the manufacturer's instructions. IEC18 cells and rat macrophage

suspensions ($10^6$–$10^8$ of cells/mL DMEM medium) were incubated with different concentrations of AHCC® at 37°C for 8 h and 24 h, respectively. LDH release was measured in the culture supernatant by colorimetric detection at 490 and 680 nm.

## Measurement of the Effect of AHCC® on Cytokine Secretion From Macrophage and IEC18 Cells Following Infection by *P. aeruginosa* PAO1

For the determination of cytokines macrophage suspensions ($10^6$–$10^8$ of cells/mL DMEM medium) and IEC18 cells were cultured with *P. aeruginosa* and incubated with non-toxic concentrations at 2 and 5 mg/mL of AHCC® for 8 h. Following centrifugation of macrophage suspensions at 4°C and 10,000 × *g* for 5 min, the resulting supernatants were frozen at −80°C. Supernatants from IEC18 cells were also collected, centrifuged and frozen. Aliquots were thawed and cytokine levels determined using ELISA-based kits (BD Biosciences, Erembodegem, Belgium) following the protocol provided by the manufacturer. In addition, macrophage cells were used for the quantification of IkB and MAP kinase by western blot as described below.

## Western Blot Assays

For the detection of p-ERK (the phosphorylated form of Extracellular Regulated Kinase), p-P38 (phosphorylated form of P38 mitogen-activated protein kinases), p-JNK (phosphorylated Jun N-terminal kinase), p-IkB (phosphorylaated form of IkappaB kinase) cells were homogenized in lysis buffer (PBS containing 0.1% (w/v) SDS, 0.1% (w/v) sodium deoxycholate, 1% (v/v) Triton X-100) with protease inhibitor cocktail (Sigma) 1:100 (v/v). Subsequently, homogenates were sonicated and centrifuged 7,000 × *g* for 5 min at 4°C. Protein concentrations were determined using the bicinchoninic acid assay (Ortega-González et al., 2014). Samples were boiled in 5 × LaemmLi buffer (220 mM Tris, 312 μM SDS, 50% (v/v) glycerol, 1% (v/v) 2-mercaptoethanol, 22.5 mM EDTA, pH 6.8, containing traces of bromophenol blue) for 5 min, separated by SDS-PAGE, electroblotted to PVDF membranes (Millipore, Madrid, Spain), and exposed to the primary antibodies against ERK, p-ERK (both from Sigma), p-P38, p-JNK and phosphorylated p-IkB, respectively (all from Cell signaling, Danvers, MA, United States). Prior to exposure to the secondary IgG Peroxidase antibody (provided by Sigma, mouse for ERK and p-ERK, rabbit in the others) the bands were visualized by enhanced chemiluminescence (PerkinElmer, United States) and quantified with the NIH software (Scion Image).

## Determination of Exotoxin A Concentration in IEC18 Cells

The cells were cultured in 6 well-plates. At confluence, cells were infected with *P. aeruginosa* at a ratio of 5 bacterial cells per eukaryotic cell in the absence and in the presence of non-toxic concentrations (2 and 5 mg/mL) of AHCC®. Plates containing cells were washed 3 times with PBS and incubated with a gentamicin solution (100 mg/mL) for 1 h to eliminate bacteria. Subsequently, plates were washed 3 times with PBS prior to cell collection using RIPA buffer containing a protease and phosphatase inhibitor cocktail (Sigma). Proteins were extracted and Western blots were carried out as outlined above using the Exotoxin A antibody (Sigma) at a 1:2,000 dilution. Following overnight incubation and washing with the primary antibody the membrane was incubated with the secondary IgG Peroxidase anti-rabbit antibody (Sigma) at a 1:10.000 dilution for 2 h. The bands were detected by enhanced chemiluminescence (PerkinElmer, Waltham, MA, United States) and quantified with NIH software (Scion Image).

## Analysis of Gene Expression by Quantitative Real Time PCR

The expression of the genes was studied using quantitative real time PCR. Total RNA of *P. aeruginosa* culture, in the presence and in the absence of 2–5 mg/mL of AHCC® for 8 h, was obtained by the TRI reagent®/BCP method (Invitrogen). AHCC® was added to *P. aeruginosa* grown to OD = 0.6. 1 μg of RNA was retrotranscribed following the protocol recommended by the manufacturer (iScript, BioRad, Alcobendas, Spain) and specific RNA sequences were amplified with MX3005P real time PCR device (Stratagene) using the set of primers pairs indicated in **Supplementary Table 1**. The genes of interest were amplified by PCR (61°C as annealing temperature, 40 cycles), through Go Taq®qPCR Master Mix (PromegaMadison, United States), using 2 ml cDNA as template. The cycle threshold values were normalized to that of the reference transcript, 16S RNA, and a fold change compared to the control group was calculated.

## Bacterial Internalization by Cultured IEC18 Cells

The internalization of viable bacteria in IEC18 cells was tested using an overnight culture of *P. aeruginosa* PAO1 strain. Subsequently, the bacteria were washed twice and diluted in the DMEM medium. For infection, a ratio of $10^6$–$10^8$ (Bacteria/IEC18 cells) was maintained. Previously, IEC18 cells were treated with cytochalasin D (CytoD) at a non-toxic concentration of 2 μM and were synchronously infected with bacteria/cell for 2 h in the presence and in the absence of AHCC® at 2 and 5 mg/mL of final non-toxic concentration. To remove the non-phagocytosed bacteria the eukaryotic cells were washed three times in ice-cold PBS and further harvested and lysed in a lysis buffer [PBS containing 0.1% (w/v) SDS, 0.1% (w/v) sodium deoxycholate, 1% (v/v) Triton X-100] with protease inhibitor cocktail (Sigma) 1:100 (v/v). The internalization of *P. aeruginosa* was analyzed by plating a series of dilutions $10^{-5}$ and $10^{-10}$ on LB agar and incubating at 37°C overnight. The number of bacteria phagocytosed into IEC18 epithelial cells was determined by counting the growth colony forming units (CFU).

## Statistical Analysis

All results are expressed as means with the corresponding standard deviations. Differences among means were analyzed for statistical significance by a one-way ANOVA analysis and *a posteriori* least significance test. All analyses were carried out

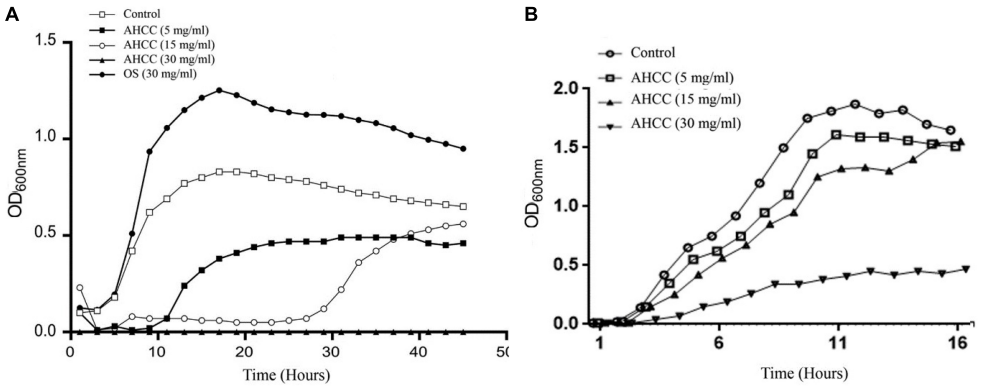


**FIGURE 1 |** Effect of AHCC® on the growth of *P. aeruginosa*. The growth curves in minimal medium M9 **(A)** and complete medium BHI **(B)** in the absence and presence of AHCC® at 5, 15 and 30 mg/mL are shown. As a control for the use of oligosaccharides as a carbon source when bacteria were grown in minimal medium M9 20 mg/mL of goat milk oligosaccharides (OS) was used. Growth curves were recorded at 37°C for 24 h. Representative data from one of three independent experiments with similar results are shown.

with the GraphPad Prism 7.0 program (Jandel Corporation, San Rafael, CA, United States). Concentration-response curves were fitted to a logarithmic curve when possible with Origin 7.0 (OriginLab Corporation, Northampton, MA, United States). Differences were considered significant at $P < 0.05$.

## RESULTS

### Effect of AHCC® on the Growth of *P. aeruginosa* PAO1

AHCC® is a standardized extract of cultured *Lentinula edodes* mycelia which contains a mixture of oligosaccharides, including digestion resistant glucans. To explore the effect of AHCC® on *P. aeruginosa*, growth curves were obtained in M9 medium (**Figure 1A**) and in BHI medium (**Figure 1B**). Two different strategies were followed using M9 medium: inoculating bacteria to the medium and following the growth for 24 h in the presence of AHCC® or growing the bacteria to exponential phase (OD = 0.6) before adding AHCC®. When bacteria were added to M9 medium (OD = 0.05) in the presence of 5 and 15 mg/mL of AHCC® a pronounced reduction in bacterial growth rate and yield was noted, suggesting antibacterial activity. However, in the presence of 30 mg/mL of AHCC® a complete growth inhibition was observed, probably due to the toxic effect of AHCC® at this high concentration (**Figure 1A**). Additionally, a growth curve was generated in the presence of 30 mg/mL of control oligosaccharides (OS) as a carbon and energy source, which showed that OS promoted bacterial growth (**Figure 1A**). The experiments carried out with BHI medium, in which AHCC® was added at OD = 0.05, indicate that the lower concentration of AHCC® (5 mg/mL) had no substantial effect on P. *aeruginosa*, and only when the bacteria were cultured with AHCC® 30 mg/mL a significant growth inhibition was observed (**Figure 1B**). Finally, when AHCC® was added to bacteria grown to OD = 0.6 no substantial effect was observed (**Figure 1B**). Therefore, our results indicate that AHCC® could be toxic at high concentrations. In addition, in a minimum medium (M9) a low concentration of AHCC® (5 mg/mL) may inhibit growth when bacteria are diluted, but this effect was essentially

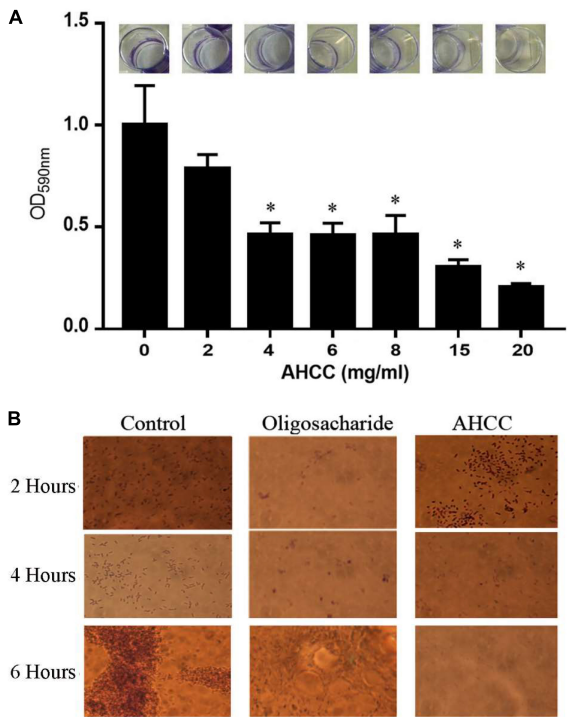


**FIGURE 2 |** Formation of *P. aeruginosa* biofilm. **(A)** Biofilm formation in the absence and in the presence of different concentrations of AHCC® in 24-well plates. Biofilm formation was monitored in M9 minimal medium supplemented with 0.2% (w/v) glucose and casamino acids and quantified after 6 h. Then, the relative amount of biofilm formation in the experiments was represented against AHCC® concentration. Data are the average of three independent assays. **(B)** Microscopic inspection of biofilm formation in the absence and in the presence of 10 mg/mL of AHCC® at 2, 4 and 6 h.

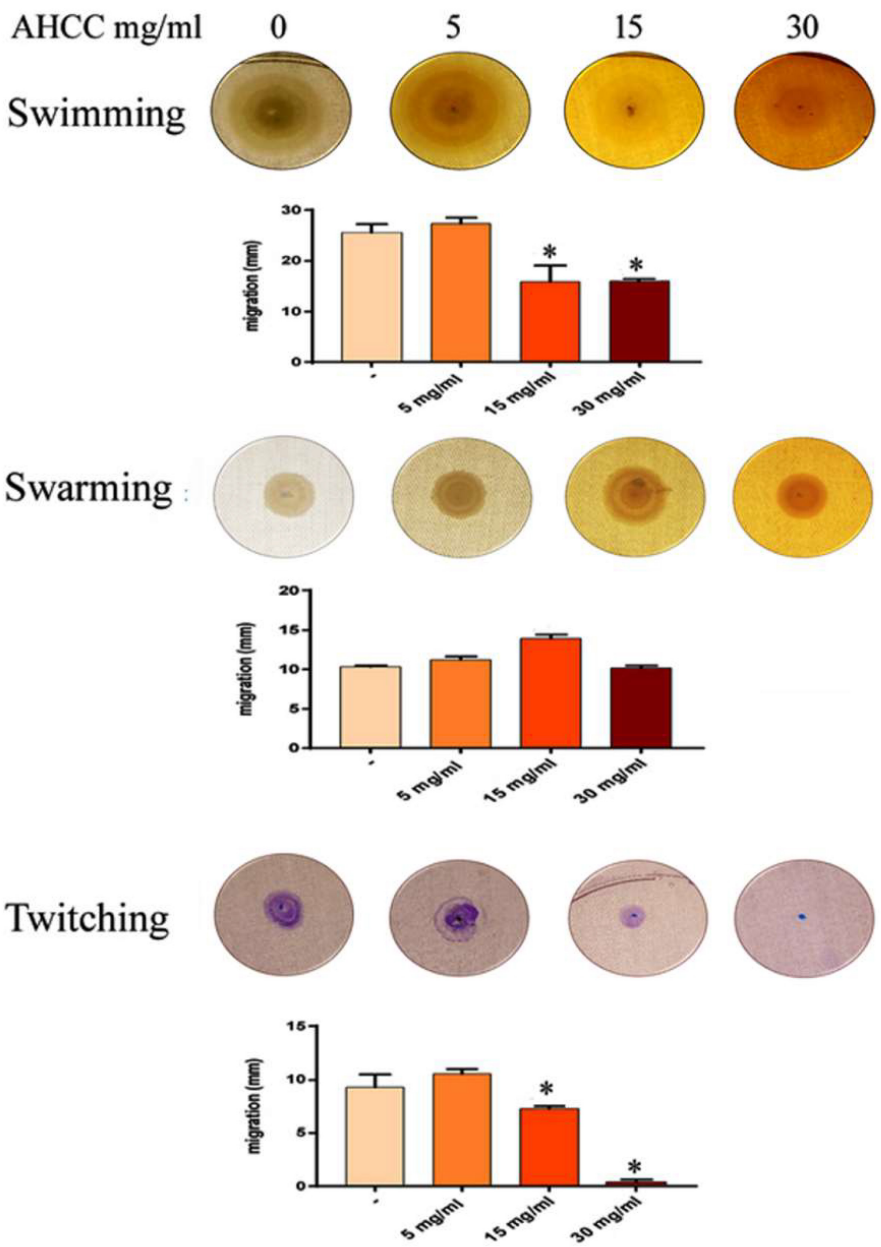


**FIGURE 3 |** Effects of AHCC® on the motility of *P. aeruginosa.* Motility assays were carried out as described in Materials and Methods. AHCC® at 5, 15 and 30 mg/mL was present in the agar plates and in the bacterial suspension. *$p < 0.05$ vs. control (ANOVA followed by least significance tests).

absent in a complete medium or with concentrated bacteria (OD = 0.6) in minimal medium, indicating that AHCC at the concentrations used in other experiments in this study is not toxic to *P. aeruginosa*.

## Biofilm Formation and Quantification in the Presence of AHCC®

Biofilm formation is a mechanism used by *P. aeruginosa* for surface colonization that leads to a significant resistance against antibiotics. To explore the inhibitory effects of AHCC® on *P. aeruginosa* biofilm formation, the growth was initiated by inoculating 500 μL of LB medium with 5 μL of suspended bacteria, from an overnight culture to reach $DO_{660nm}$ of 0.05, in individual wells of a 24-well microtiter plate and then incubated at 37°C for different times (**Figure 2** and **Supplementary Figure 1**). The biofilm formation was quantified after 4–8 h using the crystal violet (CV) method as described in material and methods (**Figure 2** and **Supplementary Figure 1**). The **Figure 2A** shows that biofilm formation was clearly inhibited (50–70 fold) in a concentration-dependent manner by AHCC® (2–20 mg/mL) for 4 h. Subsequently, this inhibitory effect was

confirmed by the inspection of biofilm formation under the microscope (**Figure 2B**). These results suggest that AHCC® is potentially useful in preventing biofilm formation either directly or indirectly by inhibiting growth.

## AHCC® Effect on Bacterial Motility

*Pseudomonas aeruginosa* exhibits three different types of motility, namely swimming, swarming and twitching, which play a key role in the colonization of surfaces by bacteria and the subsequent formation of biofilms (Mattick, 2002; Klausen et al., 2003). Initial experiments investigated the effects that AHCC® extract (5, 15 and 30 mg/mL) had on the levels of *P. aeruginosa* strain PAO1 swimming motility, surface-associated swarming and twitching motilities. Under control conditions (AHCC® free), this bacterium was able to undertake all three types of motility (**Figure 3**). Nevertheless, while AHCC® caused no change in swarming motility, it was found that it significantly inhibited (at least 50% of controls) the swimming and twitching motility at 15 and 30 mg/mL ($p < 0.05$). Interestingly, AHCC® completely blocked twitching motility when plates were incubated in the presence of 30 mg/mL of AHCC® concentration at 24 h time point (**Figure 3**). The effect on swimming and twitching motility may be due to direct modulation by AHCC®, to a growth inhibitory effect, or to a combination of both.

## AHCC® Reduces Transcript Levels for Genes That Are Related to Bacterial Pathogenicity

Quantitative real time PCR (RT-qPCR) data analysis shows that AHCC® reduces the transcript levels for PA0807 (*ampD*) and PA0908 (*alpB*), encoding proteins involved in responses to antibiotics, suggesting that AHCC® modulates the sensitivity to antibiotics (Amber and Nancy, 2008; Shah and Swiatlo, 2008; Alvarez-Ortega et al., 2010). Moreover, the results shown in **Table 1** evidence reduced transcript levels of the *dctA* gene (PA1183), associated with the normal growth of *P. aeruginosa* (Valentini et al., 2011), and of the *icmP* gene (PA4370), encoding a metalloproteinase outer membrane protein which has been shown to degrade plasminogen activator (Christian et al., 2015) and to play a key role in *P. aeruginosa* pathogenicity. However, the reduced transcript level of the gene (PA3866) encoding the pyocin S4 suggests that AHCC® acts as a signal molecule that modulates bacterial virulence through distinct signaling pathways, including partial growth inhibition.

## AHCC® Is Not Toxic to IEC18 Cells or Rat Macrophages

To assess the possible toxic effect of AHCC® in IEC18 cells and macrophages, we quantified the level of lactate dehydrogenase (LDH) activity in the culture medium, a marker of cytotoxicity. As described by Ortega-González et al. (2014), **Figure 4A** shows that AHCC® does not affect cell viability as demonstrated by the low lactate dehydrogenase activity in the medium compared to the LDH released in the presence of the positive control (**Figure 4A**). In parallel, AHCC was shown not to alter LDH activity in the medium of rat macrophages cultured for up to 24 h after exposure (**Supplementary Figure 2**). Therefore, the 5 mg/mL concentration was selected for further experiments.

**TABLE 1 |** Quantitative real time PCR experiments to quantify the effect of AHCC§on the transcript levels of genes which are related to bacterial pathogenicity in *P. aeruginosa* infected IEC18 cells.

| Gene ID | Gene | Protein | Relative expression levels | *P* value |
|---|---|---|---|---|
| PA0807 | *ampD* | *N*-acetylmuramoyl-L-alanine amidase | −3.2 | 0.1798 |
| PA0908 | *alpB* | Outer membrane protein AlpB | −4.12 | 0.175 |
| PA1183 | *dctA* | C4-dicarboxylate transport protein | −6.2 | 0.0061 |
| PA3866 | *Pyocin S4* | soluble (S-type) pyocins | −13.22 | 0.0373 |
| PA4370 | *icmP* | Insulin-cleaving metalloproteinase outer membrane | −5.64 | 0.0163 |

*Experiments were conducted using IEC18 cells infected with P. aeruginosa cells (ratio 1/5) for 4 h in either the absence or the presence of 5 mg/mL AHCC prior to carrying out the PCR-real time.*
*The cycle threshold values were normalized to that of the reference transcript, 16S RNA, and data of relative expression levels were normalized to the control lacking AHCC.*

## AHCC® Reduces Cytokine Secretion by Rat Macrophages and IEC18 Cells Infected With *P. aeruginosa*

The IL-6, IL-10 and TNF cytokines are produced by activated macrophage cells as a positive response of inflammatory reactions in the process of bacterial infection. These cytokines are also produced, although in much lower concentrations, by IEC18 cells. To examine the specific effect of AHCC® on cytokine production by rat macrophages and IEC18 cells infected with *P. aeruginosa* PAO1 strain, the secretion of cytokines (IL-6, IL-10 and TNF-α) at 8 h was investigated in the presence and in the absence of AHCC® at 5 mg/mL (**Figure 4**) using enzyme-linked immunosorbent assay (ELISA) kits (Invitrogen, Thermo Fisher Scientific). The data in **Figures 4B,D**, respectively, indicate that the presence of AHCC® reduced significantly the pro-inflammatory cytokine (IL-6 and TNF-α) and the anti-inflammatory cytokine (IL-10) (**Figure 4C**) compared with the cell infected by bacteria and without AHCC®, suggesting an anti-inflammatory effect of AHCC® in both cell types.

## AHCC® Modulated Signal Transduction Pathways in Macrophage Cells Infected With *P. aeruginosa*

The mitogen-activated protein kinase (MAPK) and the NFkB signaling pathways are implicated in the production of TNF-α and IL-6 in macrophage cells (Lee et al., 2010; Yang et al., 2007). To study the modulation exerted by AHCC® on the inflammatory response. We have therefore studied the importance of NF-kB and MAPK signaling molecules in macrophage cell infected by *P. aeruginosa* during AHCC® treatment through a western blot analysis.

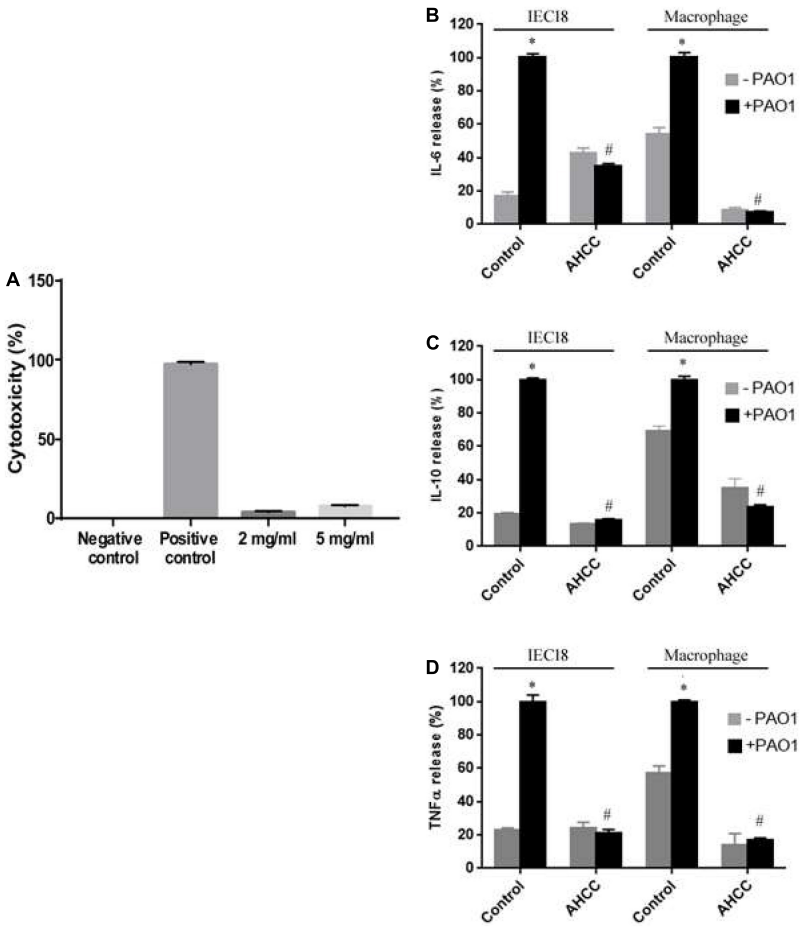


**FIGURE 4 |** Toxicity and inflammatory response of AHCC® on macrophages and IEC 18 cells. Lactate dehydrogenase (LDH) as a marker of cytotoxicity was measured in the supernatants of IEC18 cells **(A)** exposed to AHCC® at 2 or 5 mg/mL. **(B–D)** Cytokine levels in the supernatant of IEC18 or macrophages. Cells were incubated with *P. aeruginosa* PAO1 (ratio 1/5) for 8 h in either the absence or the presence of 5 mg/mL AHCC® prior to the determination of IL-6 **(B)**, IL-10 **(C)** and TNF secretion **(D)**. Values are means ± s.e.m., $n = 6–8$; $^{*}p < 0.05$ vs. cells without bacteria and $^{\#}p < 0.05$ vs. WT in the absence of AHCC® (ANOVA followed by least significance tests).

As shown in **Figure 5**, western blot analysis demonstrated that, while the NFκB pathway was not widely affected by the presence of the AHCC® at 2 and 5 mg/mL, a significant decrease was observed in the level of p-P38, pJNK and, most prominently, in p-ERK phosphorylation (**Figure 5**), pointing to a modulation of the MAPK canonical pathway resulting in a significant reduction of IL-6, IL-10 and TNF-α secretion (**Figure 4**).

## Secretion Systems and Exotoxin A of *Pseudomonas aeruginosa* Are Modulated by AHCC®

Many known natural products exert inhibitory effect on the secretion system which used by pathogenic bacteria to infect host cells (Ortega-González et al., 2014). To analyze the role of AHCC® on *P. aeruginosa* virulence, internalized exotoxin A is quantified into IEC18 cells infected by bacteria. Anti-exotoxin A western blot analysis revealed that the addition of AHCC® at 2 and 5 mg/mL to eukaryotic cells reduces significantly the levels of exotoxin A injected into the cell (**Figures 6A,B**). The data suggest that AHCC® inhibits the mechanism of the type III and VI secretion system that allows exotoxin A to be injected into the eukaryotic cell. Nevertheless, the analysis, using real time qPCR, of expression genes encoding key proteins necessary for the function of secretion systems (i.e., ExsA/VgrG and Hcp for T3SS and T6SS, respectively), shows upregulation (**Figure 6C**). Thus, a mechanistic link for AHCC®-mediated reduction in intracellular exotoxin A concentration cannot be established at this level.

## Effect of AHCC® on Inhibition of Actin Cytoskeletal Dynamics in IEC18 Cell on *P. aeruginosa* Internalization

The ability of pathogenic bacteria to interact with eukaryotic cells depends on the interaction of virulence factors such as adhesins and secretion systems (Gerlach and Hensel, 2007). To analyze whether the entry of the *P. aeruginosa* depends on the dynamics of the actin filaments, we studied bacterial internalization in the

presence of actin depolymerizing fungal toxin cytochalasin D (Cyto D) to prevent bacterial internalization. This compound binds to the positive end of the F filament and prevents the addition of G actin monomers, inhibiting polymerization (Sampath and Pollard, 1991). The standard technique for quantifying internalized bacteria in these assays is still plating a series of dilutions on solid agar and counting the growth colony forming units (CFU).

As shown in **Figure 7**, bacterial internalization was around 55% lower in the presence of the pharmacological inhibitor Cyto D. Notably, addition of AHCC® at either 2 or 5 mg/mL resulted in subtotal inhibition of bacterial internalization, suggesting that mechanisms unrelated to modulation of the cytoskeleton are involved in its effect. In fact, Cyto D had little effect compared with AHCC alone, pointing at a high impact of such mechanisms (**Figure 7**).

## DISCUSSION

Development of new strategies to treat bacterial infections has become a health target, since the therapeutic arsenal is limited, and bacteria are developing multidrug resistances. *P. aeruginosa* presents limited susceptibility to antimicrobial agents and may become multidrug resistant. *P. aeruginosa* infections are a leading cause of nosocomial infections, responsible for 10% of all hospital-acquired infections, which are often severe and even life threatening (Aloush et al., 2006). These facts make of critical importance, according to the WHO, finding new strategies to prevent and treat *P. aeruginosa* infections.

Food and food components may be a good source in the search for alternatives to conventional antibiotics, due to their variety of components with low toxicity. Among them, prebiotics, including standardized extract of cultured *Lentinula edodes* mycelia (AHCC®), are known to regulate intestinal microbiome, through the regulation of the host immune system and the growth of beneficial bacteria. Effects on pathogens have also been described (Collado et al., 2007; Aviles et al., 2008), including *P. aeruginosa* (Ortega-González et al., 2014; Rubio-Gómez et al., 2020). Here, we have evaluated AHCC® for the prevention of *P. aeruginosa* infection. The first approach has been to determine the effect of AHCC® on bacterial growth, observing a concentration dependent longer lag phase and overall growth inhibition in minimal M9 medium (**Figure 1**). Accordingly, the analysis of gene expression indicated a reduction in the expression of the gene *dctA* (PA1183), which is associated with normal growth of *P. aeruginosa* (Valentini et al., 2011). Our data indicate that AHCC® is not a good source of carbohydrates for *P. aeruginosa,* since these effects on the growth curve were observed when grown in M9 medium but not in BHI medium. In addition, we observed that once the log phase was reached (OD = 0.6) the addition of AHCC® had little effect, possibly indicating that it has little or no direct effect on cell division.

On the other hand, AHCC® affected several key aspects of the virulence of *P. aeruginosa*, including its motility and the subsequent formation of biofilms. *P. aeruginosa* utilizes flagellum-mediated swimming motility to approach a surface, where it attaches and further spreads *via* the surface-associated motilities swarming and twitching, mediated by multiple flagella and type-IV pili, respectively (**Figure 3**). AHCC® reduced swimming motility and completely blocked twitching movements, while no changes in swarming were observed in our

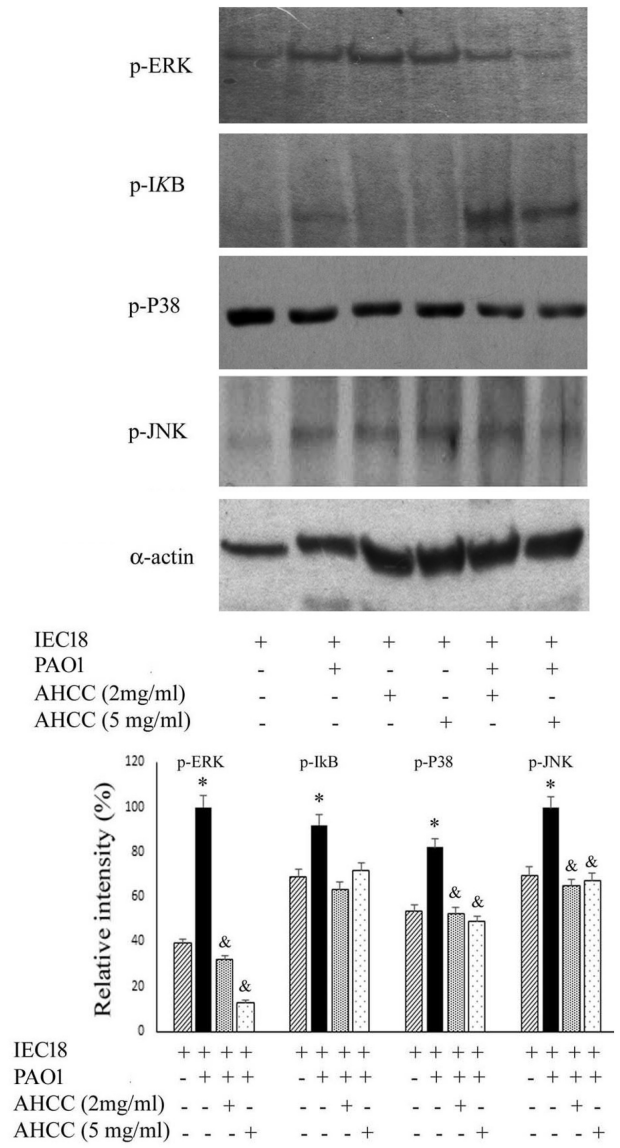


**FIGURE 5 |** Inflammatory transduction pathways are modulated by AHCC®. Macrophage cells were cultured in the presence of *P. aeruginosa* in the absence or presence of 2 and 5 mg/mL AHCC®. After 8 h growth western blots were performed using the cell extracts and the corresponding antibody against specifics proteins. The following protein were detected: p-ERK (the phosphorylated form of Extracellular Regulated Kinase), p-P38 (Activated and phosphorylated form of P38 mitogen-activated protein kinases), p-JNK (Jun N-terminal kinases), p-IkB (phosphorylated form). As control, actin was quantified in all samples using α-actin antibody. Shown are duplicate sample in the absence of added effectors and triplicate samples in the presence of AHCC®. *$p < 0.05$ vs cells without bacteria. (ANOVA followed by least significance tests).

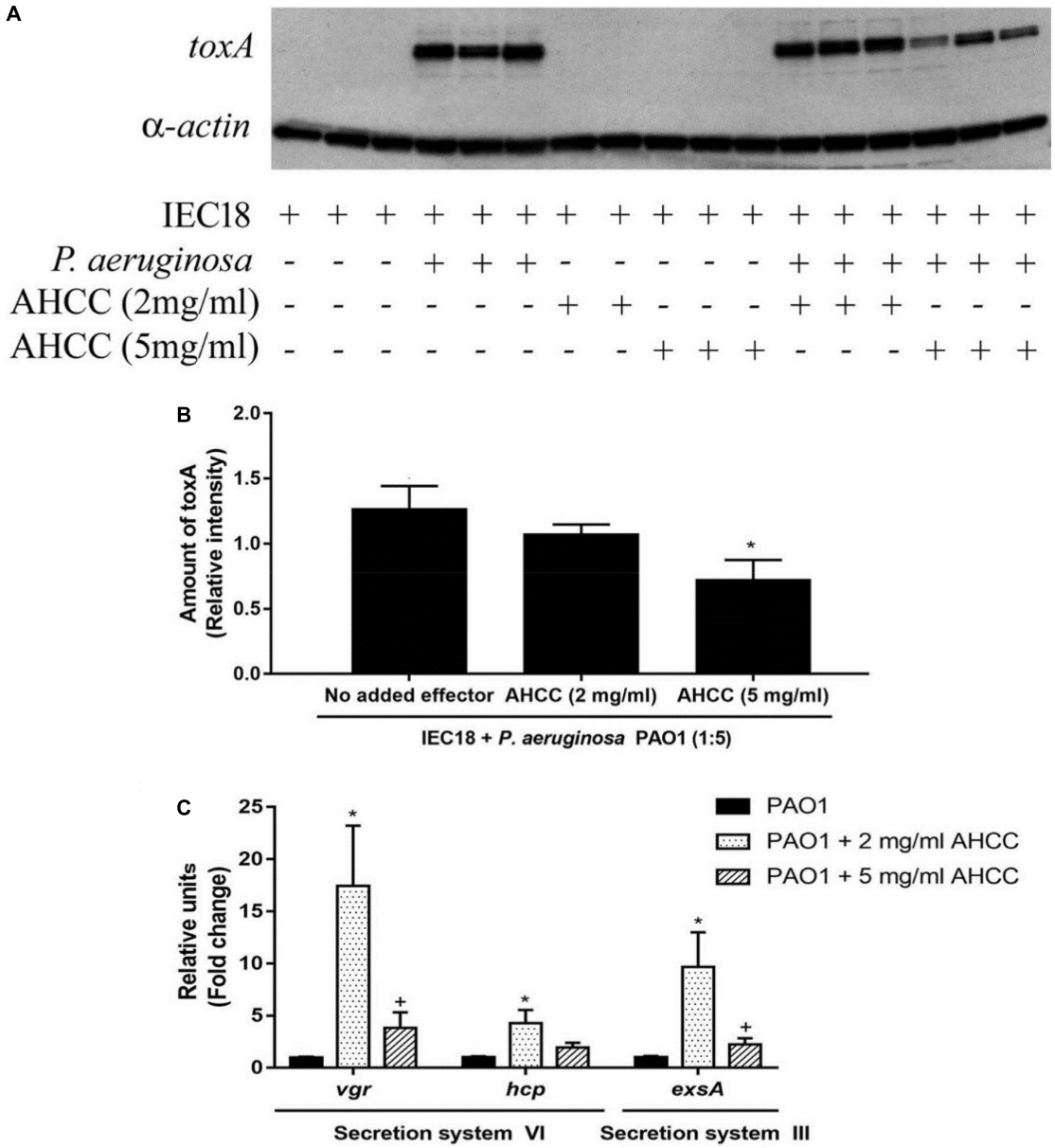


**FIGURE 6 |** The gene expression of *P. aeruginosa* secretion systems and *toxA* are modulated by AHCC®. **(A)** Western blot determination of the cellular concentration of exotoxin A in IEC18 cells following co-culture with *P. aeruginosa* in the presence and absence of AHCC® at 2 and 5 mg/mL of concentration. **(B)** Densitometric analysis of above data. Exotoxin A densities were corrected with those obtained for α-actin. **(C)** Quantitative real time PCR studies of *P. aeruginosa* of cultures grown in the presence and absence of AHCC® at 2 and 5 mg/mL of concentration. The expression of genes encoding proteins of secretion systems III and VI are shown. Values are means ± S.E.M., $n = 6–9$; $^*p < 0.05$ vs. without AHCC® (ANOVA followed by least significance tests).

experimental conditions, indicating a differential inhibitory effect of AHCC® on motility mechanisms. These may be largely related to reduced growth in the presence of AHCC®. Biofilms consist of bacteria encased within an extracellular matrix of proteins, polysaccharides, and small molecules. Biofilm formation provides increased protection of bacteria from antibiotics and host defenses (Mattick, 2002) and reduced biofilm formation has been related to the inhibition of movement capacity as swimming and twitching. Consistently with the reduced movement, a significant reduction in biofilm formation induced by AHCC® was found for the first 4 h (**Figure 2** and **Supplementary Figure 1**). The observed effects of AHCC® increasing the lag phase of *P. aeruginosa,* matching the attaching phase and beginning of biofilm formation, may at least partly account for these effects.

Direct effects of AHCC® on *P. aeruginosa* virulence were further characterized studying the expression of genes (PA0807, PA0908, PA4370 and PA3866) involved in antibiotic resistance and pathogenicity. PA0807 (*ampD*) and PA0908 (*alpB*) encode

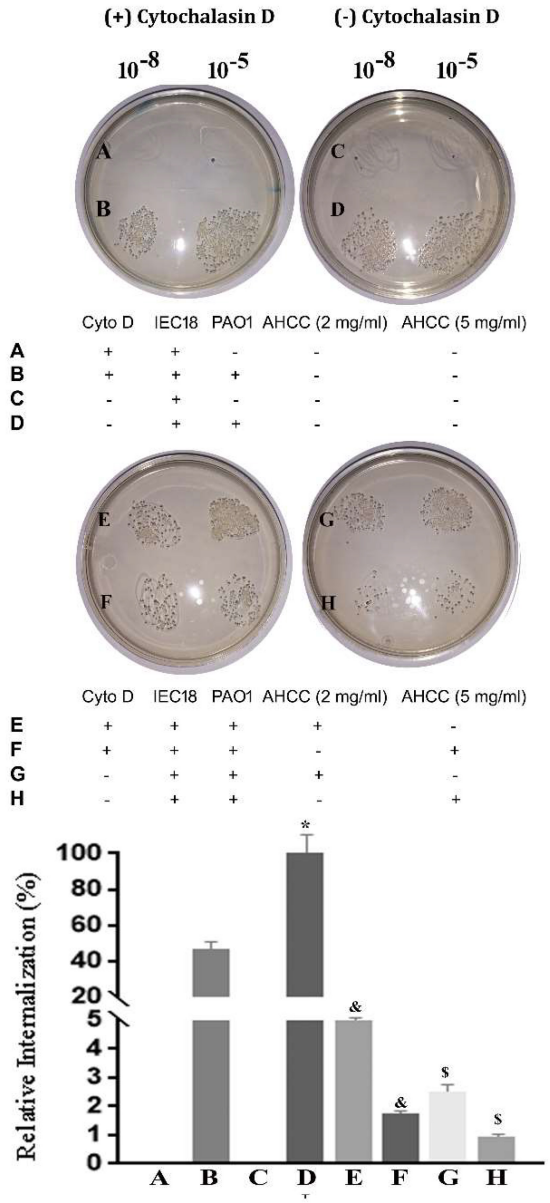


**FIGURE 7 |** Effect of AHCC® on internalization by IEC 18 *in vitro.* In the presence and in the absence of 8 μM Cyto D, the cells were synchronously infected with 10 CFU/cell for 60 min. Bacterial internalization was analyzed by automatically quantifying the growth colony forming units (CFU) (The experiment are performed in triplicated; mean ± S.E.M). The graph shows the mean percentage of bacterial internalization with respect to the sample control in the presence or absence of 20 mg/mL AHCC®. $^{*}p < 0.05$ vs. without Cyto D and $^{\&}p < 0.05$ vs. without AHCC® (ANOVA followed by least significance tests).

proteins whose increased expression is related antibiotic resistance (Amber and Nancy, 2008; Shah and Swiatlo, 2008; Alvarez-Ortega et al., 2010). The *IcmP* gene (PA4370) product is a metalloproteinase outer membrane protein which has been shown to degrade plasminogen activator (Christian et al., 2015) and to play a key role in *P. aeruginosa* pathogenicity. On the other hand, S-type pyocins are bacteriocins produced by *P. aeruginosa* isolates to antagonize or kill other strains of the same species, in other to avoid competition (Dingemans et al., 2016). These pyocins are two component systems consisting of a large and a small component, the large component being the killing subunit. Pyocin S4, encoded by the gene PA3866, is a large component with a C-terminal domain consistent with tRNase activity (Ameer et al., 2012).

The expression of all these genes was found to be reduced. This effect may be the result of a direct modulation of gene expression, or secondary to growth inhibition by AHCC®, or even to a combination of both mechanisms. At any rate, AHCC® appears to act as a signal molecule to modulate different signaling pathways resulting in lower antibiotic resistance, decreased pathogenicity and attenuated ability of *P. aeruginosa* to control the bacterial environment and to infect eukaryotic cells. Exotoxin A produced by several microorganisms, including *P. aeruginosa*, inhibits protein elongation in eukaryotic cells. Addition of AHCC® to primary IEC18 cell cultures reduced the exotoxin A levels inside the cells. This effect was unrelated to modulation of TSS3/TSS6 critical genes, i.e., those encoding ExsA, Hcp and Vgr, which were actually upregulated, suggesting AHCC® may act by a different mechanism such as altering the synthesis of the virulence factor. It should be noted that the secretion systems described above are important for adhesion to the cell.

To further confirm the results, we infected IEC18 cells in the presence AHCC®, observing that it decreased the number of bacteria inside eukaryotic cells. A number of extracellular pathogens, including *P. aeruginosa*, are able to invade epithelial cells by modulating the dynamics of host microtubules. The basic mechanism of this important strategy for improving virulence is poorly understood. Cytochalasin-induced actin alteration has been widely associated with reduction in bacterial internalization by cultured epithelial cells (Cooper, 1987. Chippendale et al., 1994. Benjamin et al., 1995). Consistent with this notion, Cyto D inhibited significantly the internalization of *P. aeruginosa* in IEC18 cells. However, the fact that this effect was greatly augmented by adding AHCC strongly suggests that the latter acts by different mechanisms.

*Pseudomonas aeruginosa* induces the production of cytokines by infected cells. This effect has been associated to the stimulation of TLR receptors, leading to activation of NFκB and MAPKs signaling pathways (Paolillo et al., 2011). We aimed to study if AHCC® regulates the effect of *P. aeruginosa* on the production of cytokines by macrophage cells. As expected, bacteria induced IL6, IL10 and TNFα production and an increased phosphorylation of IκB-α and MAPKs (ERK, p38 and JNK). These stimulatory effects were prevented by AHCC®, with high intensity in the case of the MAPKs pathway, as even in the absence of bacteria the production of cytokines was diminished (**Figure 4**). From these results an indirect effect of AHCC®, acting on macrophage to prevent or attenuate *P. aeruginosa* infection, could be ascertained.

In conclusion, our findings indicate that AHCC® may have potential as an inhibitor of *P. aeruginosa* infection, decreasing bacterial-induced virulence by modulating bacterial properties, such as growth, motility and biofilm formation, as well as decreasing the inflammatory reaction and signaling

through significantly inhibiting the ERK and NFkB pathways, and bacterial internalization. Therefore, elucidation of the mechanism whereby AHCC® inhibits the colonization of the intestinal epithelial cells by *P. aeruginosa* through the analysis of its adhesion and receptors may contribute to the prevention of endogenous *P. aeruginosa* septicemia arising from the intestinal tract.

## CONCLUSION

Our data indicate that AHCC, a nutritional supplement with prebiotic effects, acts as an anti-infective agent against *P. aeruginosa* affecting growth, motility, biofilm and virulence, resulting in a lower impact on eukaryotic cells reflected in the reduction of the secretion of inflammatory cytokines. Moreover, future preclinical and clinical investigations are needed to further validate the potential preventive and/or therapeutic efficacy of AHCC against *P. aeruginosa* infection and inflammatory conditions. We anticipate that AHCC may be employed in future therapeutic regimens to enhance the efficacy of treatment and to dampen the adverse effects of chronic treatment by antibiotics drugs currently used to alleviate immune-related and inflammatory conditions due to the *P. aeruginosa* infection.

## DATA AVAILABILITY STATEMENT

The original contributions presented in the study are included in the article/**Supplementary Material**, further inquiries can be directed to the corresponding author/s.

## ETHICS STATEMENT

The animal study was reviewed and approved by Universidad de Granada (Ref: 277-CEEA-OH-2018).

## AUTHOR CONTRIBUTIONS

MT-G: methodology and investigation. DC-H: validation and methodology. MM: writing—review and editing. FM: validation and writing—review and editing. OM-A: supervision, visualization, editing, and funding acquisition. AD: conceptualization, methodology, writing—reviewing and editing, and supervision. All authors contributed to the article and approved the submitted version.

## FUNDING

This work was supported by grants from FEDER project of Junta de Andalucía, Spain (30B572F301), Ministry of Economy and Competitivity, partly with Fondo Europeo de Desarrollo Regional FEDER funds (SAF2017-88457-R and AGL2017-85270-R), and by Junta de Andalucía (CTS235 and CTS164). MT-G was supported by the University of the Ministry of Education (Spain). CIBERehd is funded by Instituto de Salud Carlos III.

## SUPPLEMENTARY MATERIAL

The Supplementary Material for this article can be found online at: https://www.frontiersin.org/articles/10.3389/fmicb.2022.814448/full#supplementary-material

**Supplementary Figure 1 |** Formation of *P. aeruginosa* biofilm. Biofilm formation in the absence and in the presence of different concentrations of AHCC® at 8 h in glass test tube and 24-well plates.

**Supplementary Figure 2 |** Toxicity of AHCC® on macrophage cells. Macrophage cell was exposed to kit reagent (LDH positive compound) and AHCC® at 2 and 5 mg/of final concentration. Following incubation at 37°C for 24 h, the LDH activity was determined as described in Materials and Methods. $*p < 0.05$ vs. macrophage in the presence of kit toxic compound (ANOVA followed by least significance tests).

## REFERENCES

Abril, M. A., Michan, C., Timmis, K. N., and Ramos, J. L. (1989). Regulator and enzyme specificities of the TOL plasmid-encoded upper pathway for degradation of aromatic hydrocarbons and expansion of the substrate range of the pathway. *J. Bacteriol.* 171, 6782–6790. doi: 10.1128/jb.171.12.6782-6790.1989

Aloush, V., Shiri, N. V., Yardena, S. I., Shaltiel, C., and Yehuda, C. (2006). Multidrug-resistant *Pseudomonas aeruginosa*: risk factors and clinical impact. *Antimicrob. Agents Chemother.* 50, 43–48.

Alvarez-Ortega, C., Wiegand, I., Olivares, J., Hancock, R. E., and Martínez, J. L. (2010). Genetic determinants involved inthe susceptibility of *Pseudomonas aeruginosa* to beta lactam antibiotics. *Antimicrob. Agents Chemother.* 54, 4159–4167.

Amber, S. J., and Nancy, H. D. (2008). Role of ampD homologs in overproduction of AmpC in clinical isolates of *Pseudomonas aeruginosa*. *Antimicrob. Agents Chemother.* 52, 3922–3927. doi: 10.1128/AAC.00341-08

Ameer, E., Qing, W., and Pierre, C. (2012). The soluble pyocins S2 and S4 from *Pseudomonas aeruginosa* bind to the same FpvAI receptor. *Microbiologyopen* 1, 268–275. doi: 10.1002/mbo3.27

Amer, L. S., Bishop, B. M., and Van Hoek, M. L. (2010). Antimicrobial and antibiofilm activity of cathelicidins and short, synthetic peptides against Francisella. *Biochem. Biophys. Res. Commun.* 396, 246–251. doi: 10.1016/j.bbrc.2010.04.073

Aviles, H. O., Donnell, P., Orshal, J., Fujii, H., Sun, B., Sonnenfeld, G., et al. (2008). Active hexose correlated compound activates immune function to decrease bacterial load in a murine model of intramuscular infection. *Am. J. Surg.* 195, 537–545. doi: 10.1016/j.amjsurg.2007.05.045

Benjamin, P., Federman, M., and Wanke, C. A. (1995). Characterization of an invasive phenotype associated with enteroaggregative *Escherichia coli*. *Infect. Immun.* 63, 3417–3421. doi: 10.1128/iai.63.9.3417-3421.1995

Bleves, S., Viarre, V., Salacha, R., Michel, G. P., Filloux, A., Filloux, A., et al. (2010). Protein secretion systems in *Pseudomonas aeruginosa*: a wealth of pathogenic weapons. *Int. J. Med. Microbiol.* 300, 534–543. doi: 10.1016/j.ijmm.2010.08.005

Chastre, J., and Fagon, J. Y. (2002). Ventilator-associated pneumonia. *Am. J. Respir. Crit. Care Med.* 165, 867–903.

Chippendale, G. R., Warren, J. W., Trifillis, L. A., and Mobley, L. H. (1994). Internalization of *Proteus mirabilis* by human renal epithelial cells. *Infect. Immun.* 62, 3115–3121. doi: 10.1128/iai.62.8.3115-3121.1994

Choi, J. Y., Lee, S., Yun, S. M., Suh, D. H., Kim, K., No, J. H., et al. (2018). Active Hexose Correlated Compound (AHCC) inhibits the proliferation of ovarian cancer cells by suppressing signal transducer and activator of transcription 3 (STAT3) Activation. *Nutr. Cancer* 70, 109–115. doi: 10.1080/01635581.2018.1380203

Christensen, G. D., Simpson, W. A., Younger, J. J., Baddour, L. M., Barrett, F. F., Melton, M., et al. (1985). Adherence of coagulase-negative staphylococci to plastic tissue culture plates: a quantitative model for the adherence of staphylococci to medical devices. *J. Clin. Microbiol.* 22, 996–1006. doi: 10.1128/jcm.22.6.996-1006.1985

Christian, L., Melanie, B., Chaves-Moreno, D., Andreas, O., Christian, H., Stephan, F., et al. (2015). Metaproteomics approach to elucidate host and pathogen protein expression during catheter-associated urinary tract infections (CAUTIs). *Mol. Cell. Proteomics* 14, 989–1008. doi: 10.1074/mcp.M114.043463

Collado, M. C., Grzeskowiak, L., and Salminen, S. (2007). Probiotic strains and their combination inhibit *in vitro* adhesion of pathogens to pig intestinal mucosa. *Curr. Microbiol.* 55, 260–265. doi: 10.1007/s00284-007-0144-8

Cooper, J. A. (1987). Effects of cytochalasin and phalloidin on actin. *J. Cell Biol.* 105, 1473–1478.

Corradetti, B., Vaiasicca, S., Mantovani, M., Virgili, E., Bonucci, M., and Ferri, I. H. (2019). Bioactive immunomodulatory compounds: a novel combinatorial strategy for integrated medicine in oncology? BAIC exposure in cancer cells. *Integr. Cancer Ther.* 18:1534735419866908. doi: 10.1177/1534735419866908

Cossart, P., and Sansonetti, P. J. (2004). Bacterial invasion: the paradigms of enteroinvasive pathogens. *Science* 304, 242–248. doi: 10.1126/science.1090124

Daddaoua, A., Enrique, M. P., Lopez-Posadas, R., Vieites, J. M., González, M., Requena, P., et al. (2007). Active hexose correlated compound acts as a prebiotic and is anti-inflammatory in rats with hapten induced colitis. *J. Nutr.* 137, 1222–1228. doi: 10.1093/jn/137.5.1222

Daddaoua, A., Martínez-Plata, E., Ortega-González, M., Ocón, B., Aranda, C. J., Zarzuelo, A., et al. (2013). The nutritional supplement Active Hexose Correlated Compound (AHCC) has direct immunomodulatory actions on intestinal epithelial cells and macrophages involving TLR/MyD88 and NF-kappaB/MAPK activation. *Food Chem.* 136, 1288–1295. doi: 10.1016/j.foodchem.2012.09.039

Daddaoua, A., Puerta, V., Requena, P., Martinez-Ferez, A., Guadix, E., Boza, J. J., et al. (2006). Goat milk oligosaccharides are anti-inflammatory in rats with hapten-induced colitis. *J. Nutr.* 136, 672–676. doi: 10.1093/jn/136.3.672

Delattin, N., De Brucker, K., Vandamme, K., Meert, E., Marchand, A., Chaltin, P., et al. (2014). Repurposing as a means to increase the activity of amphotericin B and caspofungin against Candida albicans biofilms. *J. Antimicrob. Chemother.* 69, 1035–1044. doi: 10.1093/jac/dkt449

Dingemans, J., Ghequire, M. G. K., Michael, C., Mot, R. De, and Cornelis, P. (2016). Identification and functional analysis of a bacteriocin, pyocin S6, with ribonuclease activity from a *Pseudomonas aeruginosa* cystic fibrosis clinical isolate. *Microbiologyopen* 5, 413–423. doi: 10.1002/mbo3.339

Durand, E., Verger, D., Rego, A. T., Chandran, V., Meng, G., Fronzes, R., et al. (2009). Structural biology of bacterial secretion systems in gram-negative pathogens–potential for new drug targets. *Infect. Disord. Drug Targets* 9, 518–547. doi: 10.2174/187152609789105722

Fredheim, E. G., Klingenberg, C., Rohde, H., Frankenberger, S., Gaustad, P., Sollid, J. E., et al. (2009). Biofilm formation by *Staphylococcus haemolyticus*. *J. Clin. Microbiol.* 47, 1172–1180. doi: 10.1128/jcm.01891-08

Gerlach, R. G., and Hensel, M. (2007). Protein secretion systems and adhesins: the molecular armory of Gram-negative pathogens. *Int. J. Med. Microbiol.* 297, 401–415. doi: 10.1016/j.ijmm.2007.03.017

Ghoneum, M., Wimbley, M., Salem, F., McKlain, A., Attallah, N., and Gill, G. (1995). Immunomodulatory and anticancer effects of active hemicellulose compound (AHCC). *Int. J. Immunother.* 11, 23–28.

Goldberg, J. B. (2010). Why is *Pseudomonas aeruginosa* a pathogen? *F1000 Biol. Rep.* 2:29.

Hamood, A. N., Colmer-Hamood, J. A., and Carty, N. L. (2004). "Regulation of *Pseudomonas aeruginosa* exotoxin A synthesis," in *Pseudomonas: Virulence and Gene Regulation*, ed. J. L. Ramos (New York, NY: Academic Publisher), 2, 389–423.

Hassett, D. J., Korfhagen, T. R., Irvin, R. T., Schurr, M. J., Sauer, K., Lau, G. W., et al. (2010). *Pseudomonas aeruginosa* biofilm infections in cystic fibrosis: insights into pathogenic processes and treatment strategies. *Expert Opin. Ther. Targets* 14, 117–130. doi: 10.1517/14728220903454988

Hauser, A. R. (2009). The type III secretion system of *Pseudomonas aeruginosa*: infection by injection. *Nat. Rev. Microbiol.* 7, 654–665. doi: 10.1038/nrmicro2199

Iglewski, B. H., and Kabat, D. (1975). NAD-dependent inhibition of protein synthesis by *Pseudomonas aeruginosa* toxin. *Proc. Natl. Acad. Sci. U.S.A.* 6, 2284–2288.

Ito, T., Urushima, H., Sakaue, M., Yukawa, S., Honda, H., Hirai, K., et al. (2014). Reduction of adverse effects by a mushroom product, active hexose correlated compound (AHCC) in patients with advanced cancer during chemotherapy–the significance of the levels of HHV-6 DNA in saliva as a surrogate biomarker during chemotherapy. *Nutr. Cancer* 66, 377–382. doi: 10.1080/01635581.2014.884232

Johansson, E. M., Crusz, S. A., Kolomiets, E., Buts, L., Kadam, R. U., Camara, M., et al. (2008). Inhibition and dispersion of *Pseudomonas aeruginosa* biofilms by glycopeptide dendrimers targeting the fucose-specific lectin LecB. *Chem. Biol.* 15, 1249–1257. doi: 10.1016/j.chembiol.2008.10.009

Kidd, P. M. (2005). The use of mushroom glucan and proteoglycans in cancer treatment. *Altern. Med. Rev.* 5, 4–27.

Klausen, M., Heydorn, A., Ragas, P., Lambertsen, L., Aaes-Jorgensen, A., Molin, S., et al. (2003). Biofilm formation by *Pseudomonas aeruginosa* wild type, flagella and type IV pili mutants. *Mol. Microbiol.* 48, 1511–1524. doi: 10.1046/j.1365-2958.2003.03525.x

Lee, P. C., Stopford, C. M., Svenson, A. G., and Rietsch, A. (2010). Control of effector export by the *Pseudomonas aeruginosa* type III secretion proteins PcrG and PcrV. *Mol. Microbiol.* 75, 924–941.

Llosa, M., Roy, C., and Dehio, C. (2009). Bacterial type IV secretion systems in human disease. *Mol. Microbiol.* 73, 141–151. doi: 10.1111/j.1365-2958.2009.06751.x

Mah, T. F., Pitts, B., Pellock, B., Walker, G. C., Stewart, P. S., and O'Toole, G. A. (2003). A genetic basis for *Pseudomonas aeruginosa* biofilm antibiotic resistance. *Nature* 426, 306–310.

Matsui, Y., Uhara, J., Satoi, S., Kaibori, M., Yamada, H., Kitade, H., et al. (2002). Improved prognosis of post-operative hepatocellular carcinoma patients when treated with functional foods: a prospective cohort study. *J. Hepatol.* 37, 78–86. doi: 10.1016/s0168-8278(02)00091-0

Mattick, J. S. (2002). Type IV pili and twitching motility. *Annu. Rev. Microbiol.* 56, 289–314. doi: 10.1146/annurev.micro.56.012302.160938

Merrell, D. S., and Falkow, S. (2004). Frontal and stealth attack strategies in microbial pathogenesis. *Nature* 430, 250–256. doi: 10.1038/nature02760

Montie, T. C., Doyle-Huntzinger, D., Craven, R., and Holder, L. A. (1982a). Loss of virulence associated with absence of flagellum in an isogenic mutant of *Pseudomonas aeruginosa* in the burned mouse model. *Infect. Immun.* 38, 1296–1298. doi: 10.1128/iai.38.3.1296-1298.1982

Montie, T. C., Craven, R., and Holder, I. A. (1982b). Flagellar preparations from *Pseudomonas aeruginosa*: isolation and characterization. *Infect. Immun.* 35, 281–288.

Oelschlaeger, T. A. (2010). Mechanisms of probiotic actions. *Int. J. Med. Microbiol.* 300, 57–62. doi: 10.1016/j.ijmm.2009.08.005

Ortega-González, M., Sánchez de Medina, F., Molina-Santiago, C., López-Posadas, R., Pacheco, D., Krell, T., et al. (2014). Fructooligosacharides reduce *Pseudomonas aeruginosa* PAO1 pathogenicity through distinct mechanisms. *PLoS One* 9:e85772. doi: 10.1371/journal.pone.0085772

Ortiz-Castro, R., Pelagio-Flores, R., Méndez-Bravo, A., Ruiz-Herrera, L. F., Campos-García, J., and López-Bucio, J. (2014). Pyocyanin, a virulence factor produced by *Pseudomonas aeruginosa*, alters root development through reactive oxygen species and ethylene signaling in *Arabidopsis*. *Mol. Plant Microbe Interact.* 27, 364–378.

Paolillo, R., Romano, C. C., Sorrentino, S., Mazzola, N., Mita, L., Riza, A., et al. (2011). Expression of IL-23, VEGF and TLR2/TLR4 on mononuclear cells after exposure to *Pseudomonas aeruginosa*. *Int. J. Immunopathol. Pharmacol.* 24, 961–973. doi: 10.1177/039463201102400414

Parsot, C. (2009). *Shigella* type III secretion effectors: how, where, when, for what purposes? *Curr. Opin. Microbiol.* 12, 110–116. doi: 10.1016/j.mib.2008.12.002

Rangel-Vega, A., Bernstein, L. R., Mandujano-Tinoco, E. A., Garcia-Contreras, S. J., and Garcia-Contreras, R. (2015). Drug repurposing as an alternative for the treatment of recalcitrant bacterial infections. *Front. Microbiol.* 6:282. doi: 10.3389/fmicb.2015.00282

Roman, B. E., Beli, E., Duriancik, D. M., and Gardner, E. M. (2013). Short-term supplementation with active hexose correlated compound improves the antibody response to influenza B vaccine. *Nutr. Res.* 33, 12–17. doi: 10.1016/j.nutres.2012.11.001

Rubio-Gómez, J. M., Santiago, C. M., Udaondo, Z., Garitaonaindia, M. T., Krell, T., Ramos, J. L., et al. (2020). Full transcriptomic response of *Pseudomonas aeruginosa* to an inulin-derived fructooligosaccharide. *Front. Microbiol.* 11:202. doi: 10.3389/fmicb.2020.00202

Sampath, P., and Pollard, T. D. (1991). Effects of cytochalasin, phalloidin, and pH on the elongation of actin filaments. *Biochemistry* 30, 1973–1980.

Shah, P., and Swiatlo, E. (2008). A multifaceted role for polyamines in bacterial pathogens. *Mol. Microbiol.* 68, 4–16.

Siles, S. A., Srinivasan, A., Pierce, C. G., Lopez-Ribot, J. L., and Ramasubramanian, A. K. (2013). High-throughput screening of a collection of known pharmacologically active small compounds for identification of *Candida albicans* biofilm inhibitors. *Antimicrob. Agents Chemother.* 57, 3681–3687. doi: 10.1128/AAC.00680-13

Suarez, G., Sierra, J. C., Kirtley, M. L., and Chopra, A. K. (2010). Role of Hcp, a type 6 secretion system effector, of *Aeromonas hydrophila* in modulating activation of host immune cells. *Microbiology* 156, 3678–3688. doi: 10.1099/mic.0.041277-0

Suarez, G., Sierra, J. C., Sha, J., Wang, S., Erova, T. E., Fadl, A., et al. (2008). Molecular characterization of a functional type VI secretion system from a clinical isolate of *Aeromonas hydrophila*. *Microb. Pathog.* 44, 344–361. doi: 10.1016/j.micpath.2007.10.005

Tacconelli, E., and Magrini, N. (2017). *World Health Organization. Global Priority List of Antibiotic-Resistant Bacteria to Guide Research, Discovery, and Development of New Antibiotics.* Available Online at: http://www.who.int/medicines/publications/global-priority-list-antibiotic-resistant-bacteria/en/ [accessed on June 29, 2018]

Taylor, P. K., Yeung, A. T., and Hancock, R. E. (2014). Antibiotic resistance in *Pseudomonas aeruginosa* biofilms: towards the development of novel anti-biofilm therapies. *J. Biotechnol* 191, 121–130. doi: 10.1016/j.jbiotec.2014.09.003

Torres, N. S., Abercrombie, J. J., Srinivasan, A., Lopez-Ribot, J. L., Ramasubramanian, A. K., and Leung, K. P. (2016). Screening a commercial library of pharmacologically active small molecules against *Staphylococcus aureus* biofilms. *Antimicrob. Agents Chemother.* 60, 5663–5672. doi: 10.1128/AAC.00377-16

Valentini, M., Storelli, N., and Lapouge, K. (2011). Identification of C4-Dicarboxylate transport systems in *Pseudomonas aeruginosa* PAO1. *J. Bacteriol.* 193, 4307–4316. doi: 10.1128/jb.05074-11

Van den Driessche, F., Brackman, G., Swimberghe, R., Rigole, P., and Coenye, T. (2017). Screening a repurposing library for potentiators of antibiotics against *Staphylococcus aureus* biofilms. *Int. J. Antimicrob. Agents* 49, 315–320. doi: 10.1016/j.ijantimicag.2016.11.023

Von Klitzing, E., Bereswill, S., and Heimesaat, M. M. (2017). Multidrug-resistant *Pseudomonas aeruginosa* induce systemic pro-inflammatory immune responses in colonized mice. *Eur. J. Microbiol. Immunol.* 7, 200–209. doi: 10.1556/1886.2017.00022

Wilkinson, G. F., and Pritchard, K. (2015). In vitro screening for drug repositioning. *J. Biomol. Screen* 20, 167–179. doi: 10.1177/1087057114563024

Yanagimoto, H., Satoi, S., Yamamoto, T., Hirooka, S., Yamaki, S., Kotsuka, M., et al. (2016). Alleviating Effect of Active Hexose Correlated Compound (AHCC) on chemotherapy-related adverse events in patients with unresectable pancreatic ductal adenocarcinoma. *Nutr. Cancer* 68, 234–240. doi: 10.1080/01635581.2016.1134597

Yang, C. S., Lee, J. S., Song, C. H., Hur, G. M., Lee, S. J., Tanaka, S., et al. (2007). Protein kinase C zeta plays an essential role for Mycobacterium tuberculosis-induced extracellular signal-regulated kinase 1 / 2 activation in monocytes / macrophages via Toll-like receptor 2. *Cell Microbiol.* 9, 382–396. doi: 10.1111/j.1462-5822.2006.00797.x

Ye, S. F., Ichimura, K., Wakame, K., and Ohe, M. (2003). Suppressive effects of active hexose correlated compound on the increased activity of hepatic and renal ornithine decarboxylase induced by oxidative stress. *Life Sci.* 74, 593–602. doi: 10.1016/j.lfs.2003.06.038

Zhang, L., and Mah, T. F. (2008). Involvement of a novel efflux system in biofilm-specific resistance to antibiotics. *J. Bacteriol.* 190, 4447–4452. doi: 10.1128/JB.01655-07

**Conflict of Interest:** The authors declare that the research was conducted in the absence of any commercial or financial relationships that could be construed as a potential conflict of interest.

**Publisher's Note:** All claims expressed in this article are solely those of the authors and do not necessarily represent those of their affiliated organizations, or those of the publisher, the editors and the reviewers. Any product that may be evaluated in this article, or claim that may be made by its manufacturer, is not guaranteed or endorsed by the publisher.

frontiers in Microbiology

ORIGINAL RESEARCH
published: 16 March 2022
doi: 10.3389/fmicb.2022.818165

# Appraisal of Cinnamaldehyde Analogs as Dual-Acting Antibiofilm and Anthelmintic Agents

*Sagar Kiran Khadke†, Jin-Hyung Lee†, Yong-Guy Kim, Vinit Raj and Jintae Lee**

*School of Chemical Engineering, Yeungnam University, Gyeongsan, South Korea*

Cinnamaldehyde has a broad range of biological activities, which include antibiofilm and anthelmintic activities. The ever-growing problem of drug resistance and limited treatment options have created an urgent demand for natural molecules with antibiofilm and anthelmintic properties. Hence, we hypothesized that molecules with a scaffold structurally similar to that of cinnamaldehyde might act as dual inhibitors against fungal biofilms and helminths. In this regard, eleven cinnamaldehyde analogs were tested to determine their effects on fungal *Candida albicans* biofilm and nematode *Caenorhabditis elegans*. α-Methyl and *trans*-4-methyl cinnamaldehydes efficiently inhibited *C. albicans* biofilm formation (>90% inhibition at 50 μg/mL) with minimum inhibitory concentrations (MICs) of ≥ 200 μg/mL and 4-bromo and 4-chloro cinnamaldehydes exhibited anthelmintic property at 20 μg/mL against *C. elegans*. α-Methyl and *trans*-4-methyl cinnamaldehydes inhibited hyphal growth and cell aggregation. Scanning electron microscopy was employed to determine the surface architecture of *C. albicans* biofilm and cuticle of *C. elegans*, and confocal laser scanning microscopy was used to determine biofilm characteristics. The perturbation in gene expression of *C. albicans* was investigated using qRT-PCR analysis and α-methyl and *trans*-4-methyl cinnamaldehydes exhibited down-regulation of *ECE1*, *IFD6*, *RBT5*, *UCF1*, and *UME6* and up-regulation of *CHT4* and *YWP1*. Additionally, molecular interaction of these two molecules with UCF1 and YWP1 were revealed by molecular docking simulation. Our observations collectively suggest α-methyl and *trans*-4-methyl cinnamaldehydes are potent biofilm inhibitors and that 4-bromo and 4-chloro cinnamaldehydes are anthelmintic agents. Efforts are required to determine the range of potential therapeutic applications of cinnamaldehyde analogs.

**Keywords: antibiofilm, anthelmintic, *Candida albicans*, α-methyl cinnamaldehyde, *trans*-4-methyl cinnamaldehyde, protein interaction**

OPEN ACCESS

***Edited by:***
*Laura Quintieri,*
*Italian National Research Council, Italy*

***Reviewed by:***
*Kunal Singh,*
*Institute of Himalayan Bioresource Technology (CSIR), India*
*Sueli Fumie Yamada-Ogatta,*
*State University of Londrina, Brazil*

***Correspondence:**
*Jintae Lee*
*jtlee@ynu.ac.kr*

*† These authors have contributed equally to this work*

***Specialty section:***
*This article was submitted to Antimicrobials, Resistance and Chemotherapy, a section of the journal Frontiers in Microbiology*

***Received:*** *19 November 2021*
***Accepted:*** *02 February 2022*
***Published:*** *16 March 2022*

***Citation:***
*Khadke SK, Lee J-H, Kim Y-G, Raj V and Lee J (2022) Appraisal of Cinnamaldehyde Analogs as Dual-Acting Antibiofilm and Anthelmintic Agents. Front. Microbiol. 13:818165. doi: 10.3389/fmicb.2022.818165*

## INTRODUCTION

Plants are one of the prime sources of bioactive molecules. Cinnamaldehydes are present in the bark of trees of the genus *Cinnamomum*, which contains around 250 plant species (Shreaz et al., 2016). Highest percentages of cinnamaldehyde are found in two common species, namely, *Cinnamomum cassia* and *Cinnamomum verum* (also called *C. zeylanicum*) (Chen et al., 2017; Doyle and Stephens, 2019). *Trans*-cinnamaldehyde the predominant form in cinnamon is a phenylpropanoid and is generally recognized as safe by United States Food and Drug Administration (USFDA), and the Flavor and Extract Manufacturer's Association (FEMA), and the Council of Europe has given it

an A status for use in foodstuffs (Friedman, 2017). *Trans*-cinnamaldehyde is a yellow oil with a sweet taste and the odor of cinnamon and is primarily used as a flavoring agent as well as used in medical products, cosmetics, and perfumes (Brackman et al., 2008; Doyle and Stephens, 2019). Furthermore, *trans*-cinnamaldehyde has also been documented to have antibiofilm and anti-quorum sensing activity against *Vibrio harveyi* (Niu et al., 2006), enterohemorrhagic and uropathogenic *Escherichia coli* strains (Kim et al., 2015; Kot et al., 2015), methicillin-resistant *Staphylococcus aureus* strains (Kavanaugh and Ribbeck, 2012; Kot et al., 2018), *Pseudomonas aeruginosa* (Kavanaugh and Ribbeck, 2012), *Pseudomonas fluorescens* (Li et al., 2018), *Cronobacter sakazakii* (Amalaradjou and Venkitanarayanan, 2011), *Streptococcus pyogenes* (Beema Shafreen et al., 2014), *Salmonella typhimurium* (Silva et al., 2018), and against the pathogenic fungus *C. albicans* (Ying et al., 2019; Miranda-Cadena et al., 2021). In addition, cinnamaldehyde analogs are known to have an array of bioactivities, which include antibacterial (Firmino et al., 2018), antifungal (Da Nobrega Alves et al., 2020), antiviral (Hayashi et al., 2007), antiulcer (Tabak et al., 1999), antioxidant (Mathew and Abraham, 2006), antidiabetic (Im et al., 2014), anti-inflammatory (Srisook et al., 2019), anticancer (Fang et al., 2004) activities and insecticidal (Cheng et al., 2009; Lu et al., 2020), larvicidal (Cheng et al., 2004), nematicidal (Ferreira Barros et al., 2021), and anthelmintic (Williams et al., 2015) effects.

The failure of current antifungal treatments caused by their overuse and the consequent emergence of multidrug-resistant variants of microorganisms presents a challengeable problem (Cegelski et al., 2008; Liu et al., 2020; Lin et al., 2021). Bacteria and fungi protect themselves from antimicrobial agents, host defense systems, and nutrient limitations by forming self-organized and three-dimensional communities (biofilms) on various biotic or abiotic surfaces (Costerton et al., 1999; Tan et al., 2019), and by so doing contribute to the persistence of infections. Conventional antifungal agents inhibit planktonic fungal growth, which often results in drug resistance (Hentzer et al., 2002; Ma et al., 2020). A report published in 2019 by the Centers for Disease Control and Prevention (CDC, 2019) stated that *Candida albicans* presents a serious threat *via* the spread of life-threatening candidiasis (Ostrosky-Zeichner et al., 2010; CDC, 2019). *C. albicans* and its biofilms are found on mucosal surfaces and in the gastrointestinal and genitourinary tracts, and *C. albicans* readily colonizes host tissues and indwelling medical devices such as urinary catheters, dental implants, artificial heart valves, joint prosthetics, penile implants, and intrauterine devices (Ramage et al., 2005; Sardi et al., 2013; De Oliveira et al., 2019; Handorf et al., 2019). Highly structured *C. albicans* biofilms form on implant surfaces and subsequently the pathogen disseminate into blood to cause invasive candidiasis, which is responsible for an estimated 100,000 deaths per annum in the United States and for the replacement of over five million central nervous catheters (Sardi et al., 2013). Highly resistant fungal biofilm infections are treated using high antifungal doses and the removal of colonized medical devices, which pose risks of kidney and liver damage and substantially increase medical costs (Ramage et al., 2005; De Oliveira et al., 2019).

On the other hand, parasitic nematodes have serious impacts on global health and socio-economic development, for example, several soil-transmitted nematodes directly affect human populations, pose major threats to livestock and plants, and are responsible for huge economic losses (Hotez et al., 2014). Unfortunately, the originally limited armamentarium of anthelmintic drugs and their extensive usage have directed to drug resistance, and thus, there is an urgent need to discover new drug candidates (Diawara et al., 2013; Kotze et al., 2014; Krücken et al., 2017). The evaluation of the anthelmintic efficacies of candidate compounds against parasitic nematodes poses several challenges, which include limited access to lifecycle stages, cost-intensive laboratory studies on life cycles and host dependency, and fragile and complex *in vitro* culture (Burns et al., 2015; Hahnel et al., 2020). Free-living, transparent *Caenorhabditis elegans* has been well used as a model system for evaluation purposes. This nematode has a simple, rapid life cycle and well-annotated genes, and an extensive number of molecular tools (Brenner, 1974). *C. elegans* shares the typical anatomical characteristics of most nematode species as regards its body plan, cuticle, and nervous system organization (Harder, 2016).

Inspired by the broad-ranging biological activities of the cinnamaldehyde scaffold including antibiofilm and anthelmintic potencies as well as safety profile of naturally isolated cinnamaldehyde and the current challenges posed by drug-resistant fungi and parasites, hence it can be hypothesized that cinnamaldehyde analogs may be good alternative against *C. albicans* biofilm and nematode *C. elegans*. To check this hypothesis, we selected cost-effective eleven cinnamaldehyde analogs for the screening *in vitro* antibiofilm and *in vivo* anthelmintic activities. In order to explore surface morphological effect of two active cinnamaldehyde analogs on *C. albicans* biofilm and *C. elegans*, scanning electron microscopy (SEM) was carried out. Also, confocal laser scanning microscopy (CLSM) was utilized for biofilms of *C. albicans*. Further, the antibiofilm effects of the two most active cinnamaldehyde analogs, α-methyl cinnamaldehyde and *trans*-4-methyl cinnamaldehyde, were investigated using hyphae formation and cell aggregation assays. The molecular mechanism of α-methyl cinnamaldehyde and *trans*-4-methyl cinnamaldehyde was estimated using quantitative real-time PCR (qRT-PCR) analysis and molecular interaction of α-methyl cinnamaldehyde and *trans*-4-methyl cinnamaldehyde with proteins UCF1 (filament specific regulator) and YWP1 (yeast form wall protein 1) was predicted by molecular simulation (**Scheme 1**). To the best of our knowledge, this is the first report on the antibiofilm and anthelmintic activities of cinnamaldehyde analogs against *C. albicans* and *C. elegans*, respectively.

# MATERIALS AND METHODS

## Reagents and Culture Strains

Chemicals including eleven cinnamaldehyde analogs viz. 4-bromo cinnamaldehyde (95%), 4-chloro cinnamaldehyde (95%), cinnamaldehyde oxime (95%), 4-dimethylamino cinnamaldehyde (98%), 4-fluoro cinnamaldehyde (97%), α-methyl cinnamaldehyde (95%), 2-methoxy cinnamaldehyde

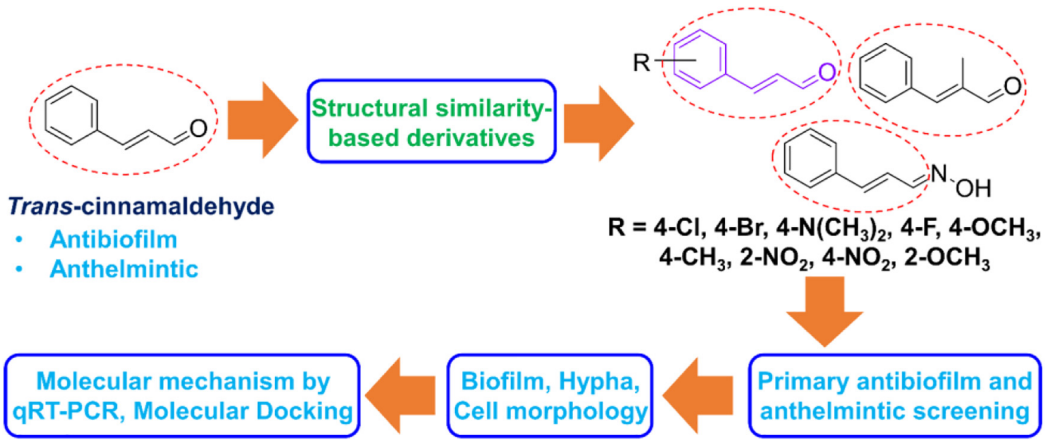


**SCHEME 1 |** Schematic representation of the strategies used in the present study.

(95%), 4-methoxy cinnamaldehyde (95%), 2-nitro cinnamaldehyde (98%), 4-nitro cinnamaldehyde (95%), *trans*-4-methyl cinnamaldehyde (95%), and one positive control; *trans*-cinnamaldehyde (99%) (**Figure 1C**), dimethyl sulfoxide (DMSO) (99%) and crystal violet (90%) were purchased from either Sigma-Aldrich (St. Louis, MO, United States), Combi Blocks, Inc., (San Diego, CA, United States) or TCI Co., (Tokyo, Japan). The fluconazole-resistant *C. albicans* strains DAY185 and ATCC 10231 used were obtained from the Korean Culture Center for Microorganisms (Seoul, South Korea) (Lee et al., 2018). For the experiments, *C. albicans* strains DAY185 and ATCC 10231 were cultured under aerobic conditions at 37°C in potato dextrose agar (PDA; Becton Dickinson, Sparks, MD, United States) and potato dextrose broth (PDB; Becton Dickinson, Sparks, MD, United States). Initially, fungal strains were taken from −80°C glycerol stock and streaked onto potato dextrose agar plates. Single fresh colonies were inoculated into PDB (2 mL) in 14 mL round-bottom tubes and incubated at 37°C at 250 rpm (Lee et al., 2018). Cinnamaldehyde analogs were dissolved in required quantities of DMSO. DMSO [0.1% (v/v)] was used as the negative control and this concentration did not inhibit fungal growth or biofilm formation.

## Biofilm Formation, Minimum Inhibitory Concentrations, and Growth Rate Measurements for the Screening of Cinnamaldehyde Analogs Against *C. albicans*

Biofilm formation assays were performed in 96-well microtiter plates using the crystal violet staining method, as previously described (Lee et al., 2021). Briefly, a 2-day-old single colony of *C. albicans* was inoculated into PDB and incubated overnight at 37°C with shaking. Overnight cultures of initial turbidity 0.1 at $OD_{600}$ nm (~$10^5$ CFU/mL) were re-inoculated into fresh PDB (final volume 300 μL) and concurrently treated individually with or without the presence of eleven cinnamaldehyde analogs at 100 μg/mL and *trans*-cinnamaldehyde. Microtiter plates were incubated at 37°C without shaking for 24 h, and biofilms that adhered to plate bottoms were stained with 0.1% crystal violet for 20 min, repeatedly washed with sterile distilled water, and resuspended in 95% ethanol. Plates were read at $OD_{570}$ nm to assess biofilm formation using a Multiskan EX microplate reader (Thermo Fisher Scientific, Waltham, MA, United States). Besides, the minimum inhibitory concentrations (MICs) of cinnamaldehyde analogs were determined as per Clinical and Laboratory Standards Institute (CLSI) guidelines (CLSI, 2017). Overnight cultures of *C. albicans* were treated with each cinnamaldehyde analog at various concentrations (0–200 μg/mL) and incubated at 37°C for 24 h. MIC was defined as the lowest concentration that inhibited yeast growth by 80%, as assessed by spectrophotometry (620 nm). The results quoted are the averages of at least two independent cultures.

Based on outcomes of biofilm experiment, cell growth analysis was carried out as follows. *C. albicans* DAY185 was re-inoculated into 96-well plates containing PDB medium (1:50 dilution) and treated with or without the eight most potent cinnamaldehyde analogs, as determined by biofilm formation assay, that is, 4-bromo, 4-chloro, 4-fluoro, α-methyl, 2-methoxy, 2-nitro, 4-nitro, *trans*-4-methyl, or *trans*-cinnamaldehydes at 50–100 μg/mL for 24 h at 37°C. Afterward, *C. albicans* ATCC 10231 was inoculated into 96-well plates containing PDB medium (1:50 dilution) and treated with or without two most potent cinnamaldehyde analogs at 50–100 μg/mL for 24 h at 37°C. Growths were assessed by spectrophotometry at $OD_{620}$. Consequently, two cinnamaldehyde analogs were selected based on their antibiofilm potency. Later, doses dependent antibiofilm effects of highly potent cinnamaldehyde analogs were revealed at 0–50 μg/mL. Results are the averages of measurements taken from at least six replicate wells.

## Colony Morphology Assay on Solid Media

Potato dextrose agar plates containing or not α-methyl, *trans*-4-methyl, or *trans*-cinnamaldehydes (0–50 μg/mL) were streaked

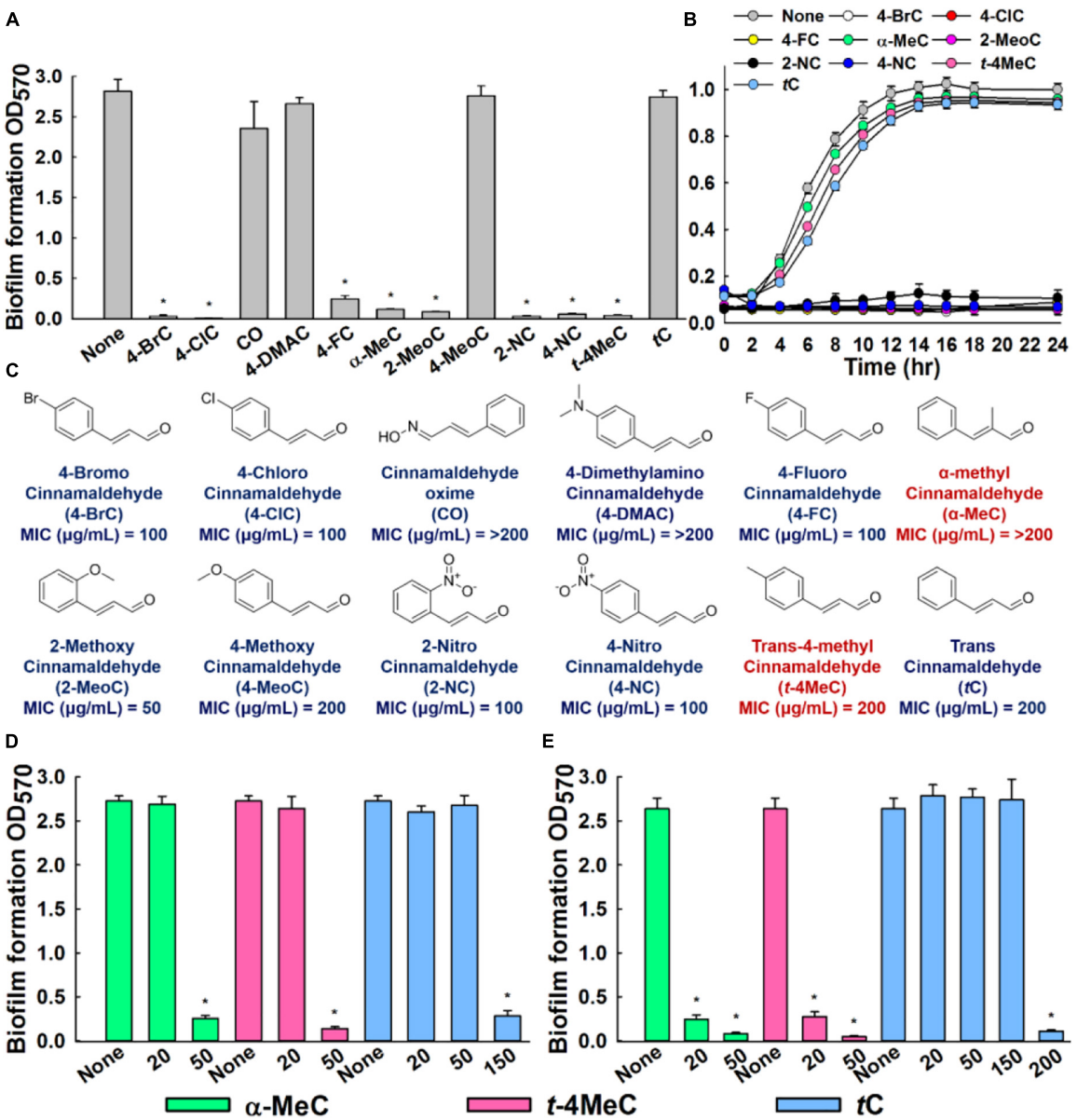


**FIGURE 1 |** *In vitro* antibiofilm activities of cinnamaldehyde analogs against *C. albicans*. Influences of eleven cinnamaldehyde analogs and *trans*-cinnamaldehyde (*t*C) on biofilm formation by the *C. albicans* DAY185 at 100 μg/mL **(A)**, *C. albicans* DAY185 cell growth was investigated in the presence of the eight antibiofilm cinnamaldehyde analogs and the *trans*-cinnamaldehyde control at 100 μg/mL **(B)**, Chemical structures and MIC **(C)**. The antibiofilm activities of α-methyl cinnamaldehyde (α-MeC) and *trans*-4-methyl cinnamaldehyde (*t*-4MeC) at 20 and 50 μg/mL, and *trans*-cinnamaldehyde (*t*C) at 20–200 μg/mL against *C. albicans* DAY185 **(D)** and *C. albicans* ATCC 10231 **(E)**. Error bars indicate standard deviations. *$P < 0.05$ vs. non-treated controls (None).

with *C. albicans* DAY185 or ATCC 10231 and incubated at 37°C for 6 days. Plates were periodically monitored for colony formation and morphology, and phenotypic changes were observed using the iRiS$^{TM}$ Digital Cell Imaging System (Logos BioSystems, South Korea) at 10x (Lee et al., 2021). At least, three independent experiments were conducted.

## Yeast-Hyphae-Transition Assay

Assays were conducted in liquid media, as previously described (Lee et al., 2021). *C. albicans* DAY185 or ATCC 10231 cells at a density of $10^5$ CFU/mL were inoculated in 2 mL of PDB medium and treated with α-methyl, *trans*-4-methyl, or *trans*-cinnamaldehydes at 0–50 μg/mL. Disposable, sterile polypropylene tubes (14 mL) with polyethylene caps were used to conduct hyphal assays in PDB. Tubes were demonstrated by the manufacturer to create aerobic (open-cap) conditions. Cultures containing cinnamaldehyde analogs or not were incubated at 37°C without shaking for 24 h, aliquoted, and imaged in bright field using the iRiS$^{TM}$ Digital Cell Imaging System at 20x. At least, four independent experiments were conducted.

## Biofilm Annotations by Confocal Laser Scanning Microscopy

*Candida albicans* biofilms were produced on 96-well polystyrene plates in the presence or absence of α-methyl, *trans*-4-methyl, or *trans*-cinnamaldehydes at 50 μg/mL without shaking for 24 h at 37°C. After incubation, planktonic cells were removed by washing (three times) with distilled water, and biofilms were stained with carboxyfluorescein diacetate succinimidyl ester (Invitrogen, Eugene, OR, United States) (Lee et al., 2019a). Plate bottoms were then visualized using a 488 nm Ar laser (emission 500–550 nm) beneath a confocal laser microscope (Nikon Eclipse Ti, Tokyo, Japan). To quantify biofilm structures, COMSTAT software (Heydorn et al., 2000) was used to determine biovolumes ($\mu m^3\ \mu m^{-2}$), mean biofilm thicknesses (μm), and percentage substratum coverages (%). Two autonomous cultures were performed for each experimental condition and at least 10 random positions were screened.

## Microscopic Architecture of *C. albicans* Biofilms and *C. elegans* Cuticles

Scanning electron microscopy was used to observe biofilms, as previously described (Kim et al., 2020). Briefly, precut pieces of a nylon membrane 0.5 × 0.5 cm were placed in 96-well plates containing *C. albicans* grown in PDB medium with or without α-methyl, *trans*-4-methyl, or *trans*-cinnamaldehydes (50 μg/mL) and incubated for 24 h at 37°C. Cells that adhered to nylon membranes for 24 h were fixed with a glutaraldehyde (2.5%) and formaldehyde (2%) solution, postfixed using osmium tetroxide, and dehydrated using an ethanol series (50, 70, 80, 90, 95, and 100%) and isoamyl acetate. After critical-point drying, cells were sputter-coated with palladium/gold and imaged using an S-4200 scanning electron microscope (Hitachi, Tokyo, Japan) at 15 kV.

To examine *C. elegans* cuticles, scanning electron microscopy was performed using an S-4800 instrument (Hitachi, Tokyo, Japan), as described previously (Ropiak et al., 2016). To investigate the effects of the highly potent anthelmintic agents, nematodes were treated with 4-bromo or 4-chloro cinnamaldehydes at 20 μg/mL for 48 h, and then 10 nematodes per treatment were processed for SEM imaging, as previously described (Ropiak et al., 2016). *Trans*-cinnamaldehyde was used as the control.

## RNA Isolation and qRT-PCR for Transcriptomic Profile of *C. albicans*

Transcript expression analysis was conducted using concentrate of 25 mL cultures of *C. albicans* at an initial turbidity of 0.1 at $OD_{600}$ (∼$10^5$ CFU/mL). These were incubated for 6 h at 37°C with agitation (250 rpm) in the presence or absence of α-methyl or *trans*-4-methyl cinnamaldehydes (50 μg/mL). RNA degradation was prevented by adding RNase inhibitor (RNAlater, Ambion, TX, United States) to cells immediately after incubation. Total RNA was isolated using a hot acidic phenol method (Amin-Ul Mannan et al., 2009) and RNA was purified using the Qiagen RNeasy mini Kit (Valencia, CA, United States).

To determine the expressions of hyphal and biofilm-related genes (*ALS3*, *CHT4*, *ECE1*, *HWP1*, *IFD6*, *RAS1*, *RBT5*, *UCF1*, *UME6*, and *YWP1*), qRT-PCR was performed as described (Kim et al., 2016) using SYBR Green master mix (Applied Biosystems, Foster City, CA, United States) and an ABI StepOne Real-Time PCR System (Applied Biosystems). The housekeeping gene (*RDN18*) and the primers used for qRT-PCR are listed in **Supplementary Table S1**. At least two independent cultures were used.

## Preparation of Ligands and Computational Screening

Ligand structures were prepared using LigPrep tools in the Schrodinger suite and optimized for minimum energy using the density functional theory (DFT) approach, as described previously (Khadke et al., 2021; Raj et al., 2021). The main reason of molecular docking was to confirm and reveal the molecular interaction between potent cinnamaldehyde analogs and highly significant genes of interest. Based on the gene expression perturbation, we have chosen *UCF1* and *YWP1* owing to their prominent downregulation (12- and 54-fold change) and upregulation (26- and 17-fold change), respectively. Hence, UCF1 and YWP1 proteins were selected for docking study to confirm that whether α-methyl and *trans*-4-methyl cinnamaldehyde can interact with these proteins. Conformations and bond orders were minimized and refined using the OPLS 2005 force field. Prepared ligands were subjected to analysis for computational screening with the active binding pocket of UCF1 and YWP1. Initially, the binding active pockets of UCF1 and YWP1 were predicted by the CASTp server[1] (Tian et al., 2018). These predicted active sites were assigned for a final grid by molecular screening by treating drug molecules as rigid entities and receptors as flexible entities. To ensure the reliability, validity, and reproducibility of docking results, molecular docking was performed using AUTODOCK (Seeliger and De Groot, 2010). Additionally, cluster analysis of these targeted molecules was carried out with UCF1 and YWP1. Further, binding energies and interactions between α-methyl, *trans*-4-methyl, or *trans*-cinnamaldehydes and UCF1 or YWP1 were determined using a computational approach, as previously described (Raj et al., 2021). BIOVIA Discovery Studio Visualizer was used to capture interactions between the cinnamaldehyde analogs and UCF1 or YWP1.

## Assessment of the *in vivo* Anthelmintic Activities of Cinnamaldehyde Analogs

*Caenorhabditis elegans fer-15(b26)*; *fem-1(hc17)* (Garigan et al., 2002) strain was obtained from Prof. Eleftherios Mylonakis (Brown University). The strain was maintained on a nematode growth medium (NGM) with *E. coli* OP50 as feed, and synchronized as previously described protocol (Lee et al., 2017). Briefly, *C. elegans* worms, eggs were collected in worm-lysis solution (2% sodium hypochlorite and 0.5 N sodium hydroxide) from adults, washed and allowed to hatch to the L1 stage in M9 buffer for 24 h at 25°C under 6 rpm rotation (Lee et al., 2017). Later, worms were transferred to fresh NGM plates containing

[1]https://www.uniprot.org/uniprot/Q59KG2 and https://www.uniprot.org/uniprot/Q59Y31, respectively, accessed 1 September 2021.

*E. coli* OP50 lawns to obtain synchronized L4 stage worms and collected in M9 buffer, washed, and transferred to 96-well plate.

*In vivo* anthelmintic activities were investigated to confirm the anthelmintic effects of the eleven cinnamaldehyde analogs and *trans*-cinnamaldehyde using a previously described *C. elegans* model (Ropiak et al., 2016; Lee et al., 2019b). In brief, synchronized *C. elegans fer-15(b26)*; *fem-1(hc17)* worms ($n$ = ∼20–30) were pipetted into the wells of a 96-well plate in M9 buffer. Cinnamaldehyde analogs (5–100 μg/mL) were then added to a final volume of 300 μL. Nematodes were incubated for 4 days at 25°C, and viabilities were determined using an iRiS$^{TM}$ Digital Cell Imaging System (Logos BioSystems, South Korea) by exposing worms to LED or UV LED light for 10–30 s (Rajasekharan et al., 2018). Three independent experiments were performed in triplicate.

## Estimation of Absorption, Distribution, Metabolism, and Excretion Properties of Cinnamaldehyde Analogs

The drug-likeness parameters of two most potent antibiofilm and anthelmintic cinnamaldehyde analogs and *trans*-cinnamaldehyde were evaluated using Swiss Absorption, Distribution, Metabolism, and Excretion (ADME) (Daina et al., 2017). According to the Lipinski rule, an orally active pharmaceutical agent should have a molecular weight of ≤ 500 g/moL, a Log $P$ of ≤ 5, ≤ 5 hydrogen bond-donating atoms, ≤ 10 hydrogen-bond accepting atoms, and a topological polar surface of ≤ 140Å$^2$ (Benet et al., 2016).

## Statistical Analysis

Replication numbers for assays are provided above, and results are presented as means ± standard deviations. The statistical analysis was performed using one-way ANOVA followed by Dunnett's test in SPSS version 23 (SPSS Inc., Chicago, IL, United States). $P$ values of $< 0.05$ were considered significant. Asterisks are used to denote significant differences between treated and untreated samples.

# RESULTS

## *In vitro* Assessments of the Antibiofilm Activities of Cinnamaldehyde Analogs Against *C. albicans*

The antibiofilm potencies of the eleven cinnamaldehyde analogs at 100 μg/mL were initially investigated using *C. albicans* DAY185 and their potencies were compared with *trans*-cinnamaldehyde (**Figure 1A**). At initial screening, eight analogs, that is, 4-bromo, 4-chloro, 4-fluoro, α-methyl, 2-methoxy, 2-nitro, 4-nitro, and *trans*-4-methyl cinnamaldehydes displayed strong antibiofilm activities (98, 99, 91, 95, 96, 98, 97, and 98%, respectively) against *C. albicans* DAY185. In contrast, cinnamaldehyde oxime, 4-dimethylamino cinnamaldehyde, and 4-methoxy cinnamaldehyde showed no or little biofilm inhibitory activity. Among the initially screened eight antibiofilm inhibitors, six had MIC in the range of 50–100 μg/mL, while two remained cinnamaldehyde analogs showed MIC of ≥ 200 μg/mL (**Figure 1C**). Usually, antifungal agents inhibit microorganism planktonic growth, and this inhibition can lead to drug resistance, thus based on MIC's and our focus relying on finding lead antibiofilm agents, we selected α-methyl and *trans*-4-methyl cinnamaldehydes for further investigations (**Figures 1A,B**).

In more detail, α-methyl and *trans*-4-methyl cinnamaldehydes dose-dependently inhibited biofilm formation by both *C. albicans* strains. For example, α-methyl and *trans*-4-methyl cinnamaldehydes at 50 μg/mL inhibited *C. albicans* DAY185 biofilm formations by > 90% (**Figure 1D**). Also, both the analogs inhibited *C. albicans* ATCC 10231 biofilm formations by > 88 and > 95%, at 20 and 50 μg/mL, respectively (**Figure 1E**). Whereas, *trans*-cinnamaldehyde at 20, and 50 μg/mL did not affect biofilm formation of *C. albicans* DAY185 but at 150 μg/mL inhibited biofilm formation by 90% (**Figure 1D**). However, when *trans*-cinnamaldehyde was tested at 20, 50, and 150 μg/mL, it did not inhibit the biofilm formation of *C. albicans* ATCC 10231 (**Figure 1E**). Additionally, the biofilm inhibitory effect of *trans*-cinnamaldehyde at 200 μg/mL on *C. albicans* ATCC 10231 was attributed to its antifungal activity (**Figures 1C,E**). Planktonic cell growths were measured to assess the antifungal activities of α-methyl and *trans*-4-methyl cinnamaldehydes (**Figure 1B**). Neither of these two analogs inhibited the planktonic growth of *C. albicans* DAY185 or ATCC 10231 at 50 or 100 μg/mL and their MICs were ≥ 200 μg/mL (**Figure 1B** and **Supplementary Figure S1**). These results show α-methyl and *trans*-4-methyl cinnamaldehydes effectively prevented biofilm formation by *C. albicans* strains at sub-inhibitory concentrations and that they are more active than *trans*-cinnamaldehyde.

## Cinnamaldehyde Analogs Impaired *C. albicans* Yeast-Hyphae Transition

A microscopic temporal study of *C. albicans* DAY185 or ATCC 10231 colonies on solid PDA revealed extensive hyphal protrusions. Colonies were monitored over 6 days in the presence or absence of α-methyl or *trans*-4-methyl cinnamaldehydes and compared with *trans*-cinnamaldehyde. In the non-treated control, progressive growth of hyphal filaments was observed. Interestingly, α-methyl and *trans*-4-methyl cinnamaldehydes prevented hyphal protrusions from *C. albicans* DAY185 colonies at 50 μg/mL and revealed colonies with smooth and curved surfaces. However, *trans*-cinnamaldehyde at 50 μg/mL had no effect (**Figure 2A**), but at 150 μg/mL prevented *C. albicans* DAY185 hyphal protrusions and revealed smooth and curved surfaces. As well as, both the analogs prevented hyphal protrusions from *C. albicans* ATCC 10231 colonies at 20 and 50 μg/mL with colonies surfaces smooth and curved. In contrast, *trans*-cinnamaldehyde at 20, 50, and 150 μg/mL exhibited characteristics similar to the non-treated control of *C. albicans* ATCC 10231 (**Supplementary Figures S2A, S3A**).

*Candida albicans* biofilm maturation is dependent on a dimorphic switch from yeast to hyphal cells and cell aggregation (Chandra et al., 2001). To examine the effects of α-methyl and *trans*-4-methyl cinnamaldehydes on *C. albicans* morphology, yeast-hyphae transition of *C. albicans* DAY185 or ATCC 10231

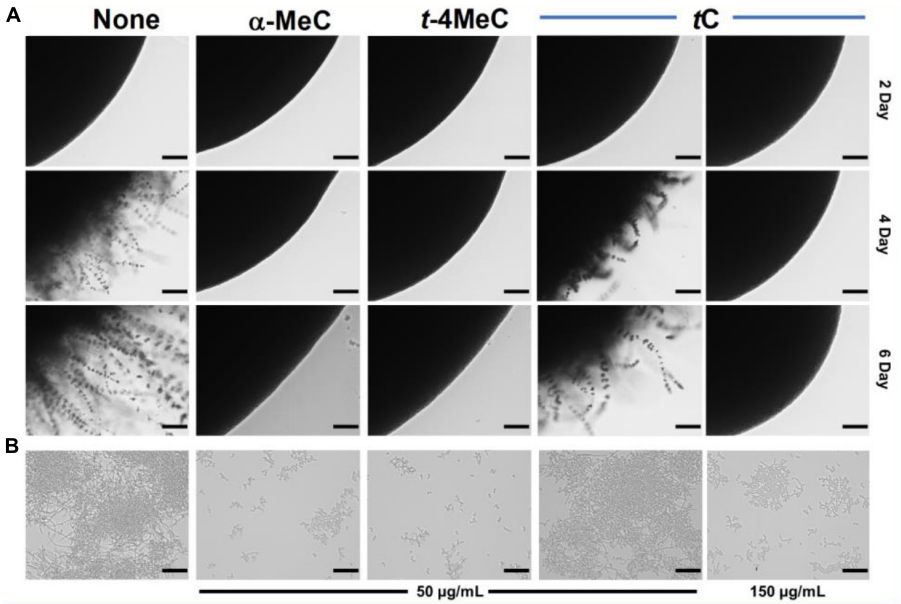


**FIGURE 2 |** Inhibition of hyphal filamentation and aggregation by α-methyl cinnamaldehyde (α-MeC) and *trans*-4-methyl cinnamaldehyde (*t*-4MeC). *C. albicans* DAY185 was streaked onto PDA solid plates in the absence or presence of α-methyl cinnamaldehyde (α-MeC; 50 μg/mL), *trans*-4-methyl cinnamaldehyde (*t*-4MeC; 50 μg/mL), or *trans*-cinnamaldehyde (*t*C; 50 and 150 μg/mL). Colony morphologies were observed periodically over 6 days at 37°C **(A)**, *C. albicans* DAY185 yeast-hyphae transition was assessed in PDB in the presence of α-methyl cinnamaldehyde (α-MeC; 50 μg/mL), *trans*-4-methyl cinnamaldehyde (*t*-4MeC; 50 μg/mL), or *trans*-cinnamaldehyde (*t*C; 50 and 150 μg/mL) after incubation for 24 h **(B)**. The scale bars in panels **(A,B)** represent 100 μm. None indicates the non-treated control.

was assessed by observing cell aggregation and hyphae formation. After 24 h incubation in PDB medium, large cell aggregates intertwined by hyphae were observed in non-treated controls. At 50 μg/mL both analogs significantly inhibited filamentation and cell aggregation of *C. albicans* DAY185 as compared with that of non-treated controls (**Figure 2B**). *Trans*-cinnamaldehyde had no effect on yeast-hyphae transition at 50 μg/mL, but at 150 μg/mL inhibited the filamentation and aggregation of *C. albicans* DAY185. In case of *C. albicans* ATCC 10231, both analogs at 20 and 50 μg/mL significantly inhibited filamentation and cell aggregation while similar filamentation was observed with *trans*-cinnamaldehyde at 20, 50, and 150 μg/mL. Thus, the *C. albicans* morphology confirms that α-methyl and *trans*-4-methyl cinnamaldehydes inhibit yeast-hypha transition and are more active than *trans*-cinnamaldehyde (**Supplementary Figures S2B, S3B**).

## Microscopic Examination of *C. albicans* Biofilm Inhibition by α-Methyl and *Trans*-4-Methyl Cinnamaldehydes

*Candida albicans* biofilm inhibition was analyzed by confocal laser scanning microscopy. In the non-treated control, *C. albicans* formed dense biofilms (thickness > 52 μm and achieved almost 100% surface coverage) after culture for 24 h, whereas the presence of α-methyl or *trans*-4-methyl cinnamaldehydes at 50 μg/mL dramatically reduced biofilm densities and thicknesses. On the other hand, *trans*-cinnamaldehyde at 50 μg/mL had no effect (**Figure 3A**). Effects on biofilm formation were also measured using COMSTAT biofilm software. Specifically, biofilm biomass, mean thickness, and substrate coverage were reduced by α-methyl and *trans*-4-methyl cinnamaldehydes by > 98% vs. non-treated controls (**Figure 3B**).

In addition, the antibiofilm activities of α-methyl and *trans*-4-methyl cinnamaldehydes at 50 μg/mL against *C. albicans* DAY185 were examined by SEM. Entirely grown biofilms containing fully formed hyphae were observed on nylon membranes in the absence of cinnamaldehydes (**Figure 3C**). Interestingly, hyphae formation significantly decreased in the presence of α-methyl or *trans*-4-methyl cinnamaldehydes, whereas no inhibition was observed in the presence of *trans*-cinnamaldehyde (**Figure 3C**). These observations were in accord with our biofilm formation assay results (**Figure 1D**). Furthermore, biofilms grown in presence of α-methyl or *trans*-4-methyl cinnamaldehydes had fewer and shorter hyphae and were predominantly composed of yeast and pseudohyphal cells, whereas treatment with *trans*-cinnamaldehyde had no observable effect. Collectively, these results show that α-methyl and *trans*-4-methyl cinnamaldehydes potently inhibit *C. albicans* hyphal formation, cell aggregation, and biofilm formation.

## Gene Expression Changes in *C. albicans* After Treatment by α-Methyl and *Trans*-4-Methyl Cinnamaldehydes

qRT-PCR was used to investigate gene expressions of ten biofilm- and hypha-related genes after treating *C. albicans* with α-methyl or *trans*-4-methyl cinnamaldehydes. Transcriptional

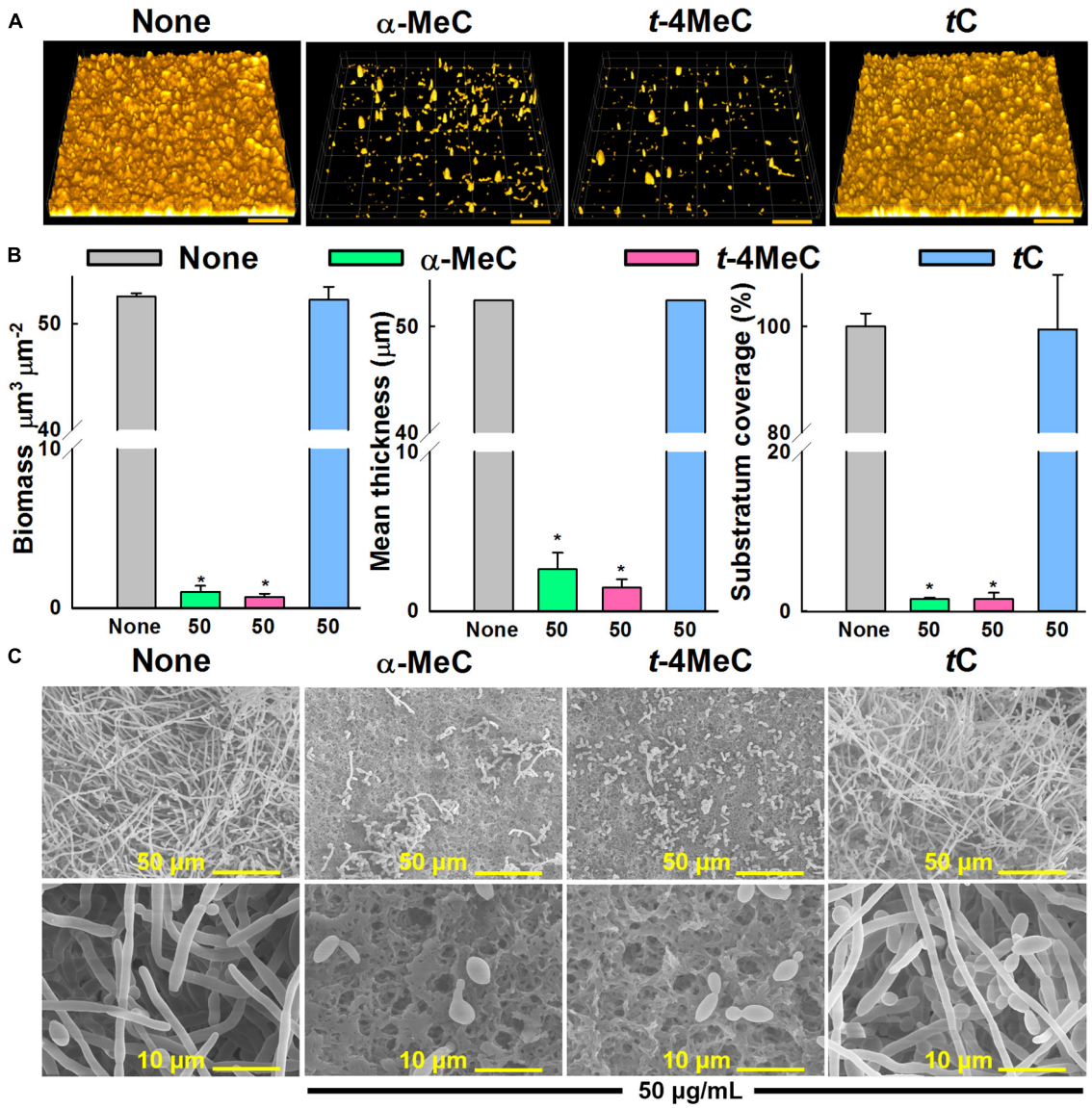


**FIGURE 3 |** Effect of α-methyl (α-MeC) and *trans*-4-methyl (*t*-4MeC) cinnamaldehydes on *C. albicans* DAY185 biofilms. *C. albicans* DAY185 biofilm formation in the presence of α-methyl cinnamaldehyde (α-MeC), *trans*-4-methyl cinnamaldehyde (*t*-4MeC), or *trans*-cinnamaldehyde (*t*C) at 50 μg/mL was examined by confocal laser microscopy **(A)**, *C. albicans* DAY185 biofilm formations were quantified by COMSTAT analysis **(B)**, *C. albicans* DAY185 biofilm formations on nylon membranes grown in the presence of α-methyl cinnamaldehyde (α-MeC), *trans*-4-methyl cinnamaldehyde (*t*-4MeC), or *trans*-cinnamaldehyde (*t*C) at 50 μg/mL were observed by SEM **(C)**. The scale bars in panel **(A)** represent 100 μm and in panel **(B)** represent 50 and 10 μm. Error bars indicate standard deviations. *$P < 0.05$ vs. non-treated controls (None). None indicates biofilm formation without treatment after 24 h incubation.

changes observed after treatment with α-methyl or *trans*-4-methyl cinnamaldehydes at 50 μg/mL were similar (**Figure 4A**). Notably, the expressions of three key biofilm- and hypha-related genes, namely, *ECE1* (hypha-specific protein, also known as *HWP2*), *UCF1* (filamentous growth), and *UME6* (filament-specific regulator) were repressed by both cinnamaldehyde analogs. For example, α-methyl cinnamaldehyde downregulated *ECE1, IFD6* (alcohol dehydrogenase), and *UCF1* by 12-, 2.8- and 48-fold respectively, and *trans*-4-methyl cinnamaldehyde downregulated *ECE1*, *RBT5* (GPI-modified cell wall protein), *UCF1*, and *UME6* by 5-, 6-, 54-, and 4-fold respectively. While, both α-methyl and *trans*-4-methyl cinnamaldehydes upregulated the expressions of *YWP1* (yeast form wall protein 1) by 26- and 17-fold, respectively (**Supplementary Table S2**). On the other hand, the expressions of other biofilm and hyphae-related genes (*ALS3*, *HWP1*, and *RAS1*) were unaffected by α-methyl and *trans*-4-methyl cinnamaldehydes. Although α-methyl cinnamaldehyde upregulated *CHT4* (chitinase 4) by 4.6-fold but did not affect *UME6*. In contrast, *trans*-4-methyl cinnamaldehyde had no effect on *CHT4* and *IFD6*. qRT-PCR findings showed that α-methyl and *trans*-4-methyl cinnamaldehydes significantly downregulated biofilm- and hyphae-related genes (i.e., *ECE1, IFD6*, *RBT5*, *UCF1,*

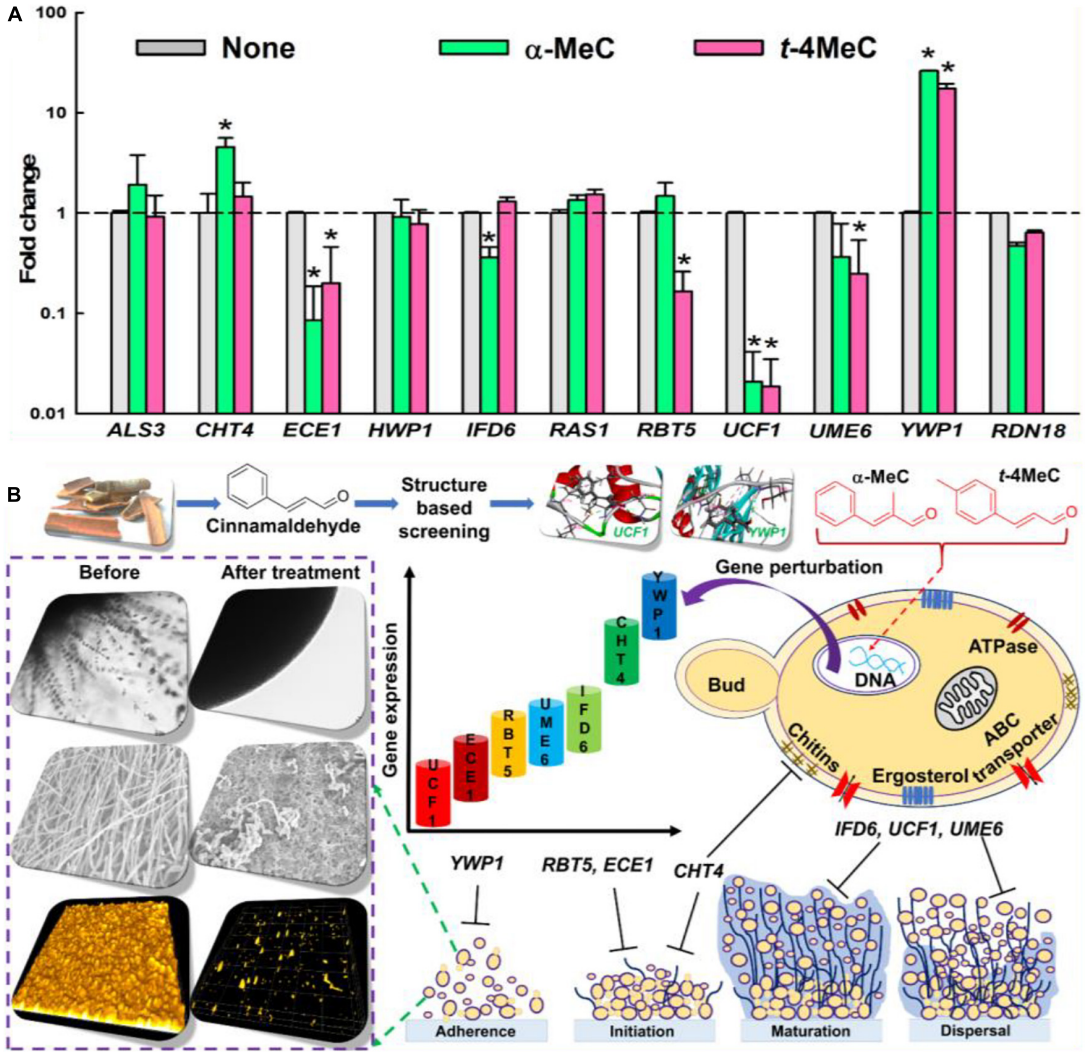


**FIGURE 4 |** The relative transcriptional profile of ten biofilm- and hypha-related genes. *C. albicans* DAY185 cells incubated with or without α-methyl cinnamaldehyde (α-MeC) or *trans*-4-methyl cinnamaldehyde (*t*-4MeC) at 50 μg/mL for 6 h and relative transcriptional expressions profiles were obtained by qRT-PCR. Fold changes represent alteration in the transcription of treated vs. untreated *C. albicans* DAY185. *RDN18* was used for endogenous normalization of expression levels and the experiment was performed in duplicate (six qRT-PCR reactions were performed per gene) **(A)**. A plausible mechanism of *C. albicans* biofilm inhibition by α-methyl cinnamaldehyde (α-MeC) and *trans*-4-methyl cinnamaldehyde (*t*-4MeC) illustrating all the phenotypic and gene expressional changes **(B).** Error bars indicate standard deviations. *$P < 0.05$ vs. non-treated controls (None).

and *UME6*) and upregulated biofilm-related genes *CHT4*, and *YWP1* (**Figure 4A**). Collectively, a plausible mode of action of *C. albicans* biofilm inhibition was depicted to illustrate all of the phenotypic and gene expressional changes caused by α-methyl and *trans*-4-methyl cinnamaldehydes (**Figure 4B**).

## Molecular Docking of α-Methyl, or *Trans*-4-Methyl Cinnamaldehydes With UCF1 or YWP1 to Reveal the Molecular Interaction Profiles

Molecular dockings were carried out to investigate the molecular interactions between α-methyl and *trans*-4-methyl cinnamaldehydes with amino acid residues of UCF1 and YWP1 proteins, respectively, based on the results obtained in qRT-PCR assay, where, potent antibiofilm agents α-methyl and *trans*-4-methyl cinnamaldehydes, highly downregulated *UCF1* and upregulated *YWP1* genes, respectively (**Figure 4A**). The binding affinities of α-methyl, *trans*-4-methyl, and *trans*-cinnamaldehydes with the predicted active binding sites of UCF1 and YWP1 fell in the ranges −5.4 to −5.9 kcal/mol and −4.4 to −4.9 kcal/mol, respectively. α-Methyl, *trans*-4-methyl, and *trans*-cinnamaldehydes exhibited binding energies of −5.78, −5.84, and −5.45 kcal/mol, respectively, with the active binding domain of UCF1 (**Figures 5A–C** and **Table 1**), and binding energies −4.86, −4.55, and −4.42 kcal/mol, respectively, with the active binding domain of YWP1 (**Figures 5D–F** and **Table 1**). α-Methyl, *trans*-4-methyl, and *trans*-cinnamaldehydes formed

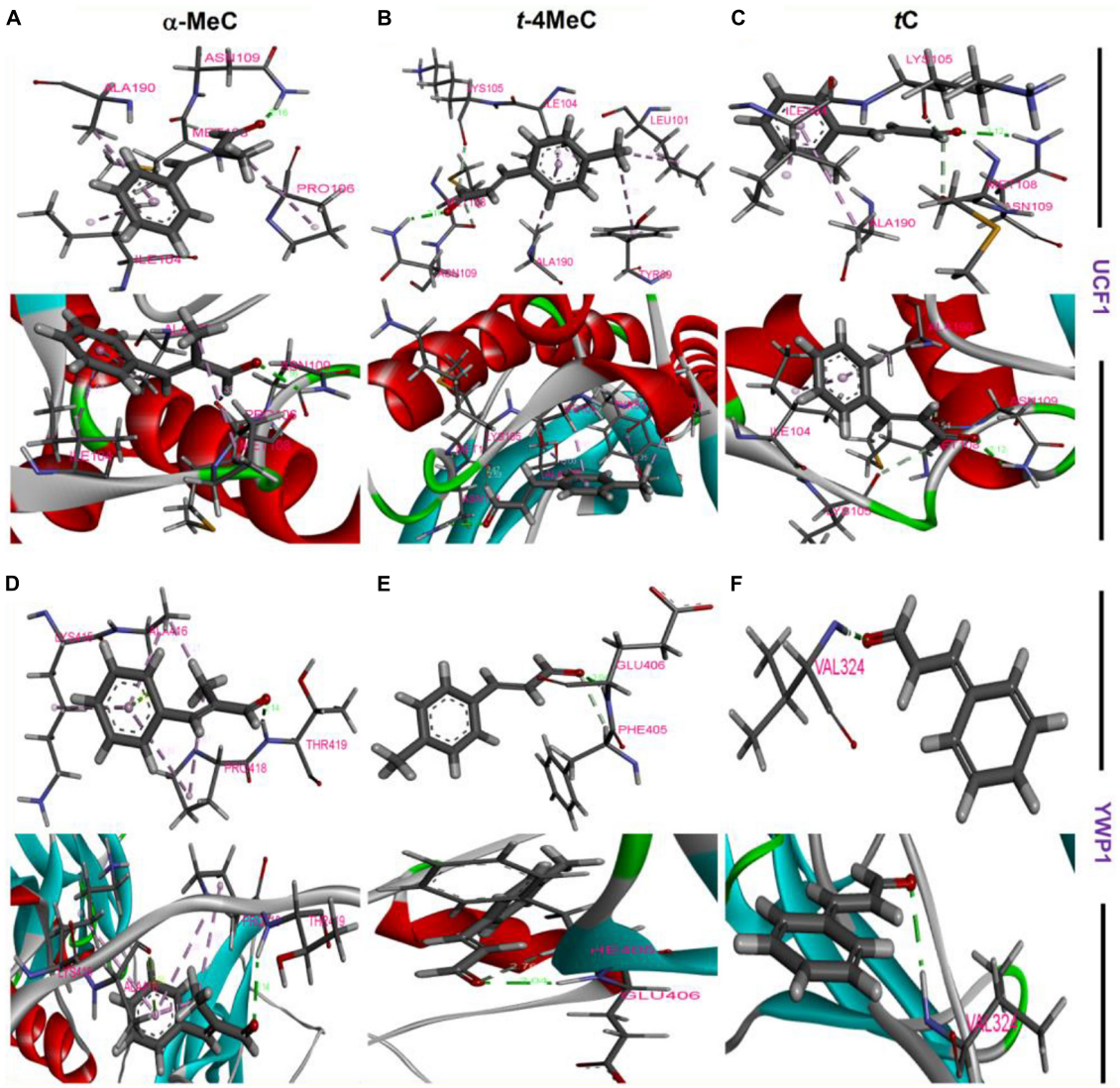


**FIGURE 5 |** Amino acid residue interactions between UCF1 receptor protein and α-methyl cinnamaldehyde (α-MeC) **(A)**, *trans*-4-methyl cinnamaldehyde (*t*-4MeC) **(B)**, and *trans*-cinnamaldehyde (*t*C) **(C)**, Amino acid residue interactions between YWP1 receptor protein and α-methyl cinnamaldehyde (α-MeC) **(D)**, *trans*-4-methyl cinnamaldehyde (*t*-4MeC) **(E)**, and *trans*-cinnamaldehyde (*t*C) **(F)**.

three π-π, six π-π, or four π-π and one hydrogen bond with Ile104, Pro106, Met108, Asn109, and Ala190; Tyr89, Leu101, Ile104, Lys105, Met108, Asn109, and Ala190; or Ile104, Lys105, Met108, Asn109, and Ala190 amino acid residues of UCF1, respectively (**Table 1**). Likewise, α-methyl, *trans*-4-methyl, or *trans*-cinnamaldehydes formed four π-π and two hydrogen bonds, one π-π and one hydrogen bond, or one hydrogen bond with Lys415, Ala416, Pro418, Thr419; Phe405, Glu406; or Val324 amino acid residues of YWP1, respectively (**Table 1**). Also, cluster analysis revealed the number of possible binding positions with UCF1 and YWP1 (**Supplementary Figure S4**). These qRT-PCR and molecular docking results are compatible for biofilm inhibition since downregulated *UCF1* plays a crucial role in filamentous growth (El Khoury et al., 2018) and upregulated *YWP1* gene has antiadhesive effect and plays a role in biofilm dispersion (Mccall et al., 2019). Overall, the molecular dockings of α-methyl and *trans*-4-methyl cinnamaldehydes were more coherent than that of *trans*-cinnamaldehyde.

## Anthelmintic Activities of the Eleven Cinnamaldehyde Analogs as Determined Using *in vivo* Nematode *C. elegans* Model

To investigate another possible application for cinnamaldehyde analogs, we investigated their anthelmintic activities using *in vivo C. elegans* model. During initial screening, several cinnamaldehyde analogs, that is, cinnamaldehyde oxime, 4-dimethylamino, 4-fluoro, α-methyl, 4-nitro, and *trans*-4-methyl cinnamaldehydes at 50 μg/mL displayed nematicidal activities

**TABLE 1 |** Binding energies of targeted ligands with UCF1 or YWP1 proteins.

| Compounds | Receptor | Binding energy (Kcal/mol) AUTODOCK | Indicating amino acids | Bonds |
|---|---|---|---|---|
| α-Methyl cinnamaldehyde | UCF1 | −5.7 | Ile104, Pro106, Met108, Asn109, Ala190 | 3π−π, 1H |
| *trans*-4-Methyl cinnamaldehyde | UCF1 | −5.84 | Tyr89, Leu101, Ile104, Lys105, Met108, Asn109, Ala190 | 6π−π, 1H |
| *trans*-Cinnamaldehyde | UCF1 | −5.45 | Ile104, Lys105, Met108, Asn109, Ala190 | 4π−π, 1H |
| α-Methyl cinnamaldehyde | YWP1 | −4.86 | Lys415, Ala416, Pro418, Thr419 | 4π−π, 2H |
| *trans*-4-Methyl cinnamaldehyde | YWP1 | −4.55 | Phe405, Glu406 | 1π−π, 1H |
| *trans*-Cinnamaldehyde | YWP1 | −4.42 | Val324 | 1H |

*Amino acid residues essentially required for binding are colored blue.*

by killing all worms over 5 days (**Figure 6**). While 2-methoxy, 2-nitro, and one positive *trans*-cinnamaldehydes exhibited only minor nematicidal activity at concentrations ≥ 100 μg/mL over 5 days. 4-Bromo and 4-chloro cinnamaldehydes had the most potent nematicidal activities and achieved 100% killing at 10 and 20 μg/mL, respectively, at 2 days of exposure (**Figure 6**).

## Surface Morphology of *C. elegans* After Treatment With 4-Bromo or 4-Chloro Cinnamaldehydes

Scanning electron microscopy was used to investigate the effects of 4-bromo and 4-chloro cinnamaldehydes on *C. elegans*. 4-Bromo and 4-chloro cinnamaldehydes induced slight structural changes to the cuticle of *C. elegans*. For example, non-treated controls showed smooth circumferential ridges (annuli) and furrows of cuticle, whereas worms treated with 20 μg/mL of 4-bromo or 4-chloro cinnamaldehydes had slightly shriveled cuticles with moderately uniform ridge formations and were shrunken as compared with non-treated controls. *Trans*-cinnamaldehyde at 20 μg/mL had little effect on *C. elegans* (**Supplementary Figure S5**). Taken together both 4-bromo and 4-chloro cinnamaldehydes caused surface morphological changes to the cuticle of *C. elegans*, which confirmed their anthelmintic potentials.

## Cinnamaldehyde Analogs Exhibit Drug-Like Properties

*In silico* pharmacokinetic properties were examined to investigate the possible therapeutic uses of the potent cinnamaldehyde analogs. All potent cinnamaldehyde analogs were scrutinized for compliance with Lipinski's "rule-of-five" to check their ADME properties. Topological polar surface area (TPSA), molecular weight, lipophilicity, and solubility were examined to predict abilities of drugs to cross membranes. All potent cinnamaldehyde analogs had a log *P* of < 5, a molecular weight < 500, and ≤ 10 hydrogen bond acceptors or ≤ 5 hydrogen bond donors, and a TPSA of < 120 $Å^2$. Specifically, 4-bromo, 4-chloro, α-methyl, *trans*-4-methyl or *trans*-cinnamaldehydes had log *P* values in the range 1.9–2.7, molecular weights in the range 130–220 g/moL, one hydrogen bond acceptor and no hydrogen bond donor and a TPSA of 17.07$Å^2$ (**Supplementary Figure S6** and **Supplementary Table S3**). Additionally, all potent cinnamaldehyde analogs exhibited an ability to cross the blood-brain barrier and high gastrointestinal absorptions (**Supplementary Figure S6** and **Supplementary Table S3**). Furthermore, none of the potent cinnamaldehyde analogs violated Lipinski's "rule-of-five," which suggested all have therapeutic potential.

# DISCUSSION

Based on structure similarities, we screened out cost-effective cinnamaldehyde analogs that inhibit biofilm formation rather than cell growth to reduce the risk of drug-resistance development. Remarkably, the substitution of methyl on aromatic ring of cinnamaldehyde may be responsible for the potent antibiofilm effect. As previously reported (Brackman et al., 2011) that electron withdrawing group enhanced the activity of cinnamaldehyde analogs, we speculate that our cinnamaldehyde analogs may work in the similar manner. Furthermore, presence of α, β-unsaturated carbonyl pharmacophore in cinnamaldehyde analog structures may serve as biological essential group (Chen et al., 2017). These electrophilic acceptors could react with nucleophiles by Michael type addition resulting in cinnamaldehyde analogs-receptor conjugates which probably suggest potent activities of the cinnamaldehyde. Meanwhile, α-methyl and *trans*-4-methyl cinnamaldehydes at sub-MIC concentrations inhibited biofilms formation more than *trans*-cinnamaldehyde by inhibiting hyphae formation. Hyphae assays and SEM results showed that α-methyl and *trans*-4-methyl cinnamaldehydes inhibited *C. albicans* filamentation markedly more than *trans*-cinnamaldehyde and that observed in non-treated controls (**Figures 2**, **3C**). Interestingly, *trans*-cinnamaldehyde at 50 μg/mL had no effect on biofilm formation by *C. albicans* DAY185 or ATCC 10231, which contrasts with reports (Ying et al., 2019; Miranda-Cadena et al., 2021) that it is effective against different strains of *C. albicans,* and suggests *trans*-cinnamaldehyde inhibits biofilm formation at higher concentrations. These results concur with the findings of Taguchi et al. (2013), who concluded cinnamaldehyde acts against *C. albicans* in two different ways, that is, by inhibiting mycelial growth and killing activity by causing membrane damage. *Trans*-cinnamaldehyde has also been reported to disrupt the activities of mitochondria, cell-wall synthesizing enzyme β-1-3-glucan, and chitin in other organisms (Bang et al., 2000; Ka et al., 2003).

Interestingly, our qRT-PCR studies showed that the down-regulations of *ECE1*, *IFD6*, *RBT5*, *UCF1*, and *UME6* in *C. albicans* cells by α-methyl and *trans*-4-methyl cinnamaldehydes (**Figure 4A**). Specifically, *ECE1* is essential for hyphal development and their expressions have been shown to be correlated with cell elongation and biofilm formation

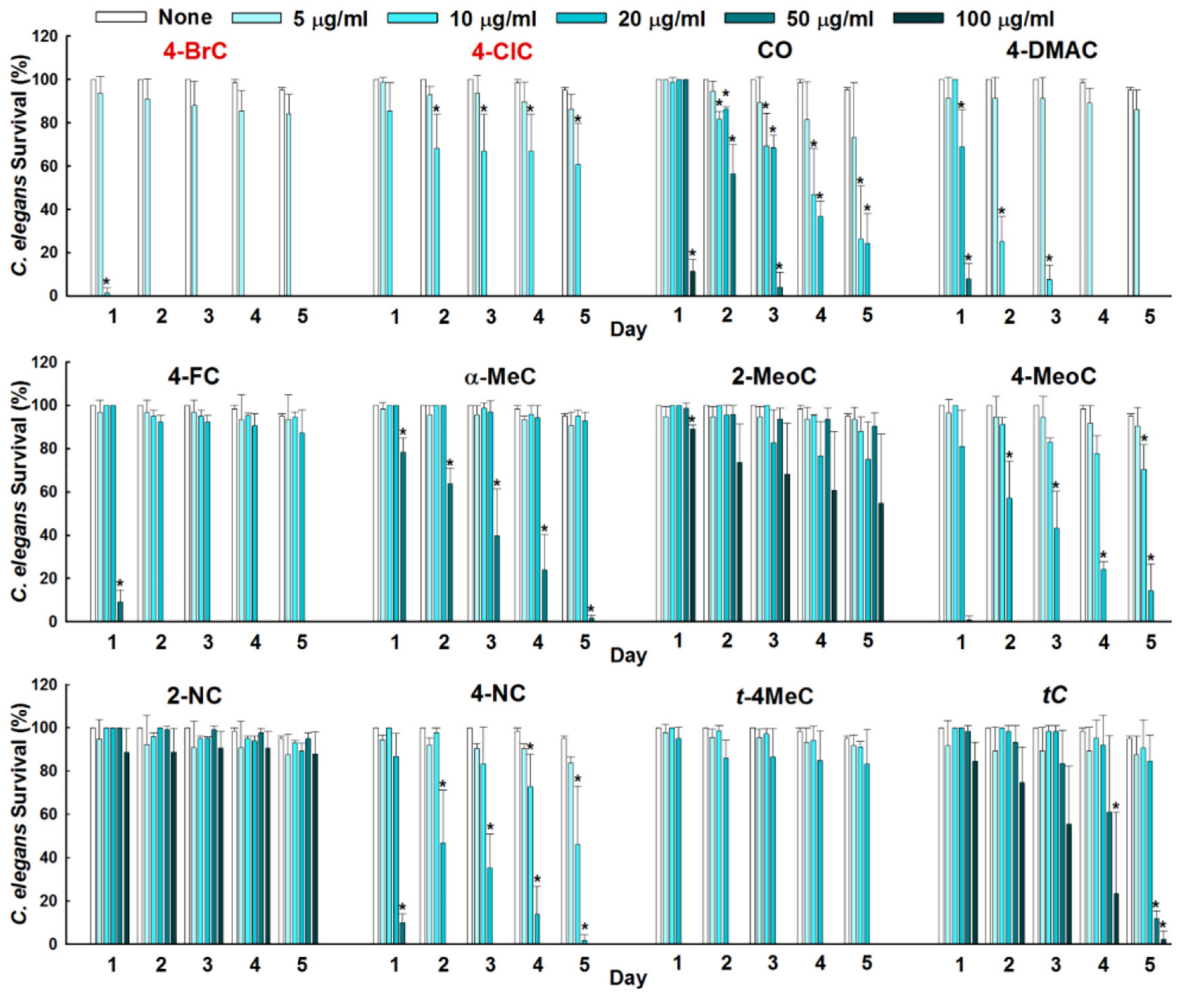


**FIGURE 6 |** Anthelmintic activities of cinnamaldehyde analogs were evaluated against *C. elegans* for 5 days. Error bars indicate standard deviations. *$P < 0.05$ vs. non-treated controls (None).

(Lee et al., 2021). *RBT5* which putatively encodes GPI-modified cell wall protein (Perez et al., 2006). *IFD6* negatively affects the matrix production (Nobile et al., 2009). *UCF1* plays major role in filamentous growth and *UME6* is a filament specific regulator of *C. albicans* hyphal extension and enhances the biofilm formation (Banerjee et al., 2013; El Khoury et al., 2018). Moreover, *CHT4*, and *YWP1* genes were upregulated in favor of biofilm inhibition, as upregulation of *CHT4* suggested the degradation of chitin in cell wall (Drakulovski et al., 2011) and *YWP1* has antiadhesive effect and plays a role in biofilm dispersion (Mccall et al., 2019). It has been reported that *C. verum* essential oils significantly downregulated the expressions of another set of biofilm or hypha related genes, namely, *RAS*, *EFG1*, *CYR*, *CPH*, *HWP1*, *ALS3*, *SAP2*, *SAP4*, *SAP5*, *SAP6*, and *HST7*, and up-regulated *NRG* in *C. albicans* (Essid et al., 2019). Also, Khan et al. (2017) reported cinnamaldehyde downregulated *HWP1* expression, whereas we found cinnamaldehyde treatment did not affect the expressions of *RAS*, *ALS3*, or *HWP1*. Consequently, it is confirmed that treatments with α-methyl and *trans*-4-methyl cinnamaldehydes inhibited biofilm formation of *C. albicans* by inducing phenotypic and gene expressional changes *via* hyphal growth inhibition.

The conformation interaction of UCF1 with α-methyl, and *trans*-4-methyl cinnamaldehydes showed that common amino acid residues such as Ile104, Met108, Asn109, and Ala190 are essential for the molecular interaction. Also, α-methyl, and *trans*-4-methyl cinnamaldehydes with YWP1 protein formed the conformation interaction with Lys415, Ala416, Pro418, Thr419, Phe405, Glu406, and Val324 amino acid residues. Gene expression and molecular interaction studies revealed that α-methyl, and *trans*-4-methyl cinnamaldehydes might work as antibiofilm agents *via* inhibiting filament and suppressing adhesive effect of *C. albicans*.

Cinnamaldehyde and its analog cinnamaldehyde oxime are well-known nematicides and natural alternatives to synthetic anthelmintic agents and pesticides against the animal and plant parasites *Ascaris suum* and *Meloidogyne incognita*

(Williams et al., 2015; Ferreira Barros et al., 2021). According to our findings, cinnamaldehyde analogs have anthelmintic activity and 4-bromo and 4-chloro cinnamaldehydes were the most active at 10 and 20 μg/mL, respectively. Lu et al. (2020) suggested that cinnamaldehyde disrupts glutathione metabolism and found that at 800 μg/mL caused 100% *C. elegans* mortality, which is several fold higher than the mortality rates observed for the cinnamaldehyde analogs tested in the present study (5–100 μg/mL). Slight surface morphological changes to the cuticle of *C. elegans* by 4-bromo and 4-chloro cinnamaldehydes confirmed their anthelmintic effects. Ropiak et al. (2016) reported that higher concentrations (2 mM) of *trans*-cinnamaldehyde are required to cause morphological changes to *C. elegans* cuticles. Also, Williams et al. (2015) reported marked damage to digestive tissues and the muscular layer in *A. suum* after treatment with cinnamaldehydes as a anthelmintic agents. Besides, Brackman et al. (2011) reported that *trans*-cinnamaldehyde has $IC_{50}$ value of 77 μM against MRC-5 cells, which suggests that the therapeutic window of cinnamaldehyde analogs may be high enough for therapeutic applications in humans and animals. Moreover, Lipinski's "rule-of-five" summarizes vital molecular pharmacokinetic properties of compounds that predict their potential applicability's as oral drugs (Benet et al., 2016). All potent cinnamaldehyde analogs examined exhibited drug-like properties and did not violate the "rule-of-five" (**Supplementary Figure S6**). These tested cinnamaldehyde analogs may work well toward human cell lines; therefore, it is needed to test their toxicity toward *in vivo* models.

Thus, our observations suggest α-methyl and *trans*-4-methyl cinnamaldehydes can be used as a potential molecule for further drug discovery as multitargets antibiofilm molecules and that 4-bromo and 4-chloro cinnamaldehydes might be used as anthelmintic agents for the development of new therapeutic candidates.

## CONCLUSION

Novel antivirulence agents are required to address the challenges posed by drug-resistant microorganisms. Our *in vitro* studies collectively showed that α-methyl and *trans*-4-methyl cinnamaldehydes inhibited *C. albicans* biofilm formation without killing *C. albicans*. Also, our potent cinnamaldehyde analogs act as suppressors of the *UCF1* and *YWP1* genes in *C. albicans*. These compounds can be considered to treat persistent infections either singly or in combination or as adjunctive treatments. In addition, 4-bromo and 4-chloro cinnamaldehydes exhibited potent anthelmintic effects and can be used as anthelmintic agents. Hence, the present study demonstrates cinnamaldehyde analogs can serve as potential molecules to provide a basis to design effective drug molecules for the treatment of multidrug-resistant microbial agents causing human infections.

## DATA AVAILABILITY STATEMENT

The original contributions presented in the study are included in the article/**Supplementary Material**, further inquiries can be directed to the corresponding author/s.

## AUTHOR CONTRIBUTIONS

SK and JL: conceptualization. SK, J-HL, and VR: methodology. SK and VR: software. SK, VR, J-HL, and Y-GK: validation and formal analysis and investigation. JL: resources. SK, VR, and JL: data curation, writing of the manuscript, and visualization. J-HL and JL: project administration. All authors have read and agreed to the published version of the manuscript.

## FUNDING

This work was supported by the Priority Research Centers Program through the National Research Foundation of Korea (NRF) funded by the Ministry of Education (Grant No. 2014R1A6A1031189), by the Basic Science Research Program through the NRF funded by the Ministry of Education (Grant No. 2021R1I1A3A04037486), and by an NRF grant funded by the Korea government (MSIT) (Grant No. 2021R1A2C1008368).

## SUPPLEMENTARY MATERIAL

The Supplementary Material for this article can be found online at: https://www.frontiersin.org/articles/10.3389/fmicb.2022.818165/full#supplementary-material

## REFERENCES

Amalaradjou, M. A., and Venkitanarayanan, K. (2011). Effect of *trans*-cinnamaldehyde on inhibition and inactivation of *Cronobacter sakazakii* biofilm on abiotic surfaces. *J. Food Prot.* 74, 200–208. doi: 10.4315/0362-028X.JFP-10-296

Amin-Ul Mannan, M., Sharma, S., and Ganesan, K. (2009). Total RNA isolation from recalcitrant yeast cells. *Anal. Biochem.* 389, 77–79. doi: 10.1016/j.ab.2009.03.014

Banerjee, M., Uppuluri, P., Zhao, X. R., Carlisle, P. L., Vipulanandan, G., Villar, C. C., et al. (2013). Expression of *UME6*, a key regulator of *Candida albicans* hyphal development, enhances biofilm formation via Hgc1- and Sun41-dependent mechanisms. *Eukaryot. Cell* 12, 224–232. doi: 10.1128/EC.00163-12

Bang, K. H., Lee, D. W., Park, H. M., and Rhee, Y. H. (2000). Inhibition of fungal cell wall synthesizing enzymes by *trans*-cinnamaldehyde. *Biosci. Biotechnol. Biochem.* 64, 1061–1063. doi: 10.1271/bbb.64.1061

Beema Shafreen, R. M., Selvaraj, C., Singh, S. K., and Karutha Pandian, S. (2014). *In silico* and *in vitro* studies of cinnamaldehyde and their derivatives against LuxS in *Streptococcus pyogenes*: effects on biofilm and virulence genes. *J. Mol. Recognit.* 27, 106–116.

Benet, L. Z., Hosey, C. M., Ursu, O., and Oprea, T. I. (2016). BDDCS, the Rule of 5 and drugability. *Adv. Drug Deliv. Rev.* 101, 89–98. doi: 10.1016/j.addr.2016.05.007

Brackman, G., Celen, S., Hillaert, U., Van Calenbergh, S., Cos, P., Maes, L., et al. (2011). Structure-activity relationship of cinnamaldehyde analogs as inhibitors of AI-2 based quorum sensing and their effect on virulence of *Vibrio* spp. *PLoS One* 6:e16084. doi: 10.1371/journal.pone.0016084

Brackman, G., Defoirdt, T., Miyamoto, C., Bossier, P., Van Calenbergh, S., Nelis, H., et al. (2008). Cinnamaldehyde and cinnamaldehyde derivatives reduce virulence in *Vibrio* spp. by decreasing the DNA-binding activity of the quorum sensing response regulator LuxR. *BMC Microbiol.* 8:149. doi: 10.1186/1471-2180-8-149

Brenner, S. (1974). The genetics of *Caenorhabditis elegans*. *Genetics* 77:71.

Burns, A. R., Luciani, G. M., Musso, G., Bagg, R., Yeo, M., Zhang, Y., et al. (2015). *Caenorhabditis elegans* is a useful model for anthelmintic discovery. *Nat. Commun.* 6:7485.

CDC (2019). *Antibiotic resistance threats in the United States*. Atlanta, GA: U.S. Department of Health and Human Services, CDC.

Cegelski, L., Marshall, G. R., Eldridge, G. R., and Hultgren, S. J. (2008). The biology and future prospects of antivirulence therapies. *Nat. Rev. Microbiol.* 6, 17–27. doi: 10.1038/nrmicro1818

Chandra, J., Kuhn, D. M., Mukherjee, P. K., Hoyer, L. L., Mccormick, T., and Ghannoum, M. A. (2001). Biofilm formation by the fungal pathogen *Candida albicans*: development, architecture, and drug resistance. *J. Bacteriol.* 183, 5385–5394. doi: 10.1128/JB.183.18.5385-5394.2001

Chen, B.-J., Fu, C.-S., Li, G.-H., Wang, X.-N., Lou, H.-X., Ren, D.-M., et al. (2017). Cinnamaldehyde analogues as potential therapeutic agents. *Mini Rev. Med. Chem.* 17, 33–43. doi: 10.2174/1389557516666160121120744

Cheng, S. S., Liu, J. Y., Huang, C. G., Hsui, Y. R., Chen, W. J., and Chang, S. T. (2009). Insecticidal activities of leaf essential oils from *Cinnamomum osmophloeum* against three mosquito species. *Bioresour. Technol.* 100, 457–464. doi: 10.1016/j.biortech.2008.02.030

Cheng, S. S., Liu, J. Y., Tsai, K. H., Chen, W. J., and Chang, S. T. (2004). Chemical composition and mosquito larvicidal activity of essential oils from leaves of different *Cinnamomum osmophloeum* provenances. *J. Agric. Food Chem.* 52, 4395–4400. doi: 10.1021/jf0497152

CLSI (2017). *CLSI. Reference method for broth dilution antifungal susceptibility testing of yeasts. 4th ed. CLSI standard M27*. Wayne,PA: Clinical and laboratory standards institute.

Costerton, J. W., Stewart, P. S., and Greenberg, E. P. (1999). Bacterial biofilms: a common cause of persistent infections. *Science* 284, 1318–1322. doi: 10.1126/science.284.5418.1318

Da Nobrega Alves, D., Monteiro, A. F. M., Andrade, P. N., Lazarini, J. G., Abilio, G. M. F., et al. (2020). Docking prediction, antifungal activity, anti-biofilm effects on *Candida* spp., and toxicity against human cells of cinnamaldehyde. *Molecules* 2020:25. doi: 10.3390/molecules25245969

Daina, A., Michielin, O., and Zoete, V. (2017). SwissADME: a free web tool to evaluate pharmacokinetics, drug-likeness and medicinal chemistry friendliness of small molecules. *Sci. Rep.* 7:42717. doi: 10.1038/srep42717

De Oliveira, D. B. C., Silva, L. B., Da Silva, B. V., Borges, T. C., Marques, B. C., Dos Santos, M. B., et al. (2019). A new acridone with antifungal properties against *Candida* spp. and dermatophytes, and antibiofilm activity against *C. albicans*. *J. Appl. Microbiol.* 127, 1362–1372. doi: 10.1111/jam.14381

Diawara, A., Halpenny, C. M., Churcher, T. S., Mwandawiro, C., Kihara, J., Kaplan, R. M., et al. (2013). Association between response to albendazole treatment and β-tubulin genotype frequencies in soil-transmitted helminths. *PLoS Negl. Trop. Dis.* 7:e2247. doi: 10.1371/journal.pntd.0002247

Doyle, A. A., and Stephens, J. C. (2019). A review of cinnamaldehyde and its derivatives as antibacterial agents. *Fitoterapia* 139:104405. doi: 10.1016/j.fitote.2019.104405

Drakulovski, P., Dunyach, C., Bertout, S., Reynes, J., and Mallié, M. (2011). A *Candida albicans* strain with high MIC for caspofungin and no *FKS1* mutations exhibits a high chitin content and mutations in two chitinase genes. *Med. Mycol.* 49, 467–474. doi: 10.3109/13693786.2010.538732

El Khoury, P., Awad, A., Wex, B., and Khalaf, R. A. (2018). Proteomic analysis of a *Candida albicans pir32* null strain reveals proteins involved in adhesion, filamentation and virulence. *PLoS One* 13:e0194403. doi: 10.1371/journal.pone.0194403

Essid, R., Gharbi, D., Abid, G., Karkouch, I., Hamouda, T. B., Fares, N., et al. (2019). Combined effect of *Thymus capitatus* and *Cinnamomum verum* essential oils with conventional drugs against *Candida albicans* biofilm formation and elucidation of the molecular mechanism of action. *Ind. Crops. Prod.* 140:111720.

Fang, S.-H., Rao, Y. K., and Tzeng, Y. (2004). Cytotoxic effect of *trans*-cinnamaldehyde from *Cinnamomum osmophloeum* leaves on human cancer cell lines. *Int. J. Appl. Sci. Eng.* 2, 136–147.

Ferreira Barros, A., Paulo Campos, V., Lopes, De Paula, L., Alaís Pedroso, L., De Jesus Silva, F., et al. (2021). The role of *Cinnamomum zeylanicum* essential oil, (*E*)-cinnamaldehyde and (*E*)-cinnamaldehyde oxime in the control of *Meloidogyne incognita*. *J. Phytopathol.* 169, 229–238.

Firmino, D. F., Cavalcante, T. T. A., Gomes, G. A., Firmino, N. C. S., Rosa, L. D., De Carvalho, M. G., et al. (2018). Antibacterial and antibiofilm activities of *Cinnamomum* Sp. essential oil and cinnamaldehyde: antimicrobial activities. *ScientificWorldJournal* 2018:7405736. doi: 10.1155/2018/7405736

Friedman, M. (2017). Chemistry, antimicrobial mechanisms, and antibiotic activities of cinnamaldehyde against pathogenic bacteria in animal feeds and human foods. *J. Agric. Food. Chem.* 65, 10406–10423. doi: 10.1021/acs.jafc.7b04344

Garigan, D., Hsu, A.-L., Fraser, A. G., Kamath, R. S., Ahringer, J., and Kenyon, C. (2002). Genetic analysis of tissue aging in *Caenorhabditis elegans*: a role for heat-shock factor and bacterial proliferation. *Genetics* 161, 1101–1112. doi: 10.1093/genetics/161.3.1101

Hahnel, S. R., Dilks, C. M., Heisler, I., Andersen, E. C., and Kulke, D. (2020). *Caenorhabditis elegans* in anthelmintic research – Old model, new perspectives. *Int. J. Parasitol. Drugs. Drug. Resist.* 14, 237–248. doi: 10.1016/j.ijpddr.2020.09.005

Handorf, O., Schnabel, U., Bösel, A., Weihe, T., Bekeschus, S., Graf, A. C., et al. (2019). Antimicrobial effects of microwave-induced plasma torch (MiniMIP) treatment on *Candida albicans* biofilms. *Microb. Biotechnol.* 12, 1034–1048. doi: 10.1111/1751-7915.13459

Harder, A. (2016). "Chapter three - The biochemistry of *Haemonchus contortus* and other parasitic nematodes," in *Advances in Parasitology*, eds R. B. Gasser and G. V. Samson-Himmelstjerna (Cambridge, MA: Academic Press), 69–94. doi: 10.1016/bs.apar.2016.02.010

Hayashi, K., Imanishi, N., Kashiwayama, Y., Kawano, A., Terasawa, K., Shimada, Y., et al. (2007). Inhibitory effect of cinnamaldehyde, derived from *Cinnamomi cortex*, on the growth of influenza A/PR/8 virus *in vitro* and *in vivo*. *Antiviral. Res.* 74, 1–8. doi: 10.1016/j.antiviral.2007.01.003

Hentzer, M., Riedel, K., Rasmussen, T. B., Heydorn, A., Andersen, J. B., Parsek, M. R., et al. (2002). Inhibition of quorum sensing in *Pseudomonas aeruginosa* biofilm bacteria by a halogenated furanone compound. *Microbiology* 148, 87–102. doi: 10.1099/00221287-148-1-87

Heydorn, A., Nielsen, A. T., Hentzer, M., Sternberg, C., Givskov, M., Ersboll, B. K., et al. (2000). Quantification of biofilm structures by the novel computer program COMSTAT. *Microbiology* 146(Pt 10), 2395–2407. doi: 10.1099/00221287-146-10-2395

Hotez, P. J., Alvarado, M., Basáñez, M.-G., Bolliger, I., Bourne, R., Boussinesq, M., et al. (2014). The global burden of disease study 2010: interpretation and implications for the neglected tropical diseases. *PLoS Negl. Trop. Dis.* 8:e2865. doi: 10.1371/journal.pntd.0002865

Im, K., Issac, A., Nm, J., Ninan, E., Maliakel, B., and Kuttan, R. (2014). Effects of the polyphenol content on the anti-diabetic activity of *Cinnamomum zeylanicum* extracts. *Food Funct.* 5, 2208–2220. doi: 10.1039/c4fo00130c

Ka, H., Park, H. J., Jung, H. J., Choi, J. W., Cho, K. S., Ha, J., et al. (2003). Cinnamaldehyde induces apoptosis by ROS-mediated mitochondrial permeability transition in human promyelocytic leukemia HL-60 cells. *Cancer Lett.* 196, 143–152. doi: 10.1016/s0304-3835(03)00238-6

Kavanaugh, N. L., and Ribbeck, K. (2012). Selected antimicrobial essential oils eradicate *Pseudomonas* spp. and *Staphylococcus aureus* biofilms. *Appl. Environ. Microbiol.* 78, 4057–4061. doi: 10.1128/AEM.07499-11

Khadke, S. K., Lee, J.-H., Kim, Y.-G., Raj, V., and Lee, J. (2021). Assessment of antibiofilm potencies of nervonic and oleic acid against *Acinetobacter baumannii* using *in vitro* and computational approaches. *Biomedicines* 9:1133. doi: 10.3390/biomedicines9091133

Khan, S. N., Khan, S., Iqbal, J., Khan, R., and Khan, A. U. (2017). Enhanced killing and antibiofilm activity of encapsulated cinnamaldehyde against *Candida albicans*. *Front. Microbiol.* 8:1641. doi: 10.3389/fmicb.2017.01641

Kim, Y. G., Lee, J. H., Gwon, G., Kim, S. I., Park, J. G., and Lee, J. (2016). Essential oils and eugenols inhibit biofilm formation and the virulence of *Escherichia coli* O157:H7. *Sci Rep* 6, 36377. doi: 10.1038/srep36377

Kim, Y. G., Lee, J. H., Kim, S. I., Baek, K. H., and Lee, J. (2015). Cinnamon bark oil and its components inhibit biofilm formation and toxin production. *Int. J. Food Microbiol.* 195, 30–39. doi: 10.1016/j.ijfoodmicro.2014.11.028

Kim, Y. G., Lee, J. H., Park, J. G., and Lee, J. (2020). Inhibition of *Candida albicans* and *Staphylococcus aureus* biofilms by centipede oil and linoleic acid. *Biofouling* 36, 126–137. doi: 10.1080/08927014.2020.1730333

Kot, B., Wicha, J., Piechota, M., Wolska, K., and Gruzewska, A. (2015). Antibiofilm activity of *trans*-cinnamaldehyde, *p*-coumaric, and ferulic acids on uropathogenic *Escherichia coli*. *Turk J. Med. Sci.* 45, 919–924. doi: 10.3906/sag-1406-112

Kot, B., Wierzchowska, K., Gruzewska, A., and Lohinau, D. (2018). The effects of selected phytochemicals on biofilm formed by five methicillin-resistant *Staphylococcus aureus*. *Nat. Prod. Res.* 32, 1299–1302. doi: 10.1080/14786419.2017.1340282

Kotze, A. C., Hunt, P. W., Skuce, P., Von Samson-Himmelstjerna, G., Martin, R. J., Sager, H., et al. (2014). Recent advances in candidate-gene and whole-genome approaches to the discovery of anthelmintic resistance markers and the description of drug/receptor interactions. *Int. J. Parasitol. Drugs. Drug. Resist.* 4, 164–184. doi: 10.1016/j.ijpddr.2014.07.007

Krücken, J., Fraundorfer, K., Mugisha, J. C., Ramünke, S., Sifft, K. C., Geus, D., et al. (2017). Reduced efficacy of albendazole against *Ascaris lumbricoides* in Rwandan school children. *Int. J. Parasitol. Drugs. Drug. Resist.* 7, 262–271. doi: 10.1016/j.ijpddr.2017.06.001

Lee, J.-H., Kim, Y.-G., Gupta, V. K., Manoharan, R. K., and Lee, J. (2018). Suppression of fluconazole resistant *Candida albicans* biofilm formation and filamentation by methylindole derivatives. *Front. Microbiol.* 9:2641. doi: 10.3389/fmicb.2018.02641

Lee, J.-H., Kim, Y.-G., Khadke, S. K., and Lee, J. (2021). Antibiofilm and antifungal activities of medium-chain fatty acids against *Candida albicans* via mimicking of the quorum-sensing molecule farnesol. *Microb. Biotechnol.* 14, 1353–1366. doi: 10.1111/1751-7915.13710

Lee, J.-H., Kim, Y.-G., Khadke, S. K., Yamano, A., Watanabe, A., and Lee, J. (2019a). Inhibition of biofilm formation by *Candida albicans* and polymicrobial microorganisms by nepodin via hyphal-growth suppression. *ACS Infect. Dis.* 5, 1177–1187. doi: 10.1021/acsinfecdis.9b00033

Lee, J.-H., Kim, Y.-G., Khadke, S. K., Yamano, A., Woo, J.-T., and Lee, J. (2019b). Antimicrobial and antibiofilm activities of prenylated flavanones from *Macaranga tanarius*. *Phytomedicine* 63:153033. doi: 10.1016/j.phymed.2019.153033

Lee, J.-H., Kim, Y.-G., Kim, M., Kim, E., Choi, H., Kim, Y., et al. (2017). Indole-associated predator–prey interactions between the nematode *Caenorhabditis elegans* and bacteria. *Environ. Microbiol.* 19, 1776–1790. doi: 10.1111/1462-2920.13649

Li, T., Wang, D., Liu, N., Ma, Y., Ding, T., Mei, Y., et al. (2018). Inhibition of quorum sensing-controlled virulence factors and biofilm formation in *Pseudomonas fluorescens* by cinnamaldehyde. *Int. J. Food Microbiol.* 269, 98–106. doi: 10.1016/j.ijfoodmicro.2018.01.023

Lin, P., Yan, Z.-F., and Li, C.-T. (2021). Biosynthesis of silver nanoparticles using *Lavandula stoechas* and an enhancement of its antibacterial activity with antibiotics. *Biotechnol. Bioproc. Eng.* 26, 650–659. doi: 10.1007/s12257-020-0379-9

Liu, Y., Ren, H., Wang, D., Zhang, M., Sun, S., and Zhao, Y. (2020). The synergistic antifungal effects of gypenosides combined with fluconazole against resistant *Candida albicans* via inhibiting the drug efflux and biofilm formation. *Biomed. Pharmacother.* 130:110580. doi: 10.1016/j.biopha.2020.110580

Lu, L., Shu, C., Chen, L., Yang, Y., Ma, S., Zhu, K., et al. (2020). Insecticidal activity and mechanism of cinnamaldehyde in *C. elegans*. *Fitoterapia* 146:104687. doi: 10.1016/j.fitote.2020.104687

Ma, S., Moser, D., Han, F., Leonhard, M., Schneider-Stickler, B., and Tan, Y. (2020). Preparation and antibiofilm studies of curcumin loaded chitosan nanoparticles against polymicrobial biofilms of *Candida albicans* and *Staphylococcus aureus*. *Carbohydr. Polym.* 241:116254. doi: 10.1016/j.carbpol.2020.116254

Mathew, S., and Abraham, T. E. (2006). Studies on the antioxidant activities of cinnamon (*Cinnamomum verum*) bark extracts, through various *in vitro* models. *Food Chem.* 94, 520–528. doi: 10.1016/j.foodchem.2004.11.043

Mccall, A. D., Pathirana, R. U., Prabhakar, A., Cullen, P. J., and Edgerton, M. (2019). *Candida albicans* biofilm development is governed by cooperative attachment and adhesion maintenance proteins. *NPJ. Biofilms. Microbiomes.* 5:21. doi: 10.1038/s41522-019-0094-5

Miranda-Cadena, K., Marcos-Arias, C., Mateo, E., Aguirre-Urizar, J. M., Quindós, G., and Eraso, E. (2021). *In vitro* activities of carvacrol, cinnamaldehyde and thymol against *Candida* biofilms. *Biomed. Pharmacother.* 143:112218. doi: 10.1016/j.biopha.2021.112218

Niu, C., Afre, S., and Gilbert, E. S. (2006). Subinhibitory concentrations of cinnamaldehyde interfere with quorum sensing. *Lett. Appl. Microbiol.* 43, 489–494. doi: 10.1111/j.1472-765X.2006.02001.x

Nobile, C. J., Nett, J. E., Hernday, A. D., Homann, O. R., Deneault, J. S., Nantel, A., et al. (2009). Biofilm matrix regulation by *Candida albicans* Zap1. *PLoS Biol.* 7:e1000133. doi: 10.1371/journal.pbio.1000133

Ostrosky-Zeichner, L., Casadevall, A., Galgiani, J. N., Odds, F. C., and Rex, J. H. (2010). An insight into the antifungal pipeline: selected new molecules and beyond. *Nat. Rev. Drug Discov.* 9, 719–727. doi: 10.1038/nrd3074

Perez, A., Pedros, B., Murgui, A., Casanova, M., Lopez-Ribot, J. L., and Martinez, J. P. (2006). Biofilm formation by *Candida albicans* mutants for genes coding fungal proteins exhibiting the eight-cysteine-containing CFEM domain. *FEMS Yeast Res.* 6, 1074–1084. doi: 10.1111/j.1567-1364.2006.00131.x

Raj, V., Park, J. G., Cho, K. H., Choi, P., Kim, T., Ham, J., et al. (2021). Assessment of antiviral potencies of cannabinoids against SARS-CoV-2 using computational and *in vitro* approaches. *Int. J. Biol. Macromol.* 168, 474–485. doi: 10.1016/j.ijbiomac.2020.12.020

Rajasekharan, S. K., Raorane, C. J., and Lee, J. (2018). LED based real-time survival bioassays for nematode research. *Sci. Rep.* 8:11531. doi: 10.1038/s41598-018-30016-5

Ramage, G., Saville, S. P., Thomas, D. P., and López-Ribot, J. L. (2005). *Candida* biofilms: an update. *Eukaryot. Cell.* 4, 633–638.

Ropiak, H. M., Desrues, O., Williams, A. R., Ramsay, A., Mueller-Harvey, I., and Thamsborg, S. M. (2016). Structure-activity relationship of condensed tannins and synergism with *trans*-cinnamaldehyde against *Caenorhabditis elegans*. *J. Agric. Food Chem.* 64, 8795–8805. doi: 10.1021/acs.jafc.6b03842

Sardi, J. C. O., Scorzoni, L., Bernardi, T., Fusco-Almeida, A. M., and Mendes Giannini, M. J. S. (2013). *Candida* species: current epidemiology, pathogenicity, biofilm formation, natural antifungal products and new therapeutic options. *J. Med. Microbiol.* 62, 10–24. doi: 10.1099/jmm.0.045054-0

Seeliger, D., and De Groot, B. L. (2010). Ligand docking and binding site analysis with PyMOL and Autodock/Vina. *J. Comput. Aided. Mol. Des.* 24, 417–422. doi: 10.1007/s10822-010-9352-6

Shreaz, S., Wani, W. A., Behbehani, J. M., Raja, V., Irshad, M., Karched, M., et al. (2016). Cinnamaldehyde and its derivatives, a novel class of antifungal agents. *Fitoterapia* 112, 116–131. doi: 10.1016/j.fitote.2016.05.016

Silva, A. F., Dos Santos, A. R., Coelho Trevisan, D. A., Ribeiro, A. B., Zanetti Campanerut-Sa, P. A., Kukolj, C., et al. (2018). Cinnamaldehyde induces changes in the protein profile of *Salmonella typhimurium* biofilm. *Res. Microbiol.* 169, 33–43. doi: 10.1016/j.resmic.2017.09.007

Srisook, K., Mankhong, S., Chiranthanut, N., Kongsamak, K., Kitwiwat, N.-T., Tongjurai, P., et al. (2019). Anti-inflammatory effect of *trans*-4-methoxycinnamaldehyde from *Etlingera pavieana* in LPS-stimulated macrophages mediated through inactivation of NF-κB and JNK/c-Jun signaling pathways and in rat models of acute inflammation. *Toxicol. Appl. Pharmacol.* 371, 3–11. doi: 10.1016/j.taap.2019.03.026

Tabak, M., Armon, R., and Neeman, I. (1999). Cinnamon extracts' inhibitory effect on *Helicobacter pylori*. *J. Ethnopharmacol.* 67, 269–277. doi: 10.1016/s0378-8741(99)00054-9

Taguchi, Y., Hasumi, Y., Abe, S., and Nishiyama, Y. (2013). The effect of cinnamaldehyde on the growth and the morphology of *Candida albicans*. *Med. Mol. Morphol.* 46, 8–13. doi: 10.1007/s00795-012-0001-0

Tan, Y., Leonhard, M., Moser, D., Ma, S., and Schneider-Stickler, B. (2019). Antibiofilm efficacy of curcumin in combination with 2-aminobenzimidazole against single- and mixed-species biofilms of *Candida albicans* and *Staphylococcus aureus*. *Colloids. Surf. B. Biointerfaces.* 174, 28–34. doi: 10.1016/j.colsurfb.2018.10.079

Tian, W., Chen, C., Lei, X., Zhao, J., and Liang, J. (2018). CASTp 3.0: computed atlas of surface topography of proteins. *Nucleic. Acids. Res.* 46, W363–W367. doi: 10.1093/nar/gky473

Williams, A. R., Ramsay, A., Hansen, T. V. A., Ropiak, H. M., Mejer, H., Nejsum, P., et al. (2015). Anthelmintic activity of *trans*-cinnamaldehyde and A- and B-type proanthocyanidins derived from cinnamon (*Cinnamomum verum*). *Sci. Rep.* 5:14791. doi: 10.1038/srep14791

Ying, L., Mingzhu, S., Mingju, Y., Ye, X., Yuechen, W., Ying, C., et al. (2019). The inhibition of *trans*-cinnamaldehyde on the virulence of *Candida albicans* via enhancing farnesol secretion with low potential for the development of resistance. *Biochem. Biophys. Res. Commun.* 515, 544–550. doi: 10.1016/j.bbrc.2019.05.165

**Conflict of Interest:** The authors declare that the research was conducted in the absence of any commercial or financial relationships that could be construed as a potential conflict of interest.

frontiers in Microbiology

ORIGINAL RESEARCH
published: 23 March 2022
doi: 10.3389/fmicb.2022.806654

# A Cationic Amphipathic Tilapia Piscidin 4 Peptide-Based Antimicrobial Formulation Promotes Eradication of Bacterial Vaginosis-Associated Bacterial Biofilms

*Wen-Chun Lin[1], Yun-Ru Chen[2], Chi-Mu Chuang[3,4,5] and Jyh-Yih Chen[1]**

[1]*Marine Research Station, Institute of Cellular and Organismic Biology, Academia Sinica, Jiaushi, Taiwan,* [2]*Academia Sinica Protein Clinic, Institute of Biological Chemistry, Academia Sinica, Taipei, Taiwan,* [3]*College of Nursing, National Taipei University of Nursing and Health Sciences, Taipei, Taiwan,* [4]*Department of Obstetrics and Gynecology, Taipei Veterans General Hospital, Taipei, Taiwan,* [5]*School of Medicine, National Yang Ming Chiao Tung University, Taipei, Taiwan*

OPEN ACCESS

**Edited by:**
*Giuseppantonio Maisetta, University of Pisa, Italy*

**Reviewed by:**
*Berthony Deslouches, University of Pittsburgh, United States*
*Annelise Emily Barron, Stanford University, United States*
*Chang-Jer Wu, National Taiwan Ocean University, Taiwan*

***Correspondence:**
*Jyh-Yih Chen*
*zoocjy@gate.sinica.edu.tw*

**Specialty section:**
*This article was submitted to Antimicrobials, Resistance and Chemotherapy, a section of the journal Frontiers in Microbiology*

**Received:** *01 November 2021*
**Accepted:** *28 February 2022*
**Published:** *23 March 2022*

**Citation:**
*Lin W-C, Chen Y-R, Chuang C-M and Chen J-Y (2022) A Cationic Amphipathic Tilapia Piscidin 4 Peptide-Based Antimicrobial Formulation Promotes Eradication of Bacterial Vaginosis-Associated Bacterial Biofilms. Front. Microbiol. 13:806654. doi: 10.3389/fmicb.2022.806654*

Bacterial vaginosis (BV) is prevalent among women of reproductive age and has a high rate of recurrence, which can be largely attributed to ineffective BV biofilm eradication by current first-line antibiotics. In this study, we report that the Nile tilapia piscidin 4 (TP4) exhibits broad-spectrum antimicrobial and antibiofilm activity against BV-associated bacteria, but not beneficial lactobacilli. In addition, BV-associated *Gardnerella vaginalis* remains susceptible to TP4 even after continual exposure to the peptide for up to 22 passages. *Gardnerella vaginalis* and *Streptococcus anginosus* are both biofilm-forming BV-associated bacteria, and we found that combining TP4 peptide and disodium EDTA with the biofilm-disrupting agent, chitosan, can eradicate biofilms formed by single or mixed *G. vaginalis* and *S. anginosus*. In addition, long-term storage of TP4 peptide in chitosan did not diminish its bactericidal activity toward *G. vaginalis*. Preformulation studies were performed using High performance liquid chromatography (HPLC) and Circular Dichroism (CD). The long-term stability of TP4 peptide was assessed under various conditions, such as different temperatures and ionic strengths, and in the presence of $H_2O_2$ and lactic acid. When exposed to sodium dodecyl sulfate (SDS), TP4 maintained its secondary structure at various temperatures, salt and disodium EDTA concentrations. Furthermore, the TP4 microbicide formulation significantly reduced the colonization density of BV-associated bacteria in mice infected with single or mixed bacteria (*G. vaginalis* and *S. anginosus*). The TP4 microbicide formulation showed biocompatibility with beneficial human vaginal lactobacilli and female reproductive tissues in C57BL/6 mice. These results suggest that the TP4 microbicide formulation could be a promising topical microbicide agent for BV treatment.

**Keywords: bacterial vaginosis, polymicrobial biofilm, vaginal microbicide formulation, amphipathic antimicrobial peptides, Nile tilapia piscidin 4**

## INTRODUCTION

Bacterial vaginosis (BV) is a common condition in reproductive-aged women, with a worldwide prevalence of over 30%. The cause of BV is microflora imbalance in the vagina, where lactic acid-producing bacteria normally play an essential role of maintaining an acidic environment (pH < 4.5) that inhibits colonization by pathogenic bacteria (O'Hanlon et al., 2013; Borges et al., 2014). One such pathogen is *Gardnerella vaginalis*, which is often increased in BV along with reductions in the proportion of lactic acid-producing bacteria (Deng et al., 2018). Patients typically present with vaginal odor and a thin milky discharge. If treatment is neglected, BV may cause pelvic inflammation, increased susceptibility to preterm birth, or even infertility (Ravel et al., 2021).

Current first-line antibiotic regimens include oral metronidazole, topical intravaginal clindamycin cream, and metronidazole gel (Workowski, 2015). These treatments are associated with a high recurrence rate (over 50% within 6 months to 1 year) for BV that may be due to an inability of antibiotics to effectively eradicate bacterial biofilms (Machado et al., 2016; Hay, 2017). In addition, metronidazole and clindamycin are used to against anaerobic bacteria. However, recent whole-metagenome sequencing studies have identified at least four *G. vaginalis* clades, of which two may be intrinsically resistant to metronidazole (Schuyler et al., 2016). *Gardnerella vaginalis* and BV-associated bacteria often form a complex polymicrobial bio-structure in the BV biofilm (Castro et al., 2019), which is not only composed of anaerobic bacteria. It has been found that some aerobic bacteria, such as *Streptococcus* spp. and *Escherichia coli*, are also involved in BV pathogenesis (Tao et al., 2019). After the patient receives antibiotic treatment, co-existing microbes that are not sensitive to the antibiotics can become dominant species within the human vaginal microbiota. For example, the side effect of antibiotic treatment is vaginal candidiasis (Sobel et al., 2006; Pappas et al., 2016). When patients suffer from vaginitis repeatedly, they are more likely to experience sexually transmitted infections (STI), such as trichomoniasis or human immunodeficiency virus (HIV; Brotman et al., 2010; Cohen et al., 2012), making it difficult to restore a healthy environment. Therefore, new treatment strategies are needed for BV treatment.

Various recent studies have proposed alternative therapeutic approaches to reduce BV recurrence, including extended antimicrobial regimens (Sobel et al., 2006), oral or vaginal administration of probiotic (Bradshaw et al., 2012; Heczko et al., 2015; Marcotte et al., 2019) or amphoteric tenside pessary (WO3191) combined with first-line regimens (Gottschick et al., 2017), and adjunctive intravaginal lactic acid (Plummer et al., 2021) or boric acid treatments (Powell et al., 2019). Although some of these approaches seem promising, there has been limited progress in terms of providing long-term cure after stopping the treatments. Therefore, the active pharmaceutical ingredient (API) for BV treatment should have broad-spectrum antimicrobial activity against relevant vaginal pathogens and not harm the normal beneficial vaginal flora (Mendling et al., 2019). Another consideration is that the broad-spectrum antimicrobial activity API should be used in combination with a biofilm disrupting agent to promote its bactericidal effects.

Antimicrobial peptides (AMPs) are important parts of the innate immune system of many plants and animals, helping to effectively kill invading pathogenic bacteria and regulate host immunity, without harming the host cells (Maróti et al., 2011; Pasupuleti et al., 2012). One group of AMPs has an α-helix configuration with an overall positive charge and amphipathic character (Wang et al., 2016). Because of the positive charge, selective attack of negatively charged pathogenic bacteria is possible. The hydrophobic peptide domains interact with the lipid bilayer to cause membrane disturbances (Toke, 2005; Lázár et al., 2018). In addition, many AMPs can effectively inhibit the formation of biofilms (Yasir et al., 2018). Nile tilapia piscidin 4 (TP4 peptide) is an AMP identified from Nile tilapia (*Oreochromis niloticus*) that exhibits broad-spectrum activity against Gram-positive and Gram-negative bacteria. It is also effective against drug-resistant bacteria (Pan et al., 2015; Hazam and Chen, 2020). Besides its direct actions as a microbicide, TP4 peptide possesses other properties, including regulating host cell immunity, biofilm eradication, and promotion of wound-healing (Huang et al., 2015; Chang et al., 2017; Hazam and Chen, 2020; Liu et al., 2021). These properties may help clear infections, reduce inflammatory responses, and promote restoration of healthy tissues (Liu et al., 2021). However, the TP4 peptide has not been thoroughly tested in the context of BV. In this study, we investigated the therapeutic potential of TP4 peptide in BV. We evaluated the effect of TP4 peptide on survival and biofilm formation of BV-associated bacteria. We also tested combinations of TP4 peptide with a biofilm-disrupting agent on mature biofilms of BV-associated bacteria. Finally, we evaluated the safety and efficacy of the TP4 microbicide formulation *in vivo*, introducing a potential new strategy for BV treatment.

## MATERIALS AND METHODS

### Peptide Synthesis and Secondary Structure Analysis

Tilapia piscidin 4 peptide (H-FIHHIIGGLFSAGKAIHRLIRRRRR-OH) was synthesized by GL Biochem Ltd (Shanghai, China). The solution structure of TP4 has been reported in a previous study (Protein Data Bank under accession number: 5H2S); peptide structure was visualized using PyMOL (DeLano, 2002).

### Bacterial Strains, Protozoa, and Culture Conditions

Bacterial vaginosis-associated bacteria *G. vaginalis* (ATCC 14018, ATCC 49145), candidiasis pathogen *Candida albicans* (ATCC 14053), trichomoniasis pathogen *Trichomonas vaginalis* (ATCC 30001), and human vagina-derived lactobacilli, *Lactobacillus crispatus* (ATCC 33820), *Lactobacillus gasseri* (ATCC 33323), *Lactobacillus plantarum* (ATCC 14917), and *Lactobacillus jensenii* (ATCC 25258), were purchased from the American Type Culture Collection (ATCC). *Gardnerella vaginalis* $M^R$ is a spontaneous

metronidazole-resistant mutant of ATCC 14018. The clinical isolates of BV-associated bacteria and healthy human vagina lactobacilli were kindly provided by Dr. Chuang at National Yang Ming Chiao Tung University, Taiwan (all bacterial isolates are listed in **Table 1**). All BV-associated bacteria were cultured in NYCIII broth (ATCC medium 1685) and grown at 37°C in anaerobic conditions, using AnaeroPack®-Anaero (MGC, Japan). All *Lactobacillus* spp. were cultured in MRS broth (Difco BD) and grown at 37°C in facultatively anaerobic conditions, using AnaeroPack®-MicroAero (MGC, Japan), except *L. gasseri* was grown in aerobic conditions. *Candida albicans* was cultured in YM broth (Difco BD) and grown at 37°C in aerobic conditions.

## Microbroth Dilution Assay

The antibacterial activities of TP4 and antibiotics were assessed by minimal inhibitory concentration (MIC) and minimum bactericidal concentration (MBC) experiments. The methods for evaluation of *in vitro* antimicrobial activity followed the Clinical and Laboratory Standards Institute (CLSI) guidelines, with minor modifications. Brain-Heart Infusion (BHI) medium (Difco BD) supplemented with 1% glucose (BHIG), RPMI1640 and MRS broth were respectively used for microbroth dilution assays of BV-associated bacteria, *C. albicans* and *Lactobacillus* spp. Serial dilutions were made of the antimicrobial agent with test medium in a round-bottom 96-well microplate (Corning), and the fresh overnight culture of bacterial were added to final inoculum of $5\times10^5$ colony-forming units (CFU)/ml ($1\times10^3$ CFU/ml in antifungal susceptibility testing, CLSI M27-A3). After a 24-h incubation, the lowest concentration of antimicrobial agent with no visible growth was defined as the MIC. Bacteria were subcultured from broth dilutions in MIC tests on agar plates to determine the lowest concentration of antimicrobial agent that is bactericidal (defined as the MBC).

## Evaluation of Biofilm-Forming Capacity

The biofilm-forming ability of BV-associated bacteria was determined as previously described with minor modifications (Gottschick et al., 2016; Jardak et al., 2017). All BV-associated bacteria were grown in BHI containing 0.3% starch (Sigma) and 1% glucose (sBHI) for biofilm formation. An overnight culture of *G. vaginalis* in growth medium (NYCIII) was subcultured in biofilm medium (sBHI). The subculture was performed several times to allow bacteria to adapt the biofilm medium; the bacteria have different gene expression and metabolism profiles in planktonic and biofilm stages. A fresh overnight culture of bacterial in sBHI was added in 200 µl to final inoculum of $1\times10^6$ CFU/ml in 96-well flat-bottom microtiter plates (Corning). After a 24-h incubation at 37°C under anaerobic conditions, medium and planktonic cells were removed, and each well was washed twice with saline. After washing, the plates were dried in an oven for 1 h. Biofilms were stained with 200 µl of 0.5% crystal violet solution, then washed twice with 200 µl saline to remove unbound dye. Biofilm-forming ability was determined by visualizing biofilms after crystal violet staining.

## Trichomonacidal Assays

*Trichomonas vaginalis* (ATCC 30001) was maintained in trypticose-yeast-maltose (TYM, ATCC medium 358) media

**TABLE 1** | Minimal inhibitory concentrations (MICs) and minimum bactericidal concentrations (MBCs) of tilapia piscidin 4 (TP4) and antibiotics tested on clinical isolates of bacterial vaginosis (BV)-associated bacteria and vaginal lactobacilli.

| No. | Clinical strain | Metronidazole | | Clindamycin | | TP4 | | Biofilm formation ability |
|---|---|---|---|---|---|---|---|---|
| | | MIC | MBC | MIC | MBC | MIC | MBC | |
| | | µg/ml | | | | | | |
| 11-1-1 | *Streptococcus intermedius* | 62.5 | 250–500 | 15.63 | 31.25–62.5 | 15.63 | 31.25 | X |
| 11-4-1 | *Streptococcus anginosus* | 125 | >500 | 15.63 | 62.5–125 | 7.81 | 15.63 | O |
| 3-1-1 | *Streptococcus anginosus* | 125 | 250–500 | 31.25 | 125–250 | 7.81 | 15.63–31.25 | O |
| 3-3-1 | *Streptococcus anginosus* | 125 | 250–500 | 15.63 | 62.5 | 7.81 | 15.63–31.25 | O |
| 3-5-8 | *Streptococcus anginosus* | >500 | >500 | 31.25 | 62.5 | 7.81–15.63 | 15.63 | O |
| 4-3-1 | *Streptococcus anginosus* | >500 | >500 | >500 | >500 | 7.81 | 7.81–15.63 | O |
| 3-2-9 | *Streptococcus agalactiae* | >500 | >500 | 500 | >500 | 15.63 | 15.63–31.25 | X |
| 11-5-11 | *Streptococcus agalactiae* | >500 | >500 | 125 | >500 | 7.81–15.63 | 7.81–15.63 | X |
| 4-4-1 | *Streptococcus agalactiae* | >500 | >500 | >500 | >500 | 7.81 | 7.81 | O |
| 12-1-1 | *Streptococcus pasteurianus* | 500 | >500 | >500 | >500 | 3.91–7.81 | 15.63–31.25 | X |
| 8-1-1 | *Escherichia coli* | 500 | >500 | >500 | >500 | 3.91–7.81 | 15.63 | X |
| 8-4-1 | *Enterococcus avium* | >500 | >500 | >500 | >500 | 1.95–3.91 | 3.91 | X |
| 1-3-16 | *Actinobaculum schaalii* | 15.63 | 500 | >500 | >500 | 1.95–3.91 | 3.91 | X |
| 6-2-4 | *Gardnerella vaginalis* | 7.81 | 15.63–31.25 | 15.63 | 31.25–62.5 | 3.91–7.81 | 7.81–15.63 | O |
| 11-5-4 | *Gardnerella vaginalis* | 62.5 | 125 | 500 | >500 | 7.81 | 7.81–15.63 | O |
| 3-2-23 | *Gardnerella vaginalis* | 3.91 | 15.63 | 3.91 | 3.91–7.81 | 3.91 | 7.81 | O |
| 4-3-11 | *Gardnerella vaginalis* | >500 | >500 | 7.81 | 15.63 | 3.91 | 7.81 | O |
| 7-2-4 | *Lactobacillus crispatus* | >500 | >500 | 125 | 250 | 125 | 250 | X |
| 8-5-12 | *Lactobacillus crispatus* | >500 | >500 | 125 | 250 | 125 | 250 | X |
| 4-5-8 | *Lactobacillus crispatus* | >500 | >500 | 500 | >500 | 62.5 | 250 | X |

*X, no biofilm formation ability; O, able to form biofilm.*

supplemented with 10% (v/v) heat-inactivated bovine serum (Sigma) in 5% $CO_2$ at 37°C. For the trichomonacidal assay, $5 \times 10^5$ cells were seeded into the wells of a 12-well plate. Then, cells were incubated with the indicated concentrations of TP4 or metronidazole for 24 h. *Trichomonas vaginalis* viability was assessed using the trypan blue exclusion test as previously described (Shaio et al., 1987). A hemocytometer was used to count the number of living cells.

## TP4 Bactericidal Activity in Vaginal Fluid Simulant

The vaginal fluid simulant (VFS) composition is shown in **Figure 1A**, and was prepared as previously described with minor modifications (Tomás and Nader-Macías, 2007). This formula of VFS does not include lactic acid and acetic acid to maintain a high survival rate of *G. vaginalis*. *Gardnerella vaginalis* (ATCC 14018), *L. crispatus* (ATCC 33820), and *L. gasseri* (ATCC 33323) inocula were prepared from fresh overnight cultures adjusted to a final concentration of $1 \times 10^6$ CFU/ml in VFS. TP4 was added to a final concentration of 0, 20, 50, and 100 μg/ml (0 μg/ml as control). The mixtures were plated for CFU quantification at different indicated time.

## Time-Kill Analysis

The *G. vaginalis* (ATCC 14018) inoculum was prepared with the fresh overnight culture in BHIG, adjusted to a final concentration of $1 \times 10^6$ CFU/ml. TP4 and antibiotics were added to concentrations of 1× MBC (metronidazole: 3.91 μg/ml, clindamycin: 7.81 μg/ml, and TP4 3.91 μg/ml) or 2× MBC (metronidazole: 7.81 μg/ml, clindamycin: 15.63 μg/ml, and TP4 7.81 μg/ml). The antimicrobial agent BHIG was not added for growth control. The number of CFUs was counted from cultures spread onto NYC III agar plates and incubated at 37°C under anaerobic conditions for 0, 0.5, 1, 2, 4, 6, 8, 12, and 24 h.

## Resistance Development Assay

The propensity for TP4 peptide treatment to induce resistance was evaluated by a microbroth dilution assay. *Gardnerella vaginalis* (ATCC 14018) was serially passaged in resistance induction studies. The experiment was performed as previously described with minor modifications (Lee et al., 2018; Elliott et al., 2020). Metronidazole and clindamycin served as antibiotic controls. The MIC test was performed first, and the bacteria were subcultured in half the MIC (1/2 MIC well) with fresh NYC-III medium. After growing bacteria to the stationary phase, the next generation MIC was measured; cells were incubated for 24 h at 37°C, according to the experimental procedure described for the microbroth dilution assay. MICs were determined in triplicate for each of 22 generations.

## Minimal Biofilm Inhibitory Concentration

Evaluation of biofilm formation inhibitory activity was performed as previously described with minor modifications (Algburi et al., 2018). Serial dilutions of the antimicrobial agent were made with sBHI in flat-bottom 96-well microtiter plates, and a fresh overnight culture of bacteria was added to a final inoculum of $1 \times 10^6$ CFU/ml. After 24 h of incubation at 37°C under anaerobic conditions, medium and planktonic cells were removed from each well, and the well was washed twice with saline. After washing, the plates were dried in oven for 1 h. Biofilms were stained with 200 μl of 0.5% crystal violet solution, then washed twice with saline to remove unbound dye. Minimal biofilm inhibitory concentrations (MBICs) were determined as the lowest concentration of an antimicrobial agent needed to inhibit the development of biofilms.

## RNA Isolation and Quantitative Real-Time PCR

Fresh overnight cultures of *G. vaginalis* in NYCIII (growth medium) and sBHI (biofilm medium) were used to assess the bacterial cells in planktonic and biofilm stages. Total RNA was extracted using the TRIzol Max Bacterial RNA Isolation Kit (Thermo Scientific) according to the manufacturer's instructions. Reverse transcription reagent (Toyobo) was used to reverse transcribe total RNA. The expression levels of sialidase, vaginolysin, bacitracin transport ATP-binding protein (BcrA), and multidrug resistance ABC transporter (ABC transporter) gene were analyzed by quantitative real-time PCR (qRT-PCR) using SYBR Green PCR Master Mix (Toyobo) and an ABI StepOnePlus Real-Time PCR System (Applied Biosystems, Foster, CA, United States). The cycling steps were: 5 min at 95°C, followed by 40 cycles of 15 s at 95°C and 60 s at 56°C. The primers used for qRT-PCR are listed in **Supplementary Table 1**.

## Biofilm Disruption Assay

The different molecular weights of chitosan (Sigma) used in this study are summarized in **Figure 2A**. Around 1.2% chitosan stock solution was dissolved in 0.1 M acetic acid in sterile saline. A fresh overnight culture of *G. vaginalis* (ATCC 14018) biofilm was prepared, with planktonic cells removed from each well and washed twice with saline. Subsequently, serially diluted chitosan was added to the mature biofilm. After overnight incubation, the biofilm was washed twice with saline, stained with crystal violet and quantified by OD at 585 nm. Biofilm mass quantification by the crystal violet staining method was performed as previously described with minor modifications (Gottschick et al., 2016).

## Biofilm Cell Viability Assay

A fresh overnight culture of *G. vaginalis* 3-2-23, *S. anginosus* 11-4-1, or *G. vaginalis* 3-2-23 combined with *S. anginosus* 11-4-1 (1:1, mixed-culture biofilm) in sBHI was added to 50 μl of final inoculum of $1 \times 10^6$ CFU/ml in a 96-well flat-bottom microtiter plate. After 24 h of incubation at 37°C under anaerobic conditions, medium and planktonic cells were removed, and each well was washed twice with saline. TP4 combined with disodium EDTA (sigma) solution in serial dilutions were added to the mature biofilm. Cells were incubated for 6 h at 37°C in anaerobic conditions, then bacterial viability was analyzed using alamarBlue (Thermo Scientific) according to the

**A**

Composition of simulating vaginal fluid

| Chemical Name | Formula | g/L |
|---|---|---|
| Glucose | $C_6H_{12}O_6.H_2O$ | 5 |
| Glycerol | $C_3H_8O_3$ | 0.16 |
| Sodium chloride | NaCl | 3.51 |
| Potassium chloride | KCl | 1.5 |
| Urea | $NH_2CONH_2$ | 0.4 |
| Albumin | | 0.018 |
| Mucin | | 0.25 |
| Lactic acid | $C_3H_6O_3$ | - |
| Acetic acid | $CH_3CO_2H$ | - |

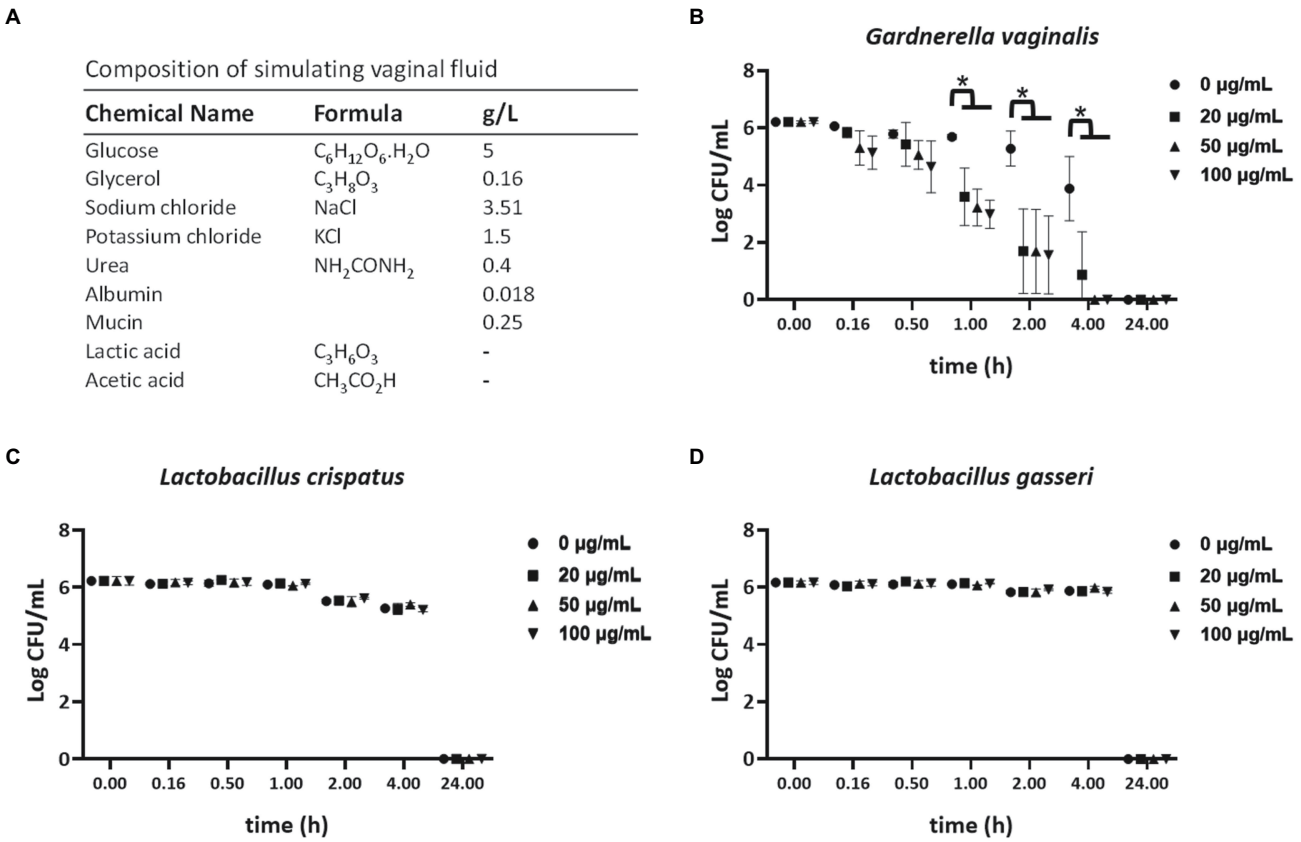


**FIGURE 1 |** Selective bactericidal activity of TP4 in vaginal fluid simulant (VFS). **(A)** VFS composition. (–): This formula of VFS does not include lactic acid and acetic acid in order to maintain a high survival rate of *Gardnerella vaginalis*. Viability of *G. vaginalis* **(B)**, *Lactobacillus crispatus* **(C)**, and *Lactobacillus gasseri* **(D)** in VFS after treatment with various TP4 concentrations (0, 20, 50, and 100 μg/ml), as determined by colony-forming unit (CFU). All values represent the mean ± SD of three individual experiments. *$p < 0.05$ compared to CFU/ml from bacteria in VFS TP4-free control, determined by one-way ANOVA.

manufacturer's instructions. In the experiment testing TP4 combined with disodium EDTA in chitosan gel against mature biofilm, a fresh overnight culture of *G. vaginalis* 3-2-23, *S. anginosus* 11-4-1, or *G. vaginalis* 3-2-23 combined with *S. anginosus*11-4-1 (1:1, mixed-culture biofilm) in sBHI was added to 400 μl of final inoculum of $1 \times 10^6$ CFU/ml in a 24-well flat-bottom microtiter plate. The experimental procedure was performed as described above. Different combinations of TP4, disodium EDTA and chitosan were added to the mature biofilm. After 6 h of incubation at 37°C under anaerobic conditions, bacterial viability was analyzed using the CFU plate count method.

## Preformulation Studies of the TP4 Peptide

High performance liquid chromatography (HPLC) and Circular Dichroism (CD) were used to investigate the stability and secondary structure of TP4 peptide under different environmental conditions. To study the long-term stability of TP4, 500 μg/ml of peptide was dissolved in various aqueous buffer solutions. The influence of temperature of the TP4 peptide was evaluated by storing peptides at −20, 4, 25, 37, and 65°C for 1 month. The effect of salt concentrations on the TP4 peptide was evaluated by storing peptide in 0, 50, 150, 250, 500 mM sodium chloride (NaCl) for 1 month. In the physiological environment, lactobacilli dominate the human vaginal flora, secreting lactic acid and hydrogen peroxide ($H_2O_2$) into the vaginal fluid. The influences of oxidation and acidic environments on TP4 peptide were evaluated. The experimental concentrations were higher than the physiological concentration ranges (O'Hanlon et al., 2011). The effect of acidic environment on TP4 peptide stability was evaluated at 0, 56.5, 113, 565, 1,130 mM lactic acid (physiological concentrations of lactic acid: 55–111 mM; O'Hanlon et al., 2011). The oxidation of TP4 peptide was assessed by exposing TP4 to 8 mM $H_2O_2$ solution (physiological concentrations of $H_2O_2 < 100$ μM) (O'Hanlon et al., 2011). Stability of the TP4 peptide under different environmental conditions was assessed for 1 month; samples were collected on day 0, 1, 2, 3, 7, 14, 21, and 28 for analysis by HPLC (Waters Corporation, Milford, MA) following a previously reported method (Sassi et al., 2011). To study of the secondary structural changes of TP4 peptide and determine its stability in different solutions, TP4 peptide (145 μg/ml) was dissolved in serially diluted membrane-mimicking sodium dodecyl sulfate (SDS) solutions (0, 1, 5, 10, 50, and 100 mM), or 100 mM SDS solution containing different

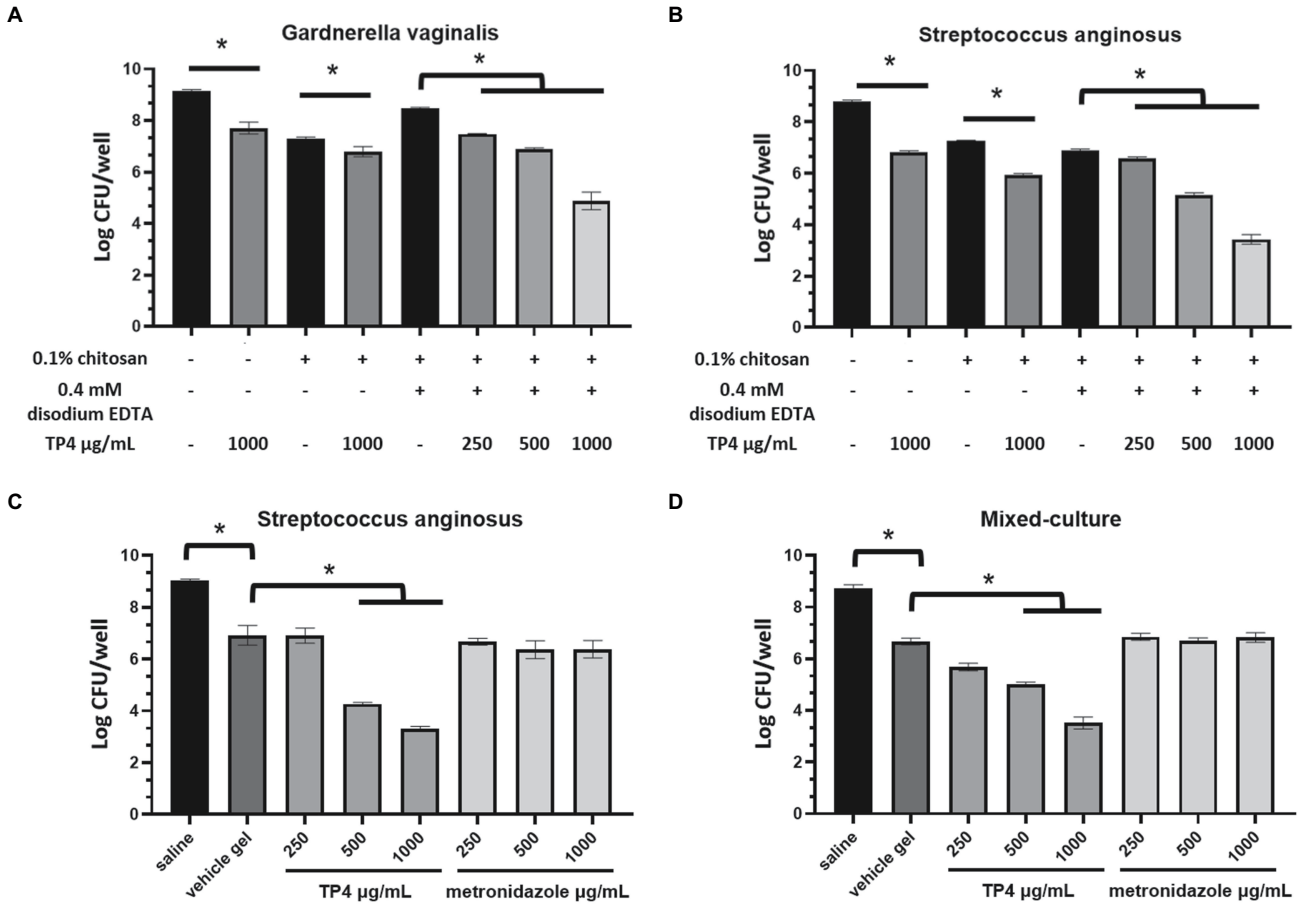


**FIGURE 2 |** Tilapia piscidin 4 and disodium EDTA formulated in chitosan reduces bacterial viability in BV-associated bacteria biofilms. Mature biofilms formed by BV-associated bacteria *Gardnerella vaginalis* **(A)** or *Streptococcus anginosus* **(B)** were treated with different combinations of TP4, disodium EDTA and chitosan. Mature biofilms formed by **(C)** *S. anginosus* or **(D)** *S. anginosus* combined with *G. vaginalis* (mixed culture) were treated with different concentrations of TP4 or metronidazole in vehicle gel (0.1% chitosan + 0.4 mM disodium EDTA). Biofilm cell viability was measured in terms of CFU counts. All values represent the mean ± SD of three individual experiments (*$p < 0.05$, one-way ANOVA).

concentrations of NaCl (0, 100, 200, and 400 mM) or different concentrations of disodium EDTA (0, 0.1, 0.4, 1.6, and 6.4 mM). The measure the effects of temperature on the structure of TP4, 145 μg/ml of peptide was pre-incubated at different temperatures (20, 37, 50, and 90°C) in 100 mM SDS solution for 1 h. The far-UV CD spectra of samples were measured using a J-815 CD spectrometer (Jasco, Japan) at 25°C with a wavelength range of 260–190 nm or 260–200 nm. For each spectrum, an average of five scans was collected using a 1 mm path length quartz cell (Hellma Analytics, Germany).

## Experimental Animals

Mouse experiments were approved by the Academia Sinica Institutional Animal Care & Utilization Committee (Protocol number: IACUC 20-12-1568). Six-week-old female C57BL/6 mice were purchased from the BioLASCO Taiwan Co., Ltd. All mice were maintained at a constant temperature and 12:12-h light–dark cycle. Mice were adapted to the environment for 2 weeks before experimentation.

## Mouse Estrus Cycle

The mouse estrus cycle is divided into four main stages, including proestrus, estrus, metestrus, and diestrus, which occur over a period of 4–5 days (Byers et al., 2012). The estrus cycle will affect the physiological characteristics of reproductive tract tissues and local immune response in mice (McLean et al., 2012; Schaefer et al., 2014). At the proestrus to estrus stage, the epithelium is completely keratinized, and superficies are detached gradually in the vaginal cavity (McLean et al., 2012; Schaefer et al., 2014). It is difficult to distinguish epithelial cell detachment caused by physiological or drug toxicity. This stage is therefore not suitable for evaluating drug toxicity. In current studies evaluating the toxicity of topical agents on the reproductive tract, Depo-Provera is administered to maintain the mice in a diestrus-like state, reducing the variability in histopathological evaluations (Ensign et al., 2012; Coulibaly et al., 2019). In the metaestrus to diestrus stage, vaginal epithelial cells become thin, and leukocyte infiltration is present in the vaginal epithelium (McLean et al., 2012;

Schaefer et al., 2014). In this stage, the amount of bacteria in the vagina flora is reduced, and the host immune responses prevent bacterial infection and colonization (Jerse et al., 2011; Vrbanac et al., 2018). β-estradiol often used for estrous synchronization in mouse vaginal infection models (Jerse et al., 2011; Gilbert et al., 2013, 2019; Hymes et al., 2013). This treatment dampens the inflammatory response (natural influx of polymorphonuclear leukocytes) and increases susceptibility to bacteria colonization in mouse vagina. Therefore, the mouse vaginal infection model in this study included as step of administering β-estradiol, which kept the mice in an estrus-like state, according to vaginal cytology. This state reduced the variability in bacteria colonization capacity. All mice were confirmed to be at estrus stage according to vaginal cytology before experimentation (**Supplementary Figure 5**).

## Toxicity Assessment of TP4 Microbicide Formulation in Mice

Evaluation of vaginal toxicity in mice followed a previous study with minor alterations (Ensign et al., 2012; Coulibaly et al., 2019). Eight-week-old female C57BL/6 mice were used to evaluate tissue toxicity after vaginal administration of the TP4 microbicide formulation. To synchronize in the diestrus phase, mice were subcutaneously injected with 2 mg of Depo-Provera (Sigma) in 200 µl of Ringer's lactate solution, 4 days prior to the drug toxicity test. After synchronization, mice vaginal smears had predominant leukocyte populations, indicating a diestrus-like state. Mice received a single vaginal administration of 20 µl saline (Negative control), 5% Nonoxynol-9 (N-9; Positive control; Sigma), 2% Benzalkonium chloride (BZK; Positive control; Sigma), TP4 at 5 or 10 mg/ml in saline, or TP4 at 5 or 10 mg/ml in gel (vehicle gel contained 0.1% chitosan and 0.4 mM disodium EDTA in saline). "Blank group" means that no drug was administered and there was no irritation of vaginal tissue. Mice were sacrificed at 24 h after drug application for histopathological examination. All animals were sacrificed by exsanguination under anesthesia with pure carbon dioxide. The female reproductive system (vagina, cervix, uterus, and ovary) was collected and preserved in 10% neutral buffered formalin (Sigma). Tissues were trimmed, dehydrated through graded ethanols, cleared in xylene, embedded in paraffin wax, sectioned to approximately 4–5 µm thickness, and stained with hematoxylin and eosin (H&E). Severity of lesions was graded according to the methods described by Shackelford et al. (2002). Degrees of lesions were graded histopathologically from 0 to 5 depending on severity: 0 = normal; 1 = minimal (<1%); 2 = slight (1–25%); 3 = moderate (26–50%); 4 = moderately severe (51–75%); and 5 = severe/high (76–100%).

## Mouse Vaginal Infection Model

In order to test the effects of TP4 microbicide formulation on BV-associated bacteria and normal human vaginal flora *in vivo*, clinical isolates of BV-associated bacteria (*G. vaginalis* 3-2-23 and *S. anginosus* 11-4-1) and *Lactobacillus* spp. (*L. crispatus* ATCC 33820 and *L. gasseri* ATCC 33323) were used to colonize mouse vaginal tissues. The procedures followed a previous study with minor modifications (Gilbert et al., 2013) All bacteria to be inoculated were streptomycin resistant mutants ($S^R$) in order to distinguish the inoculated bacteria from endogenous bacteria. Eight-week-old female C57BL/6 mice were subcutaneously injected with 100 µl sesame oil containing 0.5 mg of β-estradiol in the lower abdomen at 1 day and 3 days before the drug administration, in order to synchronize the estrous cycles. Around 2 days before the test drug administration, mice were lavaged and vaginally inoculated with 20 µl of the bacterial suspension once daily for 2 consecutive days. After 2 consecutive days of vaginal inoculation, the test drug was administered twice a day, and the bacterial load was measured by vaginal lavage on the day after administration. Bacterial inoculation doses and the experimental procedure are shown in **Supplementary Figure 6**. To quantify the bacteria load in the mice vagina after test drug administration, vaginal lavage was performed using a p200 micropipette containing 30 µl sterile saline by gently inserting it into the mouse vagina (about 5 mm deep) and repeated pipetting. The lavage was repeated five times to obtain a total of 150 µl vaginal lavage fluid. The fluid was serially diluted and spread onto NYC III (for counting *G. vaginalis* and *S. anginosus* CFU) or MRS (for counting *L. crispatus* and *L. gasseri* CFU) plates containing 1 mg/ml streptomycin (eliminates endogenous bacteria contamination). The plates were incubated anaerobically at 37°C and colonies were counted after 72 h. All colonies were confirmed by colony PCR. Colony PCR was performed in a Veriti™ 96-Well Thermal Cycler (Applied Biosystems, Foster, CA, United States) with the following cycling parameters: 5 min at 95°C, followed by 40 cycles of 20 s at 95°C, 30 s at 56°C, and 20 s at 72°C. The primers used for colony PCR are listed in **Supplementary Table 1**.

## Statistical Analysis

GraphPad Prism 8.0 software was used for statistical analyses. Data were collected from at least three independent experiments. Statistical significance was determined by one-way ANOVA with Tukey's multiple comparison test. Values of $p < 0.05$ were considered significant.

# RESULTS

## Antimicrobial Activity of TP4 Against Pathogens and Normal Vaginal Flora

Current first-line antibiotics for BV are associated with high rates of recurrence and candidiasis. Furthermore, recurrence after antibiotic treatment is associated with increased risk of STIs, such as trichomoniasis (Sobel et al., 2006; Brotman et al., 2010; Cohen et al., 2012). The TP4 peptide has a cationic amphipathic α-helical structure (**Supplementary Figure 1**) and was reported to exhibit broad-spectrum antimicrobial properties (Hazam and Chen, 2020). To investigate the effects of TP4 on vaginal pathogens, such as *G. vaginalis*, *C. albicans*, and *T. vaginalis*, and healthy human vaginal lactobacilli, the MIC, MBC, and trichomonacidal assay were performed on a panel of vaginal pathogens and lactobacilli. **Table 2** and

**Supplementary Figure 2** show that the control antibiotics exhibited highly potent microbicide activity on vaginal pathogens. The healthy human vaginal lactobacilli showed low susceptibility to antibiotics (MBCs of antibiotics were in the ranges of 1.95–7.81 μg/ml for *G. vaginalis*, <0.48 μg/ml for *C. albicans*, and >62.5 μg/ml for all lactobacilli; Metronidazole <0.98 μg/ml inhibited the growth of *trichomonads*). In contrast, TP4 peptide showed broad-spectrum microbicide activity for all vaginal pathogens, including *G. vaginalis*, *C. albicans*, and *T. vaginalis*, and it was also effective against a metronidazole-resistant strain of *G. vaginalis* (MBC of TP4 peptide against *G. vaginalis*, *G. vaginalis* $M^R$ and *C. albicans* were in the range of 3.91–7.81 μg/ml; TP4 peptide 31.25 μg/ml inhibited the growth of *trichomonads*). Notably, all the healthy human vaginal lactobacilli were resistant to TP4 peptide (MBC at >250 μg/ml in all lactobacilli). Next, we assessed the antimicrobial activity of the TP4 peptide on BV-associated bacteria and normal vaginal flora in VFS, which is used to mimic the vaginal environment. **Figure 1** shows the survival rate of *G. vaginalis* was decreased by over 90% after a 2-h TP4 treatment (TP4 20, 50, and 100 μg/ml; **Figure 1B**). In contrast, there were no significant differences in *L. crispatus* (**Figure 1C**) or *L. gasseri* (**Figure 1D**) treated with TP4 (TP4 20, 50, and 100 μg/ml) compared to untreated controls. These findings demonstrated the TP4 peptide has broad-spectrum microbicide activity for vaginal pathogens, but it does not negatively affect beneficial vaginal lactobacilli. Importantly, this selective antibacterial activity was also observed in VFS.

## TP4 Rapidly Kills *Gardnerella vaginalis* With Low Spontaneous Resistance Frequency

The bactericidal mechanism of antimicrobial drugs greatly affects their killing kinetics and resistance development. Therefore, we sought to evaluate the bacterial killing kinetics of TP4 peptides compared with antibiotics. The time-kill kinetics were studied on *G. vaginalis* treated with 1X or 2X the MBC of TP4 peptide or antibiotics. As **Figure 3A** shows, TP4 peptide killed *G. vaginalis* within 120 min. In contrast, metronidazole and clindamycin exhibited longer bactericidal action times, taking 24 h to kill *G. vaginalis*. We next investigated the propensity for TP4 peptide or antibiotic treatments to induce resistant mutants. Broth dilution was performed to determine the fold-change of MIC after bacterial passage in the presence of microbicides. *Gardnerella vaginalis* was passaged for more than 20 generations during its long-term exposure to TP4 peptide and antibiotics. As shown in **Figure 3B**, the MIC for metronidazole was increased by more than 100× after four passages (MIC > 500 μg/ml), whereas the MIC for clindamycin was increased 32× after 21 passages (MIC at 125 μg/ml). In contrast, the MIC for TP4 peptide increased only 4× after 22 passages (MIC at 15.63 μg/ml). Based on these data, we conclude that TP4 peptide kill bacteria much faster than first-line antibiotics and it does not readily induce resistance.

## TP4 Prevents BV-Associated Bacterial Biofilm Formation

During our experiments, we noted that *G. vaginalis* has a capacity to form biofilms (**Table 2**). According to a previous report (Castro et al., 2019), *G. vaginalis* has a greater propensity than other BV-associated species to form biofilms, which function like a scaffold for other BV-associated species to incorporate and colonize the vaginal epithelium. After its formation, other BV-associated bacteria can add biomass to the biofilm, ultimately forming a solid biofilm structure that confers resistance to drugs. Recent studies have found that some aerobic bacteria, such as *Streptococcus* spp. and *E. coli*, are involved in BV pathogenesis (Tao et al., 2019). Therefore, we next evaluated the antibacterial activity of TP4 and antibiotics on clinical isolates of BV-associated bacteria and human vaginal lactobacilli. As shown in **Table 1**, all *L. crispatus* were resistant to first-line antibiotics and TP4 peptide (MBCs > 250 μg/ml in antibiotics and TP4 peptide to all *L. crispatus*). However, not all the anaerobic bacteria, such as *G. vaginalis*, were sensitive to metronidazole (MICs against *G. vaginalis* ranged from 3.91 to >500 μg/ml). Not surprisingly,

**TABLE 2** | Comparative susceptibility of *Gardnerella vaginalis*, *Candida albicans*, and vaginal lactobacilli to TP4 and antibiotics.

| Strain | Metronidazole | | Clindamycin | | Amphotericin B | | TP4 | | Biofilm formation ability |
|---|---|---|---|---|---|---|---|---|---|
| | MIC | MBC | MIC | MBC | MIC | MBC | MIC | MBC | |
| | μg/ml | | | | | | | | |
| *Gardnerella vaginalis* (ATCC®14018™) | 1.95–3.91 | 3.91 | 3.91 | 7.81 | | | 3.91 | 3.91–7.81 | O |
| *Gardnerella vaginalis* $M^R$ | >500 | >500 | | | | | 7.81 | 7.81 | O |
| *Gardnerella vaginalis* (ATCC®49145™) | 1.95–3.91 | 7.81 | 1.95 | 1.95–3.91 | | | 3.91 | 3.91–7.81 | O |
| *Candida albicans* (ATCC® 14053™) | | | | | <0.48 | <0.48 | 7.81 | 15.63 | |
| *Lactobacillus crispatus* (ATCC®33820™) | >500 | >500 | 62.5 | 500 | >62.5 | >62.5 | 125 | 250 | |
| *Lactobacillus gasseri* (ATCC®33323™) | >500 | >500 | >500 | >500 | >62.5 | >62.5 | 500 | 500 | |
| *Lactobacillus plantarum* (ATCC® 14917™) | >500 | >500 | 62.5 | 250 | | | 125 | 250 | |
| *Lactobacillus jensenii* (ATCC® 25258™) | >500 | >500 | 500 | >500 | | | 250 | 250 | |

*$M^R$: spontaneous metronidazole-resistant mutant; O: able to form biofilm.*

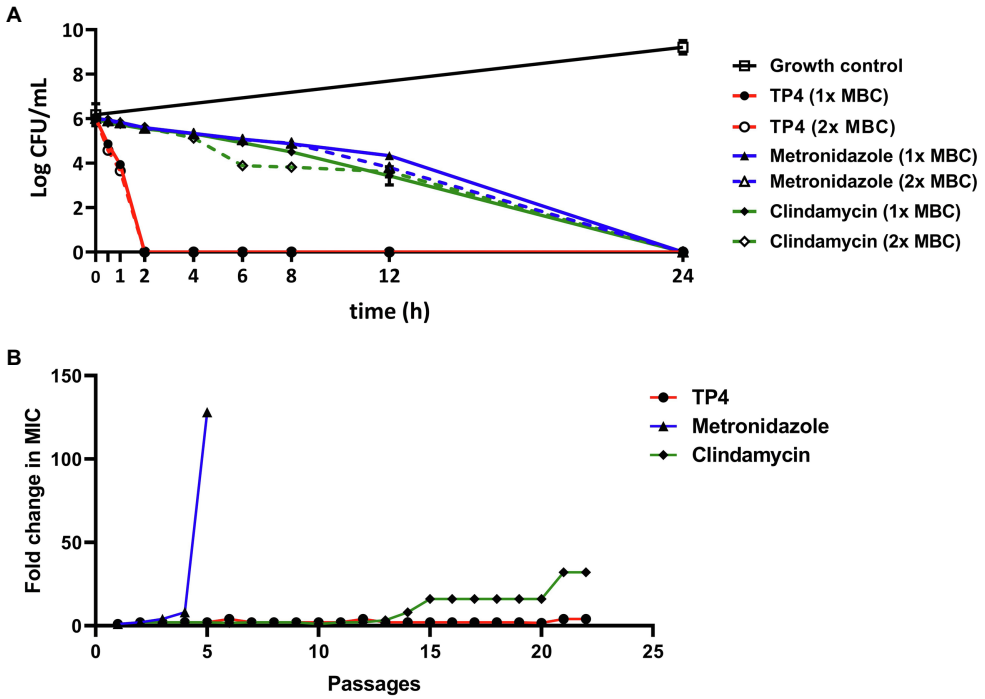


**FIGURE 3 |** Tilapia piscidin 4 rapidly kills and does not readily induce resistance in pathogenic *Gardnerella vaginalis*. **(A)** Representative time-kill curves for *G. vaginalis* exposed to TP4, metronidazole, or clindamycin at 1× MBC (7.81, 3.91, and 7.81 μg/ml, respectively) and 2× MBC (15.63, 7.81, and 15.63 μg/ml, respectively). The log CFU/ml for all groups were determined at time 0 and then at several time-points up to 24 h. **(B)** Development of resistance in *G. vaginalis* cells exposed to TP4, metronidazole, or clindamycin in an anaerobic environment. The Y-axis shows the fold-change in MIC compared to the first passage. All values represent the mean ± SD of three individual experiments.

the aerobic bacteria, i.e., *Streptococcus* spp., *E. coli* and *Enterococcus avium* were resistant to metronidazole (MICs range from 62.5 to >500 μg/ml). In addition, clindamycin only had a low MIC for some anaerobic bacteria, such as *G. vaginalis*, and aerobic bacteria. Most of the aerobic bacteria and facultative anaerobic *Actinobaculum schaalii* were resistant to clindamycin (MICs against *G. vaginalis* ranged from 3.91 to 500 μg/ml, and MICs against all aerobic bacteria or facultative anaerobic *A. schaalii* ranged from 15.63 to >500 μg/ml). In contrast, all BV-associated bacteria were sensitive to TP4 (MICs against all BV-associated bacteria ranged from 3.91 to 15.63 μg/ml). We observed that among BV-associated bacteria, *S. anginosus*, *S. agalactiae*, and *G. vaginalis* have biofilm-forming capacities (**Table 1**). Thus, we next used crystal violet staining to evaluate whether TP4 peptide and antibiotics can prevent BV-associated bacteria biofilm formation. As shown in **Figure 4**, metronidazole and clindamycin only partially prevented BV-associated bacteria biofilm formation. In contrast, TP4 peptide prevented all the BV-associated bacteria from forming biofilms. MBICs for metronidazole ranged from 3.91 to >500 μg/ml; MBICs for clindamycin ranged from 3.91 to >500 μg/ml, and MBICs for TP4 peptide ranged from 3.91 to 15.63 μg/ml. These results showed that first-line antibiotics cannot prevent all BV-associated bacteria from forming biofilms. However, TP4 can prevent all biofilm formation by all BV-associated bacteria. Most importantly, the data also revealed that *L. crispatus* clinical isolates are tolerant to TP4 peptide.

## Biofilms Increase Antibiotic Resistance Development and Associated Gene Expression in *Gardnerella vaginalis* Isolates

In general, biofilms are much more tolerant to antimicrobial agents than planktonic cells, which may a cause for failure of antibiotic treatments and disease recurrence (Hall and Mah, 2017). Biofilm-forming capacity is regarded as a virulence factor for BV pathogenesis, so we compared the biofilm-forming capacities of different *G. vaginalis* isolates. There were no significant differences in biofilm formation between different *G. vaginalis* isolates cultured in the same culture conditions (sBHI, anaerobic culture for 24 h; **Supplementary Figure 3A**). We then wanted to gather information regarding the regulation of virulence gene expression in *G. vaginalis* biofilms. We observed that in most *G. vaginalis* isolates, expression of the sialidase gene and antibiotic resistance-associated genes, such as multidrug resistance ABC transporter and BcrA were significantly increased in biofilms over planktonic cultures. Meanwhile, the cytotoxicity associated gene, vaginolysin, was significantly decreased in the biofilms compared to planktonic cells (**Supplementary Figure 3B**). These results suggest that biofilm formation may increase resistance to the intracellular actions of antibiotics.

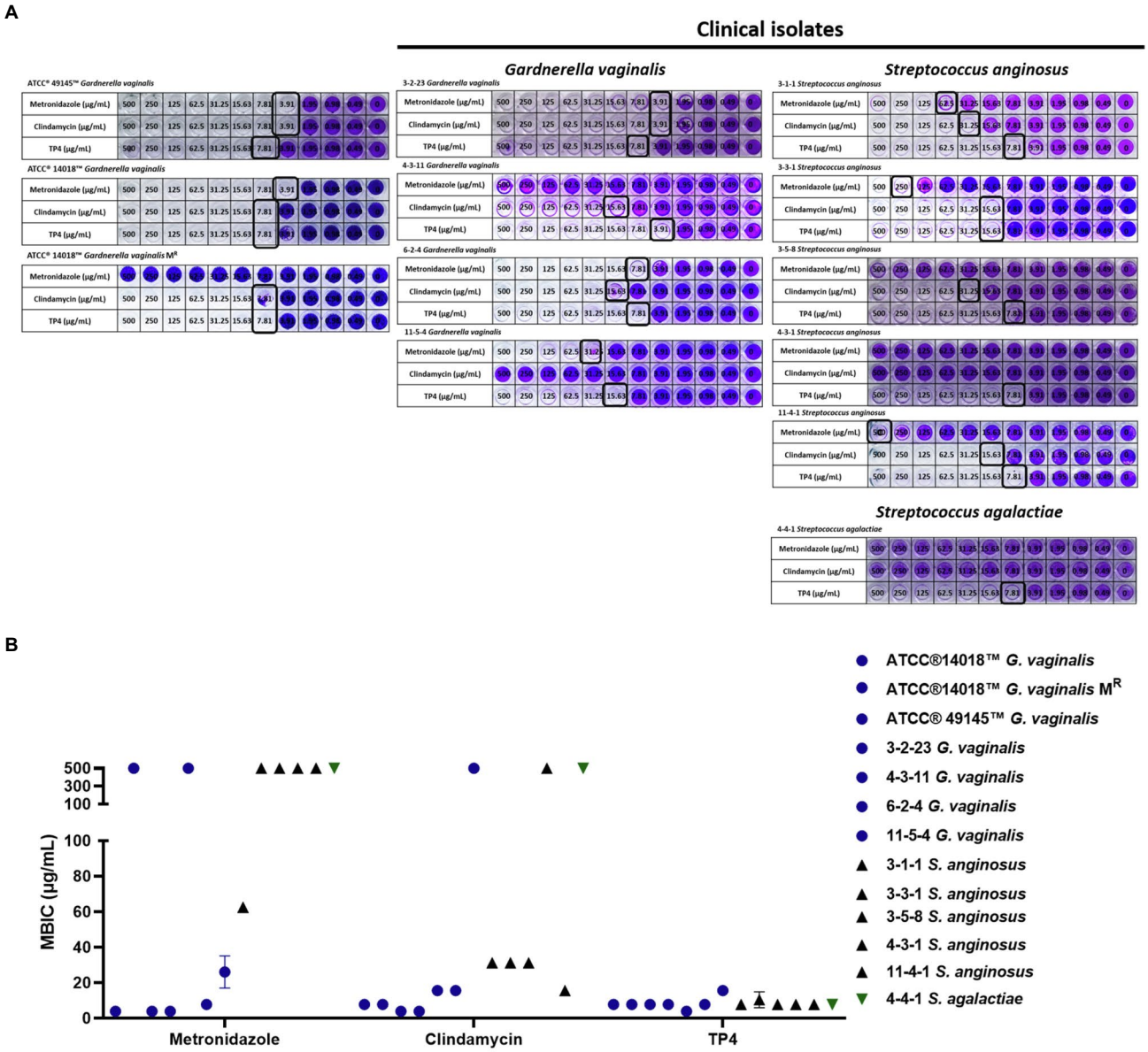


**FIGURE 4 |** Inhibitory effect of TP4 and antibiotics on BV-associated bacteria biofilm formation. Biofilms formed by BV-associated bacteria were tested with various concentrations of the TP4 and antibiotics. **(A)** The biofilm cells were stained with crystal violet; a representative result from three replicates. Black frame representative Minimal biofilm inhibitory concentration (MBIC). **(B)** Quantification of the MBIC was performed in three individual experiments. The y-axis 500 represents MBIC ≥ 500 μg/ml. All values represent the mean ± SD of three individual experiments.

## Chitosan Disrupts Biofilms and can be Used as an Excipient for TP4

Chitosan is a positively charged linear polysaccharide that is widely used in the biomedical and biotechnological fields due to its non-toxic, stable, biodegradable characteristics (Bhattarai et al., 2010). Recent studies showed that chitosan disrupts *Staphylococcus* biofilms (Felipe et al., 2019) and exhibits antifungal activity (Lo et al., 2020). To investigate whether chitosan can also disrupt *G. vaginalis* biofilm activity, we cultured biofilms with different molecular weights of chitosan (**Figure 5A**). **Figure 5B** shows that various molecular weights of chitosan disrupt *G. vaginalis* biofilm formation in a dose-dependent manner. Notably, low molecular weight (LMW) and medium molecular weight (MMW) chitosan more significantly reduced *G. vaginalis* biomass than high molecular weight (HMW) chitosan (significant difference between HMW and MMW/LMW chitosan at 0.8%; no significant differences between LMW and MMW). Next, we investigated whether the LMW and MMW chitosan would affect TP4 peptide antimicrobial activity. TP4 peptide was prepared in chitosan gel and used to determine *G. vaginalis* MBC values. **Figure 5C** shows that LMW and MMW chitosan do not affect TP4 peptide antimicrobial

**A**

| Sigma-Aldrich | Chitosan | Viscosity (10 mg/mL in 1% acetic acid ) | Molecular weight |
|---|---|---|---|
| 448869 | low molecular weight | 20-300 cP | 50,000-190,000 Da |
| 448877 | medium molecular weight | 200-800 cP | 190,000-310,000 Da |
| 419419 | high molecular weight | 800-2000 cP | 310,000-375,000 Da |

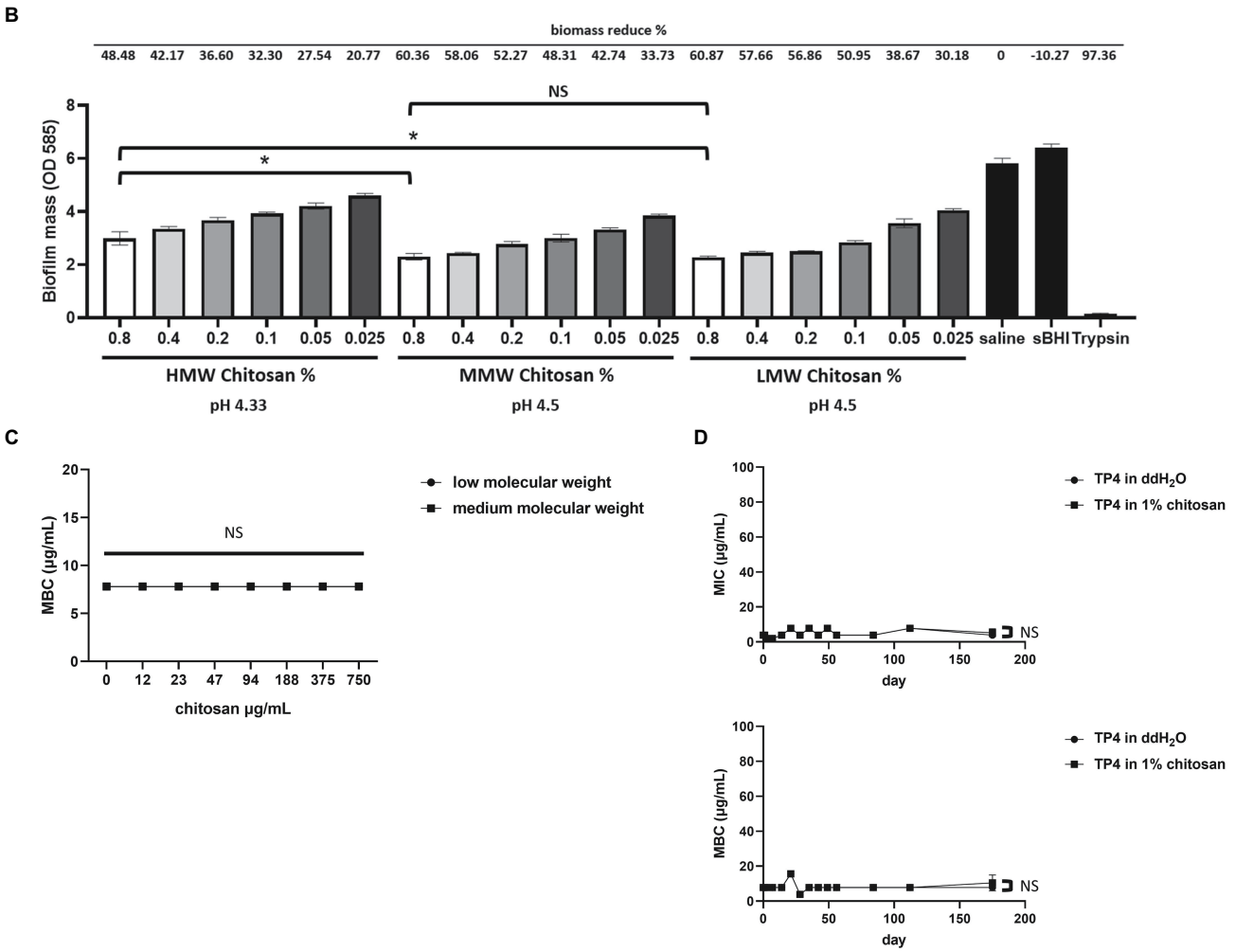


**FIGURE 5 |** Chitosan can disrupt *G. vaginalis* biofilm and does not affect TP4 bactericidal activity. **(A)** Different molecular weights of chitosan were used. **(B)** Testing the biofilm disruption activity of different molecular weights of chitosan. Different molecular weights of chitosan were added to *Gardnerella vaginalis* biofilms at different concentrations. Saline served as a vehicle control; sBHI served as a negative control; trypsin served as a positive control. Biofilm mass was determined by crystal violet staining. Data show the quantified biofilm mass and average biomass reduction (%) from three individual experiments. **(C)** TP4 bactericidal activity in Brain-Heart Infusion glucose (BHIG) with different concentrations of low molecular weight (LMW) and medium molecular weight (MMW) chitosan. **(D)** Long-term stability of TP4 stored in chitosan gel was analyzed over time. TP4 was dissolved in chitosan gel or $ddH_2O$. MICs and MBCs were determined at different time-points. All values represent the mean ± SD of three individual experiments (*$p < 0.05$, one-way ANOVA). NS, no significant differences.

activity (MBCs of 7.81 µg/ml at different concentrations of chitosan are the same as TP4 peptide dissolved in water). We then tested whether TP4 peptide stored long-term in MMW chitosan gel was stable and retained antimicrobial activity. TP4 peptide was stored in MMW chitosan gel for half a year, during which the MIC and MBC were determined at different time points. As **Figure 5D** shows, the MICs and MBCs were not significantly different between TP4 peptide in MMW chitosan gel or dissolved in water. There was no apparent change in MICs or MBCs with prolonged storage times (MICs remained in the range of 1.95–7.81 µg/ml, and MBCs remained in the range of 3.91–15.63 µg/ml). Taken together, these results showed that TP4 peptide can be stored in MMW chitosan gel for months without affecting its antimicrobial activity.

Furthermore, the biofilm-disrupting properties of chitosan may allow it to serve as an excipient for TP4 peptide.

## TP4 Peptide Combined With Chelating Agent Disodium EDTA and Chitosan Promotes Eradication of Biofilms Formed by BV-Associated Bacteria

The inability to eradicate polymicrobial BV biofilms may be largely responsible for the high disease recurrence rates associated with current first-line regimens antibiotics (Machado et al., 2016). We found that BV-associated bacteria, *G. vaginalis* and *S. anginosus*, exhibit strong biofilm-forming capacities (**Table 1**). To investigate the impact of the TP4 peptide on BV-related biofilms. *Gardnerella vaginalis*, *S. anginosus*, and mixed-culture biofilm (*G. vaginalis* combined with *S. anginosus*) were subjected to testing. EDTA is a Food and Drug Administration (FDA) approved preservative for pharmaceutical products, as it can chelate divalent ions. EDTA can destabilize the biofilm matrix and enhance susceptibility to antibacterial agents (Cavaliere et al., 2014; Field et al., 2017). Checkerboard assays showed (**Supplementary Figure 4**) that low concentration disodium EDTA (below 0.8 mM) enhanced TP4 bactericidal activity in *G. vaginalis*, *S. anginosus*, and mixed-culture biofilms (disodium EDTA >6 mM had an antagonistic effect on TP4 microbicide activity; data not shown). Next, we evaluated the bactericidal activity of TP4 peptide combined with disodium EDTA and chitosan in mature biofilms. **Figure 2** shows that TP4 peptide combined with disodium EDTA and chitosan significantly decreased the number of CFU from *G. vaginalis* (**Figure 2A**), *S. anginosus* (**Figures 2B,C**), or mixed-culture biofilms (**Figure 2D**) in a dose-dependent manner (TP4 0, 250, 500, and 1,000 μg/ml). In contrast, metronidazole is inactivated when used on *S. anginosus* (**Figure 2C**) or mixed-culture biofilms (**Figure 2D**; no significant difference between metronidazole and vehicle). These results suggest that a TP4 microbicide formulation consisting of TP4 peptide, disodium EDTA and chitosan can promote the eradication of BV-associated bacteria biofilms.

## Preformulation Studies on TP4 Peptide

Tilapia piscidin 4 peptide has broad-spectrum activity against BV-associated bacteria and is a promising agent in the treatment of BV. However, peptide drugs are susceptible to environmental influences, such as excipients or vaginal fluid that may cause conformational changes, oxidation or hydrolysis, affecting the antimicrobial activity. Long-term stability studies were performed on TP4 peptide exposed to different temperatures or different concentrations of salt, lactic acid, and oxidation conditions using HPLC. No detectable differences were observed for TP4 peptide stored at −20, 4, 25, 37, and 65°C for 28 days (**Figure 6A**). In addition, a healthy vagina is dominated by lactobacilli that produce $H_2O_2$ (physiological concentrations < 100 μM) and lactic acid (physiological concentrations 55–111 mM) to eliminate other pathogens (O'Hanlon et al., 2011). Long-term stability studies showed that TP4 peptide samples exposed to a range of $H_2O_2$ (0, 8 mM), lactic acid (0, 56.5, 113, 565, and 1,130 mM) and NaCl (0, 50, 150, 250, and 500 mM) concentrations were unaffected after 28 days (**Figures 6B–D**). This result suggests that TP4 peptide is stable in the presence of lactic acid and $H_2O_2$ as well as at a wide range of temperatures and ionic strengths. This is an important finding, as the drug will be applied in a vaginal environment (typical pH 3.5–4.5, $H_2O_2$ < 100 μM). In order to investigate potential secondary structure and conformational changes in the TP4 peptide, CD experiments were conducted under several conditions. As illustrated in **Figure 6E**, TP4 peptide dissolved in $H_2O$ exhibited negative peaks at around 198 nm in the CD spectra (SDS 0 mM), suggesting the presence of a random coil structure. With increasing SDS (membrane-mimicking condition) concentrations, a strong positive peak appeared at 191 nm, accompanied by enhancement of two negative peaks at 208 and 222 nm in the CD spectra, suggesting that the secondary structure of TP4 peptide contained an α-helix. Based on **Figure 6E** results, TP4 peptide dissolved in SDS solution (SDS 100 mM) at different temperatures (**Figure 6G**), NaCl concentrations (**Figure 6F**) or disodium EDTA concentrations (**Figure 6H**) all maintained a consistent secondary structure. The results showed that the TP4 peptide is stable and its secondary structure is maintained under many experimental conditions.

## Safety of the TP4 Microbicide Formulation in C57BL/6 Female Mice

Following the evaluation of TP4 peptide combined with disodium EDTA and chitosan on BV-associated bacteria biofilms, the *in vivo* safety of the same TP4 microbicide formulation (TP4 peptide in 0.1% chitosan with 0.4 mM disodium EDTA in saline) was tested using C57BL/6 mice. The diestrus status of Depo-Provera-treated mice was assessed by vaginal cytology before drug exposure. As shown in **Supplementary Figure 5A**, leukocytes were predominantly present in vaginal fluid of mice 4 days after Depo-Provera administration, indicating a diestrus-like state. After synchronization, mice received a single vaginal administration of the test drug. Mice were sacrificed 24 h after drug administration for histopathological examination. N-9 is a non-ionic detergent microbicide that failed in Phase 3 trials because it causes damage to the vaginal epithelium and increases pro-inflammatory mediators that subsequently increase risk of HIV and gonorrhoea infection (Hoffman et al., 2004; Obiero et al., 2012). BZK is also known to damage epithelial tissues (Patton et al., 1999). The effects of N-9 and BZK on the genital tract are well-established (Ensign et al., 2012; Podaralla et al., 2014; Coulibaly et al., 2019), so we used these two agents as positive controls in our mouse vaginal irritation experiments. The histological analysis of reproductive organs is summarized in **Figure 7** and **Supplementary Table 2**. No apparent lesions were observed in any reproductive organs of saline- or TP4-treated mice (including TP4 peptide and TP4 microbicide formulation). In contrast, vaginal irritation (epithelial thinning and erosion/necrosis) was observed in the 5% N-9 and 2% BZK groups (incidence in 5% N-9: 3/5; incidence in 2% BZK: 5/5). Furthermore, cervical irritation (epithelial

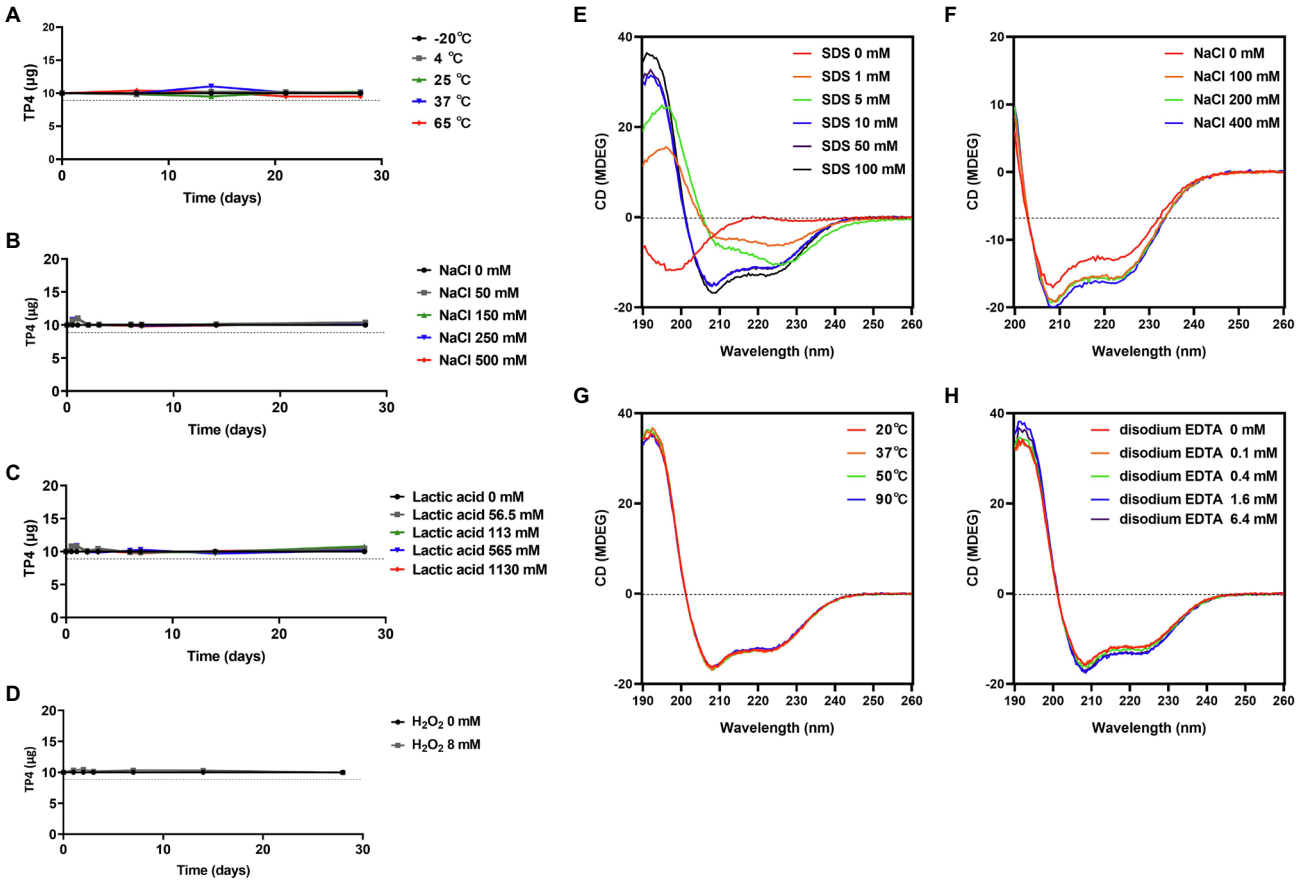


**FIGURE 6 |** Preformulation studies on TP4 peptide. High performance liquid chromatography (HPLC) of 500 μg/ml TP4 peptide dissolved in various aqueous buffer solutions or conditions and kept for various times. **(A)** TP4 was stored at −20, 4, 25, 37, and 65°C to evaluate the effects of temperature. **(B)** TP4 was incubated in different NaCl concentrations (0, 50, 150, 250, and 500 mM) to evaluate effects of ionic strength. **(C)** TP4 was stored in different lactic acid concentrations (0, 56.5, 113, 565, and 1,130 mM) to evaluate the effects of acidic physiological conditions. **(D)** TP4 oxidation was evaluated in 8 mM $H_2O_2$ solution. The dotted line represents 90% stability. Data are representative of three independent experiments and values are expressed in mean ± SD. Circular Dichroism (CD) spectra of 145 μg/ml TP4 peptide dissolved in the indicated concentrations of sodium dodecyl sulfate (SDS; **E**), in 100 mM SDS plus the indicated concentrations of NaCl **(F)**, in 100 mM SDS at 20, 37, 50, and 90°C for 1 h **(G)**, or in 100 mM SDS plus the indicated concentrations of disodium EDTA **(H)**.

thinning and erosion/necrosis) was observed in the 2% BZK group (incidence: 3/5). We also found that leukocytic exudate with cell debris, leukocyte infiltration of the subepithelial stroma, and mucification were present in both control mice and treated mice; these signs were considered to be related to the estrus cycle. The results suggest that intravaginal application of TP4 peptide (5 mg/ml and 10 mg/ml) or TP4 microbicide formulation (TP4 5 mg/ml and 10 mg/ml in gel) in mice once for 24 h did not cause toxicity or epithelial irritation in the female reproductive tissues (vagina, cervix, uterus, and ovary) when compared to known vaginal irritants (5% N-9 and 2% BZK).

## *In vivo* Effects of TP4 Microbicide Formulation

Finally, we investigated whether the TP4 microbicide formulation could be used to treat vaginal BV-associated bacteria challenges in mice. Treatment with β-estradiol improves the vaginal susceptibility of mice to infections and can be used in mouse models to evaluate the effectiveness of topical microbicides (Jerse et al., 2011; Gilbert et al., 2013). The synchronization of estrus status in β-estradiol-treated mice was assessed by vaginal cytology before treatments were administered. As shown in **Supplementary Figure 5B**, nucleated epithelial cells were predominant in vaginal fluid of mice 2 days after β-estradiol administration, indicating an estrus-like state. The mouse vaginal infection procedure and doses of bacterial strain inoculations are shown in **Supplementary Figure 6**. The β-estradiol-treated mice were challenged with *G. vaginalis* or *S. anginosus*. Of note, *S. anginosus* seemed to survive better in the mouse vagina compared to *G. vaginalis*. The inoculated doses of *G. vaginalis* and *S. anginosus* were respectively about $10^7$ and $10^6$ cells per day for each mouse (**Supplementary Figure 6B**). However, after 2 consecutive days of vaginal inoculations, the *G. vaginalis* and *S. anginosus* in the vagina of mice were respectively estimated to be about $4.1 \times 10^4$ and $4.6 \times 10^6$ cells per mouse (**Figures 8A,B**). Application of the TP4 microbicide formulation significantly decreased amount of *G. vaginalis* (**Figure 8A**) and

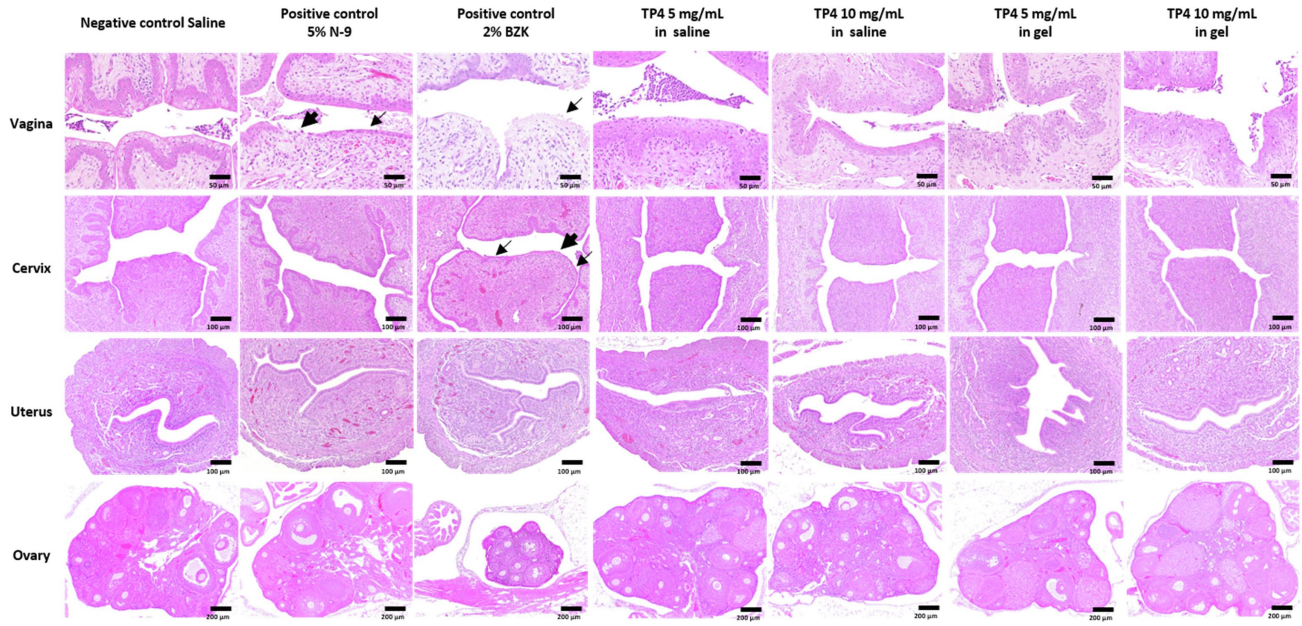


**FIGURE 7 |** Tissue toxicity following vaginal administration of TP4 microbicide formulation in mice. Eight-week-old female C57BL/6 mice were used to evaluate tissue toxicity following vaginal administration of TP4. Hematoxylin and eosin (H&E) staining of mouse reproductive organs excised 24 h after intravaginal administration of saline (negative control), 5% N-9 (positive control), 2% BZK (positive control) and TP4 at 5 or 10 mg/ml in saline or gel (TP4 microbicide formulation). Vehicle gel contains 0.1% chitosan and 0.4 mM disodium EDTA in saline. Epithelial thinning and erosion are indicated by fine arrows and arrows, respectively. Images are representative of $n = 5$ mice. Scale bar applies to all images.

*S. anginosus* (**Figure 8B**) recovered from mice vaginal lavage in a dose-dependent manner (TP4 0, 5, and 10 mg in vehicle gel).

In most cases of BV, at least two different pathogens are present in the vaginal epithelium (Castro et al., 2019). Therefore, we next investigated the effects of TP4 microbicide formulation in vaginas treated with mixed *G. vaginalis* and *S. anginosus*. TP4 was compared to metronidazole, which was prepared in the same vehicle gel. As shown in **Figure 8C**, the TP4 microbicide formulation significant decreased the total number of bacterial CFU recovered from mice vaginal lavage. In contrast, metronidazole-treated mice did not exhibit a significant difference with the vehicle group (**Figure 8C**), probably because it is inactivated on *S. anginosus* (**Figure 8D**). Next, we evaluated whether the TP4 microbicide formulation exhibited toxicity toward beneficial human vaginal lactobacilli. As shown in **Figures 8E**,**F**, no significant difference was found between TP4 microbicide formulation- and vehicle gel-treated mice that were inoculated with *L. crispatus* (**Figure 8E**) or *L. gasseri* (**Figure 8F**). Taken together, these results show that the TP4 microbicide formulation is effective at reducing BV-associated bacteria number and non-toxic to beneficial human vaginal lactobacilli *in vivo*.

## DISCUSSION

In this study, we investigate the therapeutic potential of a broad-spectrum bactericidal peptide for treating BV-associated bacteria, especially in the form of biofilms. Our findings of a biofilm-disrupting TP4 microbicide formulation may provide a new strategy for future BV treatment. The current first-line antibiotics, metronidazole, and clindamycin, cannot inhibit many BV-associated bacteria (Schuyler et al., 2016; **Table 1**). In the past, BV was thought to be dominated by *G. vaginalis*, accompanied by other anaerobic bacteria, such as *Atopobium vaginae*, *Corynebacterium amycolatum*, *Prevotella bivia*, and *Fusobacterium nucleatum* (Spiegel et al., 1983; Deng et al., 2018). However, recent studies show that aerobic bacteria, such as *S. anginosus*, are also involved in vaginitis (Tao et al., 2019). This means that current first-line antibiotic regimens, which are only effective against anaerobic bacteria, are insufficient to treat some patients. However, the development of new BV medications has been extremely slow. Although, the FDA approved Secnidazole (Solosec, a nitroimidazole derivative) in 2017, this new drug is expected to suffer from the same drawbacks as current first-line antibiotics (Aziz et al., 2019).

The TP4 peptide has broad-spectrum antimicrobial and antibiofilm activity against relevant vaginal pathogens, making it different from metronidazole and clindamycin. In particular, the lactobacilli found in healthy human vaginas are resistant to TP4 peptide (**Tables 1**, **2**; **Figure 1**). We speculate that the selective bactericidal activity of TP4 may be related to differences in cell membrane components, such as teichuronic acid, lipopolysaccharides, proteins, and phospholipids, that contribute to the overall surface charge and influence the electrostatic interactions between peptides and the membrane (Kłodzińska et al., 2010; Malmsten, 2016). *Gardnerella vaginalis* is one of the most important pathogens in BV (Schwebke et al., 2014),

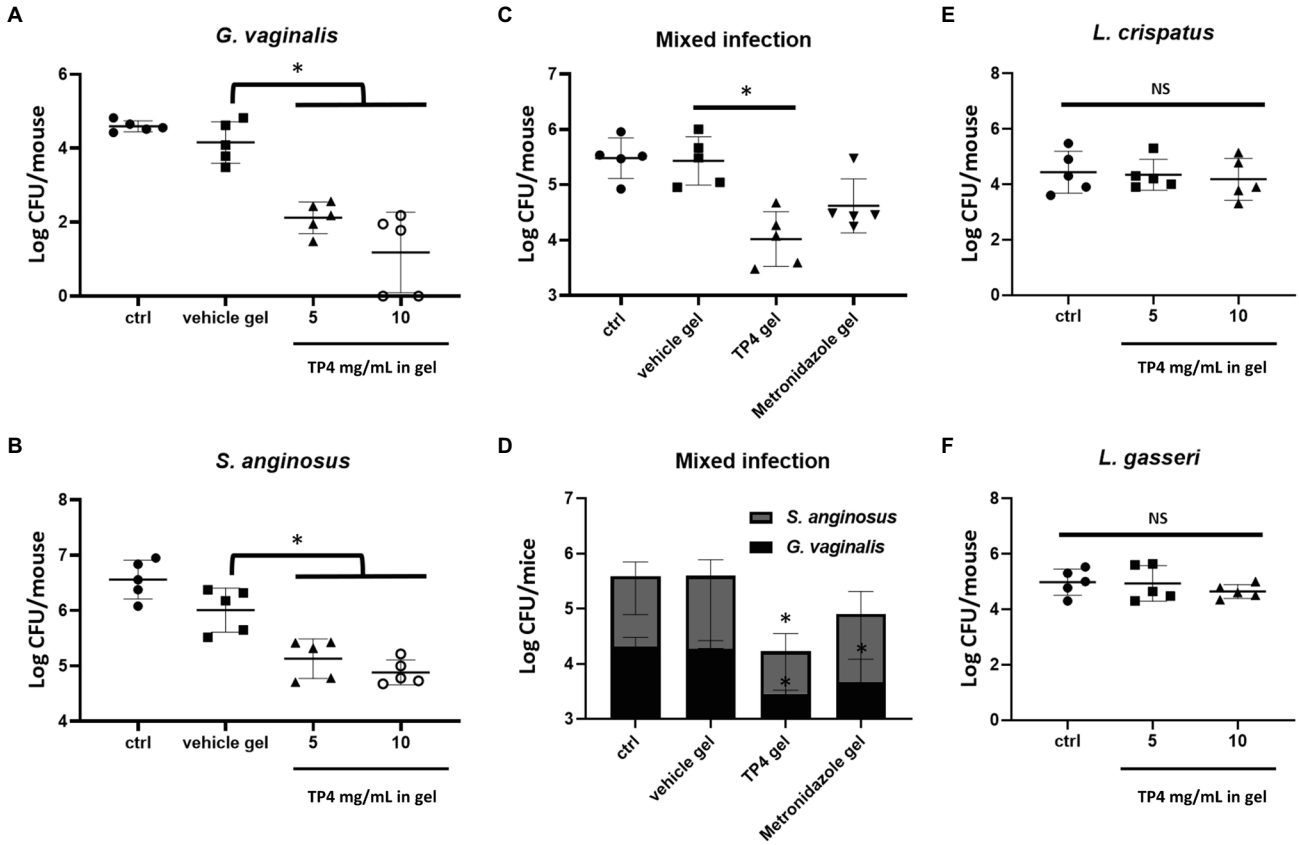


**FIGURE 8 |** *In vivo* effects of TP4 microbicide formulation. Eight-week-old female C57BL/6 mice under pseudo-estrus conditions were vaginally treated two times per day with 20 μl vehicle gel or TP4 at 5 or 10 mg/ml in gel **(A,B)**, vehicle gel or TP4 or metronidazole (7.5 mg/ml) in gel **(C,D)**, and TP4 at 5 or 10 mg/ml in gel **(E,F)** after inoculation with *Gardnerella vaginalis* **(A)**, *Streptococcus anginosus* **(B)**, *Lactobacillus crispatus* **(E)**, *Lactobacillus gasseri* **(F)** or combined *G. vaginalis* and *S. anginosus* **(C,D)**. The results show the CFUs of *G. vaginalis* and *S. anginosus*. Vehicle gel contained 0.1% chitosan and 0.4 mM disodium EDTA in saline. Bacteria viability was assessed by CFU plate counts from vaginal lavage (150 μl vaginal lavage per mouse, $n = 5$ mice per group). All values represent the mean ± SD. *$p < 0.05$ compared to vehicle gel **(A–D)** or ctrl **(E,F)**, determined by one-way ANOVA.

but its role has always been controversial because it is also present in healthy women (Hickey and Forney, 2014). Many reports show that compared with other BV-associated bacteria, *G. vaginalis* has a higher virulence potential, including cytotoxic effects and a strong propensity to form biofilms (Patterson et al., 2010; Machado et al., 2013; Alves et al., 2014). Our results demonstrated that *G. vaginalis* and *S. anginosus* exhibit some of the strongest biofilm-forming capacities among BV-associated bacteria (**Table 1**), which may promote biofilm structures that can promote growth of other BV-associated bacteria (Castro et al., 2019).

In BV, bacterial biofilms are formed by clusters of BV-associated bacteria that attach to the surface of vaginal epithelium cells (Castro et al., 2019) and are embedded in a self-produced matrix that includes proteins, polysaccharides, and extracellular DNA (Limoli et al., 2015). Studies have shown that biofilms persist on the vaginal epithelium even after putatively successful therapy with metronidazole (Swidsinski et al., 2008). The biofilms may provide a means for bacteria to evade host immune cells and reduce antimicrobial penetration. In this study, we found that the expression of drug resistance-associated genes, ABC transporter, and BcrA in the biofilm was significantly higher than in planktonic cultures for most clinical isolates (**Supplementary Figure 3**). This result is consistent with previous reports (Castro et al., 2017) and suggests that bacteria in biofilms may exhibit antibiotic resistance, which could explain the high recurrence rate with standard therapy. Therefore, new studies must focus on breaking down the biofilm structure to achieve optimal efficacy of antimicrobial therapies for BV. For instance, researchers have used DNase combined with metronidazole (Hymes et al., 2013) or amphoteric tenside pessary after metronidazole treatment to disrupt biofilms (Gottschick et al., 2017); however, this method still failed to prevent recurrence. Chitosan is an excellent excipient because it is cheap, non-toxic, and biodegradable. It has been widely used in biomedical and biotechnological fields (Muxika et al., 2017) due to its antifungal and biofilm-disrupting properties (Yang et al., 2017; Felipe et al., 2019; Araujo et al., 2021), which make it suitable as a vaginal drug carrier for BV treatment. In our study,

we demonstrated that chitosan disrupted *G. vaginalis* biofilms, and TP4 peptide stored in chitosan for up to half a year still maintained its antibacterial activity without affecting the bactericidal activity of TP4 peptide on *G. vaginalis* (**Figure 5**). Therefore, chitosan may be highly useful as a vehicle or excipient for TP4 peptide to treat BV.

Antimicrobial peptides are rarely translated into clinical use due to their poor *in vivo* stability, quick degradation and inactivation by physiological environments. However, some candidate AMPs have entered clinical trials for use in treating local infections, such as LTX-109 (Lytixar; Clinical trial identifier: NCT01223222, NCT01803035, and NCT01158235), and Pexiganan (Locilex) (NCT01590758 and NCT01594762), SGX942 (NCT02013050; Mahlapuu et al., 2020). In order to evaluate the possible clinical use of TP4 peptides as a topical microbicide, one must first consider whether the local environment affects the bactericidal activity. Therefore, we performed a preformulation evaluation of the product (Alliance for Microbicide Development, 2006). Generally, AMPs are in a random coil conformation when dissolved in water and form an active amphipathic α-helix when they come into contact with the bacterial surface, subsequently promoting membrane leakage (Beevers and Dixon, 2010). The secondary structure is highly susceptible to environmental influences, which can change the ability of the AMP to cause membrane leakage (Júnior et al., 2018). We use VFS to mimic a vaginal fluid environment and found that in this solvent, TP4 maintains selective bactericidal activity for *G. vaginalis* and does not affect healthy human vaginal lactobacilli (**Figure 1**). We also considered peptide degradation during the manufacturing process or when it enters a biological system (Volkin et al., 2002). HPLC and CD were used to evaluate the TP4 peptide stability and secondary structure, revealing that TP4 peptide is stable over a wide range of temperatures, and concentrations of salt, disodium EDTA, hydrogen peroxide, and lactic acid; it does not lose its secondary structure under these conditions (**Figure 6**). Taken together, our data show that TP4 peptide has great potential for development as a microbicide candidate.

Various vaginal microbicide formulations are unable to enter clinical trials due to safety concerns, so lead microbicide formulations need to be evaluated early in the development process (Fernández-Romero et al., 2015). The WHO recommendations the osmolality of a microbicide formulation candidates should not exceed 380 mOsm/kg to reduce the risk of vaginal epithelium damage, and pH values should be about 3.5–4.5 (around normal vaginal values) to prevent increasing BV risk and HIV survival (World Health Organization, 2012). In this study, the formulation of chitosan as a TP4 peptide excipient conforms with these WHO recommendations (TP4 microbicide formulation osmolality <380 mOsm/Kg, pH 4.5). The preclinical safety of TP4 microbicide formulation was evaluated in C57BL/6 mice, including an assessment of vaginal inflammation, swelling, mucosa damage, and local toxicity, as well as harm to vagina normal flora (Fernández-Romero et al., 2015). There was no obvious toxicity in mice receiving intravaginal administration of the TP4 microbicide formulation. Estradiol-treated mice are often used as animal models to establish the colonization of pathogens associated with human reproductive tract infections, such as *G. vaginalis* (Gilbert et al., 2013; Hymes et al., 2013), *Streptococcus agalactiae* (Vrbanac et al., 2018), and *Neisseria gonorrhoeae* (Jerse et al., 2011). The pH of estradiol-treated mouse vagina (pH range 5.8–7.2; Jerse et al., 2011) is conducive to the colonization of BV-associated bacteria, which can be inoculated to evaluate the *in vivo* microbicidal activities of TP4 microbicide formulations. In this study, we established a murine model of single- or dual-species vaginal colonization by *G. vaginalis and S. anginosus*, or lactobacilli. We demonstrated that TP4 microbicide formulation decreases the colonization density of BV-associated bacteria but not lactobacilli. Not surprisingly, metronidazole did not reduce the *S. anginosus* survival in dual-species infected mice. However, the immunomodulatory effects of TP4 microbicide formulation could not be evaluated in this model because of a non-obvious inflammatory response in vaginal tissue and fluid (data not shown) in inoculated mice (observed after *G. vaginalis, S. anginosus*, or dual-species). These results are consistent with a previous report (Gilbert et al., 2013). Overall, this study suggests that the TP4 microbicide formulation has broad-spectrum BV-associated bactericidal activity. The TP4 peptide, chelating agent disodium EDTA and biofilm-disrupting chitosan might be a potent anti-biofilm formulation to treat polymicrobial BV biofilms.

## DATA AVAILABILITY STATEMENT

The original contributions presented in the study are included in the article/**Supplementary Material**, further inquiries can be directed to the corresponding author.

## ETHICS STATEMENT

Mouse experiments were approved by the Academia Sinica Institutional Animal Care & Utilization Committee (Protocol number: IACUC 20-12-1568).

## AUTHOR CONTRIBUTIONS

W-CL designed and performed the experiments, analyzed the data, and wrote the manuscript. Y-RC performed the Far-UV CD spectrum. C-MC designed the experimental studies. J-YC obtained funding, designed the experiments, and revised the paper. All authors contributed to the article and approved the submitted version.

## FUNDING

This work was supported by a grant through the National Biotechnology Research Park, Academia Sinica (NBRP-TRP-108-1-01). This research was supported by intramural funding

from the Marine Research Station (Jiaushi, Ilan), Institute of Cellular and Organismic Biology, Academia Sinica to J-YC (Research Fellow).

## ACKNOWLEDGMENTS

The authors would like to thank Kan-Hung Lee and National Laboratory Animal Center, Taipei, Taiwan for their useful advice on pathological examination. We acknowledge Y-RC from the Academia Sinica Protein Clinic (ASPC) for supporting the data collection and analysis of Far-UV CD spectrum. ASPC is funded by Academia Sinica Core Facility and Innovative Instrument Project (AS-CFII-109-107). We would like to thank Marcus J. Calkins for English editing. We thank the Institute of Cellular and Organismic Biology Core Facility for technical support during the experiments.

## SUPPLEMENTARY MATERIAL

The Supplementary Material for this article can be found online at: https://www.frontiersin.org/articles/10.3389/fmicb.2022.806654/full#supplementary-material

## REFERENCES

Algburi, A., Zehm, S., Netrebov, V., Weeks, R., Zubovskiy, K., and Chikindas, M. L. (2018). Benzoyl peroxide inhibits quorum sensing and biofilm formation by *Gardnerella vaginalis* 14018. *Infect. Dis. Obstet. Gynecol.* 2018, 1–9. doi: 10.1155/2018/1426109

Alliance for Microbicide Development (2006) *MDS, the Microbicide Development Strategy*. MD: Silver Spring.

Alves, P., Castro, J., Sousa, C., Cereija, T. B., and Cerca, N. (2014). *Gardnerella vaginalis* outcompetes 29 other bacterial species isolated from patients with bacterial vaginosis, using in an in vitro biofilm formation model. *J. Infect. Dis.* 210, 593–596. doi: 10.1093/infdis/jiu131

Araujo, V., de Souza, M., Carvalho, G. C., Duarte, J. L., and Chorilli, M. (2021). Chitosan-based systems aimed at local application for vaginal infections. *Carbohydr. Polym.* 261:117919. doi: 10.1016/j.carbpol.2021.117919

Aziz, M. A. A., Sharifipour, F., Abedi, P., Jahanfar, S., and Judge, H. M. (2019). Secnidazole for treatment of bacterial vaginosis: a systematic review. *BMC Womens Health* 19:121. doi: 10.1186/s12905-019-0822-2

Beevers, A. J., and Dixon, A. M. (2010). Helical membrane peptides to modulate cell function. *Chem. Soc. Rev.* 39, 2146–2157. doi: 10.1039/b912944h

Bhattarai, N., Gunn, J., and Zhang, M. (2010). Chitosan-based hydrogels for controlled, localized drug delivery. *Adv. Drug Deliv. Rev.* 62, 83–99. doi: 10.1016/j.addr.2009.07.019

Borges, S., Silva, J., and Teixeira, P. (2014). The role of lactobacilli and probiotics in maintaining vaginal health. *Arch. Gynecol. Obstet.* 289, 479–489. doi: 10.1007/s00404-013-3064-9

Bradshaw, C. S., Pirotta, M., De Guingand, D., Hocking, J. S., Morton, A. N., Garland, S. M., et al. (2012). Efficacy of oral metronidazole with vaginal clindamycin or vaginal probiotic for bacterial vaginosis: randomised placebo-controlled double-blind trial. *PLoS One* 7:e34540. doi: 10.1371/journal.pone.0034540

Brotman, R. M., Klebanoff, M. A., Nansel, T. R., Yu, K. F., Andrews, W. W., Zhang, J., et al. (2010). Bacterial vaginosis assessed by gram stain and diminished colonization resistance to incident gonococcal, chlamydial, and trichomonal genital infection. *J. Infect. Dis.* 202, 1907–1915. doi: 10.1086/657320

Byers, S. L., Wiles, M. V., Dunn, S. L., and Taft, R. A. (2012). Mouse estrous cycle identification tool and images. *PLoS One* 7:e35538. doi: 10.1371/journal.pone.0035538

Castro, J., França, A., Bradwell, K. R., Serrano, M. G., Jefferson, K. K., and Cerca, N. (2017). Comparative transcriptomic analysis of *Gardnerella vaginalis* biofilms vs. planktonic cultures using RNA-seq. *NPJ Biofilms Microbiomes* 3:3. doi: 10.1038/s41522-017-0012-7

Castro, J., Machado, D., and Cerca, N. (2019). Unveiling the role of *Gardnerella vaginalis* in polymicrobial bacterial vaginosis biofilms: the impact of other vaginal pathogens living as neighbors. *ISME J.* 13, 1306–1317. doi: 10.1038/s41396-018-0337-0

Cavaliere, R., Ball, J. L., Turnbull, L., and Whitchurch, C. B. (2014). The biofilm matrix destabilizers, EDTA and DNaseI, enhance the susceptibility of nontypeable Hemophilus influenzae biofilms to treatment with ampicillin and ciprofloxacin. *Microbiologyopen* 3, 557–567. doi: 10.1002/mbo3.187

Chang, T. W., Wei, S. Y., Wang, S. H., Wei, H. M., Wang, Y. J., Wang, C. F., et al. (2017). Hydrophobic residues are critical for the helix-forming, hemolytic and bactericidal activities of amphipathic antimicrobial peptide TP4. *PLoS One* 12:e0186442. doi: 10.1371/journal.pone.0186442

Cohen, C. R., Lingappa, J. R., Baeten, J. M., Ngayo, M. O., Spiegel, C. A., Hong, T., et al. (2012). Bacterial vaginosis associated with increased risk of female-to-male HIV-1 transmission: a prospective cohort analysis among African couples. *PLoS Med.* 9:e1001251. doi: 10.1371/journal.pmed.1001251

Coulibaly, F. S., Ezoulin, M., Dim, D. C., Molteni, A., and Youan, B. C. (2019). Preclinical safety evaluation of HIV-1 gp120 responsive microbicide delivery system in C57BL/6 female mice. *Mol. Pharm.* 16, 595–606. doi: 10.1021/acs.molpharmaceut.8b00872

DeLano, W. L. (2002). Pymol: an open-source molecular graphics tool. *Ccp4 Newsl. Protein Crystallogr.* 40:11.

Deng, Z. L., Gottschick, C., Bhuju, S., Masur, C., Abels, C., and Wagner-Döbler, I. (2018). Metatranscriptome analysis of the vaginal microbiota reveals potential mechanisms for protection against metronidazole in bacterial vaginosis. *mSphere* 3, e00262–e00318. doi: 10.1128/mSphereDirect.00262-18

Elliott, A. G., Huang, J. X., Neve, S., Zuegg, J., Edwards, I. A., Cain, A. K., et al. (2020). An amphipathic peptide with antibiotic activity against multidrug-resistant gram-negative bacteria. *Nat. Commun.* 11:3184. doi: 10.1038/s41467-020-16950-x

Ensign, L. M., Tang, B. C., Wang, Y. Y., Tse, T. A., Hoen, T., Cone, R., et al. (2012). Mucus-penetrating nanoparticles for vaginal drug delivery protect against herpes simplex virus. *Sci. Transl. Med.* 4:138ra79. doi: 10.1126/scitranslmed.3003453

Felipe, V., Breser, M. L., Bohl, L. P., Rodrigues da Silva, E., Morgante, C. A., Correa, S. G., et al. (2019). Chitosan disrupts biofilm formation and promotes biofilm eradication in *Staphylococcus* species isolated from bovine mastitis. *Int. J. Biol. Macromol.* 126, 60–67. doi: 10.1016/j.ijbiomac.2018.12.159

Fernández-Romero, J. A., Teleshova, N., Zydowsky, T. M., and Robbiani, M. (2015). Preclinical assessments of vaginal microbicide candidate safety and efficacy. *Adv. Drug Deliv. Rev.* 92, 27–38. doi: 10.1016/j.addr.2014.12.005

Field, D., Baghou, I., Rea, M. C., Gardiner, G. E., Ross, R. P., and Hill, C. (2017). Nisin in combination with cinnamaldehyde and EDTA to control growth of escherichia coli strains of swine origin. *Antibiotics* 6:35. doi: 10.3390/antibiotics6040035

Gilbert, N. M., Lewis, W. G., and Lewis, A. L. (2013). Clinical features of bacterial vaginosis in a murine model of vaginal infection with *Gardnerella vaginalis*. *PLoS One* 8:e59539. doi: 10.1371/journal.pone.0059539

Gilbert, N. M., Lewis, W. G., Li, G., Sojka, D. K., Lubin, J. B., and Lewis, A. L. (2019). *Gardnerella vaginalis* and *Prevotella bivia* trigger distinct and overlapping phenotypes in a mouse model of bacterial vaginosis. *J. Infect. Dis.* 220, 1099–1108. doi: 10.1093/infdis/jiy704

Gottschick, C., Deng, Z. L., Vital, M., Masur, C., Abels, C., Pieper, D. H., et al. (2017). Treatment of biofilms in bacterial vaginosis by an amphoteric tenside pessary-clinical study and microbiota analysis. *Microbiome* 5:119. doi: 10.1186/s40168-017-0326-y

Gottschick, C., Szafranski, S. P., Kunze, B., Sztajer, H., Masur, C., Abels, C., et al. (2016). Screening of compounds against *Gardnerella vaginalis* biofilms. *PLoS One* 11:e0154086. doi: 10.1371/journal.pone.0154086

Hall, C. W., and Mah, T. F. (2017). Molecular mechanisms of biofilm-based antibiotic resistance and tolerance in pathogenic bacteria. *FEMS Microbiol. Rev.* 41, 276–301. doi: 10.1093/femsre/fux010

Hay, P. (2017). Bacterial vaginosis. *F1000Research* 6:1761. doi: 10.12688/f1000research.11417.1

Hazam, P. K., and Chen, J. Y. (2020). Therapeutic utility of the antimicrobial peptide tilapia piscidin 4 (TP4). *Aquacult. Rep.* 17:100409. doi: 10.1016/j.aqrep.2020.100409

Heczko, P. B., Tomusiak, A., Adamski, P., Jakimiuk, A. J., Stefański, G., Mikołajczyk-Cichońska, A., et al. (2015). Supplementation of standard antibiotic therapy with oral probiotics for bacterial vaginosis and aerobic vaginitis: a randomised, double-blind, placebo-controlled trial. *BMC Womens Health* 15, 1–12. doi: 10.1186/s12905-015-0246-6

Hickey, R. J., and Forney, L. J. (2014). *Gardnerella vaginalis* does not always cause bacterial vaginosis. *J. Infect. Dis.* 210, 1682–1683. doi: 10.1093/infdis/jiu303

Hoffman, I. F., Taha, T. E., Padian, N. S., Kelly, C. W., Welch, J. D., Martinson, F. E., et al. (2004). Nonoxynol-9 100 mg gel: multi-site safety study from sub-Saharan Africa. *AIDS* 18, 2191–2195. doi: 10.1097/00002030-200411050-00012

Huang, H. N., Chan, Y. L., Wu, C. J., and Chen, J. Y. (2015). Tilapia piscidin 4 (TP4) stimulates cell proliferation and wound closure in MRSA-infected wounds in mice. *Mar. Drugs* 13, 2813–2833. doi: 10.3390/md13052813

Hymes, S. R., Randis, T. M., Sun, T. Y., and Ratner, A. J. (2013). DNase inhibits *Gardnerella vaginalis* biofilms in vitro and in vivo. *J. Infect. Dis.* 207, 1491–1497. doi: 10.1093/infdis/jit047

Jardak, M., Abdelli, F., Laadhar, R., Lami, R., Stien, D., Aifa, S., et al. (2017). Evaluation of biofilm-forming ability of bacterial strains isolated from the roof of an old house. *J. Gen. Appl. Microbiol.* 63, 186–194. doi: 10.2323/jgam.2016.10.005

Jerse, A. E., Wu, H., Packiam, M., Vonck, R. A., Begum, A. A., and Garvin, L. E. (2011). Estradiol-treated female mice as surrogate hosts for neisseria gonorrhoeae genital tract infections. *Front. Microbiol.* 2:107. doi: 10.3389/fmicb.2011.00107

Júnior, N., Cardoso, M. H., Cândido, E. S., van den Broek, D., de Lange, N., Velikova, N., et al. (2018). An acidic model pro-peptide affects the secondary structure, membrane interactions and antimicrobial activity of a crotalicidin fragment. *Sci. Rep.* 8:11127. doi: 10.1038/s41598-018-29444-0

Kłodzińska, E., Szumski, M., Dziubakiewicz, E., Hrynkiewicz, K., Skwarek, E., Janusz, W., et al. (2010). Effect of zeta potential value on bacterial behavior during electrophoretic separation. *Electrophoresis* 31, 1590–15966. doi: 10.1002/elps.200900559

Lázár, V., Martins, A., Spohn, R., Daruka, L., Grézal, G., Fekete, G., et al. (2018). Antibiotic-resistant bacteria show widespread collateral sensitivity to antimicrobial peptides. *Nat. Microbiol.* 3, 718–731. doi: 10.1038/s41564-018-0164-0

Lee, J. K., Luchian, T., and Park, Y. (2018). New antimicrobial peptide kills drug-resistant pathogens without detectable resistance. *Oncotarget* 9, 15616–15634. doi: 10.18632/oncotarget.24582

Limoli, D. H., Jones, C. J., and Wozniak, D. J. (2015). Bacterial extracellular polysaccharides in biofilm formation and function. *Microbiol. Spectr.* 3, 1–30. doi: 10.1128/microbiolspec

Liu, C. W., Su, B. C., and Chen, J. Y. (2021). Tilapia piscidin 4 (TP4) reprograms M1 macrophages to M2 phenotypes in cell models of *Gardnerella vaginalis*-induced vaginosis. *Front. Immunol.* 12:773013. doi: 10.3389/fimmu.2021.773013

Lo, W. H., Deng, F. S., Chang, C. J., and Lin, C. H. (2020). Synergistic antifungal activity of chitosan with fluconazole against *Candida albicans*, *Candida tropicalis*, and fluconazole-resistant strains. *Molecules* 25:5114. doi: 10.3390/molecules25215114

Machado, D., Castro, J., Palmeira-de-Oliveira, A., Martinez-de-Oliveira, J., and Cerca, N. (2016). Bacterial vaginosis biofilms: challenges to current therapies and emerging solutions. *Front. Microbiol.* 6:1528. doi: 10.3389/fmicb.2015.01528

Machado, A., Jefferson, K. K., and Cerca, N. (2013). Interactions between *Lactobacillus crispatus* and bacterial vaginosis (BV)-associated bacterial species in initial attachment and biofilm formation. *Int. J. Mol. Sci.* 14, 12004–12012. doi: 10.3390/ijms140612004

Mahlapuu, M., Björn, C., and Ekblom, J. (2020). Antimicrobial peptides as therapeutic agents: opportunities and challenges. *Crit. Rev. Biotechnol.* 40, 978–992. doi: 10.1080/07388551.2020.1796576

Malmsten, M. (2016). Interactions of antimicrobial peptides with bacterial membranes and membrane components. *Curr. Top. Med. Chem.* 16, 16–24. doi: 10.2174/1568026615666150703121518

Marcotte, H., Larsson, P. G., Andersen, K. K., Zuo, F., Mikkelsen, L. S., Brandsborg, E., et al. (2019). An exploratory pilot study evaluating the supplementation of standard antibiotic therapy with probiotic lactobacilli in south African women with bacterial vaginosis. *BMC Infect. Dis.* 19, 1–15. doi: 10.1186/s12879-019-4425-1

Maróti, G., Kereszt, A., Kondorosi, E., and Mergaert, P. (2011). Natural roles of antimicrobial peptides in microbes, plants and animals. *Res. Microbiol.* 162, 363–374. doi: 10.1016/j.resmic.2011.02.005

McLean, A. C., Valenzuela, N., Fai, S., and Bennett, S. A. (2012). Performing vaginal lavage, crystal violet staining, and vaginal cytological evaluation for mouse estrous cycle staging identification. *J. Vis. Exp.* 67:e4389. doi: 10.3791/4389

Mendling, W., Palmeira-de-Oliveira, A., Biber, S., and Prasauskas, V. (2019). An update on the role of *Atopobium vaginae* in bacterial vaginosis: what to consider when choosing a treatment? A mini review. *Arch. Gynecol. Obstet.* 300, 1–6. doi: 10.1007/s00404-019-05142-8

Muxika, A., Etxabide, A., Uranga, J., Guerrero, P., and de la Caba, K. (2017). Chitosan as a bioactive polymer: processing, properties and applications. *Int. J. Biol. Macromol.* 105, 1358–1368. doi: 10.1016/j.ijbiomac.2017.07.087

Obiero, J., Mwethera, P. G., and Wiysonge, C. S. (2012). Topical microbicides for prevention of sexually transmitted infections. *Cochrane Database Syst. Rev.* 6:CD007961. doi: 10.1002/14651858.CD007961.pub2

O'Hanlon, D. E., Moench, T. R., and Cone, R. A. (2011). In vaginal fluid, bacteria associated with bacterial vaginosis can be suppressed with lactic acid but not hydrogen peroxide. *BMC Infect. Dis.* 11:200. doi: 10.1186/1471-2334-11-200

O'Hanlon, D. E., Moench, T. R., and Cone, R. A. (2013). Vaginal pH and microbicidal lactic acid when lactobacilli dominate the microbiota. *PLoS One* 8:e80074. doi: 10.1371/journal.pone.0080074

Pan, C. Y., Chen, J. C., Chen, T. L., Wu, J. L., Hui, C. F., and Chen, J. Y. (2015). Piscidin is highly active against carbapenem-resistant *Acinetobacter baumannii* and NDM-1-producing *Klebsiella pneumonia* in a systemic septicaemia infection mouse model. *Mar. Drugs* 13, 2287–2305. doi: 10.3390/md13042287

Pappas, P. G., Kauffman, C. A., Andes, D. R., Clancy, C. J., Marr, K. A., Ostrosky-Zeichner, L., et al. (2016). Clinical practice guideline for the management of candidiasis: 2016 update by the infectious diseases society of America. *Clin. Infect. Dis.* 62, e1–e50. doi: 10.1093/cid/civ933

Pasupuleti, M., Schmidtchen, A., and Malmsten, M. (2012). Antimicrobial peptides: key components of the innate immune system. *Crit. Rev. Biotechnol.* 32, 143–171. doi: 10.3109/07388551.2011.594423

Patterson, J. L., Stull-Lane, A., Girerd, P. H., and Jefferson, K. K. (2010). Analysis of adherence, biofilm formation and cytotoxicity suggests a greater virulence potential of *Gardnerella vaginalis* relative to other bacterial-vaginosis-associated anaerobes. *Microbiology* 156, 392–399. doi: 10.1099/mic.0.034280-0

Patton, D. L., Kidder, G. G., Sweeney, Y. C., Rabe, L. K., and Hillier, S. L. (1999). Effects of multiple applications of benzalkonium chloride and nonoxynol 9 on the vaginal epithelium in the pigtailed macaque (Macaca nemestrina). *Am. J. Obstet. Gynecol.* 180, 1080–1087. doi: 10.1016/S0002-9378(99)70598-3

Plummer, E. L., Bradshaw, C. S., Doyle, M., Fairley, C. K., Murray, G. L., Bateson, D., et al. (2021). Lactic acid-containing products for bacterial vaginosis and their impact on the vaginal microbiota: a systematic review. *PLoS One* 16:e0246953. doi: 10.1371/journal.pone.0246953

Podaralla, S., Alt, C., and Shankar, G. N. (2014). Formulation development and evaluation of innovative two-polymer (SR-2P) bioadhesive vaginal gel. *AAPS PharmSciTech* 15, 928–938. doi: 10.1208/s12249-014-0124-9

Powell, A., Ghanem, K. G., Rogers, L., Zinalabedini, A., Brotman, R. M., Zenilman, J., et al. (2019). Clinicians' use of intravaginal boric acid maintenance therapy for recurrent vulvovaginal candidiasis and bacterial vaginosis. *Sex. Transm. Dis.* 46, 810–812. doi: 10.1097/OLQ.0000000000001063

Ravel, J., Moreno, I., and Simón, C. (2021). Bacterial vaginosis and its association with infertility, endometritis, and pelvic inflammatory disease. *Am. J. Obstet. Gynecol.* 224, 251–257. doi: 10.1016/j.ajog.2020.10.019

Sassi, A. B., Bunge, K. E., Hood, B. L., Conrads, T. P., Cole, A. M., Gupta, P., et al. (2011). Preformulation and stability in biological fluids of the retrocyclin RC-101, a potential anti-HIV topical microbicide. *AIDS Res. Ther.* 8:27. doi: 10.1186/1742-6405-8-27

Schaefer, K., Brown, N., Kaye, P. M., and Lacey, C. J. (2014). Cervico-vaginal immunoglobulin G levels increase post-ovulation independently of neutrophils. *PLoS One* 9:e114824. doi: 10.1371/journal.pone.0114824

Schuyler, J. A., Mordechai, E., Adelson, M. E., Sobel, J. D., Gygax, S. E., and Hilbert, D. W. (2016). Identification of intrinsically metronidazole-resistant clades of *Gardnerella vaginalis*. *Diagn. Microbiol. Infect. Dis.* 84, 1–3. doi: 10.1016/j.diagmicrobio.2015.10.006

Schwebke, J. R., Muzny, C. A., and Josey, W. E. (2014). Role of *Gardnerella vaginalis* in the pathogenesis of bacterial vaginosis: a conceptual model. *J. Infect. Dis.* 210, 338–343. doi: 10.1093/infdis/jiu089

Shackelford, C., Long, G., Wolf, J., Okerberg, C., and Herbert, R. (2002). Qualitative and quantitative analysis of nonneoplastic lesions in toxicology studies. *Toxicol. Pathol.* 30, 93–96. doi: 10.1080/01926230252824761

Shaio, M. F., Chen, J. G., and Chang, F. Y. (1987). A comparison of various methods for the determination of viability of parasitic flagellates. *Southeast Asian J. Trop. Med. Public Health* 18, 539–546.

Sobel, J. D., Ferris, D., Schwebke, J., Nyirjesy, P., Wiesenfeld, H. C., Peipert, J., et al. (2006). Suppressive antibacterial therapy with 0.75% metronidazole vaginal gel to prevent recurrent bacterial vaginosis. *Am. J. Obstet. Gynecol.* 194, 1283–1289. doi: 10.1016/j.ajog.2005.11.041

Spiegel, C. A., Davick, P., Totten, P. A., Chen, K. C., Eschenbach, D. A., Amsel, R., et al. (1983). *Gardnerella vaginalis* and anaerobic bacteria in the etiology of bacterial (nonspecific) vaginosis. *Scand. J. Infect. Dis.* 40, 41–46.

Swidsinski, A., Mendling, W., Loening-Baucke, V., Swidsinski, S., Dörffel, Y., Scholze, J., et al. (2008). An adherent *Gardnerella vaginalis* biofilm persists on the vaginal epithelium after standard therapy with oral metronidazole. *Am. J. Obstet. Gynecol.* 198, 97.e1–97.e6. doi: 10.1016/j.ajog.2007.06.039

Tao, Z., Zhang, L., Zhang, Q., Lv, T., Chen, R., Wang, L., et al. (2019). The pathogenesis of *Streptococcus anginosus* in aerobic vaginitis. *Infect. Drug Resist.* 12, 3745–3754. doi: 10.2147/IDR.S227883

Toke, O. (2005). Antimicrobial peptides: new candidates in the fight against bacterial infections. *Biopolymers* 80, 717–735. doi: 10.1002/bip.20286

Tomás, M. S. J., and Nader-Macías, M. E. (2007). Effect of a medium simulating vaginal fluid on the growth and expression of beneficial characteristics of potentially probiotic lactobacilli. *Commun. Curr. Res. Educ. Top. Trends Appl. Microbiol.* 2, 732–739.

Volkin, D. B., Sanyal, G., Burke, C. J., and Middaugh, C. R. (2002). Preformulation studies as an essential guide to formulation development and manufacture of protein pharmaceuticals. *Pharm. Biotechnol.* 14, 1–46. doi: 10.1007/978-1-4615-0549-5_1

Vrbanac, A., Riestra, A. M., Coady, A., Knight, R., Nizet, V., and Patras, K. A. (2018). The murine vaginal microbiota and its perturbation by the human pathogen group B *Streptococcus*. *BMC Microbiol.* 18:197. doi: 10.1186/s12866-018-1341-2

Wang, G., Li, X., and Wang, Z. (2016). APD3: the antimicrobial peptide database as a tool for research and education. *Nucleic Acids Res.* 44, D1087–D1093. doi: 10.1093/nar/gkv1278

Workowski, K. A. (2015). Centers for disease control and prevention sexually transmitted diseases treatment guidelines. *Clin. Infect. Dis.* 61, S759–S762. doi: 10.1093/cid/civ771

World Health Organization (2012). Use and procurement of additional lubricants for male and female condoms: WHO/UNFPA/FHI360: advisory note. World Health Organization. Available at: https://apps.who.int/iris/bitstream/handle/10665/76580/WHO_RHR_12.33_eng.pdf?sequence=1&isAllowed=y

Yang, T. T., Cheng, Y. Z., Qin, M., Wang, Y. H., Yu, H. L., Wang, A. L., et al. (2017). Thermosensitive chitosan hydrogels containing polymeric microspheres for vaginal drug delivery. *Biomed. Res. Int.* 2017, 1–12. doi: 10.1155/2017/3564060

Yasir, M., Willcox, M. D. P., and Dutta, D. (2018). Action of antimicrobial peptides against bacterial biofilms. *Materials* 11:2468. doi: 10.3390/ma11122468

**Conflict of Interest:** The authors declare that the research was conducted in the absence of any commercial or financial relationships that could be construed as a potential conflict of interest.

**Publisher's Note:** All claims expressed in this article are solely those of the authors and do not necessarily represent those of their affiliated organizations, or those of the publisher, the editors and the reviewers. Any product that may be evaluated in this article, or claim that may be made by its manufacturer, is not guaranteed or endorsed by the publisher.

frontiers | Frontiers in Microbiology

ORIGINAL RESEARCH
published: 11 April 2022
doi: 10.3389/fmicb.2022.832919

# Complex Chronic Wound Biofilms Are Inhibited *in vitro* by the Natural Extract of *Capparis spinose*

*Silvia Di Lodovico[1], Tiziana Bacchetti[2], Simonetta D'Ercole[3], Sara Covone[1], Morena Petrini[3], Mara Di Giulio[1], Paola Di Fermo[1], Firas Diban[1], Gianna Ferretti[4] and Luigina Cellini[1]**

[1] Department of Pharmacy, University "G. d'Annunzio" Chieti-Pescara, Chieti, Italy, [2] Department of Life and Environmental Sciences, Polytechnic University of Marche, Ancona, Italy, [3] Department of Medical, Oral and Biotechnological Sciences, University "G. d'Annunzio" Chieti-Pescara, Chieti, Italy, [4] Department of Clinical Science, Research Center of Health Education and Health Promotion, Polytechnic University of Marche, Ancona, Italy

Resistant wound microorganisms are becoming an extremely serious challenge in the process of treating infected chronic wounds, leading to impaired healing. Thus, additional approaches should be taken into consideration to improve the healing process. The use of natural extracts can represent a valid alternative to treat/control the microbial infections in wounds. This study investigates the antimicrobial/antivirulence effects of *Capparis spinose* aqueous extract against the main chronic wound pathogens: *Staphylococcus aureus*, *Pseudomonas aeruginosa*, and *Candida albicans*. The extract shows phenolic characterization with rutin (1.8 ± 0.14 μg/mg) as the major compound and antibacterial effect against bacteria (*S. aureus* PECHA 10 MIC 6.25%; *P. aeruginosa* PECHA 4 MIC 12.50%) without action against *C. albicans* (MIC and MFC ≥ 50%). *Capparis spinose* also shows a significant antivirulence effect in terms of antimotility/antibiofilm actions. In particular, the extract acts (i) on *P. aeruginosa* both increasing its swimming and swarming motility favoring the planktonic phenotype and reducing its adhesive capability, (ii) on *S. aureus* and *P. aeruginosa* biofilm formation reducing both the biomass and CFU/ml. Furthermore, the extract significantly displays the reduction of a dual-species *S. aureus* and *P. aeruginosa* Lubbock chronic wound biofilm, a complex model that mimics the realistic *in vivo* microbial spatial distribution in wounds. The results suggest that *C. spinose* aqueous extract could represent an innovative eco-friendly strategy to prevent/control the wound microbial infection.

**Keywords: *Capparis spinose*, antimicrobial and antivirulence actions, dual-species biofilm, Lubbock chronic wound biofilm model, *S. aureus*, *P. aeruginosa*, *C. albicans***

OPEN ACCESS

***Edited by:***
*Giuseppantonio Maisetta, University of Pisa, Italy*

***Reviewed by:***
*Mariana Carmen Chifiriuc, University of Bucharest, Romania*
*Koshy Philip, University of Malaya, Malaysia*

****Correspondence:***
*Luigina Cellini*
*l.cellini@unich.it*

***Specialty section:***
*This article was submitted to Antimicrobials, Resistance and Chemotherapy, a section of the journal Frontiers in Microbiology*

***Received:*** *10 December 2021*
***Accepted:*** *24 February 2022*
***Published:*** *11 April 2022*

***Citation:***
*Di Lodovico S, Bacchetti T, D'Ercole S, Covone S, Petrini M, Di Giulio M, Di Fermo P, Diban F, Ferretti G and Cellini L (2022) Complex Chronic Wound Biofilms Are Inhibited in vitro by the Natural Extract of Capparis spinose. Front. Microbiol. 13:832919. doi: 10.3389/fmicb.2022.832919*

## INTRODUCTION

The increase and rapid spread of antimicrobial-resistant wound microorganisms hinder the management of microbial infections and delays wound healing. The wound microbial colonization of wound is the most frequent poly-microbial colonization, involving both aerobic and anaerobic pathogen microorganisms including bacteria and yeasts. Among the detected pathogens, *Staphylococcus aureus*, *Pseudomonas aeruginosa*, *Candida albicans*, and beta-hemolytic streptococci are the primary cause of delayed wound healing and infection (Bowler et al., 2001). In particular,

*S. aureus* and *P. aeruginosa* are the main wound bacterial isolates playing an important role in the development of poly-microbial biofilms (DeLeon et al., 2014; Di Giulio et al., 2020).

*Staphylococcus aureus* is the most problematic bacterium in wound infections (Tong et al., 2015) with a high incidence affecting the management practices. As reported by Nakamura et al. (2014), the blood stream infection by *S. aureus* is an important risk factor of wound infection. *Staphylococcus aureus* is able to express various virulence factors that facilitate cell adhesion and host response. In fact, the microorganism binds fibronectin, collagen, fibrinogen, laminin, and elastin, and thanks to its coagulase activity, it produces a fibrin network that represents a scaffold on which bacteria can adhere forming a biofilm (Arciola et al., 2005; Yung et al., 2021). Alves et al. (2018) demonstrated that *S. aureus* acts as a pioneer for the attachment of *P. aeruginosa* that, in turn, promotes an invasive phenotype in *S. aureus*.

*Pseudomonas aeruginosa* is another important pathogen responsible for infections that are difficult to treat including skin diseases. If the wound is not properly treated, *P. aeruginosa* is able to change the infection type from local to systemic. The increase in multidrug -resistant *P. aeruginosa* strains, together with their capability to form a biofilm, represents a challenge for the treatment (Yang et al., 2019). In addition, the dynamic relationship among swimming, swarming, and twitching motility represents a significant virulence bacterium trait, interfering with the biofilm formation (Zolfaghar et al., 2003). Finally, in wound biofilms, also *C. albicans* provides a synergistic microbial complex with bacteria (Di Giulio et al., 2018).

Chronic wound infections are persistent and very hard to eradicate due to the poly-microbial biofilm and the increasing resistant/tolerant microorganisms against traditional treatments. Orazi and O'Toole (2017) reported that in a poly-microbial biofilm, exoproducts of *P. aeruginosa* reduce the susceptibility of *S. aureus* to vancomycin and tobramycin, and the release of N-acetyl glucosamine (GlcNAc) by *S. aureus* stimulates the *P. aeruginosa* quinolone signal (PQS) that is responsible for the production of its virulence factors (e.g., pyocyanin, elastase, rhamnolipids, and HQNO) and quorum sensing. The increase in multidrug-resistant wound strains today represents an important worldwide challenge and new treatment strategies are urgent. New approaches have been developed to act interfering with the ability of the bacteria to produce virulence factors, such as the factors produced during growth as biofilms, which promote resistance to common drugs.

In this scenario, natural compounds could represent innovative approaches, as adjuvants and alternatives to antibiotics in the drainage or debridement to remove sloughed and devitalized tissues, which cause slow wound healing (Di Giulio et al., 2020).

Different natural compounds are proposed to treat microbial proliferation in wounds. Bioactive and antimicrobial properties of extracts of plant phenolic compounds against human pathogens have been widely studied to characterize and develop new medical and pharmaceutical products (Tungmunnithum et al., 2018). In particular, the phenolic fraction of natural compounds is responsible for the organoleptic and biological effects, such as antimicrobial and antibiofilm effects (Di Lodovico et al., 2020b).

Among the different medicinal plants, *Capparis spinose* deserves to be better investigated for its biological properties. *Capparis spinose* (*C. spinosa*), belonging to the *Capparaeae* family, is widely found in the Mediterranean area (especially in France, Spain, Italy, and Algeria) (Al-Snafi, 2015; Rahimi et al., 2020). It is a perennial spiny bush that bears rounded, fleshy leaves and big white to pinkish-white flowers. *Capparis spinose* has been used as a traditional herbal remedy since ancient times for its beneficial effects on human diseases, such as splenomegaly, mental disorders, tubercular glands, rheumatoid arthritis, and gut and skin disease. Mahboubi and Mahboubi (2014) showed that the aqueous extracts from the roots of *C. spinose* display a remarkable antimicrobial activity against *Staphylococcus* spp., *Escherichia coli*, *Helicobacter pylori*, *Candida* spp., and *Aspergillus niger*.

The aim of this study is to investigate the antimicrobial and antivirulence effects of *C. spinose* aqueous extract against the main chronic wound pathogens. The antivirulence analysis is performed by evaluating *C. spinose* antimotility/twitching and antibiofilm actions. The poly-microbial biofilm is also analyzed by using the Lubbock chronic wound biofilm (LCWB) model that mimics the realistic microbial spatial proliferation in wounds. This *in vitro* model is widely recognized as more closely resembling the *in vivo* human wound environment including the wound-simulating medium, the fibrin network produced by *S. aureus*, and the realistic nutrient and oxygen gradient (Thaarup and Bjarnsholt, 2021). This suitable *in vitro* model represents a pivotal preliminary screen useful in translating into *in vivo* detections.

The proposed study can be defined as "green research" in line with the identification of novel strategies to overcome antimicrobial resistance and for the low environmental impact in the aqueous extraction that is widely diffused in the Mediterranean area.

The innovative aspect of this work is to propose a valid and eco-friendly non-antibiotic strategy to prevent and control wound microbial infections, strongly highlighting the antimicrobial and antivirulence actions of *C. spinose* aqueous extract.

# MATERIALS AND METHODS

## Bacterial Cultures

Anonymized clinical *Staphylococcus aureus* PECHA 10, *Pseudomonas aeruginosa* PECHA 4, and *Candida albicans* X3 strains (Di Giulio et al., 2018, 2020) were used for this study. The strains were isolated from chronic wounds of patients that gave their informed consent for the study. The study was approved by the Inter Institutional Ethic Committee of University "G. d'Annunzio" Chieti-Pescara, Chieti, Italy (ID n. richycnvw). The strains were characterized for their susceptibility to antibiotics, and in particular, *S. aureus* PECHA 10 and *P. aeruginosa* PECHA 4 were resistant strains (**Supplementary Table 1**). All the methods were performed in accordance with the relevant

guidelines and regulations. For the experiments, bacteria were cultured in Trypticase Soy Broth (TSB, Oxoid, Milan, Italy) and incubated at 37°C overnight in aerobic condition and then refreshed for 2 h at 37°C in an orbital shaker. Then the broth cultures were standardized to optical density at 600 nm ($OD_{600}$) = 0.125. The broth culture of *Candida albicans*, grown on Sabouraud dextrose agar (SAB, Oxoid, Milan, Italy) was prepared in RPMI 1640 (Sigma-Aldrich, Milan, Italy) plus 2% glucose and standardized to $OD_{600}$ = 0.15.

## Chemicals

Gallic acid, catechin, chlorogenic acid, p-OH benzoic acid, vanillic acid, epicatechin, syringic acid, 3-OH benzoic acid, 3-OH-4-MeO benzaldehyde, p-coumaric acid, rutin, sinapinic acid, t-ferullic acid, naringin, 2,3-diMeO benzoic acid, benzoic acid, o-coumaric acid, quercetin, harpagoside, t-cinnamic acid, naringenin, and carvacrol were purchased from Sigma-Aldrich (Milan, Italy). Methanol (HPLC-grade) and formic acid (99%) were obtained from Carlo Erba Reagenti (Milan, Italy).

## Extract Preparation

Plants of *C. spinose* subsp. *rupestris* have been growing in Borgo Cisterna (Santa Lucia Cisterna, Macerata Feltria, PU, Italy) and managed by the Agency for Food Service Industry in the Marche (ASSAM), an institution involved in the implementation of programs for the protection of biodiversity for agriculture of the Marche Region in relation to the Regional Law No. 12 "Protection of animal and plant genetic resources of the Marche" approved June 2003. The law protects the genetic resources that are locally grown within the region. The flower bods used in this study have been kindly provided by Mario Gallarani and his family that grow *C. spinose* subsp. *rupestris* in Borgo Cisterna (Santa Lucia Cisterna, Macerata Feltria, Italy). Plants of *C. spinose* subsp. rupestris have been registered to the Regional Register of Biodiversity of Marche Region No. 70 of the Vegetal Section, Herbaceous Species. The use of *C. spinose* was in agreement with the IUCN Policy Statement on Research Involving Species at Risk of Extinction and the Convention on the Trade in Endangered Species of Wild Fauna and Flora. *Capparis spinose* flower bods were washed, frozen at –20°C, freeze-dried, and shredded. One gram of the powdered sample was incubated with 100 ml of ultrafiltered water at 80°C for 10 min (Eddouks et al., 2017). Thereafter, the aqueous extract was filtered by Millipore filter (Millipore 0.2 mm) to remove particulate matter.

## High-Performance Liquid Chromatography Analyses

High-performance liquid chromatography (HPLC) **analyses** were performed on Waters liquid chromatograph equipped with a model 600 solvent pump and a 2996 photodiode array detector, and Empower v.2 Software (Waters Spa, Milford, MA, United States) was used for acquisition of data. C18 reversed-phase packing column [Prodigy ODS(3), 4.6 × 150 mm, 5 μm; Phenomenex, Torrance, CA, United States] was used for separation, and the column was thermostated at 30 ± 1°C using a Jetstream2 Plus column oven. The UV/Vis acquisition wavelength was set in the range of 200–500 nm. The quantitative analyses were achieved at maximum wavelength for each compound. The injection volume was 20 μl. The mobile phase was directly on-line degassed by using Biotech DEGASi, mod. Compact (LabService, Anzola dell'Emilia, Italy). Gradient elution was performed using the mobile phase water–acetonitrile (93:7, v/v, 3% acetic acid) (Zengin et al., 2017). The sample solutions were centrifuged, and the supernatant was injected into HPLC.

The phenolic stock solutions were prepared at a concentration of 1 mg/ml in a final volume of 10 ml of methanol. Working solutions of mixed standards at different concentrations obtained by dilution in mobile phase were injected into the HPLC-UV/Vis system.

The lyophilized extract sample was weighted and dissolved in mobile phase, and 20 μl was injected into the HPLC-UV/Vis system. For over range samples, 1:10 dilution factor was applied.

## Assessment of Total Phenolic and Flavonoid Content and Antioxidant Activity

Total phenolic (TP) content in *C. spinose* has been evaluated by Folin–Ciocalteu assay (Ainsworth and Gillespie, 2007). Total flavonoid (TF) content in *C. spinose* was measured by spectrophotometry with aluminum chloride ($AlCl_3$) as the reagent according to Kim et al. (2003). TP and TF levels were expressed as milligrams of gallic acid equivalent (GAE) per 100 g of dry weight of *C. spinose* (mg GAE/100 gdw) and milligrams of catechin equivalent (CE) per 100 g of dry weight of *C. spinose* (mg CE/100 gdw), respectively.

Total antioxidant capacity (TAC) of *C. spinose* was determined by oxygen radical absorbance capacity (ORAC) assay, using fluorescein, as fluorescent probe, and 2,2'-azobis (2-methylpropionamide) dihydrochloride (AAPH), as oxidizing agent (Gillespie et al., 2007). Trolox was used to calibrate the assay. The final ORAC values were calculated using the net area under the curve (AUC) of decay. Results were expressed as Trolox equivalents per 100 g of dry *C. spinose* weight (mmol TE/100 gdw).

## *Capparis spinose* Aqueous Extract Antimicrobial Assays

The *C. spinose* aqueous extract MIC was performed against *S. aureus* PECHA 10, *P. aeruginosa* PECHA 4, and *C. albicans* X3 by microdilution method according to the CLSI (2018). *Capparis spinose* aqueous extract stock solution was diluted in Mueller Hinton Broth II cation adjusted (MHB, Oxoid, Milan, Italy) for bacteria and in RPMI 1640 plus 2% glucose for *C. albicans* X3 at a final concentration of from 50 to 0.78%. MBCs/MFCs were determined by subculturing 10 μl of suspensions from the MICs on Mueller Hinton agar (MHA, OXOID, Milan, Italy) for bacteria and on Sabouraud Dextrose agar (SAB, OXOID, Milan, Italy) for *C. albicans*.

As control, amikacin and amphotericin B MICs were used for bacteria and *C. albicans* X3, respectively.

## *Capparis spinose* Aqueous Extract Antivirulence Assays

The antivirulence analysis of *C. spinose* aqueous extract was performed by evaluating its effect on *P. aeruginosa* PECHA 4 motility (swimming and swarming), *P. aeruginosa* PECHA 4 twitching, *S. aureus* PECHA 10, and *P. aeruginosa* PECHA 4 biofilm formation.

### Effect on *Pseudomonas aeruginosa* PECHA 4 Motility

The *C. spinose* aqueous extract capability to interfere with the *P. aeruginosa* PECHA 4 motility was determined by swarming and swimming motility. Briefly, according to Abraham et al. (2011), for the swarming motility, the standardized cultures were inoculated at the center of swarming plates containing 1% peptone, 0.5% NaCl, 0.5% agar, and 0.5% D-glucose with the extract at sub-MICs. For swimming motility, standardized cultures were inoculated at the center of plates containing 1% tryptone, 0.5% NaCl, and 0.3% agar and extract at sub-MICs. Plates were incubated at 37°C for 24 h, and bacterial halos were recorded.

### Effect on *Pseudomonas aeruginosa* PECHA 4 Twitching

The capability of *C. spinose* aqueous extract to interfere with the *P. aeruginosa* PECHA 4 pilus retraction was determined by twitching assay. For the cultural analysis, cultures were inoculated to the bottom of the twitching plates consisting of 10 g/L of tryptone, 5 g/L of yeast extract, 10 g/L of NaCl, and 1% agar with the extract at sub-MICs. Plates were incubated at 37°C for 24 h, and then the agar was removed, and the halo was stained with 0.1% Crystal Violet and measured (Turnbull and Whitchurch, 2014). For RT-PCR *pilT* gene expression, *P. aeruginosa* PECHA 4 RNA was extracted using the RNeasy mini kit (Qiagen, Milan, Italy), according to the manufacturer's instructions. cDNA was generated using the iScript cDNA Synthesis Kit (Bio-Rad, Milan, Italy) and then stored at −20°C until use. For the quantitative PCR, the oligonucleotide used primers as follows: *pilT* Fwd: ACCGACTTCTCCTTCGAGGT; *pilT* Rev: GAGGGAATGGTCCGGAATAC (Cowles and Gitai, 2010); the housekeeping gene 5S RNA Fwd: TGACGATCATAGAGCGTTGG; 5S RNA Rev: GATAGGAGCTTGACGATGACCT (El-Sayed et al., 2020). Quantitative PCR reactions were performed according to Di Fermo et al. (2020). A melting curve was used at the end to confirm only one peak and only one product. Values of the threshold cycle (Ct) and relative expression level were normalized by the ΔCT method. Results were analyzed using the Bio-Rad CFX Manager Software, version 3.1 (Bio-Rad Laboratorie, Milan, Italy).

### Effect on *Staphylococcus aureus* PECHA 10 and *Pseudomonas aeruginosa* PECHA 4 Biofilm Formation

Considering the ineffectiveness of *C. spinose* against *C. albicans* X3, the antibiofilm effect was not detected. *Capparis spinose* aqueous extract antibiofilm effect at sub-MICs was evaluated on *S. aureus* PECHA 10 and *P. aeruginosa* PECHA 4 biofilm formation in terms of (i) biomass quantification, (ii) CFU/ml, and (iii) cell viability.

For biomass quantification, standardized cultures in TSB (Oxoid) plus 0.5% (vol/vol) glucose were inoculated in 96-well flat-bottom microtiter plates in the presence of 1/2, 1/4, 1/8 MIC, or without (control) the extract. Plates were incubated at 37°C for 24 h in aerobic condition. After incubation, dry biofilms were stained with 0.1% Crystal Violet and quantified according to Di Lodovico et al. (2020b).

For CFU/ml determination, after 24 h, each well was washed with PBS, and adhered bacteria were scraped off and resuspended in 200 μl of PBS, transferred to test tubes, vortexed for 2 min, diluted, and spread on mannitol salt (MSA, OXOID, Milan, Italy) agar for *S. aureus* PECHA 10 and on cetrimide (CET, OXOID, Milan, Italy) for *P. aeruginosa* PECHA 4. Plates were incubated for 24 h at 37°C (D'Ercole et al., 2020). Microscopic observations with Live/Dead staining prior to spreading confirmed the presence of disaggregated viable cells.

Cell viability was evaluated by using Live/Dead staining (Molecular Probes Inc., Invitrogen, San Giuliano Milanese, Italy) according to Turnbull and Whitchurch (2014) and Di Lodovico et al. (2019). The number of viable and dead cells was determined by using an image analysis software (LEICA QWin) through the examination of at least 10 random fields of view, and the counts were repeated independently by three blinded microbiologists (Di Lodovico et al., 2020a).

### Effect on Dual-Species Biofilm, Lubbock Chronic Wound Biofilm

To evaluate the effect of *C. spinose* aqueous extract in a dual-species *S. aureus* and *P. aeruginosa* biofilm, in-forming Lubbock chronic wound biofilm (LCWB) was prepared according to Di Giulio et al. (2020). Briefly, 100 μl of extract at a final concentration of 3.12%, which corresponded to 1/2 MIC of *S. aureus* PECHA 10, or 100 μl of amikacin (AMK, as a reference) at a final concentration of 8 mg/L or 100 μl of PBS (for control), was added to the Lubbock medium containing Brucella broth (BB, Oxoid, Milan, Italy) with 0.1% agar bacteriological, 50% porcine plasma (Sigma Aldrich, Milan, Italy), 5% horse erythrocytes (BBL, Microbiology System, Milan, Italy), 2% fetal calf serum (Biolife Italiana, Milan, Italy), and *S. aureus* and *P. aeruginosa* grown in TSB (Oxoid) (Di Giulio et al., 2020). The test tubes were incubated for 48 h at 37°C, and then the *S. aureus* PECHA 10 and *P. aeruginosa* PECHA 4 CFUs per mg of LCWB were determined (Di Giulio et al., 2020).

## Statistical Analysis

Data were obtained from at least three independent experiments performed in duplicate. Data were shown as the means ± standard deviation. Differences between groups were assessed with one-way analysis of variance (ANOVA). Values of $p \leq 0.05$ were considered statistically significant.

**TABLE 1 |** Total amounts (μg/mg) of phenolics in the lyophilized extract.

| | Concentration (μg/mg) |
|---|---|
| Chlorogenic acid | 0.31 ± 0.04 |
| *p*-OH benzoic acid | 0.35 ± 0.07 |
| 3-OH benzoic acid | 0.40 ± 0.05 |
| *p*-Coumaric acid | 0.54 ± 0.03 |
| Rutin | 1.83 ± 0.14 |
| 2,3-diMeO benzoic acid | 0.46 ± 0.04 |
| Total | 3.89 ± 0.18 |

# RESULTS

This study evaluates the antimicrobial and antivirulence properties of a well-characterized *C. spinose* aqueous extract against microorganisms isolated from chronic wounds.

## High-Performance Liquid Chromatography Analysis

Only quantifiable phenolic compounds greater than the limit of quantification (LOQ = 0.20 μg/ml) are shown in the **Table 1**. All other compounds are to be understood as not detected or below the detection limit (LOD = 0.10 μg/ml).

## Assessment of Total Phenolic and Flavonoid Content and Antioxidant Activity

Total phenolic (TP) and total flavonoid (TF) levels in *C. spinose* aqueous extract are 1.6 ± 0.1 g GAE/100 g and 91.1 ± 19.3 mg CE/100 g, respectively. Total antioxidant capacity, evaluated by ORAC assay, is 50.8 ± 8.4 mmol TE/100 g.

## *Capparis spinose* Aqueous Extract Antimicrobial Assays

**Table 2** shows the MIC and the MBC/MFC values of *C. spinose* aqueous extract against *S. aureus*, *P. aeruginosa*, and *C. albicans* clinical isolates.

According to *C. spinose* aqueous extract gallic acid and catechin equivalent analysis, the *S. aureus* MIC corresponds to 0.78 mg GAE/ml and 0.11 mg CE/ml, and the MBC corresponds to 1.56 mg GAE/ml and 0.22 mg CE/ml. The *P. aeruginosa* MIC corresponds to 1.56 mg GAE/ml and 0.22 mg CE/ml, and the MBC corresponds to 3.12 mg GAE/ml and 0.44 mg CE/ml. For *C. albicans*, the MIC and the MFC are more than 6.25 mg GAE/ml and 0.90 mg CE/ml.

*Capparis spinose* aqueous extract shows a relevant antibacterial effect against the tested bacterial strains.

Considering the ineffectiveness of *C. spinose* aqueous extract against *C. albicans* (MIC and MFC values are more than 50%, that is, the maximum percentage of the extract tested in this study), this microorganism is not included in the subsequent experiments.

## *Capparis spinose* Aqueous Extract Antivirulence Assays

### Effect on *Pseudomonas aeruginosa* PECHA 4 Motility

The *C. spinose* aqueous extract displays a significant increase in the swimming and swarming motility of *P. aeruginosa*. As shown in **Figures 1A,B**, the swimming and swarming halo sizes are more than the control ones. In fact, the halo diameter of swimming motility for the control is 4 ± 1 mm, whereas 10 ± 2 and 12 ± 2 mm are halo diameters recorded in the presence of 1/4 and 1/8 MIC of *C. spinose* aqueous extract, respectively. The halo diameters for swarming motility are 6 ± 1 mm for control, 11 ± 3 and 13 ± 3 mm for 1/4 and 1/8 MIC of *C. spinose* aqueous extract, respectively.

*Capparis spinose* aqueous extract enhances *P. aeruginosa* flagellar activation.

### Effect on *Pseudomonas aeruginosa* PECHA 4 Twitching

For twitching motility, relevant percentages of halo reduction with respect to the control are obtained. As shown in **Figure 2A**, the halo diameters are 12 ± 4 mm for the control and 9 ± 1 mm in the presence of both 1/4 and 1/8 MIC of *C. spinose* aqueous extract with 23% ± 15% of halo reduction. These data are also confirmed by RT-PCR that evaluates the *pilT* gene expression. *Capparis spinose* aqueous extract at sub-MIC concentrations reduces the *pilT* expression of 27% (**Figures 2B,C**).

*Capparis spinose* aqueous extract interferes with the *P. aeruginosa* pilus retraction, reducing the microorganism adhesive capability.

### Effect on *Staphylococcus aureus* PECHA 10 and *Pseudomonas aeruginosa* PECHA 4 Biofilm Formation

The *C. spinose* aqueous extract shows a significant action in antibiofilm formation against both *S. aureus* and *P. aeruginosa* detected strains. As shown in **Figure 3A**, the *C. spinose* aqueous extract, at sub-MIC values, significantly reduces the *S. aureus* biomass after 24 h of treatment. In particular, the percentages of biomass reduction with respect to the control are 92.21% ± 1.87, 90.54% ± 8.38, and 72.63% ± 6.62 at 1/2, 1/4, and 1/8 MICs, respectively. **Figure 3B** shows the *S. aureus* CFU/ml of biofilm formation after treatment with sub-MICs of *C. spinose* aqueous extract for 24 h. With respect to the control, there is a significant CFU/ml reduction ($p < 0.05$) at 1/2 and 1/4 MICs. In the presence of *C. spinose* aqueous extract at sub-MICs, there is a relevant reduction in biofilm adhesion with remarkable red cells detected in Live/Dead images (**Figure 3C**). The cells appear less clustered with about 20% of dead red cells (**Figure 3C**, histograms).

Regarding the *P. aeruginosa* antibiofilm formation activity, significant percentages of biomass reduction are obtained at sub-MICs. In detail, the percentages range from 89.97% ± 4.97 at 1/8 MIC to 99.48% ± 0.76 at 1/2 MIC (**Figure 4A**). In the presence of *C. spinose* aqueous extract, significant reductions ($p < 0.05$) in biomass and CFU/ml are observed. In fact, a few cells are detected by CFU enumeration (**Figure 4B**) and Live/Dead

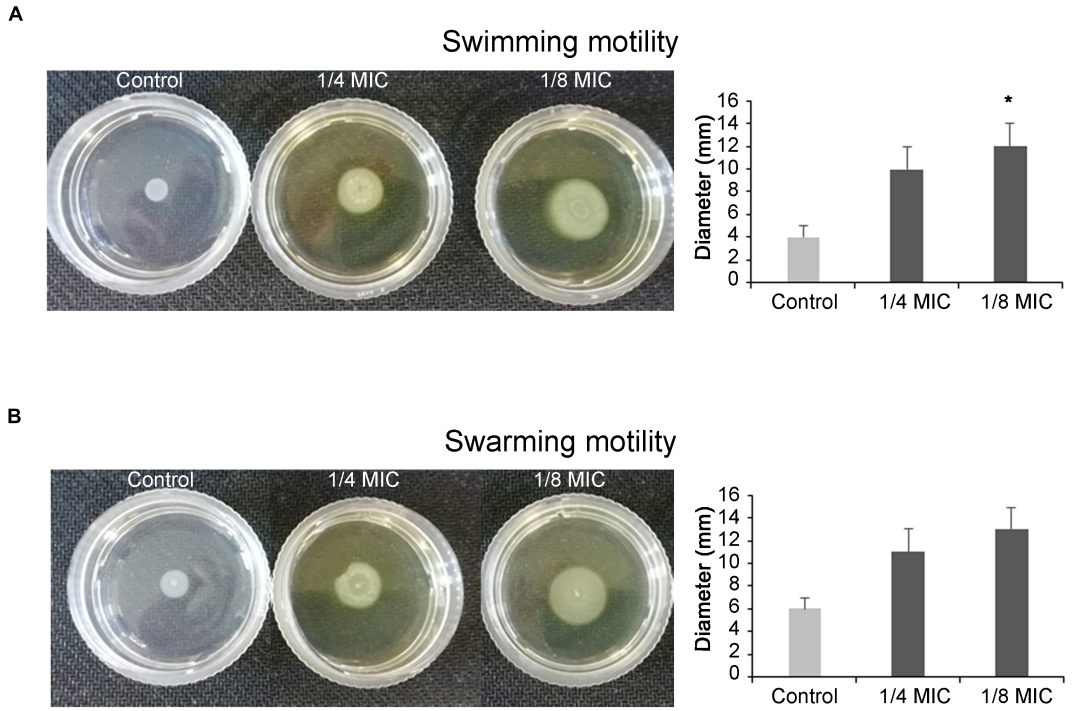


**FIGURE 1 |** Effect of sub-minimum inhibitory concentrations (MICs) of *Capparis spinose* aqueous extract on *Pseudomonas aeruginosa* PECHA 4 motility assay; representative images of swimming **(A)** and swarming **(B)** motilities on soft agar plates with diameter of obtained halos and relative histograms. *Significant with respect to the control ($p < 0.05$).

staining (**Figure 4C**). This significant *P. aeruginosa* reduction in the presence of *C. spinose* aqueous extract is confirmed by Live/Dead images (**Figure 4C**) with an almost total percentage of viable cells (**Figure 4C**, histograms).

*Capparis spinose* aqueous extract is able to inhibit the biofilm formation of *S. aureus* and *P. aeruginosa* tested strains.

### Effect on Dual-Species Biofilm, Lubbock Chronic Wound Biofilm

In a poly-microbial biofilm, *C. spinose* aqueous extract significantly reduces the microbial growth. In fact, in dual-species *S. aureus* and *P. aeruginosa* LCWB, the CFU/mg reductions are 97.32% ± 2.29 ($p < 0.05$) for *S. aureus* and 99.67% ± 0.07 ($p < 0.05$) for *P. aeruginosa* (**Table 3**). This relevant reduction is similar to those obtained with the antibiotic used as reference control.

*Capparis spinose* aqueous extract confirms its antibiofilm effect in the complex system LCWB model with a significant capability to reduce the microbial growth.

## DISCUSSION

In this study, the antimicrobial and antivirulence activities of a characterized *C. spinose* aqueous extract have been

**TABLE 2 |** Minimum inhibitory concentration (MIC) and minimum bactericidal concentration (MBC)/minimum fungicidal concentration (MFC) of *Capparis spinose* aqueous extract against *Staphylococcus aureus* PECHA 10, *Pseudomonas aeruginosa* PECHA, and *Candida albicans* X3.

| Strains | MIC | | MBC/MFC | |
|---|---|---|---|---|
| | ***C. spinose* aqueous extract (%)** | **Amikacin/amphotericin B (μg/ml)** | ***C. spinose* aqueous extract (%)** | **Amikacin/amphotericin B (μg/ml)** |
| *S. aureus* PECHA 10 | 6.25 | 16 | 12.50 | 16 |
| *P. aeruginosa* PECHA 4 | 12.50 | 32 | 25 | 32 |
| *C. albicans* X3 | >50 | 0.5 | >50 | 0.5 |

*Amikacin and amphotericin B are included as control for bacteria and C. albicans X3, respectively.*

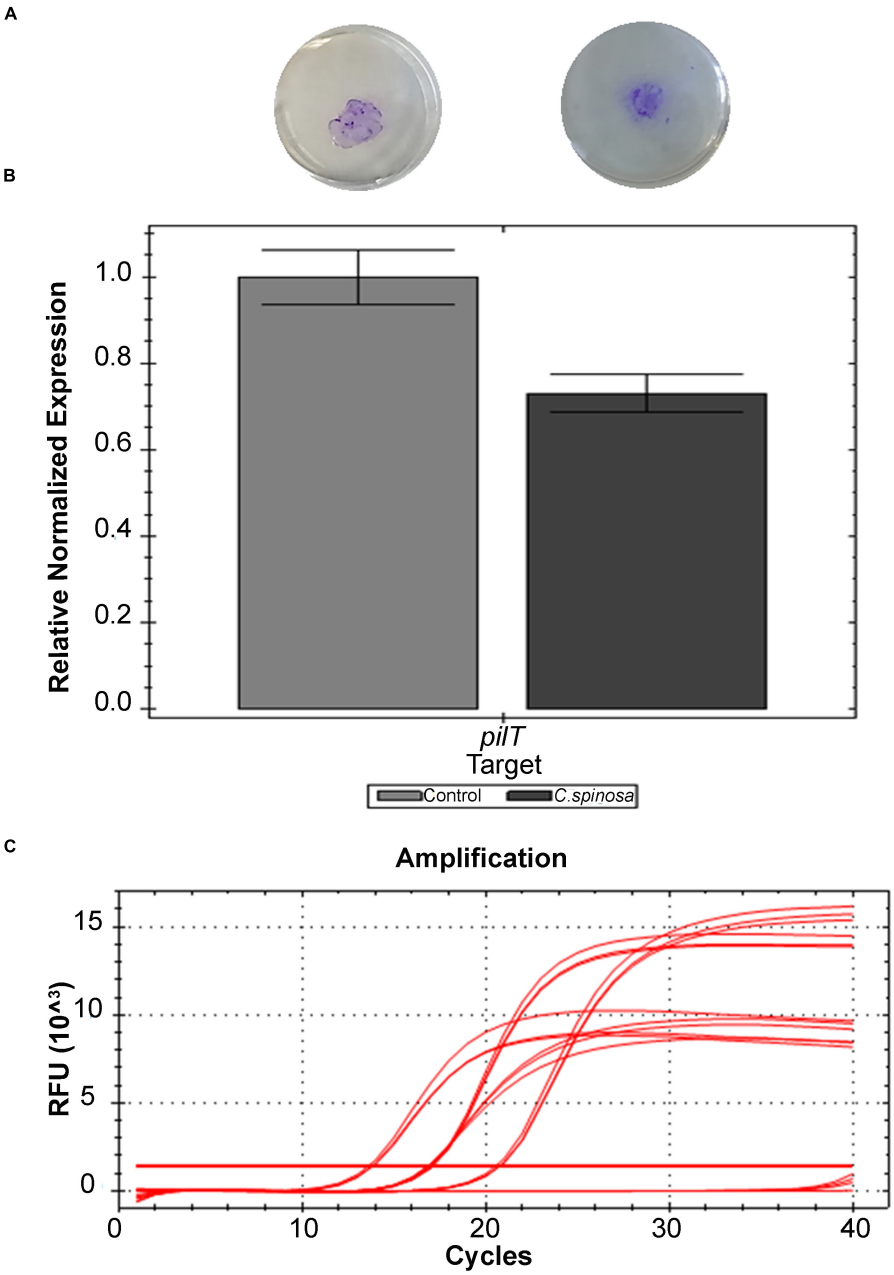


**FIGURE 2 |** Effect of sub-MICs of *Capparis spinose* aqueous extract on *Pseudomonas aeruginosa* PECHA 4 twitching assay: **(A)** representative images of macroscopic twitching assay on cultural plates; **(B)** expression of *pilT* gene; **(C)** amplification chart with the Ct values of each sample of the *pilT* gene expression.

evaluated against resistant chronic wound microorganisms. The worrying phenomenon related to the antimicrobial resistance of chronic wound microorganisms is the cause of treatments failure. In addition, the chronic wound infections are always associated with the poly-microbial biofilm delaying wound healing (Di Giulio et al., 2020).

The World Health Organization reports the use of different medicinal plants for the management of health and treatment of diseases due to their bioactive components and health-promoting effects (World Health Organization (WHO), 2013).

Caper berries contain a wide range of bioactive compounds, such as alkaloids, flavonoids, steroids, terpenoids, and tocopherols. Healthy properties and composition of phytonutrients of Capparis flower buds have been recently reviewed. Levels and composition of phytonutrients are influenced by different factors such as cultivars, genotypes (both cultivated and wild), and geographical origin (Maldini et al., 2016; Zhang and Ma, 2018; Wojdyło et al., 2019).

The profile of the main phenolic compounds, detected in the present study, is in a greater part in agreement with

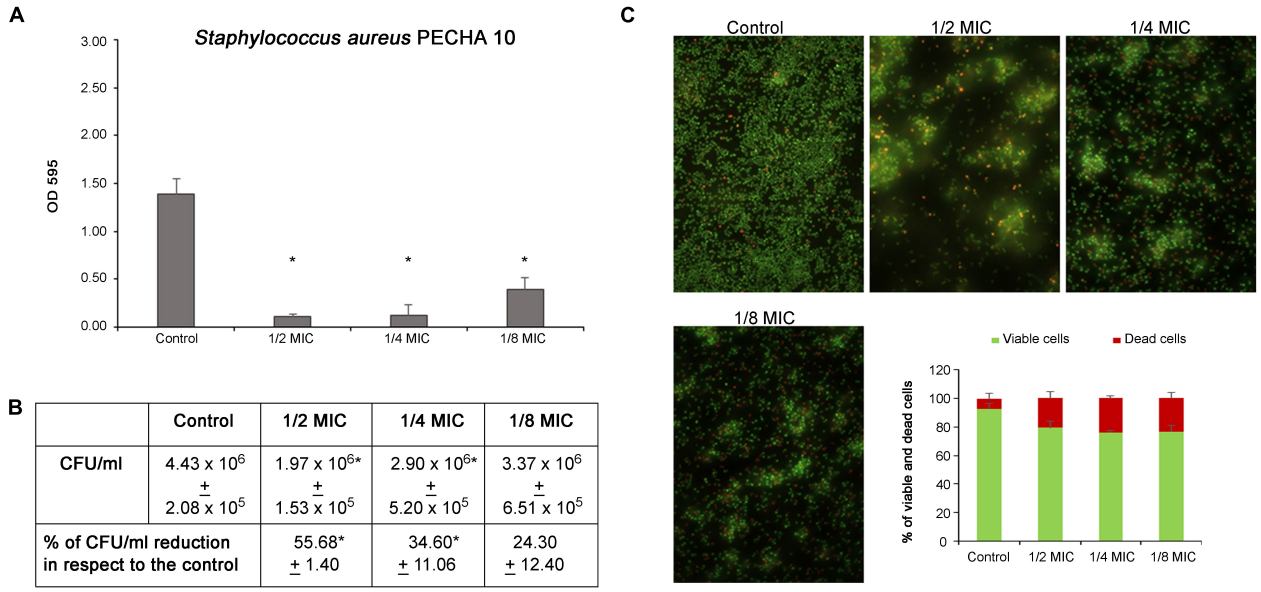


**B**

| | Control | 1/2 MIC | 1/4 MIC | 1/8 MIC |
|---|---|---|---|---|
| CFU/ml | $4.43 \times 10^6 \pm 2.08 \times 10^5$ | $1.97 \times 10^{6*} \pm 1.53 \times 10^5$ | $2.90 \times 10^{6*} \pm 5.20 \times 10^5$ | $3.37 \times 10^6 \pm 6.51 \times 10^5$ |
| % of CFU/ml reduction in respect to the control | | 55.68* ± 1.40 | 34.60* ± 11.06 | 24.30 ± 12.40 |

**FIGURE 3 |** Effect of sub-MICs of *Capparis spinose* aqueous extract on *Staphylococcus aureus* PECHA 10 biofilm formation. **(A)** Biomass evaluation; **(B)** cultivable cell count (CFU/ml); **(C)** representative images (Live/Dead stain) and quantitative analysis (histograms) of viable and dead cells. *Significant with respect to the control ($p < 0.05$).

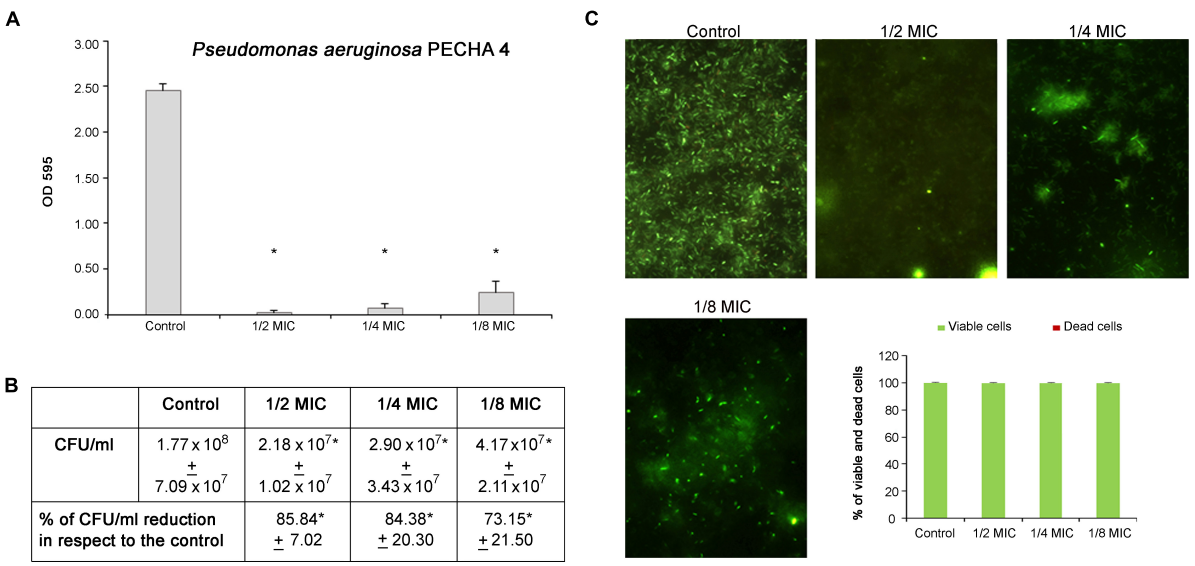


**B**

| | Control | 1/2 MIC | 1/4 MIC | 1/8 MIC |
|---|---|---|---|---|
| CFU/ml | $1.77 \times 10^8 \pm 7.09 \times 10^7$ | $2.18 \times 10^{7*} \pm 1.02 \times 10^7$ | $2.90 \times 10^{7*} \pm 3.43 \times 10^7$ | $4.17 \times 10^{7*} \pm 2.11 \times 10^7$ |
| % of CFU/ml reduction in respect to the control | | 85.84* ± 7.02 | 84.38* ± 20.30 | 73.15* ± 21.50 |

**FIGURE 4 |** Effect of sub-MICs of *Capparis spinose* aqueous extract on *Pseudomonas aeruginosa* PECHA 4 biofilm formation. **(A)** Biomass evaluation; **(B)** cultivable cell count (CFU/ml); **(C)** representative images (Live/Dead stain) and quantitative analysis (histograms) of viable and dead cells. *Significant with respect to the control ($p < 0.05$).

previous studies (Mollica et al., 2017; Stefanucci et al., 2018) with the exception of the amount of rutin that represents the compound in major amount. It is important to mention that the phenolic profile could change according to the applied extraction technique and the extraction solvent, which is confirmed by several studies in the literature (Mollica et al., 2017, 2019; Stefanucci et al., 2018). In particular, Stefanucci et al. (2018) demonstrated a large variability in rutin concentration in Capparis collected in Italy, Morocco, and Turkey (Mollica et al., 2017, 2019).

The studied *C. spinose* aqueous extract affects the bacterial growth without any impact on yeast cells, showing a selective action against bacteria. In fact, the compound shows a significant antimicrobial action against *S. aureus* and *P. aeruginosa* clinical isolates without a relevant effect against *C. albicans*. The detected MIC values are in the MIC range previously found by Taguri et al.

**TABLE 3 |** Colony-forming units (CFUs)/mg of *Staphylococcus aureus* PECHA 10 and *Pseudomonas aeruginosa* PECHA 4 in the presence of *Capparis spinose* aqueous extract in informing Lubbock chronic wound biofilm (LCWB) model [amikacin (AMK) as reference control].

| | **CFUs/mg LCWB (% reduction with respect to the control)** | |
|---|---|---|
| | ***S. aureus* PECHA 10** | ***P. aeruginosa* PECHA 4** |
| ***C. spinose*** | $7.03 \times 10^{1}$* $\pm$ $6.00 \times 10^{1}$ (97.32* $\pm$ 2.26) | $1.66 \times 10^{3}$* $\pm$ $3.55 \times 10^{2}$ (99.67* $\pm$ 0.07) |
| **AMK** | $2.56 \times 10^{2} \pm 1.03 \times 10^{2}$ (90.20* $\pm$ 1.53) | $2.32 \times 10^{4} \pm 5.88 \times 10^{3}$ (95.40* $\pm$ 1.17) |
| **Control** | $2.62 \times 10^{3} \pm 5.37 \times 10^{2}$ | $5.03 \times 10^{5} \pm 3.66 \times 10^{5}$ |

**Statistically significant with respect to the control ($p < 0.05$).*

(2006) who determined the MICs of 22 polyphenols against 26 species of bacteria with MIC values between 0.067 and 3.200 g/L.

The molecular mechanisms of antibacterial action of phytochemicals, such as phenolic compounds, are not yet fully understood, but these compounds are known to involve many sites of action at cellular level (Bouarab-Chibane et al., 2019). Several authors explained the antimicrobial activity of polyphenols by modifications in the cell membrane permeability, changes in intracellular functions due to interactions between the phenolic compounds and cell enzymes, or by the modification of the cell wall rigidity with integrity losses due to different interaction polyphenol cell membrane (Ikigai et al., 1993; Stapleton et al., 2004; Taguri et al., 2006; Cushnie and Lamb, 2011). Among polyphenols, the main category included in Capparis extract are anthocyanins. We suggest that the observed antibacterial effect could be related to these molecules and/or the synergisms with other antioxidant polyphenols, such as phenolic acids, and their mixtures of different chemical forms. Moreover, according to the *C. spinose* aqueous extract characterization, the rutin could be responsible for the action against *S. aureus* and *P. aeruginosa* growth interfering with DNA synthesis, an antibacterial mechanism of action of various flavonoids (Cushnie and Lamb, 2005). In addition, as reported by Cushnie and Lamb (2005), the flavonoid toxicity is minimal; in fact, they are widely spread in edible plant and beverages. However, for the *in vivo* application, the evaluation of the eventual toxic effect should be done.

*Capparis spinose* aqueous extract displays also a relevant antivirulence action against *P. aeruginosa* motility/twitching and *S. aureus* and *P. aeruginosa* mono- and poly-microbial biofilms. In fact, the tested extract acts both on swimming/swarming motility favoring the flagellar-mediated movement and twitching motility reducing the *P. aeruginosa* adhesion. The detected significant increase in flagellar biosynthesis, with respect to the control, favors the planktonic status leading to enhance the bacterial movement. This effect induces a phenotype more susceptible to treatments. The noticed microbial twitching reduction interferes with the *P. aeruginosa* adhesive capability. The twitching motility is an important step for bacterial colonization and biofilm formation in *P. aeruginosa* (Shreeram et al., 2018). In particular, the inactivation and loss of function in *pilT* produces a hyperpiliation and the loss of twitching motility due to the inability of pilus fiber formation. The inactivation of *pilT* determines the loss of cytotoxicity *in vitro* and the inhibition of the contact between bacteria and the host cells (Shreeram et al., 2018). Here, *C. spinose* extract acts weakening the *P. aeruginosa* adhesive capability.

The microbial biofilm mode of growth allows microbes to protect themselves against host immune system and antimicrobial agents making biofilm-related infections difficult to treat and eradicate. In this study, *C. spinose* aqueous extract significantly reduces the mono- and poly-microbial biofilms of *S. aureus* and *P. aeruginosa* with less clustered cells. On mono-microbial biofilms, the effect is more relevant against *P. aeruginosa* with a significant effect on biomass quantification and bacterial cells. On *S. aureus* biofilm formation, the compound reduces the biomass production with a slow bacterial growth reduction. Cosa et al. (2019) showed that the antibiofilm effect of *C. spinose* is correlated to its capability to reduce the quorum-sensing (QS) regulation, reducing the bacterial virulence and pathogencity. In fact, Abraham et al. (2011) showed that the *C. spinose* methanolic extract is able to reduce the production of AHL-dependent QS interfering with biofilm production. In addition, the authors demonstrated the capability of the extract to reduce the EPS production in different bacterial pathogens. In particular, Peng et al. (2018) underline the significant role of rutin in the QS regulation with AI-2 decreasing and the reduction of biofilm formation and virulence factor gene expression.

A very interesting result is obtained when the effect of *C. spinose* aqueous extract is detected in a condition of poly-microbial biofilm that reproduces the *in vivo* spatial microbial colonization of *S. aureus* and *P. aeruginosa* in a chronic wound. The used LCWB model represents a recognized *in vitro* chronic wound system for interkingdom microbial species. In this model, the presence of red blood cells, plasma, and nutrients, mimicking the wound bed environment, promotes the *S. aureus*/*P. aeruginosa* microbial growth, closely reproducing their spatial distribution in human-like environment. In this complex dual-species microbial colonization, *C. spinose* aqueous extract expresses a significant percentage of reduction of both microbial populations. This interesting data is obtained with a well-recognized *in vitro* model that resembles to the *in vivo* wound environment in terms of wound-simulating media, host matrix, several chosen species, 3D gradients, flow, grown on solid surface (Thaarup and Bjarnsholt, 2021). As a consequence, our results stimulate further studies on *in vivo* model such as porcine and human models. In fact, the limitation of our model, while considering both the presence of the most important chronic wound factors and the easy reproducibility with ethical sound, is the unshared interaction between the immune system and microorganisms. The complex and dynamic events related to the immune host defense should be taken into account in future studies (de Bont et al., 2019; Sabbatini et al., 2021).

In conclusion, the obtained findings suggest the capability of *C. spinose* aqueous extract to inhibit the growth and virulence of *P. aeruginosa* PECHA 4 and *S. aureus* PECHA 10 chronic wound microorganisms. The significant antimicrobial and antivirulence properties make the *C. spinose* a good candidate for the study

of novel medicaments in the prevention and control of chronic wound microorganisms.

*Capparis spinose* aqueous extract could represent a valid eco-friendly suggestion to overcome the worrying antimicrobial resistance phenomenon.

## DATA AVAILABILITY STATEMENT

The raw data supporting the conclusions of this article will be made available by the authors, without undue reservation.

## AUTHOR CONTRIBUTIONS

SDL, MDG, SDE, PDF and FD conducted the microbiology experiments. SC, TB, and GF performed the *Capparis spinose* characterization. MP and SDL performed the data analysis. SDL and LC wrote the manuscript. MDG, LC, and GF contributed to discussing the results and critical review of the manuscript. All authors made significant contributions to this manuscript, participated actively in the conception and design of the experiments, and read and approved the final manuscript.

## FUNDING

This study was supported by LC and MDG FAR 2020 and in part by Research Grant PRIN 2017 SFBFER from MIUR, Italy, and also supported by Programma di Sviluppo Rurale 2014–2020 Europa/Regione Marche.

## ACKNOWLEDGMENTS

We acknowledge Gloria Magi and Arianna Rapagnetta for their technical contribution. We also thank Ambra Micheletti from the Agency for Food Service Industry in the Marche (ASSAM) Region, Italy, for supporting the study and Mario Gallarani and his family for cultivating *C. spinose* subsp. *rupestris* and for kindly giving us the flower bods used in this study. We acknowledge Olivetta Del Bianco for the English revision.

## SUPPLEMENTARY MATERIAL

The Supplementary Material for this article can be found online at: https://www.frontiersin.org/articles/10.3389/fmicb.2022.832919/full#supplementary-material

## REFERENCES

Abraham, S. V. P. I., Palani, A., Ramaswamy, B. R., Shunmugiah, K. P., and Arumugam, V. R. (2011). Antiquorum sensing and antibiofilm potential of *Capparis spinosa*. *Arch. Med. Res.* 42, 658–668. doi: 10.1016/j.arcmed.2011.12.002

Ainsworth, E. A., and Gillespie, K. M. (2007). Estimation of total phenolic content and other oxidation substrates in plant tissues using Folin-Ciocalteu reagent. *Nat. Protoc.* 2, 875–877. doi: 10.1038/nprot.2007.102

Al-Snafi, A. E. (2015). The chemical constituents and pharmacological effects of *Capparis spinose* - an overwiew. *Ind. J. Pharmaceutic. Sci. Res.* 5, 93–100.

Alves, P. M., Al-Badi, E., Withycombe, C., Jones, P. M., Purdy, K. J., and Maddocks, S. E. (2018). Interaction between *Staphylococcus aureus* and *Pseudomonas aeruginosa* is beneficial for colonization and pathogenicity in a mixed biofilm. *Pathog. Dis.* 76:1. doi: 10.1093/femspd/fty003

Arciola, C. R., Campoccia, D., Gamberini, S., Baldassarri, L., and Montanaro, L. (2005). Prevalence of *cna, fnbA* and *fnbB* adhesin genes among *Staphylococcus aureus* isolates from orthopedic infections associated to different types of implant. *FEMS Microbiol. Let.* 246, 81–86. doi: 10.1016/j.femsle.2005.03.035

Bouarab-Chibane, L., Forquet, V., Lantéri, P., Clément, Y., Léonard-Akkari, L., Oulahal, N., et al. (2019). Antibacterial properties of polyphenols: characterization and QSAR (Quantitative Structure–Activity Relationship) models. *Front. Microbiol.* 10:829. doi: 10.3389/fmicb.2019.00829

Bowler, P. G., Duerden, B. I., and Armstrong, D. G. (2001). Wound microbiology and associated approaches to wound management. *Clin. Microbiol. Rev.* 14, 244–269. doi: 10.1128/CMR.14.2.244-269.2001

CLSI (2018). *Methods for Dilution Antimicrobial Susceptibility Tests for Bacteria that Grow Aerobically* 11th edn. M07, Wayne, PA: Clinical and Laboratory Standards Institute

Cosa, S., Chaudhary, S. K., Chen, W., Combrinck, S., and Viljoen, A. (2019). Exploring common culinary herbs and spices as potential anti-quorum sensing agents. *Nutrients*. 11:739. doi: 10.3390/nu11040739

Cowles, K. N., and Gitai, Z. (2010). Surface association and the MreB cytoskeleton regulate pilus production, localization and function in *Pseudomonas aeruginosa*. *Mol. Microbiol.* 76, 1411–1426. doi: 10.1111/j.1365-2958.2010.07132.x

Cushnie, T. P., and Lamb, A. J. (2005). Antimicrobial activity of flavonoids. *Int. J. Antimicrob. Agents* 26, 343–356. doi: 10.1016/j.ijantimicag.2005.09.002

Cushnie, T. P. T., and Lamb, A. J. (2011). Recent advances in understanding the antibacterial properties of flavonoids. *Int. J. Antimicrob. Agents* 38, 99–107. doi: 10.1016/j.ijantimicag.2011.02.014

de Bont, C. M., Boelens, W. C., and Pruijn, G. J. M. (2019). NETosis, complement, and coagulation: a triangular relationship. Cell Mol. Immunol. 16, 19–27. doi: 10.1038/s41423-018-0024-0

DeLeon, S., Clinton, A., Fowler, H., Everett, J., Horswill, A. R., and Rumbaugh, K. P. (2014). Synergistic interactions of *Pseudomonas aeruginosa* and *Staphylococcus aureus* in an *in vitro* wound model. *Infect. Immun.* 82, 4718–4728. doi: 10.1128/IAI.02198-14

D'Ercole, S., Di Fermo, P., Di Giulio, M., Di Lodovico, S., Di Campli, E., Scarano, A., et al. (2020). Near-infrared NIR irradiation and sodium hypochlorite: an efficacious association to counteract the *Enterococcus faecalis* biofilm in endodontic infections. *J. Photochem. Photobiol. B* 210:111989. doi: 10.1016/j.jphotobiol.2020.111989

Di Fermo, P., Di Lodovico, S., Amoroso, R., De Filippis, B., D'Ercole, S., Di Campli, E., et al. (2020). Searching for new tools to counteract the *Helicobacter* pylori resistance: the positive action of resveratrol derivatives. *Antibiotics (Basel)* 9:891. doi: 10.3390/antibiotics9120891

Di Giulio, M., Di Lodovico, S., Fontana, A., Traini, T., Di Campli, E., Pilato, S., et al. (2020). Graphene Oxide affects *Staphylococcus aureus* and *Pseudomonas aeruginosa* dual species biofilm in Lubbock Chronic Wound Biofilm model. *Sci. Rep.* 10:18525. doi: 10.1038/s41598-020-75086-6

Di Giulio, M., Zappacosta, R., Di Lodovico, S., Di Campli, E., Siani, G., Fontana, A., et al. (2018). Antimicrobial and antibiofilm efficacy of graphene oxide against chronic wound microorganisms. *Antimicrob. Agents Chemother.* 62:e00547–18. doi: 10.1128/AAC.00547-18

Di Lodovico, S., Gasparri, F., Di Campli, E., Di Fermo, P., D'Ercole, S., Cellini, L., et al. (2020a). Prebiotic combinations effects on the colonization of *Staphylococcal* skin strains. *Microorganisms* 9:37. doi: 10.3390/microorganisms9010037

Di Lodovico, S., Menghini, L., Ferrante, C., Recchia, E., Castro-Amorim, J., Gameiro, P., et al. (2020b). Hop extract: an efficacious antimicrobial and anti-biofilm agent against multidrug-resistant *Staphylococci* strains and *Cutibacterium acnes*. *Front. Microbiol.* 11:1852. doi: 10.3389/fmicb.2020.01852

Di Lodovico, S., Napoli, E., Di Campli, E., Di Fermo, P., Gentile, D., Ruberto, G., et al. (2019). *Pistacia vera* L. oleoresin and levofloxacin is a synergistic combination against resistant *Helicobacter* pylori strains. *Sci. Rep.* 9:4646. doi: 10.1038/s41598-019-40991-y

Eddouks, M., Lemhadri, A., Hebi, M., El Hidani, A., Zeggwagh, N. A., El Bouhali, B., Hajji, L., et al. (2017). *Capparis spinosa* L. aqueous extract evokes antidiabetic effect in streptozotocin-induced diabetic mice. Avicenna J. Phytomed. 7, 191–198. PMCID: PMC5355824

El-Sayed, N. R., Samir, R., Abdel-Hafez, L. J. M., and Ramadan, M. A. (2020). Olive leaf extract modulates quorum sensing genes and biofilm formation in multi-drug resistant *Pseudomonas aeruginosa*. *Antibiotics (Basel)* 9:526. doi: 10.3390/antibiotics9090526

Gillespie, K. M., Chae, J. M., and Ainsworth, E. A. (2007). Rapid measurement of total antioxidant capacity in plants. *Nat. Protoc.* 2, 867–870. doi: 10.1038/nprot.2007.100

Ikigai, H., Nakae, T., Hara, Y., and Shimamura, T. (1993). Bactericidal catechins damage the lipid bilayer. *Biochim. Biophys. Acta* 1147, 132–136. doi: 10.1016/0005-2736(93)90323-r

Kim, D. O., Chun, O. K., Kim, Y. J., Moon, H. Y., and Lee, C. Y. (2003). Quantification of polyphenolics and their antioxidant capacity in fresh plums. *J. Agric. Food Chem.* 51, 6509–6515. doi: 10.1021/jf0343074

Mahboubi, M., and Mahboubi, A. (2014). Antimicrobial activity of *Capparis spinosa* as its usages in traditional medicine. *Herba Polonica* 60, 39–48. doi: 10.2478/hepo-2014-0004

Maldini, M., Foddai, M., Natella, F., Addis, R., Chessa, M., Petretto, G. L., et al. (2016). Metabolomic study of wild and cultivated caper (*Capparis spinosa* L.) from different areas of Sardinia and their comparative evaluation. *J. Mass Spectr.* 51, 716–728. doi: 10.1002/jms.3830

Mollica, A., Stefanucci, A., Macedonio, G.,,Locatelli, M., Luisi, G., Novellino, E., et al. (2019). Chemical composition and biological activity of *Capparis spinosa* L. from Lipari Island. *S. Afr. J. Bot.* 120, 135–140. doi: 10.1016/j.sajb.2018.02.397

Mollica, A., Zengin, G., Locatelli, M., Stefanucci, A., Mocan, A., Carradori, S., et al. (2017). Anti-diabetic and anti-hyperlipidemic properties of *Capparis spinosa* L.: in vivo and in vitro evaluation of its nutraceutical potential. *J. Funct. Foods* 35, 32–42. doi: 10.1016/j.jff.2017.05.001

Nakamura, T., Daimon, T., Mouri, N., Masuda, H., and Sawa, Y. (2014). *Staphylococcus aureus* and repeat bacteremia in febrile patients as early signs of sternal wound infection after cardiac surgery. *J. Cardiothorac. Surg.* 9:80. doi: 10.1186/1749-8090-9-80

Orazi, G., and O'Toole, G. A. (2017). *Pseudomonas aeruginosa* alters *Staphylococcus aureus* sensitivity to vancomycin in a biofilm model of cystic fibrosis infection. *MBio* 8:e00873-17. doi: 10.1128/mBio.00873-17

Peng, LY., Yuan, M., Cui ZQ., Wu ZM., Yu ZJ, Song, K., Tang, B., et al . (2018). Rutin inhibits quorum sensing, biofilm formation and virulence genes in avian pathogenic *Escherichia coli*. *Microb. Pathog.* 119, 54–59. doi: 10.1016/j.micpath.2018.04.007

Rahimi, V. B., Rajabian, A., Rajabi, H., Vosough, E. M., Mirkarimi, H. R., Hasanpour, M., et al. (2020). The effects of hydro-ethanolic extract of *Capparis spinosa* (*C. spinosa*) on lipopolysaccharide (LPS)-induced inflammation and cognitive impairment: evidence from *in vivo* and *in vitro* studies. *J. Ethnopharmacol.* 256:112706. doi: 10.1016/j.jep.2020.112706

Sabbatini, M., Magnelli, V., and Renò, F. (2021). NETosis in wound healing: when enough is enough. *Cells* 10:494. doi: 10.3390/cells10030494

Shreeram, D. D., Panmanee, W., McDaniel, C. T., Daniel, S., Schaefer, D. W., and Hassett, D. J. (2018). Effect of impaired twitching motility and biofilm dispersion on performance of *Pseudomonas aeruginosa*-powered microbial fuel cells. *J. Ind. Microbiol. Biotechnol.* 45, 103–109. doi: 10.1007/s10295-017-1995-z

Stapleton, P. D., Shah, S., Hamilton-Miller J. M. T., Hara, Y., Nagaoka, Y., Kumagai, A., Uesato, S., et al. (2004). Anti-*Staphylococcus aureus* activity and oxacillin resistance modulating capacity of 3- O-acylcatechins. *Int. J. Antimicrob. Agents* 24, 374–380. doi: 10.1016/j.ijantimicag.2004.03.024

Stefanucci, A., Zengin, G., Locatelli, M., Macedonio, G., Wang CK, Novellino, E., et al. (2018). Impact of different geographical locations on varying profile of bioactives and associated functionalities of caper (*Capparis spinosa* L.). *Food Chem Toxicol.* 118, 181–189. doi: 10.1016/j.fct.2018.05.003

Taguri, T., Tanaka, T., and Kouno, I. (2006). Antibacterial spectrum of plant polyphenols and extracts depending upon hydroxyphenyl structure. *Biol. Pharm. Bull.* 29, 2226–2235. doi: 10.1248/bpb.29.2226

Thaarup, I. C., and Bjarnsholt, T. (2021). Current in vitro biofilm-infected chronic wound models for developing new treatment possibilities. *Adv. Wound Care (New Rochelle)* 10, 91–102. doi: 10.1089/wound.2020.1176

Tong, S. Y. C., Davis, J. S., Eichenberger, E., Holland, T. L., and Fowler, V. G., Jr. (2015). *Staphylococcus aureus* infections: epidemiology, pathophysiology, clinical manifestations, and management. *Clin. Microbiol. Rev.* 28, 603–661. doi: 10.1128/CMR.00134-14

Tungmunnithum, D., Thongboonyou, A., Pholboon, A., and Yangsabai A. (2018). Flavonoids and other phenolic compounds from medicinal plants for pharmaceutical and medical aspects: an overview. *Medicines (Basel)* 5:93. doi: 10.3390/medicines5030093

Turnbull, L., and Whitchurch, C. B. (2014). Motility assay: twitching motility. *Methods Mol. Biol.* 1149, 73–86. doi: 10.1007/978-1-4939-0473-0_9

World Health Organization (WHO) (2013). *Regulatory Situation of Herbal Medicines: a Worldwide Review*. Geneva: World Health Organization

Wojdyło, A., Nowicka, P., Grimalt, M., Legua, P., Almansa, M. S., Amorós, A., et al. (2019). Polyphenol compounds and biological activity of Caper (*Capparis spinosa* L.) flowers buds. *Plants (Basel)* 8:539. doi: 10.3390/plants8120539

Yang, M., Zhang, C., Hansen, S. A., Mitchell, W. J., Zhang, M. Z., and Zhang, S. (2019). Antimicrobial efficacy and toxicity of novel CAMPs against *P. aeruginosa* infection in a murine skin wound infection model. *BMC Microbiol.* 19:293. doi: 10.1186/s12866-019-1657-6

Yung, D. B. Y., Sircombe, K. J., and Pletzer, D. (2021). Friends or enemies? The complicated relationship between *Pseudomonas aeruginosa* and *Staphylococcus aureus*. *Mol. Microbiol.* 116, 1–15. doi: 10.1111/mmi.14699

Zengin, G., Locatelli, M., Stefanucci, A., Macedonio, G., Novellino, E., Mirzaie, S., Dvorácskó, S., et al. (2017). Chemical characterization, antioxidant properties, anti-inflammatory activity and enzyme inhibition of *Ipomoea batatas* L. leaf extracts. *Int. J. Food Prop.* 20, 1907–1919. doi: 10.1080/10942912.2017.1357127

Zhang, H., and Ma, Z. F. (2018). Phytochemical and pharmacological properties of *Capparis spinosa* as a medicinal plant. *Nutrients* 10:116. doi: 10.3390/nu10020116

Zolfaghar, I., Evans, D. J., and Fleiszig, S. M. J. (2003). Twitching motility contributes to the role of pili in corneal infection caused by *Pseudomonas aeruginosa*. *Infect. Immun.* 71, 5389–5393. doi: 10.1128/IAI.71.9.5389-5393.20

**Conflict of Interest:** The authors declare that the research was conducted in the absence of any commercial or financial relationships that could be construed as a potential conflict of interest.

**Publisher's Note:** All claims expressed in this article are solely those of the authors and do not necessarily represent those of their affiliated organizations, or those of the publisher, the editors and the reviewers. Any product that may be evaluated in this article, or claim that may be made by its manufacturer, is not guaranteed or endorsed by the publisher.

frontiers | Frontiers in Microbiology

ORIGINAL RESEARCH
published: 25 April 2022
doi: 10.3389/fmicb.2022.874354

# Epigallocatechin-3-Gallate Ameliorates Acute Lung Damage by Inhibiting Quorum-Sensing-Related Virulence Factors of *Pseudomonas aeruginosa*

*Huaqiao Tang[1†], Suqi Hao[1†], Muhammad Faraz Khan[2], Ling Zhao[1], Fei Shi[1], Yinglun Li[1], Hongrui Guo[1], Yuanfeng Zou[1], Cheng Lv[1], Jie Luo[3,4], Ze Zeng[3], Qiang Wu[5] and Gang Ye[1]**

[1]Department of Pharmacy, College of Veterinary Medicine, Sichuan Agricultural University, Chengdu, China, [2]Department of Botany, Faculty of Basic and Applied Sciences, University of Poonch Rawalakot, Rawalakot, Pakistan, [3]National Ethnic Affairs Commission Key Open Laboratory of Traditional Chinese Veterinary Medicine, Tongren Polytechnic College, Tongren, China, [4]Engineering Research Center of the Medicinal Diet Industry, Tongren Polytechnic College, Tongren, China, [5]Agricultural College, Yibin Vocational and Technical College, Yibin, China

OPEN ACCESS

**Edited by:**
Laura Quintieri,
Italian National Research Council, Italy

**Reviewed by:**
Mohammad Minnatul Karim,
Islamic University, Bangladesh
Mona I. Shaaban,
Mansoura University, Egypt

***Correspondence:**
Gang Ye
yegang_sicau@163.com

[†]These authors share first authorship

**Specialty section:**
This article was submitted to Antimicrobials, Resistance and Chemotherapy, a section of the journal Frontiers in Microbiology

**Received:** 12 February 2022
**Accepted:** 04 April 2022
**Published:** 25 April 2022

**Citation:**
Tang H, Hao S, Khan MF, Zhao L, Shi F, Li Y, Guo H, Zou Y, Lv C, Luo J, Zeng Z, Wu Q and Ye G (2022) Epigallocatechin-3-Gallate Ameliorates Acute Lung Damage by Inhibiting Quorum-Sensing-Related Virulence Factors of Pseudomonas aeruginosa. Front. Microbiol. 13:874354. doi: 10.3389/fmicb.2022.874354

The superbug *Pseudomonas aeruginosa* is among the most formidable antibiotic-resistant pathogens. With declining options for antibiotic-resistant infections, new medicines are of utmost importance to combat with *P. aeruginosa*. In our previous study, we demonstrated that Epigallocatechin-3-gallate (EGCG) can inhibit the production of quorum sensing (QS)-regulated virulence factors *in vitro*. Accordingly, the protective effect and molecular mechanisms of EGCG against *P. aeruginosa*-induced pneumonia were studied in a mouse model. The results indicated that EGCG significantly lessened histopathological changes and increased the survival rates of mice infected with *P. aeruginosa*. EGCG effectively alleviated lung injury by reducing the expression of virulence factors and bacterial burden. In addition, EGCG downregulated the production of pro-inflammatory cytokines, such as TNF-α, IL-1, IL-6, and IL-17, and increased the expression of anti-inflammatory cytokines IL-4 and IL-10. Thus, the experimental results supported for the first time that EGCG improved lung damage in *P. aeruginosa* infection by inhibiting the production of QS-related virulence factors *in vivo*.

**Keywords: anti-virulence, quorum sensing, EGCG, *P. aeruginosa*, acute lung infection**

## INTRODUCTION

Globally, pneumonia is a severe public health problem with a large disease burden and a major cause of mortality and morbidity. The disease burden caused by pneumonia affects more children worldwide than other diseases (O'Brien et al., 2019). Older patients have a high risk of death afflicted by pneumonia (Quinton and Mizgerd, 2015). Some of the bacterial and viral infections causing acute pneumonia or sepsis result in serious inflammatory damage to the lungs, thereby leading to the progression of acute lung injury (ALI) or acute respiratory distress syndrome (ARDS), especially in critically ill patients (Dai et al., 2018).

Multidrug-resistant microbes ("superbugs"), such as *Streptococcus pneumoniae*, group A *Streptococcus, Klebsiella* pneumoniae, *Staphylococcus aureus*, *Mycoplasma pneumoniae*, and *Pseudomonas aeruginosa* can cause severe pneumonia and were the main inducers of acute pathogenic factors (Ravi Kumar et al., 2018).

*P. aeruginosa*, a common opportunistic pathogen, can cause life-threatening respiratory infections and is responsible for hospital-acquired infections and ventilator-associated pneumonia (VAP). The high adaptability and an increasing number of multidrug-resistant *P. aeruginosa* constitute a threat for those who suffer from Chronic Obstructive Pulmonary Disease (COPD) or Cystic Fibrosis (*CF*; Aloush et al., 2006). Unfortunately, because of its intrinsic and extrinsic drug resistance and the capacity of *P. aeruginosa* to form biofilms, a *P. aeruginosa* infection is notoriously difficult to treat with antibiotics (Moore and Flaws, 2011). Multidrug-resistant pathogen-induced death is estimated to reach 10 million by 2050, and thereby exceeding deaths caused by cancer and diabetes combined worldwide. Thus, the development of alternative therapeutic methods is critical (O'Neill, 2016). The QS system is a cell-to-cell system that enables microbe populations to change their behavior based on population density. The QS system of *P. aeruginosa* plays a key role in coordinating various activities, including biofilm formation and the release of virulence factors. The QS system of *P. aeruginosa* is mainly regulated by four QS network subsystems, including *lasI*/*lasR, rhlI*/*rhlR*, PQS, and IQS systems (Lee and Zhang, 2015).

*P. aeruginosa*-induced pneumonia expresses a myriad of virulence factors, including flagella, pili, lipopolysaccharides (LPS), elastase, alkaline phosphatase, exotoxin A, as well as components of the type III secretion system (T3SS; Sadikot et al., 2005). In addition, the ability of *P. aeruginosa* to form biofilms is conducive to establishing infections in VAP and *CF* patients and is difficult to eradicate (Costerton et al., 1999). *P. aeruginosa*-induced pneumoniae is a complex process. Several surface-associated elements, including flagella, fimbriae, and LPS, contact host respiratory epithelia through a number of aggregated pilis (Gellatly and Hancock, 2013). Once contact with host epithelia has occurred, T3SS can be activated. *P. aeruginosa* T3SS is a major determinant of virulence, and its expression is frequently associated with acute invasive infections. Moreover, *P. aeruginosa* T3SS has been linked to increased mortality in infected patients (Hauser, 2009). Elastase (*lasB lasA*) has been shown to directly injure lung tissue through disruption of epithelial tight junctions and basal membranes. Elastase may increase the recruitment of neutrophils into the airways, which can result in serious inflammation (Kipnis et al., 2006). Pyocyanin induces direct damage to the respiratory tract as epithelial necrosis, and slowing tracheal mucociliary transport results from damaged ciliary movement (Lau et al., 2004). Virulence factors, such as type III secretory proteins, QS systems, and LPS, activate the host immune response. Therefore, the activation of macrophages, neutrophilic granulocytes, and T cells induces the secretion of cytokines, chemotactic factors, and another inflammatory mediator, thus leading to lung injury and mortality (Driscoll et al., 2007).

For thousands of years, tea originating from China has gained the world's taste. It has become the daily health drink for many individuals. In general, these health benefits result from the phenolic compounds that are present in green tea, particularly catechins. Numerous studies have demonstrated the diverse activities of Epigallocatechin-3-gallate (EGCG), including antioxidant, antibacterial, antiviral, antitumor and anti-inflammatory activities. In our previous study, we demonstrated that EGCG significantly acted against the expression of *P. aeruginosa* QS-regulated virulence *in vitro*, and significantly increased the survival rate of *Caenorhabditis elegans* infected with *P. aeruginosa* (Hao et al., 2021). QS quenching, called anti-virulence therapy, has been considered a suitable strategy to settle the multidrug resistance problem (Clatworthy et al., 2007). Taken together, our study provides additional support for drinking tea as an effective method against bacterial infections. These findings can pave the way for the use of EGCG as a therapeutic medicine to treat bacterial infections in the lungs.

# MATERIALS AND METHODS

## Animals, Bacterial Strains, and Chemicals

Eight-week-old male ICR mice (25–30 g) were purchased from Sibeifu Biotechnology Co. Ltd. (Beijing, China). Mice were housed at 22–25°C with a 12 h day-night cycle, were fed standard rodent chow, and sterile water *ad libitum* for 1 week of acclimation. All protocols involving animal studies were reviewed and approved by the Animal Ethical Committee of Sichuan Agricultural University (#20210020). *P. aeruginosa* (PAO1) were cultured in Luria Bertani (LB) medium (Sangon Biotech, Shanghai, China). EGCG was obtained from Shanghai Yuanye Bio-Technology Co., Ltd. (Shanghai, China); CIP was obtained from Sichuan Chuanlong Dongke Pharmaceutical Co., Ltd.

## Experimental Protocol

A total of 90 mice were randomly divided into six groups ($n = 15$ mice per group): a control group, PAO 1 group, PAO 1 + EGCG (20 mg/kg) group, PAO 1 + EGCG (40 mg/kg) group, PAO 1 + EGCG (80 mg/kg) group, and a Ciprofloxacin (CIP; 20 mg/kg) group. CIP was used as positive control. Mice were administered the same volume of saline or drugs by intragastric administration for 3 days. Mice were infected by using a previously described method with modifications (Traber et al., 2019). Briefly, mice were weighed and anesthetized, and received intratracheal instillation of PAO 1 ($2.5 \times 10^8$ CFU) in 20 μl phosphate buffered saline (PBS) to model an acute infection with PAO 1. Mice were anesthetized and sacrificed at 24 h after infection. Samples were harvested rapidly for subsequent analysis. Per group, 10 mice were randomly selected to collect blood and lung tissue; another five mice were selected for the collection of bronchial-alveolar lavage fluid (BALF).

## Colony Counting of the Lungs

To assess bacterial burden in the lung, fresh lung tissues were extracted aseptically, and homogenized in sterile NaCl 0.9%.

As previously described (Pylaeva et al., 2019), colony forming units (CFU) were enumerated by plating serial dilutions of lung homogenates on *Pseudomonas* Agar Medium for the detection of Pyocyanin (PDP, Haibo Biotech, Shandong, China). After incubation at 37°C for 24 h, CFU were counted and recorded.

## Histopathological Evaluation

Lung tissue was fixed with 4% paraformaldehyde overnight, and embedded in paraffin. Subsequently, lung tissue was cut into 5-μm-thick sections. Sections were stained with hematoxylin and eosin (H&E) and the degree of damage to lung tissue was validated (Sen-Kilic et al., 2019).

## ELISA

BALF was collected and centrifuged at 1500 g for 5 min, then the supernatant was removed and transferred to a clean tube. The expression of TNF-α, IL-10, and IL-17 in the supernatant was determined by ELISA according to the manufacturer's instructions [Multisciences (Lianke) Biotech Co., Ltd., Hangzhou, China]. The absorbance was measured using a microplate reader at 450 nm.

## RNA Extraction and qPCR

Total RNA was extracted from lung tissue homogenate using TRIzol reagent (Songon Biotech, Shanghai, China) according to the manufacturer's instructions. Then, cDNA synthesis was conducted using a RevertAid First Strand cDNA Synthesis kit (Thermo Fisher Scientific, K1622, Waltham, MA, United States) in a 20 μl volume of reaction mixture. Real-time PCR was performed in a total reaction volume of 10 μl, containing 5 μl PerfectStartTM Green qPCR SuperMix (TransGen Biotech, Beijing, China), 2 μl template cDNA, 1 μl of primers (Shenzhen Huada Gene Research Institute, Shenzhen, China), and 2 μl DNase/RNase-free water (Tiangen Biotech, Beijing, China). Finally, pvdQ of *P. aeruginosa* was chosen as the reference gene. The qRT-PCR reaction was conducted on a LightCycler® 480II Master Mix (Roche, Germany). Data from qRT-PCR experiments were analyzed using the $2^{®-\Delta\Delta CT}$ method (Yang et al., 2021). Primer sequences are listed in **Table 1**.

**TABLE 1** | PCR primers of virulence factors and inflammatory cytokines.

| Primer name | Type | Primer sequence |
|---|---|---|
| lasI | Fw | CGCACATCTGGGAACTCA |
| | Rev | CGGCACGGATCATCATCT |
| lasR | Fw | CTGTGGATGCTCAAGGACTAC |
| | Rev | AACTGGTCTTGCCGATGG |
| rhlI | Fw | GTAGCGGGTTTGCGGATG |
| | Rev | CGGCATCAGGTCTTCATCG |
| rhlR | Fw | GCCAGCGTCTTGTTCGG |
| | Rev | CGGTCTGCCTGAGCCATC |
| pqsA | Fw | GACCGGCTGTATTCGATTC |
| | Rev | GCTGAACCAGGGAAAGAAC |
| pqsR | Fw | CTGATCTGCCGGTAATTGG |
| | Rev | ATCGACGAGGAACTGAAGA |
| phzM | Fw | ACGGCTGTGGCGGTTTA |
| | Rev | CCGTGACCGTCGCATT |
| lasA | Fw | CTGTGGATGCTCAAGGACTAC |
| | Rev | AACTGGTCTTGCCGATGG |
| lasB | Fw | AACCGTGCGTTCTACCTGTT |
| | Rev | CGGTCCAGTAGTAGCGGTTG |
| phzA | Fw | AACGGTCAGCGGTACAGGGAAAC |
| | Rev | ACGAACAGGCTGTGCCGCTGTAAC |
| phzH | Fw | GCTCATCGACAATGCCGAACT |
| | Rev | GCGGATCTCGCCGAACATCAG |
| phzS | Fw | CCGAAGGCAAGTCGCTGGTGA |
| | Rev | GGTCCCAGTCGGCGAAGAACG |
| RhlA | Fw | TGGCCGAACATTTCAACGT |
| | Rev | GATTTCCACCTCGTCGTCCTT |
| RhlC | Fw | GCCATCCATCTCGACGGAC |
| | Rev | CGCAGGCTGTATTCGGTG |
| rpod | Fw | GGGCGAAGAAGGAAATGGTC |
| | Rev | CAGGTGGCGTAGGTGGAGAA |
| TNF-α | Fw | CTTCTGTCTACTGAACTTCGGG |
| | Rev | CAGGCTTGTCACTCGAATTTTG |
| IL-1 | Fw | GAAATGCCACCTTTTGACAG |
| | Rev | TGGATGCTCTCATCAGGACAG |
| IL-6 | Fw | TAGTCCTTCCTACCCCAATTTCC |
| | Rev | TTGGTCCTTAGCCACTCCTTC |
| IL-4 | Fw | GGTCTCAACCCCCAGCTAGT |
| | Rev | GCCGATGATCTCTCTCAAGTGAT |
| IL-10 | Fw | GCTGGACAACATACTGCTAACC |
| | Rev | ATTTCCGATAAGGCTTGGCAA |
| IL-17 | Fw | TTTAACTCCCTTGGCGCAAAA |
| | Rev | CTTTCCCTCCGCATTGACAC |
| GAPDH | Fw | TCAACGGCACAGTCAAGGC |
| | Rev | CTCCACGACATACTCAGCACC |

## Statistical Analysis

Data are expressed as the mean ± standard deviation (SD), and all experimental groups were compared with the control group. Data were analyzed using SPSS 20.0 by ANOVA (IBM SPSS Statistics, CA, United States), and $p < 0.05$ or $p < 0.01$ was considered significantly different.

# RESULTS

## Protective Efficacy of EGCG Against Acute Lung Infection

As shown in **Figure 1**, the survival of mice with a *P. aeruginosa*-induced acute lung infection was evaluated to test the protective effect of EGCG. Of the mice in the *P. aeruginosa* group, only 53.4% survived. The survival rates after EGCG early intervening treatment with 80 mg/kg, 40 mg/kg, 20 mg/kg, respectively, were 71.8, 66.7, 66.7%, whereas the survival rate of the positive CIP group was 60%, thus the protective effect was less compared to that of EGCG. Next, the alleviation of *P. aeruginosa*-induced pulmonary edema by EGCG was assessed. The results showed that the wet weight of mice in the *P. aeruginosa* group increased more than 2-fold compared with mice in the control group. EGCG significantly reduced the lung edema, and no significant differences in lung weight were observed between CIP and *P. aeruginosa*. The bacterial burden in the lungs was determined by plating serial dilutions and counting viable bacteria at 24 h post the challenge. As expected, the bacterial load in the lungs of EGCG-treated mice was significantly lower compared to that of mice in the *P. aeruginosa* group. These findings demonstrated the preventive effect of EGCG in decreasing acute lung infection

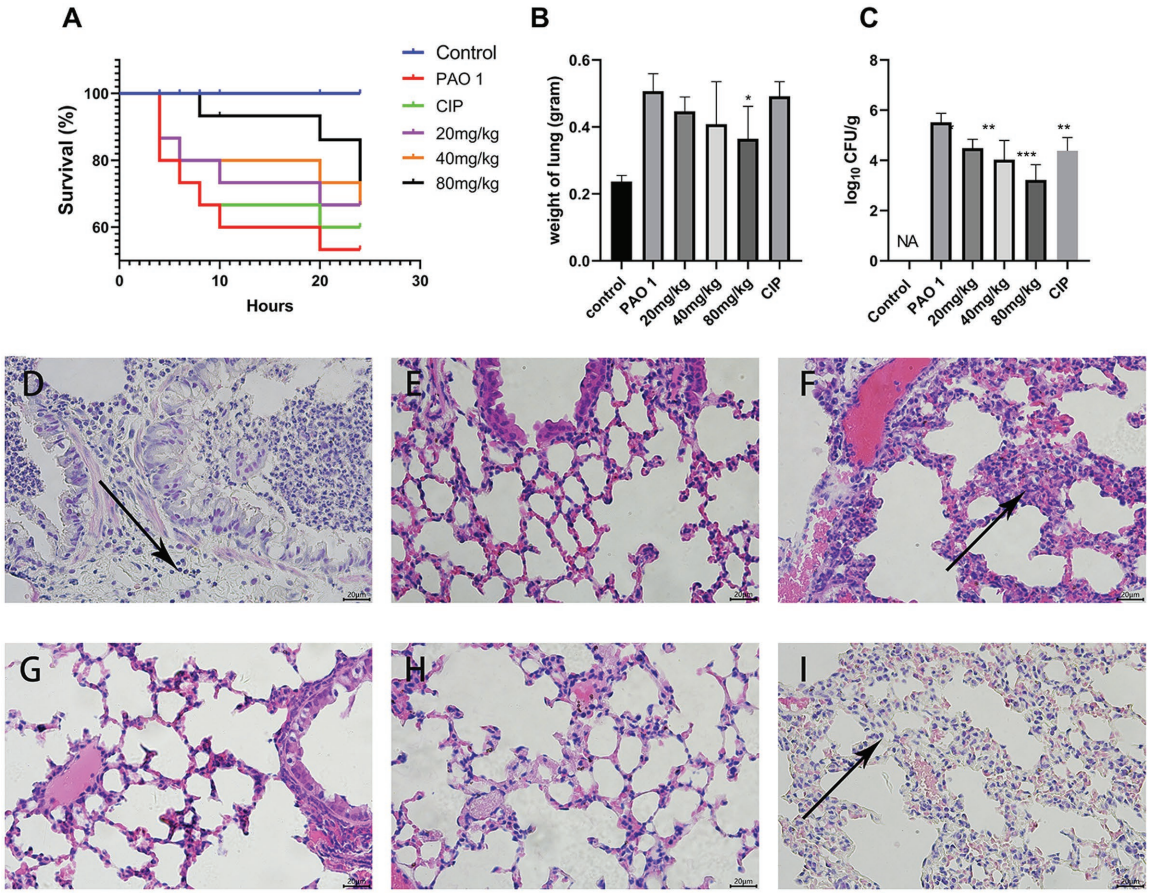


**FIGURE 1** | Protective efficacy of EGCG against acute lung infection. **(A)** The survival rate was measured at different time points post *P. aeruginosa* challenged. **(B)** The weight of the lungs after *P. aeruginosa* challenged. **(C)** Bacterial load in the lungs were evaluated at 24 h post infection. **(D–I)** Pathological changes in **(D)** *P. aeruginosa* group, **(E)** control group, **(F)** EGCG (20 mg/kg) group, **(G)** EGCG (40 mg/kg) group, **(H)** EGCG (80 mg/kg) group, **(I)** CIP was used as positive control. Data are presented as mean ± SD and analyzed with one-way ANOVA. $^{*}p < 0.05$, $^{**}p < 0.01$, $^{***}p < 0.005$ vs. PAO 1 group.

of *P. aeruginosa*. The control group did not show any histopathological changes in the lungs under the light microscope. The results indicated that lung sections after *P. aeruginosa* infection showed significant changes, including PMN infiltration, alveolar interstitial edema, interstitial hemorrhage, and alveolar wall thickening. Importantly, our results showed that EGCG treatment reduced lung damage and maintained alveolar integrity due to structural disruptions and hemorrhage in a concentration-dependent manner compared with the control. Taken together, these results demonstrated that EGCG alleviated histopathological damage in lungs of mice challenged with *P. aeruginosa*.

## EGCG Alleviated the Expression of QS System-Regulated Genes *in vivo*

In this study, the expression of QS system genes was examined in acute lung injury. As shown in **Figure 2**, EGCG and CIP significantly downregulated the expression of QS-related virulence factors *in vivo*. First, EGCG inhibited the master QS regulatory system *lasI/lasR* in a dose-dependent manner. The expression of *lasR* was significantly inhibited at 80 mg/kg. At a dose of 80 mg/kg, the expression of *lasA* and *lasB*, which are regulated *via* the *lasI/lasR* pathway, was also significantly inhibited in a dose-dependent manner. Moreover, *rhlI/rhlR* and *pqsA/pqsR* systems were downregulated as well. Our data showed that the expression level of the *pqsA/pqsR* system was lower than that of *lasI/lasR* and *rhlI/rhlR* systems. Therefore, we hypothesized that *lasI/lasR* and rhLI/rhlR systems played a dominant role in acute lung infection (**Figure 3**). The expression of virulence factors was significantly downregulated by EGCG. The expression of *phzA*, *phzS*, *phzM*, and *phzH* was also inhibited by EGCG compared with mice in the *P. aeruginosa* group. Furthermore, the *rhlA* gene, which controls the production of rhamnolipid, was significantly inhibited.

## EGCG Inhibited Biofilm Expression *in vivo*

*Pseudomonas aeruginosa* biofilm formation is regulated by the QS system (Sauer et al., 2002). The expression of biofilm matrix genes and subsequent development of biofilm structure are also adjusted by the QS system (Skariyachan et al., 2018). The expression of biofilm-regulated factors (*fila, pela, pila, pslb*) was evaluated *in vivo*. The results indicated that EGCG significantly inhibited biofilm maturation at 18 h *in vitro*, and a better inhibitory effect was found *in vivo*. The expression

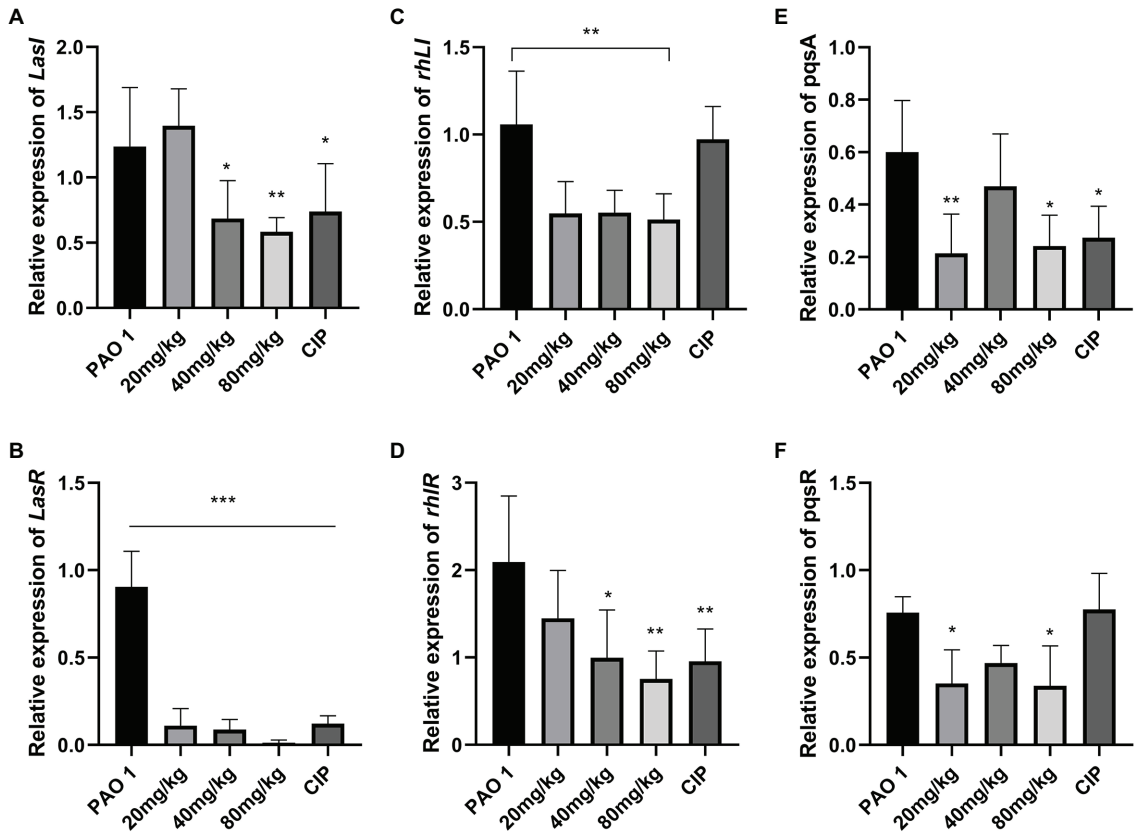


**FIGURE 2 |** The effect of EGCG on the expression of QS system *in vivo*. **(A)** *lasI*, **(B)** *lasR*, **(C)** *rhlI*, **(D)** *rhlR*, **(E)** *pqsA*, and **(F)** *pqsR*. Data are presented as mean ± SD and analyzed with one-way ANOVA. $^{*}p < 0.05$, $^{**}p < 0.01$, $^{***}p < 0.005$ vs. PAO 1 group.

of *pela*, *pila,* and *pslb* was significantly inhibited by EGCG in comparison to mice in the *P. aeruginosa* infection group. Thus, these results suggested that EGCG can effectively inhibit biofilm formation and prevent the activation of virulence factors of *P. aeruginosa in vivo*. The data are presented in **Figure 4**.

## EGCG Inhibited Inflammation in *Pseudomonas aeruginosa*-Induced Lung Injury

To assess the inflammatory state of infected mice, the expression of inflammatory cytokines was determined by real-time PCR and ELISA. Compared to the control, EGCG significantly decreased the expression of proinflammatory cytokines TNF-α, IL-1, IL-6, and IL-17. Moreover, the expression of proinflammatory cytokines in the CIP group was lower than that in the EGCG group. The EGCG group had a higher expression of anti-inflammatory cytokines IL-4 and IL-10 (**Figure 5**).

# DISCUSSION

In this study, it was demonstrated that EGCG protects mice against *P. aeruginosa*-induced lung damage by inhibiting the virulence controlled by QS systems. *P. aeruginosa* is a major cause of acute nosocomial infections and pneumonia (Kizny Gordon et al., 2017). Nosocomial bacteremia pneumonia is associated with significant mortality, morbidity, length of hospital stays and cost. In addition, despite important medical advances, there have been no improvements in the treatment of *P. aeruginosa* infections over the past two decades (Melsen et al., 2013; Jain et al., 2015). The mechanisms by which *P. aeruginosa* resists antibiotics include intrinsic, acquired and adaptive resistance, such as efflux pumps, antibiotic-inactivating enzymes, impermeable outer membrane proteins, horizontal transfer of resistance genes or mutational changes, and adaptive resistance refers to the formation of biofilms (Livermore, 2002; Breidenstein et al., 2011). *P. aeruginosa* is resistant to diverse types of antibiotics, including quinolones, aminoglycosides, and β-lactams (Hancock and Speert, 2000). Due to the increasing frequency of antibiotic resistance of *P. aeruginosa*, novel therapeutic approaches to treat *P. aeruginosa* infections are of utmost importance. Furthermore, novel treatments may be used alone or in combination with conventional therapies, such as the inhibition of QS and bacterial lectins, the use of iron chelation, phage therapy, vaccine strategies, as well as the use of nanoparticles, antimicrobial peptides and electrochemical scaffolds (Chatterjee et al., 2016). In our previous study, the minimal inhibitory concentration (MIC) of EGCG against *P. aeruginosa* was confirmed to be 512 μg/ml (Hao et al., 2021).

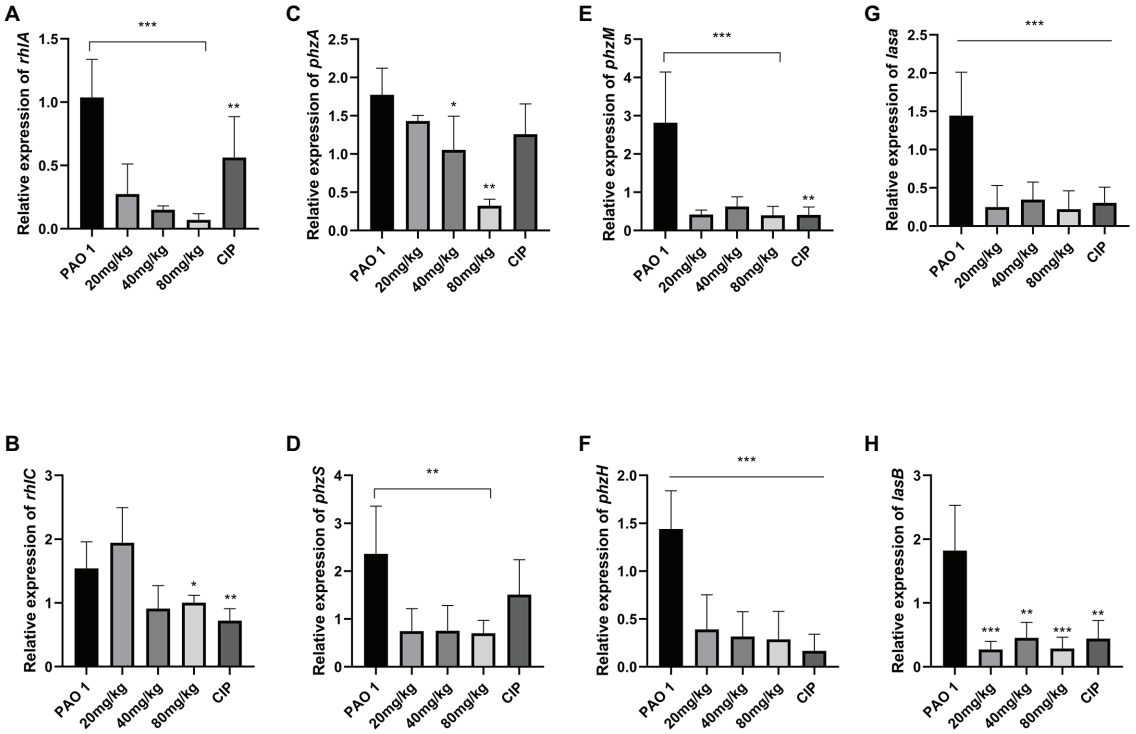


**FIGURE 3 |** The inhibition of EGCG on the expression of QS-regulated virulence factors in the lung challenged by *P. aeruginosa*. **(A)** *rhlA*, **(B)** *rhlC* **(C)** *phzA*, **(D)** *phzS*, **(E)** *phzM* **(F)** *phzH*, **(G)** *lasA*, **(H)** *lasB*. Data are presented as mean ± SD and analyzed with one-way ANOVA. $^{*}p < 0.05$, $^{**}p < 0.01$, $^{***}p < 0.005$ vs. PAO 1 group.

However, EGCG reduced virulence phenotypes, such as biofilm, protease, elastase activity, swimming, and swarming motility at concentrations where no growth inhibition was observed. In the present study, we aimed to explore the anti-infection ability of EGCG based on the QS mechanism in a mouse model of *P. aeruginosa* infection. Our results indicated that EGCG significantly alleviated *P. aeruginosa*-induced pulmonary edema, decreased the bacterial load and the level of proinflammatory cytokines in the lung, and enhanced the survival rates of mice. Moreover, EGCG significantly reduced the expression of QS-regulated virulence factors *in vivo*. Taken together, these findings showed that EGCG has the ability to mitigate the release of virulence and may alleviate inflammation-caused damage *in vivo*.

EGCG is one of the richest ingredients in green tea-derived polyphenols, and its biological activities have been extensively studied (Jigisha et al., 2012; Steinmann et al., 2013). EGCG can inhibit infections by reducing biofilm formation and toxin release in bacteria (Zhao et al., 2021). However, few studies have evaluated the clinical effect of EGCG in animal models. In several previous studies, the anti-inflammation effect of EGCG was demonstrated. Lee et al. demonstrated that EGCG protected against TNF-α-mediated lung inflammation by down-regulation of oxidative stress and expression of intercellular adhesion molecule (ICAM)-1 in A549 cells or human pulmonary alveolar epithelial cells (HPAEpiCs) as well as in mouse lungs (Lee et al., 2013). In a recent study, the effect of green tea (GTE) and EGCG on macrophage polarization was evaluated *in vitro* and it was determined whether the treatment could ameliorate inflammatory responses *in vivo*. Results showed that GTE and EGCG decreased M1-macrophages and increased Treg cells in bone marrow to inhibit inflammation. EGCG and GTE prevent LPS-induced inflammatory damage contributing to restore the immune system homeostasis through increasing M2-macrophages, N2-neutrophils and Tregs in the spleen and blood (Azambuja et al., 2022). The activation of M2 macrophages, which polarized by Th2 cytokines such as IL-4 and IL-13, can enhance the effect anti-inflammatory and immunoregulatory. Consequently, increasing the release of anti-inflammatory cytokines IL-10 and TGF-β (Shapouri-Moghaddam et al., 2018). Wang et al. (2019) demonstrated that pretreatment with EGCG attenuated LPS-induced ALI as manifested by fewer pathological changes in pulmonary edema and the expression of proinflammatory cytokines TNF-α, IL-1β, and IL-6 in the lung, serum, and BALF. The protective mechanism was associated with suppressing the TLR-4/NF-kB-p65 pathway that mediates inflammation.

These results were similar to the data obtained in our study; we demonstrated that EGCG alleviates lung damage, including pathological injury and pulmonary edema in *P. aeruginosa*-induced pulmonary infection. Moreover, EGCG decreased the *P. aeruginosa* load and infection mortality in the lung. EGCG significantly inhibited the expression of TNF-α, IL-1β, IL-6, and IL-17 in the lung but increased the expression of anti-inflammatory cytokines IL-4 and IL-10. We speculate that EGCG may improve the immunity ability through promoting the polarization of M2 macrophages. Hence EGCG increased the level of anti-inflammatory cytokines IL-4 and IL-10. Further work needs to be performed to identify the underlying

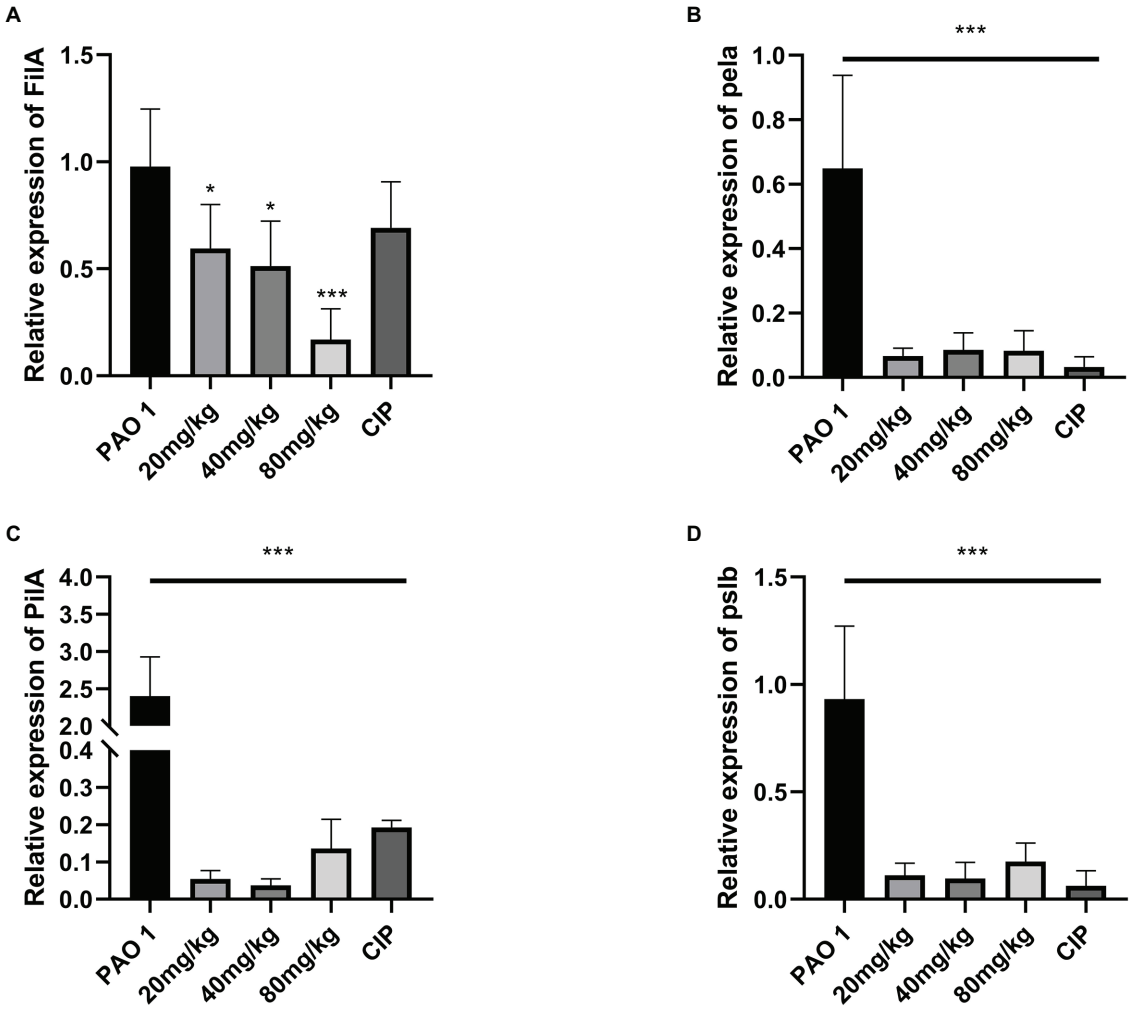


**FIGURE 4 |** EGCG significantly affected the expression of the biofilm formation relevant genes *in vivo*. **(A)** *FilA*, **(B)** *pela* **(C)** *PilA*, **(D)** *pslb*. Data are presented as mean ± SD and analyzed with one-way ANOVA. $^{*}p < 0.05$, $^{**}p < 0.01$, $^{***}p < 0.005$ vs. PAO 1 group.

mechanisms involved. The ELISA results showed that the protein expression levels of TNF-α and IL-17 decreased in a dose-dependent manner, compared with PAO 1 group. Therefore EGCG can reduce *P. aeruginosa*-induced inflammation in the lung. Liu et al. demonstrated that tea polyphenols increased the survival rate of Caenorhabditis elegans against K. pneumonia infection to 73.3 and 82.2% (Liu et al., 2020). Previous results showed that microencapsulation of EGCG exhibited therapeutic outcomes by resolution of inflammation in tuberculosis bacteria-infected lungs and a significant reduction in bacterial burden (Sharma et al., 2020). Many studies have suggested that EGCG and other polyphenol compounds could be potential antivirulence agents for pulmonary infection (Sriram et al., 2009; Ling et al., 2012). The potent anti-inflammatory activities add further appeal to the medicinal use of EGCG or other green tea polyphenol-rich products.

*P. aeruginosa* can express a plethora of virulence factors that facilitate invasion and damage host tissues (Crousilles et al., 2015), and are controlled by complex, intersecting regulatory circuits and multiple signaling systems (Nadal Jimenez et al., 2012; Balasubramanian et al., 2013). Among these, QS regulates virulence factors (proteases, elastase, rhamnolipid, exotoxins, and pyocyanin) and plays an important role in acute *P. aeruginosa* infections (Hauser, 2009; Lee and Zhang, 2015). QS participates in biofilm formation, which plays an important role during chronic infections and antibiotic resistance. In recent years, antimicrobial agents with great potential have been studied and are now known as antivirulence therapies (Hauser, 2009). This intervention targets virulence factors or virulence regulatory pathways that will not result in inhibition of bacterial growth or bacterial cell death but block their pathogenicity (Hauser, 2009). Consequently, the emergence of drug-resistant strains is decreasing. Interference with QS-mediated signaling and alleviation of virulence contribute to clearance of infecting bacteria by host defenses (Saeki et al., 2020). Our results confirmed the anti-QS ability of EGCG against *P. aeruginosa in vivo*. EGCG significantly inhibited the expression of QS-relevant genes, including *lasI*, *lasR*, *rhlI*, *rhlR*,

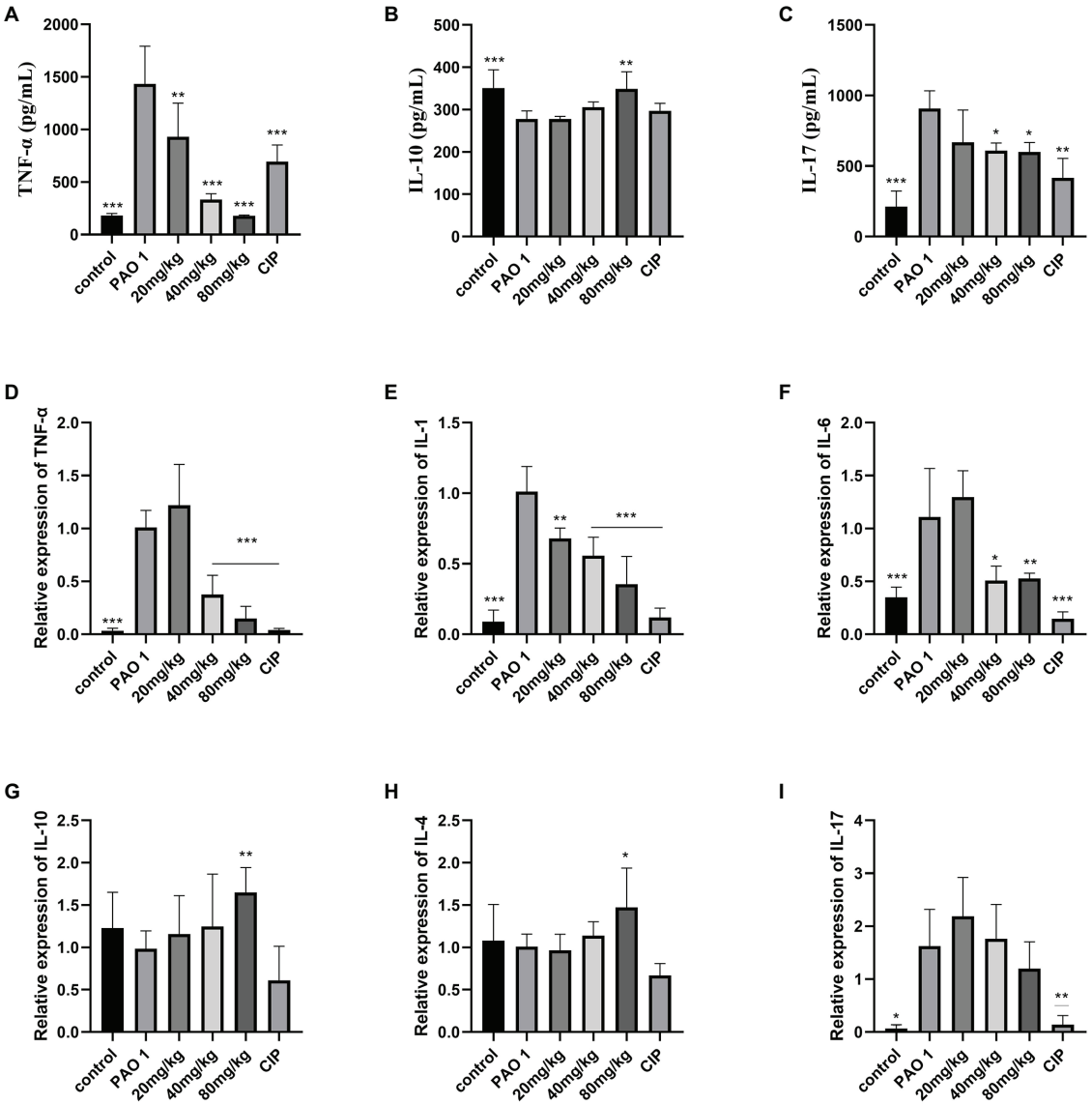


**FIGURE 5 |** Assay of inflammatory cytokines by ELISA and QRT-PCR. Secreted TNF-α, IL-10, and IL-17 from the bronchial-alveolar lavage fluid was assessed by ELISA assay kit **(A–C)**. EGCG affected the expression of cytokines with a dosage dependent manner in the lung **(D–I)**. Data are presented as mean ± SD and analyzed with one-way ANOVA. *$p < 0.05$, **$p < 0.01$, ***$p < 0.005$ vs. PAO 1 group.

*pqsA*, *pqsR*, *phzA*, *phzH*, *phzM*, *phzS*, *lasA*, *lasB*, *rhlA*, and *rhlC*. Moreover, EGCG had a better capacity to inhibit virulence than the positive CIP group. According to the gene expression results, EGCG displayed an excellent ability to inhibit proinflammatory cytokines. At 80 mg/kg, EGCG significantly increased anti-inflammatory cytokines IL-10 and IL-4, which was not observed in the CIP group. We found that the expression of *lasR*/*lasI* and *rhlR*/*rhlI* systems, the leading virulence factor during *P. aeruginosa* infection, was significantly inhibited at 80 mg/kg. Pyocyanin, a green color product of *P. aeruginosa*, can interfere with host oxidative stress responses by increasing intracellular levels of reactive oxygen species (Lau et al., 2004). Our results show that the inhibition ability of EGCG on the expression of QS-regulated virulence factors was better than that of CIP, especially in the QS systems *lasR*/*lasI*, *rhlR*/*rhlI* and *pqsR*/*pqsA*. Thus, these results suggested that EGCG not only alleviates inflammation but also reduces the damage of *P. aeruginosa* infection by targeting QS system-regulated virulence, thereby resulting in a higher protective effect than CIP. EGCG is a great potential QS inhibitor against infection that not only reduces the release of virulence factors *in vitro* but also effectively inhibits the expression of virulence factors *in vivo*.

## CONCLUSION

In conclusion, our results provide proof that EGCG alone can ameliorate acute *P. aeruginosa* infection in the lungs by QS and

inflammation inhibition. The *in vivo* results indicate that the QS inhibitor, EGCG,s may serve as a potential approach in treating bacterial infections. EGCG, a rich ingredient of tea, is indispensable to human life and may play an important role in preventing bacterial infections.

## DATA AVAILABILITY STATEMENT

The raw data supporting the conclusions of this article will be made available by the authors, without undue reservation.

## ETHICS STATEMENT

The animal study was reviewed and approved by Animal Ethical Committee of Sichuan Agricultural University.

## AUTHOR CONTRIBUTIONS

HT and SH contributed to conceptualization, methodology, validation, and investigation. LZ and FS contributed to formal analysis and investigation. YL, QW, HG, CL, JL, and ZZ contributed to writing—original draft and resources. GY contributed to writing—review and editing, supervision, resources, and funding acquisition. All authors contributed to the article and approved the submitted version.

## FUNDING

This work was supported by International Science and Technology Cooperation Program of Sichuan: 2020YFH0143; Traditional Chinese Veterinary Medicine Laboratory of the National Ethnic Affairs Commission [2020] 03.

## REFERENCES

Aloush, V., Navon-Venezia, S., Seigman-Igra, Y., Cabili, S., and Carmeli, Y. (2006). Multidrug-resistant Pseudomonas aeruginosa: risk factors and clinical impact. *Antimicrob. Agents Chemother.* 50, 43–48. doi: 10.1128/AAC.50.1.43-48.2006

Azambuja, J. H., Mancuso, R. I., Della Via, F. I., Torello, C. O., and Saad, S. T. O. (2022). Protective effect of green tea and epigallocatechin-3-gallate in a LPS-induced systemic inflammation model. *J. Nutr. Biochem.* 101:108920. doi: 10.1016/j.jnutbio.2021.108920

Balasubramanian, D., Schneper, L., Kumari, H., and Mathee, K. (2013). A dynamic and intricate regulatory network determines Pseudomonas aeruginosa virulence. *Nucleic Acids Res.* 41, 1–20. doi: 10.1093/nar/gks1039

Breidenstein, E. B., de la Fuente-Núñez, C., and Hancock, R. E. (2011). Pseudomonas aeruginosa: all roads lead to resistance. *Trends Microbiol.* 19, 419–426. doi: 10.1016/j.tim.2011.04.005

Chatterjee, M., Anju, C., Biswas, L., Kumar, V. A., Mohan, C. G., and Biswas, R. (2016). Antibiotic resistance in Pseudomonas aeruginosa and alternative therapeutic options. *Int. J. Med. Microbiol.* 306, 48–58. doi: 10.1016/j.ijmm.2015.11.004

Clatworthy, A. E., Pierson, E., and Hung, D. T. (2007). Targeting virulence: a new paradigm for antimicrobial therapy. *Nat. Chem. Biol.* 3, 541–548. doi: 10.1038/nchembio.2007.24

Costerton, J. W., Stewart, P. S., and Greenberg, E. P. (1999). Bacterial biofilms: a common cause of persistent infections. *Science* 284, 1318–1322. doi: 10.1126/science.284.5418.1318

Crousilles, A., Maunders, E., Bartlett, S., Fan, C., Ukor, E.-F., Abdelhamid, Y., et al. (2015). Which microbial factors really are important in Pseudomonas aeruginosa infections? *Future Microbiol.* 10, 1825–1836. doi: 10.2217/fmb.15.100

Dai, R.-X., Kong, Q.-H., Mao, B., Xu, W., Tao, R.-J., Wang, X.-R., et al. (2018). The mortality risk factor of community acquired pneumonia patients with chronic obstructive pulmonary disease: a retrospective cohort study. *BMC Pulm. Med.* 18, 12–10. doi: 10.1186/s12890-018-0587-7

Driscoll, J. A., Brody, S. L., and Kollef, M. H. (2007). The epidemiology, pathogenesis and treatment of Pseudomonas aeruginosa infections. *Drugs* 67, 351–368. doi: 10.2165/00003495-200767030-00003

Gellatly, S. L., and Hancock, R. E. (2013). Pseudomonas aeruginosa: new insights into pathogenesis and host defenses. *Path. Dis.* 67, 159–173. doi: 10.1111/2049-632X.12033

Hancock, R. E., and Speert, D. P. (2000). Antibiotic resistance in Pseudomonas aeruginosa: mechanisms and impact on treatment. *Drug Resist. Updat.* 3, 247–255. doi: 10.1054/drup.2000.0152

Hao, S., Yang, D., Zhao, L., Shi, F., Ye, G., Fu, H., et al. (2021). EGCG-mediated potential inhibition of biofilm development and quorum sensing in Pseudomonas aeruginosa. *Int. J. Mol. Sci.* 22:4946. doi: 10.3390/ijms22094946

Hauser, A. R. (2009). The type III secretion system of Pseudomonas aeruginosa: infection by injection. *Nat. Rev. Microbiol.* 7, 654–665. doi: 10.1038/nrmicro2199

Jain, S., Self, W. H., Wunderink, R. G., Fakhran, S., Balk, R., Bramley, A. M., et al. (2015). Community-acquired pneumonia requiring hospitalization among US adults. *N. Engl. J. Med.* 373, 415–427. doi: 10.1056/NEJMoa1500245

Jigisha, A., Nishant, R., Navin, K., and Pankaj, G. (2012). Green tea: a magical herb with miraculous outcomes. *Int. Res. J. Pharm* 3, 139–148.

Kipnis, E., Sawa, T., and Wiener-Kronish, J. (2006). Targeting mechanisms of Pseudomonas aeruginosa pathogenesis. *Med. et Mal. Infect.* 36, 78–91. doi: 10.1016/j.medmal.2005.10.007

Kizny Gordon, A. E., Mathers, A. J., Cheong, E. Y., Gottlieb, T., Kotay, S., Walker, A. S., et al. (2017). The hospital water environment as a reservoir for carbapenem-resistant organisms causing hospital-acquired infections—a systematic review of the literature. *Clin. Infect. Dis.* 64, 1435–1444. doi: 10.1093/cid/cix132

Lau, G. W., Hassett, D. J., Ran, H., and Kong, F. (2004). The role of pyocyanin in Pseudomonas aeruginosa infection. *Trends Mol. Med.* 10, 599–606. doi: 10.1016/j.molmed.2004.10.002

Lee, I.-T., Lin, C.-C., Lee, C.-Y., Hsieh, P.-W., and Yang, C.-M. (2013). Protective effects of (−)-epigallocatechin-3-gallate against TNF-α-induced lung inflammation via ROS-dependent ICAM-1 inhibition. *J. Nutr. Biochem.* 24, 124–136. doi: 10.1016/j.jnutbio.2012.03.009

Lee, J., and Zhang, L. (2015). The hierarchy quorum sensing network in Pseudomonas aeruginosa. *Protein Cell* 6, 26–41. doi: 10.1007/s13238-014-0100-x

Ling, J.-X., Wei, F., Li, N., Li, J.-L., Chen, L.-J., Liu, Y.-Y., et al. (2012). Amelioration of influenza virus-induced reactive oxygen species formation by epigallocatechin gallate derived from green tea. *Acta Pharmacol. Sin.* 33, 1533–1541. doi: 10.1038/aps.2012.80

Liu, W., Lu, H., Chu, X., Lou, T., Zhang, N., Zhang, B., et al. (2020). Tea polyphenols inhibits biofilm formation, attenuates the quorum sensing-controlled virulence and enhances resistance to Klebsiella pneumoniae infection in Caenorhabditis elegans model. *Microb. Pathog.* 147:104266. doi: 10.1016/j.micpath.2020.104266

Livermore, D. M. (2002). Multiple mechanisms of antimicrobial resistance in Pseudomonas aeruginosa: our worst nightmare? *Clin. Infect. Dis.* 34, 634–640. doi: 10.1086/338782

Melsen, W. G., Rovers, M. M., Groenwold, R. H., Bergmans, D. C., Camus, C., Bauer, T. T., et al. (2013). Attributable mortality of ventilator-associated pneumonia: a meta-analysis of individual patient data from randomised prevention studies. *Lancet Infect. Dis.* 13, 665–671. doi: 10.1016/S1473-3099(13)70081-1

Moore, N. M., and Flaws, M. L. (2011). Antimicrobial resistance mechanisms in Pseudomonas aeruginosa. *Clin. Lab. Sci.* 24, 47–51. doi: 10.29074/ascls.24.1.47

Nadal Jimenez, P., Koch, G., Thompson, J. A., Xavier, K. B., Cool, R. H., and Quax, W. J. (2012). The multiple signaling systems regulating virulence in Pseudomonas aeruginosa. *Microbiol. Mol. Biol. Rev.* 76, 46–65. doi: 10.1128/MMBR.05007-11

O'Brien, K. L., Baggett, H. C., Brooks, W. A., Feikin, D. R., Hammitt, L. L., Higdon, M. M., et al. (2019). Causes of severe pneumonia requiring hospital admission in children without HIV infection from Africa and Asia: the PERCH multi-country case-control study. *Lancet* 394, 757–779. doi: 10.1016/S0140-6736(19)30721-4

O'Neill, J. (2016). Tackling drug-resistant infections globally: final report and recommendations.

Pylaeva, E., Bordbari, S., Spyra, I., Decker, A. S., Häussler, S., Vybornov, V., et al. (2019). Detrimental effect of type I IFNs During acute lung infection With Pseudomonas aeruginosa is mediated Through the stimulation of neutrophil NETosis. *Front. Immun.* 10:2190, 2190. doi: 10.3389/fimmu.2019.02190

Quinton, L. J., and Mizgerd, J. P. (2015). Dynamics of lung defense in pneumonia: resistance, resilience, and remodeling. *Annu. Rev. Physiol.* 77, 407–430. doi: 10.1146/annurev-physiol-021014-071937

Ravi Kumar, S., Paudel, S., Ghimire, L., Bergeron, S., Cai, S., Zemans, R. L., et al. (2018). Emerging roles of inflammasomes in acute pneumonia. *Am. J. Respir. Crit. Care Med.* 197, 160–171. doi: 10.1164/rccm.201707-1391PP

Sadikot, R. T., Blackwell, T. S., Christman, J. W., and Prince, A. S. (2005). Pathogen–host interactions in Pseudomonas aeruginosa pneumonia. *Am. J. Respir. Crit. Care Med.* 171, 1209–1223. doi: 10.1164/rccm.200408-1044SO

Saeki, E. K., Kobayashi, R. K. T., and Nakazato, G. (2020). Quorum sensing system: target to control the spread of bacterial infections. *Microb. Pathog.* 142:104068. doi: 10.1016/j.micpath.2020.104068

Sauer, K., Camper, A. K., Ehrlich, G. D., Costerton, J. W., and Davies, D. G. (2002). Pseudomonas aeruginosa displays Multiple phenotypes during development as a biofilm. *SAM J.* 184, 1140–1154. doi: 10.1128/jb.184.4.1140-1154.2002

Sen-Kilic, E., Blackwood, C. B., Boehm, D. T., Witt, W. T., Malkowski, A. C., Bevere, J. R., et al. (2019). Intranasal peptide-based FpvA-KLH conjugate vaccine protects mice from Pseudomonas aeruginosa acute murine pneumonia. *Front. Immunol.* 10:2497. doi: 10.3389/fimmu.2019.02497

Shapouri-Moghaddam, A., Mohammadian, S., Vazini, H., Taghadosi, M., Esmaeili, S. A., Mardani, F., et al. (2018). Macrophage plasticity, polarization, and function in health and disease. *J. Cell. Physiol.* 233, 6425–6440. doi: 10.1002/jcp.26429

Sharma, A., Vaghasiya, K., Ray, E., Gupta, P., Gupta, U. D., Singh, A. K., et al. (2020). Targeted pulmonary delivery of the green tea polyphenol Epigallocatechin Gallate controls the growth of mycobacterium tuberculosis by enhancing the autophagy and suppressing bacterial burden. *ACS Biomater Sci. Eng.* 6, 4126–4140. doi: 10.1021/acsbiomaterials.0c00823

Skariyachan, S., Sridhar, V. S., Packirisamy, S., Kumargowda, S. T., and Challapilli, S. B. (2018). Recent perspectives on the molecular basis of biofilm formation by Pseudomonas aeruginosa and approaches for treatment and biofilm dispersal. *Folia Microbiol.* 63, 413–432. doi: 10.1007/s12223-018-0585-4

Sriram, N., Kalayarasan, S., and Sudhandiran, G. (2009). Epigallocatechin-3-gallate exhibits anti-fibrotic effect by attenuating bleomycin-induced glycoconjugates, lysosomal hydrolases and ultrastructural changes in rat model pulmonary fibrosis. *Chem. Biol. Interact.* 180, 271–280. doi: 10.1016/j.cbi.2009.02.017

Steinmann, J., Buer, J., Pietschmann, T., and Steinmann, E. (2013). Anti-infective properties of epigallocatechin-3-gallate (EGCG), a component of green tea. *Br. J. Pharmacol.* 168, 1059–1073. doi: 10.1111/bph.12009

Traber, K. E., Dimbo, E. L., Symer, E. M., Korkmaz, F. T., Jones, M. R., Mizgerd, J. P., et al. (2019). Roles of interleukin-11 during acute bacterial pneumonia. *PLoS One* 14:e0221029. doi: 10.1371/journal.pone.0221029

Wang, J., Fan, S. M., and Zhang, J. (2019). Epigallocatechin-3-gallate ameliorates lipopolysaccharide-induced acute lung injury by suppression of TLR4/NF-κB signaling activation. *Braz. J. Med. Biol. Res.* 52:e8092. doi: 10.1590/1414-431x20198092

Yang, D., Hao, S., Zhao, L., Shi, F., Ye, G., Zou, Y., et al. (2021). Paeonol attenuates quorum-sensing regulated virulence and biofilm formation in Pseudomonas aeruginosa. *Front. microbiol.* 12:692474. doi: 10.3389/fmicb.2021.692474

Zhao, Z., Meiyan, F., Juan, W., Zheng, X., Teng, C., Xinya, X., et al. (2021). Research Progress of Epigallocatechin-3-gallate (EGCG) on anti-pathogenic microbes and immune regulation. *Food Funct.* 12, 9607–9619. doi: 10.1039/D1FO01352A

**Conflict of Interest:** The authors declare that the research was conducted in the absence of any commercial or financial relationships that could be construed as a potential conflict of interest.

**Publisher's Note:** All claims expressed in this article are solely those of the authors and do not necessarily represent those of their affiliated organizations, or those of the publisher, the editors and the reviewers. Any product that may be evaluated in this article, or claim that may be made by its manufacturer, is not guaranteed or endorsed by the publisher.

frontiers | Frontiers in Microbiology

ORIGINAL RESEARCH
published: 26 April 2022
doi: 10.3389/fmicb.2022.856272

# Antifungal Activity of Sodium New Houttuyfonate Against *Aspergillus fumigatus in vitro* and *in vivo*

*Qian Zhang[1†], Fangyan Liu[1†], Meng Zeng[1], Jinping Zhang[1], Yanfei Liu[2], Caiyan Xin[1], Yingyu Mao[1*] and Zhangyong Song[1,3*]*

[1] School of Basic Medical Science, Southwest Medical University, Luzhou, China, [2] Department of Clinical Laboratory, The Affiliated Hospital of Qingdao University, Qingdao, China, [3] Molecular Biotechnology Platform, Public Center of Experimental Technology, Southwest Medical University, Luzhou, China

*Aspergillus fumigatus* is an important pathogen causing invasive aspergillosis, which is associated with high morbidity and mortality in immunocompromised people. However, the treatment of *A. fumigatus* infection is a growing challenge, owing to the limited availability antifungal agents and the continual emergence of drug-resistant strains. Drug repurposing is a potential strategy to solve this current problem. Sodium new houttuyfonate (SNH), derived from houttuynin, extracted from *Houttuynia cordata*, has anti-bacterial and anti-*Candida albicans* effects. However, whether it has anti-*A. fumigatus* activity had not been reported. In this study, the antifungal properties of SNH against *A. fumigatus*, including the standard strain AF293, itraconazole resistant clinical strains, and voriconazole resistant clinical strains, were evaluated *in vitro* and *in vivo*. Moreover, the potential mechanism of SNH was characterized. SNH exhibited significant fungicidal activity toward various *A. fumigatus* strains. SNH also inhibited fungal growth, sporulation, conidial germination and pigment formation, and biofilm formation. Further investigations revealed that SNH interfered with the *A. fumigatus* cell steroid synthesis pathway, as indicated by transcriptomic and quantitative real-time polymerase chain reaction analyses, and inhibited ergosterol synthesis, as indicated by cell membrane stress assays and ergosterol quantification. Moreover, daily gastric gavage of SNH significantly decreased the fungal burden in mice with disseminated infection (kidney, liver, and lung) and local tissue damage. In addition, the application of SNH downregulated the production of IL-6 and IL-17A. Together, these findings provided the first confirmation that SNH may be a promising antifungal agent for the treatment of *A. fumigatus* infection.

**Keywords: sodium new houttuyfonate, *Aspergillus fumigatus*, ergosterol synthesis, antifungal agent, invasive aspergillosis**

OPEN ACCESS

***Edited by:***
*Giovanni Lentini, University of Bari Aldo Moro, Italy*

***Reviewed by:***
*Daqiang Wu, Anhui University of Chinese Medicine, China*
*László Majoros, University of Debrecen, Hungary*

***Correspondence:**
*Yingyu Mao*
*tianya1000@126.com*
*Zhangyong Song*
*szy83529@163.com*

*† These authors have contributed equally to this work*

***Specialty section:***
*This article was submitted to Antimicrobials, Resistance and Chemotherapy, a section of the journal Frontiers in Microbiology*

***Received:*** *17 January 2022*
***Accepted:*** *14 March 2022*
***Published:*** *26 April 2022*

***Citation:***
*Zhang Q, Liu F, Zeng M, Zhang J, Liu Y, Xin C, Mao Y and Song Z (2022) Antifungal Activity of Sodium New Houttuyfonate Against Aspergillus fumigatus in vitro and in vivo. Front. Microbiol. 13:856272. doi: 10.3389/fmicb.2022.856272*

## INTRODUCTION

*Aspergillus fumigatus* is an opportunistic pathogen causing life-threatening infection in immunocompromised individuals (Gülmez et al., 2021). These infections can lead to a variety of pulmonary fungal diseases including allergic bronchopulmonary aspergillosis, chronic pulmonary aspergillosis, and invasive pulmonary aspergillosis (IPA; Pasula and Chandrasekar, 2021).

Among them, IPA is the most common invasive disease. The infectivity rate of IPA in hematopoietic stem cell transplantation is 43%, and that in solid-organ transplant recipients is 59% (Latgé and Chamilos, 2019). Therefore, the treatment of *A. fumigatus* infection is a clinical challenge (Benedict et al., 2019). The current therapy for *A. fumigatus* infection involves triazoles, including isavuconazole, itraconazole (ITR), posaconazole, and voriconazole (VRC; **Supplementary Figure 1**). Although VRC is the drug of choice for the treatment of IPA disease, the death rate in azole-resistant IPA patients varies from 50 to 100% (Meis et al., 2016). Moreover, the resistance of *A. fumigatus* strains to triazole is continually increasing (van der Linden et al., 2015). Therefore, new antifungal agents are urgently needed, particularly for triazole-resistant strains. Although many investigations are being conducted to develop new and effective compounds, the bioactive molecules derived from existing drugs may be promising treatments (Zhang et al., 2021).

Sodium houttuyfonate (SH) and sodium new houttuyfonate (SNH) are modified compounds derived from the plant *Houttuynia cordata* Thunb (**Supplementary Figure 1**; Shao et al., 2012), an herbal drug with antibacterial, antiviral, and antifungal effects that is clinically used in Asia. Many investigations have revealed that SH has various biological and pharmacological activities such as anti-inflammatory activity in the respiratory tract and antibacterial activity against Gram-positive bacteria (Da et al., 2019); and anti-*Candida albicans* activity (Huang et al., 2015; Shao et al., 2017; Da et al., 2019). In addition, a previous investigation has demonstrated that SH and SNH possessed highly similar structures and anti-infective biological activities (Shao et al., 2012). However, SNH has better clinical value and higher chemical stability than SH (Zhao et al., 2020). Investigations have also confirmed that SNH exhibits antibacterial effects against *Staphylococcus aureus* and methicillin-resistant *S. aureus* (Lu et al., 2013; Li et al., 2020), *Streptococcus pneumoniae* (Yang et al., 2016), and *C. albicans* (Wu et al., 2020). Although SNH acts as an anti-inflammatory medicine and has various anti-bacterial and anti-*C. albicans* activities, the anti-fungal effect against *A. fumigatus,* particularly various triazole-resistant strains, has not been reported.

In this study, the effects of SNH against *A. fumigatus* strain conidial germination and pigment formation, fungal growth, sporulation, and biofilm formation were investigated *in vitro*. Furthermore, with transcriptomic and quantitative real-time polymerase chain reaction (qRT-PCR) analyses, stress assays, and the quantification of ergosterol, the mechanism underlying the effects of SNH were investigated. Additionally, we constructed a murine model of invasive aspergillosis (IA) and the antifungal activity of SNH was demonstrated.

# MATERIALS AND METHODS

## Strains, Media, and Chemicals

The *A. fumigatus* standard strain AF293, ITR-resistant clinical isolates (AF1 and AF2), and VRC-resistant clinical strains (AF4 and AF5) were routinely grown on potato dextrose agar (PDA). Before each experiment, the strains used in this study, were cultured on PDA medium for 4 days at 37°C. The drugs, including ITR, VRC, and AmB, were purchased from *Macklin Chemicals* (Shanghai, China). SNH was obtained from *Fengyao Tonghui Chemicals* (Wuhan, China). ITR, VRC, and AmB were dissolved in DMSO to prepare a 5.12 mg/mL stock solution. SNH was dissolved in sterile distilled water with 0.05% Tween 80 to prepare a 5 mg/mL stock solution. All drug stock solutions were stored at –20°C.

## Minimal Inhibitory Concentration and Interactions Between Sodium New Houttuyfonate and Antifungal Agents

The minimal inhibitory concentration (MIC) of ITR, VRC, AmB, and SNH inhibiting growth of *A. fumigatus* were tested according to the reference Clinical and Laboratory Standards Institute M38-A2 document (CLSI, 2008; Espinel-Ingroff et al., 2010). The drug concentrations ranged from 0.06 to 32 μg/mL for both ITR and VRC, from 0.03 to 16 μg/mL for AmB, and from 0.0625 to 2 mg/mL for SNH. The conidia were dispersed in RPMI-1640 medium at a concentration of $0.4 \times 10^4$ to $5 \times 10^4$ cells/mL. The suspensions were then dispensed into triplicate wells of a 96-well microtiter plate. After incubation at 37°C for 48 h, MIC endpoints were defined as the lowest drug concentrations that caused complete visible inhibition of growth, as compared with the drug-free growth control. The criteria for determining the antifungal susceptibility of molds followed the CLSI M38-A2 document (Espinel-Ingroff et al., 2010). Experiments in each strain were performed in triplicate.

Interactions between SNH and antifungal agents (ITR or VRC) against the test strain were assessed with the MIC method as described above. The final drug concentration SNH ranged from 0.01 to 0.13 mg/mL, and those of antifungal agents (ITR or VRC) ranged from 0.03 to 32 μg/mL. The fractional inhibitory concentration index (FICI) was defined according to the M38-A2 document (Odds, 2003).

## Spot Dilution Assays

The sporulation of *A. fumigatus* was evaluated by assessment of the initial growth of a droplet of conidia from a serial dilution at final concentrations of 0 × (negative control), 1 ×, 2 ×, and 4 × MIC at two temperatures (37 and 28°C). Spot dilution experiments were performed with 3 μL of a 10-fold dilution series starting at a concentration of $10^5$ cells/mL spotted on PDA solid medium at the two temperatures for 96 h (37°C) and 120 h (28°C). Samples were collected from approximately the same three locations of colonies with an Oxford cup (Beijing Jitai Yuancheng Technology Co., Ltd., Beijing, China) and counted with a hemacytometer to estimate the average sporulation per square centimeter. Meanwhile, the conidial melanin/pigment, isolated from 4-day-old cultures with 2% NaOH, was purified and measured as described previously (Song et al., 2018).

## Effects on Germination

Fresh conidia were prepared with sterile phosphate buffered saline (PBS) and cultured at 37°C in liquid PDA medium at a concentration of $10^6$ cells/mL with various concentrations of

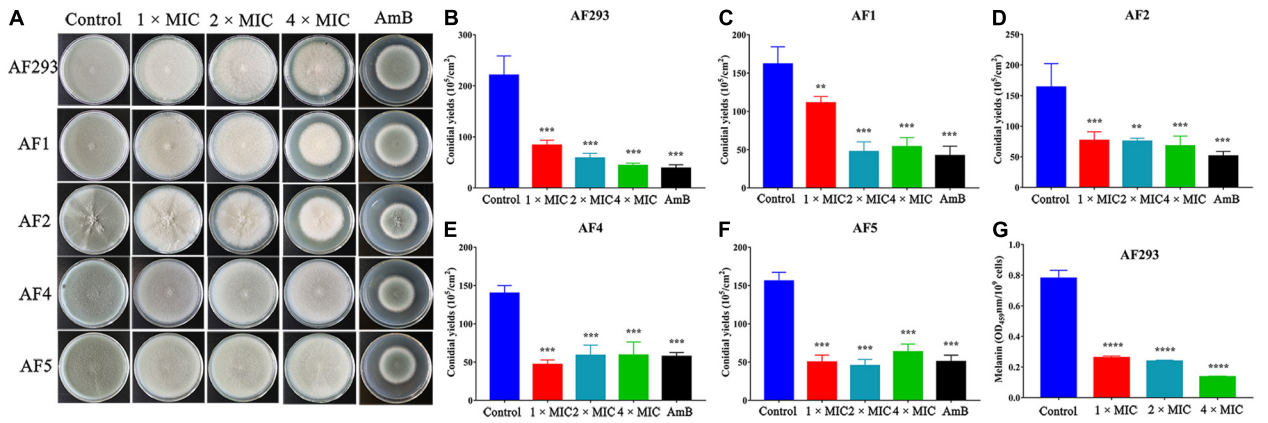


**FIGURE 1 |** Sodium new houttuyfonate (SNH) inhibits the asexual cycle of *A. fumigatus*. **(A)** Images of various concentrations of SNH treatment on PDA plates. The *A. fumigatus* strains AF293, AF1, AF2, AF4, and AF5 were incubated at a concentration of $10^5$ cells/mL. Each dilution of 3 μL was deposited on PDA solid medium with 1 ×, 2 ×, or 4 × MIC SNH; AmB (8 μg/mL, positive control); or no drugs (negative control), then incubated at 37°C for 4 days. **(B–F)** Statistical analysis of *A. fumigatus* conidia yields under SNH treatment. **(G)** Measurement of *A. fumigatus* conidial melanin. Melanin was isolated from AF293 conidia cultured on PDA solid medium with 1 ×, 2 ×, or 4 × MIC SNH. Melanin was purified with 2% NaOH, and the absorbance at 459 nm was measured spectrophotometrically. Results represent the average of three independent experiments ± SD, and the level of statistical significance was set at $^*P < 0.05$. $^{**}P < 0.01$, $^{***}P < 0.001$, and $^{****}P < 0.0001$.

SNH as described above. Then conidia were collected after 12, 16, and 20 h incubation. Germination was defined by a germ tube longer than the conidia diameter (Chen et al., 2020). The number of germinated conidia under a microscope (400 ×).

## Effect on the Metabolic Activity of Biofilm

The metabolic activity of biofilms was monitored with tetrazolium salt 2,3-bis (2-methoxy-4-nitro-5-sulfophenyl)-5-(phenylamino)-carbonyl-2*H*-tetrazoliumhydroxide (XTT; Macklin, Shanghai, China) reduction assay (Bugli et al., 2013; Bom et al., 2015; González-Ramírez et al., 2016). Briefly, for the biofilm formation assays, *A. fumigatus* spore suspension was prepared in RPMI-1640 medium supplement at a concentration of $10^6$ cells/mL with the above-described concentration of SNH, and the 96-well polystyrene plates were incubated at 37°C for 24 h. For the preformed biofilms, 200 μL of conidial suspension ($10^6$ cells/mL) was added into each well of a microtiter plate and incubated at 37°C for 24 h. Next, the plate was washed with PBS three times. Then 200 μL SNH, at the above-described concentrations, prepared in RPMI-1640 medium was added. After incubation at 37°C for 24 h, the plates were incubated with XTT-menadione solution in the dark at 37°C for 2 h. Finally, the absorbance of the supernatant was measured at 492 nm (Pumeesat et al., 2017).

The confocal laser scanning microscopy (CLSM) was performed to observe biofilm developed on the coverslips (Shanghai Baiyan Bio-Technology Co., Ltd, Shanghai, China) in 12-well plates (Shanghai Huipan Industerial Co., Ltd, Shanghai, China). Method was following the previous investigation with slight modifications (Iwahashi et al., 2020). Briefly, the biofilms were washed three times with PBS and stained with calcofluor white stain (Sigma-Aldrich Trading Co., Ltd, Shanghai, China) supplemented with 20 μL 10% KOH at room temperature for 5 min. Fluorescent images were taken and analyzed by CLSM using OLYMPUS cellSens Dimension 3.2 (Olympus Co., Ltd, Tokyo, Japan).

## Time-Kill Assays

To investigate the effects of concentration and exposure time on the activity of SNH, we performed time-kill experiments and the methodology referred to previous studies with slight modifications (Bugli et al., 2013). All strains were grown in RPMI-1640 medium with a starting inoculum of $10^6$ cells/mL. The SNH working concentrations were 1 ×, 2 ×, 4 ×, and 8 × MIC. Samples were incubated at 37°C without agitation. At predetermined time points (0, 4, 8, 12, 16, 20, and 24 h) after incubation, the samples were transferred to 96-well plates, and their metabolic activity was determined with XTT reduction assays. The method to detect the metabolic activity was as described above.

## Propidium Iodide Staining

After treatment with SNH, propidium iodide (PI) staining assays were used to investigate the *A. fumigatus* cell membrane integrity (Chen et al., 2020). The inoculum of the AF293 strain was treated with the above-described concentrations of SNH and incubated at 37°C for 12 h. Then the samples were washed with PBS three times. PI (Solarbio, Beijing, China) was incubated with *A. fumigatus* at a concentration of 20 μg/mL for 30 min in the dark. The specimens were observed under a fluorescence microscope (Leica, Germany). Results represent three independent experiments.

## Transcriptomic and qRT-PCR Analysis

Conidia of the AF293 strain were cultured in RPMI-1640 medium with or without SNH (2 × MIC) for 12 h at 37°C.

Then samples were collected, treated with liquid nitrogen, and stored at −80°C for collection of total RNA. Total RNA was prepared with RNAiso plus reagent (TaKaRa, Dalian, China) and reverse-transcribed into cDNA with a PrimeScript$^{TM}$ RT reagent kit with gDNA Eraser (TaKaRa). Illumina RNA sequencing was then conducted by Biomarker Technologies (Qingdao, China). To determine time-specific expression patterns of genes in the ergosterol synthesis pathway, we treated the AF293 conidia prepared in RPMI-1640 medium with 2 × MIC SNH and then incubated them at 37°C for 0, 6, and 12 h for RNA extraction. RT-qPCR was performed with a PrimeScript RT reagent kit with gDNA Eraser (TaKaRa, Dalian, China). Transcripts of the β-tubulin gene were used as an internal control. Transcript ratios were evaluated with the $2^{-\Delta\ \Delta\ CT}$ method (Vandesompele et al., 2002). The primer sequences are listed in **Supplementary Table 1**.

## Cell Membrane Stress Assays

Conidia of *A. fumigatus* AF293 were prepared in RPMI-1640 medium at a concentration of $10^6$ cells/mL with final concentrations of 0, 1/2 ×, and 1 × MIC SNH. Samples were incubated at 37°C for 12 h. Then a 3 μL aliquot containing $10^5$ cells/mL was inoculated onto PDA medium containing 0, 1, 2, or 4 μg/mL AmB. After inoculation at 37°C for 4 days, colony morphology was investigated with a digital camera (60-mm Macro lens, Canon Inc., Japan).

## Quantification of Ergosterol

To quantify the concentration of ergosterol, we incubated AF293 conidia in RPMI-1640 medium with different concentrations of SNH (1 ×, 2 ×, and 4 × MIC) at 37°C for 3 days. The mycelia were harvested and washed with PBS twice, as described previously (Pinto et al., 2011). Then 0.500 g samples were dispersed in 100% methanol for ultrasound-assisted extraction. The content of ergosterol was determined by high-performance liquid chromatography (HPLC; 1260 infinity II, Agilent). Ergosterol standard (Macklin, Shanghai, China) was dissolved with 100% methanol to a concentration of 100 μg/mL and used as a reference solution. The concentration of ergosterol was calculated with the following equations: (peak area of experimental group × concentration of ergosterol standard group)/peak area of ergosterol standard product. Experiments for each strain were performed in triplicate.

## Antifungal Activity *in vivo*

Male 6–8-week-old Balb/c mice (Chongqing Tengxin Biotechnology Co., Ltd., Chongqing, China) with a weight of 20–25 g was given food and water *ad libitum*. Mice were immunosuppressed by injection of cyclophosphamide at 200 mg/kg intravenously for 3 days (Denning et al., 1995, 1997). Then the mice were infected by injection of a 100 μL inoculum of *A. fumigatus* AF293 into the tail vein at a final concentration of $10^7$ cells/mL. After the successful establishment of an IA mouse model, treatment was started 2 h after inoculation and was continued for 7 days by gastric gavage with SNH at 10 mg/kg/d and 30 mg/kg/d. The same volume of normal saline and ITR with a concentration of 75 mg/kg/d were used in the control group.

Fungal burden and histopathology were used to evaluate the efficacy of SNH against IA. The liver, kidney, lung, and serum were collected after the mice were treated for 1, 4, and 7 days. One half of the collected liver, kidney, and lung samples was used to prepared dilutions of the homogenates and plated on PDA. The number of colony formation units per gram of tissue was determined after at least 48 h of incubation at 37°C. The other tissues were fixed in 10% methanol and embedded in paraffin. Thin sections were cut and stained with periodic acid-Schiff stain (PAS) for microscopic observations.

Cytokines were detected with a BD Cytometric Bead Array Mouse Inflammation Kit (Univ, Shanghai, China) in serum treated for 1 and 4 days. IL-6, IL-17A, IFN-γ, and TNF-α were detected according to the manufacturer's protocol. Then samples were measured on a BD FACSCalibur Flow Cytometer and analyzed in FCAP Array Software Version 3.0 (BD Bioscience).

## Statistical Analysis

Each experiment was performed three independent times. Graphing and statistical analyses were performed in GraphPad Prism, version 7.0 (GraphPad Software Inc., La Jolla, CA, United States) with Student's *t*-test. Cytokine data were compared with unpaired two-tailed Mann-Whitney (non-parametric) tests. Results represent the average of three independent experiments ± standard deviation (SD), and the level of statistical significance was set at $^*P < 0.05$.

# RESULTS

## Sodium New Houttuyfonate Has Antifungal Activity Against *A. fumigatus*

To evaluate the antifungal potential of SNH against *A. fumigatus*, we tested the MIC. The MIC of SNH against the AF293, AF1, and AF2 strains was 100 μg/mL, whereas that against AF4 and AF5 strains was 50 μg/mL. For AmB, the MIC for the AF293, AF1, and AF2 strains was 4 μg/mL, and was 0.5–1 μg/mL for AF4 and AF5. However, the FICI indicated that the combination ITR or VRC with SNH produced no synergistic effects against ITR- or VRC-resistant strains (data not shown). Furthermore, 1 ×, 2 ×, and 4 × MIC SNH against *A. fumigatus* was used to assess sporulation at 37 and 28°C. As shown in **Figure 1** and **Supplementary Figure 2**, strains treated with SNH showed a significant decrease in conidial yield to 40–50% that in the untreated group ($P < 0.05$). Additionally, the *A. fumigatus* had a whitish color in the SNH treatment group. Further investigations confirmed that the conidia of SNH-treated strains accumulated less melanin than those of the control group (**Figure 1G**).

The anti-biofilm activity of SNH was evaluated with XTT reduction analysis. The metabolic activity of biofilm was significantly decreased by treatment with even low concentrations of SNH (**Figure 2A**; $P < 0.05$). In the mature biofilms pretreated with 1 × MIC, XTT reduction assays demonstrated that the inhibition rate was approximately 20%. However, compared with the control treatment, 4 × MIC treatment resulted in an 80% lower inhibition rate (**Figure 2B**). Next, the fluorescent filamentous biomass of biofilms was

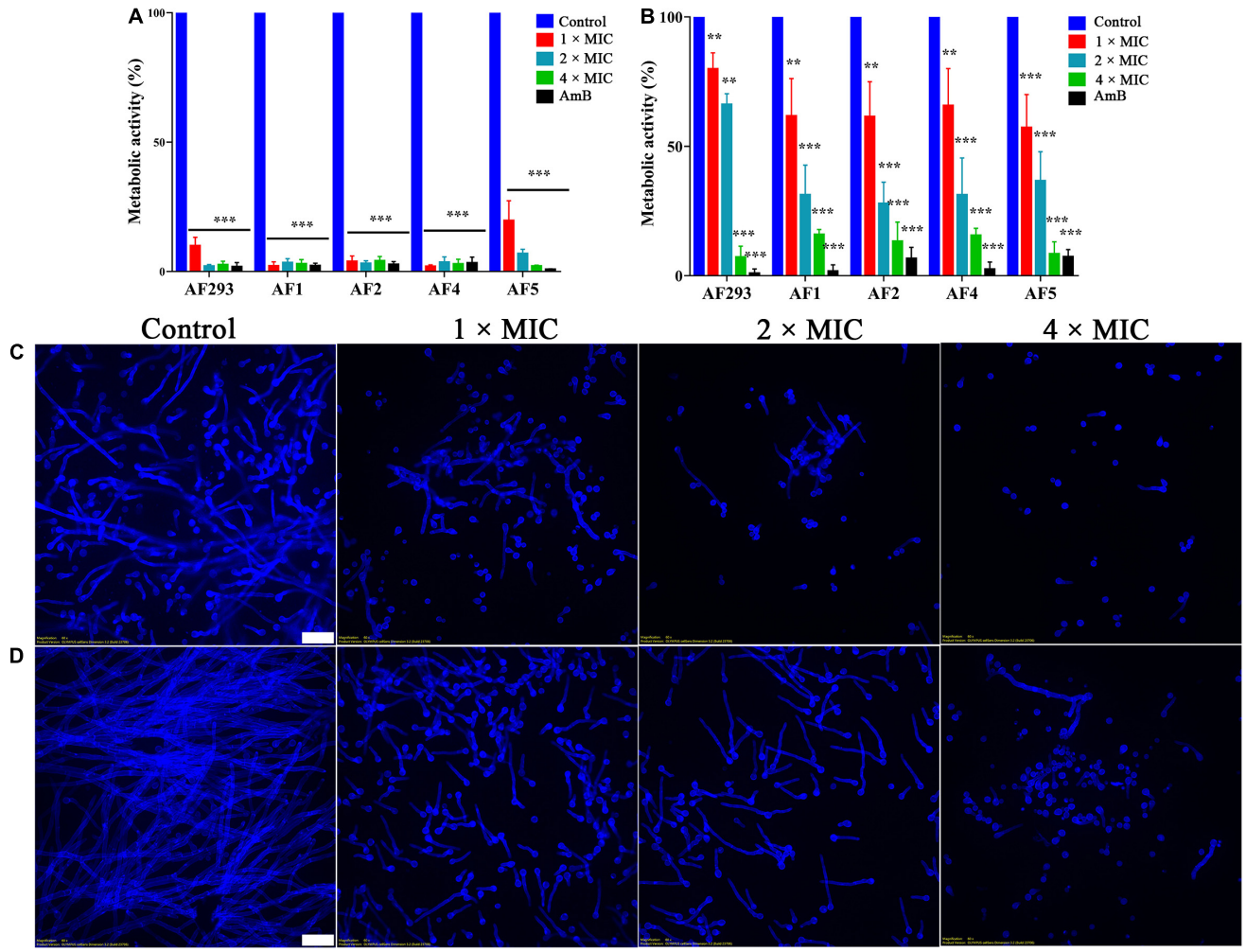


**FIGURE 2 |** Effect of sodium new houttuyfonate (SNH) on biofilm. Readings of colorimetric XTT reduction assays at 492 nm are expressed as the percentage metabolic activity of the control. **(A)** Effect of SNH on the biofilm formation of the AF293, AF1, AF2, AF4, and AF5 strains. **(B)** Effect of SNH on preformed biofilms of the AF293, AF1, AF2, AF4, and AF5 strains. Results represent the average of three independent experiments ± SD, and the level of statistical significance was set at $^{*}P < 0.05$, $^{**}P < 0.01$, and $^{***}P < 0.001$. CLSM observation of the AF293 strain in **(C)** biofilm formation and **(D)** the preformed biofilm treated with 1 ×, 2 ×, and 4 × MIC SNH, respectively. Biofilms were stained with 1mL calcofluor white stain supplemented with 20 μL 10% KOH. Scale bar = 20 μm.

examined by the CLSM. Compared with control group, as shown in **Figures 2C,D**, *A. fumigatus* mycelium length was shortened and the mature biofilm was thinner after SNH treatment. Hyphal growth, the basis of biofilm formation, was modest at 1 × and 2 × MIC; however, hyphal growth was absent at 4 × MIC (**Figure 3**). These results correlated with the results of the XXT reduction assays.

Time-kill assays were used to investigate the kinetics of SNH against *A. fumigatus* (**Figures 4A–E**). Similar to amphotericin B (AmB), SNH exhibited fungistatic activity against all tested *A. fumigatus* strains at a concentration of 0.4 mg/mL. Further investigations were evaluated with PI staining. Statistical analysis indicated that the percentage of PI-stained cells rose to 42.37, 66.23, and 79.72% after treatment with SNH at concentrations of 0.1, 0.2, and 0.4 mg/mL, respectively (**Figure 4F**). In particular, the percentage of PI-stained cells treated with the 4 × MIC approached that in the AmB treatment group. These results revealed that SNH exhibited fungicidal activity against *A. fumigatus*.

## Sodium New Houttuyfonate Inhibits Ergosterol Synthesis Affecting Cell Membrane Integrity

After verifying SNH's potent antifungal activity, we proceeded to investigate the antifungal mechanism of SNH. Transcriptomic changes in *A. fumigatus* treated with SNH were analyzed with Illumina sequencing, and 2.83 Gb clean data were obtained from each sample, with differential expression of 175 annotated genes. Raw sequence data have been deposited in the Beijing Institute of Genomics Genome Sequence Archive (accession number PRJCA007831). Genes with fold change ≥ 2 and false discovery

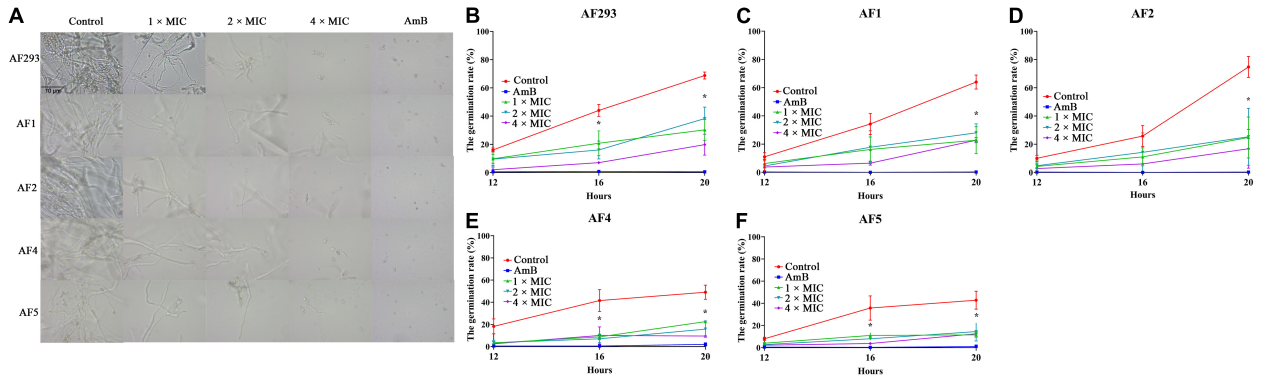


**FIGURE 3 |** Effect of sodium new houttuyfonate (SNH) on conidial generation. **(A)** Generation of *A. fumigatus* treated with SNH. **(B–F)** *A. fumigatus* germination number counted after 1 ×, 2 ×, or 4 × MIC SNH treatment at 37°C for 12, 16, and 20 h. Testing of each group was performed in triplicate, and the level of statistical significance was set at $^{*}P < 0.05$. The number of *A. fumigatus* germinations was counted under a microscope (400 ×).

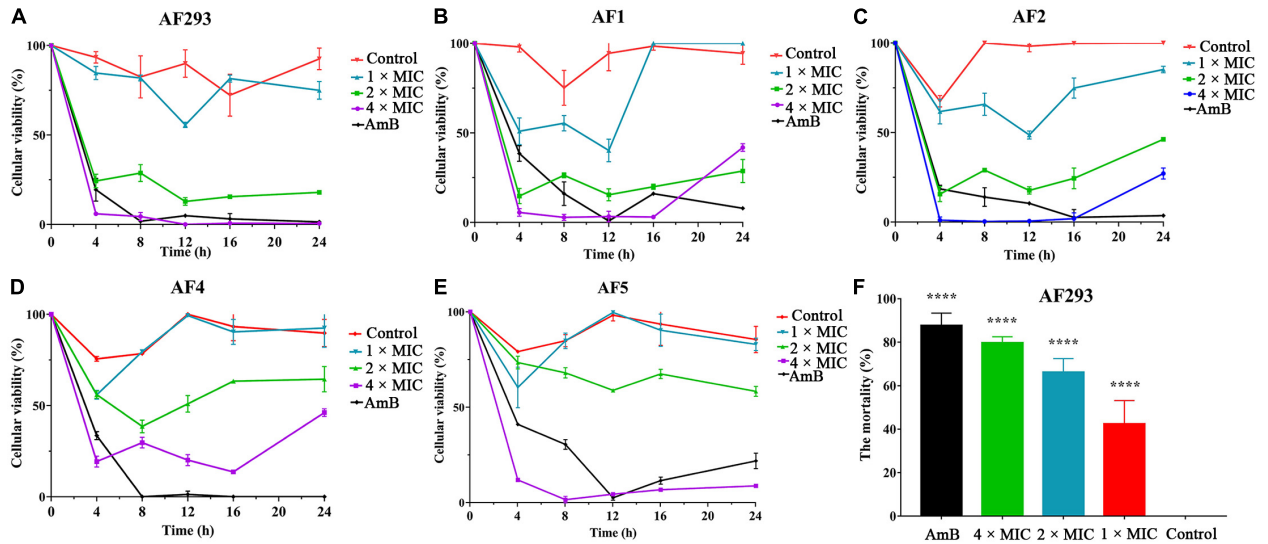


**FIGURE 4 |** Sodium new houttuyfonate (SNH) has fungicidal activity against *A. fumigatus*. **(A–E)** Time-kill curves of 1 ×, 2 ×, 4 ×, and 8 × MIC SNH against *A. fumigatus* AF293, AF1, AF2, AF4, and AF5 strains. Readings of colorimetric XTT reduction assays at 492 nm are expressed as the percentage cellular viability of the control. **(F)** The mortality of AF293 was analyzed with PI staining after treatment with SNH at 1 ×, 2 ×, and 4 × MIC. AF293 treated with 8 μg/mL AmB and no drugs were used as the control groups. Results represent the average of three independent experiments ± SD, and the level of statistical significance was set at $^{*}P < 0.05$, $^{****}P < 0.0001$.

rate (FDR) < 0.01 were considered significantly differentially expressed. The results showed that 66 genes were up-regulated and 109 genes were down-regulated (**Supplementary Figure 3A**). These differentially expressed genes (DEGs) were functionally grouped into gene ontology classes including 39 functional categories (**Supplementary Figure 3B**) and 16 clusters of orthologous groups (**Supplementary Figure 3C**). The DEGs were also assigned to 50 Kyoto Encyclopedia of Genes and Genomes (KEGG) pathways. The main KEGG enrichment pathway was the steroid biosynthesis pathway (**Figure 5A**).

To verify the transcriptomic results described above, we investigated genes associated with the ergosterol biosynthetic gene pathway through qRT-PCR analysis. In accordance with the transcriptomic data, the expression of 14 genes, including *Erg2* (C-8 sterol isomerase, putative), *Erg3* (Sterol desaturase), *Erg4* [C-24(28) sterol reductase], *Erg5* (Cytochrome P450 sterol C-22 desaturase, putative), *Erg6* (Sterol 24-c-methyltransferase, putative), *Erg7* (Oxidosqualene: lanosterol cyclase), *Erg26* (C-3 sterol dehydrogenase/C-4 decarboxylase), and *Erg27* (3-ketosteroid reductase), were down-regulated after SNH treatment. Furthermore, four other genes, *Erg1* (Squalene monooxygenase), *Erg24* (C-14 sterol reductase), *Erg25* (C-4 methyl sterol oxidase), and *Cyp51A* (14-alpha sterol demethylase), were up-regulated (**Figure 5B**). These data suggested that the antifungal activity of SNH against *A. fumigatus* involved interference with the steroid synthesis pathway. We

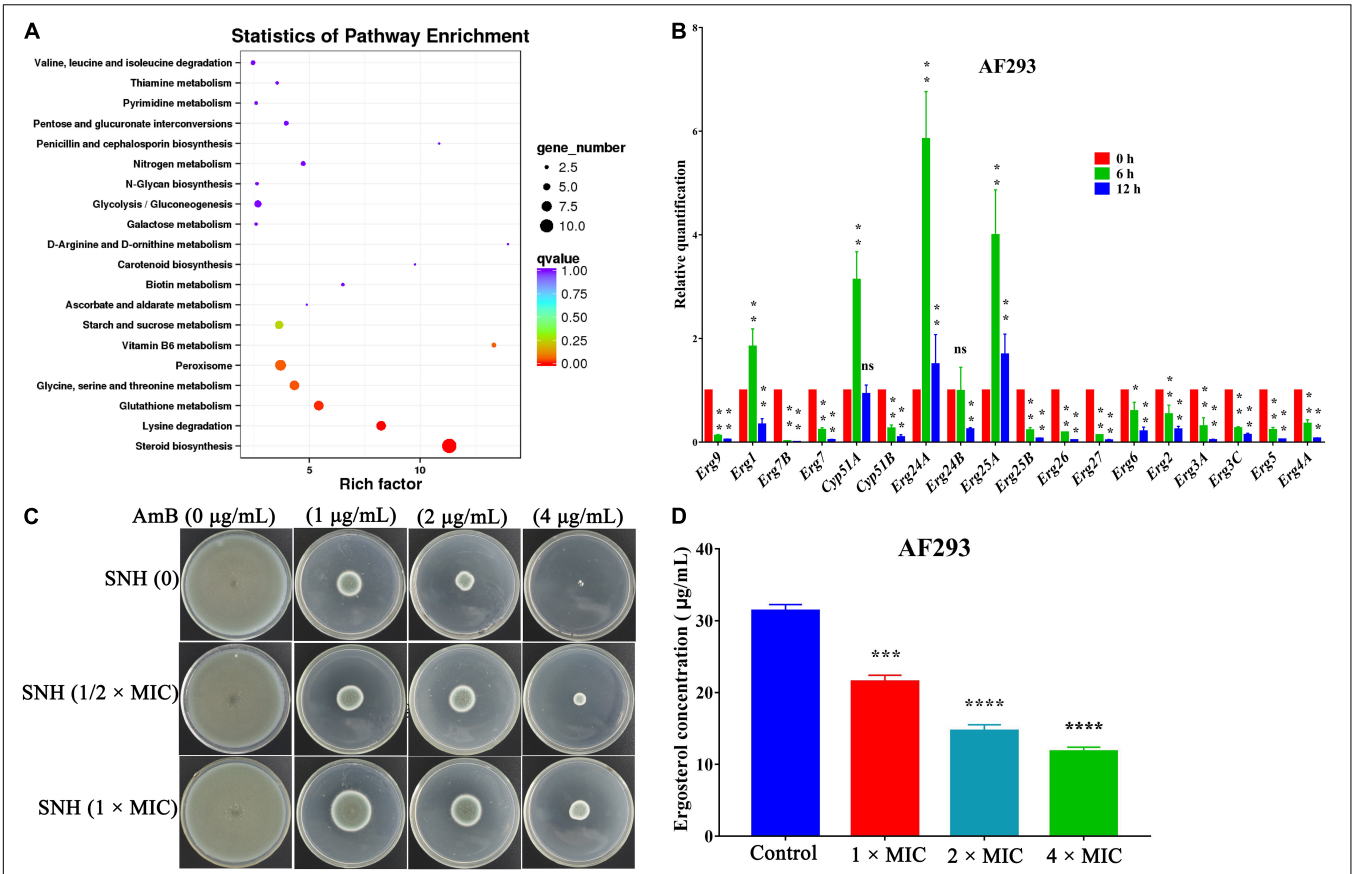


**FIGURE 5 |** Antifungal mechanism of sodium new houttuyfonate (SNH). **(A)** Scatter plot of KEGG pathway enrichment statistics for the top 20 enriched pathways. The enrichment factor is the ratio of the number of genes that were differentially expressed to the total number of genes in a certain pathway. The color and size of the dots represent the range of the q-value and the number of DEGs mapped to the indicated pathways, respectively. **(B)** qRT-PCR analysis of gene expression levels. AF293 was incubated in the absence (control) or presence (2 × MIC) of SNH in RPMI-1640 medium at 37°C for 6 and 12 h. The histogram shows the relative expression of genes after SNH treatment with respect to the control. **(C)** *A. fumigatus* treated with SNH showed significantly diminished sensitivity to the AmB drug. AF293 conidia were treated with 0, 1/2 ×, and 1 × MIC SNH for 12 h at 37°C, then inoculated on PDA solid medium supplemented with AmB (0, 1, 2, and 4 μg/mL). **(D)** Quantification of ergosterol content. AF293 conidia were grown for 3 days in RPMI-1640 medium containing 0, 1 ×, 2 ×, and 4 × MIC SNH; ergosterol was extracted with 100% methanol; and spectral profiles were determined at 280 nm. Results represent the average of three independent experiments ± SD. The level of statistical significance was set at $^{*}P < 0.05$. $^{**}P < 0.01$, $^{***}P < 0.001$, and $^{****}P < 0.0001$; ns indicates no statistical difference.

further verified the antifungal mechanism on ergosterol biosynthesis by performing cell membrane stress assays. The strain treated with SNH showed significantly diminished sensitivity to AmB (**Figure 5C**). HPLC results (**Figure 5D**) were determined after treatment with SNH by 1 ×, 2 ×, and 4 × MIC, and the concentration of ergosterol decreased by 31.31, 53.25, and 62.42%, respectively. In summary, these data indicated that SNH inhibited the growth of *A. fumigatus* by inhibiting ergosterol synthesis.

## Sodium New Houttuyfonate Has Therapeutic Effects on Murine Invasive Aspergillosis

The IA murine model was used to assess the *in vivo* efficacy of antifungal activity. Compared with treatment with normal saline, treatment with SNH at doses of 10 mg/kg/day and 30 mg/kg/day significantly decreased the fungal burden in the liver, kidney, and lung ($P < 0.05$), and had effects equal to those of ITR from day 4 to day 7 (**Figures 6A,C**). Histopathology investigations using PAS-staining were consistent with the fungal burden results. Moreover, sections of PAS-stained kidney and lung were analyzed microscopically for abnormalities. The results revealed that the SNH or ITR treatment groups, compared with the treatment with normal saline, resulted in significantly fewer inflammatory cell infiltrates (**Figure 6D**), thus suggesting that repeated treatment with SNH was efficacious in IA mice.

To determine the effect of SNH on murine cellular immunity, we analyzed the serum of sacrificed mice 1 and 4 days after *A. fumigatus* challenge and drug treatment. Overall, the levels of IL-6 and IL-17A in mice with a treatment dose of SNH of 10 mg/kg/day or 30 mg/kg/day decreased (**Figures 6E,F**). On day 1, compared with the levels in untreated IA mice, the level of the pro-inflammatory cytokine IL-6 after treatment with SNH at a dose of 10 mg/kg/day was 3.26-fold lower, and that of IL-17A was

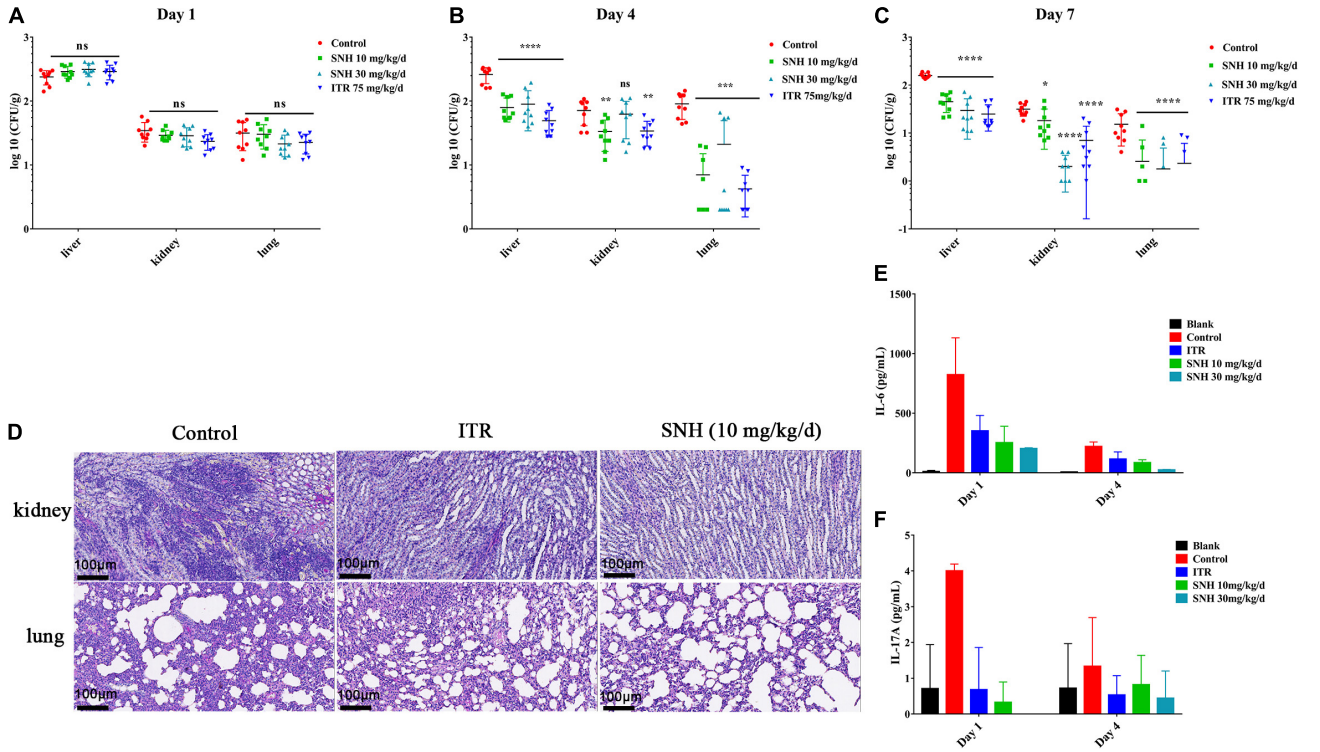


**FIGURE 6 |** Therapeutic effect of sodium new houttuyfonate (SNH) on invasive aspergillosis (IA) in mice. **(A–C)** Fungal burden of the lung, kidney, and liver. The IA model mice were treated by gastric gavage with SNH at 10 mg/kg/d and 30 mg/kg/d, and the fungal burden was measured at 1–, 4–, and 7-days posttreatment. **(D)** Histological analysis of mice with IA. PAS-stained sections were prepared from the kidneys and lungs of mice 7 days after treatment with SNH at 10 mg/kg/d. Scale bar is 100 μm. **(E,F)** Determination of cytokines. Levels of IL-6 and IL-17A in various groups of mice serum on days 1 and 4 after treatment with SNH are shown. Each cytokine assay was performed three times, and the values represent average ± SD of three data points. Normal saline and ITR-treated IA mice were used in the control group, respectively. The statistical significance level was set at $^{*}P < 0.05$. $^{**}P < 0.01$, $^{***}P < 0.001$, and $^{****}P < 0.0001$; ns indicates no statistical significance compared with untreated mice with IA.

8-fold lower. After completion of 1 day of therapy in the SNH 30 mg/kg/day group, the level of IL-6 was decreased by 4.53-fold, and the level of IL-17A was undetectable. In addition, the levels of IFN-γ, and TNF-α were unchanged with respect to those in the sham control (**Supplementary Figures 4B,C**).

## DISCUSSION

With fungal infections dramatically increasing worldwide, treatment efficacy is dependent on antifungal drugs. Unfortunately, the current antifungal agents are unsatisfactory. Drug repurposing is a promising technique to develop antifungal treatments, which has identified several non-antifungal agents with antifungal activity, such as antibacterial drugs, immunosuppressants, and statins (Kim et al., 2020; Zhang et al., 2021). SNH, initially used the treatment of respiratory infections, was also found to have anti-fungal activity against *C. albicans* (Shao et al., 2017; Wu et al., 2020). The current study demonstrated that SNH had fungistatic activity against *A. fumigatus* by inhibiting the synthesis of ergosterol. In addition, SNH exhibited potent *in vivo* antifungal activity against *A. fumigatus* infection.

Conidia are an important virulence factor of *A. fumigatus*. As many as 1,000 *A. fumigatus* conidia from the environment are inhaled into the alveoli daily (van de Veerdonk et al., 2017). The conidia can be cleared in healthy people. However, conidia can colonize the lungs of immunocompromised people and then germinate, thus causing invasive infections. Therefore, the suppression of conidia production and germination is essential to prevent *A. fumigatus* prophase infection. In our study, the conidiation and spore-to-hyphae morphological transition of *A. fumigatus* were significantly inhibited by treatment with even 1 × MIC of SNH in the spot dilution assays and in conidial germination assays (**Figures 1** and **3**). Moreover, lighter pigmentation levels and a whitish color of conidia were observed in the SNH treated group (**Figure 1G**). *A. fumigatus* conidia produce a bluish-green pigment in the cell wall to protect the fungus against the host immune defenses by shielding the fungal pathogen-associated molecular patterns or restricting the activation of reactive oxygen intermediates (Youngchim et al., 2004; Pihet et al., 2009; Schmaler-Ripcke et al., 2009; Chai et al., 2010). Notably, the albino conidia have been found to stimulate much stronger host defense mechanisms, such as increased levels of proinflammatory cytokines, such as TNF-α, IL-6, and IFN-γ (Chai et al., 2010). Furthermore, the ability to form biofilms is

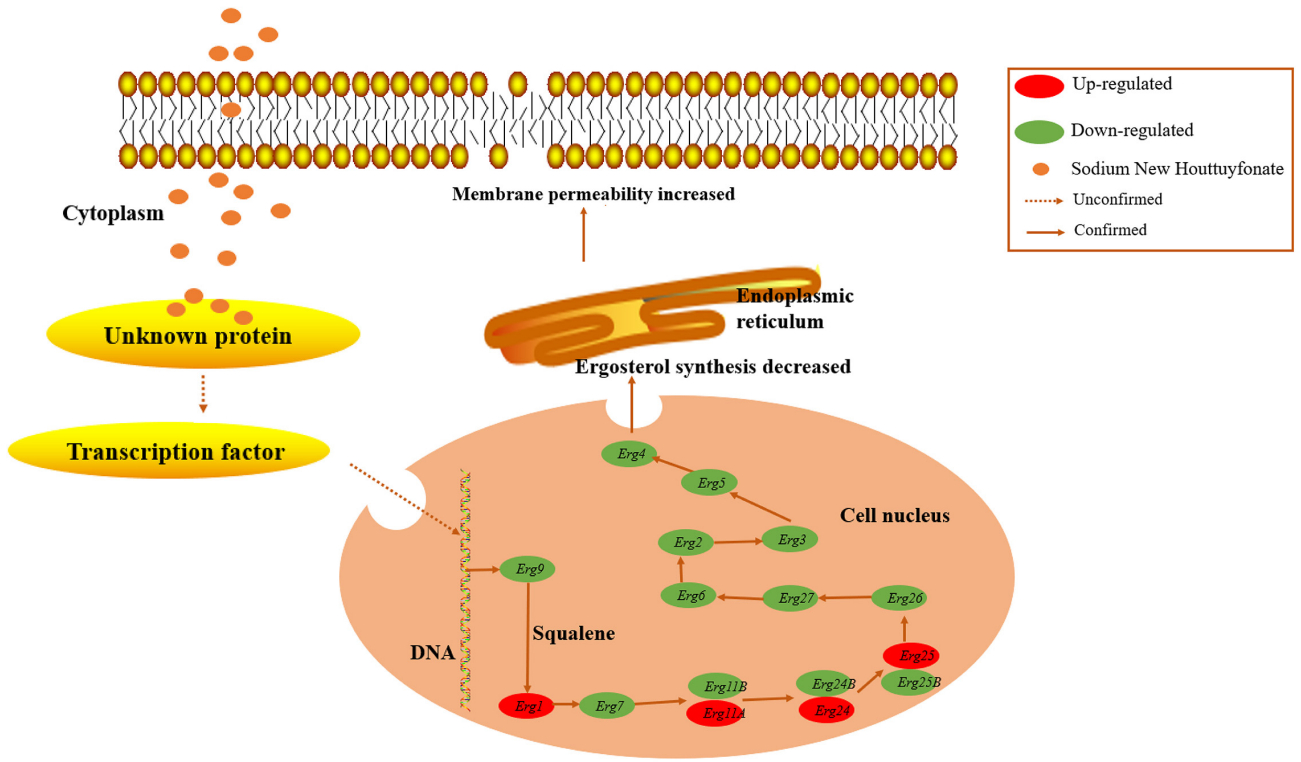


**FIGURE 7 |** Model of the anti-*A. fumigatus* mechanism. Sodium new houttuyfonate (SNH) may activate an unknown protein or transcription factor, which translocates to the nucleus and inhibits ergosterol synthesis in the endoplasmic reticulum via suppressing the expression of related genes in *A. fumigatus*. The cell membrane permeability is elevated, thus contributing to cell growth inhibition or death. Dotted arrows indicate unknown pathways, and solid arrows indicate verified pathways.

a unique aspect of fungal biology exploited by antifungal drugs. As much as 1,000-fold higher resistance has been estimated for pathogenic fungi in biofilms compared with the planktonic state (Rossoni et al., 2019; Zhang et al., 2021). The formation of hyphae is the basis for biofilm formation. In this study, SNH was found to effectively inhibit the biofilm formation of *A. fumigatus* and eradicate the formed biofilm (**Figure 2**), thus demonstrating that SNH had potent antifungal activity.

Ergosterol, an essential element of the fungal cell membrane, forms direct linkages with the phospholipid membrane and plays an important role in membrane fluidity, cell cycle progression, cell morphology, and substance transportation (Banerjee et al., 2014; Rana et al., 2019). The biosynthesis of ergosterol is regulated by ergosterol biosynthetic enzymes. The ergosterol biosynthesis pathway is divided into three parts: the mevalonate pathway, ergosterol pathway, and toxic sterol pathway (Lan et al., 2021). The ergosterol pathway is generally chosen as a target for antifungal drug design. For instance, azole and allylamine decrease the production of ergosterol for fungistasis by inhibiting the *Erg11* and *Erg1* genes, respectively (Ryder, 1992; Quiles-Melero and García-Rodríguez, 2021). According to the transcriptomic results, the main KEGG enrichment pathway was steroid biosynthesis, thus suggesting that this pathway might be the target of SNH (**Figure 5A**). Herein, the expression of genes associated with ergosterol synthesis in the ergosterol pathway was analyzed. Most genes in this pathway were down-regulated, thus illustrating an inhibitory effect of SNH toward this pathway. Further results from cell membrane stress assays and HPLC confirmed our hypothesis. However, the expression of *Erg1*, *Erg11*, *Erg24*, and *Erg25* was up-regulated. We speculate that this up-regulation transitory compensatory reaction of *A. fumigatus* to the adverse external environment. In summary, we proposed a mechanistic model for the anti-*A. fumigatus* activity of SNH summarized in **Figure 7** based on our current data. In this model, SNH may activate an unknown protein or transcription factor, which translocates to the nucleus and inhibits the ergosterol synthesis pathway. Cell membrane permeability is subsequently elevated, thus contributing to the inhibition of cell growth or inducing death. The underlying anti-*C. albicans* mechanism of SH and SNH have been reported to be closely involved with the synthesis and transport of β-1,3-glucan and the Ras1-cAMP-Efg1 pathway, respectively (Shao et al., 2017; Wu et al., 2020). However, in our transcriptomic data, the expression of these related genes showed no significant change (data not shown). How SNH affects the expression of ergosterol synthesis-related genes remains unknown and must be verified in further investigations.

A mouse model with IA was used to explore the therapeutic effects of SNH. The treatment of IA mice with SNH resulted

in a lower fungal burden (**Figures 6A–C**) and less infiltration of inflammatory cells in tissues than were observed in the negative control (**Figure 6D**), thus suggesting that SNH was an effective therapy *in vivo*. Recently, the dysregulated production of Th cell cytokines has been confirmed to be associated with the pathogenesis of invasive aspergillosis (Cenci et al., 1999). Therefore, we investigated the levels of IL-6 and IL-17A produced by $CD4^+$ Th cells (**Figures 6E,F**). In general, Th2 cytokines (e.g., IL-6) and Th17 cytokines (e.g., IL-17A) were associated with infection progression under conditions of compromised immunity, and the differentiation and immune function of Th17 cells was positively regulated by IL-6 (Egwuagu, 2009). In mice with IPA, excessive Th2-type reactivity has been found to be associated with poor prognosis in aspergillosis (Cenci et al., 2000). Moreover, Th1 cytokines (e.g., IFN-γ and TNF) are the key components of innate and adaptive immunity in anti-aspergillus defense (Singh et al., 2009; Park et al., 2009; Schmidt et al., 2011; Xu et al., 2018). Investigations have indicated that IFN-γ- and TNF-α- treated mice with IA show decreased mortality (Nagai et al., 1995). However, Th2 cells inhibited T cell activation and promoted the Th2 cell response by inhibiting proinflammatory cytokines and chemokines, thus preventing Th1-type reactivity in aspergillosis. However, in our investigation, all IA mice had high levels of IFN-γ and TNF-α, thereby suggesting a protective immune mechanism in the host. Further experiments are needed to elucidate the reason for the high levels of IFN-γ and TNF-α.

Together, the data from this study confirmed that SNH exhibited fungistatic activity and demonstrated that the effects of SNH on the ergosterol synthesis pathway inhibit *A. fumigatus* growth. However, SNH did not directly bind ergosterol and influence the cell membrane. Although further investigations are needed, the demonstration of the anti-*A. fumigatus* activity of IA *in vivo* supported that the SNH is a promising antifungal agent for the treatment of *A. fumigatus* infection.

## DATA AVAILABILITY STATEMENT

The datasets presented in this study can be found in online repositories. The names of the repository/repositories and accession number(s) can be found in the article/**Supplementary Material**.

## ETHICS STATEMENT

The animal study was reviewed and approved by Mice experimental protocols were approved by the Southwest Medical University Institutional Animal Care and Use Committee (2020540).

## AUTHOR CONTRIBUTIONS

ZS and YM conceived and designed the experiments. QZ and FL performed the experiments and drafted the manuscript. MZ analyzed the data and performed validation of relevant results. JZ and CX contributed to the revision of the manuscript. All authors read and approved the final version of the manuscript.

## FUNDING

This research was financially supported by the Sichuan Province Administration of Traditional Chinese Medicine (2020JC0129), Technology Strategic Cooperation Project of Luzhou Municipal People's Government–Southwest Medical University (2020LZXNYDJ38 and 2020LZXNYDJ23), Science and Technology Project of Luzhou (2021-JYJ-73), and Foundation of Southwest Medical University (2020ZRQNA023, 2020ZRQNA039, 2020ZRQNB066, and 2021ZKMS008).

## ACKNOWLEDGMENTS

The authors thank the Molecular Biotechnology Platform and the Large Scientific Instrument Platform, Public Center of Experimental Technology, Southwest Medical University, for technical, instrument, and equipment support related to this work.

## SUPPLEMENTARY MATERIAL

The Supplementary Material for this article can be found online at: https://www.frontiersin.org/articles/10.3389/fmicb.2022.856272/full#supplementary-material

**Supplementary Figure 1 |** Chemical structure of **(A)** sodium houttuyfonate, **(B)** sodium new houttuyfonate, **(C)** isavuconazole, **(D)** itraconazole, **(E)** posaconazole, and **(F)** voriconazole.

**Supplementary Figure 2 |** Sodium new houttuyfonate (SNH) inhibits the asexual cycle of *A. fumigatus*. **(A)** Images of treatment with various concentrations of SNH on PDA plates. The *A. fumigatus* strains AF293, AF1, AF2, AF4, and AF5 were incubated at a concentration of $10^5$ cells/mL. Each 3 μL dilution was deposited on PDA solid medium with 1 ×, 2 × , or 4 × MIC SNH; AmB (8 μg/mL, positive control); or no drugs (negative control) before incubation at 37°C for 4 days. **(B–F)** Statistical analysis of *A. fumigatus* conidia yields under SNH treatment. Results represent the average of three independent experiments ± SD, and the level of statistical significance was set at $^*P < 0.05$.

**Supplementary Figure 3 |** Transcriptomic analyses. **(A)** Volcano plot of differentially expressed genes (DEGs). The green dots indicate downregulated genes (109) and the red dots indicate upregulated genes (66), with a total of 175 DEGs. **(B)** Gene ontology terms of DEGs. The distributions are summarized in three main categories: biological process (BP), molecular function (MF), and cellular component (CC). **(C)** Clusters of orthologous groups of the consensus sequence. The highest frequencies included carbohydrate transport and metabolism; secondary metabolites biosynthesis, transport, and catabolism; and amino acid transport and metabolism.

**Supplementary Figure 4 |** Therapeutic effects of SNH on histologic analysis and determination of cytokines. **(A)** PAS-stained sections were prepared from the kidneys and lungs of mice at 4 days after treatment with SNH at 10 mg/kg/d. The black arrows indicated spores or hyphae. Scale bar is 100 μm. **(B,C)** Levels of IFN-γ and TNF-α in the serum in various groups of mice on days 1 and 4 after treatment with SNH are shown. The values represent the average ± SD of three data points. Normal saline and itraconazole (ITR)-treated IA mice were used in the control group.

## REFERENCES


Banerjee, D., Burkard, L., and Panepinto, J. C. (2014). Inhibition of nucleotide biosynthesis potentiates the antifungal activity of amphotericin B. *PloS One.* 9:e87246. doi: 10.1371/journal.pone.0087246

Benedict, K., Jackson, B. R., Chiller, T., and Beer, K. D. (2019). Estimation of direct healthcare costs of fungal diseases in the United States. *Clin. Infect. Dis.* 68, 1791–1797. doi: 10.1093/cid/ciy776

Bom, V. L., de Castro, P. A., Winkelströter, L. K., Marine, M., Hori, J. I., Ramalho, L. N., et al. (2015). The *Aspergillus fumigatus* sitA phosphatase homologue is important for adhesion, cell wall integrity, biofilm formation, and virulence. *Eukaryot. Cell* 14, 728–744. doi: 10.1128/EC.00008-15

Bugli, F., Posteraro, B., Papi, M., Torelli, R., Maiorana, A., Paroni Sterbini, F., et al. (2013). *In vitro* interaction between alginate lyase and amphotericin B against *Aspergillus fumigatus* biofilm determined by different methods. *Antimicrob. Agents Chemother.* 57, 1275–1282. doi: 10.1128/AAC.01875-12

Cenci, E., Mencacci, A., Bacci, A., Bistoni, F., Kurup, V. P., and Romani, L. (2000). T cell vaccination in mice with invasive pulmonary aspergillosis. *J. Immunol.* 165, 381–388. doi: 10.4049/jimmunol.165.1.381

Cenci, E., Mencacci, A., Del Sero, G., Bacci, A., Montagnoli, C., d'Ostiani, C. F., et al. (1999). Interleukin-4 causes susceptibility to invasive pulmonary aspergillosis through suppression of protective type I responses. *J. Infect. Dis.* 180, 1957–1968. doi: 10.1086/315142

Chai, L. Y., Netea, M. G., Sugui, J., Vonk, A. G., van de Sande, W. W., et al. (2010). *Aspergillus fumigatus* conidial melanin modulates host cytokine response. *Immunobiology.* 215, 915–920. doi: 10.1016/j.imbio.2009.10.002

Chen, L., Qu, S., Yang, K., Liu, M., Li, Y. X., Keller, N. P., et al. (2020). Perillaldehyde: a promising antifungal agent to treat oropharyngeal candidiasis. *Biochem. Pharmacol.* 180:114201. doi: 10.1016/j.bcp.2020.114201

Da, W., Shao, J., Li, Q., Shi, G., Wang, T., Wu, D., et al. (2019). Physical interaction of sodium houttuyfonate with β-1,3-glucan evokes *Candida albicans* cell wall remodeling. *Front. Microbiol.* 10:34. doi: 10.3389/fmicb.2019.00034

Denning, D. W., Hall, L., Jackson, M., and Hollis, S. (1995). Efficacy of D0870 compared with those of itraconazole and amphotericin B in two murine models of invasive aspergillosis. *Antimicrob. Agents Chemother.* 39, 1809–1814. doi: 10.1128/AAC.39.8.1809

Denning, D. W., Radford, S. A., Oakley, K. L., Hall, L., Johnson, E. M., and Warnock, D. W. (1997). Correlation between *in-vitro* susceptibility testing to itraconazole and *in-vivo* outcome of *Aspergillus fumigatus* infection. *J. Antimicrob. Chemother.* 40, 401–414. doi: 10.1093/jac/40.3.401

Egwuagu, C. E. (2009). STAT3 in CD4+ T helper cell differentiation and inflammatory diseases. *Cytokine.* 47, 149–156. doi: 10.1016/j.cyto.2009.07.003

Espinel-Ingroff, A., Diekema, D. J., Fothergill, A., Johnson, E., Pelaez, T., Pfaller, M. A., et al. (2010). Wild-type MIC distributions and epidemiological cutoff values for the triazoles and six *Aspergillus* spp. for the CLSI broth microdilution method (M38-A2 document). *J. Clin. Microbiol.* 48, 3251–3257. doi: 10.1128/JCM.00536-10

González-Ramírez, A. I., Ramírez-Granillo, A., Medina-Canales, M. G., Rodríguez-Tovar, A. V., and Martínez-Rivera, M. A. (2016). Analysis and description of the stages of *Aspergillus fumigatus* biofilm formation using scanning electron microscopy. *BMC Microbiol.* 16:243. doi: 10.1186/s12866-016-0859-4

Gülmez, D., Sığ, A. K., Akar, N., Duyan, S., and Arıkan Akdağlı, S. (2021). Changing trends in isolation frequencies and species of clinical fungal strains: what do the 12-years (2008-2019) mycology laboratory data tell about? *Mikrobiyol. Bul.* 55, 53–66. doi: 10.5578/mb.20156

Huang, W., Duan, Q., Li, F., Shao, J., Cheng, H., and Wu, D. (2015). Sodium houttuyfonate and EDTA-Na2 in combination effectively inhibits *Pseudomonas aeruginosa*, *Staphylococcus aureus* and *Candida albicans in vitro* and *in vivo*. *Bioorg. Med. Chem. Lett.* 25, 142–147. doi: 10.1016/j.bmcl.2014.10.072

Iwahashi, J., Kamei, K., and Watanabe, H. (2020). Disruption of *Aspergillus fumigatus* biofilm by *Streptococcus pneumoniae*: mycelial fragmentation by hydrogen peroxide. *J. Infect. Chemother.* 26, 831–837. doi: 10.1016/j.jiac.2020.03.015

Kim, J. H., Cheng, L. W., Chan, K. L., Tam, C. C., Mahoney, N., Friedman, M., et al. (2020). Antifungal drug repurposing. *Antibiotics.* 9:812. doi: 10.3390/antibiotics9110812

Lan, Q., Li, Y., Wang, F., Li, Z., Gao, Y., Lu, H., et al. (2021). Deubiquitinase Ubp3 enhances the proteasomal degradation of key enzymes in sterol homeostasis. *J. Biol. Chem.* 296:100348. doi: 10.1016/j.jbc.2021.100348

Latgé, J. P., and Chamilos, G. (2019). *Aspergillus fumigatus* and Aspergillosis in 2019. *Clin. Microbiol. Rev.* 33, e140–e118. doi: 10.1128/CMR.00140-18

Li, X., Wang, P., Hu, X., Zhang, Y., Lu, X., Li, C., et al. (2020). The combined antibacterial effects of sodium new houttuyfonate and berberine chloride against growing and persistent methicillin-resistant and vancomycin-intermediate *Staphylococcus aureus*. *BMC Microbiol.* 20:317. doi: 10.1186/s12866-020-02003-2

Lu, X., Yang, X., Li, X., Lu, Y., Ren, Z., Zhao, L., et al. (2013). In vitro activity of sodium new houttuyfonate alone and in combination with oxacillin or netilmicin against methicillin-resistant *Staphylococcus aureus*. *PloS One* 8:e68053. doi: 10.1371/journal.pone.0068053

Meis, J. F., Chowdhary, A., Rhodes, J. L., Fisher, M. C., and Verweij, P. E. (2016). Clinical implications of globally emerging azole resistance in *Aspergillus fumigatus*. *Philos. Trans. R. Soc. Lond. B. Biol. Sci.* 371:20150460. doi: 10.1098/rstb.2015.0460

Nagai, H., Guo, J., Choi, H., and Kurup, V. (1995). Interferon-gamma and tumor necrosis factor-alpha protect mice from invasive aspergillosis. *J. Infect. Dis.* 172, 1554–1560. doi: 10.1093/infdis/172.6.1554

Odds, F. C. (2003). Synergy, antagonism, and what the chequerboard puts between them. *J. Antimicrob. Chemother.* 52:1. doi: 10.1093/jac/dkg301

Park, S. J., Hughes, M. A., Burdick, M., Strieter, R. M., and Mehrad, B. (2009). Early NK cell-derived IFN-{gamma} is essential to host defense in neutropenic invasive aspergillosis. *J. Immunol.* 182, 4306–4312. doi: 10.4049/jimmunol.0803462

Pasula, S., and Chandrasekar, P. H. (2021). Azole resistance in *Aspergillus* species: promising therapeutic options. *Expert Opin. Pharmacother.* 22, 2071–2078. doi: 10.1080/14656566.2021.1940134

Pihet, M., Vandeputte, P., Tronchin, G., Renier, G., Saulnier, P., Georgeault, S., et al. (2009). Melanin is an essential component for the integrity of the cell wall of *Aspergillus fumigatus* conidia. *BMC Microbiol.* 9:177. doi: 10.1186/1471-2180-9-177

Pinto, E., Afonso, C., Duarte, S., Vale-Silva, L., Costa, E., Sousa, E., et al. (2011). Antifungal activity of xanthones: evaluation of their effect on ergosterol biosynthesis by high-performance liquid chromatography. *Chem. Biol. Drug Des.* 77, 212–222. doi: 10.1111/j.1747-0285.2010.01072.x

Pumeesat, P., Muangkaew, W., Ampawong, S., and Luplertlop, N. (2017). *Candida albicans* biofilm development under increased temperature. *N. Microbiol.* 40, 279–283.

Quiles-Melero, I., and García-Rodríguez, J. (2021). Antifúngicos de uso sistémico [Systemic antifungal drugs]. *Rev. Iberoam. Micol.* 38, 42–46. doi: 10.1016/j.riam.2021.04.004

Rana, R., Sharma, R., and Kumar, A. (2019). Repurposing of fluvastatin against *Candida albicans* CYP450 Lanosterol 14 α-demethylase, a target enzyme for antifungal therapy: an in silico and *in vitro* study. *Curr. Mol. Med.* 19, 506–524. doi: 10.2174/1566524019666190520094644

Rossoni, R. D., de Barros, P. P., Lopes, L., Ribeiro, F. C., Nakatsuka, T., Kasaba, H., et al. (2019). Effects of surface pre-reacted glass-ionomer (S-PRG) eluate on *Candida* spp.: antifungal activity, anti-biofilm properties, and protective effects on *Galleria mellonella* against *C. albicans* infection. *Biofouling.* 35, 997–1006. doi: 10.1080/08927014.2019.1686485

Ryder, N. S. (1992). Terbinafine: mode of action and properties of the squalene epoxidase inhibition. *Br. J. Dermatol.* 126(Suppl. 39), 2–7. doi: 10.1111/j.1365-2133.1992.tb00001.x

Schmaler-Ripcke, J., Sugareva, V., Gebhardt, P., Winkler, R., Kniemeyer, O., Heinekamp, T., et al. (2009). Production of pyomelanin, a second type of melanin, via the tyrosine degradation pathway in *Aspergillus fumigatus*. *Appl. Environ. Microbiol.* 75, 493–503. doi: 10.1128/AEM.02077-08

Schmidt, S., Tramsen, L., Hanisch, M., Latgé, J. P., Huenecke, S., Koehl, U., et al. (2011). Human natural killer cells exhibit direct activity against *Aspergillus fumigatus* hyphae, but not against resting conidia. *J. Infect. Dis.* 203, 430–435. doi: 10.1093/infdis/jiq062

Shao, J., Cheng, H., Wang, C., and Wang, Y. (2012). A phytoanticipin derivative, sodium houttuyfonate, induces *in vitro* synergistic effects with levofloxacin against biofilm formation by *Pseudomonas aeruginosa*. *Molecules* 17, 11242–11254. doi: 10.3390/molecules170911242

Shao, J., Cui, Y., Zhang, M., Wang, T., Wu, D., and Wang, C. (2017). Synergistic *in vitro* activity of sodium houttuyfonate with fluconazole against clinical *Candida albicans* strains under planktonic growing conditions. *Pharma. Biol.* 55, 355–359. doi: 10.1080/13880209.2016.1237977

Singh, M., Madan, T., Waters, P., Sonar, S., Singh, S. K., Kamran, M. F., et al. (2009). Therapeutic effects of recombinant forms of full-length and truncated human surfactant protein D in a murine model of invasive pulmonary aspergillosis. *Mol. Immunol.* 46, 2363–2369. doi: 10.1016/j.molimm.2009.03.019

Song, Z., Yang, J., Xin, C., Xing, X., Yuan, Q., Yin, Y., et al. (2018). A transcriptional factor, MrMsn2, in the dimorphic fungus *Metarhizium rileyi* is essential for dimorphism transition, aggravated pigmentation, conidiation and microsclerotia formation. *Microb. Biotechnol.* 11, 1157–1169. doi: 10.1111/1751-7915.13302

van de Veerdonk, F. L., Gresnigt, M. S., Romani, L., Netea, M. G., and Latgé, J. P. (2017). *Aspergillus fumigatus* morphology and dynamic host interactions. *Nat. Rev. Microbiol.* 15, 661–674. doi: 10.1038/nrmicro.2017.90

van der Linden, J. W., Arendrup, M. C., Warris, A., Lagrou, K., Pelloux, H., Hauser, P. M., et al. (2015). Prospective multicenter international surveillance of azole resistance in *Aspergillus fumigatus*. *Emerg. Infect. Dis.* 21, 1041–1044. doi: 10.3201/eid2106.140717

Vandesompele, J., De Preter, K., Pattyn, F., Poppe, B., Van Roy, N., De Paepe, A., et al. (2002). Accurate normalization of real-time quantitative RT-PCR data by geometric averaging of multiple internal control genes. *Genom. Biol.* 3:RESEARCH0034. doi: 10.1186/gb-2002-3-7-research0034

Wu, J., Wu, D., Zhao, Y., Si, Y., Mei, L., Shao, J., et al. (2020). Sodium new houttuyfonate inhibits *Candida albicans* biofilm formation by inhibiting the Ras1-cAMP-Efg1 pathway revealed by RNA-seq. *Front. Microbiol.* 11:2075. doi: 10.3389/fmicb.2020.02075

Xu, L. N., Xu, R. A., Zhang, D., Su, S. S., Xu, H. Y., Wu, Q., et al. (2018). The changes of expressive levels of IL-17A, STAT3, and RORγt in different invasive pulmonary aspergillosis mice. *Infect. Drug Resist.* 11, 1321–1328. doi: 10.2147/IDR.S172949

Yang, X. Y., Shi, T., Du, G., Liu, W., Yin, X. F., Sun, X., et al. (2016). iTRAQ-based proteomics revealed the bactericidal mechanism of sodium new houttuyfonate against *Streptococcus pneumoniae*. *J. Agric. Food Chem.* 64, 6375–6382. doi: 10.1021/acs.jafc.6b02147

Youngchim, S., Morris-Jones, R., Hay, R. J., and Hamilton, A. J. (2004). Production of melanin by *Aspergillus fumigatus*. *J. Med. Microbiol.* 53, 175–181. doi: 10.1099/jmm.0.05421-0

Zhang, Q., Liu, F., Zeng, M., Mao, Y., and Song, Z. (2021). Drug repurposing strategies in the development of potential antifungal agents. *Appl. Microbiol. Biotechnol.* 105, 5259–5279. doi: 10.1007/s00253-021-11407-7

Zhao, Y., Mei, L., Si, Y., Wu, J., Shao, J., Wang, T., et al. (2020). Sodium new houttuyfonate affects transcriptome and virulence factors of *Pseudomonas aeruginosa* controlled by quorum sensing. *Front. Pharmacol.* 11:572375. doi: 10.3389/fphar.2020.572375

**Conflict of Interest:** The authors declare that the research was conducted in the absence of any commercial or financial relationships that could be construed as a potential conflict of interest.

**Publisher's Note:** All claims expressed in this article are solely those of the authors and do not necessarily represent those of their affiliated organizations, or those of the publisher, the editors and the reviewers. Any product that may be evaluated in this article, or claim that may be made by its manufacturer, is not guaranteed or endorsed by the publisher.

frontiers | Frontiers in Microbiology

ORIGINAL RESEARCH
published: 24 May 2022
doi: 10.3389/fmicb.2022.815091

# Enhancing the Antibiofilm Activity of β-1,3-Glucanase-Functionalized Nanoparticles Loaded With Amphotericin B Against *Candida albicans* Biofilm

*Yulong Tan[1,2*†], Su Ma[3†], Ting Ding[1,2], Roland Ludwig[3], Jintae Lee[4] and Jiaman Xu[1,2]*

[1] Special Food Research Institute, Qingdao Agricultural University, Qingdao, China, [2] Qingdao Special Food Research Institute, Qingdao, China, [3] Food Biotechnology Laboratory, Department of Food Sciences and Technology, University of Natural Resources and Life Sciences, Vienna, Austria, [4] School of Chemical Engineering, Yeungnam University, Gyeongsan, South Korea

OPEN ACCESS

**Edited by:**
Laura Quintieri,
Institute of Sciences of Food Production (CNR), Italy

**Reviewed by:**
Leonardo Caputo,
Institute of Sciences of Food Production (CNR), Italy
Sueli Fumie Yamada-Ogatta,
State University of Londrina, Brazil

***Correspondence:**
Yulong Tan
tanyulong@qau.edu.cn

† These authors have contributed equally to this work and share first authorship

**Specialty section:**
This article was submitted to Antimicrobials, Resistance and Chemotherapy, a section of the journal Frontiers in Microbiology

**Received:** 15 November 2021
**Accepted:** 25 April 2022
**Published:** 24 May 2022

**Citation:**
Tan Y, Ma S, Ding T, Ludwig R, Lee J and Xu J (2022) Enhancing the Antibiofilm Activity of β-1,3-Glucanase-Functionalized Nanoparticles Loaded With Amphotericin B Against Candida albicans Biofilm. Front. Microbiol. 13:815091. doi: 10.3389/fmicb.2022.815091

*Candida* biofilm-related infections cause increased morbidity and mortality in patients with a reduced immune response. Traditional antifungal therapies have proven to be insufficient as the biofilm matrix acts as a perfusion barrier. Thus, novel methods are required to improve drug delivery and kill *Candida* within the biofilm. In this study, chitosan nanoparticles (CSNPs) loaded with Amphotericin B (AMB), which were functionalized with β-1,3-glucanase (Gls), were fabricated (CSNPs-AMB-Gls), and their antibiofilm activity against *Candida albicans* biofilm was evaluated *in vitro*. Scanning electron microscopy (SEM) and confocal laser scanning microscopy (CLSM) were employed to examine biofilm architecture and cell viability. CSNPs-AMB-Gls inhibited planktonic cell growth and biofilm formation effectively and exhibited the highest efficacy on the removal of a mature biofilm than free AMB or CSNPs-AMB. The created nanoparticles (NPs) were found to penetrate the biofilm so as to directly interfere with the cells inside and disassemble the biofilm matrix. CSNPs-AMB-Gls could also eradicate biofilms from clinical isolates. These results suggest the potential applicability of CSNPs-AMB-Gls for the treatment of *Candida* biofilm-related infections.

**Keywords: antibiofilm, nanoparticle, chitosan, *Candida*, amphotericin B**

## INTRODUCTION

*Candida* species are typical pathogenic microorganisms, which have been identified as the fourth most common cause of bloodstream infections in the United States and are associated with high morbidity and mortality (Gottardo et al., 2019; Nani et al., 2019). In addition to public health consequences, *Candida* is also related to food contamination, which reduces the nutritional value of products and leads to foodborne intoxications (Piccinelli et al., 2016; Rajkowska and Kunicka-Styczyńska, 2018). The predominant nosocomial fungal pathogen is *Candida albicans,* which is one of the leading causes of infections known to have a great biofilm-forming ability (Rajendran et al., 2016; Wall et al., 2019). *Candida* cells within biofilms, communities of cells embedded in a matrix, exhibit lower susceptibility to antimicrobials due to an extracellular matrix (Mitchell et al., 2016; Lohse et al., 2017). Even high therapeutic concentrations of existing antifungal drugs prove to be

less efficient in inhibiting growth or removing biofilms while the risk of causing serious side effects, such as kidney or liver damage, is increased (Lohse et al., 2017).

Amphotericin B (AMB), a broad-spectrum antifungal drug, is recommended as first-line therapy for fungal-related infections (Benincasa et al., 2011; Vikelouda et al., 2017). However, *C. albicans* in the biofilm shows high resistance to AMB, which can be 1,000-fold less susceptible than planktonic ones. Several lipid-based drug delivery systems have been employed to enhance the therapeutic effect and decrease the toxicity of AMB (Weiler et al., 2008; Nieto et al., 2018). Unfortunately, the widespread use of these new formulations is impeded due to the high production cost (Weiler et al., 2009; Steimbach et al., 2017). Therefore, there is an urgent need to precise the delivery to enhance the efficiency and improve the inhibitory effect of AMB on ergosterol in fungal membranes.

Nanobiotechnology has gained attention in the pharmaceutical and medical fields, and the nano-sizing of antimicrobial agents seems to be a promising treatment for biofilm-related infections. Because nanoparticles (NPs) can more easily penetrate the biofilm matrix due to their size and surface charge (Baelo et al., 2015). It has been reported that both positively and negatively charged NPs could bind to biofilms. Negatively charged NPs could bind to microbial cells with hydrophobic interactions, while positively charged NPs could diffuse into the biofilm through binding to negatively charged biofilm polymers, such as eDNA (Nafee et al., 2014). Therefore, they can interfere with cells inside the biofilm directly (Jamil et al., 2017; Benoit et al., 2019). Moreover, the NP structure can enclose and protect antimicrobials from endogenous and exogenous factors of microbial cells, leading to enhanced bioactivity at the proximity of target cells (Jamil et al., 2016). Chitosan (CS) is a cost-effective biopolymer suitable for the preparation of biocompatible, biodegradable, and non-cytotoxic NPs with inherent antimicrobial and antibiofilm activity (Martinez et al., 2010; Klinger-Strobel et al., 2016). In our previous work, CS nanoparticle (CSNP) has been proven to be a kind of ideal carrier for biofilm treatment (Tan et al., 2018). Furthermore, CSNP is a promising carrier to overcome the poor aqueous solubility of hydrophobic drugs (Trapani et al., 2009; Quiñones et al., 2018).

Increased drug resistance of *C. albicans* in biofilms compared to its planktonic form is mainly due to the self-produced extrapolymeric substance (EPS) matrix (Limoli et al., 2015; Flemming et al., 2016). Moreover, the inactive structure of the biofilm still promotes the adhesion and regeneration of other microorganisms (MacDonald et al., 2000). Therefore, the biofilm matrix itself should also be a target in addition to fungal cells. Recently, EPS-degrading enzymes have been proposed as a new strategy to remove the biofilm and to enhance drug efficacy (Okshevsky and Meyer, 2015; Kimura and Urata, 2016; Klinger-Strobel et al., 2016). As one of the major polysaccharides in the *C. albicans* biofilm matrix, β-1,3-glucan plays an important role in the biofilm structure and cell protection. The enzyme β-1,3-glucanase (Gls) can disrupt the *Candida* biofilm matrix by degrading β-1,3-glucan (Nett et al., 2007). Our previous work also showed that Gls can enhance the efficacy of antimicrobial drugs (De Brucker et al., 2015; Tan et al., 2018). However, to our knowledge, there are no reports showing nanosystems that combine the enzyme specifically degrading the *Candida* biofilm matrix and the antifungal that kills *Candida* within the biofilm.

Therefore, the combination of CSNPs with antimicrobials and enzymes as novel nanoantimicrobials seems to be a plausible approach for the treatment of *Candida* biofilms. In this study, CSNPs were functionalized with Gls and loaded with AMB (CSNPs-AMB-Gls) to combine enhanced antibiofilm activity with biofilm matrix disruption ability.

# MATERIALS AND METHODS

## Strains, Media, and Reagents

*Candida albicans* DAY 185 was used in the experiments. Three clinical isolates of *C. albicans*, named *C. albicans* BF1, BF2, and BF3, were obtained from the Medical University of Vienna. Each experiment was repeated three times. All of them are able to form strong biofilms, which have been confirmed by the crystal violet method. The strains were cultured in a Yeast Peptone Dextrose (YPD) medium (Sigma-Aldrich, Austria) at 30°C. RPMI 1640 medium (Thermo Fisher Scientific, Waltham, MA, United States) was used for biofilm growth. Gls (lyticase from *Arthrobacter luteus*, ≥2,000 units/mg protein), CS (low molecular weight, degree of deacetylation 75–85%), AMB, and other reagents were purchased from Sigma-Aldrich.

## Formulation of Nanoparticles

Chitosan nanoparticles were prepared as described by the ion gelation method with polyanionic sodium triphosphate (TPP) in our previous work (Pu et al., 2014). CSNP-Gls was prepared with mixing CSNPs [1 mg/ml polybutylene succinate (PBS)] and Gls (100 μg/ml PBS) while stirring overnight at 4°C. NP suspensions were centrifuged (14,000 rpm, 30 min) and freeze-dried eventually. For the preparation of CSNPs-AMB-Gls, CSNPs-Gls suspension (1 mg/ml) was mixed with AMB (100 μg/ml DMSO) and stirred for 24 h. The mixture was centrifuged and lyophilized.

## Characterization of Nanoparticles

The size of NPs was analyzed by dynamic light scattering (DLS). Laser Doppler velocimetry assays were used to determine the zeta potential (ZetaSizer Nano ZS, Malvern Instruments, United Kingdom). Morphological characterization was confirmed by scanning electron microscopy (SEM, JSM 6310, JEOL Ltd., Akishima, Tokyo, Japan).

The CSNPs-Gls suspension (prepared as reported above) was evaluated using a suspension of yeast as the substrate according to the Sigma-Aldrich protocol for Gls activity assay. The loading capacity (LC) of AMB loaded on the NP was estimated by measuring the absorption at 405 nm spectrophotometrically (Spectroscopy, Persee, TU-1810, China) and calculated as follows:

$$LC = (tAMB - fAMB)/NPs$$

Where tAMB, fAMB, and NPs, represent total AMB, free AMB, and NP amount, respectively.

## *In vitro* Release

Release kinetics *in vitro* was carried out as follows: 4 ml of CSNPs-AMB-Gls solution (1 mg/ml in a dialysis bag) was placed in 40 ml of PBS with stirring (100 rpm). At any given time point, 4 ml of PBS was taken and replaced with 4 ml of fresh PBS to maintain the sink volume. The amount of AMB in the solution was measured at 405 nm by UV spectrometry (Persee, TU-1810, China).

## Minimum Inhibitory Concentration Assay

About 100 μl of *Candida* ($1 \times 10^6$ CFU/ml), including *C. albicans* DAY 185 and three clinical isolates of *C. albicans,* was added to wells of 96-well microplates (Thermo Fisher Scientific, Waltham, MA, United States) with different concentrations of free AMB, CSNPs, and CSNPs-AMB-Gls (4, 2, 1, 0.5, 0.25, 0.125, 0.0625, or 0 μg/ml). The microplate was incubated at 37°C for 24 h at 150 rpm. Minimum inhibitory concentration (MIC) was defined as the lowest concentration of AMB at which no visible growth was detected.

## Growth of Biofilms

Biofilms in a 96-well microplate and on silicone platelets were conducted and assayed as previously described (Tan et al., 2018). In brief, *C. albicans* was diluted to $1 \times 10^6$ CFU/ml with RPMI 1640 and 100 μl of fungal culture was pipetted into each well of a 96-well microplate. Biofilms were formed at 37°C for 24 h without shaking.

## Penetration of Chitosan Nanoparticles Into Biofilms

Chitosan nanoparticles were labeled with rhodamine B isothiocyanate (CSNPs-RBITC) as previously described (Pu et al., 2014). An autoclaved medical grade silicone platelet (3-mm-diameter, Websinger, Austria) was placed in each well of the 96-well microplate. *C. albicans* DAY 185 biofilms were formed on medical grade silicone platelets for 24 h as described above in the 96-well microplate and mixed with RBITC-CSNPs (100 μg/ml) for 2 h and washed with PBS. The penetration of CSNPs was determined by confocal laser scanning microscopy (CLSM).

## Efficacy on the Biofilm Formation

Biofilms were formed in 96-well microplates as previously described. *C. albicans* DAY 185 cells were incubated with free AMB, a combination of AMB and Gls (AMB+Gls, 2 μg/ml), CSNPs-AMB, and CSNPs-AMB-Gls with different drug concentrations (0, 0.25, 0.5, and 1 μg/ml) for 24 h. Biofilms were washed with PBS and quantified with a cell counting kit-8 (CCK-8, Dojindo Molecular Technologies, Gaithersburg, MD, United States) reduction assay. The absorbance was examined at 450 nm.

## Efficacy on the Mature Biofilm

*Candida albicans* DAY 185 biofilms were formed as described above for 24 h and added with fresh medium containing different concentrations (0, 1, 2, and 4 μg/ml) of free AMB, AMB+Gls, CSNPs-AMB, and CSNPs-AMB-Gls. After another 24 h, the biofilms were washed with PBS and quantified with the CCK-8 reduction assay.

## Efficacy on Biofilms on Medical Silicone Surfaces

Biofilms on silicone platelets were treated with free AMB, AMB+Gls, CSNPs-AMB, and CSNPs-AMB-Gls (4 μg/ml) as described above.

Biofilm architecture was investigated by SEM. Biofilms on silicone platelets were fixed in 3% glutaraldehyde (v/v) in PBS solution overnight at 4°C, and then subjected to serial dehydration with 25, 50, 75, and 100% ethanol for 10 min each. The biofilms were coated with gold and examined by SEM (JSM 6310, JEOL Ltd., Akishima, Tokyo, Japan).

The cells of biofilms were stained with a LIVE/DEAD® BacLight™ Bacterial Viability and Counting kit (L34856, Invitrogen, United States) following the manufacturer's instructions. Cell viability was observed with CLSM.

## Antibiofilm Activity Against Clinical Isolates

The antibiofilm efficacy of free AMB, AMB+Gls, CSNPs-AMB, and CSNPs-AMB-Gls (2 μg/ml) was tested on three clinical isolates. Biofilms of clinical strains formed in the 96-well microplate were evaluated as described above.

## Statistical Analysis

Statistical analyses of data were determined with GraphPad Prism software program (GraphPad Software, San Diego, CA, United States). Values are given as mean ± standard deviation (SD) of the number of experiments ($n = 3$). Statistical significance was determined by the *t*-test analysis with $p < 0.05$.

# RESULTS

## Characterization of CSNPs-AMB-Gls

Scanning electron microscopy images showed that CSNPs-AMB-Gls was round particles (**Figure 1**). The average size of CSNPs-AMB-Gls was 174.47 ± 5.12 nm (size PDI 0.17), and the surface zeta potential was +15.84 ± 1.41 mV. The loading capacity of AMB on CSNPs-AMB-Gls was 3.05% ± 0.13%. Gls loaded on the NP-retained Gls activity, the activity of which was 128.6 ± 4.54 U/mg NP.

## *In vitro* Release Studies

**Figure 2** shows the release profiles of AMB from NPs. CSNPs-AMB-Gls presented an initial burst release phase in the first 1 h: 52.5% of the total AMB was released. Subsequently, the drug release was slowed down. Over 24 h, CSNPs-AMB-Gls showed a sustained release of 80.6% of the total AMB.

## Minimum Inhibitory Concentration Assay

Both free AMB and CSNPs-AMB-Gls were effective against *C. albicans* DAY 185 and the growth of clinical isolates, which

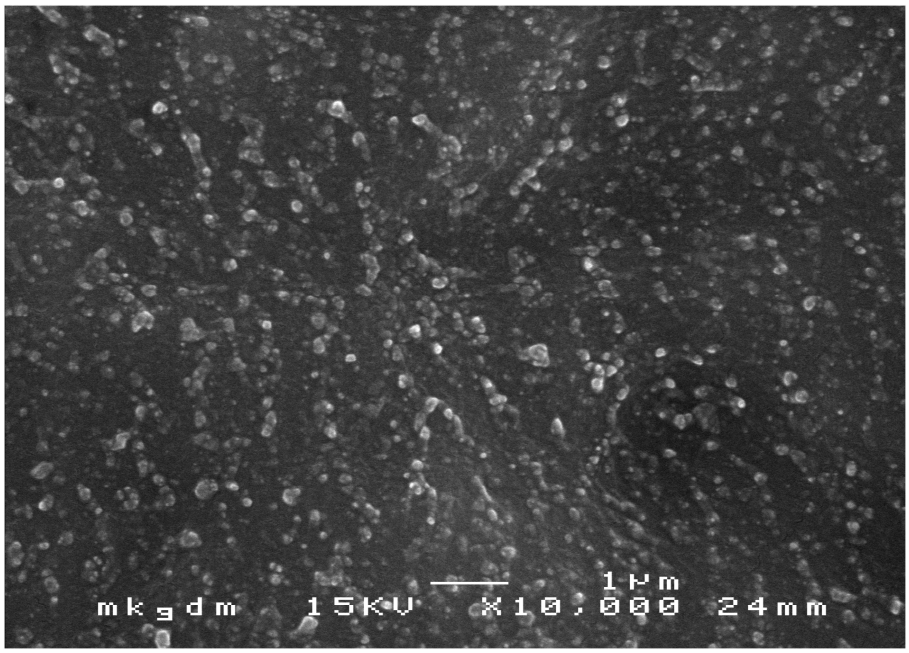


**FIGURE 1 |** Scanning electron microscopy (SEM) image of chitosan nanoparticles (CSNPs) loaded with amphotericin B (AMB), which were functionalized with β-1,3-glucanase (Gls) (CSNPs-AMB-Gls). Magnification, ×10,000.

showed the same MIC. MIC was 1 μg/ml against *C. albicans* DAY 185 and higher against clinical isolates (2, 2, and 4 μg/ml, respectively). CSNPs alone had no effect on planktonic *Candida* at the concentration used in this work (data not shown). This result suggested that AMB loading in CSNPs did not change the antifungal activity of free AMB to planktonic *Candida*.

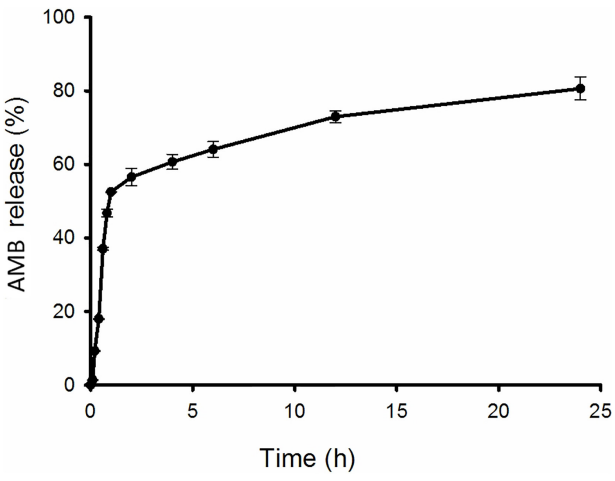


**FIGURE 2 |** *In vitro* release kinetics of AMB from the nanoparticle (NP). CSNPs-AMB-Gls was placed in polybutylene succinate (PBS) with stirring. The amount of AMB in the solution was measured at 405 nm by UV spectrometry at any given time point.

## Penetration of Chitosan Nanoparticle Into Biofilms

After 2 h treatment with CSNPs, red color (RBITC-NPs) can be observed on the surface and inside the biofilm, suggesting that the penetration of CSNPs into the biofilm (**Figure 3**).

## Inhibition Activity on Biofilm Formation

As shown in **Figure 4**, free AMB, AMB+Gls, CSNPs-AMB, and CSNPs-AMB-Gls showed concentration-dependent biofilm inhibition activity with all tested concentrations. At the concentration of 1 μg/ml, almost no biofilm formations were observed in the treatment with free AMB, AMB+Gls, CSNPs-AMB, and CSNPs-AMB-Gls. At other concentrations, CSNPs-AMB and CSNPs-AMB-Gls showed similar inhibition compared to free AMB.

## Antibiofilm Activity on the Mature Biofilm

Due to the high resistance of the biofilm to antimicrobial agents, we used 4 × MIC for evaluating the antibiofilm activity of free AMB, AMB+Gls, CSNPs-AMB, and CSNPs-AMB-Gls on the mature biofilm (**Figure 5**). As expected, *C. albicans* DAY 185 in the biofilm increases resistance to free AMB or CSNPs-AMB without Gls compared to planktonic forms. However, both free AMB with Gls (AMB+Gls) and CSNPs-AMB-Gls showed a good extent of biofilm eradication. Moreover, CSNPs-AMB-Gls exhibited the highest activity in the eradication of preformed biofilm at any of the concentrations tested. At a concentration of 4 μg/ml AMB, AMB+Gls caused a 83.1% biofilm reduction, but CSNPs-AMB-Gls reduced the biofilm by 90.9%.

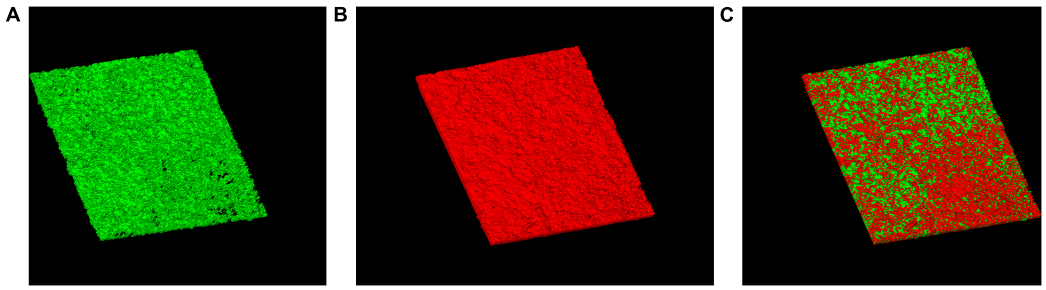


**FIGURE 3 |** Penetration of CSNPs into biofilms. CSNPs were labeled with rhodamine B isothiocyanate (RBITC) and visualized by confocal laser scanning microscopy (CLSM). SYTO 9-labeled biofilms incubated with CSNPs **(A)**. RBITC-NP penetration into biofilms **(B)**. Overlap **(C)**.

## Antibiofilm Efficacy on Silicone

Biofilm architecture and LIVE/DEAD organisms within the biofilm on silicone surfaces were investigated. The cell viability of the biofilm on silicone platelets treated with or without drugs was observed with CLSM (**Figure 6**). A large number of green-colored cells (live cells) were observed without any treatment (**Figure 6A**), which indicated that the mature biofilm was mainly composed of active cells. Treated with free AMB and CSNPs-AMB, the green-colored cells (live cells) were drastically reduced (**Figures 6B,C**). With the combination of Gls, more red-colored cells (dead cells) and less biofilm thickness were shown compared to free AMB treatment (**Figures 6D,E**).

Scanning electron microscopy images confirmed the results mentioned above and revealed changes in the biofilm structures (**Figure 7**). In the control group, we can see the typical dense composition of biofilms (**Figure 7A**). However, treatment with free AMB and CSNPs-AMB significantly reduced colonization (**Figures 7B,C**). Furthermore, AMB+Gls and CSNPs-AMB-Gls resulted in only single cells or even free of cells on silicone platelets (**Figures 7D,E**), which meant that the biofilm structure was disrupted with the killing of *Candida* cells.

## Antibiofilm Activity Against Clinical Isolates

As shown in **Supplementary Figure 1**, biofilm formations by all clinical isolates were reduced in the presence

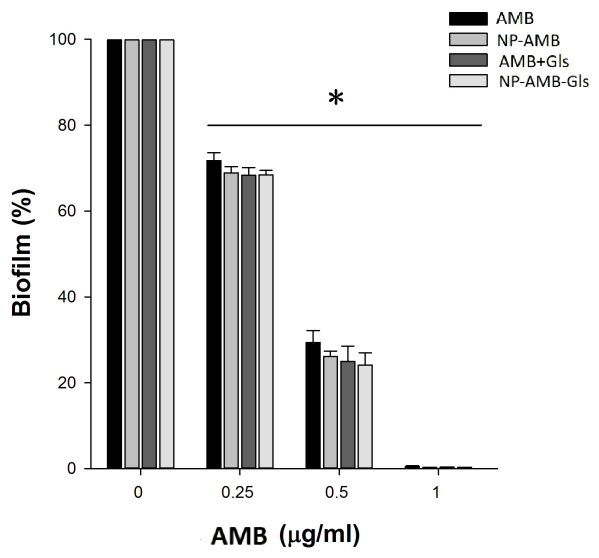


**FIGURE 4 |** Inhibition efficacy on the biofilm in a 96-well microplate. *Candida albicans* DAY 185 cells were co-incubated with free AMB, AMB+Gls, CSNPs-AMB, and CSNPs-AMB-Gls with different drug concentrations (0, 0.25, 0.5, and 1 μg/ml) for 24 h. The results represent the means and standard deviations (SDs) (error bars), $n = 3$. Statistical significance was determined by the *t*-test analysis. $^*p < 0.05$ for comparison between the untreated and treated groups.

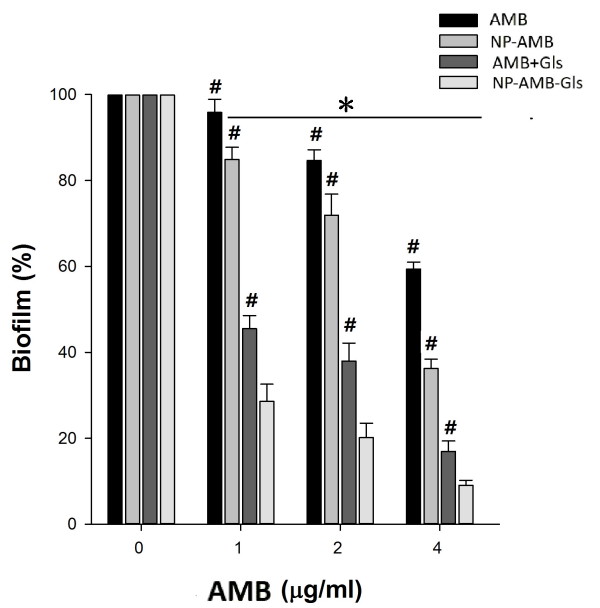


**FIGURE 5 |** Eradication efficacy of NPs on the mature biofilm by *C. albicans* DAY 185 in a 96-well microplate. Mature biofilms were treated with different concentrations (0, 1, 2, and 4 μg/ml) of free AMB, AMB+Gls, CSNPs-AMB, and CSNPs-AMB-Gls for 24 h. The results represent the means and SDs (error bars), $n = 3$. Statistical significance was determined by the *t*-test analysis. $^*p < 0.05$ for a comparison between the untreated and treated groups. $\#p < 0.05$ for a comparison between CSNPs-AMB-Gls and other treated groups.

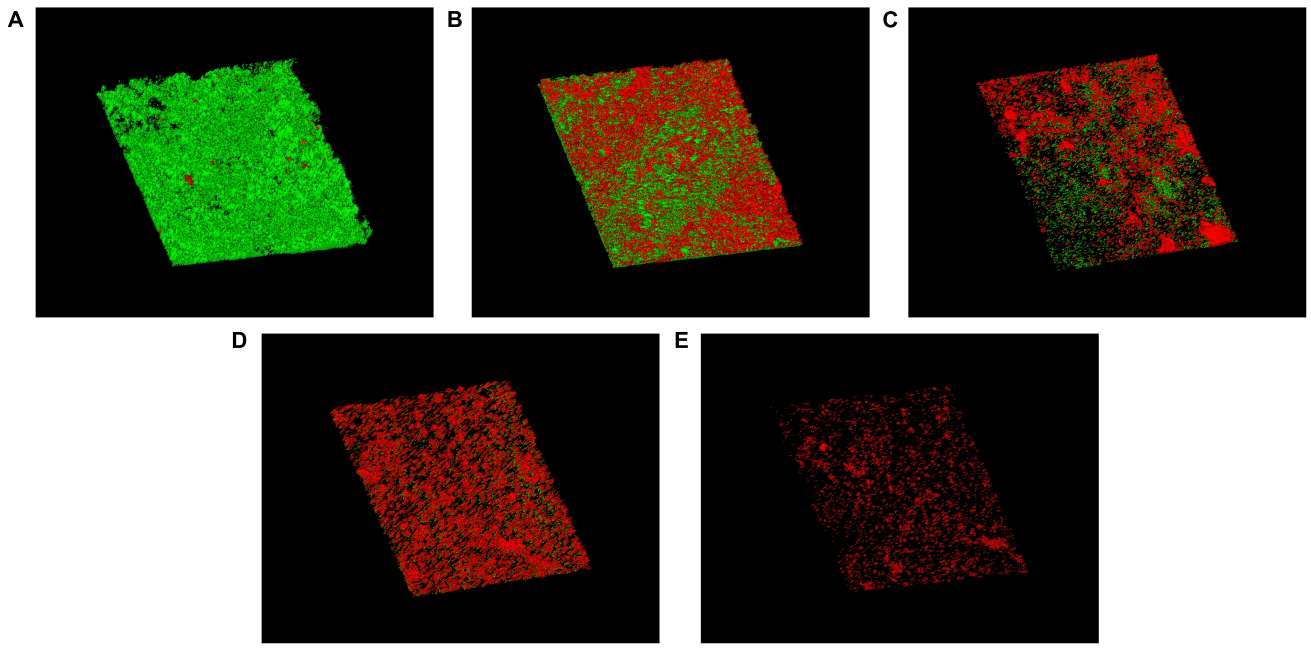


**FIGURE 6 |** CLSM images of biofilms on untreated **(A)** or free AMB **(B)**, CSNPs-AMB **(C)**, AMB+Gls **(D)**, and CSNPs-AMB-Gls **(E)** treated silicone surfaces. Biofilms were stained with the Live/Dead® BacLight™ Bacterial Viability and Counting kit. CLSM reconstructions show the three-dimensional staining pattern for live cells (SYTO-9, green) and dead cells (propidium iodide, red). Magnification, ×10.

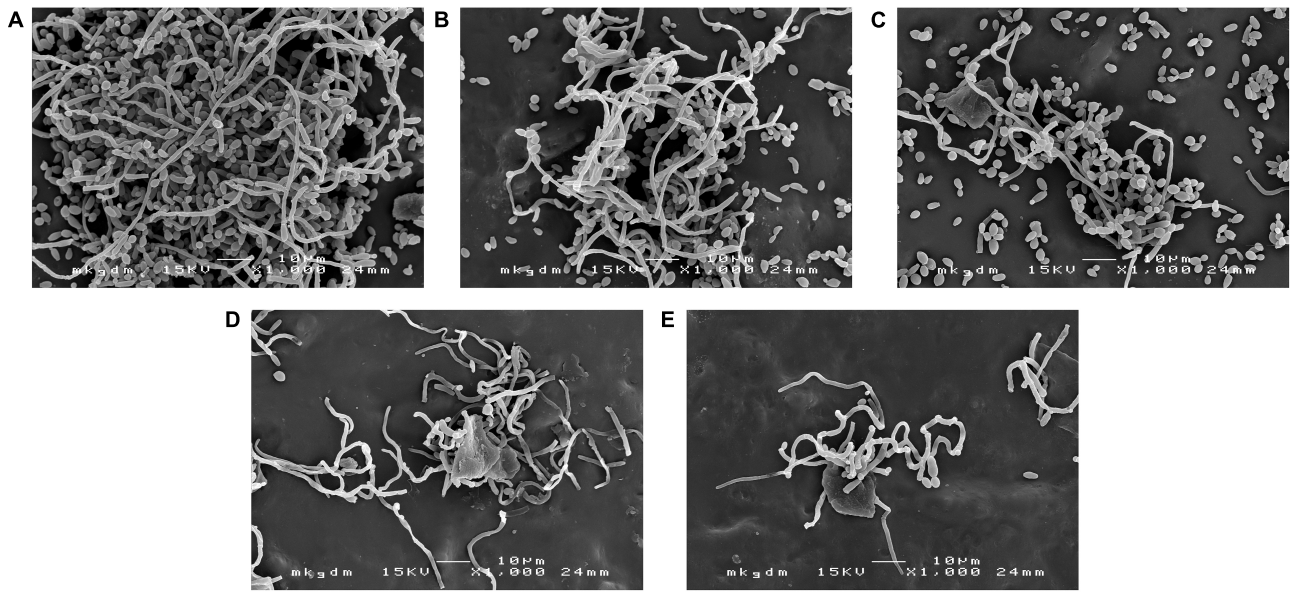


**FIGURE 7 |** SEM images of the biofilm by *C. albicans* DAY 185 on untreated **(A)** or free AMB **(B)**, CSNPs-AMB **(C)**, AMB+Gls **(D)**, and CSNPs-AMB-Gls **(E)** treated silicone surfaces.

of free AMB, AMB+Gls, CSNPs-AMB, and CSNPs-AMB-Gls (4 × MIC). CSNPs-AMB-Gls exhibited the best antibiofilm activity, which reduced 74.5, 85.2, and 59.5% biofilms of the clinical isolates BF1, BF2, and BF3, respectively.

## DISCUSSION

Recently, NPs have been employed to protect antibiofilm agents from drug sequestration and improve penetration into the matrix, so as to enhance the therapeutic effect for treating

biofilms. Here, CSNPs were functionalized with Gls and loaded with AMB to develop a new antibiofilm strategy until now.

In this work, AMB from CSNPs-AMB-Gls showed an initial burst release phase followed by a sustained release phase. This release mode is more suitable for the removal of biofilms. Because the initial burst release means a higher initial drug dose, which will reduce microbial drug tolerance (Cheow et al., 2010; Forier et al., 2014).

It has been reported that positively charged NPs could bind to negatively charged bacterial biofilm matrix components (Nafee et al., 2014; Baelo et al., 2015). Moreover, CS has the ability of penetrating into biofilms (Lu et al., 2014; Pu et al., 2014). Here, the proven ability to penetrate biofilms facilitates CSNPs to be a good drug carrier, which can carry drugs to penetrate into the biofilm as well and kill the inner cells.

For biofilm inhibition efficacy, Gls alone exhibited no obvious inhibition and CSNPs-AMB-Gls was not able to enhance the inhibition efficacy of biofilm formation relative to CSNPs-AMB. In addition, AMB alone or whenever driven with CSNPs (at all concentrations) showed similar efficacy on biofilm formation and planktonic cells, because the drug could kill planktonic fungi directly before biofilm formation.

In the preformed biofilm, our results exhibited a better eradication activity of CSNPs-AMB and CSNPs-AMB-Gls than free AMB and AMB+Gls, which indicated the superiority of NPs for biofilm treatment. NPs can protect the loaded antimicrobial agents from drug sequestration by the biofilm matrix (Forier et al., 2013; Koo et al., 2017). Moreover, NPs can deliver the drug into the biofilm matrix and directly target the microbial cells in the biofilm so as to maximize the therapeutic benefit. AMB+Gls and CSNPs-AMB-Gls showed a better detachment activity than free AMB and CSNPs-AMB, which suggested the synergistic efficacy of Gls.

β-1,3-glucan in *C. albicans* biofilm is considered to contribute to the resistance of antifungal drugs. As one of the important matrix components, β-1,3-glucan can protect cells in the biofilm by sequestering drugs (Nett et al., 2007). Similar functions of β-1,3-glucan have also been found in other *Candida* species (Tan et al., 2017). Therefore, the degradation of β-1,3-glucan resulted in the disruption of the biofilm matrix, and then improved AMB efficiency. This result is also consistent with our previous work (Tan et al., 2017, 2018). It can be ascribed to that Gls could disassemble the biofilm structure, which facilitates the mobility of positively charged NPs and binds to negatively charged biofilm components, thus providing high local concentrations of AMB to enhance the antibiofilm activity. Similarly, it has also been reported that the antibiofilm effect of antibiotic-containing NPs can be enhanced if the biofilm matrix was degraded by enzymes, such as DNase (Pu et al., 2014; Baelo et al., 2015). This interpretation could be further strengthened by SEM and CLSM images. CSNPs-AMB-Gls was more effective in killing *C. albicans* DAY 185 cells and disassembling the biofilm structure, which indicated the CSNPs-AMB-Gls better disrupted the biofilm matrix and thus increased killing of fungal cells.

Standardized and idealized laboratory conditions might make the microbe to lose some important pathophysiological characteristics when they are subcultured for decades (Fux et al., 2005). Thus, in our work, clinically isolated specimens were used to mirror clinical efficacy. The results demonstrate that CSNPs-AMB-Gls can disrupt clinically isolated biofilms as well as standard strain biofilms.

## CONCLUSION

In this study, we developed a biodegradable functional CSNP by loading AMB and Gls. CSNPs-AMB-Gls was homogeneously dispersed with a positive surface zeta potential. CSNPs-AMB-Gls was active in killing *C. albicans* cells and inhibiting biofilm formation, in addition to retaining the ability of Gls to disrupt the biofilm matrix. Excitingly, CSNPs-AMB-Gls exhibited the highest antibiofilm activity compared to free AMB and CSNPs-AMB in the mature biofilm. Although the assessment of biocompatibility and efficacy *in vivo* still needs to be evaluated, our studies pave the way for the application of CSNPs-AMB-Gls to treat *C. albicans* biofilm-related infections. Moreover, CSNPs-AMB-Gls can be employed as a platform to design more functions such as new drug delivery systems.

## DATA AVAILABILITY STATEMENT

The original contributions and additional information presented in the study are included in the article/**Supplementary Material**, further inquiries can be directed to the corresponding author.

## AUTHOR CONTRIBUTIONS

YT contributed to the conception of the study and finalized the manuscript. SM performed the experiment data and wrote the manuscript. JX contributed to analysis and manuscript preparation. RL helped to perform the analysis with constructive discussion. TD contributed to data analysis and manuscript editing. JL helped to edit the manuscript and evaluate the data. All authors contributed to the article and approved the submitted version.

## FUNDING

This research was funded by the Young Taishan Scholars Program of Shandong Province (tsqn202103094).

## SUPPLEMENTARY MATERIAL

The Supplementary Material for this article can be found online at: https://www.frontiersin.org/articles/10.3389/fmicb.2022.815091/full#supplementary-material

**Supplementary Figure 1 |** Antibiofilm activity against clinical isolates. The results represent the means and standard deviations (SDs; error bars) of three independent experiments. Statistical significance was determined by a *t*-test analysis. $*p < 0.05$ for a comparison between the untreated and treated groups. $\#p < 0.05$ for a comparison between chitosan nanoparticle (CSNP) loaded with Amphotericin B (AMB), which were functionalized with β-1,3-glucanase (Gls) (CSNP-AMB-Gls) and other treated groups.

## REFERENCES


Baelo, A., Levato, R., Julian, E., Crespo, A., Astola, J., Gavalda, J., et al. (2015). Disassembling bacterial extracellular matrix with DNase-coated nanoparticles to enhance antibiotic delivery in biofilm infections. *J. Control. Release* 209, 150–158. doi: 10.1016/j.jconrel.2015.04.028

Benincasa, M., Pacor, S., Wu, W., Prato, M., Bianco, A., and Gennaro, R. (2011). Antifungal activity of Amphotericin B conjugated to carbon nanotubes. *ACS Nano* 5, 199–208. doi: 10.1021/nn1023522

Benoit, D., Sims, K. R., and Fraser, D. (2019). Nanoparticles for oral biofilm treatments. *ACS Nano* 13, 4869–4875. doi: 10.1021/acsnano.9b02816

Cheow, W. S., Chang, M. W., and Hadinoto, K. (2010). Antibacterial efficacy of inhalable levofloxacin-loaded polymeric nanoparticles against *E. coli* biofilm cells: the effect of antibiotic release profile. *Pharm. Res.* 27, 1597–1609. doi: 10.1007/s11095-010-0142-6

De Brucker, K., Tan, Y., Vints, K., De Cremer, K., Braem, A., Verstraeten, N., et al. (2015). Fungal β-1,3-glucan increases ofloxacin tolerance of *Escherichia coli* in a polymicrobial *E. coli*/*Candida albicans* biofilm. *Antimicrob. Agents Chemother.* 59, 3052–3058. doi: 10.1128/AAC.04650-14

Flemming, H.-C., Wingender, J., Szewzyk, U., Steinberg, P., Rice, S. A., and Kjelleberg, S. (2016). Biofilms: an emergent form of bacterial life. *Nat. Rev. Microbiol.* 14, 563–75. doi: 10.1038/nrmicro.2016.94

Forier, K., Messiaen, A.-S., Raemdonck, K., Deschout, H., Rejman, J., De Baets, F., et al. (2013). Transport of nanoparticles in cystic fibrosis sputum and bacterial biofilms by single-particle tracking microscopy. *Nanomedicine* 8, 935–949. doi: 10.2217/nnm.12.129

Forier, K., Raemdonck, K., De Smedt, S. C., Demeester, J., Coenye, T., and Braeckmans, K. (2014). Lipid and polymer nanoparticles for drug delivery to bacterial biofilms. *J. Control. Release* 190, 607–623. doi: 10.1016/j.jconrel.2014.03.055

Fux, C. A., Shirtliff, M., Stoodley, P., and Costerton, J. W. (2005). Can laboratory reference strains mirror 'real-world' pathogenesis? *Trends Microbiol.* 13, 58–63. doi: 10.1016/j.tim.2004.11.001

Gottardo, B., Lemes, T. H., Byzynski, G., Paziani, M. H., Von-Zeska-Kress, M. R., Almeida, M. D., et al. (2019). One-pot synthesis and antifungal activity of nontoxic silver-loaded hydroxyapatite nanocomposites against *Candida* species. *ACS Appl. Nano Mater.* 2, 2112–2120. doi: 10.1021/acsanm.9b00091

Jamil, B., Bokhari, H., and Imran, M. (2017). Mechanism of action: how nano-antimicrobials act? *Curr. Drug Targets* 18, 363–373. doi: 10.2174/1389450116666151019101826

Jamil, B., Habib, H., Abbasi, S. A., Ihsan, A., Nasir, H., and Imran, M. (2016). Development of cefotaxime impregnated chitosan as nano-antibiotics: de novo strategy to combat biofilm forming multi-drug resistant pathogens. *Front. Microbiol.* 7:330. doi: 10.3389/fmicb.2016.00330

Kimura, Y., and Urata, M. (2016). Characterization of a eukaryotic-like protein kinase, DspB, with an atypical catalytic loop motif from *Myxococcus xanthus*. *Arch. Microbiol.* 198, 219–226. doi: 10.1007/s00203-015-1181-5

Klinger-Strobel, M., Ernst, J., Lautenschläger, C., Pletz, M. W., Fischer, D., and Makarewicz, O. (2016). A blue fluorescent labeling technique utilizing micro- and nanoparticles for tracking in LIVE/DEAD® stained pathogenic biofilms of *Staphylococcus aureus* and *Burkholderia cepacia*. *Int. J. Nanomedicine* 11, 575–83. doi: 10.2147/IJN.S98401

Koo, H., Allan, R. N., Howlin, R. P., Stoodley, P., and Hall-Stoodley, L. (2017). Targeting microbial biofilms: current and prospective therapeutic strategies. *Nat. Rev. Microbiol.* 15, 740–755. doi: 10.1038/nrmicro.2017.99

Limoli, D. H., Jones, C. J., and Wozniak, D. J. (2015). Bacterial extracellular polysaccharides in biofilm formation and function. *Microbiol. Spectr.* 3:2014. doi: 10.1128/microbiolspec.MB-0011-2014

Lohse, M. B., Gulati, M., Johnson, A. D., and Nobile, C. J. (2017). Development and regulation of single- and multi-species *Candida albicans* biofilms. *Nat. Rev. Microbiol.* 16, 19–31. doi: 10.1038/nrmicro.2017.107

Lu, Y., Slomberg, D. L., and Schoenfisch, M. H. (2014). Nitric oxide-releasing chitosan oligosaccharides as antibacterial agents. *Biomaterials* 35, 1716–1724. doi: 10.1016/j.biomaterials.2013.11.015

MacDonald, R., Santa, M., and Brozel, V. S. (2000). The response of a bacterial biofilm community in a simulated industrial cooling water system to treatment with an anionic dispersant. *J. Appl. Microbiol.* 89, 225–235. doi: 10.1046/j.1365-2672.2000.01099.x

Martinez, L. R., Mihu, M. R., Han, G., Frases, S., Cordero, R. J., Casadevall, A., et al. (2010). The use of chitosan to damage *Cryptococcus neoformans* biofilms. *Biomaterials* 31, 669–679. doi: 10.1016/j.biomaterials.2009.09.087

Mitchell, K. F., Zarnowski, R., and Andes, D. R. (2016). Fungal super glue: the biofilm matrix and its composition, assembly, and functions. *PLoS Pathog.* 12:e1005828. doi: 10.1371/journal.ppat.1005828

Nafee, N., Husari, A., Maurer, C. K., Lu, C., de Rossi, C., Steinbach, A., et al. (2014). Antibiotic-free nanotherapeutics: ultra-small, mucus-penetrating solid lipid nanoparticles enhance the pulmonary delivery and anti-virulence efficacy of novel quorum sensing inhibitors. *J. Control. Release* 192, 131–140. doi: 10.1016/j.jconrel.2014.06.055

Nani, B. D., Sardi, J., Lazarini, J. G., Silva, D. R., and Rosalen, P. L. (2019). Anti-inflammatory and anti-*Candida* effects of Brazilian organic propolis, a promising source of bioactive molecules and functional food. *J. Agric. Food Chem.* 68, 2861–2871. doi: 10.1021/acs.jafc.8b07304

Nett, J., Lincoln, L., Marchillo, K., Massey, R., Holoyda, K., Hoff, B., et al. (2007). Putative role of β-1,3 glucans in *Candida albicans* biofilm resistance. *Antimicrob. Agents Chemother.* 51, 510–520. doi: 10.1128/AAC.01056-06

Nieto, J., Alvar, J., Rodriguez, C., San Andres, M. I., San Andres, M. D., and Gonzalez, F. (2018). Comparison of conventional and lipid emulsion formulations of amphotericin B: pharmacokinetics and toxicokinetics in dogs. *Res. Vet. Sci.* 117, 125–132. doi: 10.1016/j.rvsc.2017.12.005

Okshevsky, M., and Meyer, R. L. (2015). The role of extracellular DNA in the establishment, maintenance and perpetuation of bacterial biofilms. *Crit. Rev. Microbiol.* 41, 341–352. doi: 10.3109/1040841X.2013.841639

Piccinelli, A. L., Pagano, I., Esposito, T., Mencherini, T., Porta, A., Petrone, A. M., et al. (2016). HRMS Profile of a hazelnut skin proanthocyanidin-rich fraction with antioxidant and anti-*Candida albicans* activities. *J. Agric. Food Chem.* 64, 585–595. doi: 10.1021/acs.jafc.5b05404

Pu, Y., Liu, A., Zheng, Y., and Ye, B. (2014). *In vitro* damage of *Candida albicans* biofilms by chitosan. *Exp. Ther. Med.* 8, 929–934. doi: 10.3892/etm.2014.1839

Quiñones, J. P., Peniche, H., and Peniche, C. (2018). Chitosan based self-assembled nanoparticles in drug delivery. *Polymers (Basel)* 10:235. doi: 10.3390/polym10030235

Rajendran, R., Sherry, L., Nile, C. J., Sherriff, A., Johnson, E., Hanson, M., et al. (2016). Biofilm formation is a risk factor for mortality in patients with *Candida albicans* bloodstream infection-Scotland, 2012-2013. *Clin. Microbiol. Infect.* 22, 87–93. doi: 10.1016/j.cmi.2015.09.018

Rajkowska, K., and Kunicka-Styczyńska, A. (2018). Typing and virulence factors of food-borne *Candida* spp. isolates. *Int. J. Food Microbiol.* 279, 57–63. doi: 10.1016/j.ijfoodmicro.2018.05.002

Steimbach, L. M., Tonin, F. S., Virtuoso, S., Borba, H. H., Sanches, A. C., Wiens, A., et al. (2017). Efficacy and safety of amphotericin B lipid-based formulations-a systematic review and meta-analysis. *Mycoses* 60, 146–154. doi: 10.1111/myc.12585

Tan, Y., Leonhard, M., Ma, S., Moser, D., and Schneider-Stickler, B. (2017). Dispersal of single and mixed non-albicans *Candida* species biofilms by β-1,3-glucanase in vitro. *Microb. Pathog.* 113, 342–347. doi: 10.1016/j.micpath.2017.10.057

Tan, Y., Ma, S., Leonhard, M., Moser, D., and Schneider-Stickler, B. (2018). β-1,3-glucanase disrupts biofilm formation and increases antifungal susceptibility of *Candida albicans* DAY185. *Int. J. Biol. Macromol.* 108, 942–946. doi: 10.1016/j.ijbiomac.2017.11.003

Trapani, A., Sitterberg, J., Bakowsky, U., and Kissel, T. (2009). The potential of glycol chitosan nanoparticles as carrier for low water soluble drugs. *Int. J. Pharm.* 375, 97–106. doi: 10.1016/j.ijpharm.2009.03.041

Vikelouda, A., Simitsopoulou, M., Kechagioglou, P., Papi, R., Kyriakidis, D., and Roilides, E. (2017). Antifungal activity of functionalized carbon nanotubes conjugated to Amphotericin-B against *Candida albicans* and *Candida parapsilosis* biofilms. *Mycoses* 60, 85–85. doi: 10.1021/nn1023522

Wall, G., Montelongo-Jauregui, D., Bonifacio, B. V., Lopez-Ribot, J. L., and Uppuluri, P. (2019). *Candida albicans* biofilm growth and dispersal: contributions to pathogenesis. *Curr. Opin. Microbiol.* 52, 1–6. doi: 10.1016/j.mib.2019.04.001

Weiler, S., Bellmann-Weiler, R., Dunzendorfer, S., Joannidis, M., and Bellmann, R. (2008). Levels of amphotericin B lipid formulations in ascites. *J. Antimicrob. Chemother.* 62, 1163–1164. doi: 10.1093/jac/dkn306

Weiler, S., Falkensammer, G., Hammerer-Lercher, A., Anliker, M., Vogelsinger, H., Joannidis, M., et al. (2009). Pulmonary epithelial lining fluid concentrations after use of systemic amphotericin B lipid formulations. *Antimicrob. Agents Chemother.* 53, 4934–4937. doi: 10.1128/AAC.00796-09

**Conflict of Interest:** The authors declare that the research was conducted in the absence of any commercial or financial relationships that could be construed as a potential conflict of interest.

**Publisher's Note:** All claims expressed in this article are solely those of the authors and do not necessarily represent those of their affiliated organizations, or those of the publisher, the editors and the reviewers. Any product that may be evaluated in this article, or claim that may be made by its manufacturer, is not guaranteed or endorsed by the publisher.

frontiers | Frontiers in Microbiology

ORIGINAL RESEARCH
published: 12 July 2022
doi: 10.3389/fmicb.2022.913882

# Curvularin Isolated From *Phoma macrostoma* Is an Antagonist of RhlR Quorum Sensing in *Pseudomonas aeruginosa*

*Ha-Young Choi[1,2], Duc Dat Le[1] and Won-Gon Kim[1,2]**

[1]Infectious Disease Research Center, Korea Research Institute of Bioscience and Biotechnology, Daejeon, South Korea, [2]Department of Bio-Molecular Science, KRIBB School of Bioscience, Korea University of Science and Technology (UST), Daejeon, South Korea

Quorum sensing (QS) is an attractive target for the treatment of multidrug-resistant *Pseudomonas aeruginosa*, against which new antibiotics are urgently needed. Because LasR is at the top of the QS hierarchy controlling Rhl and PQS systems, most QS inhibitors have been targeted to LasR. However, it has recently been reported that in clinical isolates of *P. aeruginosa*, LasR is frequently mutated and nonfunctional, and RhlR independently acts to produce virulent factors that maintain toxicity. Thus, for effective treatment of chronic cystic fibrosis infections, RhlR antagonists is needed to prevent the LasR-independent Rhl system, but RhlR antagonists have rarely been reported. In this study, we found that curvularin, an aromatic compound with a cyclized alkyl side chain isolated from *Phoma macrostoma*, at a low micromolar concentration of 1–30 μM potently and selectively inhibited pyocyanin and rhamnolipid production without affecting the cell viability of *P. aeruginosa*. Only high concentration (more over 100 μM) curvularin negligibly inhibited biofilm formation and elastase production, suggesting that curvularin at low concentrations selectively inhibits RhlR. The QS antagonism by curvularin was investigated in experiments using QS competition and signaling molecules assays with QS gene expression analysis, and the results showed that, indeed, at low concentrations, curvularin selectively antagonized RhlR; in contrast, it negligibly antagonized LasR only when applied at a high concentration. The exclusive RhlR antagonizing activity of curvularin at low concentrations was confirmed using QS mutants; specifically, curvularin at low concentrations inhibited pyocyanin and rhamnolipid production by selectively antagonizing N-butanoyl homoserine lactone (BHL)-activated RhlR. Moreover, by targeting RhlR, curvularin reduced the *in vivo* virulence of wild-type *P. aeruginosa* as well as *lasR* mutants in *Caenorhabditis elegans*. Overall, low-concentration curvularin is a pure RhlR antagonist in *P. aeruginosa*, and to the best of our knowledge, this is the first report describing an RhlR antagonist from natural resources. Hence, curvularin has great potential for the development of chronic *P. aeruginosa* infection therapeutics and for the study of RhlR function in the complex QS system.

**Keywords: anti-quorum sensing, curvularin, RhlR, antagonist, *Pseudomonas aeruginosa***

OPEN ACCESS

***Edited by:***
*Laura Quintieri, Italian National Research Council, Italy*

***Reviewed by:***
*Jintae Lee, Yeungnam University, South Korea*
*Song Lin Chua, Hong Kong Polytechnic University, Hong Kong SAR, China*

****Correspondence:***
*Won-Gon Kim*
*wgkim@kribb.re.kr*

***Specialty section:***
*This article was submitted to Antimicrobials, Resistance and Chemotherapy, a section of the journal Frontiers in Microbiology*

***Received:*** *06 April 2022*
***Accepted:*** *20 June 2022*
***Published:*** *12 July 2022*

***Citation:***
*Choi H-Y, Le DD and Kim W-G (2022) Curvularin Isolated From Phoma macrostoma Is an Antagonist of RhlR Quorum Sensing in Pseudomonas aeruginosa. Front. Microbiol. 13:913882. doi: 10.3389/fmicb.2022.913882*

## INTRODUCTION

*Pseudomonas aeruginosa* is a ubiquitous Gram-negative bacterium that causes many opportunistic and nosocomial infections. In particular, chronic lung infections by *P. aeruginosa* are the leading causes of mortality in cystic fibrosis (CF) patients (Finnan et al., 2004). The World Health Organization recently placed it in the 12 antibiotic-resistant "priority pathogens" (Donlan and Costerton, 2002; Davies, 2003; World Health Organization, 2017). *Pseudomonas aeruginosa* produces several virulence factors including elastase, rhamnolipid, and pyocyanin, and also forms thick biofilm in the CF lung that leads to high resistance to existing antibiotics (Davies, 2003). As most virulence traits are non-essential for bacterial survival, inhibition of bacterial virulence is an emerging strategy that does not lead to high-selective pressure and thus is less likely to cause bacterial resistance (Rasko and Sperandio, 2010; Whiteley et al., 2017).

Quorum sensing (QS) is a type of bacterial cell–cell communication through diffusible molecules called autoinducers that regulate collective behaviors such as the secretion of virulence factors, biofilm formation, bioluminescence, and antibiotic resistance (Ng and Bassler, 2009; Rutherford and Bassler, 2012; Papenfort and Bassler, 2016). QS in *P. aeruginosa* consists of three main QS systems: *las*, *rhl*, and *pqs*. Each QS system expresses autoinducer-synthesis genes, such as *lasI*, *rhlI*, and *pqsABCD*, as well as cognate-regulatory genes, including *lasR*, *rhlR*, and *pqsR* (Papenfort and Bassler, 2016). The acyl homoserine lactone (AHL) synthases LasI and RhlI produce N-(3-oxododecanoyl)-l-homoserine lactone (OdDHL) and N-butanoyl homoserine lactone (BHL), respectively, as signaling molecules whereas the quinolone synthase PqsABCD synthesizes 2-heptyl-3-hydroxy-4(1H) quinolone (PQS). The three QS systems are hierarchically regulated. Upon activation by OdDHL, the LasR-OdDHL complex activates the expression of the *rhl* and *pqs* QS systems and directs the gene expression of biofilm components and virulence factors, such as elastase (Lee and Zhang, 2015; Papenfort and Bassler, 2016). The RhlR-BHL complex, in turn, controls many QS-dependent virulence factors, such as rhamnolipid and pyocyanin. The PqsR-PQS complex direct the expression of gene cascades associated with the PQS system and virulence factors, such as pyocyanin and rhamnolipids (Jimenez et al., 2012; Lee and Zhang, 2015). Recently, 2-(2-hydroxyphenyl) thiazole-4-carbaldehyde (IQS), has been reported to be a fourth QS signaling molecule (Lee et al., 2013). The relationship between QS and biofilm formation is not fully understood (Papenfort and Bassler, 2016). The Las system is known to regulate the synthesis of exopolysaccharides, which forms the biofilm matrix (Sakuragi and Kolter, 2007). Rhamnolipids, RhlR-activated exoproducts, have been reported to be involved in the architectural development and dispersal of biofilms (Davey et al., 2003; Boles et al., 2005). Thus, the Las system appears to participate in the biofilm formation, while the Rhl system participates in the biofilm maintenance and dispersal.

LasR is at the top of the QS hierarchy in *P. aeruginosa* and activates the RhlR and PqsR pathways (Latifi et al., 1996; Pesci et al., 1997). Thus, LasR has been a primary target in the development of QS antagonists designed to prevent *P. aeruginosa* infections (Galloway et al., 2011; Welsh and Blackwell, 2016). However, mutations in *lasR* are common in *P. aeruginosa* in the lungs of chronically infected patients (Smith et al., 2006; Hoffman et al., 2009; Bjarnsholt et al. 2010). Notably, in the LasR mutants from chronic patients, RhlR independently expresses QS-regulated phenotypes, such as C4-HSL signaling molecules and virulent factors (Bjarnsholt et al. 2010; Feltner et al., 2016). In contrast, *rhlR* mutations are rare in CF lung infections. It has been reported that RhlR mutants are not viable because RhlR mutants are sensitive to cyanide produced by both LasR and PqsR mutants which are resistant to cyanide (Chen et al., 2019). Thus, for effective treatment of chronic CF infections, RhlR antagonists is needed to prevent the LasR-independent Rhl system, which is a functioning QS system in chronic *P. aeruginosa* infections (Whiteley et al., 2017). However, only a few RhlR antagonists have been reported. Recently, N-cyclopentylbutyramide (CPBA) and 1-(3,4-difluorophenyl)hex-1-yn-3-one (DFPH), which are synthetic derivatives of AHL and 4-gingerol, respectively, were reported to be RhlR antagonists (Eibergen et al., 2015; Boursier et al., 2018; Nam et al., 2020). We have also reported RhlR-selective inhibiting activity of hexyl gallate (HG) which is a synthetic alkyl ester derivative of gallate (Kim et al. 2019).

In this study, while screening for an inhibitor of *P. aeruginosa* pyocyanin production from microbial fermentation extract library, we found that fermentation extracts of a soil fungus, *Phoma macrostoma* FN413, reduced pyocyanin and rhamnolipid production but, interestingly, did not inhibit biofilm formation or elastase production in *P. aeruginosa*. This phenotype was similar to that of HG, but different from that of CPBA and DFPH that also inhibits biofilm formation. This discrepancy led to the isolation of an active compound from culture extracts, and an investigation into the QS antagonizing activity of this compound and the relationship between certain QS and virulent factors. Here, we report that curvularin is a highly RhlR-selective antagonist against *P. aeruginosa* infections, exhibiting a greater effects than that reported for other RhlR antagonists (**Figure 1**). To the best of our knowledge, curvularin is the first RhlR antagonist to be isolated from natural resources.

## MATERIALS AND METHODS

### Bacterial Strains and Reagents

The bacterial strains used in this study were *Agrobacterium tumefaciens* NT1, *Chromobacterium violaceum* CV026, *P. aeruginosa* PA14, and *P. aeruginosa* PA14 mutants (Δ*lasR*, Δ*rhlR*, and Δ*pqsR*). All bacterial strains were grown in Luria-Bertani (LB) medium. Furanone C-30 (FC), CPBA, and clofoctol (CF) were purchased from Sigma-Aldrich (St. Louis, MO, United States).

### Molecular Identification of the Fungal Strain FN70413

The genomic DNA from cultured fungal strain FN70413 was extracted using the PureHelix™ Genomic Prep Kit (Catalog #GCTN200, NanoHelix, Daejeon, South Korea). 18S rDNA was

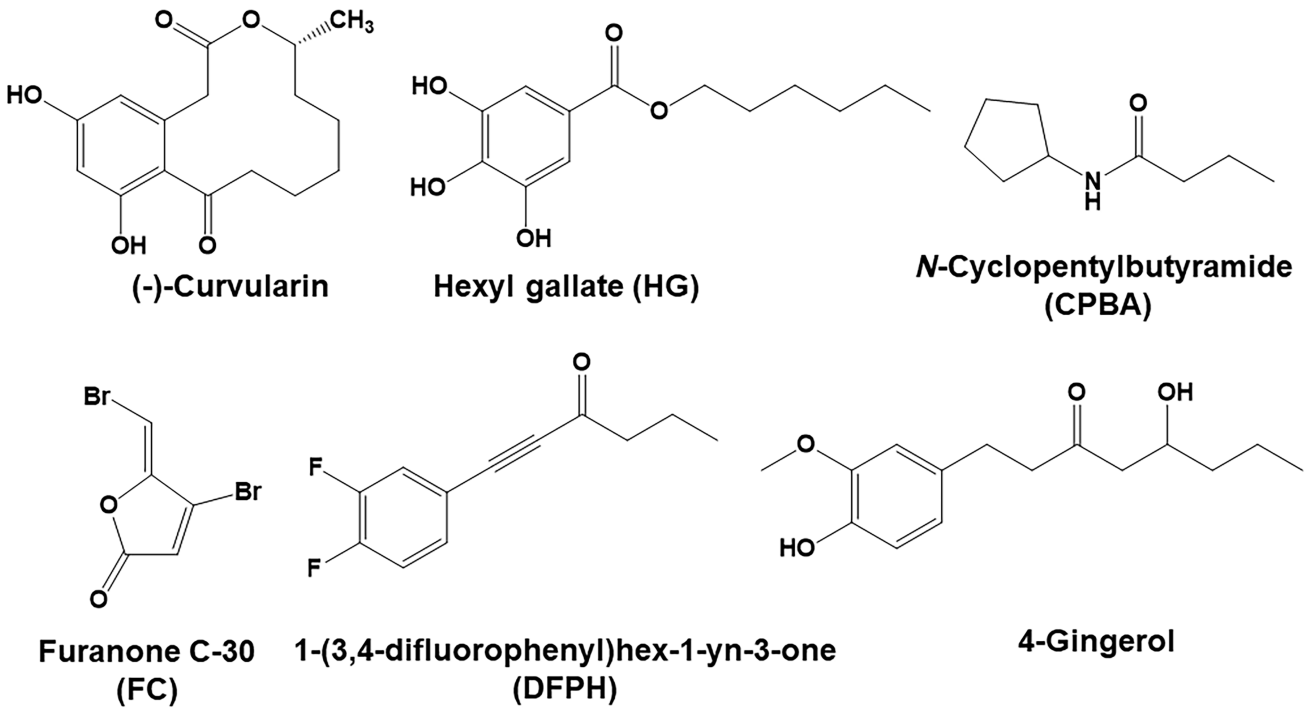


**FIGURE 1 |** (–)-Curvularin and related compounds.

amplified from the extracted gDNA by PCR using universal primer pairs of NS1 (5′-GTAGTCATATGCTTGTCTC-3′) and NS8 (5′-TCCGCAGGTTCACCTACGGA-3′). PCR reaction was carried out in 25 μl reaction volume containing 10 ng of gDNA, 2.5 mM $MgCl_2$, 0.5 μM of each primer (Macrogen, Seoul, South Korea), 200 μM of each dNTP, 0.5 U of Ex Taq DNA polymerase, and 1× Ex Taq PCR buffer (Takara, Otsu, Japan). PCR amplification were performed using a thermocycler (Dice Model TP600; Takara) under the following conditions: 94°C for 2 min, followed by 30 cycles of 94°C for 30 s, 45°C for 45 s, and 72°C for 1 min 30s with a final extension of 72°C for 5 min. The amplified PCR product was purified by PCR purification kit (Biofact, Daejeon, South Korea) and sequenced by Macrogen Inc., South Korea. Sequences were annotated and analyzed at BLAT to search the closet homolog.

## Pyocyanin Assay

The production of pyocyanin in *P. aeruginosa* PA14 was measured following a previously reported method with modification (Essar et al., 1990). *P. aeruginosa* PA14 was cultivated in LB medium overnight at 220 rpm at 37°C. The overnight cultures were diluted 100–fold in LB medium, and 0.15-ml aliquots of the diluted culture were dispensed in wells of a 96-well microtiter plate, and treated with test compounds dissolved in dimethyl sulfoxide (DMSO). After incubation at 37°C for 24 h, cell viability was assayed by measuring the optical density (OD) at 600 nm, followed by transfer of the culture medium to 2-mL Eppendorf tubes and centrifugation at 12,000 rpm at 4°C for 10 min. The supernatant was extracted with chloroform, and the chloroform layer was extracted with 0.2 N HCl. The OD of resultant aqueous fraction was measured at 520 nm.

## Rhamnolipid Assay

The production of rhamnolipid in *P. aeruginosa* PA14 was tested as previously described (Boles et al., 2005). After incubation overnight, *P. aeruginosa* PA14 cultures were diluted 100–fold in LB medium, and 5 ml of the diluted culture was dispensed into 50-ml conical tubes and treated with test compounds dissolved in DMSO. After incubation with rotation at 220 rpm at 37°C for 24 h, cell viability was assayed by measuring the OD at 600 nm, and the cultures were then centrifuged at 12,000 rpm at 4°C for 10 min. Then, 500 μl of supernatant was mixed with 500 μl of diethyl ether. The ether fraction was evaporated to dryness and dissolved in 500 μl of deionized water. Then, 100 μl of the water extract was mixed with 900 μl of Orcinol solution [0.19% Orcinol (Sigma) in 53% $H_2SO_4$]. The mixture was boiled for 30 min and cooled at room temperature for 15 min, and then the OD was measured at 421 nm with a microplate reader.

## Elastase Assay

The production of elastase in *P. aeruginosa* PA14 was assayed with Elastin-Congo red as previously described (Rust et al., 1994). *Pseudomonas aeruginosa* PA14 was cultured overnight in LB medium at 37°C with shaking. Then, the cultures were then diluted 1:100 with fresh LB medium, and the diluted culture was added at 0.1 ml/well in a 96-well microtiter plate, followed by treatment with test compounds dissolved in DMSO

and incubation for 24 h. After determination of cell viability by measuring the OD at 600 nm and subsequent centrifugation of the culture samples at 4,000 rpm for 10 min, the elastase activity in the culture supernatants was measured.

## Biofilm Assay

Biofilm formation in *P. aeruginosa* PA14 was measured as previously described (O'Toole, 2011). *Pseudomonas aeruginosa* PA14 was cultured overnight and then diluted 100-fold in M63 medium, and the diluted culture was dispensed at 0.1 ml/well in a 96-well polystyrene microplate. Test compounds or DMSO, as the negative control, were added to wells. After incubation at 37°C for 9 h without agitation, unattached cells and medium were removed, and the cells forming the biofilm, which remained attached to the well surface, were stained for 10 min with 120 μl of 0.1% crystal violet. The bound crystal violet was solubilized with 150 μl of 30% acetic acid in water for 15 min. The OD of the eluted crystal violet was measured at 550 nm with a microplate reader.

## QS Competition Assay

An AHL-based QS competition assay was performed using two reporter strains, namely, *A. tumefaciens* NT1 and *C. violaceum* CV026 (Park et al., 2006). Each strain was cultivated in LB medium overnight with a rotation of 220 rpm at 30°C and then diluted 20-fold. One milliliter of the diluted culture was then dispensed into a 15-mL conical tube, and 5 μl of X-gal (20 g/L) and 10 μl of 100 μM OdDHL (Sigma) were added to *A. tumefaciens* NT1 and 10 μl of 50 mM BHL (Cayman, Ann Arbor, MI, United States) was added to *C. violaceum* CV026. Ten microliters of each test compound dissolved in DMSO was added to the culture tubes and then incubated with 180 rpm rotation at 30°C for 36 h. After the cell viability was assayed by measuring the OD at 600 nm with a microtiter ELISA reader, color changes in *C. violaceum* CV026 and *A. tumefaciens* NT1 were measured at 590 and 545 nm, respectively.

## Measurement of QS Signaling Molecules and QS Gene Expression

QS signaling molecule production (Luo et al., 2017) and QS gene expression (Gi et al., 2014) were determined as previously described. *P. aeruginosa* PA14 was cultured and treated with test compounds following the same procedure used for the rhamnolipid assay. To measure three QS signaling molecules, 3 ml of culture supernatant was extracted with 3 ml of ethyl acetate acidified with 0.1% acetic acid, and then, the organic layer was evaporated and the remaining molecules were measured by liquid chromatography with tandem mass spectrometry (LC–MS/MS) with the spectrometer in MRM mode (Supporting Information). To determine QS gene expression, total RNA was extracted with TRIzol reagent (Invitrogen), and cDNA was then synthesized for real-time quantitative PCR (RT–qPCR) detection of target gene expression, followed by measurement *via* RT–qPCR on a Bio–Rad CFX-96 real-time PCR system (Bio–Rad, Hercules, CA, United States) with the primers listed in **Supplementary Table 1**. mRNA expression was normalized to the expression of the endogenous *rpoD* gene.

## *Caenorhabditis elegans* Life Span Assay

A *P. aeruginosa-C. elegans* infection assay was performed as previously described (O'Loughlin et al., 2013). *Caenorhabditis elegans* nematodes were propagated at 20°C for 48 h on nematode growth medium (NGM) plates containing a lawn of *E. coli* OP50 as a food source. Killing and control plates were established by spreading the overnight cultures of PA14 and OP50 cells, respectively, on a 35-mm petri plate with 4 ml of PGS agar. Test compounds dissolved in DMSO or DMSO as a negative control were added to the killing plates. The plates were then incubated at 37°C for 24 h to make a bacterial lawn and then transferred for incubation at 23°C for 24 h. Thirty L4-stage worms were placed on each plate and incubated at room temperature. The surviving nematodes were counted every 5 h for 30 h.

# RESULTS

## Screening and Isolation of an Inhibitor of Pyocyanin Production That Displayed a Phenotype Similar to a RhlR Antagonist

Screening of 3,696 microbial fermentation extracts were performed for inhibitors of pyocyanin production in *P. aeruginosa* PA14 that resulted in selection of 25 strains. Among these identified strains, the fermentation extracts of only the fungal strain FN70413, which was isolated from forest soil, inhibited the production of pyocyanin and rhamnolipid without affecting cell viability; interestingly, it did not inhibit biofilm formation by PA14. This phenotype was similar to that of HG, which we have previously reported to an RhlR-selective antagonist, but differs from that of the other reported RhlR antagonists, namely, CPBA and DFPH, which have been reported to exhibit antibiofilm activity. Additionally, the extracts inhibited pyocyanin production by a *lasR* mutant of the PA14 strain, and this inhibition was reversed when cultures were supplemented with exogenous BHL, but not with OdDHL or PQS (data not shown), suggesting that RhlR was selectively inhibited by factors in the extract fraction (Kim et al. 2019). Thus, an active compound was isolated from the culture extracts of the fungal strain *via* bioassay-guided fractionation and then identified as (−)-curvularin by mass and NMR spectral analysis; in addition, a specific rotation value ($[\alpha]_D$, −23.8, *c* 0.1, MeOH) was obtained, and it was almost the same as the value ($[\alpha]_D$, −23.4, *c* 0.1, MeOH) reported in the literature (Allu et al., 2019; **Supplementary Figures 1**, **2**; **Supplementary Table 2**). The purity of isolated curvularin was determined to be 98.3% at 220 nm by analytical HPLC (**Supplementary Figure 3**). The fungal strain FN70413 was identified as *Phoma macrostoma* using phylogenetic analysis based on 18S rDNA.

## Effect of Curvularin on Virulence Factor Production and Biofilm Formation

To determine whether curvularin selectively inhibits virulence factor production, the effects of curvularin on the production

of virulence factors, including pyocyanin, rhamnolipid and elastase, in PA14 cells were investigated. The effect of curvularin on cell viability was also examined using an optical-density-based assay of each virulence factor. Curvularin inhibited the production of pyocyanin in a concentration-dependent manner without affecting the cell growth of the PA14 strain (**Figure 2A**). Treatment with 3 and 30 μM curvularin for 24 h significantly inhibited pyocyanin production, by 31.3% and 63.2%, respectively, and this inhibitory effect was approximately three times greater than that induced by 10 and 100 μM CPBA, which reduced production by 39.2% and 60.2%, respectively, compared with pyocyanin production in untreated PA14 cells. Similarly, rhamnolipid production was significantly inhibited, by 22.8% and 66.1%, respectively, in the presence of 3 and 30 μM curvularin for 24 h, and this effect was approximately threefold greater than that induced by 10 and 100 μM CPBA, which inhibited rhamnolipid production by 38.5% and 58.4%, respectively, compared with the rhamnolipid production by the untreated cells (**Figure 2B**). Similarly, curvularin also showed more than threefold greater inhibition of pyocyanin and rhamnolipid production than the inhibition induced by HG (**Supplementary Figures 4A,B**). FC, a known LasR antagonist, exhibited inhibitory activity similar to that of curvularin.

Interestingly, at low concentrations of 1–30 μM curvularin did not inhibit elastase production, although pyocyanin and rhamnolipid production was dramatically reduced, whereas low–concentration FC, as a positive control, showed a strong inhibition as expected. However, treatment with curvularin at high concentrations, more than 100 μM, led to very weak inhibition of elastase production (**Figure 2C**). Elastase production by PA14 cells in the presence of 100 and 300 μM curvularin for 24 h was inhibited by 8.1% and 11.3%, respectively, compared to the production by untreated PA14 cells. Interestingly, at low concentrations, CPBA significantly inhibited elastase production. For example, elastase production in the presence of 3 and 30 μM CPBA for 24 h was inhibited by 8.9% and 16.1%, respectively, compared to the production by untreated PA14 cells. Similar to its effects on elastase, low-level curvularin did not affect biofilm formation, and at a high concentration, curvularin showed very weak biofilm-inhibitory ability. In contrast, low-concentration CPBA inhibited biofilm production. For example, 100 μM curvularin inhibited biofilm formation by approximately 10%, whereas only 3 μM CPBA inhibited biofilm formation by 10%. HG showed antibacterial activity in the elastase assay but did not affect biofilm formation at all as reported previously (Kim et al., 2019; **Supplementary Figures 4C,D**). As a positive control, low-concentration FC profoundly inhibited biofilm formation. Given previous reports indicating that pyocyanin and rhamnolipid are RhlR-directed exoproducts and that biofilm formation is regulated by the Las system, these results suggest that curvularin at low concentrations might selectively antagonize RhlR.

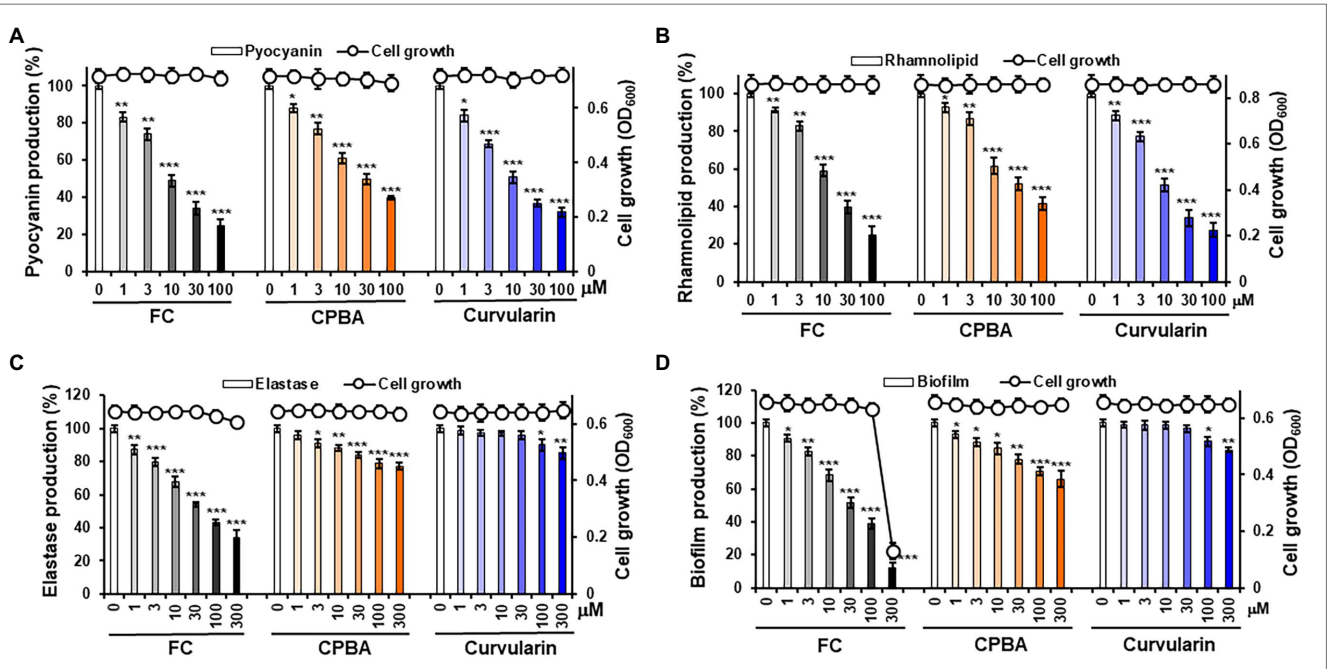


**FIGURE 2 |** Effects of curvularin on *P. aeruginosa* virulence factor production and biofilm formation. **(A–C)** Effects of curvularin on virulence factor production and cell viability in *P. aeruginosa* PA14. After PA14 cells were grown in LB medium containing various concentrations of curvularin for 24 h, cell density was measured at 600 nm and pyocyanin and rhamnolipid and elastase activity in the culture supernatants were then determined. **(D)** Effects of curvularin on *P. aeruginosa* biofilm formation and cell viability. PA14 biofilms were grown in the presence of curvularin for 9 h, followed by the measurement of planktonic cell density at 600 nm. The biofilm cells attached to the well surface were assayed using crystal violet staining. Furanone C-30 (FC) and N-cyclopentylbutyramide (CPBA) are known antagonists of LasR and RhlR, respectively. Three independent experiments were performed in triplicate, and the mean ± SD values are presented in each bar. *$p < 0.01$; **$p < 0.001$; and ***$p < 0.0001$ versus untreated cells.

## Inhibitory Effects of Curvularin on QS

To test whether curvularin selectively blocks QS receptors, an AHL-based *in vitro* QS competition assay was performed using the two reporter strains *A. tumefaciens* NT1 and *C. violaceum* CV026 (Park et al., 2006), as reported previously (Kim et al., 2018). Briefly, *A. tumefaciens* NT1 contains the TraR receptor gene fused to the *lacZ* reporter gene. The TraR receptor can sense long-chain AHLs, such as OdDHL, leading to the synthesis of a cyan pigment (Zhang et al., 1993). The *C. violaceum* CV026 strain carries the CviR receptor, which can sense short-chain AHLs, such as BHL, resulting in the production of a purple pigment violacein (McClean et al., 1997). Because the TraR and CviR receptors are homologs of the LasR and RhlR receptors, respectively, a competitive binding assay for the LasR and RhlR receptors was performed using these reporter strains (Kim et al., 2015; Srivastava et al., 2015).

Violacein pigment was produced in the CV026 cultures only when BHL was added, as expected (**Figure 3A**). Treatment with 1–100 μM curvularin inhibited the production of pigment without affecting cell growth. Treatment with 3 and 30 μM curvularin inhibited pigment production by 18.6% and 50.0%, respectively, approximately threefold greater than the effect of CPBA, with 22.4% and 50.7% inhibition at 10 and 100 μM treatment, respectively. Similarly, curvularin induced more than a threefold greater inhibition of violacein production than that induced by HG (**Supplementary Figure 5A**). FC, a LasR antagonist, did not inhibit pigment production, as expected. In contrast, in an NT1 culture, low-concentration curvularin did not inhibit pigment production, and at a concentration greater than100 μM, it showed very weak pigment production inhibition (**Figure 3B**); curvularin showed inhibition of 2.5% and 11.5% only at high concentration levels, that is at 100 and 300 μM, respectively, whereas as the positive control, FC at concentrations as low as 1 μM showed a strong inhibitory effect, as expected. However, 3 and 30 μM CPBA inhibited pigment production in NT1 cells by 16.0% and 24.5%, respectively. The effects of HG on LasR could not be determined using NT1 cells due to its antibacterial activity as reported previously (Kim et al. 2019;

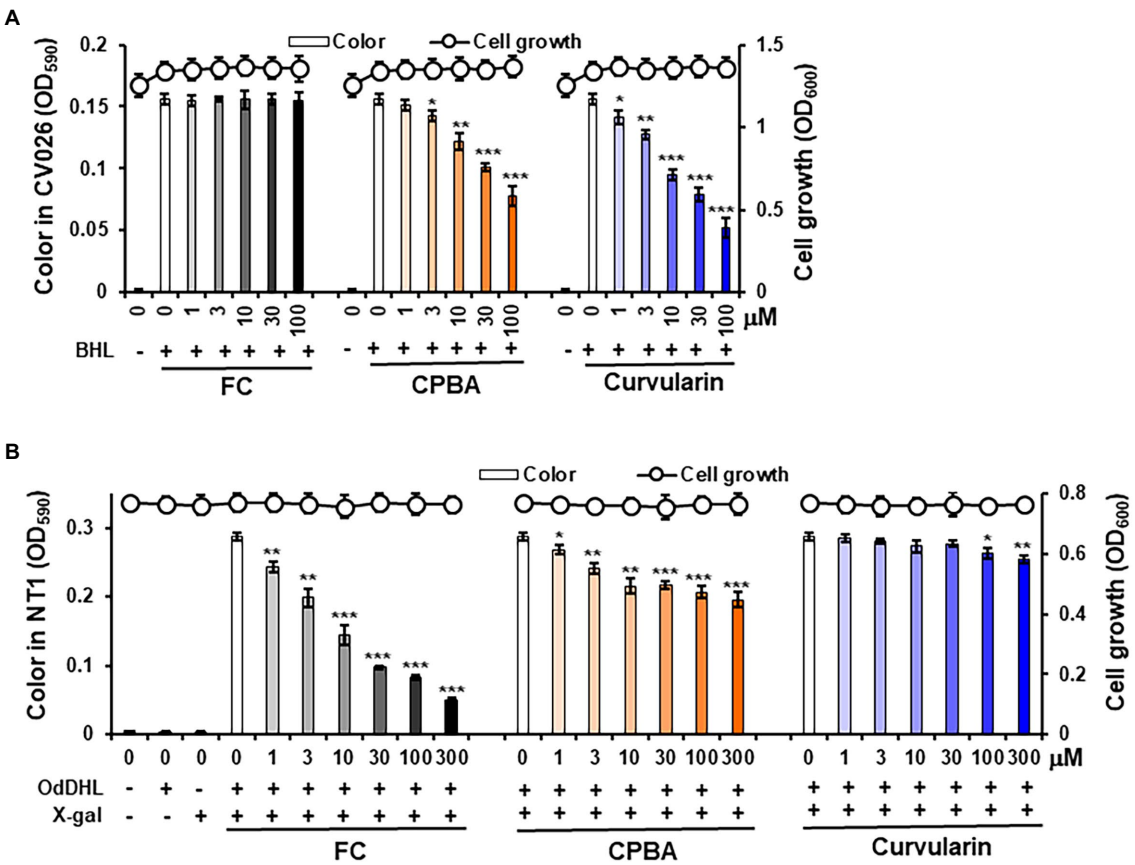


**FIGURE 3 |** Effects of curvularin on QS. QS competition against N-butanoyl homoserine lactone (BHL) and N-(3-oxododecanoyl)-l-homoserine lactone (OdDHL) was performed using the reporter strains *Agrobacterium tumefaciens* NT1 and *C. violaceum* CV026, respectively. After 1 μM OdDHL and 500 μM BHL were added to the NT1 and CV026 cultures, respectively, with various concentrations of curvularin and incubated for 24 h, cell growth at 600 nm and color change intensity were measured. **(A)** Curvularin—BHL competition. **(B)** Curvularin—OdDHL competition. Furanone C-30 (FC) and N-cyclopentylbutyramide (CPBA) are known antagonists of LasR and RhlR, respectively. The data are expressed as the mean ± SD values of three independent experiments performed in triplicate. *, $p < 0.01$; **, $p < 0.001$; and ***, $p < 0.0001$ versus untreated cells.

**Supplementary Figure 5B**). These results showed that low concentrations (1–30 μM) of curvularin antagonized only the binding of BHL to its cognate receptor RhlR, which showed threefold higher potency than that exhibited by CPBA or HG, and at concentrations greater than100 μM, curvularin weakly inhibited the binding of OdDHL to LasR, whereas CPBA at low concentrations inhibited OdDHL binding to LasR. These results indicate that low-concentration curvularin is an RhlR antagonist.

## Effect of Curvularin on QS Signaling Molecules Production and QS Gene Expression

To determine whether curvularin selectively affects QS signaling, the effects of curvularin on the production of the AHL and PQS molecules in PA14 were investigated. QS signaling molecules such as OdDHL, BHL, and PQS were quantitatively analyzed by LC–MS/MS (**Figure 4**). In the supernatants of untreated PA14 cultured for 12-h, 76.37 ± 2.65 ng/ml, 51.93 ± 0.95 ng/ml, and 1500.26 ± 46.52 ng/ml of OdDHL, BHL, and PQS, respectively, were produced. Consistent with the RhlR-specific antagonizing activity of low-concentration curvularin in the QS competition assays, only BHL production was reduced by 3–30 μM curvularin in a dose-dependent manner (**Figure 4B**), whereas OdDHL production was reduced by 15% only by high-concentration (more than 300 μM) curvularin, and PQS production was not affected (**Figures 4A,C**). As the control, low-concentration CPBA inhibited not only BHL production but also weakly inhibited OdDHL production, which was consistent with the results of the QS competition assays. Additionally, in agreement with its higher RhlR-antagonizing activity, curvularin exhibited threefold greater inhibition of BHL production than CPBA or HG (**Supplementary Figure 6B**).

The effects of curvularin on QS gene expression were also investigated by RT–qPCR. The expression levels of QS regulatory genes (*lasI*, *lasR*, *rhlI*, *rhlR*, *pqsA*, *phnB*, *pqsH*, and *pqsR*) and key QS-controlled genes (*lasA*, *lasB*, *aprE*, *rhlA*, and *phzA2*) in PA14 cells were measured (**Figure 5**; **Supplementary Figure 7**). Low-concentration curvularin selectively inhibited *rhl*-related genes, as expected. Transcription of the *rhlI*, *rhlR*, and *rhlA* genes was selectively inhibited by 3–30 μM curvularin, and transcription of *las*-related genes (*lasI*, *lasR*, *lasA*, and *lasB*) was weakly suppressed only by curvularin at a concentration higher than 100 μM. Similar to the results of the QS receptor and signaling molecule production assays, CPBA showed little selective inhibitory effect on the transcription of *rhl*-related genes, and both CPBA and HG inhibited the transcription at a rate threefold less than that of curvularin (**Supplementary Figure 8**). Transcription of *pqs*-related genes, except for the phenazine synthesis gene *phA2*, was largely unaffected by curvularin at low concentrations. As the control, FC inhibited all QS gene transcription, as expected.

Taken together, these results support the supposition that curvularin at low concentrations shows RhlR-antagonizing activity and that its inhibitory effect is greater and more selective than that of CPBA or HG.

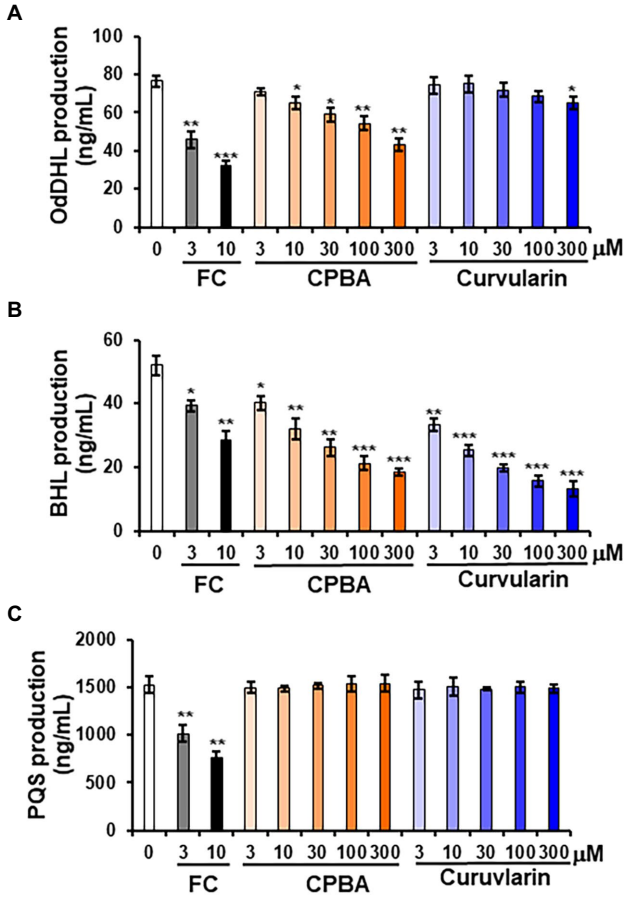


**FIGURE 4 |** Effects of curvularin on QS signaling molecule production. PA14 cells were cultured in LB medium in the presence of curvularin for 12 h. The three main QS molecules, namely, OdDHL **(A)**, BHL **(B)**, and PQS **(C)**, were extracted from the culture supernatants and quantitatively analyzed by LC–MS/MS. FC and CPBA are known antagonists of LasR and RhlR, respectively. Three independent experiments were performed in triplicate, and the mean ± SD values are presented in each bar. *$p < 0.01$; **$p < 0.001$; and ***$p < 0.0001$ versus DMSO treatment.

## Low-Concentration Curvularin Inhibits Pyocyanin and Rhamnolipid Production by Antagonizing Only RhlR

Pyocyanin and rhamnolipid synthesis is activated by both the Rhl and PQS systems (Lee and Zhang, 2015). Moreover, RhlR has been reported to direct the production of virulence factors through the RhlI-independent pathway using an alternative ligand derived from PqsE in the PQS system (Mukherjee et al., 2017). To determine whether the inhibition of pyocyanin and rhamnolipid production by curvularin is mediated exclusively through the antagonization of RhlR and to determine whether this effect is RhlI (BHL) dependent, the effects of exogenous QS ligands on low-concentration curvularin-mediated inhibition of pyocyanin or rhamnolipid production in QS mutants were investigated. In the *lasR* mutant of the PA14 strain, in which pyocyanin production is regulated by the Rhl and PQS systems, curvularin inhibited

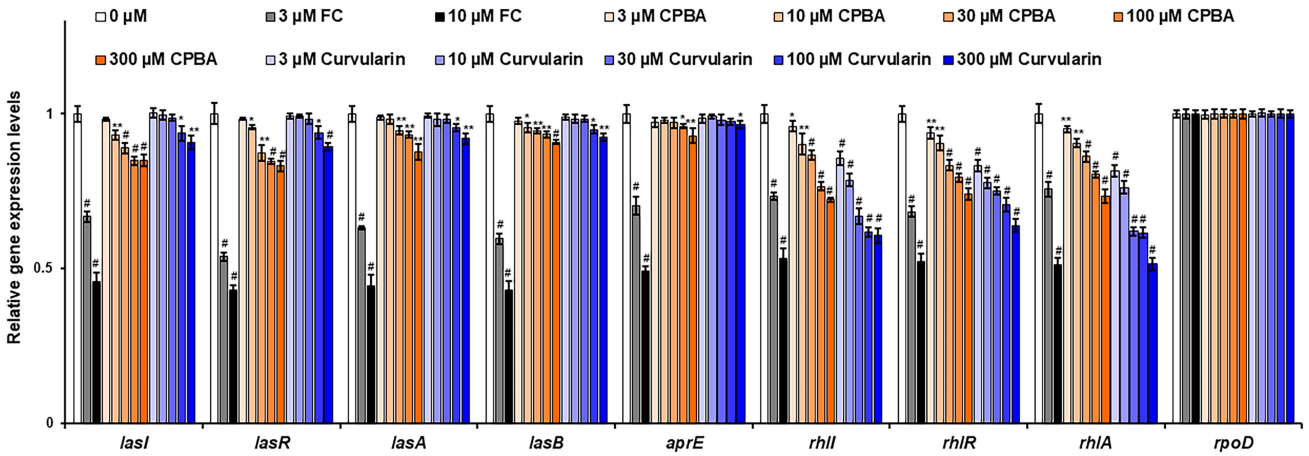


**FIGURE 5 |** Effects of curvularin on QS gene expression. PA14 cells were cultured in LB medium containing different concentrations of curvularin for 12 h. The effects of curvularin on QS gene expression were measured by RT-qPCR. FC and CPBA are known antagonists of LasR and RhlR, respectively. The experiment shown is representative of three independent experiments performed in triplicate and the mean ± SD values are presented in each bar. $^{*}p < 0.05$; $^{**}p < 0.01$; and $^{\#}p < 0.001$ versus DMSO treatment.

pyocyanin production, and this effect was reversed by supplementation with exogenous BHL, but not with OdDHL or PQS, demonstrating that low-concentration curvularin exerted its inhibitory effect by preventing BHL-mediated activation of RhlR (**Figure 6B**). As the control, FC did not inhibit pyocyanin production as expected (**Figure 6A**), whereas CPBA and CF, which are RhlR and Pqs antagonists, respectively, inhibited pyocyanin production; this effect was revered by the addition of exogenous BHL and PQS, respectively, as expected (**Figures 6B,C**). In a *rhlR* mutant in which pyocyanin production is controlled by the Las and PQS systems (**Figure 7**), curvularin lost its activity, demonstrating that curvularin exhibited inhibition by acting on only RhlR. In contrast, FC and CF, positive controls, inhibited pyocyanin production, which was reversed by exogenous supplementation with both OdDHL and PQS and with PQS, respectively, as expected (**Figures 7A,C**). On the other hand, CPBA weakly inhibited pyocyanin production, and its effect was reversed by the addition of OdDHL, similar to the results observed with FC treatment (**Figure 7A**), corroborating the finding that low-concentration CPBA acts on both LasR and RhlR. Because the *pqsR* mutant did not produce pyocyanin as previously reported (Cao et al., 2001; Diggle et al., 2003), rhamnolipid production in a *pqsR* mutant, which is regulated by the Las and Rhl systems, was analyzed (**Supplementary Figure 9**). Curvularin inhibited rhamnolipid production, and this effect was reversed by treatment with exogenous BHL, but not with OdDHL or PQS, similar to its effect on the *lasR* mutant (**Supplementary Figure 9B**). FC as the positive control inhibited rhamnolipid production, and this effect was reversed by treatment with exogenous OdDHL and BHL, whereas CF, the negative control, did not have a similar effect, as expected. CPBA inhibited rhamnolipid production, which was reversed by the addition of OdDHL and BHL, similar to the effect of FC (**Supplementary Figures 9A,B**). Overall, these results indicate that low-concentration curvularin inhibited pyocyanin and rhamnolipid production by antagonizing only BHL-activated RhlR, whereas CPBA inhibited this production by antagonizing both RhlR and LasR, although weakly.

## Reduction in Biofilm Formation and Elastase Production Is Due to Inhibition of LasR

After treatment with high-concentration curvularin (more than 100 μM), biofilm formation and elastase production were negligibly inhibited, each by ~10% (**Figures 2C,D**). Additionally, a very weak inhibition of LasR was observed in the QS competition, QS signaling molecules, and QS gene expression assays with concentrations of curvularin higher than 100 μM. Formation of *P. aeruginosa* biofilms is regulated by the Las system (Davies et al., 1998; Sakuragi and Kolter, 2007), but the regulatory mechanism of elastase synthesis is the Las system and, to a lesser degree, the Rhl system (Ochsner et al., 1994; Pearson et al., 1997). To test whether the weak reduction in biofilm formation and elastase production at high curvularin concentrations is due to the corresponding curvularin inhibition of LasR, the effects of exogenous QS ligands on the curvularin-mediated inhibition of biofilm formation and elastase production were investigated. In wild-type PA14, inhibition of biofilm formation by FC, the positive control, was reversed by supplementation with exogenous OdDHL, but not BHL, as expected (**Figure 8A**). Similarly, curvularin and CPBA treatment at 300 μM inhibited biofilm formation by 15.6% and 33.2%, respectively, which was reversed by the exogenous addition of OdDHL, but not BHL, suggesting that the reduction in biofilm formation was due to the inhibition of the OdDHL-mediated activation of LasR (**Figure 8A**). This outcome was confirmed with experiments on QS mutants. In the *lasR* mutant,

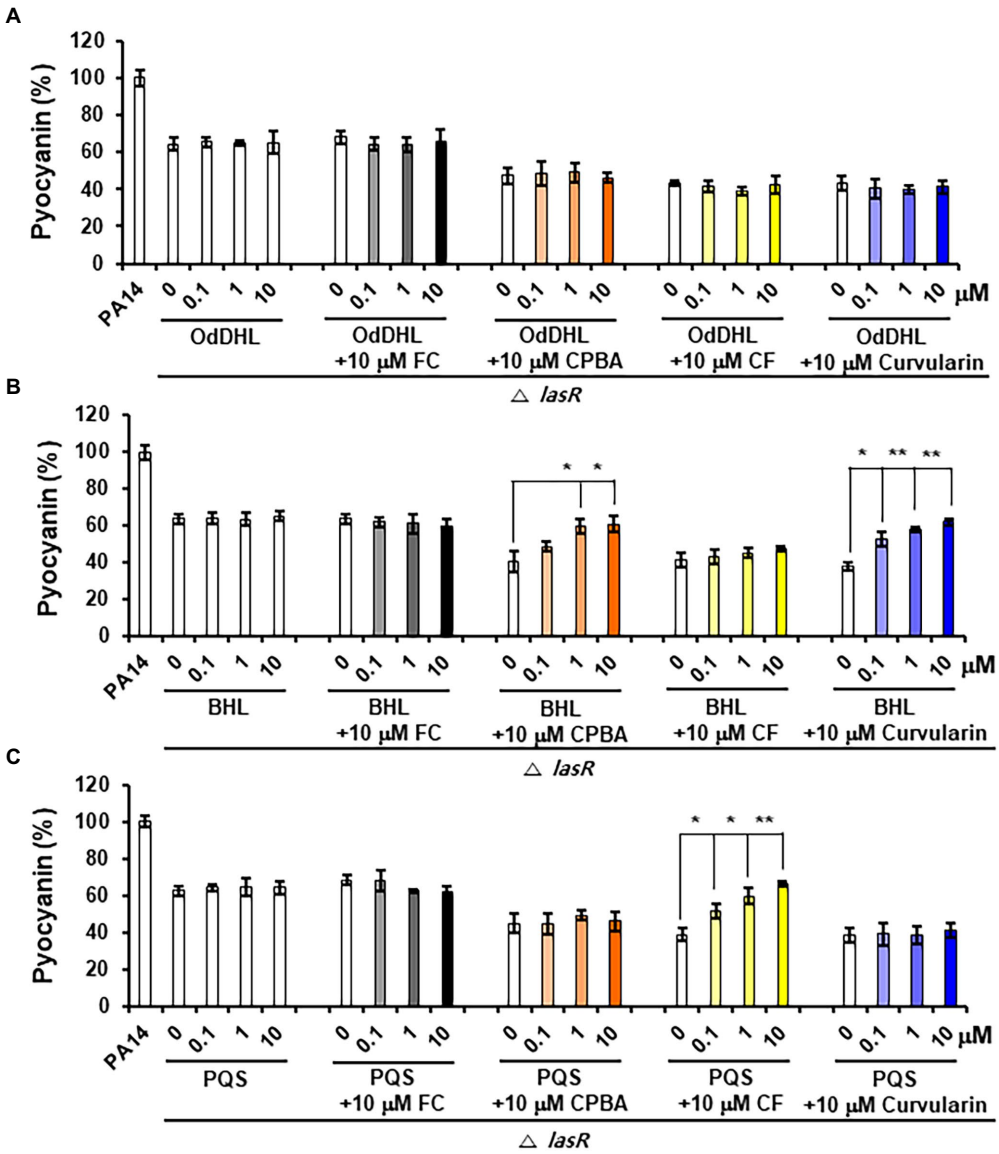


**FIGURE 6 |** Effects of exogenous QS ligands on curvularin-mediated inhibition of pyocyanin production in the Δ*lasR* mutant. Pyocyanin production in the Δ*rhlR* mutant cultured with curvularin (10 μM) in the presence or absence of different concentrations of OdDHL **(A)**, BHL **(B)**, or PQS **(C)** for 18 h. FC, CPBA, and clofoctol (CF) are known antagonists of LasR, RhlR, and PqsR, respectively. The data are representative of three independent experiments performed in triplicate and expressed as the mean ± SD values in each bar. $^{*}p < 0.01$ and $^{**}p < 0.001$ versus DMSO treatment.

all tested compounds failed to inhibit biofilm formation, demonstrating that, similar to FC, curvularin and CPBA act on LasR to inhibit biofilm formation (**Figure 8B**). In a *rhlR* mutant, all tested compounds had the same effect as they did in the wild-type strain, demonstrating that curvularin and CPBA targeted LasR, not RhlR, to inhibit of biofilm formation (**Figure 8C**). For elastase production, the same results were obtained (**Supplementary Figure 10**). Taken together, these data indicate that the negligible inhibition of biofilm formation and elastase production induced by the high concentration of curvularin was due to its corresponding inhibition of LasR.

## Confirmation of the RhlR Antagonistic Activity of Low-Concentration Curvularin in *Pseudomonas aeruginosa* PAO1

To confirm the RhlR antagonistic activity of low-concentration curvularin in another *P. aeruginosa*, the effects of exogenous QS ligands on the curvularin-induced inhibition of virulent factor production and biofilm formation were investigated in PAO1 strain. First, the effects of curvularin on virulence factor production and biofilm formation were tested in PAO1. Curvularin potently inhibited production of pyocyanin and rhamnolipid with around threefold higher inhibition than CPBA, whereas biofilm formation was weakly inhibited by only high-concentration

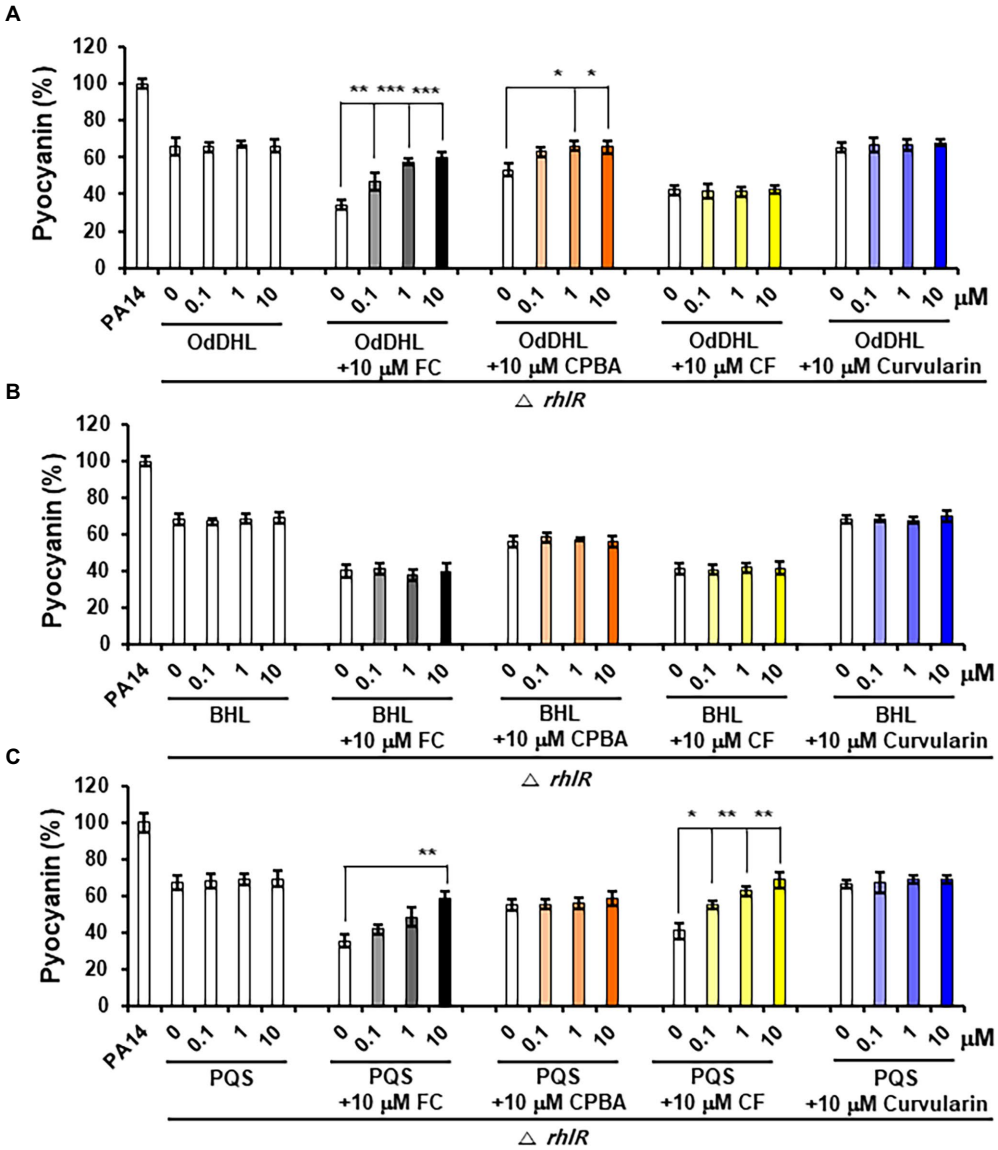


**FIGURE 7 |** Effects of exogenous QS ligands on curvularin-mediated inhibition of pyocyanin production in the Δ*rhlR* mutant. Pyocyanin production in the Δ*rhlR* mutant cultured with curvularin (10 μM) in the presence or absence of different concentrations of OdDHL **(A)**, BHL **(B)**, or PQS **(C)** for 18 h. FC, CPBA, and CF are known antagonists of LasR, RhlR, and PqsR, respectively. The data are representative of three independent experiments performed in triplicate and expressed as the mean ± SD values in each bar. *$p < 0.01$; **$p < 0.001$; and ***$p < 0.0001$ versus DMSO treatment.

curvularin, like in PA14 (**Supplementary Figure 11**). Interestingly, curvularin inhibited elastase production at both low and high concentrations unlike in PA14 which suggested a differential regulation of elastase between PA14 and PAO1. Exogenous supplementation of BHL (0.1–10 μM), not OdDHL and PQS, reversed the inhibition of pyocyanin and rhamnolipid production by low-concentration curvularin in a dose-dependent manner (**Supplementary Figures 12**, **13**). In contrast, the inhibition of pyocyanin and rhamnolipid production by CPBA was reversed by exogenous addition of OdDHL and BHL. As controls, the inhibition of pyocyanin and rhamnolipid production by FC and CF was reversed by supplementation of the three ligands and PQS, respectively, as expected. In contrast, the inhibition of biofilm formation by high-concentration curvularin was reversed by supplementation of both OdDHL and BHL (**Supplementary Figure 14A**). These results indicated the RhlR-selective antagonism of low-concentration curvularin in PAO1 like in PA14. Additionally, it was confirmed by analyzing QS signaling molecules production and QS gene expression. Low-concentration curvularin selectively inhibited the production of BHL and the transcription of *rhl*-related genes (**Supplementary Figures 15**, **16**). Taken together, these results corroborated that low-concentration curvularin selectively antagonized RhlR in PAO1 like in PA14.

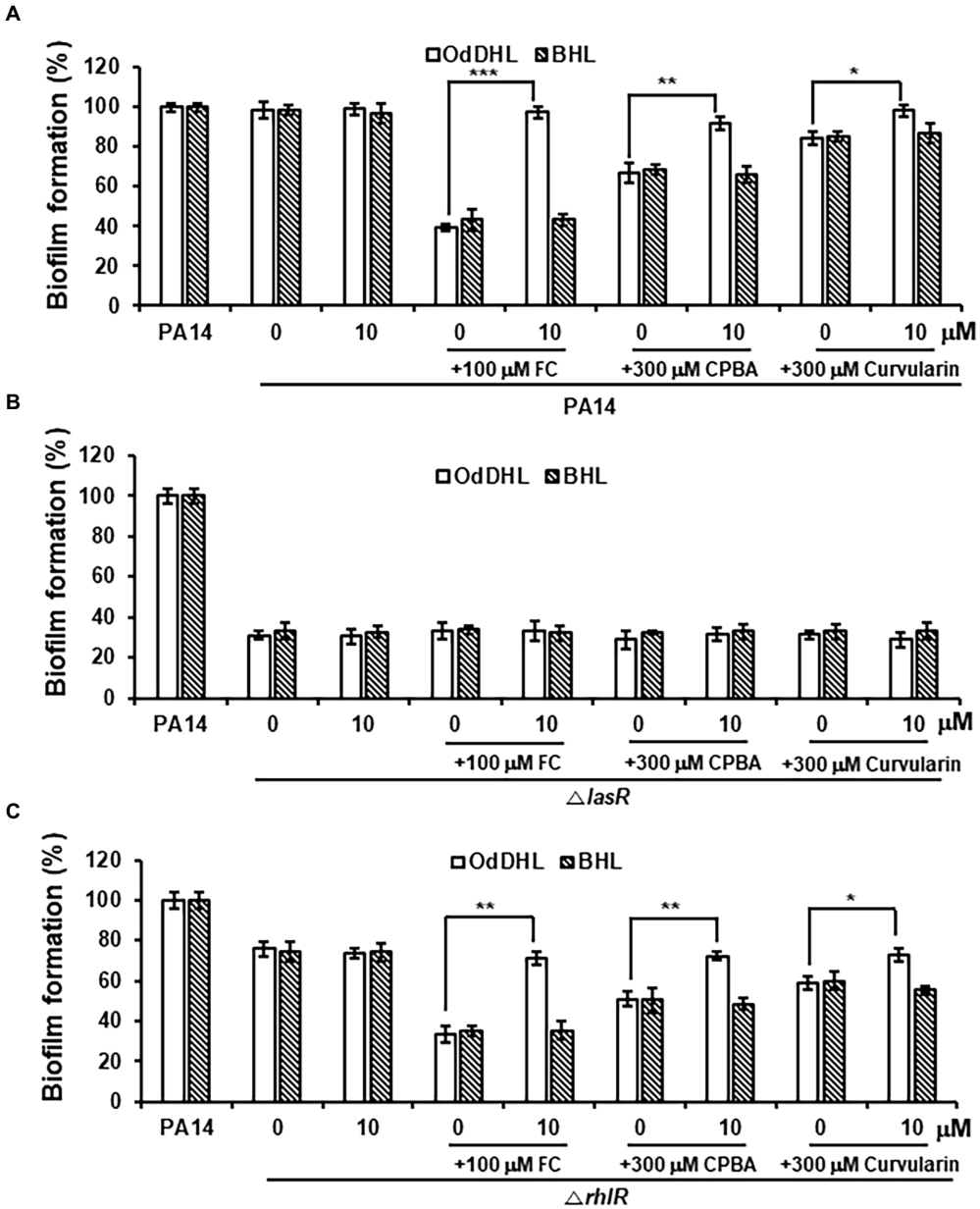


**FIGURE 8 |** Effects of exogenous QS ligands on curvularin-mediated inhibition of biofilm formation in Δ*lasR* and Δ*rhlR* mutants. Biofilm formation in wild-type PA14 **(A)**, the Δ*lasR* mutant **(B)**, and the Δ*rhlR* mutant **(C)** cultured with curvularin (300 μM) in the presence or absence of different concentrations of OdDHL or BHL for 18 h. FC and CPBA are known antagonists of LasR and RhlR, respectively. The data are representative of three independent experiments performed in triplicate and expressed as the mean ± SD values in each bar. $^{*}p < 0.01$; $^{**}p < 0.001$; and $^{***}p < 0.0001$ versus DMSO treatment.

## Antivirulence Activity of Curvularin in a *Caenorhabditis elegans* Infection Model

The effects of curvularin on the *in vivo* virulence of *P. aeruginosa* were examined using a *C. elegans* fast-kill infection assay. *Caenorhabditis elegans* rapidly died when fed with *P. aeruginosa* PA14, as evidenced by the death of 85.6% of the nematodes 36 h postinfection (**Figure 9**). Treatment with curvularin (0.1–10 μM) and *P. aeruginosa* at the same time prevented the death of the nematodes in a dose-dependent manner. Nematode death significantly decreased by 31.1% and 50.6% after curvularin treatment of 1 and 10 μM, respectively (**Figure 9A**). Additionally, the protective effects of curvularin was 1.70- and 2.34-fold greater than those of FC and CPBA, respectively, at 36 h treatment (**Supplementary Figure 17**). These results clearly indicated that curvularin protected *C. elegans* against infection with *P. aeruginosa*. We then tested whether curvularin prevents the *in vivo* virulence of the *lasR* mutant toward *C. elegans*. When infected with the *lasR* mutant, 75.6% of the nematodes died after 36 h. As the control, the LasR antagonist FC exerted no effect on *C. elegans* infected with

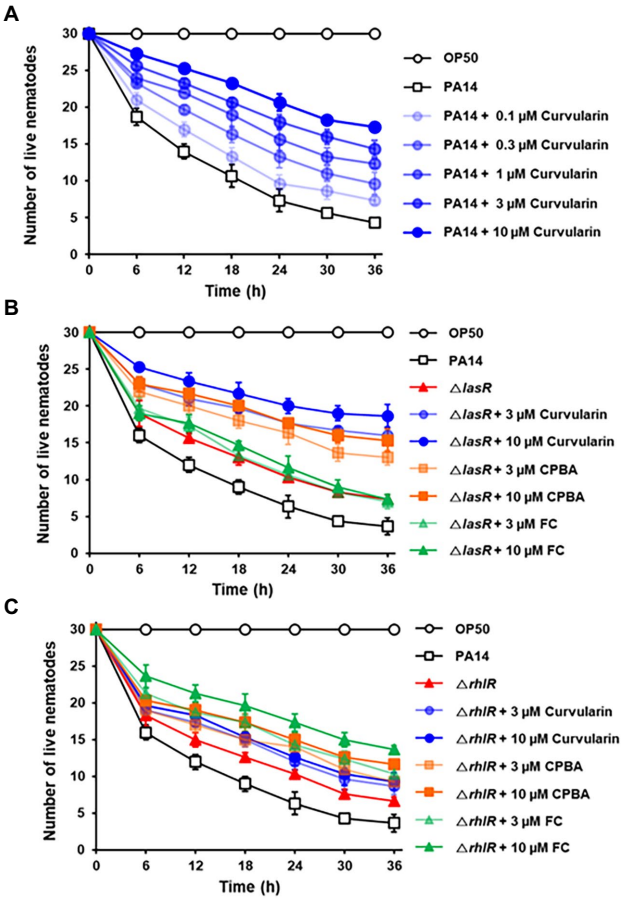


**FIGURE 9 |** *In vivo* antivirulence activity of curvularin. Antivirulence activity of curvularin in a *C. elegans* infection model. Thirty worms were introduced on lawns of *E. coli* OP50, wild-type PA14 **(A)**, Δ*lasR* mutant **(B)**, or Δ*rhlR* mutant **(C)** on plates in the presence of different concentrations of curvularin. Live nematodes were counted every 5 h for 30 h. FC and CPBA are known antagonists of LasR and RhlR, respectively. Two independent experiments were performed in triplicate, and the mean ± SD values are displayed in each graph.

the *lasR* mutant strain, as expected (**Figure 9B**). In contrast, curvularin (3 and 10 μM) significantly reduced the virulence of the *lasR* mutant with threefold greater potency than CPBA (**Figure 9B**). Additionally, to confirm that the protective effects of curvularin on *C. elegans* subjected to PA14 resulted from inhibition of RhlR, the effects of curvularin on the virulence of the *rhlR* mutant were investigated. Indeed, curvularin failed to protect *C. elegans* infected with the *rhlR* mutant strain, while FC protected the worms from death, as expected (**Figure 9C**). Taken together, these results indicated that curvularin prevented the *in vivo* virulence of the wild-type strain and *lasR* mutant in *C. elegans* by acting on RhlR.

## DISCUSSION

Virulence factor production and biofilm formation in *P. aeruginosa* are regulated by the hierarchical QS network in which the Las system activates both the Rhl and Pqs systems (Lee and Zhang, 2015). However, recent studies have shown that the Rhl system can be activated through a Las-independent mechanism (Lee et al., 2013). Importantly, in clinical isolates of *P. aeruginosa* from CF patients, the Las system was frequently nonfunctional due to *lasR* mutations, and therefore, RhlR independently activated QS-dependent genes (Feltner et al., 2016). Additionally, it has been reported that RhlR plays a central role in mediating *in vivo* QS (O'Loughlin et al., 2013; Waters and Goldberg, 2019). Thus, RhlR antagonists are needed to prevent and treat chronic *P. aeruginosa* infections.

In this study, curvularin showed differential inhibition of virulence factor production and biofilm formation, a previously unreported outcome. At the low concentrations of 1–30 μM, curvularin potently inhibited pyocyanin and rhamnolipid production at a level similar to that of FC without affecting cell growth, but did not inhibit biofilm formation or elastase production in *P. aeruginosa* PA14 and PAO1. Elastase production and biofilm formation were negligibly inhibited by curvularin at concentrations greater than 100 μM. On the other hand, low-concentration CPBA, which has been reported to an RhlR antagonist in *E. coli* reporter strains, not only inhibited pyocyanin and rhamnolipid production but also weakly inhibited biofilm formation and elastase production in PA14 and PAO1. Considering that pyocyanin and rhamnolipid are RhlR-directed exoproducts and that biofilm formation is regulated by the Las system, these results suggested that curvularin had more selective RhlR inhibition than that exhibited by CPBA. By analyzing the antagonistic activities of curvularin on QS receptors using reporter strains, the production of QS signaling molecules, and the transcription of QS-related genes, we demonstrated that low-concentration curvularin selectively antagonized RhlR, and it very weakly antagonized LasR, but only at high concentrations. On the other hand, low-concentration CPBA antagonized not only RhlR but also LasR. Additionally, curvularin exhibited threefold greater inhibitory effects than CPBA or HG on the production of virulence factors and on RhlR. Because pyocyanin and rhamnolipid synthesis are regulated by both RhlR and PqsR, the exclusive RhlR-antagonizing activity of low-concentration curvularin was confirmed by investigating the effects of exogenous AHLs and PQS on curvularin-mediated inhibition of pyocyanin and rhamnolipid production in QS mutants. Indeed, low-concentration curvularin potently inhibited the production of pyocyanin and rhamnolipid through the selective inhibition of BHL-activated RhlR, whereas CPBA inhibited RhlR and LasR weakly. Additionally, using exogenous ligands and QS mutants, we showed that the negligible inhibition of elastase production and biofilm formation by high-concentration curvularin (more than 100 μM) was due to inhibition of OdDHL-activated LasR. Taken together, the results of this study indicate that low-concentration curvularin is an RhlR-exclusive antagonist, whereas CPBA is not an RhlR-exclusive antagonist and shows weak LasR-antagonizing activity in, at least, *P. aeruginosa*. In particular, curvularin exhibited an *in vivo* antivirulence effect by acting on RhlR with 1.25-fold higher potency than that of FC, a well-known LasR antagonist, in a *P. aeruginosa*-infected *C. elegans* model.

Previous reports have shown that elastase synthesis is activated by the *las* system and to some extent by the *rhl* system. In the *rhlI* mutant of the PAO1 strain, elastase production was reported to be partially reduced, and it was recovered by supplementation with BHL (Pearson et al., 1997). The *rhlR* mutants of the PA PG201 strain lacked elastase activity, which was restored by introducing a wild-type *rhlR* gene into the mutants (Ochsner et al., 1994; Ochsner and Reiser, 1995). However, in the present study, in the PA14 strain, low-concentration curvularin profoundly antagonized RhlR and only high-concentration curvularin (more than 100 μM) antagonized LasR and inhibited elastase, but its effects were weak (**Figure 2C**). Additionally, the inhibition of elastase by curvularin was reversed by adding OdDHL but not BHL (**Supplementary Figure 10A**). These data strongly suggest that elastase synthesis is regulated by the *las* system, not the *rhl* system, in the PA14 strain, which is inconsistent with previous reports indicating that elastase was regulated by both LasR and RhlR in *P. aeruginosa* PAO1 and PA PG201. Indeed, regulation of elastase production by the *las* system was demonstrated using QS mutants; the *lasR* mutant of the PA14 strain exhibited a remarkable reduction in elastase production compared to the wild-type strain, whereas the *rhlR* mutant showed nearly normal elastase production (**Supplementary Figures 10B,C**). These results strongly suggest that the regulation in elastase synthesis differs between PA14 and PAO1. Indeed, at the low concentration of 3 μM, curvularin inhibited elastase production at in PAO1, but not in PA14 (**Supplementary Figure 11**). The elastase inhibition by low-concentration curvularin in PAO1 was reversed by the addition of BHL, but elastase inhibition by high-concentration curvularin was reversed by supplementation with both OdDHL and BHL (**Supplementary Figures 14B,C**), indicating that elastase production is regulated by both LasR and RhlR in PAO1, as reported previously. Taken together, these results indicate that elastase synthesis is regulated by LasR in PA14 but by LasR and RhlR in PAO1. To the best of our knowledge, this is the first report showing that elastase synthesis in *P. aeruginosa* is differentially regulated by QS on the basis of the strain.

The relationship between QS and biofilm formation has not yet been fully determined. The Las system has been reported to play an important role in the formation of *P. aeruginosa* biofilm by regulating the expression of the *pel* or *psl* exopolysaccharide biosynthesis gene (Davies et al., 1998; Sakuragi and Kolter, 2007). Biofilm formation in the *lasI* mutant was dramatically decreased, whereas biofilm formation in the *rhlI* mutant was almost unchanged in the PAO1 strain (Davies et al., 1998). Biofilm formation in PA14 was reduced by 60% in the *lasI* and *lasR* mutant, similar to that of the *pel* mutant, whereas it is not reduced in the *rhlI* mutant and weakly reduced, by ~10%, in the *rhlR* mutant of the PA14 strain (Sakuragi and Kolter, 2007). It seems that biofilms are regulated mainly by LasR, partially by RhlR, and not regulated by RhlI. In this study, the *lasR* mutant of the PA14 strain exhibited a remarkable reduction in biofilm formation compared to the wild-type strain (**Figure 8B**), but the *rhlR* mutant also showed a weak reduction in biofilm formation, of ~20% (**Figure 8C**). These QS mutant experiments suggest partial involvement of RhlR in biofilm formation, as reported previously. However, interestingly, low-concentration curvularin did not inhibit biofilm formation but did profoundly inhibit RhlR and it very weakly inhibited biofilm formation only at a high concentration, when it very weakly inhibited LasR. These results suggest that biofilm formation is regulated by the *las* system, not the *rhl* system, in PA14. This was proven using QS mutants; the inhibition of biofilm formation by curvularin was due to inhibition of OdDHL-activated LasR, not by inhibition of RhlR (**Figure 8**). These results clearly demonstrate that biofilm formation is regulated by the *las* system, not the *rhl* system, in PA14. Hence, how can the possible partial involvement of RhlR in biofilm formation, as suggested by the QS mutant experiments, be explained? Considering recent reports suggesting that another RhlR pathway, which is independent of RhlI (BHL), is involved in the development of colony biofilms and the production of virulence factors (Mukherjee et al., 2017), the possibility of partial involvement of RhlI-independent RhlR in biofilm formation by PA14 is suggested; however, this question remains to be answered.

Curvularin is an aromatic compound with a cyclized alkyl side chain. It has been reported that the substitution of the homoserine lactone head group in OdDHL with an aromatic group resulted in OdDHL analogs with QS antagonism (McInnis and Blackwell, 2011; Hodgkinson et al., 2012). 6-Gingerol, a natural aromatic compound with a long alkyl side chain, was reported to show LasR antagonism by binding to LasR in a similar way to that of OdDHL (Kim et al., 2015). 4-Gingerol with a shorter side chain than that of 6-gingerol has RhlR antagonistic properties (Choi et al., 2017). Among alkyl gallates, HG, a RhlR antagonist, has the same alkyl chain length as 4-gingerol. Recent structure–activity relationship study of 4-gingerol analogs for improvement of RhlR antagonism shows that rotational rigidity between the aromatic ring and the carbonyl group of the alkyl side chain is important for enhancement of RhlR antagonism (Nam et al., 2020). Additionally, the hydroxyl moiety of the aromatic ring and the carbonyl group of the alkyl chain are important for binding to RhlR. Because a double or triple bond between the aromatic ring and the carbonyl group of the alkyl side chain increase the rotational rigidity, DFPH, a 4-gingerol analog with a triple bond, has a higher antagonism for RhlR than that of 4-gingerol analogs with a single or double bond. Considering that structurally the cyclized side chain in curvularin could restrict the rotational flexibility of the side chain more strongly than the double or triple bond, it was suggested that the higher specificity of curvularin for RhlR than that of HG or CPBA might be due to its more rotational rigidity of the cyclized side chain.

Many small-molecule inhibitors of QS have been reported to be derived from natural sources, including bacteria, cyanobacteria, fungi, algae, and plants (Zhao et al., 2019; Hemmati et al., 2020). Brominated furanone, the first natural product obtained from marine algae, competitively inhibits the

LuxR receptor. Penicillic acid, patulin, equisetin, and terrein extracted from fungi inhibit both LasR and RhlR (Rasmussen et al., 2005; Kim et al., 2018). Coumarin, curcumin, berberine, cinnamic acid, and 6-gingerol extracted from plants inhibit LasR, while flavonoids inhibit both LasR and RhlR (Kim et al., 2015). All the reported natural QS inhibitors inhibit both biofilm formation and virulence factor production in *P. aeruginosa*. To the best of our knowledge, curvularin is the first RhlR antagonist isolated from natural sources.

Many synthetic QS inhibitors have been developed to block QS in *P. aeruginosa* (Galloway et al., 2011; Kalia, 2013). Most of these QS inhibitors have been focused on LasR because of its location at the top of the *P. aeruginosa* QS receptor hierarchy where it regulates *rhl*- and pqs-associated genes. Synthetic analogs of halogenated furanones including furanone C-30, or synthetic compounds of nonnatural origin such as V-06-018 and PD12, have been reported (Galloway et al., 2011). However, although RhlR plays an important role in QS in *P. aeruginosa*, RhlR antagonists have rarely been reported. Recently, Bassler et al. reported mBTL to be a partial antagonist of RhlR that inhibits pyocyanin production and prevents nematode death in a *P. aeruginosa* infection model, suggesting that RhlR may be a promising target for antivirulence treatment (O'Loughlin et al., 2013). Blackwell et al. extensively screened a focused library of synthetic, nonnative BHL analogs to use in the development of small-molecule probes that can alter the activities of individual QS receptors (Welsh et al., 2015; Boursier et al., 2018), and they thus identified CPBA and 4-iodo phenoxyacetyl L-homoserine lactone (4-iodo POHL) as RhlR antagonists in *E. coli* reporter strains. Park et al. reported an alkynyl ketone class compound, 1-(3,4-difluorophenyl)hex-1-yn-3-one (DFPH), to be a RhlR antagonist, a synthetic analog of 4-gingerol, in *E. coli* reporter strains (Nam et al., 2020). Interestingly, at low micromolar concentrations, CPBA, which has been proposed to be an RhlR antagonist, has been reported to inhibit pyocyanin and rhamnolipid production as well as biofilm formation in *P. aeruginosa* (Nam et al., 2020), exhibiting the same phenotype as CPBA in this study. However, in the present study, CPBA antagonized not only RhlR but also LasR, although weakly. CPBA inhibited pyocyanin and rhamnolipid production by antagonizing both LasR and RhlR (**Figures 6B, 7A**; **Supplementary Figures 5A,B**) and biofilm formation by antagonizing LasR but not RhlR (**Figures 8A,C**), as shown with the QS mutants in this study. Because DFPH has also been reported to inhibit both virulent factor production and biofilm formation at the same low concentrations (Nam et al., 2020), which reflect the same phenotype as that induced by CPBA, it was suggested that both CPBA and DFPH are not exclusive RhlR antagonists and that they retain weak LasR-antagonizing activity in *P. aeruginosa*. Taken together, the results of this study suggest that, at low micromolar concentrations, curvularin is an RhlR-exclusive antagonist, whereas CPBA is an RhlR antagonist with weak LasR-antagonizing activity in *P. aeruginosa*.

Antagonizing effects on QS receptors have generally been investigated in QS reporter strains of *E. coli*, *C. violaceum* CV026/*A. tumefaciens NT1* pair, or *P. aeruginosa*. The QS-antagonizing activity of CPBA and DFPH have been reported in *E. coli* QS reporter strains (Boursier et al., 2018; Nam et al., 2020). CPBA reportedly antagonized RhlR with a half-maximal inhibitory concentration ($IC_{50}$) of 52.2 μM, but it did not antagonize LasR even when it was applied at 1 mM in an *E. coli* QS reporter strain (Boursier et al., 2018), which is inconsistent with the results of CPBA in *C. violaceum* CV026 and *A. tumefaciens* NT1 and in *P. aeruginosa* QS mutants in this study. These results suggest that the *E. coli* QS reporter strain might be less sensitive to LasR antagonists than *P. aeruginosa*. Indeed, 4-iodo POHL has been reported to show a similar antagonizing activity toward RhlR but a different antagonizing activity toward LasR in *E. coli* and *P. aeruginosa* reporter strains; specifically, this compound did not antagonize LasR at 100 μM in *E. coli* reporter strains but did antagonize LasR by 60% at 100 μM in *P. aeruginosa* reporter strains (Eibergen et al., 2015; Welsh et al., 2015). Taken together, these data suggest that reporter strains of *P. aeruginosa* may yield more accurate QS competition assay results than *E. coli*, especially with respect to LasR.

Under standard laboratory conditions, the Las system directs the expression of both the Rhl and Pqs systems. However, it has been reported that this regulatory hierarchy can be nutritionally and environmentally rewired. Under low-phosphate growth conditions, Rhl and Pqs are activated independently of Las (Meng et al., 2020). Depletion of phosphate, an essential component of energy molecules, such as ATP and nucleic acids, is evident after surgical injury, increasing virulence of *P. aeruginosa* (Long et al., 2008; Chekabab et al., 2014). When responding to phosphate depletion stress, the PhoRB regulator of the two-component system activates Rhl and Pqs by profoundly competing against LasR (Meng et al., 2020). Additionally, *lasR* is frequently mutated and nonfunctional in clinical isolates of *P. aeruginosa* in the CF lung environment. In contrast, RhlR independently activates some QS-dependent genes, suggesting RhlR plays a central role in the *in vivo* QS of *P. aeruginosa* during infections of patients with CF (Bjarnsholt et al., 2010; Feltner et al., 2016). Kostylev et al. (2019) and Oshri et al. (2018) also suggested a primary mechanism by which RhlR can be activated when LasR is nonfunctional under laboratory conditions. However, more information on QS circuits under clinical *lasR*-nonfunctional conditions is needed; what are the connections between RhlR and the PQS system, what genes are regulated by RhlR, do RhlR-regulated genes depend on BHL? Because low micromolar concentrations curvularin is a potent and exclusive inhibitor of BHL-mediated activation of RhlR, curvularin can be useful for the development of novel agents to treat *P. aeruginosa* infections as well as for elucidation of the RhlR-mediated QS circuits in *P. aeruginosa*.

(−)-Curvularin has been reported to be produced by many endophytic and soil fungal species, such as *Penicillium* spp. (Yao et al., 2003), *Aspergillus* spp. (Caputo and Viola, 1977), *Curvularia* spp. (Greve et al., 2008), *Alternaria* spp. (Robeson et al., 1985), and *Epicoccum* spp. (Abdel-Hafez et al., 2017). This is the first study to isolate curvularin from *Phoma* sp. Curvularin was isolated

as a white powder in this study and soluble in methanol, ethanol, and acetone. Curvularin has no antimicrobial activity including Gram-positive and -negative bacteria and *Candida albicans* (Kumar et al., 2013). The compound is weak cytotoxic or inactive against human tumor cell lines whereas some curvularin analogs including α,β-dehydrocurvularin show potent cytotoxicity (Kumar et al., 2013; Meng et al., 2013), but is nontoxic to mice and chick embryo (Vesonder et al., 1976). Curvularin exhibits anti-inflammatory activities by inhibiting human inducible nitric oxide synthase (iNOS) expression and iNOS-dependent NO production (Schmidt et al., 2010). However, the antivirulence activity of curvularin against bacteria had not been previously reported.

## CONCLUSION

Curvularin potently inhibited pyocyanin and rhamnolipid production, showing activity similar to that of FC, by antagonizing only RhlR when administered at the low micromolar concentrations of 1–30 μM, without affecting the cell viability of *P. aeruginosa*. Furthermore, curvularin showed threefold greater inhibition of virulent factor production and more selective antagonism against RhlR than CPBA, which retained a weak LasR-antagonizing activity in *P. aeruginosa*, and hexyl gallate. Additionally, the QS mutant-based investigation into the inhibitory relationship between QS and virulent factors by low-concentration curvularin indicated that curvularin inhibited pyocyanin and rhamnolipid production by selectively antagonizing RhlI-dependent RhlR. In particular, curvularin exhibited an *in vivo* antivirulence effect by acting on RhlR with 1.7-fold greater potency than that of FC in a *P. aeruginosa*-infected *C. elegans* model. Overall, low-concentration curvularin is an RhlR-exclusive antagonist in *P. aeruginosa*, and to the best of our knowledge, this is the first report describing an RhlR antagonist from natural resources. Hence, curvularin may be useful for developing novel agents that inhibit the LasR-independent Rhl QS system, which functions in chronic *P. aeruginosa* infections, and for studying the role of RhlR in complex QS networks.

## DATA AVAILABILITY STATEMENT

The datasets presented in this study can be found in online repositories. The names of the repository/repositories and accession number(s) can be found at: figshare, https://figshare.com/s/9111198a877d87c2a642.

## AUTHOR CONTRIBUTIONS

W-GK conceived and designed the experiments and wrote the manuscript. H-YC performed most of the experiments. DL identified the structure of curvularin. H-YC and W-GK analyzed the experimental data. All authors contributed to the article and approved the submitted version.

## FUNDING

This work was supported by Basic Science Research Program through the National Research Foundation of Korea (NRF) funded by the Ministry of Education (grant number NRF-2021R1I1A2048905) and the Korea Research Institute of Bioscience & Biotechnology (KRIBB) Research Initiative Program, South Korea.

## ACKNOWLEDGMENTS

*Pseudomonas aeruginosa* PA14, *P. aeruginosa* PA14 (pUCP18), and *P. aeruginosa* PA14 mutants (Δ*lasR*, Δ*lasI*, Δ*rhlR*, and Δ*rhlI*) were kindly provided by Y. H. Cho (Cha University, Seoul, South Korea).

## SUPPLEMENTARY MATERIAL

The Supplementary Material for this article can be found online at: https://www.frontiersin.org/articles/10.3389/fmicb.2022.913882/full#supplementary-material

## REFERENCES

Abdel-Hafez, S. I., Nafady, N. A., Abdel-Rahim, I. R., Shaltout, A. M., Daròs, J.-A., and Mohamed, M. A. (2017). Biosynthesis of silver nanoparticles using the compound curvularin isolated from the endophytic fungus Epicoccum nigrum: characterization and antifungal activity. *J. Pharm. Appl. Chem.* 3, 135–146. doi: 10.18576/jpac/030207

Allu, S. R., Banne, S., Jiang, J., Qi, N., Guo, J., and He, Y. (2019). A unified synthetic approach to optically pure curvularin-type metabolites. *J. Org. Chem.* 84, 7227–7237. doi: 10.1021/acs.joc.9b00776

Bjarnsholt, T., Jensen, P. Ø., Jakobsen, T. H., Phipps, R., Nielsen, A. K., Rybtke, M. T., et al. (2010). Quorum sensing and virulence of *Pseudomonas aeruginosa* during lung infection of cystic fibrosis patients. *PLoS One* 5:e10115. doi: 10.1371/journal.pone.0010115

Boles, B. R., Thoendel, M., and Singh, P. K. (2005). Rhamnolipids mediate detachment of *Pseudomonas aeruginosa* from biofilms. *Mol. Microbiol.* 57, 1210–1223. doi: 10.1111/j.1365-2958.2005.04743.x

Boursier, M. E., Moore, J. D., Heitman, K. M., Shepardson-Fungairino, S. P., Combs, J. B., Koenig, L. C., et al. (2018). Structure–function analyses of the n-butanoyl l-homoserine lactone quorum-sensing signal define features critical to activity in RhlR. *ACS Chem. Biol.* 13, 2655–2662. doi: 10.1021/acschembio.8b00577

Cao, H., Krishnan, G., Goumnerov, B., Tsongalis, J., Tompkins, R., and Rahme, L. G. (2001). A quorum sensing-associated virulence gene of *Pseudomonas aeruginosa* encodes a LysR-like transcription regulator with a unique self-regulatory mechanism. *Proc. Natl. Acad. Sci. U. S. A.* 98, 14613–14618. doi: 10.1073/pnas.251465298

Caputo, O., and Viola, F. (1977). Isolation of α, β–dehydrocurvularin from Aspergillus aureofulgens. *Planta Med.* 31, 31–32. doi: 10.1055/s-0028-1097485

Chekabab, S. M., Harel, J., and Dozois, C. M. (2014). Interplay between genetic regulation of phosphate homeostasis and bacterial virulence. *Virulence* 5, 786–793. doi: 10.4161/viru.29307

Chen, R., Deziel, E., Groleau, M. C., Schaefer, A. L., and Greenberg, E. P. (2019). Social cheating in a *Pseudomonas aeruginosa* quorum-sensing variant. *Proc. Natl. Acad. Sci. U. S. A.* 116, 7021–7026. doi: 10.1073/pnas.1819801116

Choi, H., Ham, S. Y., Cha, E., Shin, Y., Kim, H. S., Bang, J. K., et al. (2017). Structure-activity relationships of 6- and 8-gingerol analogs as anti-biofilm agents. *J. Med. Chem.* 60, 9821–9837. doi: 10.1021/acs.jmedchem.7b01426

Davey, M. E., Caiazza, N. C., and O'Toole, G. A. (2003). Rhamnolipid surfactant production affects biofilm architecture in *Pseudomonas aeruginosa* PAO1. *J. Bacteriol.* 185, 1027–1036. doi: 10.1128/JB.185.3.1027-1036.2003

Davies, D. (2003). Understanding biofilm resistance to antibacterial agents. *Nat. Rev. Drug Discov.* 2, 114–122. doi: 10.1038/nrd1008

Davies, D. G., Parsek, M. R., Pearson, J. P., Iglewski, B. H., Costerton, J. W., and Greenberg, E. P. (1998). The involvement of cell-to-cell signals in the development of a bacterial biofilm. *Science* 280, 295–298. doi: 10.1126/science.280.5361.295

Diggle, S. P., Winzer, K., Chhabra, S. R., Worrall, K. E., Camara, M., and Williams, P. (2003). The *Pseudomonas aeruginosa* quinolone signal molecule overcomes the cell density-dependency of the quorum sensing hierarchy, regulates rhl-dependent genes at the onset of stationary phase and can be produced in the absence of LasR. *Mol. Microbiol.* 50, 29–43. doi: 10.1046/j.1365-2958.2003.03672.x

Donlan, R. M., and Costerton, J. W. (2002). Biofilms: survival mechanisms of clinically relevant microorganisms. *Clin. Microbiol. Rev.* 15, 167–193. doi: 10.1128/cmr.15.2.167-193.2002

Eibergen, N. R., Moore, J. D., Mattmann, M. E., and Blackwell, H. E. (2015). Potent and selective modulation of the RhlR quorum sensing receptor using non-native ligands:an emerging target for virulence control in *Pseudomonas aeruginosa*. *Chembiochem* 16, 2348–2356. doi: 10.1002/cbic.201500357

Essar, D. W., Eberly, L., Hadero, A., and Crawford, I. P. (1990). Identification and characterization of genes for a second anthranilate synthase in *Pseudomonas aeruginosa*: interchangeability of the two anthranilate synthases and evolutionary implications. *J. Bacteriol.* 172, 884–900. doi: 10.1128/jb.172.2.884-900.1990

Feltner, J. B., Wolter, D. J., Pope, C. E., Groleau, M. C., Smalley, N. E., Greenberg, E. P., et al. (2016). LasR variant cystic fibrosis isolates reveal an adaptable quorum-sensing hierarchy in *Pseudomonas aeruginosa*. *mBio* 7, e01513–e01516. doi: 10.1128/mBio.01513-16

Finnan, S., Morrissey, J. P., O'Gara, F., and Boyd, E. F. (2004). Genome diversity of *Pseudomonas aeruginosa* isolates from cystic fibrosis patients and the hospital environment. *J. Clin. Microbiol.* 42, 5783–5792. doi: 10.1128/JCM.42.12.5783-5792.2004

Galloway, W. R., Hodgkinson, J. T., Bowden, S. D., Welch, M., and Spring, D. R. (2011). Quorum sensing in Gram-negative bacteria: small-molecule modulation of AHL and AI-2 quorum sensing pathways. *Chem. Rev.* 111, 28–67. doi: 10.1021/cr100109t

Gi, M., Jeong, J., Lee, K., Lee, K. M., Toyofuku, M., Yong, D. E., et al. (2014). A drug-repositioning screening identifies pentetic acid as a potential therapeutic agent for suppressing the elastase-mediated virulence of *Pseudomonas aeruginosa*. *Antimicrob. Agents Chemother.* 58, 7205–7214. doi: 10.1128/AAC.03063-14

Greve, H., Schupp, P. J., Eguereva, E., Kehraus, S., Kelter, G., Maier, A., et al. (2008). Apralactone A and a new stereochemical class of curvularins from the marine-derived fungus *Curvularia* sp. *Eur. J. Org. Chem.* 2008, 5085–5092. doi: 10.1002/ejoc.200800522

Hemmati, F., Salehi, R., Ghotaslou, R., Kafil, H. S., Hasani, A., Gholizadeh, P., et al. (2020). Quorum quenching: A potential target for antipseudomonal therapy. *Infect. Drug Resist.* 13, 2989–3005. doi: 10.2147/IDR.S263196

Hodgkinson, J. T., Galloway, W. R., Wright, M., Mati, I. K., Nicholson, R. L., Welch, M., et al. (2012). Design, synthesis and biological evaluation of non-natural modulators of quorum sensing in *Pseudomonas aeruginosa*. *Org. Biomol. Chem.* 10, 6032–6044. doi: 10.1039/c2ob25198a

Hoffman, L. R., Kulasekara, H. D., Emerson, J., Houston, L. S., Burns, J. L., Ramsey, B. W., et al. (2009). *Pseudomonas aeruginosa* lasR mutants are associated with cystic fibrosis lung disease progression. *J. Cyst. Fibros.* 8, 66–70. doi: 10.1016/j.jcf.2008.09.006

Jimenez, P. N., Koch, G., Thompson, J. A., Xavier, K. B., Cool, R. H., and Quax, W. J. (2012). The multiple signaling systems regulating virulence in *Pseudomonas aeruginosa*. *Microbiol. Mol. Biol. Rev.* 76, 46–65. doi: 10.1128/MMBR.05007-11

Kalia, V. C. (2013). Quorum sensing inhibitors: an overview. *Biotechnol. Adv.* 31, 224–245. doi: 10.1016/j.biotechadv.2012.10.004

Kim, H. S., Lee, S. H., Byun, Y., and Park, H. D. (2015). 6-Gingerol reduces *Pseudomonas aeruginosa* biofilm formation and virulence via quorum sensing inhibition. *Sci. Rep.* 5:8656. doi: 10.1038/srep08656

Kim, B., Par, K. J., Choi, H. Y., Kwak, J. H., and Kim, W. G. (2019). Differential effects of alkyl gallates on quorum sensing in *Pseudomonas aeruginosa*. *Sci. Rep.* 9, 7741. doi: 10.1038/s41598-019-44236-w

Kim, B., Park, J. S., Choi, H. Y., Yoon, S. S., and Kim, W. G. (2018). Terrein is an inhibitor of quorum sensing and c-di-GMP in *Pseudomonas aeruginosa*: a connection between quorum sensing and c-di-GMP. *Sci. Rep.* 8:8617. doi: 10.1038/s41598-018-26974-5

Kostylev, M., Kim, D. Y., Smalley, N. E., Salukhe, I., Greenberg, E. P., and Dandekar, A. A. (2019). Evolution of the *Pseudomonas aeruginosa* quorum-sensing hierarchy. *Proc. Natl. Acad. Sci. U. S. A.* 116, 7027–7032. doi: 10.1073/pnas.1819796116

Kumar, C. G., Mongolla, P., Sujitha, P., Joseph, J., Babu, K. S., Suresh, G., et al. (2013). Metabolite profiling and biological activities of bioactive compounds produced by Chrysosporium lobatum strain BK-3 isolated from Kaziranga National Park, Assam, India. *Springerplus* 2, 122. doi: 10.1186/2193-1801-2-122

Latifi, A., Foglino, M., Tanaka, K., Williams, P., and Lazdunski, A. (1996). A hierarchical quorum-sensing cascade in *Pseudomonas aeruginosa* links the transcriptional activators LasR and RhlR (VsmR) to expression of the stationary-phase sigma factor RpoS. *Mol. Microbiol.* 21, 1137–1146. doi: 10.1046/j.1365-2958.1996.00063.x

Lee, J., Wu, J., Deng, Y., Wang, J., Wang, C., Wang, J., et al. (2013). A cell-cell communication signal integrates quorum sensing and stress response. *Nat. Chem. Biol.* 9, 339–343. doi: 10.1038/nchembio.1225

Lee, J., and Zhang, L. (2015). The hierarchy quorum sensing network in *Pseudomonas aeruginosa*. *Protein Cell* 6, 26–41. doi: 10.1007/s13238-014-0100-x

Long, J., Zaborina, O., Holbrook, C., Zaborin, A., and Alverdy, J. (2008). Depletion of intestinal phosphate after operative injury activates the virulence of *P. aeruginosa* causing lethal gut-derived sepsis. *Surgery* 144, 189–197. doi: 10.1016/j.surg.2008.03.045

Luo, J., Dong, B., Wang, K., Cai, S., Liu, T., Cheng, X., et al. (2017). Baicalin inhibits biofilm formation, attenuates the quorum sensing-controlled virulence and enhances *Pseudomonas aeruginosa* clearance in a mouse peritoneal implant infection model. *PLoS One* 12:e0176883. doi: 10.1371/journal.pone.0176883

McClean, K. H., Winson, M. K., Fish, L., Taylor, A., Chhabra, S. R., Camara, M., et al. (1997). Quorum sensing and *Chromobacterium violaceum*: exploitation of violacein production and inhibition for the detection of N-acylhomoserine lactones. *Microbiology* 143, 3703–3711. doi: 10.1099/00221287-143-12-3703

McInnis, C. E., and Blackwell, H. E. (2011). Design, synthesis, and biological evaluation of abiotic, non-lactone modulators of LuxR-type quorum sensing. *Bioorg. Med. Chem.* 19, 4812–4819. doi: 10.1016/j.bmc.2011.06.072

Meng, X., Ahator, S. D., and Zhang, L. H. (2020). Molecular mechanisms of phosphate stress activation of *Pseudomonas aeruginosa* quorum sensing systems. *mSphere* 5, e00119–e00120. doi: 10.1128/mSphere.00119-20

Meng, L. H., Li, X. M., Lv, C. T., Li, C. S., Xu, G. M., Huang, C. G., et al. (2013). Sulfur-containing cytotoxic curvularin macrolides from *Penicillium sumatrense* MA-92, a fungus obtained from the rhizosphere of the mangrove *Lumnitzera racemosa*. *J. Nat. Prod.* 76, 2145–2149. doi: 10.1021/np400614f

Mukherjee, S., Moustafa, D., Smith, C. D., Goldberg, J. B., and Bassler, B. L. (2017). The RhlR quorum-sensing receptor controls *Pseudomonas aeruginosa* pathogenesis and biofilm development independently of its canonical homoserine lactone autoinducer. *PLoS Pathog.* 13:e1006504. doi: 10.1371/journal.ppat.1006504

Nam, S., Ham, S.-Y., Kwon, H., Kim, H.-S., Moon, S., Lee, J.-H., et al. (2020). Discovery and characterization of pure RhlR antagonists against *Pseudomonas aeruginosa* infections. *J. Med. Chem.* 63, 8388–8407. doi: 10.1021/acs.jmedchem.0c00630

Ng, W. L., and Bassler, B. L. (2009). Bacterial quorum-sensing network architectures. *Annu. Rev. Genet.* 43, 197–222. doi: 10.1146/annurev-genet-102108-134304

Ochsner, U. A., Koch, A. K., Fiechter, A., and Reiser, J. (1994). Isolation and characterization of a regulatory gene affecting rhamnolipid biosurfactant synthesis in *Pseudomonas aeruginosa*. *J. Bacteriol.* 176, 2044–2054. doi: 10.1128/jb.176.7.2044-2054.1994

Ochsner, U. A., and Reiser, J. (1995). Autoinducer-mediated regulation of rhamnolipid biosurfactant synthesis in *Pseudomonas aeruginosa*. *Proc. Natl. Acad. Sci. U. S. A.* 92, 6424–6428. doi: 10.1073/pnas.92.14.6424

O'Loughlin, C. T., Miller, L. C., Siryaporn, A., Drescher, K., Semmelhack, M. F., and Bassler, B. L. (2013). A quorum-sensing inhibitor blocks *Pseudomonas aeruginosa* virulence and biofilm formation. *Proc. Natl. Acad. Sci. U. S. A.* 110, 17981–17986. doi: 10.1073/pnas.1316981110

Oshri, R. D., Zrihen, K. S., Shner, I., Omer Bendori, S., and Eldar, A. (2018). Selection for increased quorum-sensing cooperation in *Pseudomonas aeruginosa* through the shut-down of a drug resistance pump. *ISME J.* 12, 2458–2469. doi: 10.1038/s41396-018-0205-y

O'Toole, G. A. (2011). Microtiter dish biofilm formation assay. *J. Vis. Exp.* 47:2437. doi: 10.3791/2437

Papenfort, K., and Bassler, B. L. (2016). Quorum sensing signal-response systems in Gram-negative bacteria. *Nat. Rev. Microbiol.* 14, 576–588. doi: 10.1038/nrmicro.2016.89

Park, S. Y., Hwang, B. J., Shin, M. H., Kim, J. A., Kim, H. K., and Lee, J. K. (2006). N-acylhomoserine lactonase producing *Rhodococcus* spp. with different AHL-degrading activities. *FEMS Microbiol. Lett.* 261, 102–108. doi: 10.1111/j.1574-6968.2006.00336.x

Pearson, J. P., Pesci, E. C., and Iglewski, B. H. (1997). Roles of *Pseudomonas aeruginosa* las and rhl quorum-sensing systems in control of elastase and rhamnolipid biosynthesis genes. *J. Bacteriol.* 179, 5756–5767. doi: 10.1128/jb.179.18.5756-5767.1997

Pesci, E. C., Pearson, J. P., Seed, P. C., and Iglewski, B. H. (1997). Regulation of las and rhl quorum sensing in *Pseudomonas aeruginosa*. *J. Bacteriol.* 179, 3127–3132. doi: 10.1128/jb.179.10.3127-3132.1997

Rasko, D. A., and Sperandio, V. (2010). Anti-virulence strategies to combat bacteria-mediated disease. *Nat. Rev. Drug Discov.* 9, 117–128. doi: 10.1038/nrd3013

Rasmussen, T. B., Skindersoe, M. E., Bjarnsholt, T., Phipps, R. K., Christensen, K. B., Jensen, P. O., et al. (2005). Identity and effects of quorum-sensing inhibitors produced by Penicillium species. *Microbiology* 151, 1325–1340. doi: 10.1099/mic.0.27715-0

Robeson, D. J., Strobel, G. A., and Strange, R. N. (1985). The identification of a major phytotoxic component from Alternaria macrospora as αβ-dehydrocurvularin. *J. Nat. Prod.* 48, 139–141. doi: 10.1021/np50037a028

Rust, L., Messing, C. R., and Iglewski, B. H. (1994). Elastase assays. *Methods Enzymol.* 235, 554–562. doi: 10.1016/0076-6879(94)35170-8

Rutherford, S. T., and Bassler, B. L. (2012). Bacterial quorum sensing: its role in virulence and possibilities for its control. *Cold Spring Harb. Perspect. Med.* 2:a012427. doi: 10.1101/cshperspect.a012427

Sakuragi, Y., and Kolter, R. (2007). Quorum-sensing regulation of the biofilm matrix genes (pel) of *Pseudomonas aeruginosa*. *J. Bacteriol.* 189, 5383–5386. doi: 10.1128/JB.00137-07

Schmidt, N., Pautz, A., Art, J., Rauschkolb, P., Jung, M., Erkel, G., et al. (2010). Transcriptional and post-transcriptional regulation of iNOS expression in human chondrocytes. *Biochem. Pharmacol.* 79, 722–732. doi: 10.1016/j.bcp.2009.10.012

Smith, E. E., Buckley, D. G., Wu, Z., Saenphimmachak, C., Hoffman, L. R., D'Argenio, D. A., et al. (2006). Genetic adaptation by *Pseudomonas aeruginosa* to the airways of cystic fibrosis patients. *Proc. Natl. Acad. Sci. U. S. A.* 103, 8487–8492. doi: 10.1073/pnas.0602138103

Srivastava, A., Singh, B. N., Deepak, D., Rawat, A. K., and Singh, B. R. (2015). Colostrum hexasaccharide, a novel *Staphylococcus aureus* quorum-sensing inhibitor. *Antimicrob. Agents Chemother.* 59, 2169–2178. doi: 10.1128/AAC.03722-14

Vesonder, R. F., Ciegler, A., Fennell, D., and Tjarks, L. W. (1976). Curvularin from penicillium baradicum Baghdadi NRRL 3754, and biological effects. *J. Environ. Sci. Health B* 11, 289–297. doi: 10.1080/03601237609372044

Waters, C. M., and Goldberg, J. B. (2019). *Pseudomonas aeruginosa* in cystic fibrosis: A chronic cheater. *Proc. Natl. Acad. Sci. U. S. A.* 116, 6525–6527. doi: 10.1073/pnas.1902734116

Welsh, M. A., and Blackwell, H. E. (2016). Chemical probes of quorum sensing: from compound development to biological discovery. *FEMS Microbiol. Rev.* 40, 774–794. doi: 10.1093/femsre/fuw009

Welsh, M. A., Eibergen, N. R., Moore, J. D., and Blackwell, H. E. (2015). Small molecule disruption of quorum sensing cross-regulation in *Pseudomonas aeruginosa* causes major and unexpected alterations to virulence phenotypes. *J. Am. Chem. Soc.* 137, 1510–1519. doi: 10.1021/ja5110798

Whiteley, M., Diggle, S. P., and Greenberg, E. P. (2017). Progress in and promise of bacterial quorum sensing research. *Nature* 551, 313–320. doi: 10.1038/nature24624

World Health Organization (2017). *Global Priority List of Antibiotic-Resistant Bacteria to Guide Research D, and Development of New Antibiotics*. Geneva: WHO Press, p. 1–7.

Yao, Y., Hausding, M., Erkel, G., Anke, T., Förstermann, U., and Kleinert, H. (2003). Sporogen, S14-95, and S-curvularin, three inhibitors of human inducible nitric-oxide synthase expression isolated from fungi. *Mol. Pharmacol.* 63, 383–391. doi: 10.1124/mol.63.2.383

Zhang, L., Murphy, P. J., Kerr, A., and Tate, M. E. (1993). Agrobacterium conjugation and gene regulation by N-acyl-L-homoserine lactones. *Nature* 362, 446–448. doi: 10.1038/362446a0

Zhao, J., Li, X., Hou, X., Quan, C., and Chen, M. (2019). Widespread existence of quorum sensing inhibitors in marine bacteria: potential drugs to combat pathogens with novel strategies. *Mar. Drugs* 17:50275. doi: 10.3390/md17050275

**Conflict of Interest:** The authors declare that the research was conducted in the absence of any commercial or financial relationships that could be construed as a potential conflict of interest.

frontiers | Frontiers in Microbiology

TYPE Original Research
PUBLISHED 02 September 2022
DOI 10.3389/fmicb.2022.922444



OPEN ACCESS

EDITED BY
Giuseppantonio Maisetta,
University of Pisa, Italy

REVIEWED BY
Guiyang Xia,
Beijing University of Chinese Medicine, China
Da-Le Guo,
Chengdu University of Traditional Chinese Medicine, China
Satish Sreedharamurthy,
University of Mysore, India
Zhangshuang Deng,
China Three Gorges University, China

*CORRESPONDENCE
Zheng-Hui Li
lizhenghui@mail.scuec.edu.cn
Xin-Xiang Lei
xxlei@mail.scuec.edu.cn

†These authors have contributed equally to this work

SPECIALTY SECTION
This article was submitted to Antimicrobials, Resistance and Chemotherapy, a section of the journal Frontiers in Microbiology

RECEIVED 01 June 2022
ACCEPTED 15 August 2022
PUBLISHED 02 September 2022

CITATION
Wei P-P, Ai H-L, Shi B-B, Ye K, Lv X, Pan X-Y, Ma X-J, Xiao D, Li Z-H and Lei X-X (2022) Paecilins F–P, new dimeric chromanones isolated from the endophytic fungus *Xylaria curta* E10, and structural revision of paecilin A.
*Front. Microbiol.* 13:922444.
doi: 10.3389/fmicb.2022.922444



# Paecilins F–P, new dimeric chromanones isolated from the endophytic fungus *Xylaria curta* E10, and structural revision of paecilin A

Pan-Pan Wei†, Hong-Lian Ai†, Bao-Bao Shi, Ke Ye, Xiao Lv, Xiao-Yan Pan, Xu-Jun Ma, Dan Xiao, Zheng-Hui Li* and Xin-Xiang Lei*

School of Pharmaceutical Sciences, South-Central University for Nationalities, Wuhan, China

A total of eleven new dimeric chromanones, paecilins F-P (**2**–**12**), were isolated from the endophytic fungus *Xylaria curta* E10, along with four known analogs (**1**, **13**–**15**). Their structures and absolute configurations were determined by extensive experimental spectroscopic methods, single-crystal X-ray diffraction, and equivalent circulating density (ECD) calculations. In addition, the structure of paecilin A, which was reported to be a symmetric C8-C8′ dimeric pattern, was revised by analysis of the nuclear magnetic resonance (NMR) data, and single-crystal X-ray diffraction. Compound **1** showed antifungal activity against the human pathogenic fungus *Candida albicans* with a minimum inhibitory concentration of 16 μg/mL, and Compounds **8** and **10** showed antibacterial activity against the gram-negative bacterium *Escherichia coli* with the same minimum inhibitory concentration of 16 μg/mL.

KEYWORDS

**dimeric chromanones, endophytic fungus, *Xylaria curta* E10, antimicrobial activities, structural identification**

## Introduction

Chromanones are a class of compounds with benzo-γ-pyranone skeletons. They are widely distributed in plants, fungi, and lichens (Duan et al., 2019). Chromanones usually form homodimers or heterodimers with xanthones, the biosynthetic precursors of chromanones, with different linkages, including C6-C6, C6-C8, and C8-C8 (Wu et al., 2015; Cao et al., 2022). To unambiguously determine the absolute or even relative configurations of these dimers remains challenging because of the presence of various chiral centers, sometimes with axial chirality. These compounds have been reported to have good biological activities,

such as antitumor (Pinto et al., 2014; El-Elimat et al., 2015; Wu et al., 2015; Arora et al., 2017; Nguyen et al., 2020; Tuong et al., 2020; Lünne et al., 2021; Wang et al., 2021), antifungal (da Silva et al., 2018) and antibacterial (Pontius et al., 2008; Kumla et al., 2017; Wang et al., 2021) activities. Their dimers have attracted much attention from scientists in the fields of chemical synthesis and biosynthesis for many years because of their complex structures and remarkable biological activity (Xiao et al., 2017; Wei and Matsuda, 2020; Wei et al., 2021).

Endophytic fungi are microorganisms that live in healthy plant tissues and do not cause any loss or disease to the host plant (Ribeiro et al., 2021). Endophytic fungi are an important resource of natural bioactive compounds (Li et al., 2008; Liu et al., 2014; Chen et al., 2016; Nalin Rathnayake et al., 2019). For many years, they have attracted much attention because of their ability to produce new bioactive secondary metabolites (Liu et al., 2019). *Xylaria curta* E10 is an endophytic fungus isolated from *Solanum tuberosum*. A previous investigation of this fungus led to the isolation of several cytochalasans with novel scaffolds and intriguing biological activity. Curtachalasins A and B are two cytochalasans with 5/6/6/6 tetracyclic skeletons (Wang et al., 2018), curtachalasins C-E have an unprecedented bridged 6/6/6/6 ring system with significant resistance reversal activity against fluconazole-resistant *Candida albicans* (Wang et al., 2019a), and xylarichalasin A possesses a 6/7/5/6/6/6 fused polycyclic system with remarkable anti-proliferative activity (Wang et al., 2019b).

In our ongoing research on mining structurally interesting and biologically active constituents from natural resources, a chemical study on the endophytic fungus *Xylaria curta* E10 was carried out. As a result, eleven new dimeric chromanones named paecilins F-Q (**2**–**12**), together with four known compounds, paecilin A (**1**) (Guo et al., 2007), versixanthone F (**13**) (Wu et al., 2015), versixanthone A (**14**) (Wu et al., 2015), and versixanthone E (**15**) (Wu et al., 2015) (**Figure 1**) were isolated. Herein, the details of the isolation, structural elucidation, and antimicrobial activities of these compounds are presented.

# Materials and methods

## Fungal material

The strain required in this study was isolated from fresh healthy potato tissues collected from Dali City, Yunnan Province, China, and identified as *Xylaria curta* E10 according to the ITS sequence (GenBank Accession No. KJ883611.1, query cover 100%, maximum identity 99%). At present, the strain is stored in the microbial seed bank of the School of Pharmacy, South-Central University for Nationalities. The fungus *Xylaria curta* E10 was fermented in a solid rice medium (100 g of rice and 100 ml of water, in each 500 ml culture flask, with a total of 15 kg of rice) and was cultured at 24°C for one month.

## Fungal fermentation, extraction, and isolation

The fermented materials were soaked in absolute MeOH (20 L × 5). The combined extracts were evaporated under reduced pressure to afford a crude extract, which was further dissolved in water and partitioned against EtOAc (10 L × 5) to yield 130 g of the extract. Five fractions (A-E) were eluted by gradient elution of chloroform/methanol (1:0-0:1, V/V) by normal silica gel column chromatography.

Fraction B (30 g) was eluted by MPLC (MeOH-$H_2O$, 10:90-100:0, V/V) to obtain nine subfractions ($B_1$–$B_9$). Fraction $B_3$ (380 mg) was separated by preparative HPLC using a reversed-phase column ($CH_3CN$-$H_2O$ from 35:65 to 50:50 in 20 min, flow rate 4 mL/min) to yield **1** (20.3 mg, $t_R$ = 15.6 min). Fraction $B_4$ (6.7 g) was purified over Sephadex LH-20 eluted with MeOH to give six subfractions ($B_{4-1}$–$B_{4-6}$). Fraction $B_{4-3}$ (198 mg) was further purified by preparative HPLC with $CH_3CN$-$H_2O$ (from 32:68 to 52:48 in 20 min, flow rate 4 mL/min) to obtain Compounds **2** (30 mg, $t_R$ = 16.8 min), **3** (7.8 mg, $t_R$ = 17.2 min), **4** (6.6 mg, $t_R$ = 28.3 min), and **5** (7.3 mg, $t_R$ = 29.6 min). Fraction $B_{4-4}$ (600 mg) was separated on a silica gel column and eluted with petroleum ether and ethyl acetate (10:1) to yield five subfractions ($B_{4-4-1}$-$B_{4-4-5}$). $B_{4-4-3}$ was purified by prep-HPLC ($CH_3CN$-$H_2O$ from 39:61 to 55:45 in 25 min, flow rate 4 mL/min) to give **6** (6.8 mg, $t_R$ = 15.6 min), **7** (17.2 mg, $t_R$ = 17.9 min) and **8** (20.4 mg, $t_R$ = 20.8 min).

Fraction C (43 g) was eluted by MPLC (MeOH-$H_2O$, 10:90-100:0, V/V) to obtain eleven subfractions ($C_1$–$C_{11}$). Fraction $C_5$ (3.6 g) was separated on a silica gel column and eluted with petroleum ether and ethyl acetate (8:1), to yield eight subfractions ($C_{5-1}$–$C_{5-8}$). $C_{5-5}$ was purified by prep-HPLC ($CH_3CN$-$H_2O$ from 37:63 to 56:44 in 20 min, flow rate 4 mL/min) to give **9** (11.8 mg, $t_R$ = 18.2 min) and **10** (9.5 mg, $t_R$ = 19.7 min). Fraction $C_6$ (12 g) was purified over Sephadex LH-20 eluted with MeOH to give nine subfractions ($C_{6-1}$–$C_{6-9}$). Fraction $C_{6-5}$ (300 mg) was further purified by preparative HPLC with $CH_3CN$-$H_2O$ (from 40:60 to 54:46 in 20 min, flow rate 4 mL/min) to obtain Compounds **11** (28 mg, $t_R$ = 18.4 min), **12** (6.1 mg, $t_R$ = 19 min) and **13** (10.4 mg, $t_R$ = 23.6 min). Fraction $C_7$ (380 mg) was separated by preparative HPLC using a reversed-phase column ($CH_3CN$-$H_2O$ from 42:58 to 57:43 in 20 min, flow rate 4 mL/min) to yield **14** (16.3 mg, $t_R$ = 18.5 min) and **15** (7.5 mg, $t_R$ = 21.6 min).

## General experimental procedures

Both 1D and 2D spectra were run on Bruker Avance III 600 MHz and Bruker Avance III 500 MHz spectrometers. IR spectra were obtained with a Tenor 27 spectrophotometer using KBr pellets. UV spectra were measured on a UH-5300 spectrometer. CD spectra were recorded by a Chirascan-plus

10.3389/fmicb.2022.922444

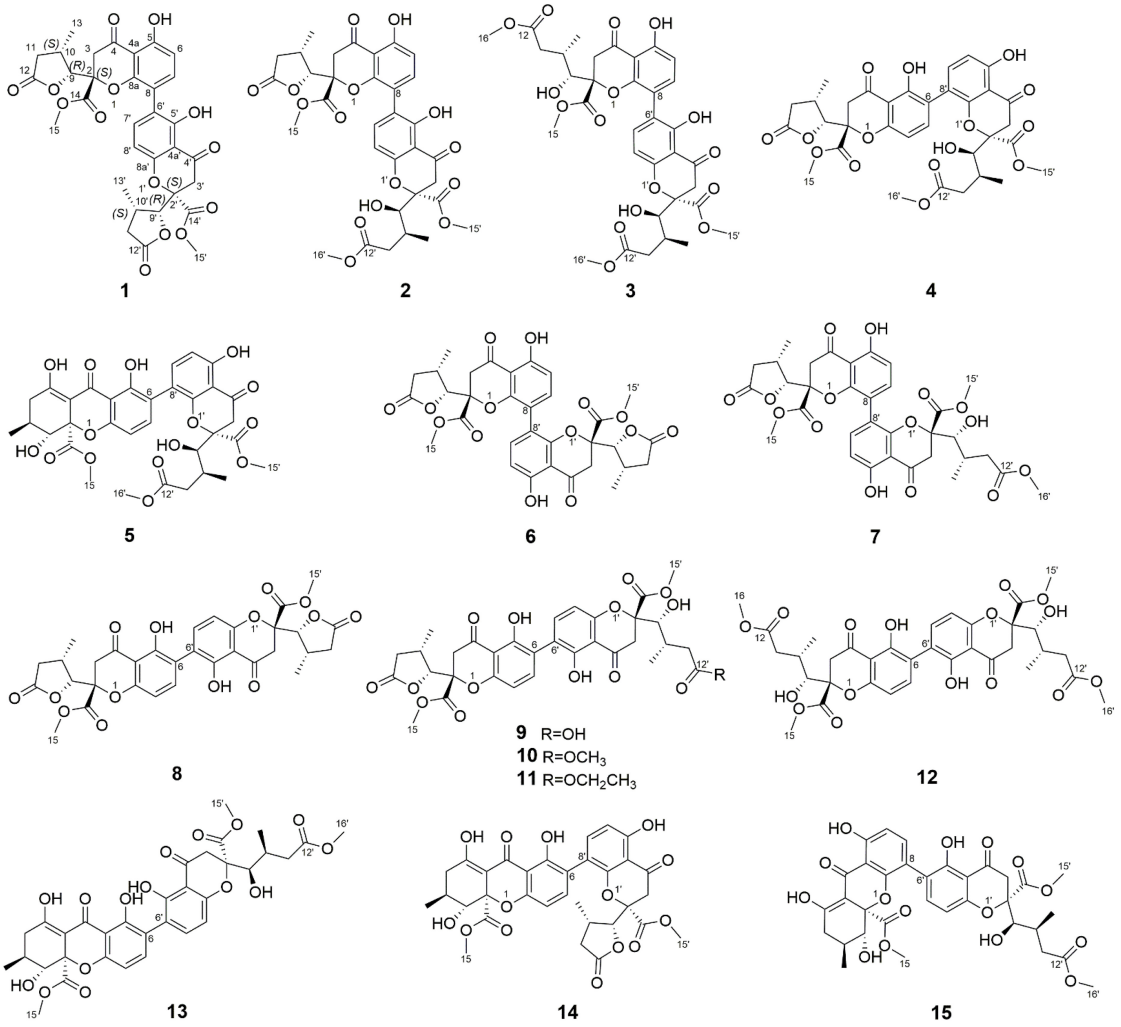


FIGURE 1
Structures of Compounds **1**–**15**.

circular dichromatic spectrometer. The optical rotations were measured with a Horiba Sepa-300 polarimeter. According to the solvent signal, the chemical shifts were expressed in ppm. The mass spectra were recorded on a mass spectrometer (Thermo Fisher Scientific, Bremen, Germany). Medium-pressure liquid chromatography (MPLC) was applied to the Biotage SP1 system and packed with RP-18 gel. Preparative high-performance liquid chromatography (prep-HPLC) was performed on an Agilent 1260 liquid chromatography system equipped with Zorbax SB-C18 columns (5 μm, 9.4 mm × 150 mm, or 21.2 mm × 150 mm) and a DAD detector. Column chromatography (CC) separations were carried out in silica gel (200–300 mesh, Qingdao Haiyang Chemical Co., Ltd., Qingdao) and Sephadex LH-20 (Sweden's France Asia Fine Chemical Co., Ltd.). The components were monitored by TLC ($GF_{254}$, Qingdao Haiyang Chemical Co., Ltd., Qingdao) and the spots were observed by heating the silica gel plate and spraying with vanillin and 10% $H_2SO_4$ in ethanol.

## Spectroscopic characterization of Compounds 2–12

Paecilin F (**2**): light yellow crystal (MeOH); $[\alpha]^{25.1}{}_D$ + 2.3 (*c*.5, MeOH); UV (MeOH) $\lambda_{max}$ (log ε) 260 (3.28) nm; IR (KBr) $\nu_{max}$ 3500, 3000, 2950, 1794, 1736, 1647, 1458, and 1320 $cm^{-1}$; $^1H$ nuclear magnetic resonance (NMR) (500 MHz, $CDCl_3$) and $^{13}C$ NMR (125 MHz, $CDCl_3$) data, see **Table 1**; positive ion HRESIMS *m/z* 693.1814 $[M + Na]^+$ (calcd for $C_{33}H_{34}O_{15}Na$, 693.1795).

Paecilin G (**3**): pale yellow gum; $[\alpha]^{21.5}{}_D$ + 66.9 (*c*.5, MeOH); UV (MeOH) $\lambda_{max}$ (log ε) 260 (2.70) nm; IR (KBr) $\nu_{max}$ 3500, 1734, 1647, 1472, 1437, 1356, 1281, 1233, 1198, 1177, 1070, 1049, and 1011 $cm^{-1}$; $^1H$ NMR (500 MHz, $CDCl_3$) and $^{13}C$ NMR (125 MHz, $CDCl_3$) data, see **Table 1**; positive ion HRESIMS *m/z* 725.2048 $[M + Na]^+$ (calcd for $C_{34}H_{38}O_{16}Na$, 725.2058).

TABLE 1 $^{1}H$ and $^{13}C$ NMR spectroscopic data of Compounds 1–3 ($CDCl_3$).

| No. | 1[a] | | 2[b] | | 3[b] | |
|---|---|---|---|---|---|---|
| | $\delta_C$, type | $\delta_H$, mult (*J* in Hz) | $\delta_C$, type | $\delta_H$, mult (*J* in Hz) | $\delta_C$, type | $\delta_H$, mult (*J* in Hz) |
| 2 | 84.4, C | | 86.0, C | | 87.0, C | |
| 3 | 40.0, $CH_2$ | 3.27, d (17.2)<br>3.15, d (17.2) | 40.1, $CH_2$ | 3.28, d (17.3)<br>3.16, d (17.3) | 40.7, $CH_2$ | 3.23, d (17.3)<br>3.19, d (17.3) |
| 4 | 194.2, C | | 194.2, C | | 196.1, C | |
| 4a | 107.9, C | | 107.9, C | | 107.8, C | |
| 5 | 161.9, C | | 161.9, C | | 161.8, C | |
| 6 | 110.4, CH | 6.62, d (8.6) | 110.4, CH | 6.63, d (8.6) | 110.1, CH | 6.60, d (8.6) |
| 7 | 141.4, CH | 7.45, d (8.6) | 141.7, CH | 7.48, d (8.6) | 141.2, CH | 7.47, d (8.6) |
| 8 | 115.3, C | | 115.3, C | | 115.2, C | |
| 8a | 156.2, C | | 156.1, C | | 156.2, C | |
| 9 | 82.9, CH | 4.86, d (6.6) | 82.4, CH | 4.65, d (7.6) | 76.6, CH | 3.87, s |
| 10 | 33.4, CH | 2.95, m | 34.1, CH | 2.88, m | 30.6, CH | 2.27, m |
| 11 | 37.0, $CH_2$ | 2.73, dd (17.3, 8.2)<br>2.43, dd (17.3, 7.0) | 35.4, $CH_2$ | 2.28, dd (17.3, 8.4)<br>1.94, dd (17.3, 11.2) | 40.0, $CH_2$ | 2.46, dd (15.7, 6.6)<br>2.23, dd (15.7, 6.1) |
| 12 | 175.0, C | | 174.7, C | | 173.3, C | |
| 13 | 14.9, $CH_3$ | 1.29, d (7.2) | 14.7, $CH_3$ | 1.23, d (7.2) | 13.3, $CH_3$ | 0.83, d (6.6) |
| 14 | 169.0, C | | 168.8, C | | 170.6, C | |
| 15 | 53.8, $CH_3$ | 3.79, s | 53.8, $CH_3$ | 3.75, s | 53.5, $CH_3$ | 3.74, s |
| 16 | | | | | 51.9, $CH_3$ | 3.66, s |
| 5-OH | | 11.58, s | | 11.60, s | | 11.69, s |
| 2′ | 85.9, C | | 87.2, C | | 87.0, C | |
| 3′ | 39.6, $CH_2$ | 3.33, d (17.2)<br>3.20, d (17.2) | 40.1, $CH_2$ | 3.31, d (17.3)<br>3.24, d (17.3) | 40.4, $CH_2$ | 3.30, d (17.3)<br>3.25, d (17.3) |
| 4′ | 194.7, C | | 196.5, C | | 196.0, C | |
| 4a′ | 107.4, C | | 107.5, C | | 107.6, C | |
| 5′ | 159.0, C | | 158.9, C | | 159.3, C | |
| 6′ | 117.7, C | | 117.4, C | | 117.7, C | |
| 7′ | 141.2, CH | 7.58, d (8.6) | 141.0, CH | 7.62, d (8.6) | 141.2, CH | 7.68, d (8.6) |
| 8′ | 107.9, CH | 6.61, d (8.6) | 108.0, CH | 6.61, d (8.6) | 107.3, CH | 6.62, d (8.6) |
| 8a′ | 158.4, C | | 158.9, C | | 159.0, C | |
| 9′ | 82.4, CH | 4.65, d (7.5) | 76.3, CH | 4.08, s | 76.5, CH | 4.06, s |
| 10′ | 33.9, CH | 2.87, m | 30.9, CH | 2.35, m | 30.9, CH | 2.38, m |
| 11′ | 35.3, $CH_2$ | 2.28, dd (17.3, 8.5)<br>1.93, dd (17.3, 11.1) | 40.0, $CH_2$ | 2.60, dd (18.0, 9.1) 2.38, m | 40.1, $CH_2$ | 2.61, dd (17.8, 9.0)<br>2.41, dd (17.8, 5.7) |
| 12′ | 174.7, C | | 173.3, C | | 173.3, C | |
| 13′ | 14.6, $CH_3$ | 1.22, d (7.1) | 13.9, $CH_3$ | 1.06, d (6.6) | 13.8, $CH_3$ | 1.07, d (6.4) |
| 14′ | 168.8, C | | 170.5, C | | 170.5, C | |
| 15′ | 53.7, $CH_3$ | 3.73, s | 53.5, $CH_3$ | 3.77, s | 53.5, $CH_3$ | 3.72, s |
| 16′ | | | 51.9, $CH_3$ | 3.70, s | 51.9, $CH_3$ | 3.70, s |
| 5′-OH | | 11.82, s | | 11.95, s | | 11.96, s |

[a]Measured on 600/150 MHz; [b]Measured on 500/125 MHz.

Paecilin H (**4**): pale yellow gum; $[\alpha]^{21.4}_{D}$ + 69.6 (*c*.5, MeOH); UV (MeOH) $\lambda_{max}$ (log ε) 260 (3.20) nm; IR (KBr) $\nu_{max}$ 3500, 1792, 1738, 1651, 1472, 1437, 1356, 1281, 1223, 1196, 1177, 1067, 1007, 837, 785, 584, and 536 $cm^{-1}$; $^{1}H$ NMR (500 MHz, $CDCl_3$) and $^{13}C$ NMR (125 MHz, $CDCl_3$) data, see Table 2; positive ion HRESIMS *m/z* 693.1791 $[M + Na]^+$ (calcd for $C_{33}H_{34}O_{15}Na$ 693.1795).

Paecilin I (**5**): pale yellow gum; $[\alpha]^{21.4}_{D}$ + 147.3 (*c*.5, MeOH); UV (MeOH) $\lambda_{max}$ (log ε) 265 (2.39) nm; IR (KBr) $\nu_{max}$ 3500, 1734, 1653, 1616, 1458, 1356, 1273, 1233, 1067, 1049, 1016, and 820 $cm^{-1}$; $^{1}H$ NMR (600 MHz, $CDCl_3$) and $^{13}C$ NMR (150 MHz, $CDCl_3$) data, see Table 2; positive ion HRESIMS *m/z* 693.1810 $[M + Na]^+$ (calcd for $C_{33}H_{34}O_{15}Na$, 693.1795).

TABLE 2 $^{1}H$ and $^{13}C$ NMR spectroscopic data of Compounds 4, 5, and 7 ($CDCl_3$).

| No. | 4[a] | | 5[b] | | 7[b] | |
|---|---|---|---|---|---|---|
| | $\delta_C$, type | $\delta_H$, mult (*J* in Hz) | $\delta_C$, type | $\delta_H$, mult (*J* in Hz) | $\delta_C$, type | $\delta_H$, mult (*J* in Hz) |
| 2 | 84.7, C | | 85.0, C | | 85.7, C | |
| 3 | 39.9, $CH_2$ | 3.31, d (17.2)<br>3.19, d (17.2) | 101.7, C | | 40.9, $CH_2$ | 3.27, d (17.3)<br>3.19, d (17.3) |
| 4 | 194.3, C | | 187.3, C | | 194.3, C | |
| 4a | 107.6, C | | 107.0, C | | 107.8, C | |
| 5 | 159.3, C | | 159.4, C | | 161.9, C | |
| 6 | 118.0, C | | 118.2, C | | 110.4, CH | 6.63, d (8.7) |
| 7 | 141.6, CH | 7.72, d (8.6) | 140.5, CH | 7.66, d (8.6) | 141.6, CH | 7.76, d (8.7) |
| 8 | 107.4, CH | 6.63, d (8.6) | 107.8, CH | 6.64, d (8.6) | 114.5, C | |
| 8a | 158.6, C | | 158.5, C | | 155.7, C | |
| 9 | 82.8, CH | 4.83, d (6.9) | 77.2, CH | 3.95, d (11.3) | 82.6, CH | 4.68, d (7.2) |
| 10 | 33.6, CH | 3.00, m | 29.4, CH | 2.44, m | 33.8, CH | 2.88, m |
| 11 | 36.8, $CH_2$ | 2.72, dd (17.3, 8.3)<br>2.50, dd (17.3, 8.0) | 36.4, $CH_2$ | 2.75, dd (19.3, 6.4)<br>2.33, dd (19.3, 10.6) | 36.1, $CH_2$ | 1.97, dd (17.2, 9.9)<br>2.42, dd (17.2, 8.3) |
| 12 | 175.0, C | | 177.9, C | | 174.5, C | |
| 13 | 15.0, $CH_3$ | 1.35, d (7.2) | 18.2, $CH_3$ | 1.18, d (6.6) | 14.8, $CH_3$ | 1.18, d (7.2) |
| 14 | 169.1, C | | 170.4, C | | 168.8, C | |
| 15 | 53.5, $CH_3$ | 3.76, s | 53.5, $CH_3$ | 3.73, s | 53.9, $CH_3$ | 3.79, s |
| 16 | | | | | | |
| 5-OH | | 11.86, s | | 11.67, s | | 11.70, s |
| 9-OH | | | | 2.83, s | | |
| 12-OH | | | | 13.76, s | | |
| 2′ | 87.0, C | | 87.0, C | | 87.0, C | |
| 3′ | 40.8, $CH_2$ | 3.24, d (17.2)<br>3.20, d (17.2) | 40.5, $CH_2$ | 3.24, d (17.5)<br>3.20, d (17.5) | 40.0, $CH_2$ | 3.27, d (17.3)<br>3.19, d (17.3) |
| 4′ | 196.0, C | | 196.0, C | | 195.8, C | |
| 4a′ | 107.8, C | | 107.8, C | | 107.7, C | |
| 5′ | 161.9, C | | 161.8, C | | 161.8, C | |
| 6′ | 110.1, CH | 6.61, d (8.6) | 110.2, CH | 6.61, d (8.6) | 110.9, CH | 6.65, d (8.7) |
| 7′ | 141.1, CH | 7.47, d (8.6) | 141.2, CH | 7.47, d (8.6) | 142.2, CH | 7.92, d (8.7) |
| 8′ | 115.0, C | | 115.4, C | | 114.9, C | |
| 8a′ | 156.2, C | | 156.1, C | | 155.8, C | |
| 9′ | 76.7, CH | 3.88, d (2.0) | 76.6, CH | 3.88, s | 76.8, CH | 3.89, dd (7.9, 1.6) |
| 10′ | 30.6, CH | 2.29, m | 30.8, CH | 2.26, m | 30.8, CH | 2.28, m |
| 11′ | 40.0, $CH_2$ | 2.46, dd (15.7, 6.5)<br>2.23, dd (15.7, 6.0) | 39.9, $CH_2$ | 2.46, dd (15.6, 6.5)<br>2.22, dd (15.6, 6.3) | 39.9, $CH_2$ | 2.22, dd (15.6, 6.3)<br>2.46, dd (15.6, 6.3) |
| 12′ | 173.3, C | | 173.2, C | | 173.2, C | |
| 13′ | 13.9, $CH_3$ | 0.84, d (6.7) | 13.6, $CH_3$ | 0.87, d (6.6) | 13.3, $CH_3$ | 0.83, d (6.5) |
| 14′ | 170.5, C | | 170.4, C | | 170.5, C | |
| 15′ | 53.8, $CH_3$ | 3.72, s | 53.4, $CH_3$ | 3.73, s | 53.6, $CH_3$ | 3.78, s |
| 16′ | 51.9, $CH_3$ | 3.66, s | 51.9, $CH_3$ | 3.65, s | 51.9, $CH_3$ | 3.65, s |
| 5′-OH | | 11.70, s | | 11.70, s | | 11.68, s |
| 9′-OH | | | | 2.55, s | | 2.50, d (7.9) |

[a]Measured on 600/150 MHz; [b]Measured on 500/125 MHz.

Paecilin J (**6**): brown crystal (MeOH); $[\alpha]^{22.5}_D$ + 36.9 (*c*.5, MeOH); UV (MeOH) $\lambda_{max}$ (log ε) 260 (1.40) nm; IR (KBr) $\nu_{max}$ 3500, 2922, 2851, 1790, 1742, 1647, 1466, 1383, 1346, 1234, 1202, 1179, 1049, and 1024 $cm^{-1}$; $^{1}H$ NMR (500 MHz, $CD_3COCD_3$) and $^{13}C$ NMR (125 MHz, $CD_3COCD_3$) data, see Table 3; positive ion HRESIMS *m/z* 661.1526 $[M + Na]^+$ (calcd for $C_{32}H_{30}O_{14}Na$ 661.1533).

Paecilin K (**7**): pale yellow gum; $[\alpha]^{21.3}_D$ + 46 (*c*.5, MeOH); UV (MeOH) $\lambda_{max}$ (log ε) 260 (1.76) nm; IR (KBr) $\nu_{max}$ 3500, 1794, 1740, 1647, 1468, 1348, 1283, 1236, 1051, 1020, 837, 783, 758, 737, 648, and 550 $cm^{-1}$; $^{1}H$ NMR (500 MHz, $CDCl_3$) and $^{13}C$ NMR (125 MHz, $CDCl_3$) data, see Table 2; positive ion HRESIMS *m/z* 693.1785 $[M + Na]^+$ (calcd for $C_{33}H_{34}O_{15}Na$, 693.1795).

TABLE 3 $^{1}H$ and $^{13}C$ NMR spectroscopic data of Compounds 6, 8, and 12 ($CDCl_3$).

| No. | 6[ac] | | 8[ad] | | 12[bd] | |
|---|---|---|---|---|---|---|
| | $\delta_C$, type | $\delta_H$, mult (*J* in Hz) | $\delta_C$, type | $\delta_H$, mult (*J* in Hz) | $\delta_C$, type | $\delta_H$, mult (*J* in Hz) |
| 2,2′ | 86.9, C | | 84.6, C | | 86.9, C | |
| 3,3′ | 40.4, $CH_2$ | 3.56, d (17.6)<br>3.18, d (17.6) | 39.8, $CH_2$ | 3.27, d (17.3)<br>3.19, d (17.3) | 40.3, $CH_2$ | 3.26, d (17.3)<br>3.23, d (17.3) |
| 4,4′ | 195.9, C | | 194.2, C | | 196.1, C | |
| 4a,4a′ | 108.4, C | | 107.6, C | | 107.6, C | |
| 5,5′ | 162.3, C | | 159.2, C | | 159.3, C | |
| 6,6′ | 110.8, CH | 6.54, d (8.7) | 117.7, C | | 117.6, C | |
| 7,7′ | 142.5, CH | 7.89, d (8.7) | 141.3, CH | 7.52, d (8.6) | 141.0, CH | 7.50, d (8.5) |
| 8,8′ | 115.4, C | | 107.5, CH | 6.62, d (8.6) | 107.3, CH | 6.61, d (8.5) |
| 8a,8a′ | 156.7, C | | 158.6, C | | 158.9, C | |
| 9,9′ | 82.9, CH | 4.89, d (7.2) | 82.7, CH | 4.80, d (6.8) | 76.5, CH | 4.05, s |
| 10,10′ | 34.4, CH | 3.03, m | 33.6, CH | 2.98, m | 30.9, CH | 2.37, m |
| 11,11′ | 36.6, $CH_2$ | 2.39, dd (17.0, 8.3)<br>1.85, dd (17.0, 9.9) | 36.8, $CH_2$ | 2.70, dd (17.3, 8.3)<br>2.47, dd (17.3, 8.3) | 40.1, $CH_2$ | 2.60, dd (17.9, 9.1)<br>2.40, dd (17.9, 9.1) |
| 12,12′ | 175.1, C | | 175.0, C | | 173.3, C | |
| 13,13′ | 15.0, $CH_3$ | 1.20, d (7.2) | 15.0, $CH_3$ | 1.33, d (7.2) | 13.8, $CH_3$ | 1.06, d (6.5) |
| 14,14′ | 170.0, C | | 169.1, C | | 170.6, C | |
| 15,15′ | 53.9, $CH_3$ | 3.80, s | 53.8, $CH_3$ | 3.76, s | 53.6, $CH_3$ | 3.76, s |
| 16,16′ | | | | | 51.9, $CH_3$ | 3.70, s |
| 5/5′-OH | | 11.70, brs | | 11.91, s | | 12.00, s |
| 9/9′-OH | | | | | | 2.77, s |

[a]Measured on 500/125 MHz; [b]Measured on 600/150 MHz; [c]Measured in $CD_3COCD_3$; [d]Measured in $CDCl_3$.

Paecilin L (**8**): pale yellow gum; $[\alpha]^{21.0}_D$ + 52.9 (*c*.5, MeOH); UV (MeOH) $\lambda_{max}$ (log ε) 265 (1.85) nm; IR (KBr) $\nu_{max}$ 3500, 2920, 1792, 1740, 1645, 1626, 1435, 1362, 1215, 1177, 1150, 1061, 1024, 804, and 586 $cm^{-1}$; $^{1}H$ NMR (500 MHz, $CDCl_3$) and $^{13}C$ NMR (125 MHz, $CDCl_3$) data, see Table 3; positive ion HRESIMS m/z 661.1538 $[M + Na]^+$ (calcd for $C_{32}H_{30}O_{14}Na$, 661.1533).

Paecilin M (**9**): pale yellow gum; $[\alpha]^{20.8}_D$ – 96.9 (*c*.5, MeOH); UV (MeOH) $\lambda_{max}$ (log ε) 265 (1.66) nm; IR (KBr) $\nu_{max}$ 3500, 2924, 1788, 1736, 1626, 1578, 1437, 1362, 1288, 1271, 1250, 1217, 1119, 1065, 839, 816, 785, and 586 $cm^{-1}$; $^{1}H$ NMR (600 MHz, $CDCl_3$) and $^{13}C$ NMR (150 MHz, $CDCl_3$) data, see Table 4; positive ion HRESIMS *m/z* 679.1627 $[M + Na]^+$ (calcd for $C_{32}H_{32}O_{15}Na$, 679.1639).

Paecilin N (**10**): pale yellow gum; $[\alpha]^{25.1}_D$ – 62.7 (*c*.5, MeOH); UV (MeOH) $\lambda_{max}$ (log ε) 260 (1.88) nm; IR (KBr) $\nu_{max}$ 3500, 2960, 1800, 1736, 1624, 1540, 1437, 1320, 1063, and 800 $cm^{-1}$; $^{1}H$ NMR (500 MHz, $CDCl_3$) and $^{13}C$ NMR (125 MHz, $CDCl_3$) data, see Table 4; positive ion HRESIMS *m/z* 671.2001 $[M + H]^+$ (calcd for $C_{33}H_{35}O_{15}$, 671.1976).

Paecilin O (**11**): pale yellow gum; $[\alpha]^{25.1}_D$ – 46.7 (*c*.5, MeOH); UV (MeOH) $\lambda_{max}$ (log ε) 260 (1.37) nm; IR (KBr) $\nu_{max}$ 3500, 2970, 1792, 1734, 1626, 1520, 1480, and 1204 $cm^{-1}$; $^{1}H$ NMR (600 MHz, $CDCl_3$) and $^{13}C$ NMR (150 MHz, $CDCl_3$) data, see Table 4; positive ion HRESIMS *m/z* 707.1934 $[M + Na]^+$ (calcd for $C_{34}H_{36}O_{15}Na$, 707.1952).

Paecilin P (**12**): pale yellow gum; $[\alpha]^{21.4}_D$ – 59.6 (*c*.5, MeOH); UV (MeOH) $\lambda_{max}$ (log ε) 265 (3.25) nm; IR (KBr) $\nu_{max}$ 3500, 1736, 1647, 1626, 1437, 1364, 1204, 1119, 1065, 1011, and 584 $cm^{-1}$; $^{1}H$ NMR (600 MHz, $CDCl_3$) and $^{13}C$ NMR (150 MHz, $CDCl_3$) data, see Table 3; positive ion HRESIMS *m/z* 725.2049 $[M + Na]^+$ (calcd for $C_{34}H_{38}O_{16}Na$, 725.2058).

## X-ray crystallographic analysis of Compounds 1, 2 and 6

### X-ray crystallographic analysis of paecilin A (1)

$C_{32}H_{30}O_{14}$, *M* = 638.56, *a* = 13.492(2) Å, *b* = 8.2053(15) Å, *c* = 14.726(3) Å, α = 90°, β = 114.945(5)°, γ = 90°, *V* = 1488.7(5) $Å^3$, *T* = 294(2) K, space group P1211, *Z* = 2, μ(Cu Kα) = 1.54178 $mm^{-1}$. The final anisotropic full-matrix least-squares refinement on $F^2$ with 424 variables converged at $R_1$ = 2.99% for the observed data and $wR^2$ = 8.38% for all data. The goodness-of-fit was 1.061. The absolute configuration was determined by the Flack parameter = 0.03(5). CCDC: 2155089. Available online: https://www.ccdc.cam.ac.uk (accessed on 28 February 2022).

### X-ray crystallographic analysis of paecilin F (2)

$C_{33}H_{34}O_{15}$, *M* = 670.6, *a* = 14.3975(11) Å, *b* = 14.4598(11) Å, *c* = 15.2705(12) Å, α = 90°, β = 90°, γ = 90°, *V* = 3179.1(4) $Å^3$, *T* = 295(2). K, space group P212121, *Z* = 4, μ(Cu

TABLE 4 $^{1}H$ and $^{13}C$ NMR spectroscopic data of Compounds 9, 10, and 11 ($CDCl_3$).

| No. | 9[a] | | 10[b] | | 11[a] | |
|---|---|---|---|---|---|---|
| | $\delta_C$, type | $\delta_H$, mult (*J* in Hz) | $\delta_C$, type | $\delta_H$, mult (*J* in Hz) | $\delta_C$, type | $\delta_H$, mult (*J* in Hz) |
| 2 | 84.5, C | | 84.5, C | | 84.6, C | |
| 3 | 39.9,$CH_2$ | 3.26, d (17.3)<br>3.23, d (17.3) | 39.7, $CH_2$ | 3.26, d (17.3)<br>3.22, d (17.3) | 39.9, $CH_2$ | 3.27, d (17.2)<br>3.20, d (17.2) |
| 4 | 196.1, C | | 196.2, C | | 194.2, C | |
| 4a | 107.7, C | | 107.6, C | | 107.7, C | |
| 5 | 159.3, C | | 159.2, C | | 159.3, C | |
| 6 | 117.5, C | | 117.3, C | | 117.4, C | |
| 7 | 141.0, CH | 7.49, d (8.6) | 140.9, CH | 7.47, d (8.6) | 141.4, CH | 7.53, d (8.5) |
| 8 | 107.5, CH | 6.62, d (8.6) | 107.4, CH | 6.61, d (8.6) | 107.5, CH | 6.63, d (8.5) |
| 8a | 159.0, C | | 159.0, C | | 158.5, C | |
| 9 | 82.8, CH | 4.80, d (6.9) | 82.7, CH | 4.79, d (6.9) | 82.8, CH | 4.80, d (6.9) |
| 10 | 33.6, CH | 2.98, m | 33.6, CH | 2.99, m | 33.7, CH | 2.98, m |
| 11 | 36.8, $CH_2$ | 2.70, dd (17.3, 8.3)<br>2.49, dd (17.3, 8.1) | 36.7, $CH_2$ | 2.69, dd (17.3, 8.3)<br>2.47, dd (17.3, 8.1) | 36.8, $CH_2$ | 2.70, dd (17.3, 8.3)<br>2.49, dd (17.3, 8.1) |
| 12 | 175.1, C | | 175.2, C | | 175.0, C | |
| 13 | 15.0, $CH_3$ | 1.33, d (7.2) | 14.9, $CH_3$ | 1.32, d (7.2) | 15.0, $CH_3$ | 1.34, d (7.2) |
| 14 | 169.2, C | | 169.2, C | | 169.2, C | |
| 15 | 53.9, $CH_3$ | 3.75, s | 53.8, $CH_3$ | 3.75, s | 53.9, $CH_3$ | 3.77, s |
| **16** | | | | | | |
| 5-OH | | 12.00, s | | 12.00, s | | 12.00, s |
| 2′ | 86.9, C | | 87.0, C | | 87.0, C | |
| 3′ | 40.1, $CH_2$ | 3.24, d (17.3)<br>3.19, d (17.3) | 40.2, $CH_2$ | 3.25, d (17.3)<br>3.18, d (17.3) | 40.3, $CH_2$ | 3.27, d (17.5)<br>3.23, d (17.5) |
| 4′ | 194.3, C | | 194.2, C | | 196.1, C | |
| 4a′ | 107.6, C | | 107.5, C | | 107.7, C | |
| 5′ | 159.3, C | | 159.2, C | | 159.3, C | |
| 6′ | 117.8, C | | 117.8, C | | 117.9, C | |
| 7′ | 141.4, CH | 7.52, d (8.6) | 141.3, CH | 7.51, d (8.6) | 141.0, CH | 7.50, d (8.5) |
| 8′ | 107.4, CH | 6.60, d (8.6) | 107.3, CH | 6.58, d (8.6) | 107.4, CH | 6.62, d (8.5) |
| 8a′ | 158.5, C | | 158.5, C | | 159.1, C | |
| 9′ | 76.3, CH | 4.08, s | 76.3, CH | 4.03, d (2.0) | 76.5, CH | 4.06, dd (5.9, 1.5) |
| 10′ | 30.8, CH | 2.39, m | 30.9, CH | 2.35, m | 30.9, CH | 2.39, m |
| 11′ | 39.9, $CH_2$ | 2.65, dd (16.9, 7.0)<br>2.42, dd (16.9, 5.3) | 40.0, $CH_2$ | 2.58, dd (17.9, 9.2)<br>2.38, dd (17.9, 5.9) | 40.4, $CH_2$ | 2.58, dd (17.7, 9.1)<br>2.36, dd (17.7, 5.8) |
| 12′ | 173.3, C | | 173.3, C | | 172.9, C | |
| 13′ | 13.8, $CH_3$ | 1.09, d (6.6) | 13.8, $CH_3$ | 1.05, d (6.4) | 13.7, $CH_3$ | 1.07, d (6.6) |
| 14′ | 170.6, C | | 170.6, C | | 170.6, C | |
| 15′ | 53.6, $CH_3$ | 3.74, s | 53.5, $CH_3$ | 3.74, s | 53.6, $CH_3$ | 3.76, s |
| 16′ | | | 51.9, $CH_3$ | 3.68, s | 60.9, $CH_2$ | 4.16, q (7.1) |
| 17′ | | | | | 14.4, $CH_3$ | 1.28, t (7.1) |
| 5′-OH | | 11.89, s | | 11.87, s | | 11.87, s |

[a]Measured on 600/150 MHz; [b]Measured on 500/125 MHz.

Kα) = 1.54178 $mm^{-1}$. The final anisotropic full-matrix least-squares refinement on $F^2$ with 448 variables converged at $R_1$ = 3.63% for the observed data and $wR^2$ = 10.01% for all data. The goodness-of-fit was 1.058. The absolute configuration was determined by the Flack parameter = 0 (3). CCDC: 2155090. Available online: https://www.ccdc.cam.ac.uk (accessed on 28 February 2022).

## X-ray crystallographic analysis of paecilin J (6)

$C_{32}H_{30}O_{14}$, $M$ = 638.56, $a$ = 12.0791(14) Å, $b$ = 13.3887(17) Å, $c$ = 18.223(2) Å, α = 90°, β = 126.144(2)°, γ = 90°, $V$ = 2947.1(6) $Å^3$, $T$ = 299(2) K, space group C2221, $Z$ = 4, μ(Cu Kα) = 1.54178 $mm^{-1}$. The final anisotropic full-matrix least-squares refinement on $F^2$ with 212 variables converged at $R_1$ = 3.67% for the observed data and $wR^2$ = 11.05%

for all data. The goodness-of-fit was 1.18. The absolute configuration was determined by the Flack parameter = 0.04(8). CCDC: 2155091. Available online: https://www.ccdc.cam.ac.uk (accessed on 28 February 2022).

## Equivalent circulating density calculations

Equivalent circulating density (ECD) calculations were carried out by the Gaussian 16 software package (Frisch et al., 2013). The conformation of the system was analyzed by Spartan 14 and calculated by the MMFF94s molecular mechanics' force field. The cutoff energy was 10 kcal/mol. The conformational optimization and frequency were calculated at the B3LYP/def2svp theoretical level by using the IEFPCM solvent model (MeOH). The optimized conformations with proportions greater than 2% were selected for ECD calculations. Compounds **3**, **4**, **8**, **10**, **11**, and **12** used the IEFPCM solvent model (MeOH) to calculate ECD (TDDFT) at the wB97xd/def2svp theoretical level. Compounds **5** and **9** used the IEFPCM solvent model (MeOH) to calculate ECD (TDDFT) at the B3LYP/DGD2VP theoretical level. Compound **7** used the IEFPCM solvent model (MeOH) to calculate ECD (TDDFT) at the wB97xd/TZVP theoretical level. The ECD curves were simulated in SpecDis v1.71 using a Gaussian function (Bruhn et al., 2013). The calculated ECD data of all conformers were Boltzmann averaged by Gibbs free energies.

## Antimicrobial activity assays

The Microbroth dilution drug sensitivity test was used for MIC determination of the tested compounds. The bacterial liquid growth was observed on a clean workbench when the concentrations of the compounds to be measured were 8, 16, 32, 64, 128, 256, and 512 μg/mL. The concentrations of *Escherichia coli* ATCC 25922 and *Salmonella enteritidis* ATCC 25923 after secondary activation were adjusted to $1.0 \times 10^8$ CFU/mL using MH medium (Qingdao High-tech Industrial Park Haibo Biotechnology Co., Ltd.). The concentration of *C. albicans* ATCC 10231 was adjusted to $1.0 \times 10^5$ CFU/mL using a PDB medium (Qingdao High-tech Industrial Park Haibo Biotechnology Co., Ltd.). The 96-well plate was rationally planned, and the experimental groups were set as 100 μL compound and 100 μL bacterial solution, with two multiple Wells. The first group of negative control medium was 200 μL MH or PDB medium, which was evaluated in a single well. In the second group, 100 μL DMSO and 100 MH or PDB medium were used as negative controls. The positive control was a

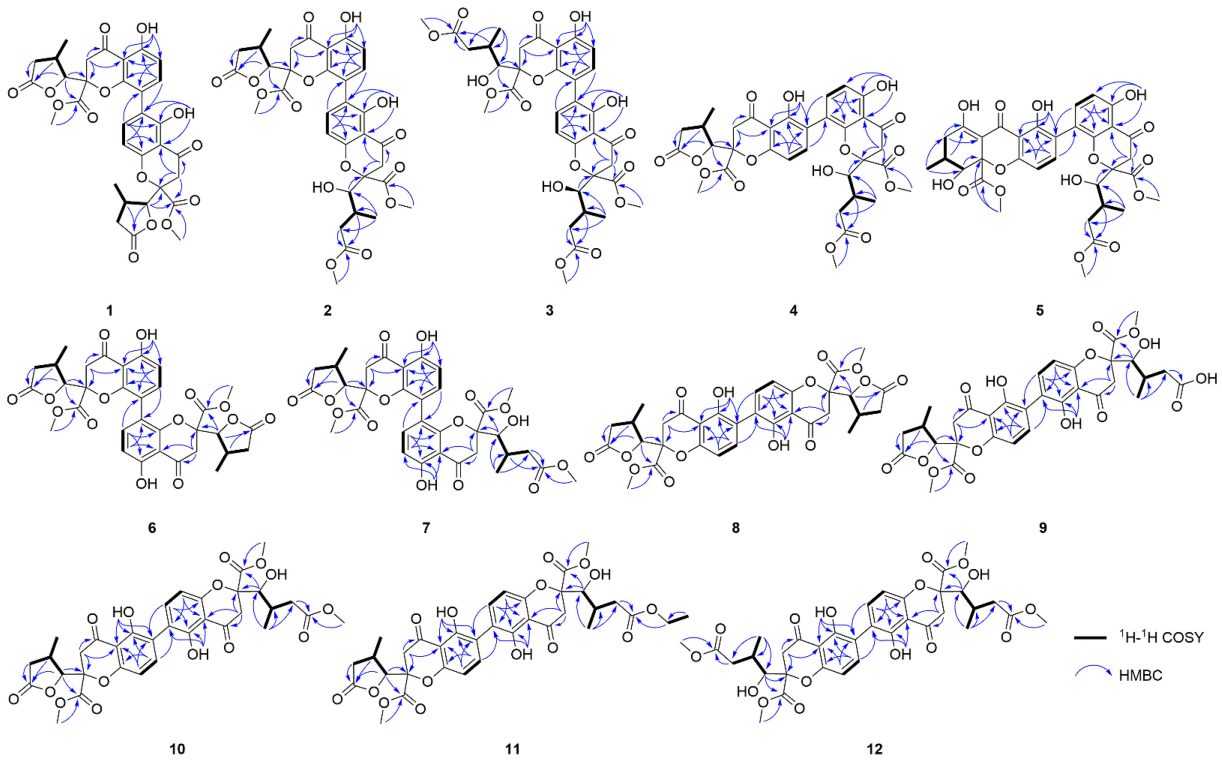


FIGURE 2
Key $^1$H-$^1$H COSY and HMBC correlations for **1**–**12**.

200 μL bacterial solution with two duplicate wells. Amphenicol, penicillin, and fluconazole were used as positive controls for *E. coli*, *S. enteritidis*, and *C. albicans*, respectively. The 96-well plate was cultured in a high-throughput growth curve analyzer for 24 h, and the results were observed. The positive control well showed turbidity, while the negative control was clear. The quality control was within the specified range, and the MIC values of compounds were the lowest concentrations without bacterial growth observed by the naked eye.

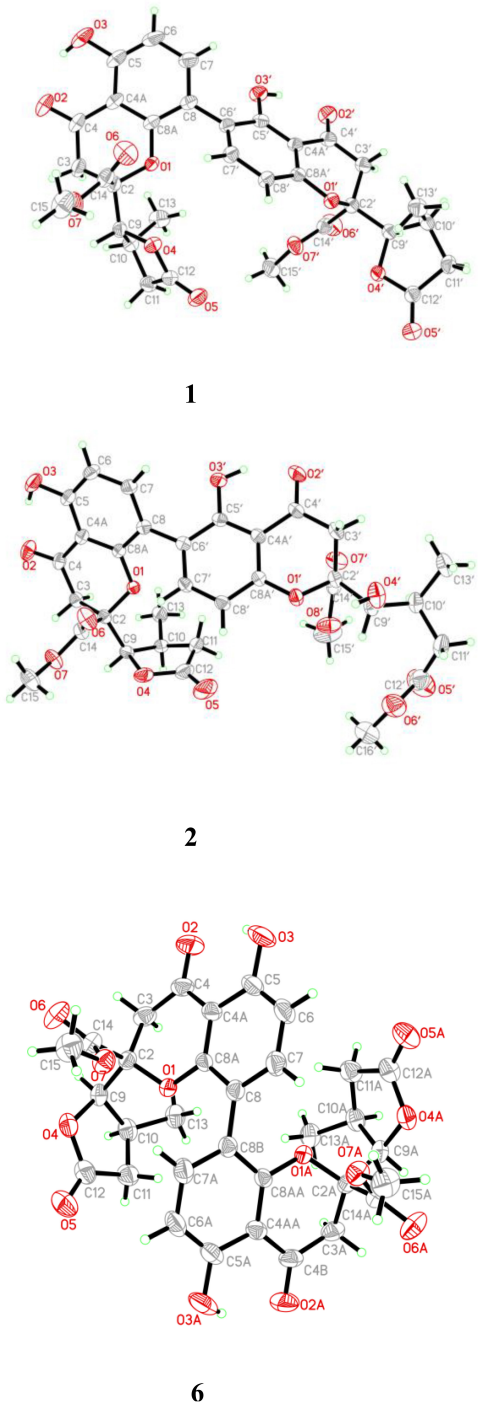

FIGURE 3
ORTEP drawing of Compounds **1**, **2**, and **6**.

## Results and discussion

### Structure elucidations

Compound **1** was obtained as light-yellow crystals, whose molecular formula was determined to be $C_{32}H_{30}O_{14}$ by HRESIMS at *m/z* 661.1532 $[M + Na]^+$ (calcd for $C_{32}H_{30}O_{14}Na^+$, 661.1533), with 18 degrees of unsaturation. In the $^1H$ NMR spectrum (Table 1), two hydroxy protons at $\delta_H$ 11.58 (1H, s, 5-OH) and 11.82 (1H, s, 5′-OH), two pairs of adjacent aromatic protons at $\delta_H$ 7.58 (1H, d, $J$ = 8.6 Hz, H-7′), 6.61 (1H, d, $J$ = 8.6 Hz, H-8′), 7.45 (1H, d, $J$ = 8.6 Hz, H-7) and 6.62 (1H, d, $J$ = 8.6 Hz, H-6), two methoxy protons at $\delta_H$ 3.79 (3H, s, H-15) and 3.73 (3H, s, H-15′), two methyl doublets at $\delta_H$ 1.29 (3H, d, $J$ = 7.2 Hz, H-13) and 1.22 (3H, d, $J$ = 7.1 Hz, H-13′), two oxymethine protons at $\delta_H$ [4.86 (1H, d, $J$ = 6.6 Hz, H-9) and 4.65 (1H, d, $J$ = 7.5 Hz, H-9′) were clearly shown. The $^{13}C$ NMR and DEPT spectra (Table 1) of **1** showed oxymethine carbons, including four methyl carbons (two oxygenated carbons), four methylene carbons, eight methine carbons (four $sp^2$ carbons), and 16 quaternary carbons (two ketone carbonyl carbons, four ester carbonyl carbons, and eight $sp^2$ carbons). The $^1H$ NMR and $^{13}C$ NMR spectral data (Table 1) of Compound **1** were nearly the same as those of paecilin A (Guo et al., 2007). Paecilin A is a symmetric dimer and should have one set of NMR data; however, there are two sets of data in its nuclear magnetic attribution table in the reference (Guo et al., 2007), so the structure of paecilin A was incorrectly assigned by erroneously linking C-8 with C-8′. Actually, C-8 was linked with C-6′, which was confirmed by the HMBC correlations from 5′-OH ($\delta_H$ 11.82) to $\delta_C$ C-6′ ($\delta_C$ 117.7)/C-4a' ($\delta_C$ 107.4), from H-7 ($\delta_H$ 7.45) to C-6′ ($\delta_C$ 117.7), and from H-7′ ($\delta_H$ 7.58) to C-8 ($\delta_C$ 115.3) (Figure 2). The *cis* configurations of H-9/H-10 and H-9′/H-10′ in the γ-butyrolactone moiety were supported by the coupling constants ($^3J_{H-9,H-10}$ = 6.6 Hz, $^3J_{H-9',H-10'}$ = 7.5 Hz) (Wu et al., 2015). In addition, the relative configuration of Compound **1** was deduced as 2*S**,9*R**,10*S**,2′*S**,9′*R**,10′*S** by comparing the chemical shifts of H-2′/H-3′/H-4′ and the coupling constants of the four differential isomers in the reference (Tietze et al., 2014). Finally, the structure of **1** was confirmed by single-crystal X-ray diffraction analysis [Flack parameter = 0.03(5), CCDC: 2155089; Figure 3]. The absolute configuration of **1** was determined to be 2*S*,9*R*,10*S*,2′*S*,9′*R*,10′*S*. Therefore, the structure of paecilin A was revised.

Compound **2** was obtained as light-yellow crystals, whose molecular formula was determined to be $C_{33}H_{34}O_{15}$ by HRESIMS analysis at *m/z* 693.1814 $[M + Na]^+$ (calcd for

$C_{33}H_{34}O_{15}Na^+$, 693.1795), with 17 degrees of unsaturation. Analysis of the $^1H$ and $^{13}C$ NMR data (Table 1) suggested that the structure of **2** was similar to that of **1**, and the only observed difference was that **2** has an additional methoxy group compared to that of **1.** Combined with the unsaturation degree, the γ-butyrolactone ring of one monomer part was opened. This change was confirmed by the key HMBC correlations (Figure 2) from $H_3$-16′ ($\delta_H$ 3.70) to C-12′ ($\delta_C$ 173.3). By comparing the chemical shifts and coupling constants of H-9′ of Compound **2** ($\delta_H$ 4.08, s) with H-5′ in versixanthones E and F ($\delta_H$ 4.06, d, $J$ = 1.8 Hz) (Wu et al., 2015), the relative configuration of Compound **2** was thus determined to be 2*S**,9*R**,10*S**,2′*S**,9′*R**,10′*S**. Finally, the absolute configuration of Compound **2** was determined to be 2*S*,9*R*,10*S*,2′*S*,9′*R*,10′*S* by single-crystal X-ray diffraction [Flack parameter = 0.00(3), CCDC: 2155090; Figure 3]. In conclusion, Compound **2** was named paecilin F.

Compound **3** was obtained as a pale-yellow gum, whose molecular formula was determined to be $C_{34}H_{38}O_{16}$ by HRESIMS analysis at *m/z* 725.2048 $[M + Na]^+$ (calcd for

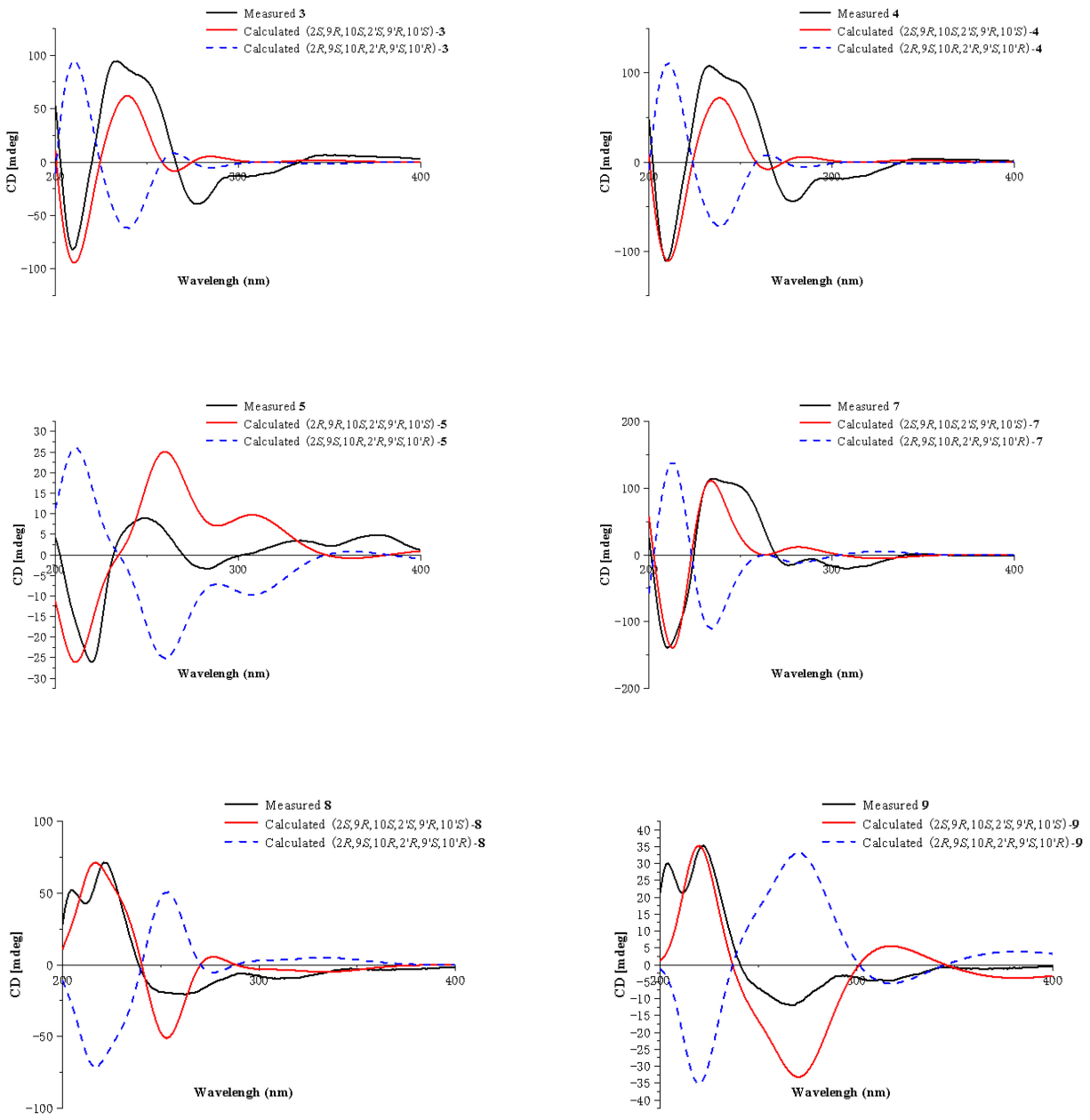


FIGURE 4
ECD calculations of **3**, **4**, **5**, **7**, **8,** and **9**.

$C_{34}H_{38}O_{16}Na^+$, 725.2058), with 16 degrees of unsaturation. The $^1H$ and $^{13}C$ NMR spectroscopic data of **3** (Table 1) showed that **3** was a congener of **2**. The only difference was that Compound **3** has an additional methoxy group compared to **2**. By considering the degrees of unsaturation, it was suggested that the γ-butyrolactone groups of the two monomer moieties were opened. These changes were confirmed by the key HMBC correlations (Figure 2) from $H_3$-16 ($\delta_H$ 3.66) to C-12 ($\delta_C$ 173.3) and $H_3$-16′ ($\delta_H$ 3.70) to C-12′ ($\delta_C$ 173.3). Referring to the chemical shifts and coupling constants of **2**, the relative configuration of Compound **3** was deduced as 2*S**,9*R**,10*S**,2′*S**,9′*R**,10′*S**. Finally, the absolute configuration of Compound **3** was determined to be 2*S*,9*R*,10*S*,2′*S*,9′*R*,10′*S* by ECD calculations (Figure 4). In summary, the structure of **3** was established and named paecilin G.

Compound **4** was obtained as a pale-yellow gum. Its molecular formula of $C_{33}H_{34}O_{15}$ was determined based on the HRESIMS data (found at *m/z* 693.1791 $[M + Na]^+$, calcd for $C_{33}H_{34}O_{15}Na^+$ 693.1795), corresponding to 17 degrees of unsaturation. Compound **4** had the same molecular formula and highly similar 1D NMR data (Table 2) to those of **2**. The only difference was that the two monomers of Compound **4** were connected by C-6 and C-8′. The $^1H$-$^1H$ COSY cross peaks (Figure 2) of H-7 ($\delta_H$ 7.72)/H-8 ($\delta_H$ 6.63), H-6′ ($\delta_H$ 6.61)/H-7′ ($\delta_H$ 7.47), and the key HMBC correlations from H-7′ ($\delta_H$ 7.47) to C-6 ($\delta_C$ 118), from H-7 ($\delta_H$ 7.72) to C-8′ ($\delta_C$ 115), from 5-OH ($\delta_H$ 11.86) to C-4a ($\delta_C$ 107.6)/C-5 ($\delta_C$ 159.3)/C-6 ($\delta_C$ 118), and from 5′-OH ($\delta_H$ 11.7) to C-4a' ($\delta_C$ 107.8)/C-5′ ($\delta_C$ 161.9)/C-6′ ($\delta_C$ 110.1) confirmed the above inference. The relative configuration of Compound **4** was deduced by comparison with the chemical shifts and coupling constants of **2**. Finally, the absolute configuration of Compound **4** was determined to be 2*S*,9*R*,10*S*,2′*S*,9′*R*,10′*S* by ECD calculations (Figure 4). In summary, the structure of **4** was established and named paecilin H.

Compound **5** was obtained as a pale-yellow gum, and it possessed the molecular formula of $C_{33}H_{34}O_{15}$ as indicated by the HRESIMS analysis at *m/z* 693.1810 $[M + Na]^+$ (calcd for $C_{33}H_{34}O_{15}Na^+$, 693.1795), with 17 degrees of unsaturation. The $^1H$ and $^{13}C$ NMR spectroscopic data of Compound **5** (Table 2) were highly similar to those of versixanthone B (Wu et al., 2015). The mass spectrometry data showed that Compound **5** had one more methoxy group than versixanthone B, which suggested that Compound **5** was the γ-butyrolactone ring-opening analog of versixanthone B. This conclusion was confirmed by the correlation between H-11′ ($\delta_H$ 2.46, 2.22) and H-16′ ($\delta_H$ 3.65 to C-12′) ($\delta_C$ 173.2) in the HMBC spectrum (Figure 2). Therefore, the planar structure of **5** was determined. The relative configuration of the tetrahydroxanthone monomer was readily established to be the same as that of versixanthone A by the coupling constant ($^3J_{H-9,H-10}$ = 11.3 Hz), the NOESY correlation between H-9 and $H_3$-13 (Figure 5), and the chemical shifts. By considering the biosynthesis of this family of congeners, together with the chemical shifts, and coupling constants of H-5′, H-6′, and H-7′ in versixanthone E (Wu et al., 2015), it was deduced that the relative configuration of Compound **5** was 2*R**,9*R**,10*S**,2′*S**,9′*R**,10′*S**. Finally, the absolute configuration was deduced as 2*R*,9*R*,10*S*,2′*S*,9′*R*,10′*S* by ECD calculations (Figure 4). Therefore, Compound **5** could be fully assigned and named paecilin I.

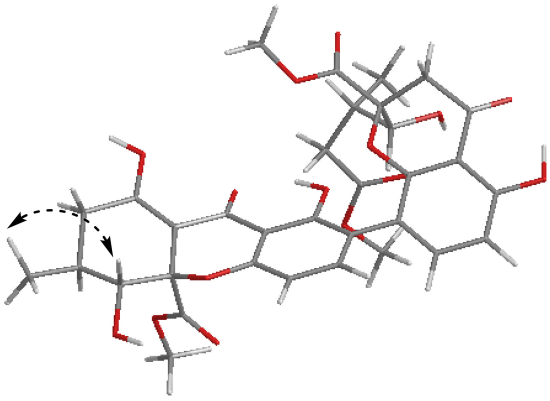

FIGURE 5
Key ROESY correlations for **5**.

Compound **6** was obtained as a brown crystal, whose molecular formula was determined to be $C_{32}H_{30}O_{14}$ by HRESIMS analysis at *m/z* 661.1526 $[M + Na]^+$ (calcd for $C_{32}H_{30}O_{14}Na^+$, 661.1533), with 18 degrees of unsaturation. According to the $^1H$ NMR and $^{13}C$ NMR data (Table 3) and the mass spectra, it could be inferred that Compound **6** was also a dimeric compound that was structurally similar to Compound **1**. There was only one set of $^1H$ and $^{13}C$ NMR spectroscopic data for **6**, indicating that the structure of **6** was symmetric. Therefore, Compound **6** had either a C8-C8′ or a C6-C6′ linkage pattern. Due to the lack of the key HMBC correlations of the signals 5-OH and 5′-OH, the connection position of its monomer remained to be determined. Fortunately, single-crystals of **6** were obtained, which finally enabled us to determine the absolute configuration as 2*S*,9*R*,10*S*,2′*S*,9′*R*,10′*S* [Flack parameter = 0.04(8), CCDC: 2155091; Figure 3]. In summary, the structure of **6** was established and named paecilin J.

Compound **7** was obtained as a pale-yellow gum, whose molecular formula was determined to be $C_{33}H_{34}O_{15}$ by HRESIMS analysis at *m/z* 693.1785 $[M + Na]^+$ (calcd for $C_{33}H_{34}O_{15}Na^+$, 693.1795), with 17 degrees of unsaturation. By comparing the $^1H$ and $^{13}C$ NMR spectra of Compound **7** (Table 2) with those of **2** (Table 1), it was found that **7** was a structural congener of **2**. The only difference between the two compounds was that Compound **7** was linked *via* C8-C8′ while **2** was linked by C8-C6′. This change was proved

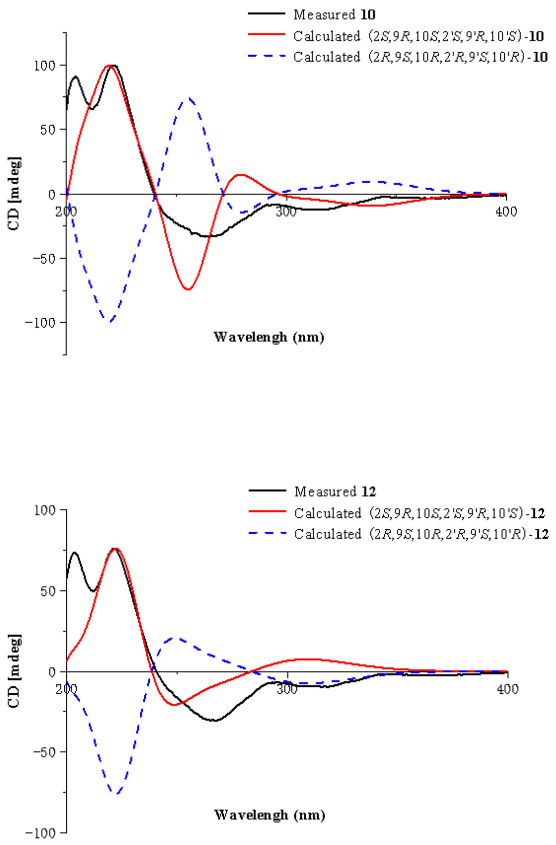


FIGURE 6
ECD calculations of **10**–**12**.

by the key HMBC correlations (Figure 2) from H-7′ ($\delta_H$ 7.92) to C-8 ($\delta_C$ 114.5), from H-7 ($\delta_H$ 7.76) to C-8′ ($\delta_C$ 114.9), from 5-OH ($\delta_H$ 11.70) to C-4a ($\delta_C$ 107.8)/C-5 ($\delta_C$ 161.9)/C-6 ($\delta_C$ 110.4), and from 5′-OH ($\delta_H$ 11.68) to C-4a′ ($\delta_C$ 107.7)/C-5′ ($\delta_C$ 161.8)/C-6′ ($\delta_C$ 110.9). By comparison of the coupling constants of Compounds **7** and **2**, it was deduced that the relative configuration of Compound **7** was 2*S**,9*R**,10*S**,2′*S**,9′*R**,10′*S**. Finally, the absolute configuration of Compound **7** was determined to be 2*S*,9*R*,10*S*,2′*S*,9′*R*,10′*S* by ECD calculations (Figure 4). Therefore, Compound **7** was elucidated and named paecilin K.

Compound **8** was obtained as a pale-yellow gum, whose molecular formula was determined to be $C_{32}H_{30}O_{14}$ by the HRESIMS analysis at *m/z* 661.1538 $[M + Na]^+$ (calcd for $C_{32}H_{30}O_{14}Na^+$, 661.1533), with 18 degrees of unsaturation. The 1D NMR spectrum of Compound **8** (Table 3) showed high similarity to that of Compound **6** (Table 3). The only difference was that the two monomers of Compound **6** were C8-C8′ linked, while the two monomers of Compound **8** were C6-C6′ linked. This conclusion was established by the key HMBC correlations (Figure 2) from H-7/H-7′ ($\delta_H$ 7.52) to C-6/C-6′ ($\delta_C$ 117.7), from 5-OH/5′-OH ($\delta_H$ 11.91) to C-4a/C-4a' ($\delta_C$ 107.6), C-5/C-5′ ($\delta_C$ 159.2), and C-6/C-6′ ($\delta_C$ 117.7). By biosynthetic considerations, and comparison with the chemical shifts and coupling constants with those of **6**, the relative configuration of Compound **8** was deduced as 2*S**,9*R**,10*S**,2′*S**,9′*R**,10′*R**. The ECD calculation for **8** was performed, and the results of **8** matched well with the experimental ECD curve (Figure 4). Therefore, the absolute configuration of **8** was 2*S*,9*R*,10*S*,2′*S*,9′*R*,10′*S*, and it was named paecilin L.

Compound **9** was obtained as a pale-yellow gum, whose molecular formula was determined to be $C_{32}H_{32}O_{15}$ by HRESIMS analysis at *m/z* 679.1627 $[M + Na]^+$ (calcd for $C_{32}H_{32}O_{15}Na^+$, 679.1639), with 17 degrees of unsaturation. Comparing the $^1H$ and $^{13}C$ NMR data of Compounds **8** (Table 3) and **9** (Table 4), it was found that these two compounds are structural analogs. The mass spectrum showed that Compound **9** was 18 Da more than Compound **8**, corresponding to a molecule of $H_2O$. Combined with the degrees of unsaturation, it was speculated that one of the γ-butyrolactone rings was opened. In the HMBC spectrum (Figure 2), H-9′ ($\delta_H$ 4.80) of Compound **8** was correlated with C-12′ ($\delta_C$ 175.0), while for Compound **9**, this correlation was absent. This evidence helped to prove the above conclusion.

The relative configurations in the two monomeric units of **9** were proposed to be the same as **8**, as indicated by the similar chemical shifts and coupling constants and by consideration of the biogenetic origin. Finally, the absolute configuration of Compound **9** was determined to be 2*S*,9*R*,10*S*,2′*S*,9′*R*,10′*S* by ECD calculations (Figure 2). In summary, Compound **9** was named paecilin M.

Compounds **10** and **11** were obtained as pale-yellow gum. The molecular formula of **10** was determined to be $C_{33}H_{34}O_{15}$ by HRESIMS at *m/z* 671.2001 $[M + H]^+$ (calcd for $C_{33}H_{35}O_{15}^+$, 671.1976), with 17 degrees of unsaturation. The molecular formula of **11** was determined to be $C_{34}H_{36}O_{15}$ by HRESIMS at *m/z* 707.1934 $[M + Na]^+$ (calcd for $C_{34}H_{36}O_{15}Na^+$, 707.1952), also with 17 degrees of unsaturation. By comparing the $^1H$ and $^{13}C$ NMR spectroscopic data of Compounds **9**-**11** (Table 4), it was found that the data of these three compounds were highly similar, with the only difference being that Compound **10** had one additional methoxy group compared to **9**, while Compound **11** had one additional ethoxy group compared to **9**. The key HMBC correlations (Figure 2) from H-10′ ($\delta_H$ 2.35)/H-11′ ($\delta_H$ 2.58, 2.38)/H-16′ ($\delta_H$ 3.68) to C-12′ ($\delta_C$ 173.3) indicated that the carboxylic acid group at C-12′ was methyl-esterified in Compound **10**. The key HMBC correlations (Figure 2) from H-10′ ($\delta_H$ 2.39)/H-11′ ($\delta_H$ 2.58, 2.36)/H-16′ ($\delta_H$ 4.16) C-12′ ($\delta_C$ 172.9) and from H-17′ ($\delta_H$ 1.28) to C-16′ ($\delta_C$ 60.9), in combination with the key $^1H$-$^1H$ COSY correlations (Figure 2) between H-16′ ($\delta_H$ 4.16) and H-17′ ($\delta_H$ 1.28) indicated that the carboxylic acid group at C-12′ was ethyl-esterified in Compound **11**. Combining the chemical shifts and coupling constants of Compound **9**, it was deduced that the relative configurations of Compounds **10** and **11** were 2*S**,9*R**,10*S**,2′*S**,9′*R**,10′*S**. Finally, by ECD calculations (Figure 6), the absolute configurations of Compounds **10** and **11** were determined to be 2*S*,9*R*,10*S*,2′*S*,9′*R*,10′*S*. Therefore, Compounds **10** and **11** were named paecilin N and paecilin O, respectively.

Compound **12** was obtained as a pale-yellow gum, and it possessed the molecular formula of $C_{34}H_{38}O_{16}$, as indicated by the HRESIMS analysis at *m/z* 725.2049 $[M + Na]^+$ (calcd for $C_{34}H_{38}O_{16}Na$, 725.2058). By comparing the 1D spectroscopic data of Compound **12** (Table 3) with those of Compound **8** (Table 3), it was suggested that Compound **12** was highly similar to Compound **8**. The only difference was that Compound **12** has two additional methoxyl groups compared to Compound **8**. Considering the reduction of two degrees of unsaturation, it was assumed that both γ-butyrolactone groups of **12** were opened. This conclusion was established by the key HMBC correlations (Figure 2) from H-10/H-10′ ($\delta_H$ 2.37), H-11/H-11′ ($\delta_H$ 2.60, 2.40), and H-16/H-16′ ($\delta_H$ 3.70) to C-12/C-12′ ($\delta_C$ 173.3). By comparison with the chemical shifts and coupling constants of the ring-opening monomer of Compound **10**, it was deduced that the relative configuration of Compound **12** was 2*S**,9*R**,10*S**,2′*S**,9′*R**,10′*S**. Finally, the absolute configuration of Compound **12** was determined to be 2*S*,9*R*,10*S*,2′*S*,9′*R*,10′*S* by ECD calculations (Figure 6). In summary, Compound **12** was named paecilin P.

TABLE 5 Antimicrobial activity from Compounds 1–12 (MIC, μg/mL).

| Compounds | *Escherichia coli* ATCC 25922 | *Salmonella enteritidis* ATCC 25923 | *Candida albicans* ATCC 10231 |
|---|---|---|---|
| **1** | 64 | 64 | 16 |
| **2** | 64 | 128 | 64 |
| **3** | 256 | > 512 | 64 |
| **4** | > 512 | >512 | > 512 |
| **5** | >512 | > 512 | >512 |
| **6** | 256 | 256 | 256 |
| **7** | 128 | 256 | > 512 |
| **8** | 16 | 32 | 32 |
| **9** | 256 | 128 | > 512 |
| **10** | 16 | 32 | 32 |
| **11** | 128 | 128 | > 512 |
| **12** | 256 | 128 | 64 |
| Chloramphenicol[a] | 1 | – | – |
| Penicillin[a] | – | 0.78 | – |
| Fluconazole[a] | – | – | 5 |

[a]Positive controls.

The other known analogs isolated in this study were identified as versixanthone F (**13**) (Wu et al., 2015), versixanthone A (**14**) (Wu et al., 2015), and versixanthone E (**15**) (Wu et al., 2015) by comparison of their NMR data with those reported in the literature.

## Antimicrobial activities

Compound **1** and new compounds (**2**–**12**) were evaluated for their antimicrobial activities against the bacteria *E. coli* and *S. enteritidis* and the fungus *C. albicans*. As a result, Compound **1** showed significant inhibitory activity against *C. albicans*, with an MIC of 16 μg/mL, while Compounds **8** and **10** showed inhibitory activity against the gram-negative bacterium *E. coli*, with the same MIC value of 16 μg/mL (Table 5).

# Conclusion

In conclusion, a total of 15 compounds, including 11 new compounds, were identified from the endophytic fungus *Xylaria curta* E10. The absolute configurations of Compounds **1**, **2,** and **6** were determined by single-crystal X-ray diffraction analysis. The absolute configurations of **3**, **4**, **5**, **7**, **8**, **9**, **10**, **11,** and **12** were determined by ECD calculations and referred to the NMR data with their structural analogs. In the antimicrobial activity assays, Compound **1** showed antifungal activity against *C. albicans*,

and Compounds **8** and **10** showed antibacterial activity against *Escherichia coli*.

## Data availability statement

The original contributions presented in this study are included in the article/**Supplementary material**, further inquiries can be directed to the corresponding authors.

## Author contributions

H-LA isolated and provided the fungus. Z-HL and X-XL designed experiments. P-PW was responsible for compound isolation, elucidated the structures and wrote the manuscript. P-PW, B-BS, KY, X-YP, X-JM, and DX performed chemical calculations. XL and Z-HL were responsible for the evaluation of the immunosuppressive activity. All authors read and approved the final manuscript.

## Funding

This work was financially supported by the National Natural Science Foundation of China (31870513 and 32000011) and the Fundamental Research Funds for the Central University, South-Central MinZu University (CZD21003).

## Acknowledgments

We thank the Analytical & Measuring Centre, South-Central University for Nationalities for the spectra measurements.

## Conflict of interest

The authors declare that the research was conducted in the absence of any commercial or financial relationships that could be construed as a potential conflict of interest.

## Publisher's note

All claims expressed in this article are solely those of the authors and do not necessarily represent those of their affiliated organizations, or those of the publisher, the editors and the reviewers. Any product that may be evaluated in this article, or claim that may be made by its manufacturer, is not guaranteed or endorsed by the publisher.

## Supplementary material

The Supplementary Material for this article can be found online at: https://www.frontiersin.org/articles/10.3389/fmicb.2022.922444/full#supplementary-material

## References

Arora, D., Chashoo, G., Singamaneni, V., Sharma, N., Gupta, P., and Jaglan, S. (2017). *Bacillus amyloliquefaciens* induces production of a novel blennolide K in coculture of *Setophoma terrestris*. *J. Appl. Microbiol.* 124, 730–739. doi: 10.1111/jam.13683

Bruhn, T., Schaumloffel, A., Hemberger, Y., and Bringmann, G. (2013). SpecDis: Quantifying the comparison of calculated and experimental electronic circular dichroism spectra. *Chirality* 25, 243–249. doi: 10.1002/chir.22138

Cao, H. Y., Cheng, Y., Sun, S. F., Li, Y., and Liu, Y. B. (2022). Anti-inflammatory dimeric tetrahydroxanthones from an endophytic *Muyocopron laterale*. *J. Nat. Prod.* 85, 148–161. doi: 10.1021/acs.jnatprod.1c00878

Chen, L., Zhang, Q. Y., Jia, M., Ming, Q. L., Yue, W., Rahman, K., et al. (2016). Endophytic fungi with antitumor activities: Their occurrence and anticancer compounds. *Crit. Rev. Microbiol.* 42, 454–473. doi: 10.3109/1040841X.2014.959892

da Silva, P. H., de Souza, M. P., Bianco, E. A., da Silva, S. R., Soares, L. N., Costa, E. V., et al. (2018). Antifungal polyketides and other compounds from Amazonian endophytic *Talaromyces* fungi. *J. Braz. Chem. Soc.* 29, 622–630. doi: 10.21577/0103-5053.20170176

Duan, Y. D., Jiang, Y. Y., Guo, F. X., Chen, L. X., Xu, L. L., Zhang, W., et al. (2019). The antitumor activity of naturally occurring chromones: A review. *Fitoterapia* 135, 114–129. doi: 10.1016/j.fitote.2019.04.012

El-Elimat, T., Figueroa, M., Raja, H. A., Graf, T. N., Swanson, S. M., Falkinham, J. O. III, et al. (2015). Biosynthetically distinct cytotoxic polyketides from *Setophoma terrestris*. *Eur. J. Org. Chem.* 2015, 109–121. doi: 10.1002/ejoc.201402984

Frisch, M. J., Trucks, G. W., Schlegel, H. B., Scuseria, G. E., Robb, M. A., Cheeseman, J. R., et al. (2013). *Gaussian 09, revision E. 01*. Wallingford, CT: Gaussian, Inc.

Guo, Z. Y., She, Z. G., Shao, C. L., Wen, L., Liu, F., Zheng, Z. H., et al. (2007). $^{1}$H and $^{13}$C NMR signal assignments of paecilin A and B, two new chromone derivatives from mangrove endophytic fungus *Paecilomyces* sp (tree 1-7). *Magn. Reson. Chem.* 45, 777–780. doi: 10.1002/mrc.2035

Kumla, D., Shine Aung, T., Buttachon, S., Dethoup, T., Gales, L., Pereira, J. A., et al. (2017). A new dihydrochromone dimer and other secondary metabolites from cultures of the marine sponge-associated fungi *Neosartorya fennelliae* KUFA 0811 and *Neosartorya tsunodae* KUFC 9213. *Mar. Drugs.* 15:375. doi: 10.3390/md15120375

Li, E., Tian, R., Liu, S. C., Chen, X. L., Guo, L. D., and Che, Y. S. (2008). Pestalotheols A-D, bioactive metabolites from the plant endophytic fungus *Pestalotiopsis theae*. *J. Nat. Prod.* 71, 664–668. doi: 10.1021/np700744t

Liu, S., Zhao, Y. P., Heering, C., Janiak, C., Müller, W. E. G., Akoneì, S. H., et al. (2019). Sesquiterpenoids from the endophytic fungus *Rhinocladiella similis*. *J. Nat. Prod.* 82, 1055–1062. doi: 10.1021/acs.jnatprod.8b00938

Liu, Y., Wray, V., Abdel-Aziz, M. S., Wang, C. Y., Lai, D., and Proksch, P. (2014). Trimeric anthracenes from the endophytic fungus *Stemphylium globuliferum*. *J. Nat. Prod.* 77, 1734–1738. doi: 10.1021/np500113r

Lünne, F., Koöhler, J., Stroh, C., Müller, L., Daniliuc, C. G., Mück-Lichtenfeld, C., et al. (2021). Insights into ergochromes of the plant pathogen *Claviceps purpurea*. *J. Nat. Prod.* 84, 2630–2643. doi: 10.1021/acs.jnatprod.1c00264

Nalin Rathnayake, G. R., Savitri Kumar, N., Jayasinghe, L., Araya, H., and Fujimoto, Y. (2019). Secondary metabolites produced by an endophytic fungus *Pestalotiopsis microspora*. *Nat. Prod. Bioprospect.* 9, 411–417. doi: 10.1007/s13659-019-00225-0

Nguyen, V. K., Genta-Jouve, G., Duong, T. H., Beniddir, M. A., Gallard, J. F., Ferron, S., et al. (2020). Eumitrins C-E: Structurally diverse xanthone dimers from the vietnamese lichen *Usnea baileyi*. *Fitoterapia* 141:104449. doi: 10.1016/j.fitote.2019.104449

Pinto, M. M., Castanheiro, R. A., and Kijjoa, A. (2014). Xanthones from marine-derived microorganisms: Isolation, structure elucidation and biological activities. *Encycl. Anal. Chem.* 27, 1–21. doi: 10.1002/9780470027318.a9927

Pontius, A., Krick, A., Kehraus, S., Foegen, S. E., Müller, M., Klimo, K., et al. (2008). Noduliprevenone: A novel heterodimeric chromanone with cancer chemopreventive potential. *Chem. Eur. J.* 14, 9860–9863. doi: 10.1002/chem.200801574

Ribeiro, B. A., da Mata, T. B., Canuto, G. A. B., and Silva, E. O. (2021). Chemical diversity of secondary metabolites produced by Brazilian endophytic fungi. *Curr. Microbiol.* 78, 33–54. doi: 10.1007/s00284-020-02264-0

Tietze, L. F., Ma, L., Jackenkroll, S., Reiner, J. R., Hierold, J., Gnanaprakasam, B., et al. (2014). The paecilin puzzle enantioselective synthesis of the proposed structures of paecilin A and B. *Heterocycles* 88, 1101–1119. doi: 10.3987/COM-13-S(S)68

Tuong, T. L., Do, L. T., Aree, T., Wonganan, P., and Chavasiri, W. (2020). Tetrahydroxanthone–chromanone heterodimers from lichen *Usnea aciculifera* and their cytotoxic activity against human cancer cell lines. *Fitoterapia* 147:104732. doi: 10.1016/j.fitote.2020.104732

Wang, W. X., Lei, X. X., Ai, H. L., Bai, X., Li, J., He, J., et al. (2019a). Cytochalasans from the endophytic fungus *Xylaria cf. curta* with resistance reversal activity against fluconazole-resistant *Candida albicans*. *Org. Lett.* 21, 1108–1111. doi: 10.1021/acs.orglett.9b00015

Wang, W. X., Lei, X. X., Yang, Y. L., Li, Z. H., Ai, H. L., Li, J., et al. (2019b). Xylarichalasin A, a halogenated hexacyclic ytochalasin from the fungus *Xylaria cf. curta*. *Org. Lett.* 21, 6957–6960. doi: 10.1021/acs.orglett.9b02552

Wang, W. X., Li, Z. H., Feng, T., Li, J., Sun, H., Huang, R., et al. (2018). Curtachalasins A and B, two cytochalasans with a tetracyclic skeleton from the endophytic fungus *Xylaria curta* E10. *Org. Lett.* 20, 7758–7761. doi: 10.1021/acs.orglett.8b03110

Wang, Z. J., Jiang, Y., Xin, X. J., and An, F. L. (2021). Bioactive indole alkaloids from insect derived endophytic *Aspergillus lentulus*. *Fitoterapia* 153:104973. doi: 10.1016/j.fitote.2021.104973

Wei, X., and Matsuda, Y. (2020). Unraveling the fungal strategy for tetrahydroxanthone biosynthesis and diversification. *Org. Lett.* 22, 1919–1923. doi: 10.1021/acs.orglett.0c00285

Wei, X. X., Chen, X. X., Chen, L., Yan, D. X., Wang, W. G., and Matsuda, Y. (2021). Heterologous biosynthesis of tetrahydroxanthone dimers: Determination of key factors for selective or divergent synthesis. *J. Nat. Prod.* 84, 1544–1549. doi: 10.1021/acs.jnatprod.1c00022

Wu, G. W., Yu, G. H., Kurtán, T., Mándi, A., Peng, J. X., Mo, X. M., et al. (2015). Versixanthones A–F, cytotoxic xanthone–chromanone dimers from the marine-derived fungus *Aspergillus versicolor* HDN1009. *J. Nat. Prod.* 78, 2691–2698. doi: 10.1021/acs.jnatprod.5b00636

Xiao, Z. M., Li, Y. Y., and Gao, S. H. (2017). Total synthesis and structural determination of the dimeric tetrahydroxanthone ascherxanthone A. *Org. Lett.* 19, 1834–1837. doi: 10.1021/acs.orglett.7b00592

frontiers | Frontiers in Microbiology

TYPE Original Research
PUBLISHED 14 September 2022
DOI 10.3389/fmicb.2022.896687



OPEN ACCESS

EDITED BY
Laura Quintieri,
Italian National Research Council, Italy

REVIEWED BY
Yue Qu,
The Alfred Hospital, Australia
Zhijun Song,
Sydvestjysk Sygehus, Denmark

*CORRESPONDENCE
Liang Yang
yangl@sustech.edu.cn
Guobao Li
feisanke-01@szsy.sustech.edu.cn

†These authors have contributed equally to this work

SPECIALTY SECTION
This article was submitted to Antimicrobials, Resistance and Chemotherapy, a section of the journal Frontiers in Microbiology

RECEIVED 15 March 2022
ACCEPTED 16 August 2022
PUBLISHED 14 September 2022

CITATION
Jia T, Liu D, Bi X, Li M, Cai Z, Fu J, Liu Z, Wu P, Ke X, Jia A, Zhang G, Li G and Yang L (2022) The AhR ligand phthiocol and vitamin K analogs as *Pseudomonas aeruginosa* quorum sensing inhibitors. *Front. Microbiol.* 13:896687. doi: 10.3389/fmicb.2022.896687



# The AhR ligand phthiocol and vitamin K analogs as *Pseudomonas aeruginosa* quorum sensing inhibitors

Tianyuan Jia[1†], Dongjing Liu[2†], Xianbiao Bi[1], Menglu Li[1,2], Zhao Cai[1], Jiapeng Fu[2], Zhi Liu[2], Pengyao Wu[2], Xue Ke[2], Aiqun Jia[3], Guoliang Zhang[2], Guobao Li[2]* and Liang Yang[1,2,4]*

[1]School of Medicine, Southern University of Science and Technology, Shenzhen, China, [2]Shenzhen Third People's Hospital, National Clinical Research Center for Infectious Disease, The Second Affiliated Hospital of Southern University of Science and Technology, Shenzhen, China, [3]School of Pharmaceutical Sciences, Hainan University, Haikou, China, [4]Shenzhen Key Laboratory of Gene Regulation and Systems Biology, Southern University of Science and Technology, Shenzhen, China

The aryl hydrocarbon receptor (AhR) protein senses microbial-secreted metabolites to trigger the host's innate immune system. The *Pseudomonas* quinolone signal (PQS) and *Mycobacterium tuberculosis* (MTb) metabolite phthiocol (Pht) are both ligands of AhR with similar chemical structures. As PQS is an essential quorum-sensing molecule that regulates a wide range of virulence factors in *Pseudomonas aeruginosa*, we hypothesized that Pht and its analogs are potential *P. aeruginosa* quorum-sensing inhibitors (QSIs) with immune-modulating functions. In this study, we demonstrated that Pht was able to inhibit the *P. aeruginosa pqs* QS system and reduce both biofilm formation and the production of pyocyanin. Molecular docking analysis suggested that Pht competes with PQS at the binding site of its receptor, PqsR. An electrophoretic mobility shift assay confirmed the Pht-PqsR interaction and showed that Pht attenuated PqsR from binding to the *pqsA* promoter. Proteomic analysis showed that synthesis of the key *pqs* QS proteins decreased upon the addition of Pht to the bacterial cultures. Furthermore, Pht analogs vitamins $K_1$ (Phylloquinone), $K_2$ (Menaquinones), and $K_3$ (Menadione) were also showed to inhibit the *P. aeruginosa pqs* QS system while able to activate the AhR signaling pathways. Our study suggests that the AhR ligands Pht and its vitamin K analogs are promising QSIs for the alternative treatment of *P. aeruginosa* infections.

KEYWORDS

**aryl hydrocarbon receptor, phthiocol, vitamin K, *Pseudomonas aeruginosa*, *Pseudomonas* quinolone signal**

## Introduction

The aryl hydrocarbon receptor (AhR) protein is a highly conserved ligand-dependent transcription factor that senses xenobiotics to activate detoxifying monooxygenase cytochrome P4501 (CYP1) for degrading ligands to metabolites; it also plays a key role in immune control (Leclerc et al., 2021). Besides its well-known

ligands-environmental pollutants, AhR can also sense secreted microbial metabolites such as pigments and signaling molecules. Recent studies showed that AhR can recognize the *Pseudomonas aeruginosa* quorum-sensing molecule 2-heptyl-3-hydroxy-4 (1H)-quinolone (*Pseudomonas* quinolone signal, PQS) (Moura-Alves et al., 2019) and *M. tuberculosis* (MTb) metabolite 2-hydroxy-3-methyl-1,4-naphthoquinone (phthiocol, Pht) (Moura-Alves et al., 2014) as its ligands. After binding, AhR either activates or suppresses the expression of its regulated genes that are involved in a wide range of pathways, such as cell signaling, innate immune response, and the control of inflammation levels against bacterial infections. Since PQS and Pht are both ligands of AhR with similar chemical structures, we hypothesized that these two molecules may be competitive in binding the native PQS receptor in *P. aeruginosa*, PqsR. A very early study reported that Pht inhibits the growth of *Streptococcus pyogenes*, *Escherichia coli,* and other bacteria (Lichstein and Van De Sand, 1946). Recently, Pht was shown to exhibit moderate anti-*P.aeruginosa* activity due to its metal ion chelating capacity (Shinde and Wadekar, 2018), which is also a feature of the PQS molecule. However, it remains unclear whether Pht is indeed able to interfere with *P. aeruginosa* PQS signaling.

*Pseudomonas aeruginosa* is a widespread opportunistic gram-negative bacterium responsible for many human infections (Curran et al., 2018). The chronic infection caused by multi-drug resistant *P. aeruginosa* is the leading cause of death in patients with cystic fibrosis (Holmes et al., 2021). *Mycobacteria* (such as MTb and *Mycobacterium abscessus*) and *P. aeruginosa* both cause diseases in human lungs and share the same ecological niche (Ehrt et al., 2018). Recent studies suggest that these two pathogens are likely to cause co-infection and aggravate inflammatory lung disease (Falkinham et al., 2015). Clinical studies on tuberculosis with recurrent *P. aeruginosa* infection in the lower respiratory tract showed that these patients have refractory sepsis and low immunity (Dos Santos et al., 2012). Moreover, the incidence of *P. aeruginosa* infection in patients with tuberculosis is very high, significantly increasing the risk of in-hospital death among patients with pulmonary TB (Martiniano et al., 2014). As MTb and *P. aeruginosa* share the same ecological niche in the human body, they may compete for limited nutrients in the lung (Devi et al., 2021). Thus, we hypothesized that there may be some mechanism of agonism between these two species.

Several strategies to combat *P. aeruginosa* biofilm infections have been developed in recent years, including compounds that do not affect the growth of bacterial cells but can inhibit or disperse biofilms, which are believed to reduce the emergency of "new drug resistance" (Majik and Parvatkar, 2014). The quorum sensing (QS) systems mediated by diffusible signaling molecules are among the most efficient regulatory mechanisms for *P. aeruginosa*, which regulate biofilm formation, secretion mechanisms, and the release of a large set of virulence factors such as pyocyanin (Lau et al., 2004a), elastase (Galloway, 1991), and rhamnolipids (Soberón-Chávez et al., 2005). A few classes of *P. aeruginosa* QS inhibitors (QSIs) have been shown to act as efficient biofilm inhibitors, including meta-bromo-thiolactone (mBTL) (O'loughlin et al., 2013), triazole-containing 2-phenylindole, salicylic acid (Srinivasarao et al., 2018), and 6-gingerol (Kim et al., 2015). However, most of the QSI compounds for *P. aeruginosa* were identified from synthetic compound libraries (Kalia, 2013), which may have the problem of high toxicity to the human body (Kalia et al., 2019). It makes sense to identify QSIs from microbial metabolites secreted by microorganisms colonizing the human body. *Pseudomonas aeruginosa* PQS can be found in the sputum of patients during infections (Pesci et al., 1999). After binding to its specific receptor PqsR, PQS can activate the expression of the *pqs* QS regulated genes (Soheili et al., 2019), including those responsible for the biosynthesis of pyocyanin and pyoverdine (García-Reyes et al., 2020). Therefore, blocking the *pqs* QS system will impair the ability of *P. aeruginosa* to form biofilms and produce virulence factors, thus attenuating infections.

In this study, Pht was shown to reduce the *pqsA-gfp* bioreporter expression in a dose-dependent manner in *P. aeruginosa*. Moreover, we showed that Pht can decrease biofilm formation and pyocyanin production of *P. aeruginosa*. The molecular docking analysis suggested that PQS and Pht bind to the same cavity of PqsR. The EMSA assay showed that Pht can inhibit PqsR protein from binding to the *pqsA* promoter. The production of the key *pqs* QS proteins, including PqsB, PqsD, and PqsA, was decreased by adding Pht into the bacterial culture according to the proteomic analysis. We further revealed that Pht analogs and vitamins $K_1$, $K_2$, and $K_3$, could also inhibit the *P. aeruginosa pqs* QS system. Thus, our data suggested that the AhR ligand Pht and its vitamin K analogs are dual-functional molecules that can interfere with the *P. aeruginosa pqs* QS system and promote an AhR-dependent innate defense mechanism against bacteria.

# Materials and methods

## Cell cultivation

THP-1 (human monocytes, ATCC TIB-202) and THP-1 AhR reporter (Moura-Alves et al., 2019) cells were grown in RPMI 1,640 (GIBCO), supplemented with 10% (v/v) heat-inactivated fetal calf serum (FCS; GIBCO), and 1% (v/v) penicillin-streptomycin (GIBCO). All AhR reporter cell lines were maintained with an additional 5 mg/mL of Puromycin (Calbiochem). Cells were kept at 37°C in 5% $CO_2$. Lentiviral infection was performed as described previously (Moura-Alves et al., 2019) and according to the protocols available on the RNAi Consortium website (https://portals.broadinstitute.org/gpp/public/). A similar protocol was used to generate the THP-1 Control and THP-1 AhR-Knockdown (KD) cell lines.

## RNA isolation and real-time quantitative-PCR

To quantify the expression of genes of interest, the THP-1 cells were grown in 24-well plates for 24 h with or without PQS/Pht/vitamin K addition. Total RNA was extracted using the TRIzol LS reagent (Invitrogen, California, USA). The qRT-PCR assay was performed using the ABI 7500 sequence detection system (Applied Biosystems, California, USA). Three replicates were performed with the glyceraldehyde-3-phosphate dehydrogenase gene (*GAPDH*) as the internal control gene.

## Molecular docking

The AhR and PqsR PDB structure files were downloaded from the Uniprot database and modified in PyMOL v. 1.4 (Schrodinger, LLC) (Seeliger and De Groot, 2010). The PQS, Pht, and vitamin K molecule files were downloaded from the Pubchem database. The docking process between proteins and potential ligands was performed in the Autodock Vina plug-in inside Chimera (Pettersen et al., 2004) (UCSF). The software program LIGPLOT v.4.5.3 (Wallace et al., 1995) was used to map the interactions between proteins and potential ligands. Open babel software (O'boyle et al., 2011) was used to transfer proper file formats.

## Microscale thermophoresis

The human recombinant AhR protein with Val128-Asn399 and N-terminal His-Tag was purchased from ImmunoClone (New York, USA). The binding of ligands to the AhR protein was assessed by microscale thermophoresis (MST) experiments using the Monolith® NT.LabelFree (NanoTemper Technologies GmbH). MST measurements were performed according to the manufacturer's instructions previously described (Moura-Alves et al., 2019). The interaction affinity of the dissociation constant Kd for each ligand was analyzed using the NanoTemper Affinity software by the changes in the normalized fluorescence (fraction bound) vs. the ligand concentration.

## Bacterial strains and media

Bacterial strains and plasmids used in this study are described in Supplementary Table 1. Bacteria were cultured in Luria–Bertani (LB) broth (1% tryptone, 0.5% yeast extract, 0.5% NaCl) and ABTGC (B-medium (0.1% $MgCl_2$, 0.1% $CaCl_2$, 0.1% $FeCl_3$) supplemented with 10% A10, 0.2% glucose, and 0.2% casamino acids). The media were solidified with 1.5% Bacto Agar (Difco). Kings' medium [Milli-Q water supplemented with proteose peptone (20 g/L), potassium sulfate (10 g/L), magnesium chloride, anhydrous (1.640 g/L), and glycerol (10% v/v)] were used for the pyocyanin quantification assay.

## *P. aeruginosa* mutant construction

*Pseudomonas aeruginosa* mutant strains Δ*pqsC* and Δ*pqsR* were generated by homologous recombination using the previously described protocol (Choi and Schweizer, 2005). The mutants were constructed by overlapping PCR to contain a gentamicin-resistance cassette. The mutant fragments were inserted into pK18, a suicide vector, to produce gene knockout plasmids. Each knockout plasmid was transformed into *E. coli* strain RK600 and conjugally transferred from RK600 to PAO1. The resultant integrants were selected on agar containing 30 μg/mL gentamicin (Gm30). To resolve merodiploids, we streaked the Gm-resistant colonies for single colonies on LB+Gm30 plates containing 5% sucrose. Potential mutants were screened by PCR using corresponding flanking primers and were confirmed by Sanger sequencing.

## *P. aeruginosa* QS inhibition and growth curve assays

PQS and Pht compounds were prepared in a 96-well microtiter plate (Nunc, Denmark) at a concentration of 100 mM in DMSO. PQS and Pht were then mixed with ABTGC medium and serial dilutions to give a concentration of 125, 250, 500, 750, 1,000, 1,500, and 2,000 nM, respectively. An overnight culture of the PAO1-*pqsA-gfp* strain (grown in LB medium at 37°C, 200 rpm) was diluted in ABTGC medium to a final optical density at 600 nm ($OD_{600nm}$) of 0.02 (~$2.5 \times 10^8$ CFU/mL). A DMSO control (0.1% final concentration) and blank control (ABTGC medium) were used. The microtiter plate was incubated at 37°C in a Tecan Infinite 200 Pro plate reader (Tecan Group Ltd., Mannedorf, Switzerland) to measure the cell density ($OD_{600nm}$) and GFP fluorescence (excitation at 485 nm, emission at 535 nm) at 30 min intervals for at least 12 h. The inhibition assay for PQS and Pht was done in triplicate. Growth curve assays were performed only by measuring the cell density ($OD_{600nm}$) using the same method above.

## Pyocyanin quantification assay

Overnight cultures of *P. aeruginosa* WT and Δ*lasI*Δ*rhlI* mutant strains were standardized to an $OD_{600nm}$ of 0.1 and diluted 100 times into 25 mL of fresh King's Medium in a 250 mL flask. The PQS and Pht compounds were added to give a final concentration of 750 nM. The cultures were grown for 48 h at 37°C in shaking conditions (200 rpm). The cultures were

monitored every 24 h to observe any color change from light-yellow to greenish-yellow in the untreated flask. The mutant strain Δ*lasI*Δ*rhlI* was used as the negative control. The final cell density was measured at 600 nm ($OD_{600nm}$) using a Tecan Infinate 200 Pro plate reader (Tecan Group Ltd., Mannedorf, Switzerland). The cultures were then centrifuged for 10 min at 10,000 rpm, and 7.5 mL of the supernatants were transferred into new Falcon tubes. Pyocyanin extraction was conducted using chloroform (3 mL) and 0.2 M HCl (1.5 mL). The top aqueous layer of HCl containing pyocyanin was pipetted into a microtiter plate, and absorbance was measured at 520 nm. The data was normalized by dividing the $OD_{520nm}$ reading by the final $OD_{600nm}$ values.

## Biofilm formation assay

Biofilm formation was quantified by crystal violet staining. Overnight LB-grown cultures were diluted in fresh medium (1:100) and incubated in 2 mL of LB in 15 mL tubes at 37°C for 24 h, statically allowing biofilm formation. After removing the spent media, we removed the loosely associated bacteria by washing them with water two times, and the remaining bacteria were stained with 0.1% crystal violet for 20 min. Then, the crystal violet stain was discarded while the stained biofilms were washed twice thoroughly with $ddH_2O$ and air-dried. The stained biofilm was then dissolved into 200 μL of 95% ethanol and quantified at 630 nm using a Tecan Infinate 200 Pro plate reader (Tecan Group Ltd., Mannedorf, Switzerland).

## The electrophoretic mobility shift assay

EMSA assays were performed using cell lysates of PAO1 and *pqsR* mutants as previously described (Gruber et al., 2016). For each sample, cell-lysate was incubated with biotinylated 248-bp *pqsA* promoter DNA (pqsA′), which was generated by PCR using biotinylated forward primer (TTCTTGCTTGGTTGCCG) and reverse primer (GACAGAACGTTCCCTCTT). The reaction mixture contained 10 mM Tris–HCl (pH 8.0), 1 mM EDTA, 50 mM NaCl, 1 mM DTT, 1 μg/μL Poly (dI-dC) and was incubated at room temperature (24°C) for 20 min. Samples were separated on a 5% polyacrylamide gel in 0.5 × Tris Borate EDTA (TBE) run at 100 V for 120 min and transferred onto a positively-charged nylon membrane at 40 V for 1 h. Biotinylated DNA on the nylon membrane was probed by streptavidin-HRP conjugate, detected by a chemiluminescent substrate (Beyotime EMSA kit; Shanghai, China), and visualized by exposing it to a GE ImageQuant RT-ECL instrument.

## Tandem mass tag-based quantitative proteomic analysis

Overnight PAO1 cultures were diluted 100 times into 25 mL of fresh LB medium. A Pht compound was added to one sample to give a final concentration of 750 nM. Then, total proteins were extracted from bacterial samples and trypsin digested. Then, the digested sample was labeled with a TMT reagent. Next, TMT labeled peptide was separated by a RIGOL L-3000 dual gradient High-Performance Liquid Chromatography (HPLC) using an Agela Durashell-C18 column. An HPLC-separated peptide was identified by nano UPLC-MS/MS consisting of a Nanoflow HPLC system (EASY-nLC 1000 system from Thermo Scientific) with an EASY-Spray C18 column and an Orbitrap Fusion Lumos mass spectrometer (Thermo Scientific). Then, the protein was identified using the Uniprot_HUMAN database. The resulting MS/MS data were processed using Proteome Discoverer 2.4. The final results were functionally annotated by Gene Ontology (GO) (Zhang et al., 2019), KEGG (https://www.genome.jp/kegg/) (Jones et al., 2014), and STRING (https://www.string-db.org) (Franceschini et al., 2013).

## Statistical analyses

All statistical analyses were performed using GraphPad Prism software with a two-sided Mann-Whitney *U*-test and Benjamini-Hochberg-corrected *P*-values. Data represent the mean ± standard deviation (SD) of three independent experiments unless otherwise indicated. *P*-values $< 0.05$ were considered statistically significant. All false discovery rate controls were performed with the Benjamini-Hochberg procedure, and a false-discovery rate of 10% ($q < 0.1$) was selected as the significant threshold. Statistical details for all tests performed can be found in the figure legends.

# Results

## PQS inhibited while Pht activated AhR downstream genes *CYP1B1* and *AHRR* in THP-1 human monocytes

*Pseudomonas aeruginosa* QS signal molecule PQS has been reported to downregulate AhR-induced cytochrome P4501 (CYP1) enzyme and CYP1A1 enzymatic activities in mouse liver cells (Hepa-1c1c7) (Moura-Alves et al., 2019). We demonstrated by qRT-PCR that the transcription of two AhR downstream genes, *CYP1B1* and AhR repressor (*AHRR*), was repressed 2.3- and 2.5-fold with the addition of 10 μM PQS in THP-1 human monocytes compared to control (additional of DMSO alone) (Figures 1A,B). In addition, there were no significant

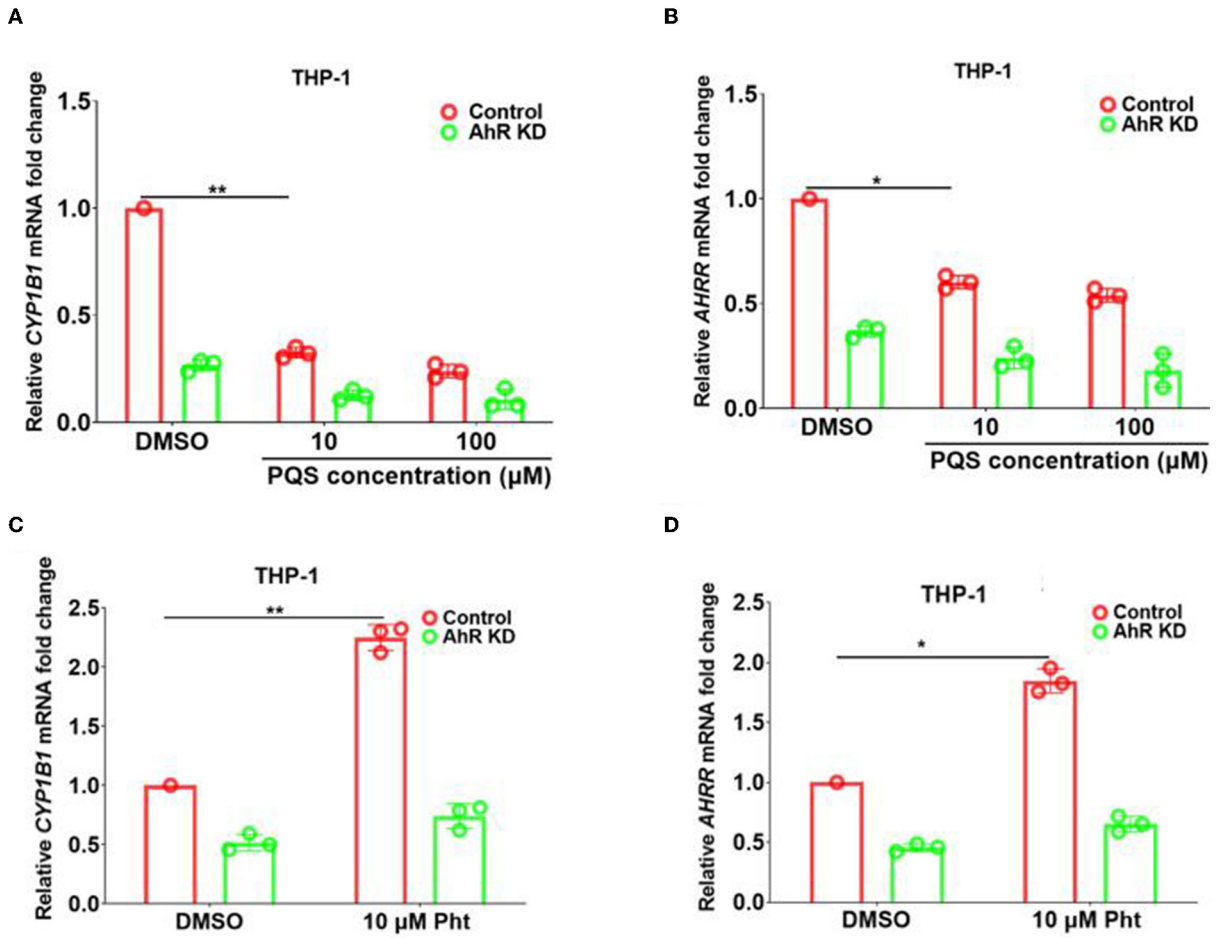


FIGURE 1
PQS inhibited while Pht activated AhR downstream genes in THP-1 human monocytes. **(A,B)** qRT-PCR quantification of the expression of *CYP1B1* and *AHRR* in THP-1 Control and AhR KD cells with PQS addition. **(C,D)** qRT-PCR quantification of the expression of *CYP1B1* and *AHRR* in THP-1 Control and AhR KD cells with Pht addition. Data are presented as means ± SD; *n* = three independent experiments (*$P \leq 0.05$ and **$P \leq 0.01$, Mann-Whitney *U*-test).

expression changes of these genes in the THP-1 KD cells upon PQS addition.

The MTb natural metabolite Pht was found to activate *CYP1B1* and *AHRR* transcription in THP-1 cells in an AhR-dependent manner (Moura-Alves et al., 2014). Our qRT-PCR results also confirmed that *CYP1B1* and *AHRR* transcription were promoted by 2.2- and 1.9-fold with the addition of 10 μM Pht in THP-1 human monocytes compared to control (DMSO only), respectively (Figures 1C,D). These results demonstrated that PQS and Pht adversely affected AhR regulatory pathways.

## *In vitro* assays of PQS or Pht interactions with AhR

The chemical structures of the *P. aeruginosa* auto-inducer PQS and MTb Pht are shown in Figures 2A,D. Molecular docking was performed using the ligands PQS and Pht against the ligand-binding domain of the human AhR protein. These compounds and their structures are shown in Figures 2B,E. To map the interactions between PQS and the residues within the ligand-binding site on AhR, we used the software LIGPLOT v. 4.5.3 (Wallace et al., 1995). This program provides a 2-dimensional map showing the hydrogen-bond and hydrophobic interactions between atoms in the ligand and those of the binding partner.

The results showed that PQS binds to the AhR protein through hydrophobic forces, and they appear to interact at residues Gln 277, Tyr 221, Pro 200, Ile 281, Ser 220, Phe 228, Phe 201, Ala 224, Lys 225, and Tyr 264 (Figure 2C). However, the docking analysis suggested that Pht and AhR appeared to interact at residues Tyr 84, Ala 46, Ile 101, Pro 22, Phe 23, Tyr 43, Ser 42, and Leu 39 (Figure 2F).

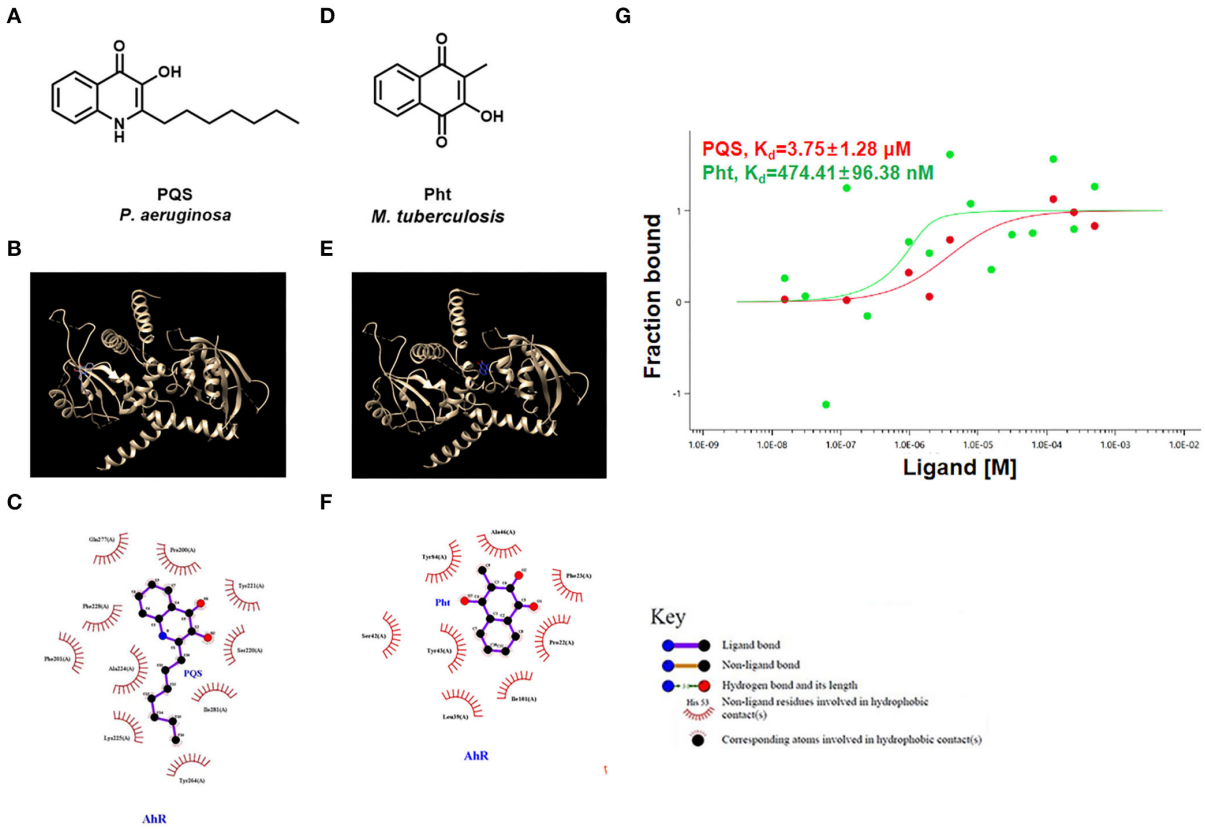


FIGURE 2
PQS and Pht were able to bind to AhR protein. **(A,D)** Molecular structures of *P. aeruginosa* PQS and MTb Pht. **(B,E)** The interaction model of the AhR protein with PQS or Pht. **(C,F)** Interaction map between residues within the AhR protein with PQS or Pht. **(G)** Quantifying the binding affinity of AhR protein with PQS or Pht using microscale thermophoresis assay.

Next, we used an MST assay to quantify the AhR binding affinity with different ligands, including PQS and Pht. The MST results indicated that the dissociation constant (Kd) values of AhR protein with PQS and Pht were 3.75 μM and 474.41 nM, respectively (Figure 2G). These results confirmed that PQS and Pht directly bind to AhR protein as ligands.

## Effects of Pht on *P. aeruginosa pqs* QS system, pyocyanin production, and biofilm formation

To engineer a PQS auto-inducer reporter system, we first made a PQS deficient Δ*pqsC* mutant by deleting the *pqsC* gene. The *pqsA-gfp* reporter plasmid (Yang et al., 2007) was next transferred into the Δ*pqsC* mutant to make the PQS biosensor strain Δ*pqsC* $P_{pqsA-gfp}$. In addition, the *pqsA-gfp* reporter plasmid was transferred into the PAO1 WT to make the PQS bioreporter strain PAO1 $P_{pqsA-gfp}$. Induction of the *pqsA* gene is mainly controlled by PqsR (the signal receptor of the *pqs* QS system), which is activated by the presence of PQS (Soheili et al., 2019). Thus, in the PAO1 $P_{pqsA-gfp}$ strain, a decrease in GFP fluorescence would indicate the presence of an antagonist of PQS, while exogenous PQS was needed to induce the GFP fluorescence of the Δ*pqsC* $P_{pqsA-gfp}$ strain.

Pht was exogenously added to both the above reporter strains to evaluate its impact on the *pqs* QS system. As shown in Figure 3A, both PQS and Pht could not affect the growth of the *P. aeruginosa* strain. PQS—not Pht—induced the *pqsA-gfp* expression in a dose-dependent manner in the PAO1 Δ*pqsC* strain (Figure 3B). In contrast, Pht was able to inhibit *pqsA-gfp* expression in a dose-dependent manner in the PAO1 $P_{pqsA-gfp}$ strain, with the optimal effect at a concentration of 750 nM (Figure 3C). These results showed that PQS activated while Pht inhibited the *P. aeruginosa pqs* QS system.

The production of pyocyanin and the formation of biofilms are *pqs* QS system-regulated phenotypes related to virulence in *P. aeruginosa* (Pearson et al., 1997). Pyocyanin is a key virulence factor produced by *P. aeruginosa* that plays a major role in cystic fibrosis (CF) lung infections (Lau et al., 2004a). Pyocyanin was shown to cause tissue damage and necrosis in a *P. aeruginosa* murine model for a lung infection (Lau et al., 2004b). Biofilm

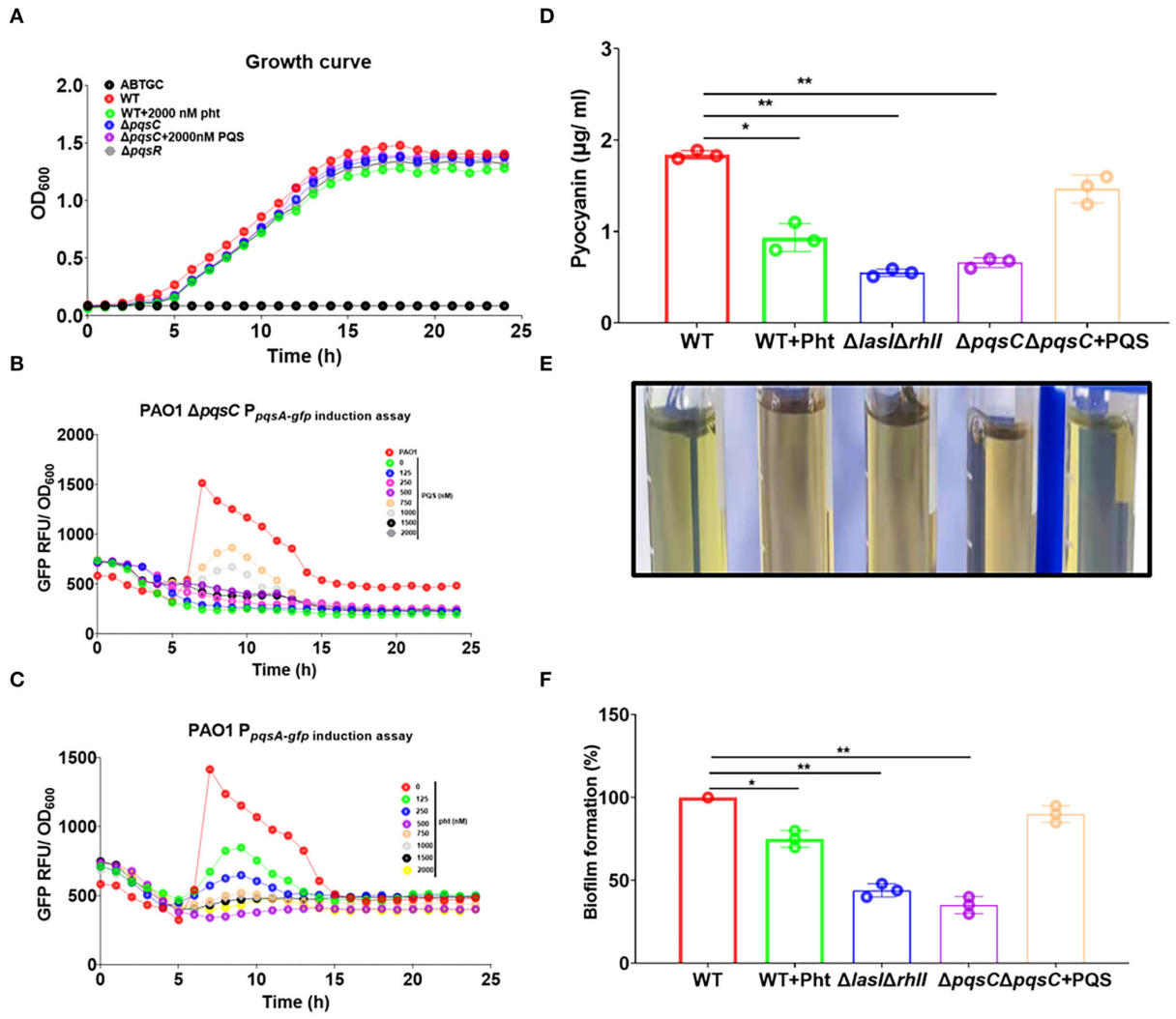


FIGURE 3
Pht inhibited *P. aeruginosa pqs* QS system, pyocyanin production, and biofilm formation. **(A)** Growth curves of *P. aeruginosa* PAO1 WT and QS mutant strain under different conditions. **(B)** Dose-dependent induction curves of PQS in Δ*pqsC* $P_{pqsA-gfp}$. **(C)** Dose-dependent inhibition curves of Pht in PAO1 $P_{pqsA-gfp}$. **(D)** The production of pyocyanin by *P. aeruginosa* WT, WT+750 nM Pht, Δ*lasI*Δ*rhlI*, Δ*pqsC*, Δ*pqsC*+750 nM PQS strains. **(E)** Photos of visualization of the green pigment corresponding to the upper panel. **(F)** The biofilm formation of *P. aeruginosa* WT, WT+750 nM Pht, Δ*lasI*Δ*rhlI*, Δ*pqsC*, Δ*pqsC*+750 nM PQS strains. Data are presented as means ± SD; *n* = three independent experiments (*$P \leq 0.05$ and **$P \leq 0.01$, Mann-Whitney *U*-test).

formation by *P. aeruginosa* is well known as the cause of chronic infections (Costerton et al., 2005). We thus evaluated the effects of Pht on these two phenotypes.

As expected, the pyocyanin production by *P. aeruginosa* PAO1 strain was found to be suppressed by Pht to a level comparable to that of PAO1 Δ*lasI*Δ*rhlI* strain and the Δ*pqsC* strain. It could be seen from the intensity of the green pigment in the supernatants of different samples that the PAO1 WT culture exhibited a dark green, Δ*lasI*Δ*rhlI* and Δ*pqsC* cultures exhibited light green, and the WT+Pht culture did not have a visible green color. These results indicated that Pht inhibited pyocyanin production (Figure 3D). Crystal violet staining showed that the biofilm formation of *P. aeruginosa* PAO1 WT was suppressed by Pht to a level comparable to that of the PAO1 Δ*lasI*Δ*rhlI* and the Δ*pqsC* strains (Figures 3E,F). Besides, we detected that Pht did not inhibit *P. aeruginosa* rhamnolipid productions (Supplementary Figure 1). These results indicated that Pht repressed *P. aeruginosa pqs* QS system, pyocyanin production, and biofilm formation.

## Investigation of the interaction of Pht with PqsR protein

The interactions between alkyl quinolones with PqsR are simulated by the crystal structure of PqsR complexed

with its ligand, which suggests the influence of ligand binding on PqsR affinity to its DNA-binding site (Ilangovan et al., 2013). Molecular docking was first performed using the reference ligand PQS and potential ligand Pht against the ligand-binding domain of the *P. aeruginosa* PqsR protein. These compounds and their structures were shown (Figures 4A,C). To map the interactions between PQS and the residues within the ligand-binding site on PqsR, the software program LIGPLOT v. 4.5.3 was used.

The results showed that PQS binds to PqsR protein by hydrophobic forces, and they appeared to interact at residues Leu 189, Tyr 258, Val 170, Ile 236, Ile 149, Ala 168, Thr 265, and Leu 207 (Figure 4B). While the docking analysis suggested that Pht and PqsR appeared to interact at residues Ile 56, Leu 114, r103 (A), n101 (A), Met 131, Ile 143, Phe 128, and Leu 104 (Figure 4D). Except for hydrophobic forces, Pht and PqsR are also predicted to be bound by a hydrogen bond at Leu 115 (A). These molecular docking results revealed that the QS signaling molecule PQS and Pht competed for the same active pocket in the PqsR protein. The hydrogen bond between Pht and PqsR might offer Pht an advantage when competing with PQS. Thus, we suspected that Pht competitively disrupted the PQS-mediated PqsR activation and signaling in *P. aeruginosa*. These predicted binding modes of PqsR and Pht need further experimental verification.

The electrophoretic mobility shift assay (EMSA) is a rapid and sensitive experimental method to detect protein-nucleic acid interactions (Hellman and Fried, 2007). The protein-nucleic acid complexes migrate more slowly than the corresponding free nucleic acid in the gel. To test whether Pht will interact with PqsR and further affect its DNA binding capacity, we performed EMSA with the biotinylated-*pqsA* promoter (Bio-*pqsA*) using cell lysates of PAO1 WT and Δ*pqsR* strains. The results showed that only PAO1 cell lysates shifted Bio-*pqsA* migration, while Δ*pqsR* cell lysates did not show any effect. The addition of Pht attenuated the interaction between PAO1 cell lysates and Bio-*pqsA*, whereas there was no effect by adding the cell lysates of Δ*pqsR* (Figures 4E,F). These results indicated that Pht could indeed block the binding of PqsR protein to the *pqsA* promoter, which further leads to the inhibitory effect against *P. aeruginosa pqs* QS systems.

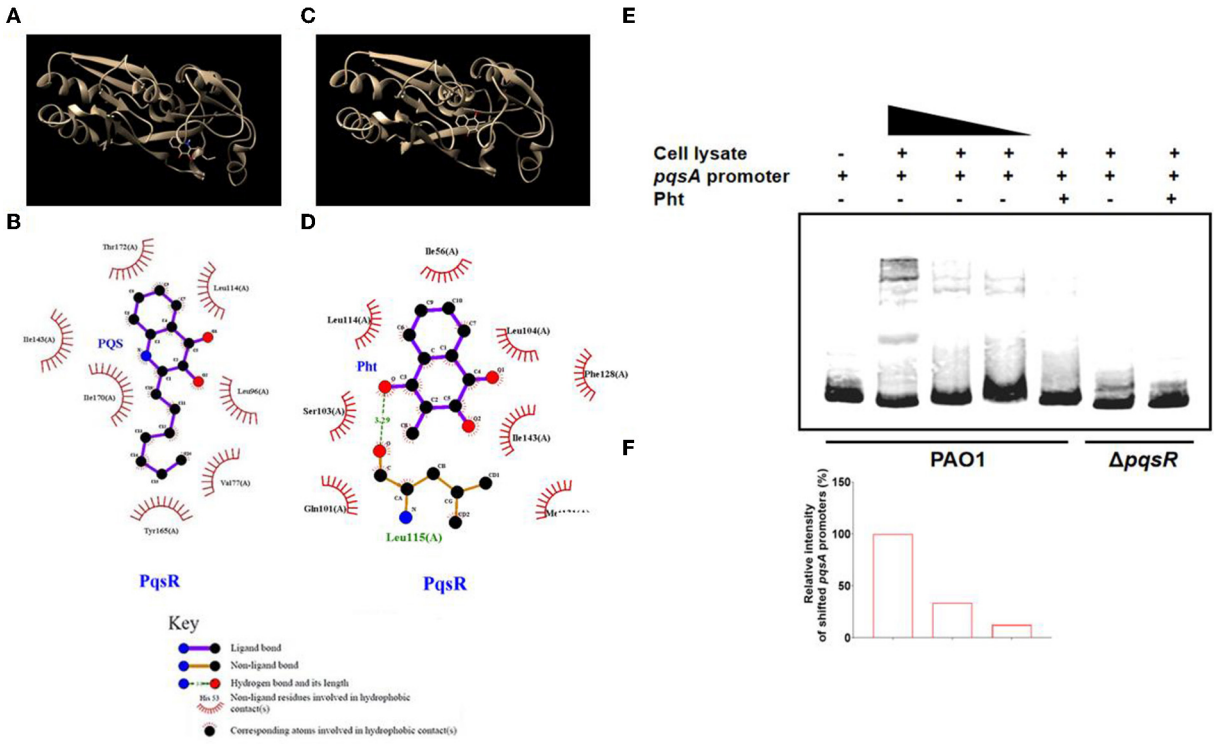


FIGURE 4
Interaction of Pht with PqsR protein. Molecular docking of the PqsR protein with PQS or Pht. **(A,C)** The interaction model of the PqsR protein with PQS or Pht. **(B,D)** Interaction map between residues within the PqsR protein with PQS or Pht. **(E)** EMSA assays with biotinylated-*pqsA* promoters incubated with cell-lysates of PAO1 and Δ*pqsR* strains. **(F)** The abundance of shifted cell-lysates corresponding to the upper panel was determined by measuring the densitometry in Image J.

## Pht down-regulated the expression of *pqs* QS regulated proteome

To study the changes in the proteomic profile of *P. aeruginosa* PAO1 upon Pht addition, TMT was used as the labeling strategy for comparative quantitative proteomic analysis (performed with a false discovery rate below 1%). The following cutoffs were used for protein identification: an unused protein score of at least 2 (i.e., 99% confidence of identification) and having more than 1 peptide identified. Using these cutoffs, we identified 2,203 proteins. Using a *p*-value cutoff of 0.05, 37 proteins were found to be significantly affected by Pht. The expression of 10 proteins was upregulated, whereas the expression of 27 proteins was downregulated (Supplementary Table 2).

Table 1 shows the 27 proteins whose abundances were significantly decreased in the Pht-treated *P. aeruginosa* PAO1 strain compared to those in the control PAO1 strain without Pht addition. Of these 27 proteins, five have been previously found to be *pqs* QS regulated: *phnA* (Anthranilate synthase component 1), *pqsB* (Anthraniloyl-CoA anthraniloyltransferase), *phzD2* (Phenazine biosynthesis protein PhzD2), *pqsD* (Anthraniloyl-CoA anthraniloyltransferase), and *pqsA* (Anthranilate–CoA ligase). These results further confirmed that Pht directly attenuates *P. aeruginosa pqs* QS regulated global proteome network.

## Vitamins $K_1$ upregulated AhR downstream genes *CYP1B1* and *AHRR* through AhR in THP-1 human monocytes

By comparing the online PubChem compound library (https://pubchem.ncbi.nlm.nih.gov/), we found several structural analogs of the Pht molecule, including vitamins $K_1$, $K_2$, and $K_3$ (Figures 5A–C). Vitamin K is a fat-soluble vitamin that participates in blood clotting (Palermo et al., 2017). Vitamin K deficiency may lead to prolonged blood clotting time, bleeding, and even death in severe cases (Palermo et al., 2017). Vitamin K not only has protective effects on the heart and the cerebrovascular system but also has a maintenance effect on the normal elasticity of blood vessel walls and participates in the metabolism of bone for the prevention and cure of osteoporosis and fracture (Fusaro et al., 2020). However, no evidence has yet shown that vitamin K can directly affect bacterial pathogenesis.

To reveal whether Pht analogs vitamin K families influence the AhR pathway, we performed qRT-PCR experiments to measure the transcription of AhR downstream genes. The results showed that *CYP1B1* and *AHRR* transcription was increased by 1.9- and 1.6-fold with the addition of 10 μM vitamin $K_1$ in THP-1 human monocytes compared to that with DMSO (Figures 5D,E). Besides, there is no change in AhR KD cells with vitamin $K_1$ stimulation. These results indicated that vitamin $K_1$ promoted AhR downstream genes *CYP1B1* and *AHRR* through AhR in THP-1 human monocytes.

## *In vitro* assays examining the interactions of vitamin K with AhR protein

Molecular docking was performed using the ligands vitamins $K_1$, $K_2$, and $K_3$ against the ligand-binding domain of the human AhR protein. Figures 6A,C,E show these compounds and their structures. The LIGPLOT results showed that vitamin $K_1$ and AhR protein were bound by hydrophobic forces that appeared to interact at residues Tyr 221, Lys 225, Gln 277, Phe 201, Ala 224, Pro 200, Tyr 264, Phe 228, Val 253, Val 255, and Ile 281 (Figure 6B). Similarly, the docking analysis suggested that vitamins $K_2$ and $K_3$ with AhR appeared to interact at several vital residues (Figures 6D,F).

We further used the MST assay to detect AhR protein binding with vitamins $K_1$, $K_2$, and $K_3$. The MST results indicated that the dissociation constant (Kd) values of AhR protein with vitamins $K_1$, $K_2$, and $K_3$ were 1.99 μM, 586.14 nM, and 2.17 μM, respectively (Figure 6G). These findings showed that vitamins $K_1$, $K_2$, and $K_3$ were able to bind AhR and are likely to modulate its activity.

## Effects of Pht analog vitamins $K_1$, $K_2$, and $K_3$ on the *P. aeruginosa pqs* QS system

We then tested whether Pht analogs, vitamins K1, K2, and K3, had an inhibitory effect on the *P. aeruginosa pqs* QS system. The growth of the reporter strain ($OD_{600nm}$) was monitored to ensure that vitamins $K_1$, $K_2$, or $K_3$ would not affect the growth of *P. aeruginosa* strains (Figure 7A). GFP expression was normalized by dividing the GFP values by the OD values measured at respective time points. Vitamin $K_1$, $K_2$, and $K_3$ were found to inhibit *pqsA-gfp* expression dose-dependently without affecting growth (Figures 7B–D). In conclusion, Pht and its analogs, vitamins K1, K2, and K3, inhibited the *P. aeruginosa pqs* QS system. In addition, we performed molecular docking to predict the binding modes of vitamins $K_1$, $K_2$, and $K_3$ to PqsR protein (Supplementary Figure 2).

# Discussion

QSI compounds are effective agents for inhibiting *P. aeruginosa* virulence and biofilms, and the mode of action of some QSIs has been extensively investigated *in vivo* (Kalia et al., 2019). For example, the sulfur-containing compound ajoene (4,5,9-trithiadodeca-1,6,11-triene 9-oxide) purified from garlic extract was shown *in vitro* to significantly inhibit a

TABLE 1 Protein expression changed in PAO1 WT with the addition of Pht[a].

| Gene name | Protein description | Protein expression fold change |
|---|---|---|
| **Down-regulated:** | | |
| *pqsA* | Anthranilate–CoA ligase | 0.84 |
| PA2379 | Probable oxidoreductase | 0.83 |
| PA4046 | Uncharacterized protein | 0.83 |
| *tatA* | Sec-independent protein translocase protein TatA | 0.83 |
| *uvrC* | UvrABC system protein C | 0.83 |
| PA5220 | Uncharacterized protein | 0.83 |
| *pqsD* | Anthraniloyl-CoA anthraniloyltransferase | 0.83 |
| PA1668 | DotU domain-containing protein | 0.82 |
| PA0752 | Uncharacterized protein | 0.82 |
| *sdhC* | Succinate dehydrogenase cytochrome b556 subunit | 0.81 |
| PA3331 | Cytochrome P450 | 0.81 |
| *nusG* | Transcription termination/antitermination protein NusG | 0.81 |
| PA4357 | FeoC domain-containing protein | 0.81 |
| *hcnC* | Hydrogen cyanide synthase subunit HcnC | 0.81 |
| *pilP* | Type IV pilus inner membrane component PilP | 0.81 |
| *citA* | Citrate transporter | 0.80 |
| *pmrB* | Sensor protein kinase PmrB | 0.80 |
| PA4591 | HlyD_D23 domain-containing protein | 0.80 |
| PA2526 | Probable Resistance-Nodulation-Cell Division (RND) efflux transporter | 0.79 |
| PA1655 | Probable glutathione S-transferase | 0.79 |
| PA2252 | Probable AGCS sodium/alanine/glycine symporter | 0.78 |
| *pilO* | Type IV pilus inner membrane component PilO | 0.77 |
| *phnA* | Anthranilate synthase component 1, pyocyanin specific | 0.76 |
| PA1654 | Probable aminotransferase | 0.76 |
| *wspC* | Probable biofilm formation methyltransferase WspC | 0.76 |
| *roxS* | Histidine kinase | 0.75 |
| PA3677 | Probable Resistance-Nodulation-Cell Division (RND) efflux membrane fusion protein | 0.72 |
| *phzD2* | Phenazine biosynthesis protein PhzD2 | 0.68 |
| *purE* | N5-carboxyaminoimidazole ribonucleotide mutase | 0.64 |
| *pqsB* | 2-heptyl-4(1H)-quinolone synthase subunit PqsB | 0.59 |
| **Up-regulated:** | | |
| PA1224 | Probable NAD(P)H dehydrogenase | 1.56 |
| *fabZ* | 3-hydroxyacyl-[acyl-carrier-protein] dehydratase FabZ | 1.39 |
| *ribH* | 6,7-dimethyl-8-ribityllumazine synthase | 1.33 |
| PA5076 | Probable binding protein component of ABC transporter | 1.32 |
| PA4880 | Probable bacterioferritin | 1.29 |
| PA4739 | BON domain-containing protein | 1.25 |
| *nalC* | NalC | 1.23 |
| *speD* | S-adenosylmethionine decarboxylase proenzyme | 1.22 |
| *ihfB* | Integration host factor subunit beta | 1.22 |
| PA3779 | Uncharacterized protein | 1.22 |

[a]Three replicates per sample in the log phase were performed for proteomics analysis.

subclass of QS-regulated *P. aeruginosa* genes and rhamnolipid production in a dose-dependent manner. Besides, in a murine pulmonary infection model, a significant clearing of infecting *P. aeruginosa* was detected in ajoene-treated mice compared to a nontreated control group (Jakobsen et al., 2012). Additionally, mBTL is a chemical molecule synthesized

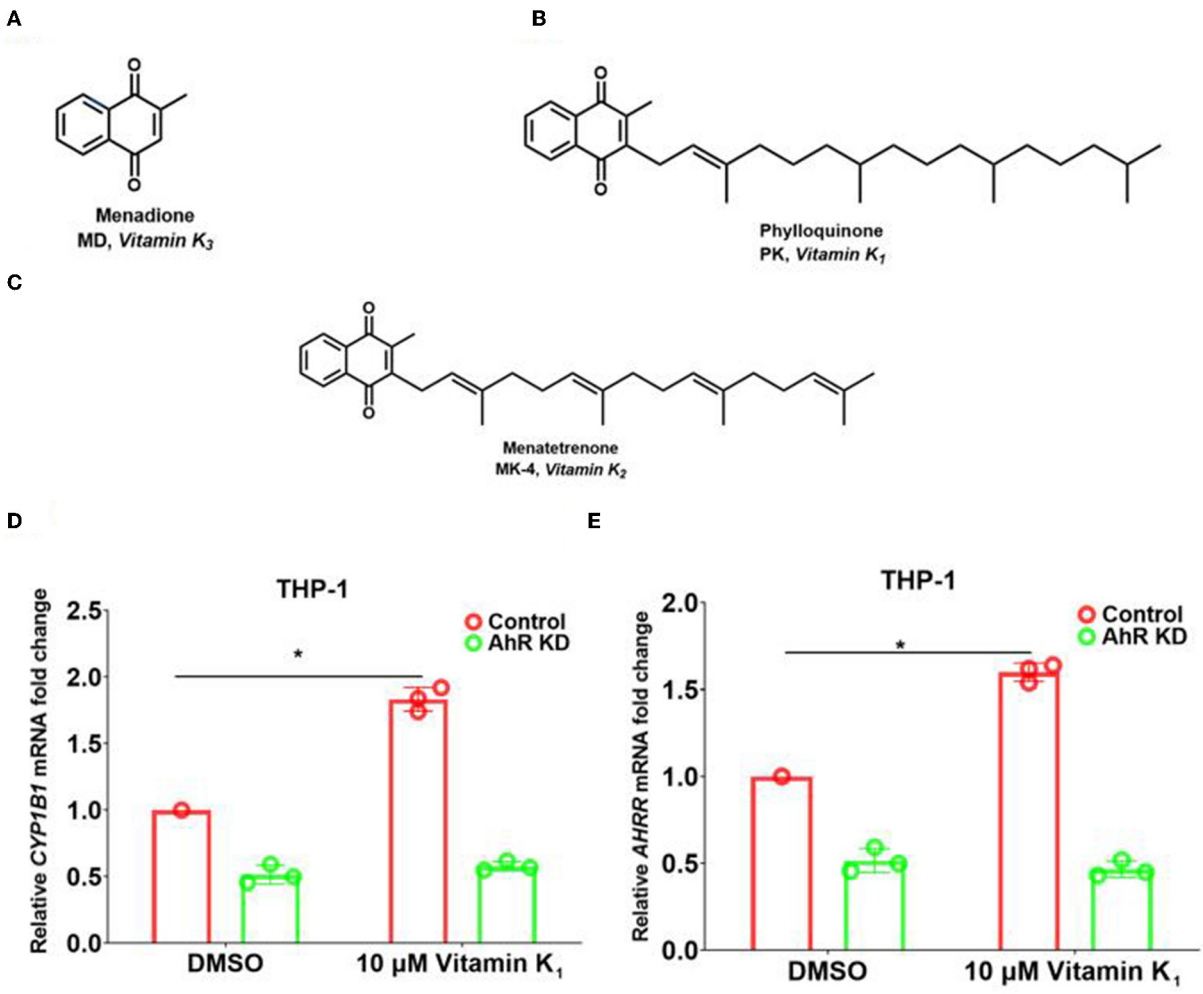


FIGURE 5
Pht analog vitamins $K_1$ increased the expression of AhR downstream genes in THP-1 human monocytes through AhR. **(A–C)** The chemical construction of molecules of vitamins $K_1$, $K_2$, and $K_3$. **(D,E)** qRT-PCR of the expression of *CYP1B1* and *AHRR* in THP-1 control and AhR KD cells with vitamin $K_1$ addition. Data are presented as means ± SD; $n$ = three independent experiments (*$P \leq 0.05$, Mann-Whitney $U$-test).

to inhibit the two *P. aeruginosa* QS regulators, LasR and RhlR, which were shown to reduce the production of the virulence factor pyocyanin and biofilm formation, protecting *Caenorhabditis elegans* from killing by *P. aeruginosa* (O'loughlin et al., 2013). However, most QSIs are discovered from screening chemical compound libraries and may be highly toxic to the human body. Therefore, it is urgent to discover and develop harmless QSI compounds such as microbial metabolites that could be detected in human lung tissues at high concentrations.

Recently, one MTb natural metabolite Pht analog Plumbagin secreted by *Plumbago zeylanica* L. was identified to inhibit *P. aeruginosa* LasR protein-regulated *las* QS system (Qais et al., 2021). In this study, we reported the dual-functional *P. aeruginosa* PQS and MTb Pht interact with host AhR and bacterial PqsR proteins (Figure 8). Pht and its analog, vitamin K, promote AhR to facilitate innate immune defense against bacteria through *CYP1B1* and *AHRR*, while PQS had the opposite effect. Moreover, Pht and its analogs, vitamins $K_1$, $K_2$, and $K_3$, were also effective QSIs that can inhibit *P. aeruginosa pqs* QS system, pyocyanin, and biofilm. Pht has been detected in the bronchoalveolar fluid with a concentration of up to 50 μM in most patients with tuberculosis (Gardner, 1996). The toxicity of Pht was previously tested in mice at a dose of 200 mg/kg oral and 150 mg/kg intraperitoneal, which is believed to be safe for *in vivo* usage (https://pubchem.ncbi.nlm.nih.gov/compound/10221). Besides, Pht analogs and vitamin K also naturally exist in the human body and have been proven to boost the human immune system by preventing calcium deposition, elastic fiber degradation, thrombosis, and inflammation in blood vessels or lungs (Janssen et al., 2021). The vitamin K family has been approved by the FDA and long-term

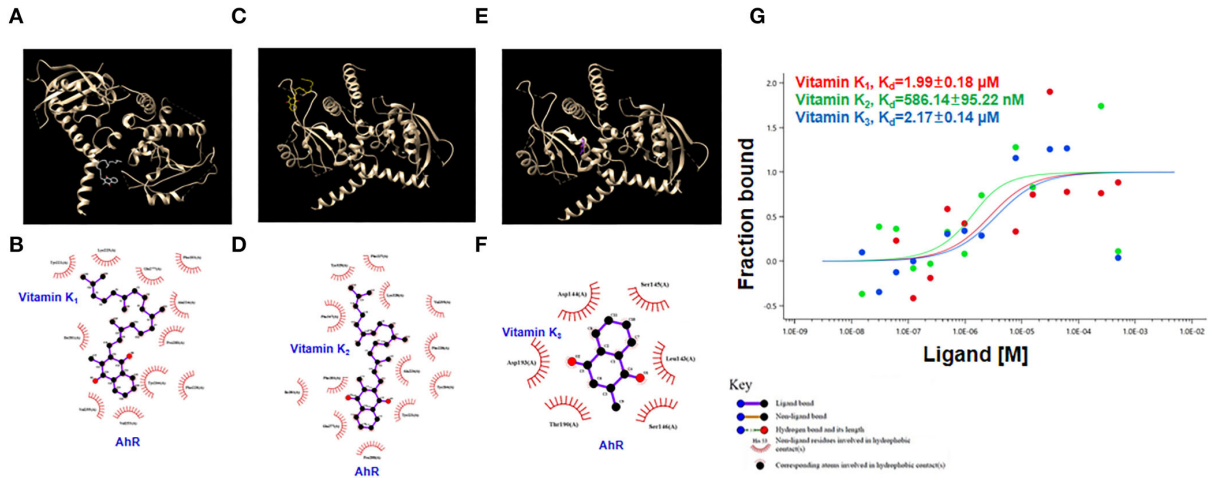


FIGURE 6
Interaction of vitamins $K_1$, $K_2$, and $K_3$ with AhR protein. **(A,C,E)** The interaction model of the AhR protein with vitamins $K_1$, $K_2$, or $K_3$. **(B,D,F)** Interaction map between residues within the AhR protein with vitamins $K_1$, $K_2$, or $K_3$. **(G)** Quantification of the binding affinity of AhR protein with vitamins $K_1$, $K_2$, or $K_3$ using microscale thermophoresis assay.

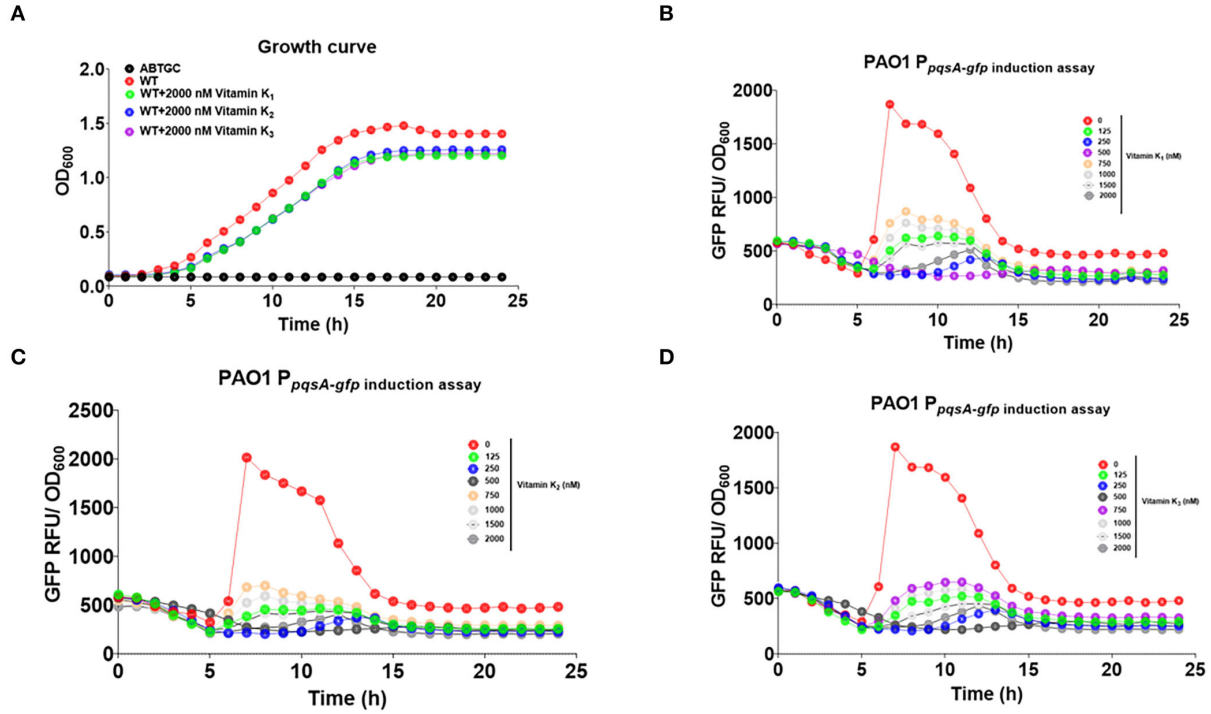


FIGURE 7
Vitamins $K_1$, $K_2$, and $K_3$ inhibited *P. aeruginosa pqs* QS system. **(A)** Growth curve of ABTGC media (Blank), *P. aeruginosa* WT, WT+2000 nM vitamins $K_1$, $K_2$, and $K_3$ strains. **(B)** Dose-dependent inhibition curves of vitamins $K_1$ with QS monitor PAO1 $P_{pqsA-gfp}$. **(C)** Dose-dependent inhibition curves of vitamins $K_2$ with QS monitor PAO1 $P_{pqsA-gfp}$. **(D)** Dose-dependent inhibition curves of vitamins $K_3$ with QS monitor PAO1 $P_{pqsA-gfp}$.

used as human drugs and healthy foods without toxicity. Thus, Pht and Vitamin K could be potentially harmless QSI drugs for controlling *P. aeruginosa* infections and increasing human immune systems.

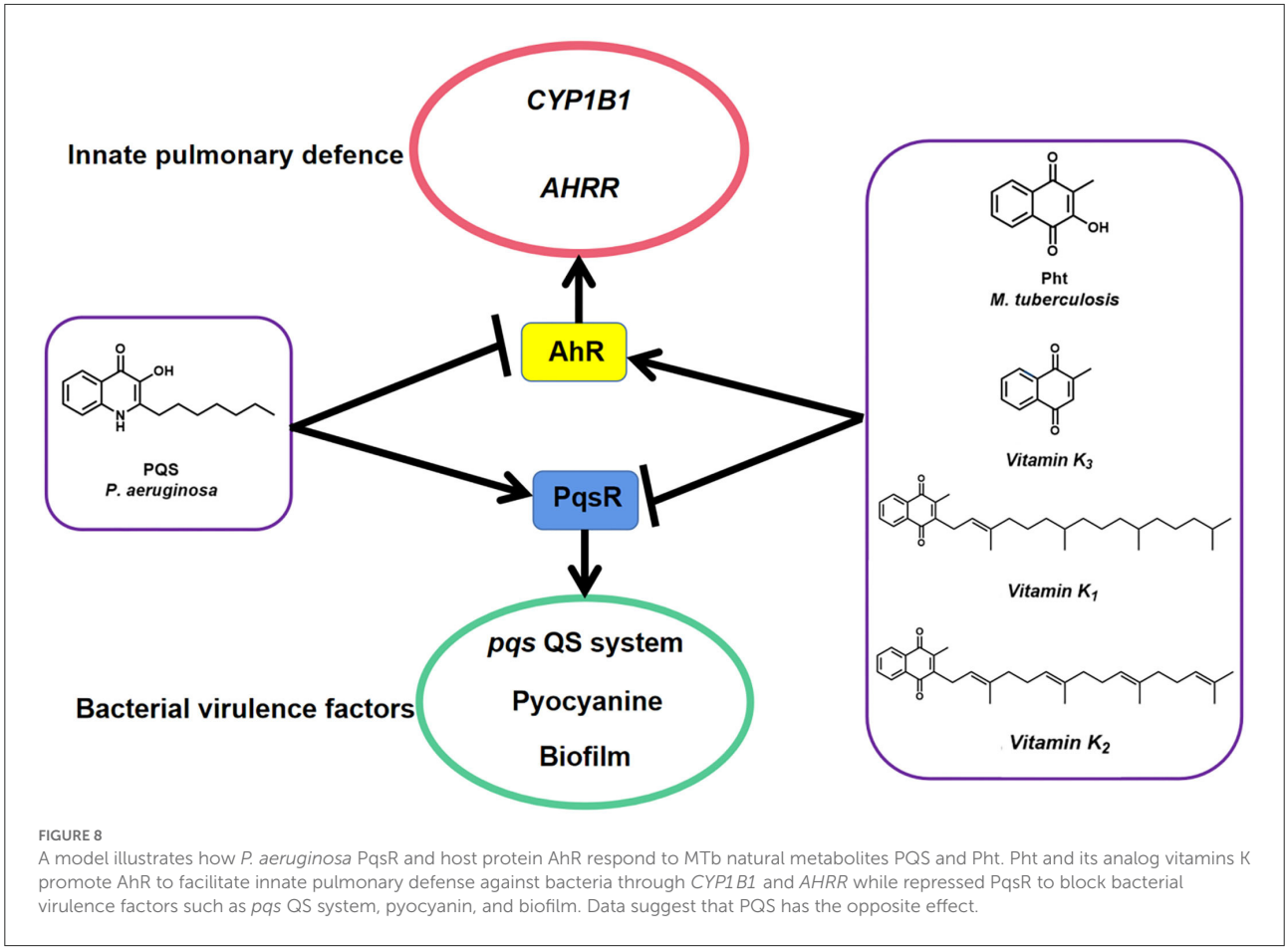


FIGURE 8
A model illustrates how *P. aeruginosa* PqsR and host protein AhR respond to MTb natural metabolites PQS and Pht. Pht and its analog vitamins K promote AhR to facilitate innate pulmonary defense against bacteria through *CYP1B1* and *AHRR* while repressed PqsR to block bacterial virulence factors such as *pqs* QS system, pyocyanin, and biofilm. Data suggest that PQS has the opposite effect.

Carbapenems, including imipenem, meropenem, and ertapenem, are common antibiotics to treat *P. aeruginosa* biofilm-associated infections in patients with CF (Yan and Bassler, 2019). However, due to the long-term use of these antibiotics, *P. aeruginosa* evolved multidrug resistance mechanisms to them, such as expression of efflux pumps and overexpression of biofilm structural components (Hall and Mah, 2017). Specifically, QSIs are newly developed specific drugs that interfere with *P. aeruginosa* virulent gene expression without affecting bacterial growth (Carradori et al., 2020). Therefore, using a combination of QSI drugs and antibiotics is a promising strategy for treating chronic biofilm infections caused by *P. aeruginosa*. The treatment of an *in vivo P. aeruginosa* foreign-body biofilm infection with a combination of QSI drugs such as Furanone C30, ajoene, or horseradish juice extract and tobramycin showed a synergistic clearing effect on the bacteria (Christensen et al., 2012). It also has been shown that *in vitro*-grown *P. aeruginosa* biofilms in the absence of an active QS system (either by mutation of crucial QS genes or by using QSI drugs) are more susceptible to tobramycin, indicating that QSI drugs and tobramycin have combinational effects on eradicating bacterial biofilms (Høiby et al., 2010). Besides, QSIs such as patulin, penicillic acid, baicalin hydrate, and cinnamaldehyde are effective in increasing the susceptibility of *P. aeruginosa* to antibiotics (Hentzer and Givskov, 2003). These findings suggest that the synergistic treatment of *P. aeruginosa* infections is an effective strategy to prevent biofilm by first disabling the QS system by reducing bacterial virulence with QSI drugs and then killing the bacteria with antibiotics. However, there is no evidence of Pht synergistic treatment with antibiotics for *P. aeruginosa* infections. Thus, we will further examine the efficiency of Pht and its analogs in combination with antibiotics to treat *P. aeruginosa* infections.

In conclusion, using small molecules targeting the QS systems is a potential strategy for eradicating and preventing *P. aeruginosa* infections. MTb natural metabolite Pht and *P. aeruginosa* PQS are both ligands of human AhR receptors with structural similarity. In this study, Pht was confirmed as an inhibitor of the *pqs* QS system of *P. aeruginosa* with an optimal working concentration of 750 nM and is likely to compete with PQS in binding with PqsR. *Pseudomonas aeruginosa*'s key virulence factor, pyocyanin, and biofilm formation could be reduced with Pht treatment. Pht analog vitamins $K_1$, $K_2$, and $K_3$ were also shown to inhibit the *P. aeruginosa pqs* QS system.

## Data availability statement

The original contributions presented in the study are publicly available. This data can be found in the ProteomeXchange Consortium with the dataset identifier PXD032384.

## Author contributions

TJ, LY, and GL designed the study. TJ, DL, XB, and ML performed experiments. TJ, ZC, JF, ZL, PW, XK, GZ, and AJ analyzed the results. TJ, ZC, and LY drafted and revised the manuscript. All authors contributed to the article and approved the submitted version.

## Funding

This work was supported by the National Key R&D Program of China (2021YFA1300902); Guangdong Natural Science Foundation for Distinguished Young Scholar (2020B1515020003); the Shenzhen Key Laboratory of Gene Regulation and Systems Biology, Southern University of Science and Technology (ZDSYS20200811144002008); and Shenzhen Science and Technology Program KQTD20200909113758004.

## Conflict of interest

The authors declare that the research was conducted in the absence of any commercial or financial relationships that could be construed as a potential conflict of interest.

## Publisher's note

All claims expressed in this article are solely those of the authors and do not necessarily represent those of their affiliated organizations, or those of the publisher, the editors and the reviewers. Any product that may be evaluated in this article, or claim that may be made by its manufacturer, is not guaranteed or endorsed by the publisher.

## Supplementary material

The Supplementary Material for this article can be found online at: https://www.frontiersin.org/articles/10.3389/fmicb.2022.896687/full#supplementary-material

## References

Carradori, S., Di Giacomo, N., Lobefalo, M., Luisi, G., Campestre, C., and Sisto, F. (2020). Biofilm and Quorum Sensing inhibitors: the road so far. *Expert Opin. Ther. Pat.* 30, 917–930. doi: 10.1080/13543776.2020.1830059

Choi, K. H., and Schweizer, H. P. (2005). An improved method for rapid generation of unmarked *Pseudomonas aeruginosa* deletion mutants. *BMC Microbiol.* 5, 30. doi: 10.1186/1471-2180-5-30

Christensen, L. D., Van Gennip, M., Jakobsen, T. H., Alhede, M., Hougen, H. P., Høiby, N., et al. (2012). Synergistic antibacterial efficacy of early combination treatment with tobramycin and quorum-sensing inhibitors against *Pseudomonas aeruginosa* in an intraperitoneal foreign-body infection mouse model. *J. Antimicrob. Chemother.* 67, 1198–1206. doi: 10.1093/jac/dks002

Costerton, J. W., Montanaro, L., and Arciola, C. R. (2005). Biofilm in implant infections: its production and regulation. *Int. J. Artif. Organs* 28, 1062–1068. doi: 10.1177/039139880502801103

Curran, C. S., Bolig, T., and Torabi-Parizi, P. (2018). Mechanisms and targeted therapies for *Pseudomonas aeruginosa* lung infection. *Am. J. Respir. Crit. Care Med.* 197, 708–727. doi: 10.1164/rccm.201705-1043SO

Devi, P., Khan, A., Chattopadhyay, P., Mehta, P., Sahni, S., Sharma, S., et al. (2021). Co-infections as modulators of disease outcome: minor players or major players? *Front. Microbiol.* 12, 664386. doi: 10.3389/fmicb.2021.664386

Dos Santos, G., Kutuzov, M. A., and Ridge, K. M. (2012). The inflammasome in lung diseases. *Am. J. Physiol. Lung Cell Mol. Physiol.* 303, L627–633. doi: 10.1152/ajplung.00225.2012

Ehrt, S., Schnappinger, D., and Rhee, K. Y. (2018). Metabolic principles of persistence and pathogenicity in Mycobacterium tuberculosis. *Nat. Rev. Microbiol.* 16, 496–507. doi: 10.1038/s41579-018-0013-4

Falkinham, J. O., III, Hilborn, E. D., Arduino, M. J., Pruden, A., and Edwards, M. A. (2015). Epidemiology and ecology of opportunistic premise plumbing pathogens: *Legionella pneumophila*, *Mycobacterium avium*, and *Pseudomonas aeruginosa*. *Environ. Health Perspect.* 123, 749–758. doi: 10.1289/ehp.1408692

Franceschini, A., Szklarczyk, D., Frankild, S., Kuhn, M., Simonovic, M., Roth, A., et al. (2013). STRING v9.1: protein-protein interaction networks, with increased coverage and integration. *Nucleic Acids Res.* 41, D808–815. doi: 10.1093/nar/gks1094

Fusaro, M., Cianciolo, G., Brandi, M. L., Ferrari, S., Nickolas, T. L., Tripepi, G., et al. (2020). Vitamin K and osteoporosis. *Nutrients* 12, 625. doi: 10.3390/nu12123625

Galloway, D. R. (1991). *Pseudomonas aeruginosa* elastase and elastolysis revisited: recent developments. *Mol. Microbiol.* 5, 2315–2321. doi: 10.1111/j.1365-2958.1991.tb02076.x

García-Reyes, S., Soberón-Chávez, G., and Cocotl-Yanez, M. (2020). The third quorum-sensing system of *Pseudomonas aeruginosa*: *Pseudomonas* quinolone signal and the enigmatic PqsE protein. *J. Med. Microbiol.* 69, 25–34. doi: 10.1099/jmm.0.001116

Gardner, P. R. (1996). Superoxide production by the mycobacterial and pseudomonad quinoid pigments phthiocol and pyocyanine in human lung cells. *Arch. Biochem. Biophys.* 333, 267–274. doi: 10.1006/abbi.1996.0390

Gruber, J. D., Chen, W., Parnham, S., Beauchesne, K., Moeller, P., Flume, P. A., et al. (2016). The role of 2,4-dihydroxyquinoline (DHQ) in *Pseudomonas aeruginosa* pathogenicity. *PeerJ* 4, e1495. doi: 10.7717/peerj.1495

Hall, C. W., and Mah, T. F. (2017). Molecular mechanisms of biofilm-based antibiotic resistance and tolerance in pathogenic bacteria. *FEMS Microbiol. Rev.* 41, 276–301. doi: 10.1093/femsre/fux010

Hellman, L. M., and Fried, M. G. (2007). Electrophoretic mobility shift assay (EMSA) for detecting protein-nucleic acid interactions. *Nat. Protoc.* 2, 1849–1861. doi: 10.1038/nprot.2007.249

Hentzer, M., and Givskov, M. (2003). Pharmacological inhibition of quorum sensing for the treatment of chronic bacterial infections. *J. Clin. Invest.* 112, 1300–1307. doi: 10.1172/JCI20074

Høiby, N., Bjarnsholt, T., Givskov, M., Molin, S., and Ciofu, O. (2010). Antibiotic resistance of bacterial biofilms. *Int. J. Antimicrob. Agents* 35, 322–332. doi: 10.1016/j.ijantimicag.2009.12.011

Holmes, C. L., Anderson, M. T., Mobley, H. L. T., and Bachman, M. A. (2021). Pathogenesis of gram-negative bacteremia. *Clin. Microbiol. Rev.* 34, e00234–20. doi: 10.1128/CMR.00234-20

Ilangovan, A., Fletcher, M., Rampioni, G., Pustelny, C., Rumbaugh, K., Heeb, S., et al. (2013). Structural basis for native agonist and synthetic inhibitor recognition by the *Pseudomonas aeruginosa* quorum sensing regulator PqsR (MvfR). *PLoS Pathog.* 9, e1003508. doi: 10.1371/journal.ppat.1003508

Jakobsen, T. H., Van Gennip, M., Phipps, R. K., Shanmugham, M. S., Christensen, L. D., Alhede, M., et al. (2012). Ajoene, a sulfur-rich molecule from garlic, inhibits genes controlled by quorum sensing. *Antimicrob. Agents Chemother.* 56, 2314–2325. doi: 10.1128/AAC.05919-11

Janssen, R., Visser, M. P. J., Dofferhoff, A. S. M., Vermeer, C., Janssens, W., and Walk, J. (2021). Vitamin K metabolism as the potential missing link between lung damage and thromboembolism in Coronavirus disease 2019. *Br. J. Nutr.* 126, 191–198. doi: 10.1017/S0007114520003979

Jones, P., Binns, D., Chang, H. Y., Fraser, M., Li, W., Mcanulla, C., et al. (2014). InterProScan 5: genome-scale protein function classification. *Bioinformatics* 30, 1236–1240. doi: 10.1093/bioinformatics/btu031

Kalia, V. C. (2013). Quorum sensing inhibitors: an overview. *Biotechnol. Adv.* 31, 224–245. doi: 10.1016/j.biotechadv.2012.10.004

Kalia, V. C., Patel, S. K. S., Kang, Y. C., and Lee, J. K. (2019). Quorum sensing inhibitors as antipathogens: biotechnological applications. *Biotechnol. Adv.* 37, 68–90. doi: 10.1016/j.biotechadv.2018.11.006

Kim, H. S., Lee, S. H., Byun, Y., and Park, H. D. (2015). 6-Gingerol reduces *Pseudomonas aeruginosa* biofilm formation and virulence *via* quorum sensing inhibition. *Sci. Rep.* 5, 8656. doi: 10.1038/srep08656

Lau, G. W., Hassett, D. J., Ran, H., and Kong, F. (2004a). The role of pyocyanin in Pseudomonas aeruginosa infection. *Trends Mol. Med.* 10, 599–606. doi: 10.1016/j.molmed.2004.10.002

Lau, G. W., Ran, H., Kong, F., Hassett, D. J., and Mavrodi, D. (2004b). *Pseudomonas aeruginosa* pyocyanin is critical for lung infection in mice. *Infect. Immun.* 72, 4275–4278. doi: 10.1128/IAI.72.7.4275-4278.2004

Leclerc, D., Staats Pires, A. C., Guillemin, G. J., and Gilot, D. (2021). Detrimental activation of AhR pathway in cancer: an overview of therapeutic strategies. *Curr. Opin. Immunol.* 70, 15–26. doi: 10.1016/j.coi.2020.12.003

Lichstein, H. C., and Van De Sand, V. F. (1946). The antibiotic activity of violacein, prodigiosin, and phthiocol. *J. Bacteriol.* 52, 145–146. doi: 10.1128/jb.52.1.145-146.1946

Majik, M. S., and Parvatkar, P. T. (2014). Next generation biofilm inhibitors for *Pseudomonas aeruginosa*: Synthesis and rational design approaches. *Curr. Top. Med. Chem.* 14, 81–109. doi: 10.2174/1568026613666131113152257

Martiniano, S. L., Sontag, M. K., Daley, C. L., Nick, J. A., and Sagel, S. D. (2014). Clinical significance of a first positive nontuberculous mycobacteria culture in cystic fibrosis. *Ann. Am. Thorac. Soc.* 11, 36–44. doi: 10.1513/AnnalsATS.201309-310OC

Moura-Alves, P., Faé, K., Houthuys, E., Dorhoi, A., Kreuchwig, A., Furkert, J., et al. (2014). AhR sensing of bacterial pigments regulates antibacterial defence. *Nature* 512, 387–392. doi: 10.1038/nature13684

Moura-Alves, P., Puyskens, A., Stinn, A., Klemm, M., Guhlich-Bornhof, U., Dorhoi, A., et al. (2019). Host monitoring of quorum sensing during *Pseudomonas aeruginosa* infection. *Science* 366, aaw1629. doi: 10.1126/science.aaw1629

O'boyle, N. M., Banck, M., James, C. A., Morley, C., Vandermeersch, T., and Hutchison, G. R. (2011). Open babel: an open chemical toolbox. *J. Cheminform.* 3, 33. doi: 10.1186/1758-2946-3-33

O'loughlin, C. T., Miller, L. C., Siryaporn, A., Drescher, K., Semmelhack, M. F., and Bassler, B. L. (2013). A quorum-sensing inhibitor blocks *Pseudomonas aeruginosa* virulence and biofilm formation. *Proc. Natl. Acad. Sci. U. S. A.* 110, 17981–17986. doi: 10.1073/pnas.1316981110

Palermo, A., Tuccinardi, D., D'onofrio, L., Watanabe, M., Maggi, D., Maurizi, A. R., et al. (2017). Vitamin K and osteoporosis: myth or reality? *Metabolism* 70, 57–71. doi: 10.1016/j.metabol.2017.01.032

Pearson, J. P., Pesci, E. C., and Iglewski, B. H. (1997). Roles of *Pseudomonas aeruginosa* las and rhl quorum-sensing systems in control of elastase and rhamnolipid biosynthesis genes. *J. Bacteriol.* 179, 5756–5767. doi: 10.1128/jb.179.18.5756-5767.1997

Pesci, E. C., Milbank, J. B., Pearson, J. P., Mcknight, S., Kende, A. S., Greenberg, E. P., et al. (1999). Quinolone signaling in the cell-to-cell communication system of *Pseudomonas aeruginosa*. *Proc. Natl. Acad. Sci. U. S. A.* 96, 11229–11234. doi: 10.1073/pnas.96.20.11229

Pettersen, E. F., Goddard, T. D., Huang, C. C., Couch, G. S., Greenblatt, D. M., Meng, E. C., et al. (2004). UCSF Chimera–a visualization system for exploratory research and analysis. *J. Comput. Chem.* 25, 1605–1612. doi: 10.1002/jcc.20084

Qais, F. A., Khan, M. S., Ahmad, I., Husain, F. M., Al-Kheraif, A. A., Arshad, M., et al. (2021). Plumbagin inhibits quorum sensing-regulated virulence and biofilms of Gram-negative bacteria: *in vitro* and *in silico* investigations. *Biofouling* 37, 724–739. doi: 10.1080/08927014.2021.1955250

Seeliger, D., and De Groot, B. L. (2010). Ligand docking and binding site analysis with PyMOL and Autodock/Vina. *J. Comput. Aided Mol. Des.* 24, 417–422. doi: 10.1007/s10822-010-9352-6

Shinde, V., and Wadekar, M. (2018). Spectral and antibacterial investigations of Er(III) Juglonates. *Inter. J. ChemTech. Res.* 10, 740–748.

Soberón-Chávez, G., Lépine, F., and Déziel, E. (2005). Production of rhamnolipids by *Pseudomonas aeruginosa*. *Appl. Microbiol. Biotechnol.* 68, 718–725. doi: 10.1007/s00253-005-0150-3

Soheili, V., Tajani, A. S., Ghodsi, R., and Bazzaz, B. S. F. (2019). Anti-PqsR compounds as next-generation antibacterial agents against *Pseudomonas aeruginosa*: a review. *Eur. J. Med. Chem.* 172, 26–35. doi: 10.1016/j.ejmech.2019.03.049

Srinivasarao, S., Nizalapur, S., Yu, T. T., Wenholz, D. S., Trivedi, P., Ghosh, B., et al. (2018). Design, synthesis and biological evaluation of triazole-containing 2-phenylindole and salicylic acid as quorum sensing inhibitors against *Pseudomonas aeruginosa*. *ChemistSelect* 3, 9170–9180. doi: 10.1002/slct.201801622

Wallace, A. C., Laskowski, R. A., and Thornton, J. M. (1995). LIGPLOT: a program to generate schematic diagrams of protein-ligand interactions. *Protein Eng.* 8, 127–134. doi: 10.1093/protein/8.2.127

Yan, J., and Bassler, B. L. (2019). Surviving as a community: antibiotic tolerance and persistence in bacterial biofilms. *Cell Host Microbe.* 26, 15–21. doi: 10.1016/j.chom.2019.06.002

Yang, L., Barken, K. B., Skindersoe, M. E., Christensen, A. B., Givskov, M., and Tolker-Nielsen, T. (2007). Effects of iron on DNA release and biofilm development by *Pseudomonas aeruginosa*. *Microbiology* 153, 1318–1328. doi: 10.1099/mic.0.2006/004911-0

Zhang, X., Xu, X., Li, P., Zhou, F., Kong, L., Qiu, J., et al. (2019). TMT based proteomic analysis of human follicular fluid from overweight/obese and normal-weight patients with polycystic ovary syndrome. *Front. Endocrinol.* 10, 821. doi: 10.3389/fendo.2019.00821

frontiers | Frontiers in Microbiology

TYPE Original Research
PUBLISHED 03 October 2022
DOI 10.3389/fmicb.2022.939390



OPEN ACCESS

EDITED BY
Laura Quintieri,
Italian National Research Council, Italy

REVIEWED BY
Jun Mei,
Shanghai Ocean University, China
Anupam Roy,
Indian Institute of Technology Kharagpur, India

*CORRESPONDENCE
Moupriya Nag
moupriya.nag@uem.edu.in
Muhammad Rajaei Ahmad Mohd Zain
rajaei@usm.my

†These authors have contributed equally to this work

SPECIALTY SECTION
This article was submitted to Antimicrobials, Resistance and Chemotherapy, a section of the journal Frontiers in Microbiology

RECEIVED 09 May 2022
ACCEPTED 11 August 2022
PUBLISHED 03 October 2022

CITATION
Lahiri D, Ray RR, Sarkar T, Upadhye VJ, Ghosh S, Pandit S, Pati S, Edinur HA, Abdul Kari Z, Nag M and Ahmad Mohd Zain MR (2022) Anti-biofilm efficacy of green-synthesized ZnO nanoparticles on oral biofilm: *In vitro* and *in silico* study. *Front. Microbiol.* 13:939390. doi: 10.3389/fmicb.2022.939390



# Anti-biofilm efficacy of green-synthesized ZnO nanoparticles on oral biofilm: *In vitro* and *in silico* study

Dibyajit Lahiri[1†], Rina Rani Ray[2], Tanmay Sarkar[3†], Vijay Jagdish Upadhye[4], Sujay Ghosh[5], Soumya Pandit[6], Siddhartha Pati[7,8], Hisham Atan Edinur[9], Zulhisyam Abdul Kari[10], Moupriya Nag[1*] and Muhammad Rajaei Ahmad Mohd Zain[11*]

[1]Department of Biotechnology, University of Engineering & Management Kolkata, Kolkata, India, [2]Department of Biotechnology, Maulana Abul Kalam Azad University of Technology, Haringhata, West Bengal, India, [3]Department of Food Processing Technology, Malda Polytechnic, West Bengal State Council of Technical Education, Government of West Bengal, Malda, India, [4]Parul University, Vadodara, Gujrat, India, [5]AMH Energy Pvt. Ltd., Kolkata, India, [6]Department of Biotechnology, Sharda University, Noida, India, [7]Natnov Bioscience Private Limited, Balasore, India, [8]Skills Innovation & Academic Network (SIAN) Institute, Association for Biodiversity Conservation & Research (ABC), Balasore, India, [9]School of Health Sciences, Health Campus, Universiti Sains Malaysia, Kubang Kerian, Kelantan, Malaysia, [10]Department of Agricultural Science, Faculty of Agro-Based Industry, Universiti Malaysia Kelantan, Kota Bharu, Kelantan, Malaysia, [11]Department of Orthopaedics, School of Medical Sciences, Universiti Sains Malaysia, Kubang Kerian, Kelantan, Malaysia

The development of biofilm on the biotic and abiotic surfaces is the greatest challenge for health care sectors. At present times, oral infection is a common concern among people with an unhealthy lifestyle and most of these biofilms-associated infections are resistant to antibiotics. This has increased a search for the development of alternate therapeutics for eradicating biofilm-associated infection. Nanobiotechnology being an effective way to combat such oral infections may encourage the use of herbal compounds, such as bio-reducing and capping agents. Green-synthesis of ZnO nanoparticles (ZnO NP) by the use of the floral extract of *Clitoria ternatea*, a traditionally used medicinal plant, showed stability for a longer period of time. The NPs as depicted by the TEM image with a size of 10 nm showed excitation spectra at 360 nm and were found to remain stable for a considerable period of time. It was observed that the NPs were effective in the eradication of the oral biofilm formed by the major tooth attacking bacterial strains namely *Porphyromonsas gingivalis* and *Alcaligenes faecalis*, by bringing a considerable reduction in the extracellular polymeric substances (EPS). It was observed that the viability of the *Porphyromonsas gingivalis* and *Alcaligenes faecalis* was reduced by NP treatment to 87.89 ± 0.25% in comparison to that of amoxicillin. The results went in agreement with the findings of modeling performed by the use of response surface methodology (RSM) and artificial neural network (ANN). The microscopic studies and FT-IR analysis revealed that there was a considerable reduction in the biofilm after NP treatment. The *in silico* studies further confirmed that the ZnO NPs showed considerable interactions with

the biofilm-forming proteins. Hence, this study showed that ZnO NPs derived from *Clitoria ternatea* can be used as an effective alternative therapeutic for the treatment of biofilm associated oral infection.

KEYWORDS

**antibiofilm, dental biofilm, *Clitoria ternatea*, response surface methodology, artificial neural network**

## Introduction

The oral cavity provides an ideal environment for the growth of a large number of microbial communities that are responsible for the development of oral biofilm (Caputo et al., 2018; Morse et al., 2018; Quintieri et al., 2020). The development of oral biofilm takes place under the influence of the salivary glycoproteins, which act as adhering material for the sessile communities (Lahiri et al., 2021a). The sessile communities remain entangled with the help of a self-secreted polymeric substance (EPS) that acts as a natural glue. The EPS not only provides nourishment to the indwelling cells but also prevents the penetration of drug-like molecules resulting in the development of antimicrobial resistance (Khatoon et al., 2018). Thus, the use of alternative therapeutics has become an important way of combating biofilm-associated oral infections. Bio-nanotechnology is an upcoming and booming area in the field of Biotechnology and is coming up as an important part of clinical dentistry and dental practices (Thrall, 2004). Nano-particles are more effective than conventional antimicrobial agents and are used in mouth-wash, toothpaste, mouth-freshener, etc., and also in many oral clinics as a healthcare technology for reducing the risk factor of any kind of surgery (Thrall, 2004). Nano-particle technology or rather bio-nano-particle technology is especially used in the processes of dental filling, enamel polishing for prevention of caries, implantation technology as nano implant particles, which has more effectiveness than the regular type of nanoparticles, etc (Sahoo and Labhasetwar, 2003). A significant part of the nano-strategy lies in their role in the prevention of bacterial growth and bacterial biofilm formation. This nanoparticle technology is getting more and more popular among people as this technology is cost-effective, time-saving, and its application may avoid major surgery (Vasir and Labhasetwar, 2005). Among various types of metallic and non-metallic nanoparticles used, there are many added values of using the zinc oxide nanoparticles as the type selection of the nanoparticle. In comparison to the other types of nanoparticles like silver oxide nanoparticles or copper oxide nanoparticles that are organic or bulk oxide, it is seen that the zinc-oxide nanoparticles are robust, chemically more stable with marked thermal resistance, and have a long shelf life (Vasir et al., 2005). Also, many studies have confirmed that the selective toxicity of ZnO nanoparticles is almost negligible in comparison to the other kinds of nanoparticles, and also while comparing them with other nanoparticles, they show the minimal effect of toxicity on human cells (Maeda et al., 2000). Zinc oxide nanoparticles also show microbicidal properties against Gram-positive and Gram-negative bacteria and fungal spores that are usually resistant to a higher temperature and higher pressure (Allaker, 2011). The advancement of modern nano-strategy due to its effectiveness and preciseness can solve many dental disturbances. The efficiency of nanoparticles can be further increased once they are mixed with some bioactive compounds derived from natural phytoextracts having high medicinal properties and are used traditionally for cleaning and whitening teeth enamel (Allen and Cullis, 2004).

Nanobiotechnology based on a phytocompound-induced synthesis of nanoparticles is becoming a rising tendency in green chemistry due to its simple, non-toxic, and inexpensive nature (Bala et al., 2015). Amongst the preferred nanoparticles, the use of biogenically synthesized ZnO nanoparticles having diverse biomedical applications (Jan et al., 2020) is considered an environment-friendly and convenient technique.

In this study, the flowers of *Clitoria ternatea*, known for their medicinal values, were used as the biogenic source for ZnO nanoparticle production. Traditionally this plant is known mainly for its antistress, antidepressant, and anticonvulsant activities. The ZnO nanoparticles, biogenically formed from this plant extract, are evaluated for their antibiofilm activities against dental biofilm-forming bacterial strains and their superiority will be confirmed over conventional antibiotics. Such appraisal was confirmed by simulation-based studies with some statistical and computational model-based analysis. The *in silico* study helped in understanding the optimum condition for the production of nanoparticles and also helped in understanding the interaction of the ZnO NP with the targeted biofilm-forming proteins.

## Materials and methods

### Microorganism

*Porphyromonsas gingivalis* and *Alcaligenes faecalis* were used in this study. The bacterial cells were cultured in Luria Bertani Broth (LB broth) at 37°C for 24 h.

## Preparation of plant extract

The dried petals of the flower *C. ternatea* were pulverized in water and incubated for a period of 24 h. This was followed by filtering using the gauge filter and the filtrate was stored at 0–4°C for further use (Lahiri et al., 2021c).

## Synthesis of zinc-oxide nanoparticles

Synthesis of ZnO NPs was performed by dissolving 5 mM zinc nitrate in 50 mL Mili Q water and was kept in a stirrer for a period of 1 h (Jamdagni et al., 2018). This was followed by the addition of 25 mL of sodium hydroxide. There was an observed change in the coloration of the solution after incubation for 1 h with plant extract at a volume of 25 mL. The solution was kept under the stirring condition at least for a period of 3 h. The precipitate was separated from the mixture by centrifugation at 8,000 *g* for 15 min. The pellets were dried using a hot air oven at 80°C for 2 h.

# Response surface methodology (RSM) for ZnO NP optimization

The Box–Behnken design (BBD) was considered to model the production of ZnO NP. The pH, volume of extract (mL), reaction time (min), temperature (°C), and concentration of zinc nitrate (mM) were the input parameters, while the absorption characteristics of the synthesized NP were optimized with Design-Expert Version 7.0.0 (Statease Inc; Minneapolis, USA) (Sarkar et al., 2021b).

# Artificial neural network (ANN) teaching-learning based optimization (TLBO) for ZnO NP optimization

The multilayer perception (MLP) neural network along with error backpropagation was considered in this study using MATLAB R2014b (Math Works Inc., USA) (Sarkar et al., 2020; Lahiri et al., 2021c). The neural network model was built of 5 (input layer)−3 (hidden layer)−1 (output layer) architecture (Figure 3), learning range varied from 0.5 to 0.9. For non-linear activation functions, the Levenberg–Marquardt ANN tool was used, along with the ANN backpropagation technique for feed-forward neural networks.

The environment of classroom learning and improvement of the student's performance has been simulated in the teaching–learning based optimization (TLBO). The input variables, fitness value, and the initial solution have been assumed as the subject, marks obtained by the students, and the size of the student batch, respectively. In this study, the temperature, pH, time, concentration of $ZnNO_3$, and volume of the plant extract were considered as the subject. The values of those parameters were assumed by the student. The evaluation criteria to measure the performance of each student was maximization. In the teacher phase, the teaching factor was introduced to improve the performance of the students. Two random students with unequal performance were selected in the learner phase, in this phase higher performance was attained by learning. Learning from their own interactions as well from the teacher was considered as the iteration. The best-performing student was identified in each iteration. The process continued till the attainment of a maximum number of iterations selected or attainment of the constant best value for the last 50 generations (Morse et al., 2018; Stalin et al., 2019). Here, the absorbance value was assumed as the student's performance and maximization of the absorbance value. The best-performing student was selected from the batch of the absorbance value was considered as the TLBO objective. The TLBO parameters considered for the study are provided in Table 1.

TABLE 1 The parameters selected to conduct the TLBO.

| Attributes for TLBO | Value/range |
|---|---|
| Student | The set of temperature, pH, time, the concentration of $ZnNO_3$, and volume of the plant extract. |
| Size of the student batch | 40 |
| Teaching factor | 1–2 |
| Stopping criteria | Attainment of the constant best value for the last 50 generations. |

The proposed ANN-TLBO methodology to find the value of the optimum input parameters for maximum absorbance is illustrated in Figure 1. The ANN model was developed with the dataset of the input parameter–response combined with the aim of maximizing the coefficient of correlation ($R$) value. The TLBO was employed considering the size of the student batch of 40, and the student's performance was boosted in the teacher and learner phase till the attainment of the stopping criteria.

## Characterization of the nanoparticles

Aliquots were taken for analyzing the UV–vis spectra at time intervals of 24 h. The UV–vis spectra were analyzed within the range of 200–1,000 nm. Transmission electron microscopy was performed for analyzing the dimension and size of the ZnO NPs (Tailor et al., 2019; Bharadwaj et al., 2021). An X-ray diffractometer is used for the purpose of analyzing crystalline phase and purity between 20° and 80°.

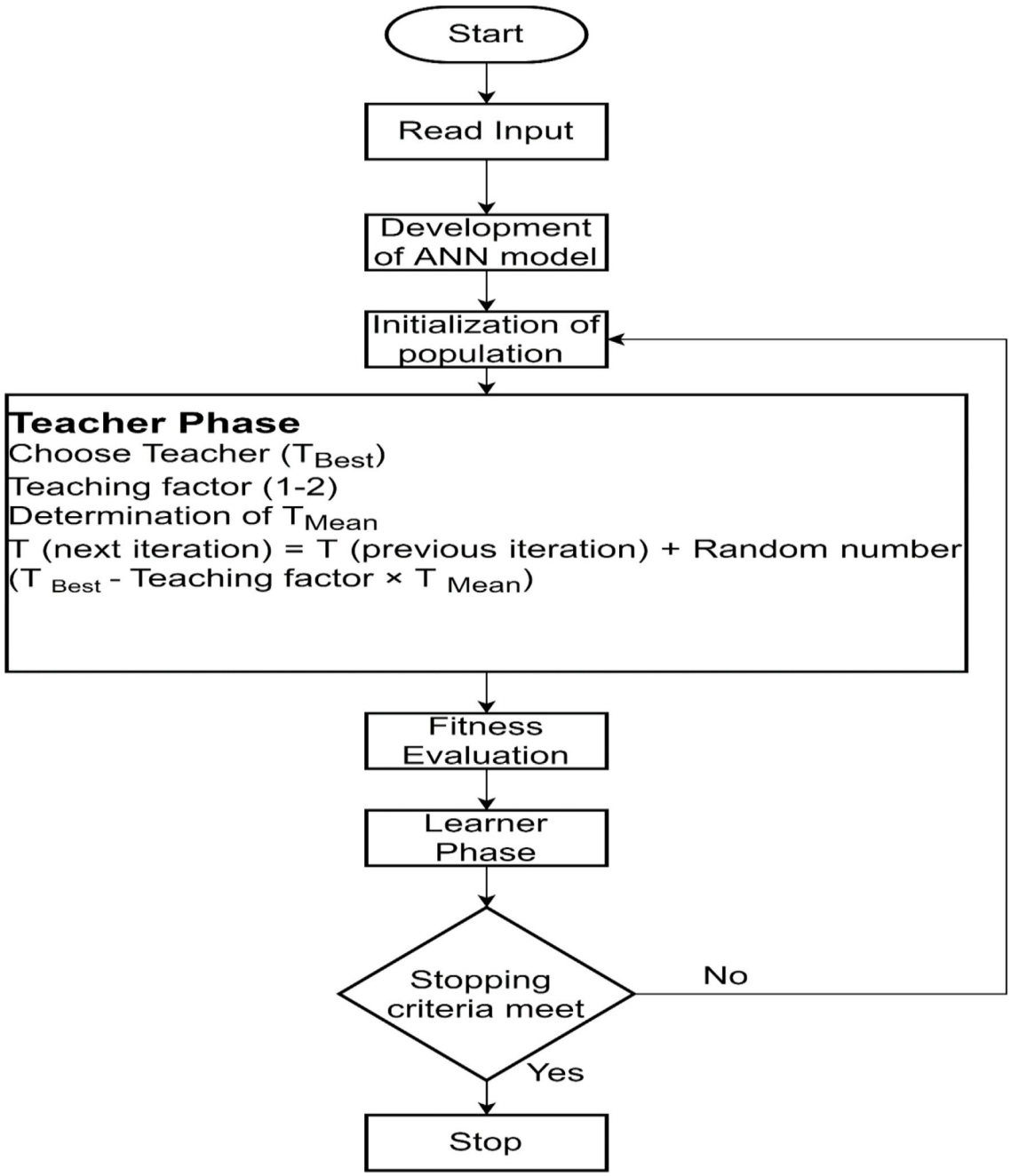


FIGURE 1
Flowchart for the proposed ANN-TLBO algorithm.

## Biofilm inhibition by ZnO NPs

The antibiofilm effect of the aqueous extract, biogenically synthesized ZnO NPs from *C. ternatea* on *Porphyromonsas gingivalis* and *Alcaligenes faecalis,* was analyzed using the microdilution method (Balouiri et al., 2016). The bacterial cells were grown within the wells of a 96-well plate at a concentration of $1 \times 10^6$ CFU/ml followed by incubation at 37°C for a period of 72 h to allow the development of biofilm (Lahiri et al., 2021b,c). After the development of biofilm, it was followed by the addition of ZnO NPs, plant extract, and amoxicillin as standard antibiotics. This was followed by

the addition of 3-[4,5-dimethyl-2-thiazolyl]-2, 5-diphenyl-2H-tetrazolium bromide (MTT dye) to quantify the viability of the bacterial cells in the presence of the challenge using the ELISA plate reader (2018 GEN-NET).

$$\text{Percentage Biofilm Inhibition} = \frac{[(\text{OD of untreated control}) - (\text{OD of the treated sample})]}{(\text{OD of untreated control})} \times 100 \quad (1)$$

### Destruction of carbohydrates and proteins associated with biofilm

The density of the sessile population associated with the biofilm is dependent on the total amount of carbohydrates and proteins that are associated with the EPS (Limoli et al., 2015). The process of extracting the carbohydrates and proteins from the biofilm comprises cell incubation in accordance with the biofilm assay. After the incubation period, the biofilm was washed gently using the PBS and boiled for a period of 30 min within 0.5 N NaOH for the purpose of extracting the surface protein. This was followed by centrifugation at 10,000 *g* for a period of 5 min followed by the collection of clear solution. The protein concentration was determined using the Lowry method. The carbohydrate concentration was analyzed by taking the sample of EPS within the test tube followed by the addition of 900 µl of distilled water and 5 mL of 98% of sulphuric acid. The color intensity was analyzed spectrophotometrically at 490 nm.

## Databases and information retrieval

The three-dimensional X-ray crystallographic structures of proteins responsible for biofilm formation, quorum sensing, and motility-related proteins in the EPS, with an approximate resolution of 1.5–2Å, were collected from the Protein Data Bank (https://www.rcsb.org/). The structure of receptor protein PDB ID: 5OLJ is associated with dental biofilm forming bacterial species *Porphyromonas gingivalis*. Another dental biofilm-forming protein was obtained from the isolated bacterial species *Alcaligenes faecalis,* using the phyre2 web server (http://www.sbg.bio.ic.ac.uk/phyre2/) in the.pdb format.

## Determination of the viability count of the sessile group of cells

The working strain grown on 0.1% chitin flakes (w/v) for a period of 72 h was washed with 0.1% (w/v) normal saline to eliminate planktonic groups of cells. After treating the sessile cells with plant extracts and bioactive compounds, the growth was determined spectrophotometrically at 590 nm at varying intervals of time (Baishya et al., 2016).

## ADME evaluation

The prediction of the ADME characteristics of the selected ligands was achieved through the SwissADME web server (http://www.swissadme.ch/). Swiss ADME is an open-source free web tool that computes the drug-likeness of compounds through their physicochemical and pharmacokinetic properties of small molecules (Daina et al., 2017). The input format consisted of the canonical SMILES of the selected compounds and the output from SwissADME containing the descriptors was obtained in.csv file format.

## Nanoparticle drawing with VESTA

In this study, VESTA (Momma and Izumi, 2008) was used for drawing the three-dimensional structure of Zinc oxide nanoparticles (ZnO) in space-filling representation. Visualization for Electronic Structural Analysis or VESTA is a three-dimensional visualization programme for structural models, volumetric data, such as electron or nuclear densities, and crystal morphologies. The software is managed and controlled by the Windows workstations *via* WPKG. ZnO nanoparticle has the lattice parameters $a = b = 3.24940$ and $c = 5.20380$ with alpha = beta = 90 and gamma = 120. Atomic position of Zn in unit cell is [0.33333, 0.66667, 0.00000] and O in unit cell situated at [0.33333, 0.66667, 0.38210].

## Preparation of molecules

The macromolecule preparation for the pre-processing of proteins before docking was achieved by AutoDockTools (ADT), which is a part of MGLTools, from the Molecular Graphics Laboratory at The Scripps Research Institute (Morris et al., 2008). Using ADT, the bound ligands were manually visualized using the Python Molecule Viewer (PMV). Removal of water molecules and addition of hydrogen were also carried out using the same. Finally, Gasteiger charges were added to the cleaned-up protein. Energy minimization of the ligands was achieved using the Auto Optimize tool of the Avogadro molecule editor and visualizer (Hanwell et al., 2012). Auto optimization continuously optimizes molecular geometry through molecular mechanics (Hanwell et al., 2012). The UFF or Universal Force Field was used along with a default value of 4 for "Steps per Update" and the energy minimization was achieved with a dE value of 0. The optimized ligands were written in.pdb format

10.3389/fmicb.2022.939390

TABLE 2 Process parameters for production of biogenic ZnO NP as per Box-Behnken design.

| Run | Temp (°C) | pH | Time (min) | Conc of Zinc nitrate (mM) | Vol of Extract (mL) | Absorbance |
|---|---|---|---|---|---|---|
| 1 | 25 | 8 | 90 | 50 | 25 | 0.742 |
| 2 | 40 | 6 | 90 | 30 | 10 | 0.698 |
| 3 | 10 | 6 | 180 | 30 | 25 | 0.778 |
| 4 | 40 | 6 | 90 | 50 | 25 | 0.784 |
| 5 | 25 | 4 | 0 | 30 | 25 | 0.008 |
| 6 | 25 | 8 | 180 | 30 | 25 | 0.756 |
| 7 | 25 | 4 | 90 | 30 | 40 | 0.638 |
| 8 | 10 | 8 | 90 | 30 | 25 | 0.612 |
| 9 | 10 | 6 | 90 | 50 | 25 | 0.743 |
| 10 | 40 | 6 | 90 | 30 | 40 | 0.796 |
| 11 | 40 | 6 | 180 | 30 | 25 | 0.843 |
| 12 | 25 | 8 | 0 | 30 | 25 | 0.01 |
| 13 | 25 | 4 | 90 | 50 | 25 | 0.789 |
| 14 | 25 | 8 | 90 | 30 | 40 | 0.824 |
| 15 | 40 | 4 | 90 | 30 | 25 | 0.756 |
| 16 | 25 | 6 | 90 | 30 | 25 | 0.425 |
| 17 | 25 | 6 | 0 | 30 | 10 | 0.009 |
| 18 | 25 | 6 | 0 | 50 | 25 | 0.012 |
| 19 | 25 | 6 | 180 | 50 | 25 | 0.921 |
| 20 | 40 | 8 | 90 | 30 | 25 | 0.655 |
| 21 | 25 | 6 | 90 | 10 | 10 | 0.512 |
| 22 | 25 | 6 | 90 | 30 | 25 | 0.768 |
| 23 | 10 | 6 | 90 | 30 | 10 | 0.626 |
| 24 | 10 | 4 | 90 | 30 | 25 | 0.678 |
| 25 | 25 | 6 | 90 | 50 | 10 | 0.684 |
| 26 | 10 | 6 | 90 | 10 | 25 | 0.712 |
| 27 | 25 | 6 | 180 | 10 | 25 | 0.801 |
| 28 | 25 | 4 | 180 | 30 | 25 | 0.814 |
| 29 | 10 | 6 | 90 | 30 | 40 | 0.842 |
| 30 | 25 | 6 | 0 | 10 | 25 | 0.012 |
| 31 | 10 | 6 | 0 | 30 | 25 | 0.014 |
| 32 | 40 | 6 | 90 | 10 | 25 | 0.234 |
| 33 | 25 | 6 | 90 | 50 | 40 | 0.744 |
| 34 | 25 | 4 | 90 | 10 | 25 | 0.521 |
| 35 | 25 | 6 | 90 | 30 | 25 | 0.667 |
| 36 | 25 | 4 | 90 | 30 | 10 | 0.7 |
| 37 | 25 | 6 | 90 | 10 | 40 | 0.734 |
| 38 | 25 | 6 | 90 | 30 | 25 | 0.746 |
| 39 | 25 | 6 | 90 | 30 | 25 | 0.742 |
| 40 | 25 | 8 | 90 | 30 | 10 | 0.745 |
| 41 | 25 | 6 | 0 | 30 | 40 | 0.012 |
| 42 | 25 | 6 | 180 | 30 | 40 | 0.845 |
| 43 | 25 | 6 | 180 | 30 | 10 | 0.848 |
| 44 | 40 | 6 | 0 | 30 | 25 | 0.018 |
| 45 | 25 | 8 | 90 | 10 | 25 | 0.661 |
| 46 | 25 | 6 | 90 | 30 | 25 | 0.621 |

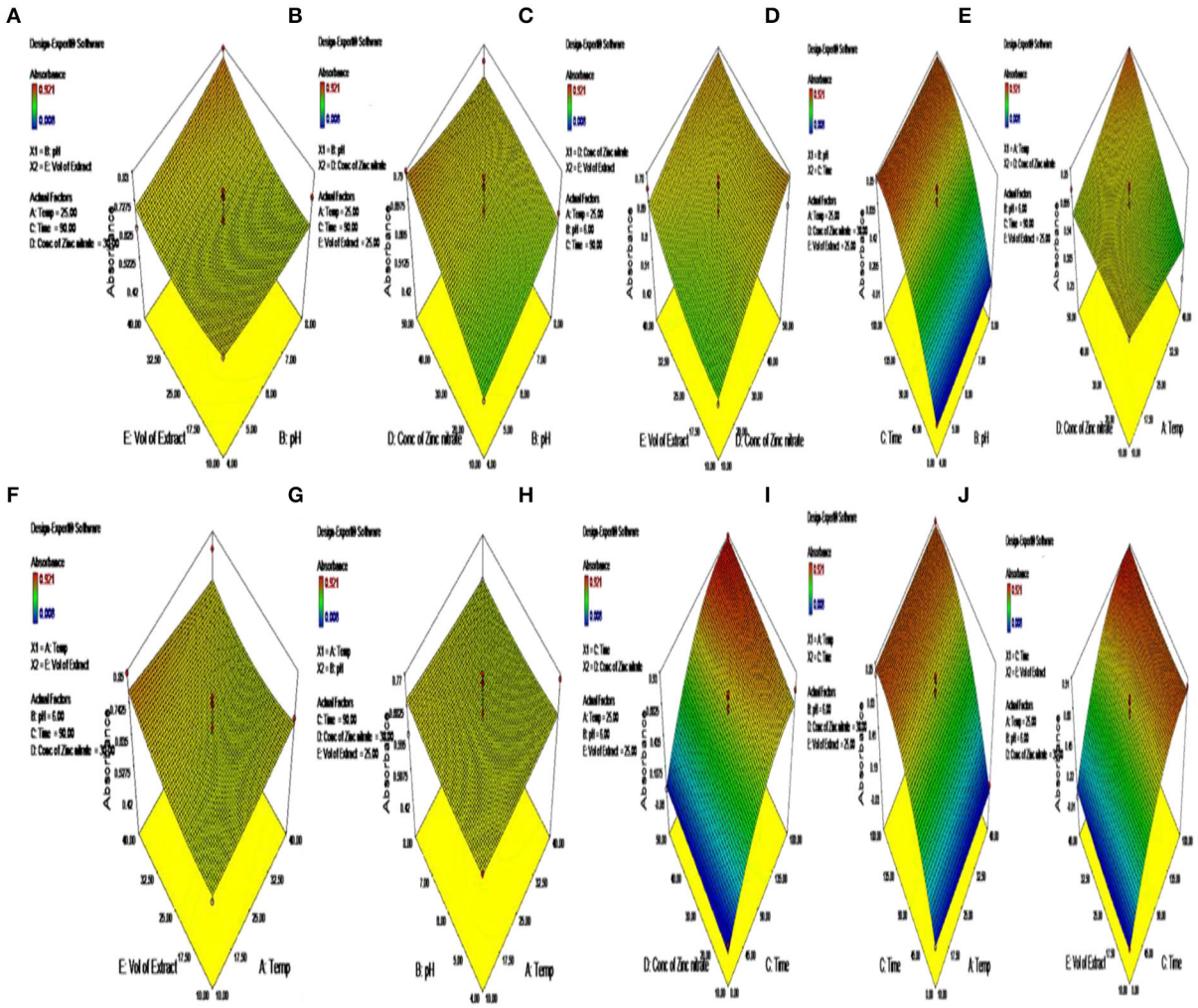


FIGURE 2
**(A–J)** Optimization of parameters for the synthesis of green-synthesized ZnO by *C. ternatea*.

and were subjected to automatic preparation by AutoDock Tools. ADT checked for and merged non-polar hydrogens with the heavier atoms to which they are attached and added Gasteiger charges.

## Grid preparation and molecular docking

To understand how the nanoparticles affected the interactions between the biofilm-associated proteins and the phytocompounds, a double-docking approach was followed, wherein, docking was first performed between the protein and ligand, and the resultant protein–ligand complex with the best cluster and lowest energy rank was further re-docked with zinc-oxide nanoparticles (ZnO-NPs). The whole procedure was carried out using the AutoDockTools software package (Morris et al., 2009). AutoDock is a molecular modeling simulation software specialized for effective protein–ligand docking, which is available under the GNU General Public License and is one of the most cited software used for docking applications in the research community.

AutoGrid was used to pre-calculate the three-dimensional grid of interaction energy based on macromolecular coordinates. AutoGrid constructs a three-dimensional grid surrounding the coordinates for the protein target and calculates the interaction energy of each grid point within it, thus creating a three-dimensional "array" of interaction energies called a "grid map" (Morris et al., 2008). This is done for the rapid evaluation of interaction energies as the completed grid of energies provided a quick lookup table (Goodsell et al., 1996). For both the docking studies, the entire macromolecule or the

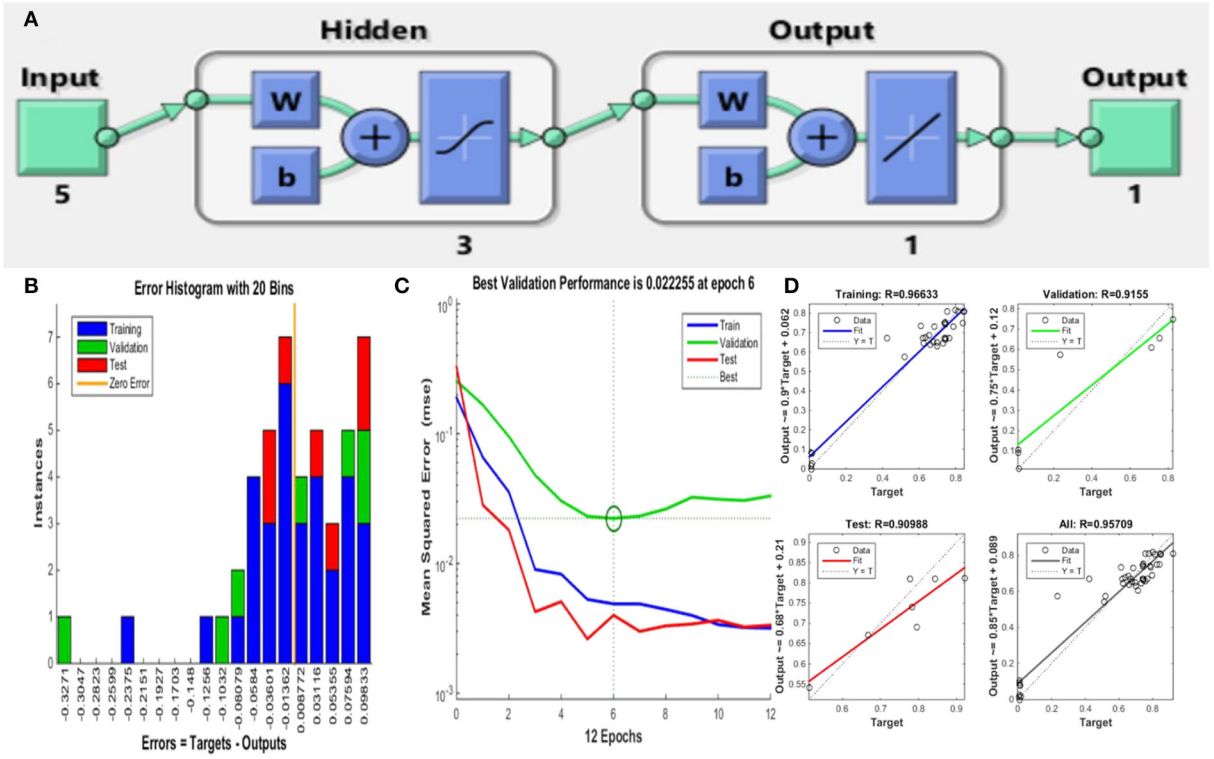


FIGURE 3
ANN-TLBO approach for ZnO NP synthesis. **(A)** Model architecture, **(B)** error histogram of the proposed model, **(C)** performance plot of the proposed model, and **(D)** regression plot for training, testing, and validation.

protein complex was enclosed within the grid box for the programme to create a larger amount of grid maps and search for the best interaction residues instead of limiting it to selective space.

The actual docking simulation was achieved with AutoDock4 for both rigid docking of protein and phytochemical ligand, and the resultant complex with the nanoparticle. A total of 1,000 runs of genetic algorithm (GA) with default parameters were used as search parameters and the output was set to the Lamarckian genetic algorithm (LGA) docking, also known as a hybrid genetic algorithm-local search (GA-LS).

## Attenuation of biofilm by atomic force microscope (AFM)

The biofilm was developed on the surface of the glass slip and was rinsed with phosphate buffer saline maintained at pH 7.4. Green synthesized ZnO NP was used for treating the biofilm being casted on the surface of the glass slide. Both treated and untreated samples of biofilm were scanned by the use of AFM (NT-MDT, Russia) at a speed of 1 Hz.

## Results and discussions

### Optimization in the production of biogenic ZnO NP

The parameters that were used for the purpose of optimizing the synthesis of ZnO NPs include pH, the volume of the extract of the plant used, and the concentration of zinc nitrate, which plays an essential role in the mechanism of synthesizing ZnO NPs. Thus, these three important parameters were taken into consideration for further study with RSM. RSM was used to optimize the use of three operational variables: pH, the volume of the extract, and the concentration of zinc nitrate for the purpose of better production of the ZnO NPs (Table 2). The values at *Y* showed that the parameters had a significant effect on the production of ZnO NPs (Table 3). The Box-Behnken design was used for the purpose of optimizing the three variables comprising 46 runs with five replicates of the central point (Figure 2). The optimization of the parameters was conducted one-factor-at-time and the results were in ignorance of the interactions between the process variables. The model helped in predicting the maximum absorbance of the biogenic ZnO

TABLE 3 RSM optimization model for optimizing the green synthesis of ZnO NPs from *C. ternatea*.

| Nanoparticle | Types of Response | Response | $R^2$ value | Adjusted $R^2$ value |
|---|---|---|---|---|
| Green-synthesized ZnO NP from *C. ternatea* | Absorbance = Absorbance +0.12747 −0.010575 * Temp −0.015677 * pH +9.91644E-003 * Time +3.74688E-003 * Conc of Zinc Nitrate −6.42454E-003 * Vol of Extract −2.91667E-004 * Temp * pH +1.12963E-005 * Temp * Time +4.32500E-004 * Temp * Conc of Zinc nitrate −1.31111E-004 * Temp * Vol of Extract −8.33333E-005 * pH * Time −1.16875E-003 * pH * Conc of Zinc Nitrate +1.17500E-003 * pH * Vol of Extract +1.66667E-005 * Time * Conc of Zinc nitrate −1.11111E-006 * Time * Vol of Extract −1.35000E-004 * Conc of Zinc Nitrate * Vol of Extract +1.37963E-005 * $Temp^2$ +3.27604E-003 * $pH^2$ −3.13863E-005 * $Time^2$ −3.03646E-005 * Conc of Zinc $Nitrate^2$ +1.87130E-004 * Vol of $Extract^2$ | Absorbance | 0.9723 | 0.8755 |

NPs that showed an F-value of 15.97 and a *p*-value of <0.01 that greatly implies that the model was used for the purpose of optimizing the conditions of NPs synthesis is significant (Figure 2, Table 2).

## ANN-TLBO prediction

The training of the neural network by a subset of various data matrices along with validation and testing regulates the performance of ANN-TLBO (training: testing: validation = 70:15:15). Thus, the ANN-TLBO model is implemented on the investigational data obtained from the executed BBD, the data set was split into three subsets (32:7:7) for the purpose of training, testing and validating the model. The mean square obtained from the analysis is considered as an indicator of performance, and $R^2$ (Correlation coefficient) is considered the precision index (Sarkar et al., 2020, 2022). The regression plots of the neural networks help in the representation of the training set, testing set, and validation set. The ANN-TLBO model for determining the biogenic ZnO nanoparticle synthesis comprises five input neuron layer that represents the process parameters, three hidden, and one output layer with the correlation coefficient value of 0.99939. On the other hand, *Staphylococcus aureus* comprises one input and four hidden neuron layers with a correlation coefficient value of 0.95709. It was further observed that the predicted values by ANN-TLBO were in close proximity with the actual run and the higher $R^2$ value in comparison to that of the RSM model illustrated that it was able to build a more robust model in comparison to that of the RSM technique (Figure 3, Table 3).

# Characterization of the green synthesized ZnO NPs

## Characterization of green synthesized ZnO NP

The green synthesis of ZnO nanoparticles from *C. ternatea* extract includes plant secondary metabolites those act as reducing as well as stabilizing agents of Zn ions in solutions of zinc oxide. The green synthesis of ZnO NPs from *C. ternatea* showed a broad peak at 335 nm (Figure 4) when scanned in the wavelength range of 300–450 nm. For ZnO nanoparticles, the absorbance peak is reported between 310 and 360 nm of wavelength (Song and Yang, 2016; Jayachandran and Nair, 2021) (Figure 4). The XRD patterns obtained by XRD (Figure 5) showed the synthesis of ZnO NP. The pattern of the crystalline peaks corresponding to (002), (101), (102), (110), (103), and (112) was almost similar to the work performed by previously published work (Alahmdi, 2022).

The green synthesized ZnO NPs thus formed were observed to be spherical in shape within the size range of 10–20 nm when observed with TEM (Figure 6).

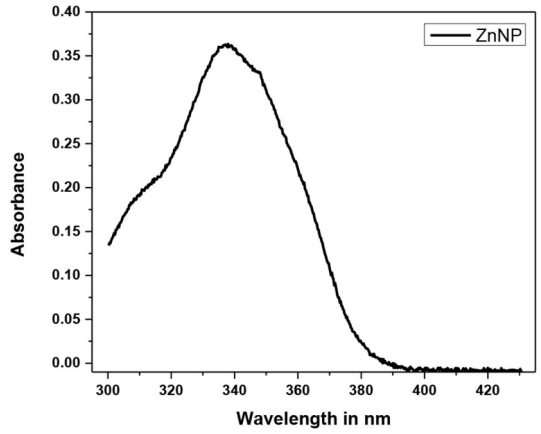


FIGURE 4
UV–visible spectroscopic analysis Green synthesized ZnO NP.

## Enfeeblement of the biofilm

The green-synthesized ZnO NPs were able to bring about the degradation of the biofilm with the enfeeblement of the structural components of the EPS constituting the biofilm (Hsueh et al., 2015). It was observed that the green-synthesized ZnO NPs were able to reduce the biofilm formed by *A. faecalis* and *P. gingivalis* by 92.27 ± 1.22% and 95.27 ± 1.28%, respectively. This was similar to the work done by Husain et al. (2022), which showed that the biosynthesized ZnO NPs were able to bring about degradation of the biofilm formed by *E.*

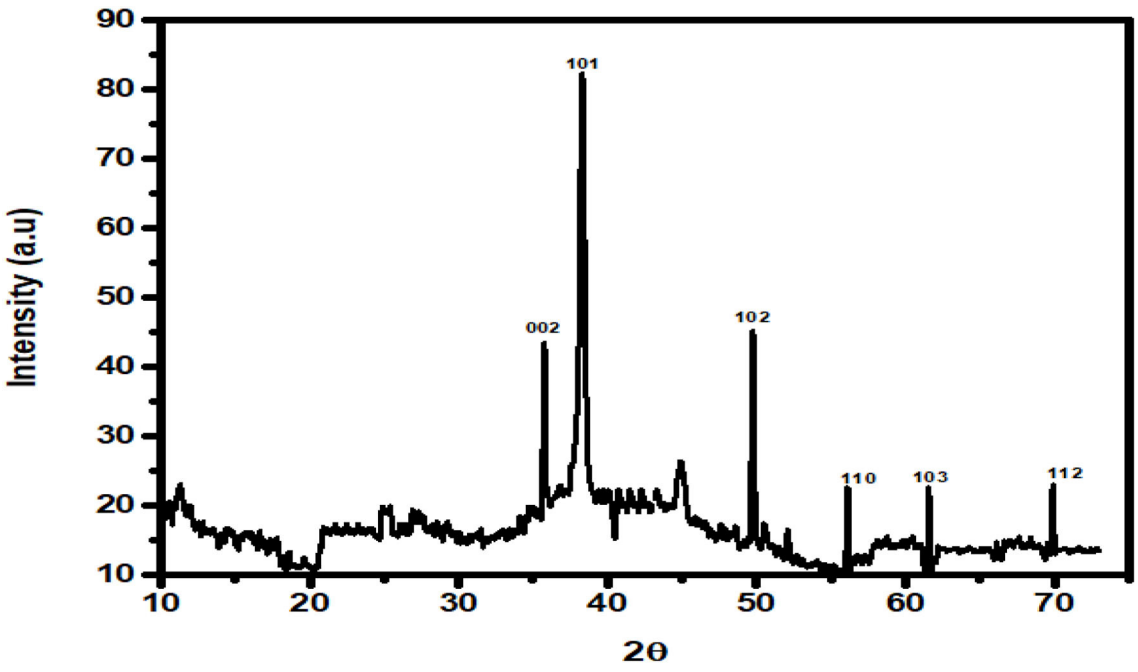


FIGURE 5
XRD analysis of the green synthesized ZnO NPs.

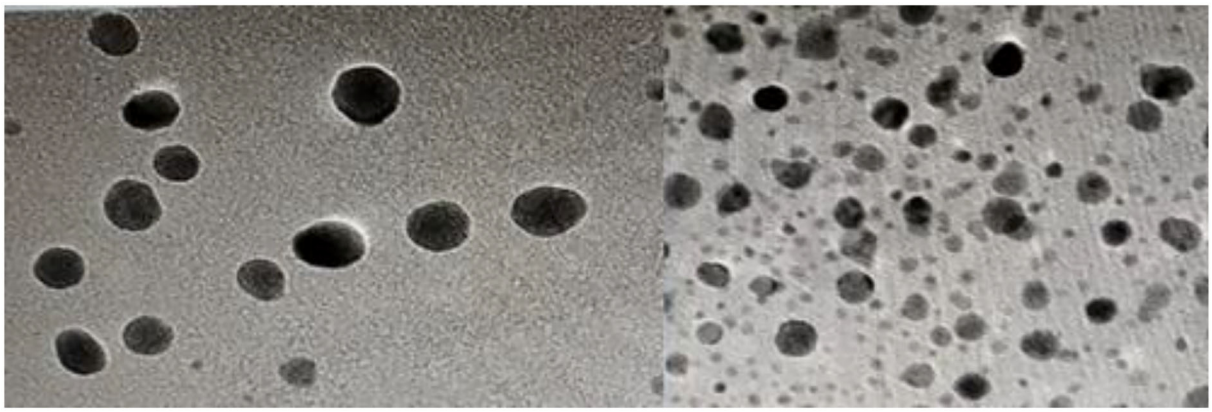

FIGURE 6
TEM images of green-synthesized ZnO NP from *C. ternatea*.

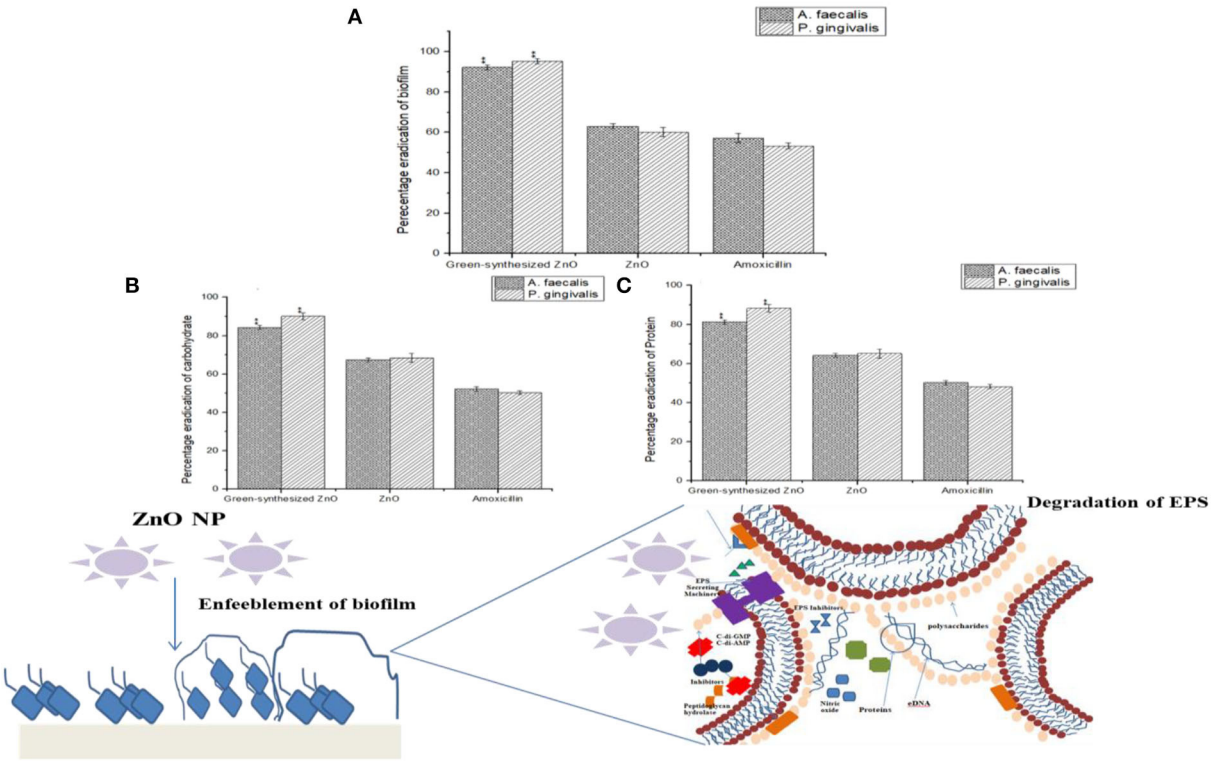


FIGURE 7
**(A)** Reduction of biofilm formed by *A. faecalis* and *P. gingivalis* in the presence of green-synthesized ZnO NPs. The ZnO NPs were also responsible for a marked reduction in the EPS with the degradation of **(B)** the carbohydrate and **(C)** protein content.

*coli, S. aureus,* and *P. aeruginosa* (Husain et al., 2022). The destabilization of biofilm architecture can be possible with the degradation of the EPS matrix (Pinto et al., 2020). The EPS has two architectural components, carbohydrates and proteins, which provide strength to the biofilm structure (Flemming et al., 2007). It was observed that the green-synthesized ZnO NPs were able to bring a marked reduction in the carbohydrate and protein content of the EPS. It was observed that the carbohydrate content within the EPS of *A. faecalis* and *P. gingivalis* was markedly reduced by 84.26 ± 1.09 % and 90.12 ± 1.09%,

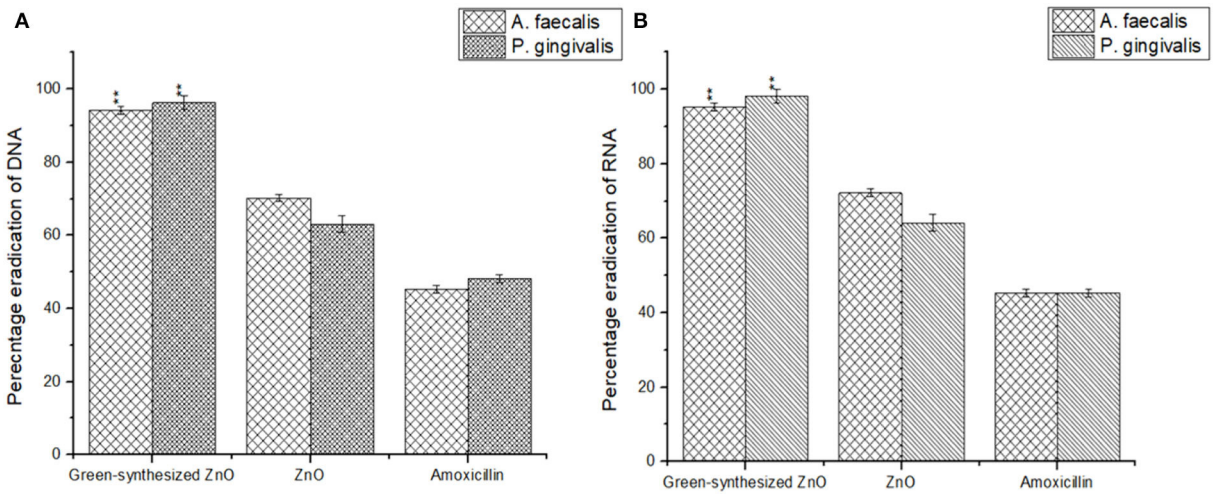


FIGURE 8
Biogenic ZnO NPs were responsible for a marked reduction in the DNA **(A)** and RNA **(B)** content of the sessile microbial colonies of *A. faecalis* and *P. gingivalis*.

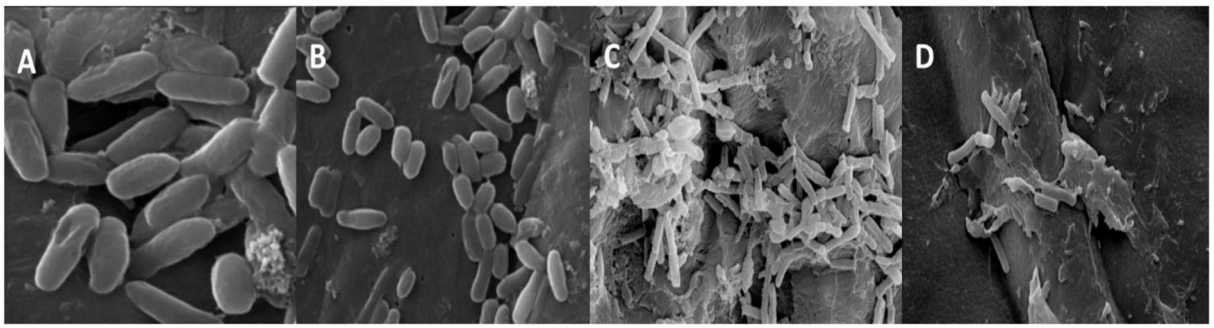


FIGURE 9
SEM images of *P. gingivalis* **(A,B)** control and treated with biogenic ZnO NPs and *A. faecalis* control and treated **(C,D)** with biogenic ZnO NPs.

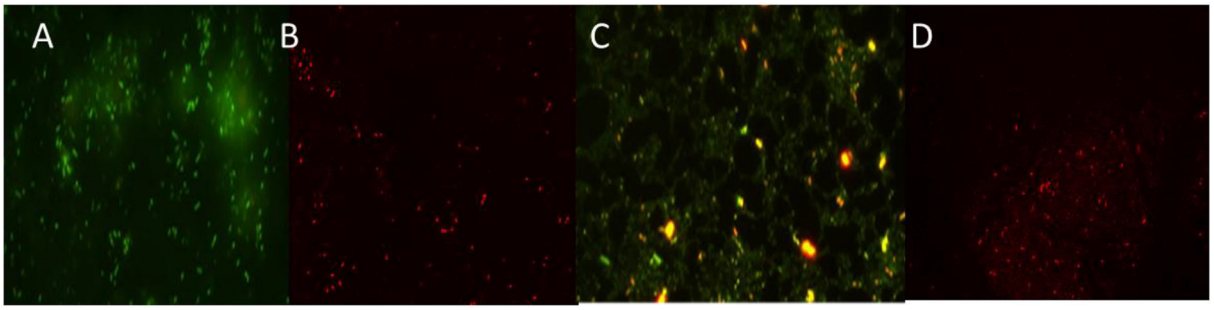


FIGURE 10
Fluorescence images of untreated and treated sessile cells by ZnO NPs of *P. gingivalis* **(A,B)** and *A. faecalis* **(C,D)**.

TABLE 4 Drug-like properties of phytocompounds.

| Bioactive compounds | Structure | Mol. Wt. | H-bond acceptors | H-bond donors | TPSA | Rotatable bonds | Bio-availability Score | Lipinski violations |
|---|---|---|---|---|---|---|---|---|
| Azadirachtin | 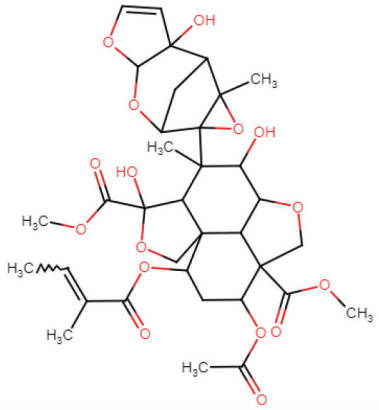 | 720.71 | 16 | 3 | 215.34 | 10 | 0.17 | 2 |
| Quercetin | 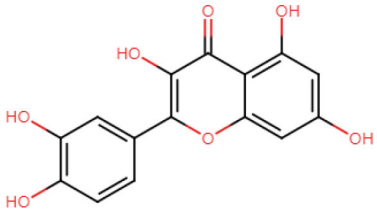 | 302.24 | 7 | 5 | 131.36 | 1 | 0.55 | 0 |

respectively, on the action of green-synthesized ZnO NPs. The NPs were also responsible for a marked reduction in the protein content of the EPS by 81.26 ± 1.09% and 88.23 ± 1.89%, respectively. This observation greatly portrayed the biogenic ZnO NPs were effective in the enfeeblement of biofilm by bringing about the destruction of the EPS (Lahiri et al., 2021d) (Figure 7).

## Degradation of genomic DNA and RNA content

The biogenic ZnO NPs possess the ability to penetrate through the biofilm and act on the cells by bringing degradation in the genomic DNA and RNA content of the cell (Kamli et al., 2021). The biogenic ZnO NPs brought a marked reduction in the genomic DNA content of *A. faecalis* and *P. gingivalis* by 94.26 ± 1.09% and 96.23 ± 1.89%, respectively. It was also observed that the NPs were further responsible to reduce the RNA content of the sessile cells in both *A. faecalis* and *P. gingivalis* by 95.26 ± 1.01% and 98.23 ± 1.83%, respectively (Figure 8).

# Influence on sessile cell viability in the presence of ZnO NP

## Disruption of biofilm under static conditions: Microscopic studies

### SEM analysis

The morphological and numerical alterations of biofilm-producing cells of the *A. faecalis* and *P. gingivalis* imparted by the green-synthesized ZnO NP were reflected by the scanning electron micrographs (Figure 9). The ZnO NP brought about a significant reduction in the number of biofilm-producing cells but also brought about a notable shrinkage in the cellular morphology and fewer colonization areas were visible compared to the control. Bacterial cells were found to form different layers of extracellular polymeric substance (EPS) in the control set which upon treatment with ZnO NP was reduced to single layers of cells showing a visible loss of the EPS and release of the cytoplasmic content. This shows that the NP brings about a substantial reduction in the biofilm along with considerable elimination of the sessile microcolonies.

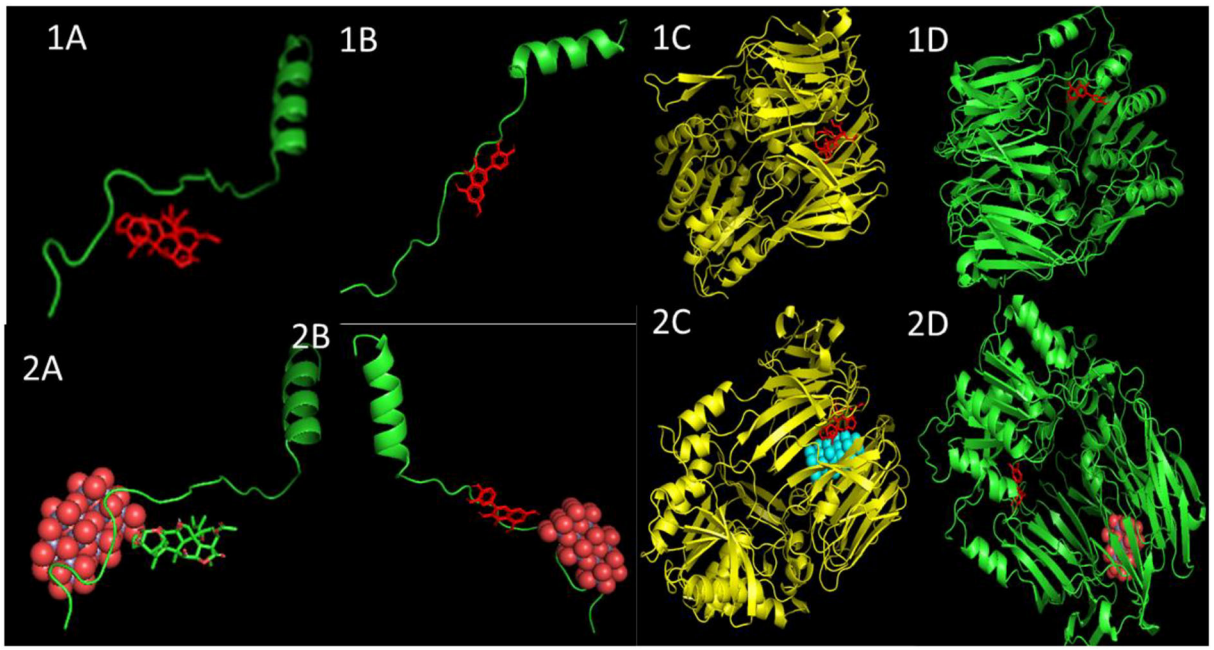


FIGURE 11
Docked poses and three-dimensional interactions of biofilm producing bacterial protein *P. gingivalis* and *A. faecalis* with phytochemical: **(1A,C)** Azadirachtin, **(1B,D)** Quercetin and the respective phytocompounds along with nanoparticles **(2A,C)** and **(2B,D)**.

TABLE 5 The binding energy values of molecular docking interaction.

| Protein | Ligand | Lowest binding energy | Lowest binding energy (NP) | Mean binding energy | Mean binding energy (NP) | Inhibition Constant Ki (ligand) | Inhibition Constant Ki (NP) |
|---|---|---|---|---|---|---|---|
| *P. gingivalis* | Azadirachtin | −8.12 | −13.19 | −8.11 | −12.76 | 1.12 uM | 216.08 pM |
| | Quercetin | −7.54 | −12.31 | −7.09 | −12.08 | 2.95 uM | 953.67 pM |
| *A. faecalis* | Azadirachtin | −7.89 | −9.77 | −7.87 | −9.74 | 8.96 uM | 159.60 nM |
| | Quercetin | −5.80 | −8.59 | −5.77 | −8.46 | 55.94 uM | 506.93 nM |

## Fluorescence microscopic analysis

The loss of biofilm production ability by the green synthesized ZnO-challenged cells of *A. faecalis* and *P. gingivalis* was checked by the fluorescence microscopic study (Figure 10). It showed a thick coating of biofilm in untreated conditions, whereas the treatment with ZnO NP resulted in a scattered appearance with a much lesser number of cells and a significantly reduced amount of biofilm. The application of the ZnO NP resulted in the killing of the cells as they appeared reddish in color in the presence of propidium iodide.

## ADME analysis

In this study, all the selected ligands were observed to have <10 hydrogen donors; however, azadirachtin was observed to have 16 hydrogen acceptors that resulted in a Lipinski violation. Apart from that, azadirachtin also had a molecular weight >500. Except for azadirachtin and nimbin, all the compounds had zero violations of Lipinski's rule of drug-likeness. However, azadirachtin was found to have the highest synthetic accessibility. All the compounds except the same had high gastrointestinal absorption, and none of the compounds are permeable to the blood brain barrier (Table 4).

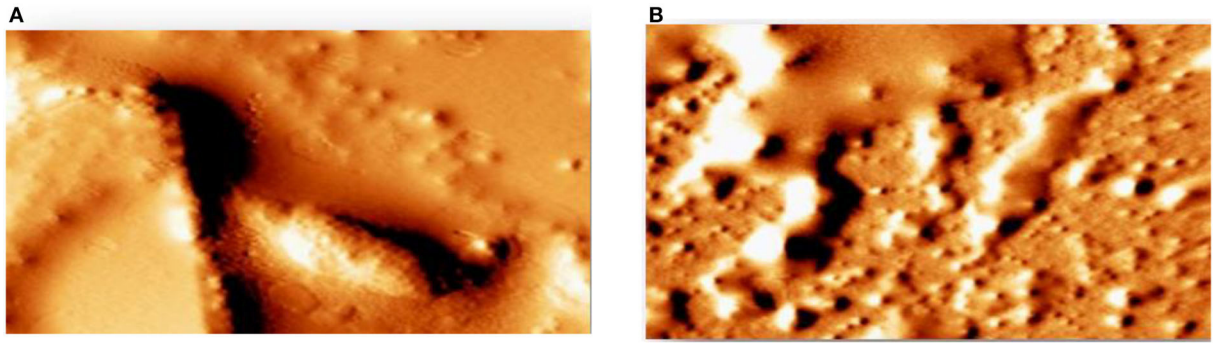


FIGURE 12
Detection of attenuation of biofilm by Atomic force microscope **(A)** tested strains was able to form a biofilm **(B)** green synthesized ZnO NP decreased significantly the adherence to glass.

### Docking analysis

AutoDock uses a "hybrid" force field that employs a "full" desolvation model, and also considers directionality in hydrogen bonds (Sarkar et al., 2021a). To estimate the interaction energy, it calculates the energy of ligand and protein in the unbound state first and then calculates the energy of the protein-ligand complex. Finally, these values are collectively used to compute the lowest and mean binding energy values. The lowest the energy value, the better is the interaction score of docking. In this study, nimbolide was found to have the best interaction with both 5OLJ and DMR19 proteins. Each of the compounds is observed to have inhibition constants in the micromolar range (uM). The inhibition concentration is a measure of the potency of an inhibitor. Mathematically, it is the concentration required to produce half the maximum inhibition.

The binding energy values of all complexes significantly decreased by ∼3 units. Double-docking with the ZnO nanoparticle was also found to enhance the number of cluster formations in all the complexes. In nimbolide, the number of clusters was found to be enhanced by a factor of 21 on docking with nanoparticles. ZnO nanoparticles also had a considerably lower inhibition constant (Ki), which was in the picoMolar and nanoMolar concentrations for biofilm forming proteins *P. gingivalis* and *A. faecalis*, respectively. This implies that a very low concentration of ZnO nanoparticles can be used to get the desired strong inhibition of the biofilm formation (Figure 11, Table 5).

## Detection of attenuation of biofilm by atomic force microscope (AFM)

AFM revealed that the tested strains was able to form biofilm and had the potency to adhere to a glass surface (Figure 12A). On the other hand, green synthesized ZnO NP decreased significantly the adherence to glass (Figure 12B). In addition, the combination of green synthesized ZnO NP decreased significantly the biofilm formation. AFM clearly showed the disrupted surface topology and height distribution profile of the biofilm developed in the presence of NP compared to the control biofilm.

## Conclusion

This study is focused on the efficiency of the green-synthesized ZnO NPs in the elimination of biofilm formed by *A. faecalis* and *P. gingivalis*. This was further ratified by the *in silico* studies. The recent study focused on the bioaugmented production of ZnO-NPs using floral extract of *C. ternatea* revealed the fact that it has a great possibility for making a nano-based herbal mouthwash with antibiofilm activities, which may be used for checking oral biofilm-induced diseases like periodontitis and tooth loss.

## Data availability statement

The original contributions presented in the study are included in the article/supplementary material, further inquiries can be directed to the corresponding author/s.

## Author contributions

Conceptualization and writing—review and editing: DL, MN, SPat, TS, and RR. Methodology: DL, MN, TS, SPan, SG, and MM. Formal analysis: DL, MN, MM, and RR. Investigation: DL, MN, and RR. Writing—original draft preparation: DL, MN, ZA, HE, SPat, TS, and RR. All

authors have read and agreed to the published version of the manuscript.

## Acknowledgments

The authors would like to acknowledge the University of Engineering and Management, Kolkata and Universiti Sains Malaysia for funding the work carried out in this manuscript.

## Conflict of interest

Author SPat was employed by NatNov Bioscience Private Ltd. and VU was employed by AMH Energy Pvt. Ltd.

The remaining authors declare that the research was conducted in the absence of any commercial or financial relationships that could be construed as a potential conflict of interest.

## Publisher's note

All claims expressed in this article are solely those of the authors and do not necessarily represent those of their affiliated organizations, or those of the publisher, the editors and the reviewers. Any product that may be evaluated in this article, or claim that may be made by its manufacturer, is not guaranteed or endorsed by the publisher.

## References

Alahmdi, M. I. (2022). *In Vitro Anticancer and Antibacterial Activity of Green Synthesized ZnO NPs Using Clitorea Ternatea Flower Extract : Inhibits MCF-7 Cell Proliferation Via Intrinsic Apoptotic Pathway*. 1–21. doi: 10.21203/rs.3.rs-1269775/v1

Allaker, R. P. (2011). "The use of antimicrobial nanoparticles to control oral infections," in *Nano-Antimicrobials* eds N. Cioffi, and M. Rai (Berlin, Heidelberg: Springer), 395–425. doi: 10.1007/978-3-642-24428-5_14

Allen, T. M., and Cullis, P. R. (2004). Drug delivery systems: entering the mainstream. *Science* 303, 1818–1822. doi: 10.1126/science.1095833

Baishya, R., Bhattacharya, A., Mukherjee, M., Lahiri, D., and Banerjee, S. (2016). Establishment of a simple reproducible model for antibiotic sensitivity pattern study of biofilm forming staphylococcus aureus. *Mater. Today Proc.* 3, 3461–3466. doi: 10.1016/j.matpr.2016.10.028

Bala, N., Saha, S., Chakraborty, M., Maiti, M., Das, S., Basu, R., et al. (2015). Green synthesis of zinc oxide nanoparticles using Hibiscus subdariffa leaf extract: effect of temperature on synthesis, anti-bacterial activity and anti-diabetic activity. *RSC Adv.* 5, 4993–5003. doi: 10.1039/C4RA12784F

Balouiri, M., Sadiki, M., and Ibnsouda, S. K. (2016). Methods for in vitro evaluating antimicrobial activity: a review. *J. Pharm. Anal.* 6, 71–79. doi: 10.1016/j.jpha.2015.11.005

Bharadwaj, K. K., Rabha, B., Pati, S., Choudhury, B. K., Sarkar, T., Gogoi, S. K., et al. (2021). Green synthesis of silver nanoparticles using diospyros malabarica fruit extract and assessments of their antimicrobial, anticancer and catalytic reduction of 4-nitrophenol (4-NP). *Nanomaterials* 11, 1999. doi: 10.3390/nano11081999

Caputo, L., Quintieri, L., Cavalluzzi, M. M., Lentini, G., and Habtemariam, S. (2018). Antimicrobial and antibiofilm activities of citrus water-extracts obtained by microwave-assisted and conventional methods. *Biomedicine* 6, 70. doi: 10.3390/biomedicines6020070

Daina, A., Michielin, O., and Zoete, V. (2017). SwissADME: a free web tool to evaluate pharmacokinetics, drug-likeness and medicinal chemistry friendliness of small molecules. *Sci. Rep.* 7, 42717. doi: 10.1038/srep42717

Flemming, H.-C., Neu, T. R., and Wozniak, D. J. (2007). The EPS matrix: the "house of biofilm cells". *J. Bacteriol.* 189, 7945–7947. doi: 10.1128/JB.00858-07

Goodsell, D. S., Morris, G. M., and Olson, A. J. (1996). Automated docking of flexible ligands: applications of AutoDock. *J. Mol. Recognit.* 9, 1–5.3. doi: 10.1002/(SICI)1099-1352(199601)9:1andlt;1::AID-JMR241andgt;3.0.CO;2-6

Hanwell, M. D., Curtis, D. E., Lonie, D. C., Vandermeersch, T., Zurek, E., and Hutchison, G. R. (2012). Avogadro: an advanced semantic chemical editor, visualization, and analysis platform. *J. Cheminform.* 4, 17. doi: 10.1186/1758-2946-4-17

Hsueh, Y.-H., Ke, W.-J., Hsieh, C.-T., Lin, K.-S., Tzou, D.-Y., and Chiang, C.-L. (2015). ZnO nanoparticles affect bacillus subtilis cell growth and biofilm formation. *PLoS ONE* 10, e0128457. doi: 10.1371/journal.pone.0128457

Husain, F. M., Qais, F. A., Ahmad, I., Hakeem, M. J., Baig, M. H., Masood Khan, J., et al. (2022). Biosynthesized zinc oxide nanoparticles disrupt established biofilms of pathogenic bacteria. *Appl. Sci.* 12, 710. doi: 10.3390/app12020710

Jamdagni, P., Khatri, P., and Rana, J. S. (2018). Green synthesis of zinc oxide nanoparticles using flower extract of Nyctanthes arbor-tristis and their antifungal activity. *J. King Saud Univ. Sci.* 30, 168–175. doi: 10.1016/j.jksus.2016.10.002

Jan, H., Shah, M., Usman, H., Khan, M. A., Zia, M., Hano, C., et al. (2020). Biogenic Synthesis and characterization of antimicrobial and antiparasitic zinc oxide (ZnO) nanoparticles using aqueous extracts of the himalayan columbine (*Aquilegia pubiflora*). *Front. Mater.* 7, 249. doi: 10.3389/fmats.2020.00249

Jayachandran, A., T., R., A., and Nair, A. S. (2021). Green synthesis and characterization of zinc oxide nanoparticles using *Cayratia pedata* leaf extract. *Biochem. Biophys. Rep.* 26, 100995. doi: 10.1016/j.bbrep.2021.100995

Kamli, M. R., Malik, M. A., Srivastava, V., Sabir, J. S. M., Mattar, E. H., and Ahmad, A. (2021). Biogenic ZnO nanoparticles synthesized from origanum vulgare abrogates quorum sensing and biofilm formation in opportunistic pathogen *Chromobacterium violaceum*. *Pharmaceutics* 13, 1743. doi: 10.3390/pharmaceutics13111743

Khatoon, Z., McTiernan, C. D., Suuronen, E. J., Mah, T. F., and Alarcon, E. I. (2018). Bacterial biofilm formation on implantable devices and approaches to its treatment and prevention. *Heliyon* 4, e01067. doi: 10.1016/j.heliyon.2018.e01067

Lahiri, D., Nag, M., Banerjee, R., Mukherjee, D., Garai, S., Sarkar, T., et al. (2021a). Amylases: biofilm inducer or biofilm inhibitor? *Front. Cell. Infect. Microbiol.* 11, 660048. doi: 10.3389/fcimb.2021.660048

Lahiri, D., Nag, M., Dutta, B., Sarkar, T., and Ray, R. R. (2021b). Artificial Neural Network and Response Surface Methodology-Mediated Optimization of Bacteriocin Production by Rhizobium leguminosarum. *Iran. J. Sci. Technol. Trans. A Sci.* 45, 1509–1517. doi: 10.1007/s40995-021-01157-6

Lahiri, D., Nag, M., Sarkar, T., Dutta, B., and Ray, R. R. (2021c). Antibiofilm activity of α-amylase from bacillus subtilis and prediction of the optimized conditions for biofilm removal by Response Surface Methodology (RSM) and Artificial Neural Network (ANN). *Appl. Biochem. Biotechnol.* 193, 1853–1872. doi: 10.1007/s12010-021-03509-9

Lahiri, D., Nag, M., Sheikh, H. I., Sarkar, T., Edinur, H., atan, Siddhartha, P., et al. (2021d). Microbiologically synthesized nanoparticles and their role in silencing the biofilm signaling cascade. *Front. Microbiol.* 12, 636588. doi: 10.3389/fmicb.2021.636588

Limoli, D. H., Jones, C. J., and Wozniak, D. J. (2015). Bacterial extracellular polysaccharides in biofilm formation and function. *Microbiol. Spectr.* 3, 1–30. doi: 10.1128/9781555817466.ch11

Maeda, H., Wu, J., Sawa, T., Matsumura, Y., and Hori, K. (2000). Tumor vascular permeability and the EPR effect in macromolecular therapeutics: a review. *J. Control. Release* 65, 271–284. doi: 10.1016/S0168-3659(99)00248-5

Momma, K., and Izumi, F. (2008). VESTA: a three-dimensional visualization system for electronic and structural analysis. *J. Appl. Crystallogr.* 41, 653–658. doi: 10.1107/S0021889808012016

Morris, G. M., Huey, R., Lindstrom, W., Sanner, M. F., Belew, R. K., Goodsell, D. S., et al. (2009). AutoDock4 and AutoDockTools4: automated docking with selective receptor flexibility. *J. Comput. Chem.* 30, 2785–2791. doi: 10.1002/jcc.21256

Morris, G. M., Huey, R., and Olson, A. J. (2008). Using AutoDock for ligand-receptor docking. *Curr. Protoc. Bioinforma. Chapter* 8, 14. doi: 10.1002/0471250953.bi0814s24

Morse, D. J., Wilson, M. J., Wei, X., Lewis, M. A. O., Bradshaw, D. J., Murdoch, C., et al. (2018). Denture-associated biofilm infection in three-dimensional oral mucosal tissue models. *J. Med. Microbiol.* 67, 364–375. doi: 10.1099/jmm.0.000677

Pinto, R. M., Soares, F. A., Reis, S., Nunes, C., and Van Dijck, P. (2020). Innovative strategies toward the disassembly of the EPS matrix in bacterial biofilms. *Front. Microbiol.* 11, 952. doi: 10.3389/fmicb.2020.00952

Quintieri, L., Fanelli, F., Zühlke, D., Caputo, L., Logrieco, A. F., Albrecht, D., et al. (2020). Biofilm and pathogenesis-related proteins in the foodborne *P. fluorescens* ITEM 17298 with distinctive phenotypes during cold storage. *Front. Microbiol.* 11, 991. doi: 10.3389/fmicb.2020.00991

Sahoo, S. K., and Labhasetwar, V. (2003). Nanotech approaches to drug delivery and imaging. *Drug Discov. Today* 8, 1112–1120. doi: 10.1016/S1359-6446(03)02903-9

Sarkar, T., Bharadwaj, K. K., Salauddin, M., Pati, S., and Chakraborty, R. (2021a). Phytochemical characterization, antioxidant, anti-inflammatory, anti-diabetic properties, molecular docking, pharmacokinetic profiling, and network pharmacology analysis of the major phytoconstituents of raw and differently dried *Mangifera indica* (Himsaga). *Appl. Biochem. Biotechnol.* 194, 950–987. doi: 10.1007/s12010-021-03669-8

Sarkar, T., Salauddin, M., Choudhury, T., Um, J. S., Pati, S., Hazra, S. K., et al. (2021b). Spatial optimisation of mango leather production and colour estimation through conventional and novel digital image analysis technique. *Spat. Inf. Res.* 29, 439–453. doi: 10.1007/s41324-020-00377-z

Sarkar, T., Salauddin, M., Hazra, S., and Chakraborty, R. (2020). Artificial neural network modelling approach of drying kinetics evolution for hot air oven, microwave, microwave convective and freeze dried pineapple. *SN Appl. Sci.* 2, 1621. doi: 10.1007/s42452-020-03455-x

Sarkar, T., Salauddin, M., Mukherjee, A., Shariati, M. A., Rebezov, M., Tretyak, L., et al. (2022). Application of bio-inspired optimization algorithms in food processing. *Curr. Res. Food Sci.* 5, 432–450. doi: 10.1016/j.crfs.2022.02.006

Song, Y., and Yang, J. (2016). Preparation and in-vitro cytotoxicity of zinc oxide nanoparticles against osteoarthritic chondrocytes. *Trop. J. Pharm. Res.* 15, 2321. doi: 10.4314/tjpr.v15i11.4

Stalin, B., Ramesh Kumar, P., Ravichandran, M., Siva Kumar, M., and Meignanamoorthy, M. (2019). Optimization of wear parameters using Taguchi grey relational analysis and ANN-TLBO algorithm for silicon nitride filled AA6063 matrix composites. *Mater. Res. Express* 6, 106590. doi: 10.1088/2053-1591/ab3d90

Tailor, G., Chaudhay, J., Verma, D., and Kr. Sarma, B. (2019). Microscopic study of zinc nanoparticles synthesised using thermosetting polymer. *Appl. Microsc.* 49, 20. doi: 10.1186/s42649-019-0018-0

Thrall, J. H. (2004). Nanotechnology and medicine. *Radiology* 230, 315–318. doi: 10.1148/radiol.2302031698

Vasir, J. K., and Labhasetwar, V. (2005). Targeted drug delivery in cancer therapy. *Technol. Cancer Res. Treat.* 4, 363–374. doi: 10.1177/153303460500400405

Vasir, K. J., Reddy, K. M., and Labhasetwar, D. V. (2005). Nanosystems in drug targeting: opportunities and challenges. *Curr. Nanosci.* 1, 47–64. doi: 10.2174/1573413052953110

# Frontiers in Microbiology

**Explores the habitable world and the potential of microbial life**

The largest and most cited microbiology journal which advances our understanding of the role microbes play in addressing global challenges such as healthcare, food security, and climate change.

---

## Discover the latest Research Topics

See more →


**Frontiers**

Avenue du Tribunal-Fédéral 34
1005 Lausanne, Switzerland
frontiersin.org

**Contact us**

+41 (0)21 510 17 00
frontiersin.org/about/contact